
This item was submitted to [Loughborough's Research Repository](#) by the author.
Items in Figshare are protected by copyright, with all rights reserved, unless otherwise indicated.

A methodology to support elbow flesh deformation for ergonomics modelling

PLEASE CITE THE PUBLISHED VERSION

PUBLISHER

Loughborough University

LICENCE

CC BY-NC-ND 4.0

REPOSITORY RECORD

Hermawati, Setia. 2011. "A Methodology to Support Elbow Flesh Deformation for Ergonomics Modelling".
Loughborough University. <https://hdl.handle.net/2134/9271>.

This item was submitted to Loughborough's Institutional Repository (<https://dspace.lboro.ac.uk/>) by the author and is made available under the following Creative Commons Licence conditions.



For the full text of this licence, please go to:
<http://creativecommons.org/licenses/by-nc-nd/2.5/>

A Methodology to Support Elbow Flesh Deformation for Ergonomics Modelling

by

Setia Hermawati

A Doctoral Thesis

Submitted in partial fulfillment of the requirements

for the award of

Doctor of Philosophy of Loughborough University

July 2011

© by Setia Hermawati 2011

Abstract

A human centric approach to the design of products and workplaces is essential to ensure the appropriate accommodation of the people who interact with such designs. Digital human models (DHM) in ergonomic simulation are commonly used within design and development to ensure product suitability. DHM for ergonomic simulation has improved in terms of its reliability and appearance in recent years. However, there appears to be a need to improve how the flesh of the DHM deforms around the joint to support improved ergonomics simulations. Supported by data acquired through the use of a 3D body scanner, this PhD research aimed to address this need by developing a methodology to simulate body deformation due to joint movements that suited the needs of ergonomics simulation. To anticipate the large scope of the research, this research focused on modelling a single joint: the elbow.

To ensure the suitability of the proposed flesh deformation method a literature review and user study was performed to derive a set of DHM specifications. Six DHM specifications were proposed i.e. accuracy, realism, minimum user intervention, accommodating different body types and sizes, real time, and whole body modelling. An existing flesh deformation method (FDM) which had the potential to conform to the DHM specifications was determined and chosen to be developed further so that it matched the requirements of DHM for ergonomics simulation. The development resulted in a new FDM which required the provision of several elements to create a surface flesh deformation at the elbow. These were: five cross sections and their locations from four key postures (full extension, 135° flexion, 90° flexion and maximum flexion); the carrying angle; and perpendicular profiles from all of the four key postures. To avoid having to obtain these elements for every person for whom the elbow was to be modelled, a supporting data framework was developed. The framework utilised a database and a limited number of inputs (race, gender, BMI and a 3D scan data of a fully extended arm) to predict the FDM's elements from which flesh deformation at the elbow was created. The database stored five key cross sections, profiles, a parameter for the carrying angle and a parameter of the locations of UAF, UAM, LAM for two race groups i.e., Caucasian and Asian. A total of 23 subjects (11 males and 12 females) were carefully chosen to represent a variety of height and body type for each race and gender. The algorithm for the new FDM and the framework is supplied in the accompanying CD.

DHM specifications were utilised to review the suitability of the new FDM for ergonomics simulation. The review results showed that the new FDM had a level of error < 3mm and was able to recreate flesh deformation around the elbow joint with a representative level of surface realism when compared to the 3D scan data. The review result also showed that the new FDM was able to accommodate different body types and sizes with a slightly larger error, < 4mm. The new FDM also demonstrated that it could be used to create flesh deformation with limited user intervention. A retrospective analysis for real time modelling and whole body modelling showed that the new FDM had a potential to conform to these two specifications. The overall result of the review demonstrated that the new FDM and framework had the potential to suit ergonomics simulation.

The thesis has made a contribution to the field of DHM research for ergonomics simulation by proposing a flesh deformation approach for the elbow that allows the integration of carrying angle; and was built based on specification for the use of DHM's in ergonomics simulation and the utilisation of 3D scan data.

Acknowledgement

I would like to thank the following people for their invaluable assistance and support:

- ❖ My partner in crime and dearest husband, Peter Chesney, who has given me tremendous support during the writing up process of this thesis.
- ❖ My parents, who have given me continuous support through their prayers.
- ❖ My supervisor, Dr. Russell Marshall, who has given me constant guidance and invaluable feedback throughout my PhD.

Table of Contents

Certificate of Originality

Abstract

Acknowledgements

List of Figures i

List of Tables xx

1.	Introduction	1
1.1	Background of research	1
1.2	Research Motivation	2
1.2.1	The trend towards DHM that is able to represent humans as closely as possible	3
1.2.2	Emergence of new technologies	3
1.2.3	A gap between DHM development in ergonomics simulation and entertainment.....	4
1.3	Research scope	5
1.4	Aim and objectives	6
1.5	Thesis outline	6
2	Literature Review	8
2.1	Digital human models (DHM) in ergonomics applications	8
2.1.1	DHM's role in ergonomics.....	9
2.1.2	DHM's characteristics in ergonomics	12
2.1.3	Existing DHM for ergonomics application	12
2.1.4	Current and future research of DHM for ergonomics application	15
2.2	Flesh Deformation around the joint for DHM	16
2.2.1	Anatomic approach to flesh deformation	16
2.2.2	Physical approach to flesh deformation.....	18
2.2.3	Geometric approach to flesh deformation	19
2.2.4	Example based	23
2.2.5	Sweep based	25
2.3	Surface Creation.....	27
2.3.1	Polygonal surface.....	27
2.3.2	Subdivision surface	28
2.3.3	Implicit	30
2.3.4	Parametric surfaces	30
2.4	Joints movements in DHM	31
2.4.1	Representing the orientation and movement of a joint	33

2.4.2	Effect of the relative orientation of a joint to its parent upon its movement	36
2.5	3D body scanning	38
2.6	Summary	40
3	User Study	43
3.1	Methodology for the user study	44
3.1.1	Sampling groups.....	45
3.1.2	Questionnaire	46
3.2	User study result	49
3.2.1	Response rate	49
3.2.2	Respondents' backgrounds.....	49
3.2.3	Questionnaires Result	50
3.3	Summary	59
4	Methodology for FDM Development	64
4.1	DHM specifications	66
4.1.1	Accuracy.....	66
4.1.2	Realism.....	67
4.1.3	Whole body modelling.....	68
4.1.4	Real time	68
4.1.5	Accommodation of different body sizes and types	69
4.1.6	Minimum user intervention	69
4.2	Comparing DHM specifications and existing FDM.....	70
4.2.1	Anatomical approach	70
4.2.2	Physical approach	70
4.2.3	Geometrical approach	71
4.2.4	Shape by example approach	71
4.2.5	Sweep blend approach	71
4.2.6	Discussion	72
4.3	Summary	74
5	First Design Phase	76
5.1	First design phase strategy.....	76
5.2	3D data capture	77
5.3	Analysis of 3D data capture integration into the Shen et al. (1994) method	79
5.3.1	Bones	79
5.3.2	Cross Sections	81

5.4	Summary	90
6	Second Design Phase.....	92
6.1	Determining the carrying angle.....	94
6.1.1	A mini literature study on the carrying angle.....	94
6.1.2	The strategy to determine the carrying angle.....	95
6.1.3	Determining the carrying angle for a fully extended and pronated arm.....	96
6.1.4	Determining the carrying angle for a posture other than a fully extended and pronated arm.....	98
6.1.5	Integrating carrying angle into upper and lower arm bone movements	100
6.2	Determining the boundaries of the region for flesh deformation at the elbow.....	102
6.2.1	Investigating the flesh deformation area at the elbow and establishing boundaries for flesh deformation at the elbow	102
6.2.2	Studying the boundaries for flesh deformation at the elbow	104
6.3	Determining a set of posture examples to govern the flesh deformation	106
6.3.1	General study of the flesh deformation at the elbow	107
6.3.2	Establishing a detail pattern of the flesh deformation.....	109
6.3.3	Choosing a suitable type of interpolation and determining a set of posture examples to interpolate the flesh deformation pattern	112
6.4	Establishing a method to acquire the cross sections from the key postures.....	114
6.4.1	Reviewing alternative methods to capture cross sections.....	114
6.4.2	Developing the chosen method to capture cross sections.....	116
6.5	Determining cross section planes' orientation.....	119
6.6	Determining number of cross sections and their location	119
6.6.1	Reviewing relevant factors to the determination of cross sections' number and location	120
6.6.2	Mini study to determine number and locations of cross sections	123
6.7	Optimum number of sampling points for cross sections.....	126
6.8	Summary	127
7	Third Design Phase.....	130
7.1	Integrating joint information and digitised cross sections	130
7.1.1	The strategy to integrate joint information and digitised cross sections	131
7.1.2	Mini study to investigate the robustness of the 3D body scanner's joint locations ...	133
7.1.3	A protocol for integration of a 3D scan of a fully extended arm with its joint information and digitised cross sections.....	134

7.1.4	A protocol for integration of joint information and digitised cross sections where a 3D scanned arm was not available	138
7.1.5	Discussion	142
7.2	Generating the additional cross sections	144
7.2.1	Investigating the possibility of utilising five key cross sections to generate additional cross sections	145
7.2.2	Proposing the general outline of the method to create additional cross sections	149
7.2.3	Establishing protocols from the general outline of the method	150
7.3	Interpolation to govern the flesh deformation	158
7.3.1	Reviewing the elements to model an arm surface	159
7.3.2	Establishing protocols for the proposed interpolation methods	162
8	Review of the Proposed FDM	174
8.1	Feasibility testing of the proposed FDM	174
8.1.1	Methodology of the proposed FDM's feasibility testing	174
8.1.2	Data collection	175
8.1.3	Data preparation	175
8.1.4	Software programming (phase 1)	180
8.1.5	Evaluation of programming results (phase 1)	182
8.1.6	Software programming (phase 2)	187
8.1.7	Evaluation of programming results (phase 2)	190
8.2	Methodology of proposed FDM's review	192
8.2.1	Review of the proposed FDM's accuracy	194
8.2.2	Review of the proposed FDM's realism	202
8.2.3	Review of the proposed FDM for minimum user intervention	214
8.2.4	Review of the proposed FDM against the real time modelling specification	216
8.2.5	Review of the proposed FDM against the whole body modelling specification	219
9	Application of the Proposed FDM for Different Body Types and Sizes	221
9.1	Strategy to apply the new FDM for different body types and sizes	221
9.2	The general outline of the framework	222
9.3	Stages to detail the general outline of the framework	224
9.4	Predicting the carrying angle at a full flexion	225
9.5	Predicting the locations of UAF, UAM, LAM and LAF for all key postures	226
9.5.1	Study on the locations of UAF, UAM, LAM and LAF	227

9.5.2	Proposing a method to predict the location of UAF, UAM, LAM and LAF for all key postures	232
9.6	Predicting five key cross sections at 135°, 90° and maximum flexion	234
9.6.1	Study on five key cross sections of all key postures	236
9.6.2	Proposing a method to predict five key cross sections at 135°, 90° and maximum flexion	243
9.7	Predicting profiles at 135°, 90° and maximum flexion	255
9.7.1	Study on profiles of all key postures	256
9.7.2	Proposing a method to predict profiles at 135°, 90° and maximum flexion	268
9.8	Database Design.....	277
9.9	Data collection for the database	279
9.10	Data processing for the database	283
9.10.1	Data processing for database items that were linked to the locations of UAF, UAM, LAM and LAF	283
9.10.2	Data processing for database items that were linked to the shape of five key cross sections	292
9.10.3	Data processing for database items linked to the shape of profiles	300
9.11	Software programme development	304
9.11.1	Programming for template matching and sampling of 3D scan data	304
9.11.2	Programming to predict five key cross sections for 135°, 90° and maximum flexion	308
9.11.3	Programming to predict profiles at 135°, 90° and maximum flexion	310
9.11.4	Integration of FDM's programming with the programming from section 9.11.1, 9.11.2 and 9.11.3.	317
9.11.5	Discussions	318
9.12	Summary	318
10	Review of the New FDM's Ability to Accommodate Different Body Sizes and Shapes.....	320
10.1	Methodology.....	320
10.2	Data collection and preparation	321
10.3	Review on the accuracy of the new FDM's ability to accommodate different body sizes and shapes	325
10.3.1	Comparison for the five key cross sections	326
10.3.2	Comparison for the profile.....	327
10.3.3	Discussions on the accuracy review	329

10.4	Review on the realism of the new FDM's ability to accommodate different body sizes and shapes	329
10.4.1	Comparison with the 3D scanned arm (full extension-135° and 135°-90°)	329
10.4.2	Comparison with the side view photographs (90°-maximum flexion)	333
10.4.3	Discussions on the realism review	344
10.5	Summary	344
11	Discussions	346
11.1	Key stages of the adopted research methodology	347
11.1.1	The literature review	348
11.1.2	The user study	351
11.1.3	The establishment of DHM specifications	358
11.1.4	The comparison of existing DHMs against the DHM specifications	359
11.1.5	The development of the new FDM	360
11.1.6	The review of FDM	369
11.1.7	The development of the framework (the application of FDM to accommodate flesh deformation for different body types and sizes)	371
11.1.8	The review of the framework	383
11.2	The advantages and disadvantages of the new FDM	384
11.3	The advantages and disadvantages of the framework	385
11.4	Research contribution and limitation	386
11.5	Future studies	388
11.5.1	Application of the FDM methodology to other joints	388
11.5.2	Application of the FDM methodology to support flesh deformation due to external forces	391
12	Conclusions and Future Studies	393
12.1	Conclusions	393
12.2	Future applications and studies	396
	References	398
	Accompanying CD (contains appendix; and algorithm of the new FDM and the framework)	

List of Figures

Figure 1. Thesis outline	6
Figure 2. An example of link and joint structure in JACK (adapted from Blanchonette (2010)) and some of the anthropometric measurements which are used to create the size of DHM	9
Figure 3. Unrealistic flesh deformation that occurs at the shoulder and elbow area due to postures adopted by DHMs (Adapted from Lämkuill, Örtengren and Malmsköld (2008))	10
Figure 4. Functions of ergonomics application throughout stages of a product life cycle (adapted from Sundin and Örtengren (2006))	11
Figure 5. Integration of motion capture in JACK to create realistic motion and posture (adapted from Sundin and Örtengren (2006))	13
Figure 6. RAMSIS's overlay technology to fit posture and anthropometric data (adapted from Seidl (2004))	14
Figure 7. SAMMIECAD created an additional database which preserved individual data which allowed virtual fitting trial (adapted from Porter et al. (2004)).....	14
Figure 8. SANTOS, a virtual soldier which had advanced features for its functionalities and realism (adapted from Abdel-Malek et al. (2006))	15
Figure 9. Upper arm model (adapted from Maurel (1998))	16
Figure 10. Skeleton model (top left image), muscle model (top middle image), muscle actuator of one of the muscle at the back (right image) and the result of flesh deformation (adapted from Leet at al. (2009))	17
Figure 11. Left image shows ellipsoids that represent muscle in Scheepers et al. (1997) study whereas the right image show deformed cylinder which represent muscles from Wilhelms and Gelder (1997).....	18
Figure 12. Two classical problems with skinning collapsed joint due to extreme and twisting posture (adapted from Lewis et al. (2000)).....	20
Figure 13. Curve skeleton, shown as thin line inside the body mesh, at the initial pose (adapted from Yang et al. (2006)).....	21
Figure 14. The left image shows a selected region to create a patch and the right image shows the created patch (adapted from Lee et al. (2009))	21
Figure 15. The left image shows half of the control surface created in Capell et al. (2002) study whereas the right image shows a cage based deformation from Ju et al. (2008) which consists of four “skinning templates”	22

Figure 16. The process of inversing an example pose (bent arm) to an initial pose (straight arm) in order to acquire location of vertices of the example pose at a new pose (straight arm) which was then used to acquire displacement maps in Lewis et al. (2000) (adapted from Sloan et al. (2001)) ..	24
Figure 17. Left image: cross section contours of the body. Middle and right images: cross section orientation and ray-casting (adapted from Shen et al. (1994)).....	26
Figure 18. Left figure shows the fitting of ellipses into the cross section of an arm while right figure shows the self intersection area detection in various postures (adapted from Hyun et.al., 2005).....	26
Figure 19. The left image shows the template of the bespoke hand model from Lee and Kim (2007) whereas the right image shows characteristic curves from You et al. (2008) which were created from a given horse skin mesh.....	27
Figure 20. (a) Low resolution polygon mesh (b) High resolution polygon mesh	28
Figure 21. Accuracy vs number of straight lines to represent a curve. From left to right, the accuracy increases as the number used to represent the curve increases	28
Figure 22. Comparison for various subdivision surfaces	28
Figure 23. Interaction between metaballs (adapted from http://www.studio-pon.com/en/products/digimeta/index.html)	30
Figure 24. (a). A Bezier curve with its control points (b) B-splines curves created from 4 control points (left) and the basis functions used to create the curve (right). The polynomial degree of the upper curve is 1 while the lower one is 2. The knot vectors are equally spaced	30
Figure 25. (a) C0 continuity, there is sharp point between two curves (b) C1 continuity. (c) C2 continuity.....	31
Figure 26. Forward and inverse kinematics illustrations.....	32
Figure 27. Skeletal hierarchy for legs-feet and shoulder-arms-a part of hands (adapted from http://h-anim.org , 2009)	32
Figure 28. Rotation matrix	33
Figure 29. Results of interpolation from some possible rotation matrix interpolation between the starting point (the most left point) and the end point (the most right point)	34
Figure 30. (a) Fixed angle rotation, YXZ order of (-45°, 45°,90°). (b) angle rotation, YXZ order of (-45°, 0, 45°)	35
Figure 31. Gimbal lock effect	35
Figure 32. Axis angle representation.....	35
Figure 33. Illustration of the zero reference position and joints orientation (adapted from Centre for Digital Arts and Experimental Media - University of Washington, 2009).....	36
Figure 34. Case example to illustrate joint movement	38

Figure 35. Steps in performing 30° rotations for bone 1: i) translate the bone to (0,0,0), ii) align the bone coordinate system with the world coordinate system by rotating it 45° anticlockwise, iii) perform the 30°, iv) return the bone coordinate system by rotating it 45° clockwise, and v) translate the bone to its original location	38
Figure 36. The left figure is projected light scanner (adapted from [TC] ² 3D Body Scanner, TC), mid figure is projected light scanner with 6 light sources/sensors (adapted from Capturor, Inspeck) and the right figure is body points cloud (adapted from [TC] ² 3D Body Scanner, 2010).....	39
Figure 37. Main application areas for body scanning technology (adapted from Lerch et al. (2007)) 40	
Figure 38. Left image shows new individuals created based on height and weight specification whereas the right image shows the modification of original whole body data by changing the weight and height (adapted from Allen et al. (2003))	40
Figure 39. Importance level of DHM characteristics/functionalities for all groups	51
Figure 40. Usage of various DHM's characteristics	52
Figure 41. Respondents desire of various DHM's characteristics.....	53
Figure 42. Respondents' response about the uniform accuracy/detail for DHM	53
Figure 43. Respondents' responses about non-uniform accuracy/detail of DHM	54
Figure 44. Respondents' response about the effect of unrealistic joint flesh	54
Figure 45. Respondents' responses about waiting time in which a real time interaction is required. 55	
Figure 46. Respondents' willingness to trade some accuracy for real time interaction.....	55
Figure 47. Respondents' view regarding the future trend of realistic DHM.....	56
Figure 48. Effect of DHM realism on accuracy	56
Figure 49. The use of realistic DHM for aesthetics purposes	56
Figure 50. Effect of realistic DHM on ergonomics CAD choices disregarding other issues.....	57
Figure 51. Flesh deformation due to contact with external sources and DHM future trend	57
Figure 52. Effect of flesh deformation due to external forces on accuracy	58
Figure 53. Flesh deformation and object deformation	58
Figure 54. Whole body implementation of the flesh deformation due to external forces	59
Figure 55. Flow chart of the research methodology	64
Figure 56. First design phase.....	76
Figure 57. Strategy for the first design phase	77
Figure 58. Raw data of 3D whole body data and final output of 3D body data from [TC] ² NX-12.....	78
Figure 59. Joint extraction from 3D whole body with [TC] ² NX-12.....	78
Figure 60. A 3D scanned arm with its joint location in Pro-Engineer Wildfire 4.0 and bones which are created from them.....	79

Figure 61. Anatomy of the upper and lower arm and the carrying angle which is created from ulna and humerus (adapted from Watkins (2010)).....	80
Figure 62. 3D arm data from a 3D body scanner preserves the carrying angle	80
Figure 63. Rays, originating from a point along the upper arm segments, were intersected with the scanned arm surface (facets)	81
Figure 64. (a) A facet of a 3D scanned arm polygonal surface. (b) A facet with its normal vector	82
Figure 65. Illustration which shows that for each ray, two intersection points could be acquired i.e. intersection point in front of and behind the ray origin; only the intersection point in front of the ray origin is used.....	82
Figure 66. Obtaining intersection points by employing the pseudo code to create a cross section with the spline function	83
Figure 67. Uniform distance between cross sections.....	84
Figure 68. Illustration of the interpolated planes for cross sections along a bone	85
Figure 69. Illustration of the bijective plane at the elbow and end planes at the wrist and shoulder	85
Figure 70. Creases development as the arm flexes	86
Figure 71. Experimental setting for the mini study (top view, side view)	87
Figure 72. (a). Photograph analysis shows the arm bones, elbow line, upper arm-elbow _{angle} and arm _{angle} (b). Elbow plane orientation for different arm postures	87
Figure 73. The relationship between elbow line _{angle} and arm _{angle} shows that the ratio changes as the arm flexes	88
Figure 74. Cross section deformation in Shen et al. (1994) (adopted from Shen et al. (1994))	88
Figure 75. Flesh deformation changes at the posterior of the upper arm as the arm was flexed	89
Figure 76. Second phase, relatives to other stages in the research	92
Figure 77. Strategy for second design phase	93
Figure 78. Detail steps on carrying angle determination	96
Figure 79. A 3D arm data from a 3D body scanner preserves the carrying angle	97
Figure 80. X-Y plane for carrying angle measurement and X-Y axis with respect to the arm	98
Figure 81. The carrying angle is measured from an additional plane and the lower arm bone	98
Figure 82. Illustration of the second and the third assumptions	99
Figure 83. The upper arm bone orientation. The lower arm bone orientation would be identical as that of the upper arm bone orientation	100
Figure 84. Adoption of zero reference position causes the lower and upper arm bones being located on a straight line. As the consequences, there is a certain degree of flexion and carrying angle even for a fully extended arm	101

Figure 85. Step by step process for the lower arm bone movements.....	101
Figure 86. The proposed strategy to determine the region for flesh deformation at the elbow	102
Figure 87. Upper arm outline comparison for various postures	103
Figure 88. Lower arm outline comparison for various postures	103
Figure 89. The area difference for the upper and lower arm during maximum flexion	104
Figure 90. Attaching markers to signify flesh deformation area	105
Figure 91. The boundaries movement during extension-flexion movements.....	105
Figure 92. An example of how distances of the lower arm boundary and upper arm boundary are being measured	105
Figure 93. Relationship between upper arm boundaries and arm angle	106
Figure 94. Relationship between lower arm boundaries and arm angles	106
Figure 95. Flow chart which shows steps in determining a set of examples to govern flesh deformation.....	107
Figure 96. Result of the 3D body scanner for arms with $\pm 90^\circ$ flexion	107
Figure 97. Flesh deformation at different stages: (a) between neutral- $\approx 135^\circ$ (b) between $\approx 135^\circ$ - $\approx 90^\circ$ and (c) between $\approx 90^\circ$ -maximum flexion.....	108
Figure 98. The proposed method to quantify the flesh deformation changes.....	109
Figure 99. Usage of a fully extended arm FDA as a reference to determine the quantification area for other arm postures	109
Figure 100. An illustration of the distribution of the 10 tracked locations on the arm outline while the arm is fully flexed	110
Figure 101. Result of the flesh deformation changes quantification and non-linear regression lines for all of the quantification areas from the five subjects	111
Figure 102. Using linear interpolation to interpolate non-linear data	112
Figure 103. A strategy to establish the method to acquire cross sections from the key posture	114
Figure 104. The first proposed setting to acquire side view photographs	117
Figure 105. Results of the first setting of the side view photographs	117
Figure 106. Second setting to obtain photographs of front and side view of the arm	118
Figure 107. Variation in cross sections capture result	118
Figure 108. Factors which affect the decision concerning the number and location of cross sections	119
Figure 109. Strategy to determine the cross sections' number and location	120
Figure 110. Growth of posterior area as the arm flexes	120
Figure 111. Illustration of the bounded area for the cross sections.....	121

Figure 112. Gaps at the elbow joint which are caused by orientation of the cross section planes..	122
Figure 113. Insertion of cross sections at 50% of the upper and lower arm FDA length onto the pre-determined cross sections' location i.e. UAF, E, and LAF	123
Figure 114. Locations for the inserted cross sections for both upper and lower arms are 50%, 33.33%, 66.66%, [33.33%-50%], [50%-66.66%], [25%-50%], [50%-75%], [33.33%-66.66%] and [35%-75%], from right to left	124
Figure 115. Effect of cross section's location to 3D shape using simplified cross sections	125
Figure 116. An illustration of sampling 16 points from the elbow cross sections	126
Figure 117. Effect of sample points number on the error level of the cross sections for endomorphs body type.....	127
Figure 118. Effect of sample points number on the error level of the cross sections for mesomorphs body type.....	127
Figure 119. Effect of sample points number on the error level of the cross sections for ectomorph body type.....	127
Figure 120. Third design phase, relatives to other stages in the research	130
Figure 121. Two stages of joints information and digitise cross sections integration	132
Figure 122. The proposed strategy to integrate digitised cross sections and joint locations	133
Figure 123. The proposed protocol to integrate joint locations of 3D scanned arm and digitised cross sections.....	134
Figure 124. Scaling the front view photograph to match the size of the arm of the front view photograph.....	135
Figure 125. Using the wires to capture the cross sections at five locations while the arm is fully extended and the digitised cross sections	136
Figure 126. Embedding joints from 3d scanned arm onto the photographs	137
Figure 127. Locations of UAF, UAM, LAM and LAF on the side view photograph of a fully extended arm	137
Figure 128. a) Creating common plane from upper and lower arm bone; b) Creating E line, which passed through elbow and crease of the anterior elbow, on the common plane; c) Creating the elbow plane which passed through E line and perpendicular with respect to the common plane...	138
Figure 129. Five cross sections were manually located and orientated	138
Figure 130. The proposed procedure to extend the joint information of a fully extended arm to other key postures.....	139
Figure 131. Arrangement of other key postures photographs.....	140

Figure 132. (a) The board in the side view photograph was used to create the plane for the front view photograph. (b) The front view and side view photograph after rescaling	140
Figure 133. Left image: creating two planes on the side view photograph. Right image: creating a plane on the front view photograph.....	141
Figure 134. Extending joint location of a fully extended arm into other key postures	141
Figure 135. Locating UAM and LAM for all key postures	141
Figure 136. Final result of the integration between joint locations and digitised cross sections for 135° flexion.....	142
Figure 137. Vitus Smart LC (Human Solutions, 2011) 3D laser scanner.....	142
Figure 138. The carrying angle of different key posture from Figure 134	143
Figure 139. The strategy to create additional cross sections from digitised cross section or their interpolation.....	144
Figure 140. Surface creation from two lines (A and B); a finite number of surface lines (x_i) which connects the line A and B were formed. Sampling at different locations along the surface lines allows the surface creation.....	145
Figure 141. Initial location of surface creation and its effect	146
Figure 142. Positive and negative shape deviation of the surface creation result (bold line shows the correct shape of the elbow deformation)	147
Figure 143. Surface lines which determine the maximum width of the arm at one location would be different from another location.....	148
Figure 144. (a) Some surface lines which cause deviation at the posterior of the elbow, shown with bold red lines (b) Another parameter is required to guide the additional cross section creation, even after the surface lines which caused arm shape deviation is discarded (c) Profile, the new parameter to assist creating the additional cross sections.....	148
Figure 145. Illustration to show that an outline obtained from side view (bold line) is not necessarily produced by prominent points which lay at the same plane (side, front and top view, respectively)	149
Figure 146. The proposed method to create additional cross sections	150
Figure 147. The protocol for surface lines creation	150
Figure 148. The common plane and the initial locations of the surface lines	151
Figure 149. The 16 points from UAF showed uniform division of its perimeter	151
Figure 150. Creating a surface line at the initial location	152
Figure 151. The protocol to incorporate a profile to the surface lines	152
Figure 152. Creating a plane for the profile by using prominent points of UAF, E and LAF	153

Figure 153. Left hand image: rays were created from points on the profile that were located on the side view plane; middle image: intersection between the rays and UAF-E-LAF plane.....	153
Figure 154. The final result of incorporating a profile to the surface lines	154
Figure 155. The protocol to obtain points for additional cross sections at the elbow	154
Figure 156. Part of the surface lines which were located at LAM-E and UAM-E sections	154
Figure 157. Obtaining points at 1/3 of surface lines of UAM-E section.....	155
Figure 158. The protocol to obtain points for additional cross sections at the elbow	155
Figure 159. Choosing 2 points which determine the maximum width of the arm of additional cross section's.....	156
Figure 160. Discarding the posterior points using the two chosen two points determined in Figure 159.....	156
Figure 161. An example of additional cross sections, which were created in Pro-Engineer, based on the output of the algorithm in Matlab 7.0.....	157
Figure 162. A protocol to integrate additional cross sections with five key cross sections	157
Figure 163. Arm surface that is created from both the digitised and additional cross sections	158
Figure 164. The strategy to resolve the issue of interpolation to govern the flesh deformation.....	159
Figure 165. The proposed interpolation methods	162
Figure 166. Protocol to interpolate carrying angle	162
Figure 167. The proposed protocol for cross section interpolation	163
Figure 169. Creating planes to determine the initial locations for two cross sections	164
Figure 170. Creating 15 rays of vectors that were originated from the bone point of the cross section in a clockwise direction.....	165
Figure 171. E cross section at 120° and comparing it with E_{90° and E_{135°	166
Figure 172. The protocol to interpolate the locations of UAF, UAM, LAM and LAF for a given arm angle	167
Figure 173. Relationship between arm_{angle} and $upper\ arm-elbow_{angle}$	167
Figure 174. Predicting the elbow orientation plane by using the linear equation that relates the angle between $upper\ arm-elbow_{angle}$ and arm_{angle}	168
Figure 175. The proposed protocol to interpolate profiles	168
Figure 176. (a). Initial points were assigned to mark the segments i.e. UAF-UAM, UAM-E, E-LAM, LAM-LAF (b). A closer look of initial points at the elbow	169
Figure 177. The 15 locations of the profile that would be used during the comparison process.....	170

Figure 178. (a)An example of adding a location in a segment while searching for the optimum number and placement of points on the profile. (b) The created profile was shown together with the original profile	170
Figure 179. Final sampling points of 1 st segment to the 4 th segment.....	171
Figure 180. Examples of the profile interpolation results	173
Figure 181. The relationship of the proposed FDM's review with the previous and next stages of the research	174
Figure 182. Detail processes to create the programming to review some of the FDM specifications	175
Figure 183. Steps to parameterise the digital cross sections	176
Figure 184. Steps to parameterise the flesh deformation area	177
Figure 185. Steps to parameterise the profile	178
Figure 186. Steps to obtain the coordinates of the joint location for a fully flexed arm	179
Figure 187. Misplacement of the five key cross sections for 60° flexion.....	183
Figure 188. Predicted UAF, UAM and LAM, for arm posture in the range of 90°-maximum flexion, are compared to the side view photograph.....	184
Figure 189. The proposed suggestion to solve the incorrect prediction of UAF, UAM, LAM and LAF for arm posture between 90°-maximum flexion.....	185
Figure 190. Adjusting UAF, UAM, LAM and LAF (white line) after interpolating them (red line)	185
Figure 191. Upper arm distortion for an arm angle between a full extension-135° for all participants	186
Figure 192. The cross sections which are resulted from the surface lines exclusion algorithm (dashed line) and a single exclusion of the surface lines (solid line).....	186
Figure 193. The cross section which is created with an additional set of points is able to mimic the actual shape of the additional cross section, compare to the current method of surface lines exclusion.....	187
Figure 194. Processes to translate the UAF and UAM cross sections.....	187
Figure 195. Steps to adjust the UAF, UAM, LAM and LAF for the arm posture between 90°-maximum flexion.....	188
Figure 196. Left image is UAM at 60° (dashed line) and UAM at 90° (solid line). Right image is UAM at 90° after lateral and medial width adjustment (solid line) compared to UAM at 90° before adjustment (thin line)	189
Figure 197. Result of the five key cross sections translation, which shows that they coincide with the corresponding profile	190

Figure 198. Results of the proposed modification for UAF, UAM, LAM and LAF for arm angle between 90°-maximum flexion.....	190
Figure 199. Effect of body type to the arm angle.....	191
Figure 200. Comparing the result between the original (transparent surface) and modified (solid surface) surface lines exclusion's programming for a 145° flexion	191
Figure 201. The review process of the proposed FDM for the current chapter	194
Figure 202. Proposed methodology for validating the accuracy of the proposed FDM	195
Figure 203. Proposed method to measure the offset for between the five key cross sections and 3D scan data.....	196
Figure 204. Details of the proposed steps to measure the offset of the five key cross sections between 3D scanned arm and the proposed FDM	196
Figure 205. The offset measurement between the five key cross sections and the side view photographs	197
Figure 206. Detail of steps for the offset measurement between the five key cross sections and the side view photograph	197
Figure 207. Proportion of different error level for the first interval of key postures i.e. maximum extension-135°	198
Figure 208. Proportion of different error level for the second interval of key postures i.e. 135°-90°	198
Figure 209. Proportion of different error level for the third interval of key postures i.e. 90°-maximum flexion	199
Figure 210. The offset measurement between profile of the proposed FDM (thin line) and profile of the side view photograph (bold line)	199
Figure 211. The proposed offset measurement for the profile.....	200
Figure 212. The proposed FDM was able to capture details at the elbow i.e. indentation at the posterior of the elbow area, which is highlighted by the solid lined circles.....	203
Figure 214. The effect of inaccurate manual measurement of the five key cross sections to the final result of the proposed FDM on both the anterior and posterior of the elbow area (highlighted by solid lined circles)	204
Figure 215. Visual observation on the arm postures between 135°-90°. Solid lined circles highlight the anterior of the elbow area whereas the dashed lined circles highlighted the posterior of the elbow area	204
Figure 216. Less realistic result, highlighted by the solid lined circles, due to the inaccurate five key cross sections which were obtained through manual measurement	205

Figure 217. Images of the proposed FDM for an arm posture between a fully extended arm-135° for participant 1	205
Figure 218. Images of the proposed FDM for an arm posture between a fully extended arm-135° for participant 2	206
Figure 219. Images of the proposed FDM for an arm posture between a fully extended arm-135° for participant 3	206
Figure 220. Images of the proposed FDM for an arm posture between a fully extended arm-135° for participant 4	207
Figure 221. Images of the proposed FDM for an arm posture between a fully extended arm-135° for participant 5	207
Figure 222. Images of the proposed FDM for an arm posture between 135°-90° for participant 1.	208
Figure 223. Images of the proposed FDM for an arm posture between 135°-90° for participant 2.	208
Figure 224. . Images of the proposed FDM for an arm posture between 135°-90° for participant 3	209
Figure 225. Images of the proposed FDM for an arm posture between 135°-90° for participant 4.	209
Figure 226. Images of the proposed FDM for an arm posture between 135°-90° for participant 5.	210
Figure 227. The ability of the proposed FDM (thin white line) to capture details at the posterior of the elbow area depends on how complex the profile (bold black line) is at that area	211
Figure 228. A mixed result of the proposed FDM (thin white line) regarding its ability to capture details at the anterior of the elbow area (bold black line)	211
Figure 229. Images of the proposed FDM for arm postures between 90°- maximum flexion for the five participants	212
Figure 230. The programming from section 8.4 demonstrates that the proposed FDM allow a user to specify body type/size i.e. choosing the subject and arm angle	214
Figure 231. The output of the programming that was developed in section 8.4 is coordinates of five key cross sections and additional cross sections for the specified participant and arm angle.....	215
Figure 232. Using the output of the programming as input in Pro-Engineer to visualise the result	215
Figure 233. The application of the new FDM with respect to other activities in the research.....	221
Figure 234. Methodology to create the application of the new FDM	221
Figure 235. Relationship between the inputs, database, prediction of the elements for flesh deformation and the new FDM	222
Figure 236. Stages in framework development	224
Figure 237. The prediction method to determine the carrying angle for an arm posture other than a fully extended arm.....	226

Figure 238. Strategy to produce a method to predict UAF, UAM, LAM and LAF location for all key postures.....	227
Figure 239. FDA for the upper arm, from a fully extended arm to a fully flexed arm, for five participants with various body size and type.....	228
Figure 240. The relationship between body size and type with respect of FDA for the lower arm also yields a similar result as that of the upper arm	228
Figure 241. Relationship between UAF and LAF	229
Figure 242. Relationship between UAF and UAM	229
Figure 243. Relationship between LAM and LAF.....	230
Figure 244. The proposed prediction method to determine the location of UAF, UAM, LAM and LAF	232
Figure 245. Five key cross sections from different key postures, top row: a fully extended arm, bottom row: a fully flexed arm	234
Figure 246. Strategy to develop a prediction method of five key cross sections for 135°, 90° and maximum flexion	235
Figure 247. Utilising the centre of both key cross sections to overlaying them.....	236
Figure 248. Examples of the comparison results of five key cross sections between participant 3 (dashed line) and participant 4 (solid line) of which participant 3 has higher BMI than the other participant	237
Figure 249. Examples of the comparison result of five key cross sections comparison between participant 1 (solid lines) and the rest of participants (dashed line) which shows that participant 1, with the least body size, generally has smaller cross sections.....	237
Figure 250. Images of UAF, UAM,LAM and LAF from different key postures for participant 1 to participant 5	238
Figure 251. Steps to scale cross section of a fully extended arm to match the size of those from other key postures.....	239
Figure 252. Images of E from different key postures for participant 1 to participant 5 shows apparent shape changes from one key posture to another.....	240
Figure 253. Overlays result from participant 1, which shows that there is dependency for UAM-UAF and LAM-LAF.....	241
Figure 254. General outline of the proposed method to predict the five key cross sections.....	243
Figure 255. Procedures of the algorithm from section 5.3.2.1 to acquire key cross sections of 3D scanned arm	244

Figure 256. Proposed method to predict cross sections of UAF, UAM, LAM and LAF for 135°, 90° and maximum flexion	245
Figure 257. Unit vector directions and coordinates to recreate cross sections of 3D scanned arm	246
Figure 258. Example of the utilisation of bounding boxes to measure the maximum vertical and horizontal dimension for UAF _{full extension} from participant 2	247
Figure 259. Example of Cartesian coordinates depiction for ratio of UAF-UAM for 3D scanned arm and database data. The identification of closest match is performed by measuring the Euclidean distance of the 3D scanner arm towards each database and choosing the database data with the smallest Euclidean distance	248
Figure 260. Top images: the anterior-posterior resizing for vertical dimension; bottom first two images: the medial-lateral resizing for horizontal dimension; bottom rightmost image: the final outcome of the four ways dimensional resizing	249
Figure 261. Example of the four dimensions of a key cross section's bounding box	250
Figure 262. Initial point and sample point 9 remain constant during the scaling of horizontal dimensions, whereas sample point 5 and 13 remained constant during the scaling resizing of vertical dimension	251
Figure 263. The proposed prediction method for E utilised the database and the 3d scan of a fully extended arm	252
Figure 264. Expressing the 16 sample points as distances towards the centre of E's bounding box	253
Figure 265. Euclidean distances of E of fully extended arms from participant 1 to participant 4	254
Figure 266. Principal component which represent 90% of variation among the Euclidean distances from participant 1 to participant 4	254
Figure 267. Strategy to develop a prediction method of five key cross sections for 135°, 90° and maximum flexion	255
Figure 268. The whole extent of profile compares to the actual profile that is used in the new FDM	257
Figure 269. Using the whole length of upper and lower arm as the limit of the profile would eliminate the effect of FDA on the profile (left image, bold lines). However, the profile of the 3D scanned arm is prone to distortion especially around the shoulder area (right image, bold lines) ..	257
Figure 270. Using 2/3 of the upper and lower arm length as the limit of the profile would minimise the distortion of the 3D scanned arm's profile around the shoulder and yet ensure that profile for the flesh deformation area is included	257
Figure 271. The orientation of the 3D scanned arm is not the same as that in the side view and front view photograph which would result in compatibility.....	259

Figure 272. Optimum number and placement of points on the profile for the five participants' data	259
Figure 273. The profile of a fully flexed arm from participant 2 and participant 3 before and after the upper arm alignment took place.....	260
Figure 274. Images of profiles of four key postures from five participants show that although variation occurs, a general pattern or shape is also apparent for each key posture	260
Figure 275. Images show how inclination of profiles from two participants is different for profiles at 135°. Middle image shows inclination difference for upper arm whereas the image at the most right shows the inclination difference for the lower arm.....	261
Figure 276. Images show how the profile changes from one key posture to another for all participants.....	262
Figure 277. Comparison between the profiles of participant 1 (bold lines) and the rest of the participants for 135°, 90° and maximum flexion (left to right)	262
Figure 278. Profile comparison between participant 3 (dash line) and participant 4 (solid lines) for all key postures	263
Figure 279. Result of profile prediction at 135° by direct application of distance changes i.e. <i>d135CM-dmax extensionCM</i> to the profile of the 3D scan data i.e. <i>dmax extension3D</i> ...	265
Figure 280. The cut point for upper and lower arm profiles is located at the middle of E region....	267
Figure 281. The general outline of the proposed method to predict the profiles at 135°, 90° and maximum flexion	268
Figure 282. The template concept was introduced as a procedure to obtain the profile of a 3D scanned arm that is compatible to the database's profiles	268
Figure 283. The integration between the digitised cross sections and joint information of the 3D scanned arm for participant 1. The result of the integration is shown in the rightmost image	269
Figure 284. Translation and rotation of a 3D scanned arm so that its elbow joint and upper arm (dashed lines) coincide with the template's elbow joint and upper arm (solid lines)	269
Figure 285. Left image shows an example of elbows from the template (solid line) and 3D scanned arm (dashed line) prior the refinement. Right image shows prominent characteristics of elbow cross sections from the five participants	270
Figure 286. The procedures to find the closest match for a 3D scanned arm	272
Figure 287. The procedures for predicting profiles of 3D scanned arm at 135°, 90° and maximum flexion.....	274
Figure 288. Examples of side-front view photographs from participants for the database	282
Figure 289. Examples of 3D scan data from participants for the database	282

Figure 290. Examples of the results of manually tracing the shapes of wires that were circled around the arms.....	282
Figure 291. Existing procedure which was adopted to obtain the locations of UAF, UAM, LAM and LAF	283
Figure 292. Relationships between the location of UAF and LAF for fully extended arm for all groups	287
Figure 293. Relationships between locations of UAF and LAF for fully flexed arms for all groups....	287
Figure 294. UAF locations are charted for each key posture and each participant in the groups....	289
Figure 297. Relationship between LAF and LAM throughout the range of arm movement for each gender and race	291
Figure 298. Existing procedure to express the shape of cross sections which was partly adopted .	293
Figure 300. Steps to obtain ratio values of maximum vertical and horizontal dimension of UAF-UAM and LAM-LAF for fully extended arms.....	294
Figure 302. Steps to acquire two vertical and horizontal dimension of UAF, UAM, LAM and LAF ...	295
Figure 303. An example of quadrant vertical and horizontal dimensions for UAF of a fully extended arm	296
Figure 304. Steps to obtain transform values of distances from E sampling points.....	297
Figure 305. Transformed values of each race and gender are being charted using their principal components.....	298
Figure 306. The existing procedure to express the shape of profiles in section 8.1.3 which was partly adopted	300
Figure 307. The 33 points on the profile for participant 6 of Asian female group	301
Figure 308. Processes in the programming for template matching and sampling of 3D scan data .	305
Figure 309. Data of participant 4 from the Asian male group	306
Figure 310. Screenshot of the programming which shows the programming prompts participant's information on: (i) 3D scan and its joint data, (ii) gender and race and (iii) BMI. Screenshots also captures some of the programming's results	306
Figure 311. 3D scan data and joint coordinates of participant 4 after template matching as well as the predicted location of UAF, UAM, LAM and LAF	307
Figure 312. Orientation of upper and lower arm bones	307
Figure 313. Examples of five key cross sections and profile which are extracted from the 3D scan data.....	307
Figure 314. Processes to predict the five key cross sections for 135°, 90° and maximum flexion ...	308

Figure 315. Predicted UAF, UAM, E, LAM and LAF for participant 4 from the Asian male group (dashed line is the original cross section from the 3D scan data, bold line is the prediction of cross sections for key posture of 135°, 90° and maximum flexion)	309
Figure 316. Transforming the predicted UAF, UAM, E, LAM and LAF into 3D coordinates	309
Figure 317. Processes in the programming to predict profiles of 135°, 90° and maximum flexion..	310
Figure 318. Results of profile prediction for 135 (thin line), 90 (dashed thin line) and maximum flexion (dashed bold line)	310
Figure 319. The bone points, which was required to guide the placement of UAF cross sections to their corresponding planes changed from one key posture to another	311
Figure 320. Cross sections do not coincide with the profiles for the predicted key postures	312
Figure 321. The effect of incorrect placement of the five key cross sections is also observable from the front view	312
Figure 322. Using the front view profile of 3D scan data to guide translations of UAF, UAM and E to adjust their front view placement	315
Figure 323. Final side view placement of five key cross sections for 135°, 90° and maximum flexion	317
Figure 324. Final front view placement of five key cross sections for 135°, 90° and maximum flexion	317
Figure 325. Examples of the result from the integration of FDM's software programme with the software programmes in section 9.11.1, 9.11.2, and 9.11.3 (arm angles, from right to left: 142°, 128° and 86°)	318
Figure 326. 3D scanned arms and their joint information of fully extended arms for all participants	322
Figure 327. 3D scanned arms of all participants for arm posture in between full extension -135°..	323
Figure 328. 3D scans of arms of all participants for arm posture in between 135°-90°	323
Figure 329. Side view photographs for participant 1 of Asian female.....	324
Figure 330. Side view photographs for participant 2 of Asian female.....	324
Figure 331. Side view photographs for participant 1 of Asian male.....	324
Figure 332. Side view photographs for participant 2 of Asian male.....	324
Figure 333. Side view photographs for participant 1 of Caucasian female	325
Figure 334. Side view photographs for participant 2 of Caucasian female	325
Figure 335. Side view photographs for participant 1 of Caucasian male	325
Figure 336. Side view photographs for participant 2 of Caucasian male	325

Figure 337. Proportion of different error level for the first interval of key postures i.e. maximum extension-135°.....	326
Figure 338. Proportion of different error level for the second interval of key postures i.e. 135°-90°	327
Figure 339. Proportion of different error level for the third interval of key postures i.e. 90°-maximum flexion	327
Figure 340. The profile prediction result for participant 2 of Asian Female (bold line: prediction result, thin line: original data).....	328
Figure 341. The profile prediction result for participant 1 of Caucasian Male (bold line: prediction result, thin line: original data).....	328
Figure 342. The profile prediction result for participant 1 of Caucasian Female (bold line: prediction result, thin line: original data).....	328
Figure 343. The profile prediction result for participant 2 of Asian Male (bold line: prediction result, thin line: original data).....	328
Figure 344. The framework was able to capture details at the elbow i.e. indentation at the posterior of the elbow area, which is highlighted by the solid lined circles	330
Figure 345. Visual observation shows the ability of the framework to capture details the area where the crease starts to develop as the arm flexes, which is highlighted by solid lined circles	330
Figure 346. Sudden width changes between immediate cross sections before and after the elbow joint result in surface discontinuation (highlighted by solid lined circles)	331
Figure 347. Distortion on the 3D scan of a fully extended arm (leftmost image) would cause unrealistic result of the framework result (middle image)	331
Figure 348. Visual observation on the arm postures between 135°-90° (solid lined circles highlight the anterior of the elbow area whereas the dashed lined circles highlighted the posterior of the elbow area).....	332
Figure 349. Further effect of distorted 3D scan of a fully extended arm on the result of the framework for arm angles between 135°-90°.....	333
Figure 350. Shape discrepancies between predicted (thin lines) and actual (bold lines) profiles are concentrated on the elbow area for arm postures between 90-maximum flexion	333
Figure 351. Shape discrepancies between predicted (thin lines) and actual (bold lines) profiles also occur on the anterior of the elbow area for arm postures between 90-maximum flexion.....	334
Figure 352. Images of framework's result for an arm posture between a fully extended arm-135° for participant 1 of Asian female group.....	335

Figure 353. Images of framework's result for an arm posture between a fully extended arm-135° for participant 2 of Asian female group.....	335
Figure 354. Images of framework's result for an arm posture between a fully extended arm-135° for participant 1 of Asian male group.....	336
Figure 355. Images of framework's result for an arm posture between a fully extended arm-135° for participant 2 of Asian male group.....	336
Figure 356. Images of framework's result for an arm posture between a fully extended arm-135° for participant 1 of Caucasian female group	337
Figure 357. Images of framework's result for an arm posture between a fully extended arm-135° for participant 2 of Caucasian female group	337
Figure 358. Images of framework's result for an arm posture between a fully extended arm-135° for participant 1 of Caucasian male group	338
Figure 360. Images of framework's result for an arm posture between 135°-90° for participant 1 of Asian female group	339
Figure 361. Images of framework's result for an arm posture between 135°-90° for participant 2 of Asian female group	339
Figure 362. Images of framework's result for an arm posture between 135°-90° for participant 1 of Asian male group	340
Figure 363. Images of framework's result for an arm posture between 135°-90° for participant 2 of Asian male group	340
Figure 365. Images of framework's result for an arm posture between 135°-90° for participant 2 of Caucasian female group.....	341
Figure 366. Images of framework's result for an arm posture between 135°-90° for participant 1 of Caucasian male group.....	342
Figure 367. Images of framework's result for an arm posture between 135°-90° for participant 2 of Caucasian male group.....	342
Figure 368. Images of framework's result for an arm posture between 90°-maximum flexion for Asian female group	343
Figure 369. Images of framework's result for an arm posture between 90°-maximum flexion for Asian male group	343
Figure 370. Images of framework's result for an arm posture between 90°-maximum flexion for Caucasian female group.....	343
Figure 371. Images of framework's result for an arm posture between 90°-maximum flexion for Asian female group	344

Figure 372. Mechanism of the new FDM for the elbow joint	346
Figure 373. The mechanism for the framework.....	347
Figure 374. Adopted methodology to create a new FDM	348
Figure 375. Two images which were used to investigate the required level of detail of a realistic DHM.....	353
Figure 376. The image used to investigate the effect of unrealistic flesh deformation	354
Figure 377. An example of one of the graphs for quantitative measures and example of images used for qualitative measures	361
Figure 378. Non-linear relationship between arm angle and the plane orientation of the cross section at the elbow	363
Figure 379. Location and orientation of UAF, UAM, LAM and LAF.....	366
Figure 380. Depiction of processes in the framework.....	371
Figure 381. The prediction method to determine the carrying angle for an arm posture other than a fully extended arm.....	377
Figure 382. The prediction methods for the location of UAF, UAM, LAM and LAF	378
Figure 383. The prediction method for UAF, UAM, LAM and LAF.....	379
Figure 384. The prediction method for E cross sections	380
Figure 385. Principal components of E cross sections for Caucasian male group which show the tendency towards scattered data	381
Figure 386. The proposed prediction method for profiles	382
Figure 387. The process to modify closest match's profile at 135° in order to provide profiles at 135°, 90° and maximum flexion for the 3D scan data	382
Figure 388. Top: the profile prediction result for participant 2 of Asian female and bottom: the profile prediction result for participant 1 of Caucasian Male (bold line: prediction result, thin line: original data).....	383
Figure 389. Creating key cross sections for each type of joint movement for the shoulder, from left to right: outward-inward medial rotation; adduction-abduction; and flexion-extension.....	389
Figure 390. Simulation of flesh deformation at the lower arm due to external force application on the skin (adapted from Shin and Badler (2002))	391

List of Tables

Table 1. Detailed description for each subdivision method	28
Table 2. Thirteen characteristics which were presented in the questionnaire	47
Table 3. Characteristic that define overall quality of ergonomics CAD	61
Table 4. Quantification of comparison between existing FDMs and DHM specification for flesh deformation.....	73
Table 5. Van Roy et al. (2005) data	98
Table 6. Variations of upper and lower arm bone length from the 3D scanned arms	134
Table 7. Linear interpolation for distance of location in E_{120}°	166
Table 8. An example of quantification result for the profile of a fully extended arm	172
Table 9. Detail of the five participants who were involved to review the accuracy and realism of the proposed FDM	175
Table 10. Example of the result of digital cross sections' parameterisation	176
Table 11. Results of cross sections location towards the elbow joint for all key postures and participants.....	177
Table 12. Distances of points along the profile and bones for all participant 1's key postures	178
Table 13. The angular range of the arm movement for all participants.....	179
Table 14. Complete results of joint coordinates for fully extended and flexed arms (in mm units)	180
Table 15. Average of total error of the proposed FDM	198
Table 16. Average error of the offset measurement for the profile interpolation.....	200
Table 17. Amount of data to be processed in real time to generate flesh deformation at the elbow	218
Table 18. Amount of data processing in real time to generate flesh deformation at the elbow	218
Table 19. Differences between the proposed FDM and Shen et al. (1994) method	219
Table 20. Characteristics of five existing participants which were involved in the development of the new FDM	224
Table 21. Data from Van Roy et al. (2005) which was used to assist the prediction of the carrying angle for full flexion.....	225
Table 22. Mean error between scaled cross section of a fully extended arm and those from other key postures	240
Table 23. FDA, which determines the location of UAF and LAF, is always less than 2/3 of the upper and upper arm length for all participant and key postures.....	258

Table 24. Distances for the case example, where the distances of 135° of the 3D scanned arm is predicted by direct application of <i>d135CM-dmax extensionCM</i> (closest match data) to is <i>dmax extension3D</i> (3D scan data)	265
Table 25. The proposed step by step process to perform refinement of lateral-medial orientation of the 3D scanned arm	271
Table 26. Steps to predict 135° profile through scaling and readjustment of the closest match 135°	275
Table 27. BMI classification (adapted from WHO (1995, 2000) and WHO Expert Consultation (2004))	280
Table 28. Participant's height, weight, BMI and arm length	280
Table 29. Comparing anthropometrical data of arm lengths for Asian i.e. Sri Lankan and Caucasian i.e. United Kingdom (adopted from Peebles and Norris, 1998) to the arm length's range from each group	281
Table 30. UAF location at fully extended arm, BMI, and upper arm length for participant in each gender and race group.....	284
Table 31. UAF location at fully flexed arm, BMI, and upper arm length for participant in each gender and race group.....	285
Table 32. Result of multiple regressions for UAF's location at fully <i>extended</i> arms.....	285
Table 33. Result of multiple regressions for UAF's location at fully <i>flexed</i> arms.....	285
Table 34. UAF and LAF locations of fully extended arms from all groups	286
Table 35. Data for establishing the relationship between the location of UAF and LAF for fully flexed arms.....	286
Table 36. Data to establish relationship between UAF and LAF from fully extended to fully flexed arm	288
To determine the mathematical equation that captured the relationship of UAF-UAM and LAF-LAM, the locations of UAF, UAM, LAM and LAF of all key postures were required from each participant. Table 37 shows an example of these locations for the Asian Female group. Table 37. Data to establish the relationship of UAF-UAM and LAF-LAM for Asian Female group.....	
Table 37. Data to establish the relationship of UAF-UAM and LAF-LAM for Asian Female group.....	290
Table 38. Ratio of UAF-UAM for each gender and race	295
Table 39. Vertical and horizontal dimension for UAF, UAM, LAM and LAF for fully extended arm for Asian female group	296
Table 40. Transformed values of E cross sections' distances	298
Table 41. Results of transformation of E cross sections' distances for other key postures.....	299

Table 42. Example of profile distances for participant 6 from the Asian female group and an illustration of some profile distances for a fully flexed arm	302
Table 43. Transformed values of profiles' distances for fully extended arms	303
Table 44. Transformed values of profiles distances from other key postures	303
Table 45. Coordinates of joints and upper/lower arm bone orientation for each key posture.....	309
Table 46. Steps to perform translation for UAF and UAM	313
Table 47. Steps to perform translation for E.....	314
Table 48. Steps to translate LAM and LAF.....	316
Table 49. Data from recruited participants	322
Table 50. Average error of the FDM application from the offset measurement result.....	326
Table 51. Average error of the offset measurement for the profile interpolation.....	328
Table 52. Difference of cross sections concept between the new FDM and the Shen et al. (1994) method	367
Table 53. Suggested minimum number of sample size for the framework's database	375
Table 54. Data from Van Roy et al. (2005) which was used to assist the prediction of the carrying angle for full flexion	376
Table 55. Data from Zampagni et al. (2008) study	377

1. Introduction

Human modelling could be defined as an attempt to represent the complex human being as a model that encompasses both physical and cognitive performance of human aspects (Sundin and Örtengren, 2006). According to Sundin and Örtengren (2006), a model could be defined as:

“A copy or an image of something, often miniature representation of a physical object, but it can equally well be used to replicate a function or a process.”

They also highlighted the purpose of a model which is to substitute a reality with a cheaper or simpler form in order to study the effect of any changes or modification of a reality.

In the last decade, human modelling has become widely used, driven by increasing need and enabled by an increase in powerful and affordable computer systems as well the software itself. The development of human modelling began in 1959 by Boeing Airplane when a figure consisting of 12 point silhouettes and lines representing two dimensional edges was created (Fetter, 1982). This ‘digital’ human model (DHM) was later improved by the development of a “First Man” in 1968 and was later followed by the development of a “Second Man”, “Third Man and Woman”; and “The Fourth Man” in the subsequent years (Fetter, 1982). This early development of DHM prompted the broad ranging DHM development across various systems and for various applications and fields that we see today (Badler et al., 1993).

1.1 Background of research

According to Tost and Pueyo (1988), the main applications of DHM can be categorised into two types: (i) entertainment; and (ii) simulation. For the first application, DHM could be used for the production of films, games or publicity purposes. For this type of application, the artistic quality of the model (i.e. the ability to visualise the human as close as possible to reality) is crucial. As a result, a user of such a DHM system will typically have to modify the parameters of the DHM for each movement in order to achieve a realistic result for body deformation or motion. Thus, any incorrect body deformation or motion, which may occur in certain motion sequences, can be corrected beforehand. Various types of commercial software e.g. Maya (Autodesk, 2011), 3ds MAX (Autodesk, 2011), MakeHuman™ (Makehuman.org, 2011), etc., are available for designers to perform this task (Hearn and Baker, 1994). For the second application, DHM is used to simulate situations in which a human is, or could be, involved e.g. industrial processes, surgical simulation, crash simulations etc. DHM for simulation applications is commonly based on predefined scientific values and parameters

which were obtained through studies or experiments. As a result, there is little desire or capability for the user to modify the predefined scientific values and parameters.

One specific DHM application within the simulation field, which is the focus of this research, is the human models used in ergonomics simulation. Ergonomics simulation is used to assist the design and evaluation of appropriate products or environments by taking human characteristics, capabilities and limitations into consideration. Previously, ergonomics software only focused on limited aspects of human performance, e.g. software that was aimed to assess manual lifting, software that was aimed to assess work postures, etc. This resulted in the use of multiple tools to aid various analyses. This condition prompted a further integrated software development which was known as “ergonomics CAD”. By combining various ergonomics analysis features into computer aided design (CAD) software, ergonomics assessments such as reach, vision, and postural comfort are able to be performed at once (Porter et al., 1995). Most ergonomics simulation software satisfies basic requirements to integrate ergonomics principles within the design process. Some of these are the ability to create 3D environment/objects around the human model, generate a human model based on anthropometric data/body type, integrate dynamic anthropometric feature/joint constraints and perform ergonomics analysis (Porter et al., 1995). Examples of ergonomics simulation software include: JACK (Siemens PLM software, 2011), MANNEQUIN-PRO (NexGen Ergonomics Inc., 2011), RAMSIS (Human Solutions GmbH., 2011), and SAMMIE (SAMMIE-CAD Limited, 2011), etc.

The typical usage of human models in Ergonomic CAD is to test if an object/workplace is appropriate for people with various anthropometric measurements. During object/workplace design, a human model, or virtual human is added. By changing the posture of the virtual human, any hazardous or inconvenient posture may be spotted and a necessary change to the design is then employed. Therefore, an accurate representation of body shape, body deformation and movement range are of importance. Several researchers have made use of ergonomic simulation software to evaluate either product or working environment e.g., Barone and Curcio (2004); Carey and Gallwey (2002), Feyen et al., (2000), etc. Chaffin (2001) has summarised some case studies addressing ergonomics problems which were successfully resolved through the support of ergonomics simulation software.

1.2 Research Motivation

This research is motivated by three factors: (i) the trend towards DHM that is able to represent humans as closely as possible; (ii) emergence of new technologies to support improved DHM development; and (iii) a gap between DHM development in ergonomics and entertainment. Each of these factors is discussed separately in the following subsections.

1.2.1 The trend towards DHM that is able to represent humans as closely as possible

One of the first DHM for ergonomics application is Cyberman which was developed to analyse and determine acceptable limb and body locations for a human model within a defined environment (Blakeley, 1980). Other early versions of DHM for ergonomics applications were Combiman (Bapu et al., 1980), SAMMIE (Kingsley et al., 1981), Boeman (Boeing Company, 1970) and JACK (Philips and Badler, 1988). Although these early versions of DHM lacked realism i.e. likeliness to a real human form and shape, they provided a foundation for the skeleton models and the underlying skeletal structures of today's computer animation (Dooley, 1982).

Due to continuous research on DHM in ergonomics applications, current DHM has improved quality and functionality in various areas including: simulation of motion and posture (Zheng et al., 2002; Andreoni et al., 2002; Debril et al., 2002; Dong et al., 2002; etc), discomfort modelling (Fritzsche and Bubb, 2007; Wang et al., 2007; etc.), hand grasp and strength modelling (Guo and Liu, 2007; Li and Zhang, 2007, etc.), amongst others. All of these developments ultimately aimed to create a human model that resembled a real human, which would eventually increase the accuracy of the simulation outcome. However, despite these latest developments, there appears to have been a lack of attention paid to the development of flesh deformation modelling either due to joint movement or contact with external forces/objects. Simulation of flesh deformation is a key component in the presentation of a human model with a greater resemblance to a real human form as opposed to a cartoon or manikin form that has been prevalent in the development of DHM systems. Simulating flesh deformation would also be useful to address further advanced analysis capabilities such as the motion restrictions due to clothing, and the deformation of the body due to interacting with an external object such as the surface of a seat. It is proposed that as flesh deformation is part of a real human behaviour, this aspect of DHM development should not be left unaddressed.

1.2.2 Emergence of new technologies

In order to achieve improved DHM for ergonomics applications, recent technology developments have been utilised. An example of this is the usage of motion capture in JACK to model human reaching motion. Chaffin (2002) used motion capture technology to gather motion data from a diverse population which would then be analysed to determine prominent sources of variation in the data. The output was then used to create a prediction model of human motion which takes into account data variation. He argued that this approach is better than current motion prediction methods as they tend to be computationally complex and will be less suitable for real time simulation.

Another example is the utilisation of 3D body scanning technologies to gather 3D anthropometric data which was adopted to overcome problems related to traditional anthropometric measurements. Currently, DHM is based on univariate traditional anthropometric measurements e.g. heights, lengths, breadths, etc., which are then extrapolated to create a three dimensional DHM. According to the Committee of Human Factors (1998), the end result is compromised due to the dependency on a series of approximation and assumptions with respect to the relationship between individual dimensions. This was supported by a recent study by Oudenhuijzen et al. (2008). Using several ergonomics CAD software, they created three dimensional DHMs based on a number of univariate anthropometric measurements from live subjects. The three dimensional DHMs were then compared with the live subjects. Their study showed that error is greater in anthropometric measurements that were not part of the original measurements. They also found that some ergonomics CAD even generated errors from the original measurement value that was provided as part of the DHM's measurement inputs. Another problem with current traditional anthropometric measurements is that, although manual 2D anthropometric measurements are considered to be accurate, they are also known to contain errors which are caused by variability of measurers' skills, difference in posture, compressed soft tissue, etc. (Gordon and Bradtmiller, 1996; Mckinnon and Istook, 2002).

The use of these technologies is becoming widespread for the collection of anthropometric measures. The CAESAR (Civilian American and European Surface Anthropometry Resource) project collected 3D scan data on 2400 US and Canadian individuals as well as 2000 European civilians (SAE International, 2011). Meanwhile, SizeUK collected 3D scan data of both sitting and standing postures from over 11,000 people in the UK, whereas SizeUSA is collecting 12000 scans of male and female throughout United States (Lerch et al., 2007).

A number of DHM systems now support the use of body scan data, for example Vis JACK that allows the incorporation of 3D body scanner data to generate a more accurate and realistic virtual human. However, to the extent of this research's knowledge, the recent development of 3D body scanner technologies had not been utilised in other aspects of DHM in ergonomics modelling such as flesh deformation modelling.

1.2.3 A gap between DHM development in ergonomics simulation and entertainment

Human modelling for entertainment focuses primarily on the aesthetic aspect of modelling the human figure. This includes realistic modelling of the human body, hands, face, hair, clothes as well as towards the development of specific techniques for their realistic animation (Maurel, 1998). An extensive amount of research has also been dedicated to create realistic flesh deformation due to

joint movement or contact with external forces/objects. Recent research has also taken advantage of the available 3D body scanning technologies. Research has also been done to use 3D body scanning technologies to synthesise new body forms or shapes from existing data (Seo and Thalmann, 2003; Allen et al., 2003; etc.). In addition, research has also utilised 3D body scanning technologies to create more realistic flesh deformation (Allen et al., 2002; Wang and Phillips, 2002; etc.). Despite an abundance of pre-existing methods to create flesh deformation, to the extent of this research's knowledge, the adopted flesh deformation methods (FDMs) used by existing DHM in ergonomics simulation are limited. JACK adopted free-form deformation (Azuola et al., 1994) whereas RAMSIS adopted a combination of rigid flesh deformation and torsion deformation for vertices around the joint (Bandouch et al., 2008). SANTOS (Abdel-Malek et al., 2006) adopted linear skinning which involves assigning weights to the outer skin surface based on the outer skin surface relationship with the nearby skeleton. All of the above adopted methods produce flesh deformation that is purely based on sculpting the flesh form with little or no regard to ergonomics principles.

1.3 Research scope

There is clear need for the development of a model that would provide a higher precision body shape and form to assist ergonomics CAD's role to accommodate a greater accuracy in product and environment assessment. As the human body is not a rigid object, body deformation will take place whenever the joints change their orientation or interaction with external objects occurs. Efforts were made to take flesh deformation into account by creating models for specific body parts (Assassi et al., 2009; Lee et al., 2009; etc.), and modelling the interaction between specific body parts and external objects (Mehta and Tewari, 2000; Verver and Mooi, 2004; Moes, 2007; Grujicic et al., 2009; etc.), etc. These efforts were made because simply disregarding the body deformation during posture extrapolation will yield an undesired poor precision of the simulation result. However, for ergonomics simulation where flesh deformation modelling of the whole body was required, these efforts would not be sufficient. Thus the scope of this research is to establish a methodology for joint deformation for ergonomics simulation purposes that could be part of a whole body modelling approach. To facilitate this, 3D body scanning technology will be utilised in order to obtain human form data. The focus will be to ensure that any resulting joint deformation method can simulate deformation as closely as possible to the original 3D body scan data in terms of its geometrical correctness. This will ensure that the flesh deformation due to joint movement directly addresses the needs of ergonomics simulation.

1.4 Aim and objectives

Supported by a 3D body scanner which permits capturing a realistic human body form, this study aims to develop a methodology to simulate body deformation due to joint movements which suits the needs of ergonomics simulation. To anticipate the large scope of the study, the study will focus on modelling a single joint: the movement of the elbow joint without additional load.

The objectives of the study are as follows:

1. *To review the state of the art on topics of the use of DHM in ergonomics and body deformation.*
2. *To develop a set of specifications for DHM to guide the development of flesh deformation modelling of the elbow that suits the needs of ergonomic simulation.*
3. *To propose a method to create flesh deformation at the elbow joint that suits the needs of ergonomic simulation.*
4. *To review the proposed method to deform the elbow against the set of specifications for DHM.*

1.5 Thesis outline

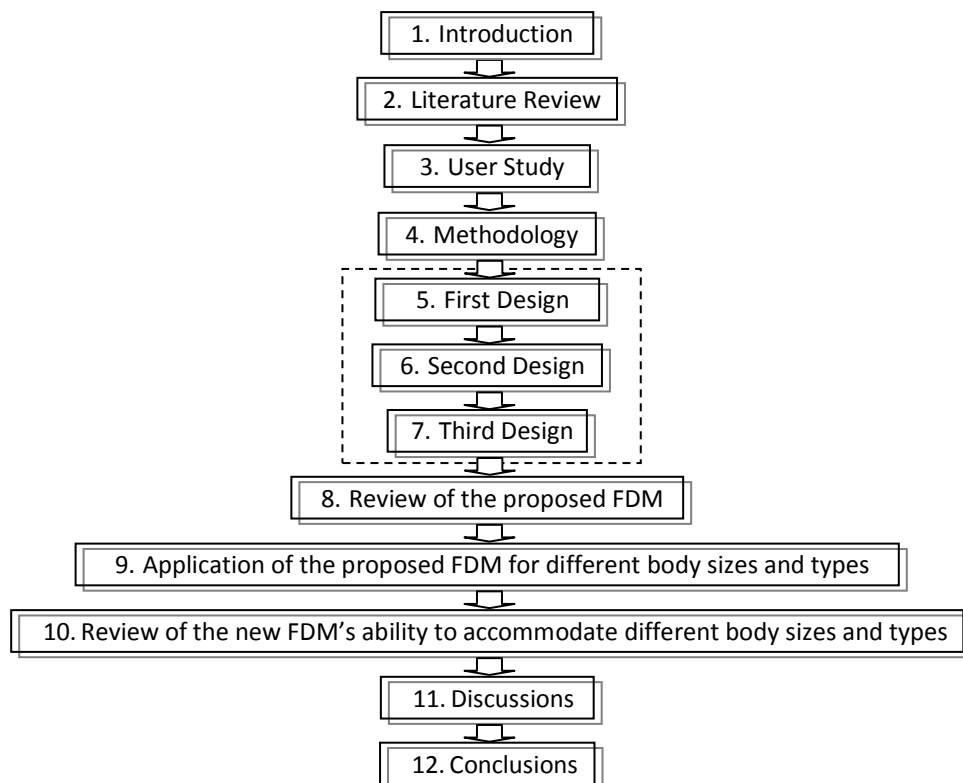


Figure 1. Thesis outline

The thesis outline is shown in Figure 1. After the introduction, a thorough literature review of an up to date usage of DHM in ergonomics and body deformation methods is presented in chapter 2. Chapter 2 also provides a concise explanation about 3D body scanning and other basic theories

related to this study. The literature review in chapter 2 is then followed by a user study in chapter 3 where views of the end users of DHM for ergonomics simulation is elicited and findings from the literature review is followed up. Chapter 4 highlights the adopted methodology used to develop the proposed FDM. In this chapter, a set of DHM specifications are determined based on the results of the literature review on the DHM usage in ergonomics and the results of the user study. This chapter also assesses existing body deformation methods against the previously determined DHM specifications. Based on the assessment result, a method to deform the elbow is proposed.

The development of the proposed method is outlined in the next three design phase chapters: chapters 5, 6 and 7. The output of the design phase chapters is then reviewed in chapter 8. This chapter aims to review the suitability of the proposed FDM against the identified DHM specifications. This chapter also identifies additional research required to measure the suitability of the proposed FDM to accommodate different body sizes and types. The additional research is explored in chapters 9 and 10. Chapter 9 elucidates on how the proposed FDM could be utilised to accommodate different body sizes and types. This chapter explains in detail a framework that would allow the proposed FDM application to accommodate different body sizes and types. Chapter 10 reviews the proposed framework by investigating the level of accuracy and realism of the flesh deformation. Chapter 11 discusses issues that were encountered during the research as well as alternative approaches that could have been pursued for this research. This chapter also discusses how this research achieved the aim and objectives which had been set up in the beginning of this research. The discussion chapter is then followed by chapter 12 which provides the conclusions of this research.

2 Literature Review

The literature review of this thesis is divided into six sections. The first section reviews the role and characteristics of DHM as well as their current development and future. The second section investigates existing approaches to flesh deformation. The third section provides a basic theory on surface creation. This is then followed by a brief theory on the representation of kinematics and rotation in section four. Next, a brief theory on DHM's joint movement and a review of 3D body scan technology are presented in sections five and six, respectively. This chapter is then concluded with a summary of the literature review. A part of the literature review was published in Hermawati and Marshall (2007).

2.1 Digital human models (DHM) in ergonomics applications

Ergonomics application/simulation is used to assist the design of appropriate products or workplaces by taking human capabilities and limitations into consideration. Previously, ergonomics applications only focused on a limited aspect of human performance hence a particular analysis would require the use of more than one tool. This condition prompted a further integrated software development which was known as "ergonomics CAD". By combining various ergonomics analysis features into a computer aided design (CAD) application, various ergonomics assessments are able to be performed at once (Porter et al., 1995). Ergonomic CAD allowed ergonomics assessments by enabling the creation of DHM in a CAD environment.

Sundin and Örtengren (2006) distinguished DHM for ergonomics applications into two kinds: i) cognitive and performance DHM and ii) Physical DHM. Cognitive and performance DHM involves the modelling and simulation of the cognitive and performance aspects of the human being. For instance, the modelling of human behaviour during interaction with a computer or machine. Physical DHM, which was categorised further into biomechanical models and computer manikins, emphasise traditional ergonomics aspects such as applied physiology, occupational ergonomics, energy expenditure, vision and safety. The main interest of this research was computer manikins which were defined as: "A 2D or 3D computer representation of the human body based on anthropometric measurements, link and joint structure, and movement characteristics, which is incorporated in software and acts in a digital environment" (CEN, 2003). However, the term DHM, instead of computer manikins, was used in this thesis for practicality.

Following the definition of DHM above, there are three fundamental features which comprise a DHM. The first one is the link and joint structure which is used to represent the kinematics of the

human being. In addition to the link and joint structure, a limit of angle range is also introduced for each joint. Figure 2 shows an example of the link and joint structure from JACK, a commercially available DHM for ergonomics application. JACK is represented by 71 links, 69 joints and 135 degrees of freedom for its joints. The second fundamental feature is the anthropometric measures which are used to model humans of various sizes, races, nationality, etc. The anthropometric measurement is essentially a one dimensional measurement which is then extrapolated to create a 3D DHM. Figure 2 shows an example of some anthropometric measurements which are used to create a 3D DHM. The last fundamental feature relates to movement characteristics which are used to model biomechanical posture and movement simulation. To accommodate this, DHM utilises inverse kinematics which predicts the link and joint location when a user specifies a posture.

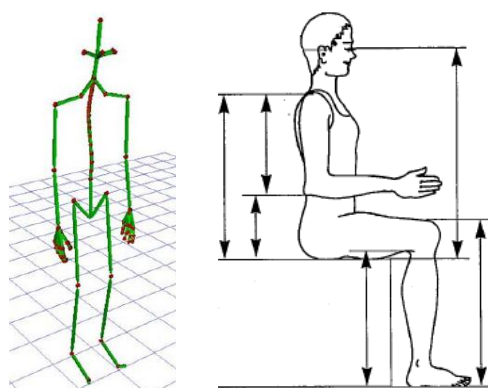


Figure 2. An example of link and joint structure in JACK (adapted from Blanchonette (2010)) and some of the anthropometric measurements which are used to create the size of DHM

2.1.1 DHM's role in ergonomics

In general, the main role of DHM in ergonomics applications is to evaluate the accommodation of a product or workplace. Naumann and Roetting (2007) briefly described the role of human models in product design i.e. to seek out answers concerning the fitness of the products before building a physical prototype, for instance, questions about visibility, ingress/egress, reaching/grasping, multi person interaction, strength assessment and comfort in relation to a product. Supporting this view, Chaffin (2001) stated that a human model is “a means to create, manipulate and control human representations and human-machine systems scenes on computers for interactive ergonomics and design problem solving”. Furthermore, utilising human models within the design phase helps the identification of ergonomics problems at an earlier stage of the design process as well as reducing or eliminating the necessity of physical mock-ups and testing with real human subjects (Badler et al., 1993; Morrissey, 1998; Zhang and Chaffin, 2000; Feyen et al., 2000). According to Chaffin (2001), despite a higher initial added cost from the usage of virtual humans compared to a traditional serial design process, a significant gain can be achieved within the prototyping, testing and the redesigning phases. Thus, the ability to simulate the interaction of a

human with a product or workplace environment virtually can lead to cost and time savings. Several researchers have made use of human models to evaluate either a product or a working environment (Fulder et al., 2005; Wichert et al., 2004; Barone and Curcio, 2004; Carey and Gallwey, 2002; Feyen et al., 2000). Chaffin (2001) summarised some ergonomics case studies which were successfully resolved through the application of ergonomics simulation software support. The main role of DHM in ergonomics application suggests that DHM accuracy is of importance in order to provide a reliable means of evaluation within prototyping, testing as well as the redesigning phase.

Chaffin (2001) also pointed out that the most common use of virtual humans is to assist in designing products which can accommodate people of varying size and shape. This common usage of DHM is supported by one of the three fundamental features of DHM in ergonomics application i.e. anthropometric measurement, which is aimed to model humans of various sizes, races, nationality, etc. (see section 2.1). Usage of DHM to design products for a variety of users implies that DHM in ergonomics should be supported with the ability to model people of different sizes and shapes.

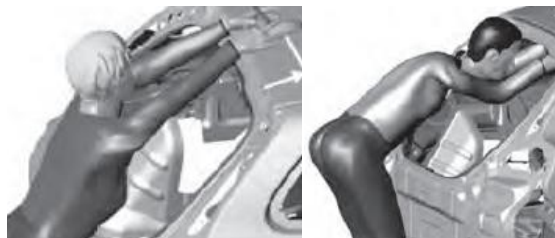


Figure 3. Unrealistic flesh deformation that occurs at the shoulder and elbow area due to postures adopted by DHMs (Adapted from Lämkkull, Örtengren and Malmköld (2008))

In relation with the role of DHM in ergonomics to assist evaluation and design of products, Green (2000) proposed general processes or work methods which are commonly adopted to perform analysis with existing ergonomics applications. The proposed work methods consist of five stages: (1) understanding the task, work environment, and the worker population; (2) understanding the limits of the software used for analysis; (3) performing analysis; (4) analysing and applying judgement to the results; and (5) reporting the results of the analysis. Ergonomics applications are used mainly in the third stage where DHM and its environment are created and ergonomics analysis such as analysis of reach, fit, posture, strength, vision etc. are performed. To perform an analysis, a user would typically need to: (1) decide the DHM's size and shape e.g. 5th percentile British female, 95th percentile British male, etc; (2) place a DHM in its environment by deciding its starting point and orientation; and (3) posture a DHM. These three processes are commonly performed in real time by a user. While performing an analysis, a user is not expected to correct any unrealistic flesh deformation or appearance that occurs due to a certain posture adopted by the DHM (see Figure 3).

Green's (2000) general processes in performing analysis with existing ergonomics applications suggests that the level of user intervention for ergonomics application is mostly limited to: creating the environment for the DHM, specifying the size and shape of DHM, controlling the posture and location of DHM, and performing a set of analysis from the given tools. This implies that, in contrast to graphic design tools, users of ergonomics applications are not expected to have to correct unrealistic flesh deformation resulting from a posture by tweaking the skin or surface representation of the DHM. Green's (2000) general processes in performing analysis with existing ergonomics application also implies that the posturing is expected to be performed within a short time scale i.e. a real time modelling.

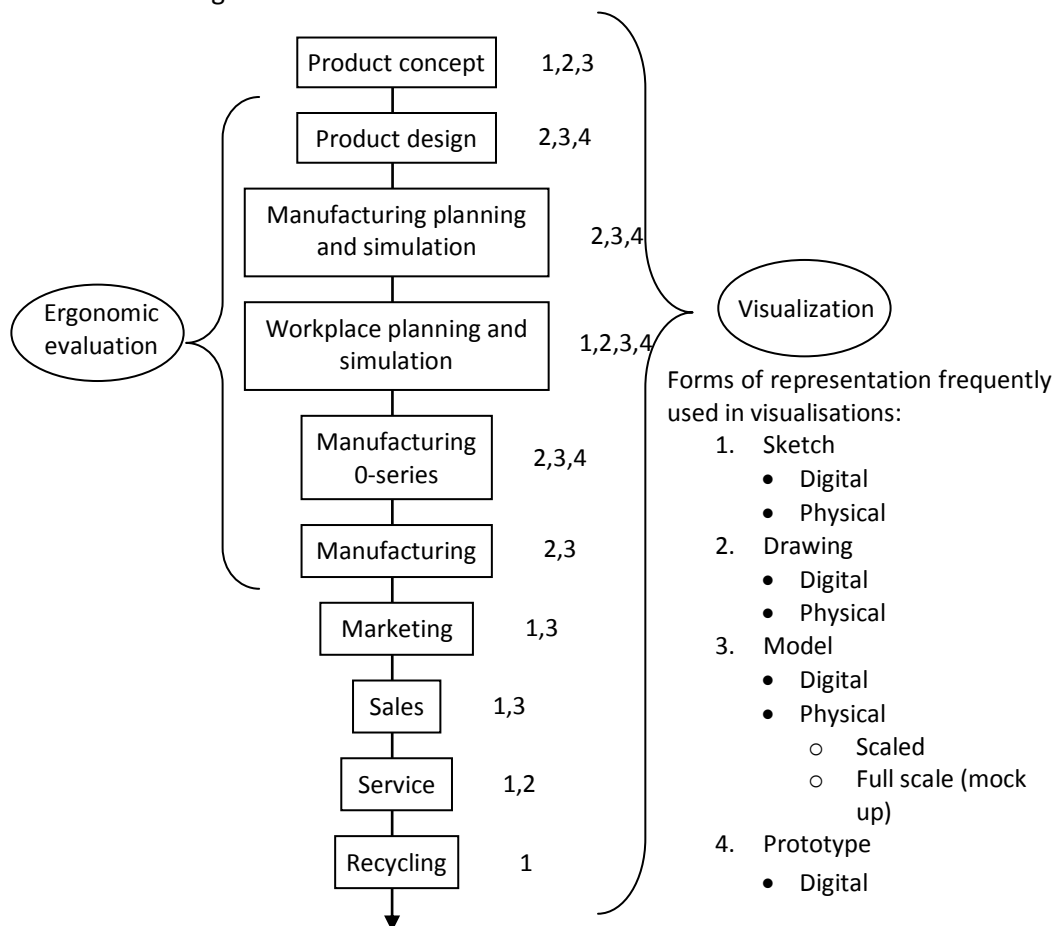


Figure 4. Functions of ergonomics application throughout stages of a product life cycle (adapted from Sundin and Örtengren (2006))

Locket et al. (2005) and Sundin and Sjöberg (2002) also argued that ergonomics human modelling tools are used for visualisation throughout product design (Figure 4). A visualisation tool is defined as a tool to support creation and presentation of a workplace, product or solution (Sundin and Örtengren, 2006). The visualisations provide information about body posture, reach ability, field of view and clearances which serve as a basis for ergonomics evaluation and decision making (Wegner et al., 2007). As a visualisation tool, DHM in ergonomics applications was found to improve participation and communication regarding ergonomics issues (Sundin and Sjöberg, 2002; Sundin et

al., 2004); and also assist the passing of information between the ergonomist and department managers or designers (Boozer and Raschke, 1998; Sundin and Örtengren, 2006). Hamilton and Nowak (2009); and Yang (2008) argued that the realistic appearance of DHM is an important aspect for visualisation of digital humans. They revealed that the user trusts the visualisation results more if the DHM looks like a real human. This implies that DHM in ergonomics simulation calls for the ability to produce a realistic DHM i.e. resemble a real human as close as possible.

2.1.2 DHM's characteristics in ergonomics

According to Locket et al. (2005), the important characteristics of DHM to simulate human activities realistically include: 1) anthropometry; 2) biomechanical and kinematics models; 3) posture/motion realism and manipulation; 4) load exertion capacity; 5) environment interactions; 6) object grasping and carrying; and 7) field of view. These characteristics were in accordance with the view of Naumann and Roetting (2007). Chaffin (2005) added: 1) additional clothing; gloves and helmets; 2) reach and fit analysis; and 3) compatibility of virtual human and CAD software, to the list above. Furthermore, Wegner et al. (2007) also provided more detailed characteristics such as: 1) detailed hand, foot, spine and shoulder model; 2) realistic skin and ability for skin deflection; 3) behavioural programming; 4) motion restriction from additional clothing etc.; 5) automatic posture optimisation; and 6) collision detection between DHM and virtual objects. Seidl and Bubb (2005) listed five fundamental characteristics of DHM in ergonomics. These are 1) kinematics of the model which involves the number and mobility of the joints, 2) a realistic outer surface simulation of the human skin surface to support the presentation of analysis results, 3) biomechanical posture and movement simulation, 4) ability to analyse the product to be developed, 5) seamless integration into design process.

The DHM's characteristics above seem to suggest that DHM characteristics are driven by the DHM's role in ergonomics application as discussed in section 2.1.1. For instance, Seidl and Bubb (2005) and Wegner et al. (2007) suggested realistic outer surface simulation of the human skin surface as one of DHM's characteristics because it supports the role of a DHM as a visualisation tool. Their suggestion also indicates that realistic outer surface simulation of the human skin is indeed required by a DHM in ergonomics application.

2.1.3 Existing DHM for ergonomics application

Most ergonomics simulation softwares satisfy basic requirements to integrate ergonomics principles within the design process. Some of these are the abilities in creating 3D environment/objects around the DHM, generating DHM based on anthropometric data/body type, integrating dynamic anthropometric features/joint constraints and performing ergonomics analysis

(Porter et al., 1995). Examples of ergonomics simulation software include JACK (Siemens PLM software, 2011), ManneQuinPro (NexGen Ergonomics Inc., 2011), RAMSIS (Human Solutions GmbH., 2011), Safework (Safework Inc., 2011), SAMMIE (SAMMIE CAD Limited, 2011) and Santos (SantosHuman™ Inc., 2011) amongst others.

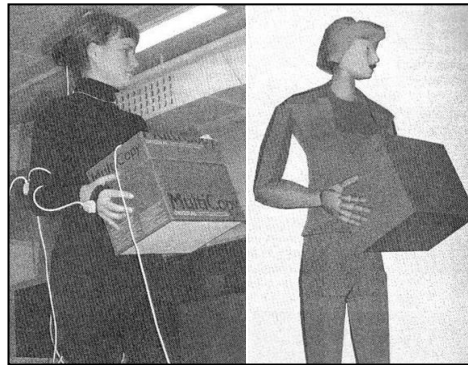


Figure 5. Integration of motion capture in JACK to create realistic motion and posture (adapted from Sundin and Örtengren (2006))

A key resource from JACK is its ability to create motion in real time through the use of motion capture and hence enabling dynamic ergonomics analysis (Figure 5). Despite the potential to produce a realistic posture and motion, Johansson and Åström (2004) identified some drawbacks of the use of motion capture to drive JACK movement such as: (1) the difficulty to create the exact anthropometry of a person from whom the motion was captured, (2) trial and error was required to ensure that the sensor of the motion capture system were placed correctly. Ergonomics analysis which could be performed in JACK includes National Institute for Occupational Safety and Health/NIOSH lifting equation (CDC, 2011), low back injury risk assessment, psychosocial strength tool, fatigue assessment, metabolic energy expenditure, Rapid Upper Limb Assessment/RULA (McAtamney and Corlett, 1993), Ovako Working Posture Analysing System/OWAS (Karhu et al., 1977) and comfort. An effort to integrate three dimensional body scan data into JACK also takes place by morphing the figure surface polygons to match the surface topography from the 3D scan data. In return, it is expected to enhance JACK's visual look and allow additional analysis such as clothing studies (Raschke, 2004). The integration of three dimensional body scan data is offered as a separate add-on application tool kit (3D Bodyscan Module) of the original version of JACK (Classic JACK). JACK consists of 68 joints to represent its skeleton and uses polygons to represent its skin representation. Flesh deformation modelling for JACK is achieved by modifying free form deformation, one of the existing flesh deformation approaches which are explained in section 2.2. Although JACK produces a DHM that bears a resemblance to a real human, Badler et al. (1993) indicated that they "bypassed" accurate skin models due to the difficulty in modelling the body figure that is dependent upon muscle/fat ratio, gender, etc. They argued that: "for the kind of

analyses done with the whole body models, error of a centimetre or so in skin surfaces are subordinate to anthropometric errors in locating true joint centres and joint geometry”.

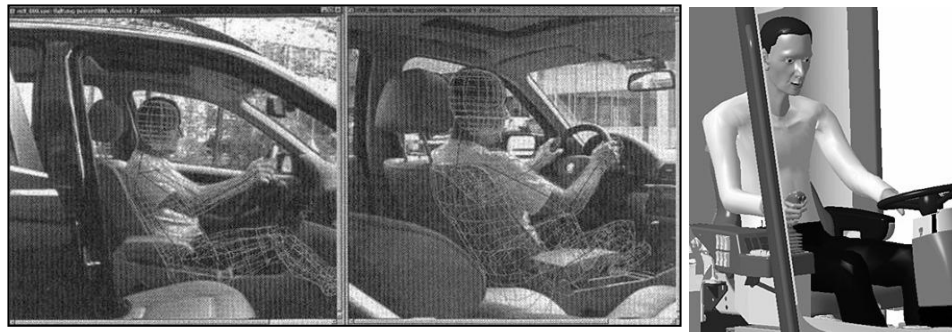


Figure 6. RAMSIS's overlay technology to fit posture and anthropometric data (adapted from Seidl (2004))

While JACK is created to assist simulation for various conditions, RAMSIS is meant to provide efficient design of interiors of cars, trucks, and airplanes (Seidl, 1997). One of the key features of RAMSIS, aside of its large number of degrees of freedom, is its overlay technology to fit posture and anthropometric data (see the first two images in Figure 6). Given two pictures simultaneously taken from two different viewpoints e.g. side and front, RAMSIS could be used to automatically fit posture and anthropometric data. Postural discomfort assessment, vehicle seating spinal postures and seat belt factors are also available in RAMSIS (Seidl, 2004). RAMSIS consists of 28 joints and its skin surface is represented with polygons. RAMSIS adopts a combination of rigid flesh deformation and torsion flesh deformation for vertices of tangential body parts that undergo rotation. The flesh deformation result is on par with JACK's flesh deformation, as shown in the right hand image in Figure 6.

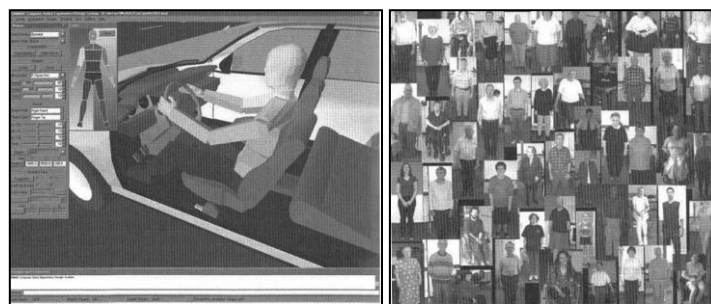


Figure 7. SAMMIECAD created an additional database which preserved individual data which allowed virtual fitting trial (adapted from Porter et al. (2004)).

Another commonly used DHM is SAMMIE. A key feature of SAMMIE is its add-on package HADRIAN (Human Anthropometric Data Requirements Investigation and Analysis) which contains a database of individuals i.e. anthropometry, mobility/capability, disability, coping strategies, and background data with a simple task analysis tool. This allows virtual fitting trials and to some extent can eliminate the need for prototyping/user trials (Porter et al., 2004). SAMMIE consists of 21 joints and 23 body segments. As shown from Figure 7, SAMMIE's skin surface is represented by a low number

of polygon surfaces and rigid deformation is employed to model its flesh deformation. As a result, SAMMIE's flesh deformation is less realistic compared to both JACK and RAMSIS.

Santos, a virtual soldier (Figure 8), is more advanced in terms of its functionality and realism. In addition to the usual features for physical DHM, it is also equipped with fatigue and endurance evaluation, volitional cognition and situation awareness, behaviour representation, object avoidance, and clothing simulation (Abdel-Malek et al., 2006). For its flesh deformation, Santos adopts a linear blend skinning approach, which is discussed later in section 2.2. As shown in Figure 8, the DHM in Santos has a more realistic appearance in comparison to DHMs discussed above. Despite its enhanced features and appearance, it has not taken the advantage of 3D body scanner availability to create a DHM.



Figure 8. SANTOS, a virtual soldier which had advanced features for its functionalities and realism (adapted from Abdel-Malek et al. (2006))

The literature review concerning the existing DHM for ergonomics application demonstrates that existing DHM generally involves whole body modelling. This is likely prompted by the need to model a whole body model to simulate a working posture so that reach and fit or visual sight line analysis could be performed.

2.1.4 Current and future research of DHM for ergonomics application

Based on the brief description of existing DHM for ergonomics applications, some of the DHM's characteristics above are already addressed whereas others still require further research. Badler (1997) summarised some studies which would be required in the future such as the inclusion of auditory information processing and environmental factors, injury assessment, ability to learn etc. In addition to this, a comprehensive review of current DHM research in Ergonomics was also given by Naumann and Roetting (2007) which showed that the recent research covered issues on modelling eye movement, comfort/discomfort assessment, hands modelling and motor behaviour /motion sequences modelling.

Chaffin (2006) regarded dynamic human motion modelling as a research area that required further development. Another area which received attention recently is DHM standardisation

(Sundin and Örtengren, 2006). Wegner et al. (2007) also highlighted the necessity of standardisation for DHM while Ruiter (2000) presented the need for educating users with less ergonomics knowledge who were not aware of underlying assumptions and simplification involved in DHM creation. He argued that the lack of understanding would lead to application mishandling and suggested to look further into what was required from DHM as well as what and how DHM were used.

Current and future research of DHM for ergonomics application suggests that there is a lack of attention paid on enhancing the appearance of DHM. This was in contrast to the findings in section 2.1.1, 2.1.2 and 2.1.3 which shows that enhancing the appearance of existing DHM in ergonomics application would be beneficial, especially with relation to its role in visualisation. To enhance the appearance of DHM, in addition to creating a DHM that resembles a human as close as possible, a realistic flesh deformation due to joint movement and interaction with external objects/pressure would likely be required.

2.2 Flesh Deformation around the joint for DHM

Currently, there are five main categories of approaches to deform the human models' flesh around the joint. These are anatomic, physical, geometric, example based and sweep based approaches. The following sections provide a brief description of each category, their strengths/weaknesses and examples of existing methods.

2.2.1 Anatomic approach to flesh deformation

The most realistic, but complicated and computationally expensive approach for flesh deformation is the anatomic approach. The anatomic approach strives to create accurate and realistic flesh deformation through accurate creation of bone, muscle and skin with respect to their shape, material properties and material behaviour. Aside of its high accuracy in depicting flesh deformation, the anatomic approach is also capable in simulating deformation when forces are applied on the skin surface. Nevertheless, deformation must be recalculated for every joint movement and needs substantial processing time. Therefore, this type of deformation model is less suitable for the deformation of a whole body model, especially for real time application with current technology.

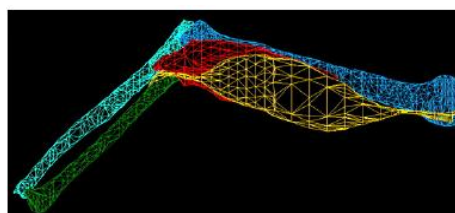


Figure 9. Upper arm model (adapted from Maurel (1998))

Dong et al. (2002) utilised Computer Tomography (CT) scan images as the base to remodel various shapes of muscles. These muscles were then combined, if needed, to reconstruct a human body. Thus, beside volume preservation, muscle deformations took into account collision detection and collision response between muscles which substantially slowed down the deformation process. Maurel (1998) went further by building a finite element model of the shoulder joint which consisted of bones, joints, muscles and skin based on Magnetic Resonance Imaging (MRI) images (Figure 9).

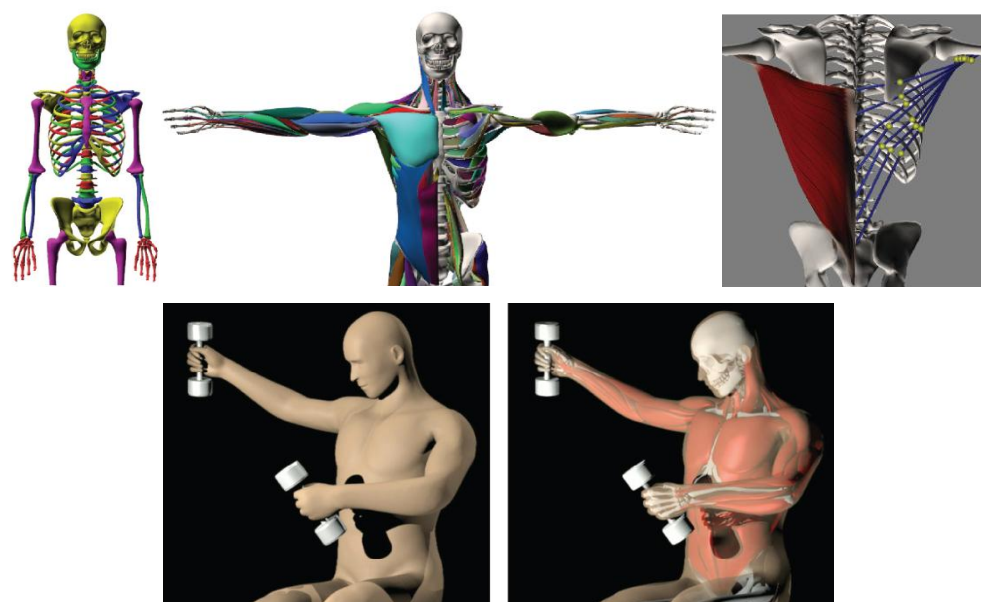


Figure 10. Skeleton model (top left image), muscle model (top middle image), muscle actuator of one of the muscle at the back (right image) and the result of flesh deformation (adapted from Leet et al. (2009))

In a more recent study, Sueda et al. (2008) developed a musculotendon simulation for hand animation. For their study, they developed an anatomically correct model of a hand which involved accurate representation of 17 bones and 54 musculotendons. The deformation is created by determination of the appropriate activation levels for each muscle. In a study by Kasap et al. (2009), MRI and Electromyography (EMG) signals were used to create accurate flesh deformation on the hip joint. Firstly, MRI data was used to reconstruct bones, muscles, ligaments, and cartilage at the hip joint. The MRI data was also used to create a so-called muscle map. The muscle map is created by calculating the distance between each muscle contour and its corresponding bounding ellipse. EMG signals are then used to modify the muscle map, hence altering the size of the muscles. Their research produced an accurate representation of skin deformation. However as EMG signals are required to control the skin deformation, this means that EMG signals had to be obtained for each new set of movements. In addition to this, the existing model could not be directly used for a different person. In another study by Lee et al. (2009), an anatomically correct upper body was created (see Figure 10). The dynamic skeleton consists of 68 bones with 147 degrees of freedom, including the vertebrae and ribs. Realistic flesh deformation is simulated by embedding 3D

anatomical geometries of the hard and soft tissues. Muscle deformation is based on automatic calculation of activated muscle signals in accordance to the pose specified by the user whereas skin deformation is based on a finite element model.

2.2.2 Physical approach to flesh deformation

In physical deformation simulation, a mass and spring system, derived from the mechanical laws of particles, is commonly used. The muscle or skin is represented as a set of particles with mass and connected with a spring which generates forces during the particles' interaction. Similar to the anatomic approach, the physical approach is able to model the interaction between a virtual human's skin and its environment. Although this approach is less computationally demanding than anatomical approach due to some simplifications in skin, muscle and bone representation, it is considered to be less suitable for real time application and is mainly for off-line simulation and animation (Hyun et al, 2003).

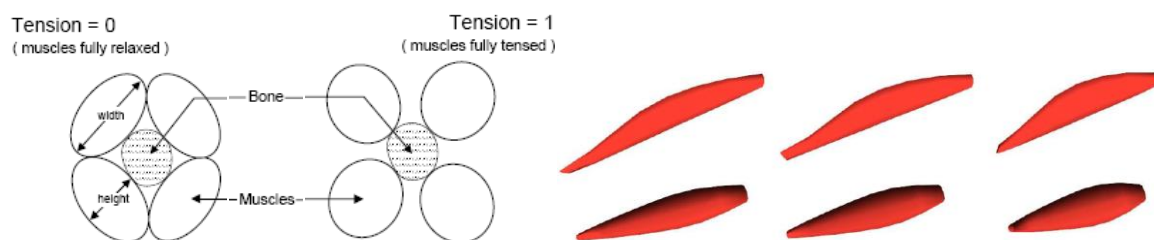


Figure 11. Left image shows ellipsoids that represent muscle in Scheepers et al. (1997) study whereas the right image show deformed cylinder which represent muscles from Wilhelms and Gelder (1997)

Nedel and Thalmann (2000) developed an “angular spring”, connecting the particles on the surface of the muscle, which caused the particle to create curvature in horizontal and vertical direction and defined the shape of the muscle. Vassilev and Spanlang (2002) introduced “support string”, modelling the matter inside an object, so that no explicit volume preservation computations during the simulation are needed during run time. Another method for the physical approach is by creating 3D objects which mimic volume preservation of the muscle during the movement. Scheepers et al. (1997) modelled the muscle as ellipsoids (sweeping the varying ellipses) while Wilhelms and Gelder (1997) used deformed cylinders (see Figure 11).

In another study by Guo and Wong (2005), given a skin mesh and its skeleton, so-called “deformable chunks” were created automatically to represent the internal structure of a human model i.e. muscles. A finite element method was applied to deform the deformable chunks. Altering the skeleton of the human model drives the deformation of the deformable chunks and results in the flesh deformation. Tang (2010) proposed a different approach to produce flesh deformation. Instead of creating an internal layer to mimic muscle deformation, he utilised a

boundary element method. Given an initial and target pose and the pre-determined locations of landmarks on the skin, he solved the deformation of the skin as a boundary element problem

Recently, there has been research towards mesh-less deformation. Guo and Qin (2005) also proposed mesh-less deformation. 3D objects are expressed as a set of points which represent the objects' interior and boundary geometry. A continuum mechanics model was used to represent the dynamic elastic behaviour of the points. A similar approach was also proposed by Adam et al. (2010). However, instead of using continuum mechanics, mesh-less finite element model was used to create flesh deformation.

2.2.3 Geometric approach to flesh deformation

A geometric approach is essentially based on geometric manipulation of the skin's vertex location. Thus, the determination of the skin's vertex location is based on neither anatomic principles nor physical properties of muscle/skin. As a consequence, this method is less complex when compared to the two previous approaches and is more suitable for applications that demand real time and yet realistic flesh deformation. This approach has also drawn more research interest compared to the two previous approaches. Hence, to ease the explanation of existing methods, the existing methods will be divided further into several sub categories. These are: i) linear blend skinning, and ii) free form deformation.

2.2.3.1 Linear Blend Skinning

This particular approach is adopted largely due to its cheap computational cost. It goes by various names such as "skinning", "smooth deformation", or "skeleton-subspace deformation". A human model in smooth deformation consists of a skin layer and articulated skeleton (joints and skeleton segments), governing the skin layer deformation. To deform the surface vertices, a weighted average of the vertex rigidly transformed by the influencing bones is computed.

Equation 1 to 3 show the formula that underlies linear blend skinning and is assigned to each vertex. First of all, linear blend skinning requires each vertex to be expressed in its local coordinate system and in a pose commonly referred to as a "rest pose". The local coordinate systems of a vertex are determined by which bone(s) it is assigned to (see equation 1). For example, a vertex that is located around the elbow joint would have two local coordinates systems i.e. local coordinates system of the upper arm and lower arm. When corresponding bones are moved, each vertex is transformed back to the world coordinate system and multiplied by the new dynamic position of those bones. This is shown by equation 2. The final location of the vertex is calculated by blending using the bone weight, as shown in equation 3. The total sum of weight of the bone(s) for a vertex is always 1.

$$\hat{v}_j = \hat{G}_j^{-1} \hat{v}, \quad (1)$$

where:

\hat{v} = the coordinates of vertex v in its local coordinates system for the bone j in the rest pose,

$$\hat{G}_j^{-1} =$$

inverse of transformation matrix that transform \hat{v} back to the world coordinate system,

\hat{v}_j = the coordinates of vertex v in the world coordinate system for the bone j in the rest pose

$$v_j = G_j \hat{G}_j^{-1} \hat{v}, \quad (2)$$

where:

v_j = the coordinates of vertex v in the world coordinates system due to the movement of bone j ,

G_j = transformation matrix that transform v to a new location due to the movement of bone j ,

$$v = \sum_{j=0}^{b-1} w_j G_j \hat{G}_j^{-1} \hat{v}, \quad (3)$$

where:

v = the final coordinates of vertex v in the world coordinates system

w_j = weight (influence) of bone j on the vertex v

The weaknesses of this method are a lack of muscle bulging/swelling and collapsing joints for extreme positions (Figure 12) which require user intervention to correct them. In spite of its speed, a linear blend skinning approach accuracy is less applicable to ergonomics simulation as the main goal of this approach is primarily driven by a visually convincing appearance.

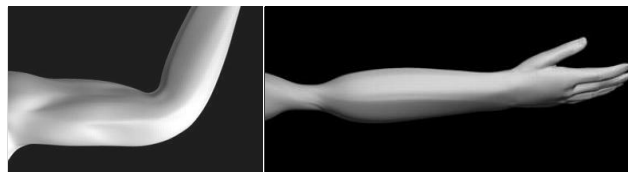


Figure 12. Two classical problems with skinning collapsed joint due to extreme and twisting posture (adapted from Lewis et al. (2000))

Several studies were directed to overcome the lack of muscle bulging/swelling and collapsing joints for extreme positions. Mohr et al. (2003) proposed an additional joint to allow more control for the animator/user to modify the location of vertices. Rohmer et al. (2008) introduced a local volume preservation which is embedded onto the existing linear blend skinning. Given a mesh and its skeleton model, their method automatically segments the mesh and pre-computes the volume of each segment. The calculated segments' volume was then used to correct the artefact of linear blend skinning. Their method also generates local bulges to the required area. Yang et al. (2006) proposed a curve skeleton to remediate artefacts of linear blend skinning. Given a mesh and its skeleton, their technique creates the curve skeleton and assigns automatic weights to the skin vertices based on their distance towards the corresponding segments of the curve skeleton. Figure 13 shows a curve skeleton at the initial pose.



Figure 13. Curve skeleton, shown as thin line inside the body mesh, at the initial pose (adapted from Yang et al. (2006))

Kavan et al. (2008) proposed dual quaternion blending which modifies the way the weights of the vertices are blended when corresponding bones of the vertices are animated. Lee et al. (2009) proposed patches to correct artefacts of linear blend skinning (see Figure 14). Their approach allows the user/animator to specify the location of patches, which once created will move together with the joint and skin. The patches are equipped with physical properties which are able to simulate elastic deformation and muscle bulge. Unrealistic deformation could be corrected by the user/animator's direct manipulation on the generated patches. Figure 14 shows an example of patch creation.

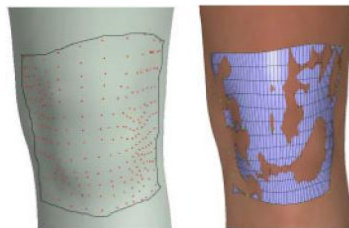


Figure 14. The left image shows a selected region to create a patch and the right image shows the created patch (adapted from Lee et al. (2009))

2.2.3.2 Free Form Deformation (FFD)

FFD was introduced first by Chadwick et al. (1989) and developed further by Sederberg and Parry (1986). FFD is a multilayered deformable animated character of which a control surface enclosing an object is created and the relation between the object inside and the surface is established. By deforming the control surface, a user sculpts the object inside. Free form deformation is efficient for designing simple characters but is less suitable for realistic modelling of a human body (Chadwick et al., 1989).

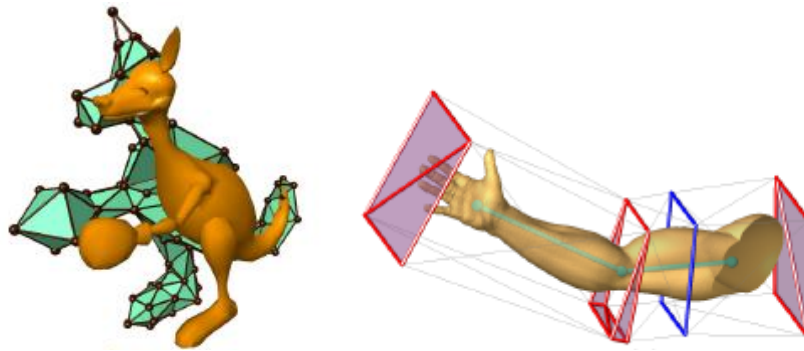


Figure 15. The left image shows half of the control surface created in Capell et al. (2002) study whereas the right image shows a cage based deformation from Ju et al. (2008) which consists of four “skinning templates”

To generate natural deformation, Summer et al. (2007) proposed the use of positional constraints on the embedded objects. The use of positional constraints allows feature preservation and hence a more natural deformation through direct manipulation. The drawback of this method was that the positional constraints of a certain body part could influence other body parts when the body parts were close to each other e.g. when the arm was by the side of the leg. To solve this problem, user intervention was required. Capell et al. (2002) proposed the use of a skeleton to drive the deformation of the control surface (see left image in Figure 15) which in turns leads to the skin mesh deformation of the corresponding skeleton. The application of their approach required the creation of a skeleton and control surface for every 3D object for which flesh deformation was needed. This could potentially be a drawback, especially for an application such as ergonomics modelling where flesh deformation was required for different body types and sizes. Ju et al. (2008) introduced a control surface, a so- called “cage based deformation”. A cage (see right image in Figure 15) is defined as a mesh with low resolution which encloses the skin mesh and skeleton of the model. A cage consists of smaller templates, so-called “skinning templates”, which wrap around a specific skeleton joint or bone. A skinning template achieves a particular skinning effect, such as a muscle bulging or artefact-free elbow bending and is defined in a way that is not specific to any given object/model. Given a skin mesh and skeleton of an object, a cage is created semi-automatically and its relationship towards the skin mesh and skeleton of an object is established. As the skeleton moves, the cage will deform. The cage deformation will then lead to the deformation of the skin mesh. As user intervention was needed to fine tune the cage fitting, this could likely be the drawback of this approach, especially for application that required minimum user intervention. Also, as the flesh deformation was based on establishing the relationship between the cage with the skin mesh and skeleton, it could potentially create a problem for applications where flesh deformation was required for various 3D objects e.g. different body types and sizes. Pushkar et al. (2007) also proposed the use of cage based deformation. However, the skin deformation is controlled purely by modification of the cage as their method did not require a skeleton

establishment for a given skin mesh. A slightly different approach is proposed by Landreneau and Schaefer (2010) who embedded a low resolution control mesh that approximated a given high-resolution mesh. Deformation of the high resolution mesh is achieved by modifying the control mesh. The automatically created low resolution control mesh of an object would likely be applicable only for that particular object. Thus, this could potentially limit the application for this approach in ergonomics modelling that covered different body types.

2.2.4 Example based

The example based method is based on extraction of flesh deformation information from a set of examples i.e. different poses/postures and using this information to create flesh deformation for new poses. The example based approach has a useful feature in that a set of examples could easily be acquired from 3D scan data (using body scanner, hand held laser scanner, etc.). As flesh deformation is based on a set of examples, the deformation result tends to be more realistic and could be performed automatically as the flesh deformation information has already been pre-processed. However, flesh deformation information which is extracted from a set of examples is likely to only produce a realistic result for that particular set of data. Also, vertex correspondence between the examples has to be established in order to allow extraction of the flesh deformation information.

Lewis et al. (2000) proposed “pose space deformation” (PSD) which requires an initial pose and various example poses. The idea was to provide flesh deformation as a scattered interpolation function of pose and allow flesh deformation to be sculpted at a desired pose, rather than a function of time. Firstly, the vertices of various example poses are inverted by means of linear blend skinning back into the initial poses. The displacement of vertices between the initial poses and various example poses are saved as displacement maps. The displacement maps, the pose and the joint angles of the pose were then stored in the pose space. To produce displacement at a desired pose, displacements of the example poses are interpolated. The interpolation is performed by weighting the contribution of each example pose. Example poses that are closer to the desired pose would have bigger contribution and vice versa. The interpolated displacement would then be used to adjust the result of linear blend skinning for the desired pose. The determination of how close a sample is, is done by simply subtracting each example pose and the desired pose. This means that all joints and vertices would have the same weights which would result in an unexpected result (Rhee et al., 2006). Kurihara et al. (2004) modified PSD further into a so-called “Weighted Pose Space Deformation” (WPSD). They modified the distance definition between poses such that joints that are relevant to a desired pose would have more weight and vice versa. This means that weight is not only assigned to a pose but also to how relevant its joints are. As a result, a more accurate

pose distance is obtained and it generates better skinning in arbitrary poses, especially when the poses are far from the examples (Rhee et al., 2006). A rather similar example based approach was also proposed by Sloan et al. (2001). However, instead of using displacement maps, a blending function was used to produce flesh deformation. In another study by Mohr and Gleicher (2003), given an initial pose and set of examples, they assigned additional joints to accommodate muscle bulging and avoid twisting. In their study, they only required a static mesh with a skeleton, which is different from Lewis et al. (2000) and Sloan et al. (2001) where a skin mesh of examples poses should already be assigned with weights of the joints. A recent study by Hong et al. (2010) also applied a similar approach to Mohr and Gleicher (2003) i.e. inserting additional joints to accommodate muscle bulge and avoid twisting.

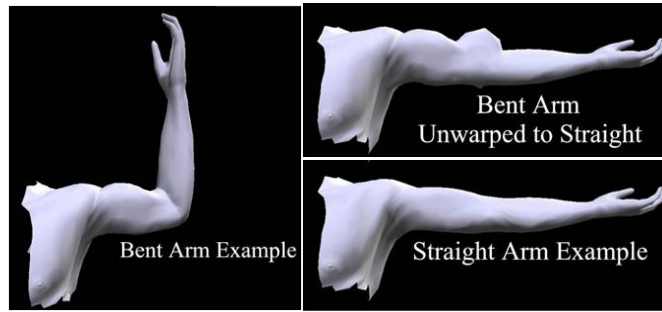


Figure 16. The process of inverting an example pose (bent arm) to an initial pose (straight arm) in order to acquire location of vertices of the example pose at a new pose (straight arm) which was then used to acquire displacement maps in Lewis et al. (2000) (adapted from Sloan et al. (2001))

All of the above research is based on interpolation of example data. A drawback of using interpolation from an example is that the motion representation will be more complex as the number of examples increases (Wang and Phillips, 2002). Hence, an approximation approach, a so-called “Multi Weight Enveloping” (MWE) is proposed by Wang and Phillips (2002). Although an approximation approach would be less accurate than interpolation, they argued that the approximation approach was able to handle more poses without increasing its complexity. Furthermore, it could process poses which were close in the pose space. They decomposed the linear blend skinning such that a weight is assigned for each joint movement. Referring to the equation 3 in 2.2.3.1, a matrix that determines how a bone moves relative to the rest pose is created (N_j), as shown in equation 4. Weights are assigned to each element of matrix N_j . An optimum weight of each element of the matrix is optimised from the set of example provided.

$$\begin{aligned} \mathbf{v} &= \sum_{j=0}^{b-1} w_j G_j \hat{G}_j^{-1} \hat{\mathbf{v}} \\ &= \sum_{j=0}^{b-1} w_j N_j \hat{\mathbf{v}} = \sum_{j=0}^{b-1} w_j \begin{bmatrix} n_{j,11} & \cdots & n_{j,14} \\ n_{j,21} & \cdots & n_{j,24} \\ n_{j,31} & \cdots & n_{j,34} \\ 0 & \cdots & 1 \end{bmatrix} \hat{\mathbf{v}} \end{aligned}$$

$$= \sum_{j=0}^{b-1} \begin{bmatrix} w_{j,11}n_{j,11} & w_{j,12}n_{j,12} & w_{j,13}n_{j,13} & w_{j,14}n_{j,14} \\ \cdots & \cdots & \cdots & \cdots \\ 0 & 0 & 0 & 1 \end{bmatrix} \quad (4)$$

Merry et al. (2006) also proposed an approximation of the example-based approach, so called “Animation Space”. They essentially decomposed the linear blend skinning method such that weight, inverse rest-pose matrix and vertex merged into a single vector which represents the animation space (p_j). Referring to the equation 3 in 2.2.3.1, the final location of vertex v is expressed as:

$$v = \sum_{j=0}^{b-1} G_j w_j \hat{G}_j^{-1} \hat{v} = \sum_{j=0}^{b-1} G_j p_j = [G_0 \ G_1 \ \dots \ G_{b-1}] \begin{bmatrix} p_0 \\ \cdots \\ p_{b-1} \end{bmatrix} = \mathbf{G} \mathbf{p}$$

By using the principle above, an optimum value of \mathbf{p} could be approximated from a set of examples and could then be used to create flesh deformation given \mathbf{G} from a desired pose. The approximation approach has a lower computational cost compared to the example-based interpolation approach. However, it will not be able to produce the same result as the example pose due to its approximation nature (Wang and Phillips (2002)).

In a recent study by Shi et al. (2008), the concept of the example based approach is combined with the physical approach. The skin mesh has material properties and is modelled physically by adding elastic forces from the surface neighbours and interior of the mesh, which was represented by forces to maintain the distance between surface vertices and corresponding bones. Given a set of examples, the motion and parameters of the materials are extracted and used to create flesh deformation. However, as it is physically based, their method could only be applied to an existing mesh and hence limits its usage.

2.2.5 Sweep based

The sweep based approach is characterised by the usage of cross sections to reconstruct and express the deformation. The use of cross sections to create a surface means that the final surface could be expressed in a various way e.g. polygon mesh, NURBS surface, etc. The deformation is mainly driven by modifying the shape of the cross sections or the orientation of the cross section and could be applied locally. For instance, to change an element of a 3D model, modification of cross sections' shape and orientation would only need to be applied to that particular element. The sweep surface is aimed to accommodate intuitive needs of users/animators to achieve desired 3D objects. This means that this method only applies minimum constraints. For instance, a user can change cross sections to any shape or orientation desired. As a consequence, to model deformation of a human body where the deformation has to follow certain constraints e.g. muscle bulge etc, a user intervention would be required to create a realistic deformation.

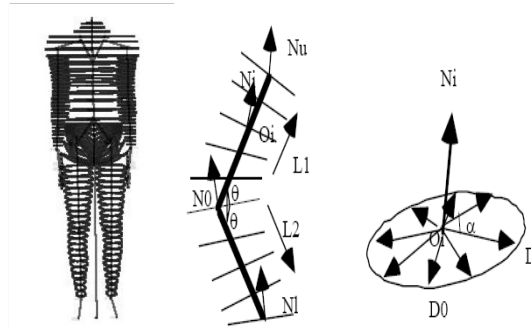


Figure 17. Left image: cross section contours of the body. Middle and right images: cross section orientation and ray-casting (adapted from Shen et al. (1994))

In a study by Shen et al. (1994), he divided the human body into 6 parts (torso, left-right arm, left-right leg and hips) and defined cross sections (contours) for each part (left image in Figure 17). Each contour is located on a different plane and no intersection between planes was allowed. Figure 17b demonstrates this principle. Normal orientation of the end planes (N_0 and N_u) were defined so that linear direction interpolation of the in-between planes can be calculated. The in-between planes were evenly distributed along the segment (L_1 or L_2) using linear distance interpolation. A bisection orientation was applied to the joint (intersection of two or more skeleton segments). As the planes were located/oriented, ray-centred along the sample points cast on the polygon surface of pre-determined human model (middle and right images in Figure 17). B-splines surfaces gave a smoother appearance with fewer vertices in comparison to the polygonal representation. Later on, these cross sections were blended to create B-splines surfaces for each body part. Because B-splines surfaces were incapable of handling human branch topology, Shen et al (1994) created a B-splines patch between the branches which had continuous tangency across the common boundaries.

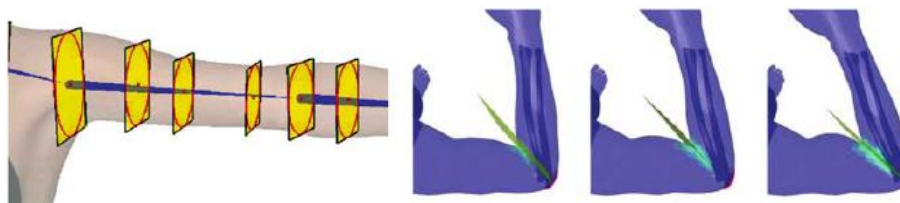


Figure 18. Left figure shows the fitting of ellipses into the cross section of an arm while right figure shows the self intersection area detection in various postures (adapted from Hyun et.al., 2005)

Hyun et al. (2003, 2005) later adopted this approach by using ellipses which fit tightly to the cross section and sweep them along the link between the joints. These ellipses were then used to govern the deformation by changing its orientation, accordingly to the joint angle changes (Figure 18). To give a higher precision and visually convincing appearance, displacement maps between the input surface and sweep blend surface were acquired. In special cases in which self intersection took place, collision detection was performed to determine the bisecting planes and pull back the vertices to the bisecting plane. The advantage of using this approach is its ability to preserve the volume when no self intersection happens. However, due to the collision detection algorithm, the

interactive speed is slow. Furthermore, user intervention is sometimes needed while blending the body segments together.

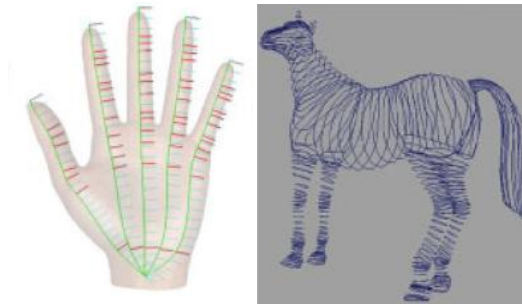


Figure 19. The left image shows the template of the bespoke hand model from Lee and Kim (2007) whereas the right image shows characteristic curves from You et al. (2008) which were created from a given horse skin mesh

Lee and Kim (2007) proposed a sweep based method to create a bespoke hand model. They create a sweep based template which could be adjusted to match a 2D image of the real hand. The sweep based template consists of a control sweep for each finger which originates from the base of the palm to the finger tip (see left image in Figure 19). You et al. (2008) proposed deformation with characteristics curves (see right image in Figure 19). Given a skin mesh of any 3D object, characteristic curves are created and their relationship to vertices of the skin mesh is established automatically. Flesh deformation is performed through modification of the characteristic curves which results in deformation of vertices of the skin mesh. Given an initial and final poses, the characteristics curves of the in-between poses could be calculated and utilised to create flesh deformation.

2.3 Surface Creation

There are various ways in representing a 3D object surface. The advantages and disadvantages of each surface representation will be discussed in the following sections.

2.3.1 Polygonal surface

A polygonal surface/polygonal mesh (Figure 20) comprises of vertices (points), edges and facets (faces). A polygonal surface is the most common way of representing an object's surface due to its high-speed rendering time. However, when a polygonal surface is used to represent organic objects with curvy surfaces, due to a polygon's piecewise linear behaviour, a high number of polygons will be needed. This also means an increment in the number of points to process (Hearn and Baker, 1994). A clearer illustration on the effect of polygon number to its accuracy in representing a curved surface is shown in Figure 21. JACK, RAMSIS, SAMMIE and Santos utilises polygonal surfaces to represent their DHMs' skin surface. As shown in the given DHM figures (see section 2.1.3), a higher count of polygonal mesh would result in a smoother surface for the DHM and vice versa.

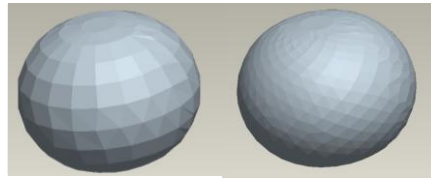


Figure 20. (a) Low resolution polygon mesh (b) High resolution polygon mesh



Figure 21. Accuracy vs number of straight lines to represent a curve. From left to right, the accuracy increases as the number used to represent the curve increases

2.3.2 Subdivision surface

A subdivision surface is an extension of a polygonal surface which smoothes out the appearance of the polygonal surface. In principal, there are two types of subdivision surfaces, approximating (Loop, 1994; Catmull-Clark, 1978; and Doo-Sabin, 1978) and interpolating i.e. Butterfly (Dyn et al., 1990). Both are shown in Figure 22.

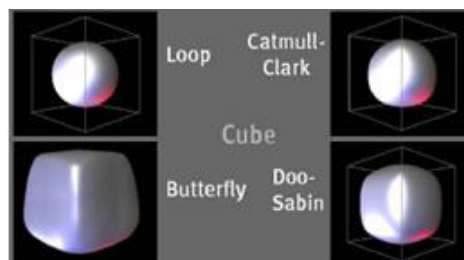
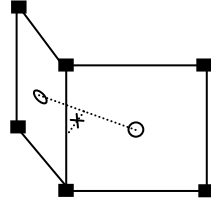
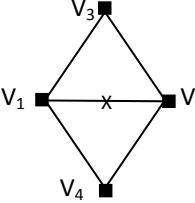
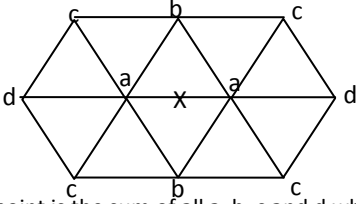


Figure 22. Comparison for various subdivision surfaces

The mechanism for each subdivision surface method is shown in Table 1. Butterfly is categorised as interpolating because the original vertices are kept and the smooth appearance is achieved by applying a certain algorithm on the calculated edge points. As the original vertices are kept, it is easy to predict the final outcome of Butterfly subdivision. Subdivision surfaces are commonly used by artists as it allows them to create smooth 3D objects from low resolution models, and are commonly found in digital sculpting applications.

Table 1. Detailed description for each subdivision method

Methods	Descriptions	Illustrations
Doo-Sabin	For each face, a face point and edge points are created. Face point is the average of all vertices of the corresponding face. The edge points are the midpoints of edges of the corresponding face. The new vertex is the average of the old vertex, two edge points (of edges which touches the old vertex) and the face point.	<ul style="list-style-type: none"> ■ : original vertices x : edge points O : face point ● : new vertex

Catmull-Clark	<p>Face point is the average of all vertices of the corresponding face. The edge point is created for each original edge and is defined as the average of the midpoint of corresponding original edge and the midpoint of the two face points (the adjoining polygons of the original edge). The new vertex is calculated using the formula in the right column.</p> <p>The new face is created from two edge point, new vertex, and face point.</p>	 <p>■ : original vertices x : edge points O : face point</p> <p>New vertex is calculated as:</p> $\frac{n-3}{n}V + \frac{1}{n}(\bar{F}) + \frac{2}{n}(\bar{M})$ <p>Where:</p> <p>N = number of adjoining polygons for the corresponding vertices V = vertex original position \bar{F} = average of face points of adjoining polygons \bar{M} = average of the midpoints of adjoining polygons.</p>
Loop	<p>Loop is only applicable for triangle polygon. For each triangle, 3 new vertices and 3 edge points are created. Edge point is constructed on each edge and defined by formula shown on the right. The new vertex is constructed for each original vertex and calculated by the formula shown on the right. When 3 new vertices and 3 edge points are connected (new vertex-edge-edge), four smaller triangles will be created within old triangle.</p>	 <p>x : edge points (E) ■ : original vertex point</p> $E = \frac{3}{8}(V_1 + V_2) + \frac{1}{8}(V_3 + V_4)$ $V = (1 - n\alpha) \times \text{original vertex} + \alpha \sum_{i=0}^n V_i$ $\alpha = \frac{1}{n} \left(\frac{5}{8} - \left(\frac{3}{8} - \frac{1}{4} \cos \frac{2\pi}{n} \right)^2 \right) \quad \text{if } n > 3$ $\alpha = 3/16 \quad \text{if } n \leq 3$ <p>Where n is the number of polygons that shares the corresponding vertex.</p>
Butterfly	<p>The smooth appearance is created through extensive mask application for the edge points. The edge point calculation depends on the characteristic of the end points of each edge. For edge with both endpoints is of valence 6, the first method is used. While for edge with one end point is not valence 6, the second method is used. For edge with both end points, the average value of the second method application for each end point is used. Detailed of the extensive mask is outlined in Sharp (2000).</p>	 <p>Edge point is the sum of all a, b, c and d where:</p> $a = \frac{1}{2} - w; b = \frac{1}{8} + 2w; c = -\frac{1}{16} - w; d = w$ <p>where w is the tension parameter, defining how tight the edge point is pulled towards the original vertices.</p> <p>Method 2:</p> $N = 3; v = \frac{3}{4}V; e_0 = \frac{5}{12}V_0; e_1 = \frac{1}{12}V_1; e_2 = -\frac{1}{12}V_2$ $N = 4; v = \frac{3}{4}V; e_0 = \frac{3}{8}V_0; e_2 = -\frac{1}{8}V_2; e_1, e_3 = 0$ $N \geq 5; v = \frac{3}{4}V; e_i = \frac{0.25 + \cos(\frac{2\pi i}{N}) + 0.5 \cos(\frac{4\pi i}{N})}{N} V_i$ <p>where N is the number of adjoining polygons.</p>

2.3.3 Implicit

An implicit surface is formed by a set of solutions from a function, $f(x,y,z) = 0$. A technique that uses implicit surfaces is metaball. Metaballs are special spheres with additive density distributions which mean that when two or more metaballs are close to each other, the density function of each metaball is additive (see Figure 23). A threshold parameter defines the radius of the iso-density surface. An isolated metaball appears as a common sphere but in the presence of other metaballs, the density functions add and generate a smooth transition between them (Hearn and Baker, 1994). Despite its realistic appearance, this approach needs full user intervention to manipulate the locations and sizes of the metaballs. Metashapes are an extension of metaballs. The difference lies on the shape varieties of metashapes which are not limited to spheres.

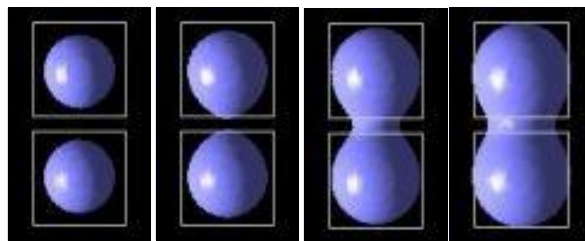


Figure 23. Interaction between metaballs (adapted from <http://www.studio-pon.com/en/products/digimeta/index.html>)

2.3.4 Parametric surfaces

Parametric surfaces are built from parametric curves. Popular parametric curves are Bezier, B-splines and Non-Uniform Rational B-splines (NURBS). For Bezier curves, a set of control points are needed. Figure 24a shows a cubic Bezier curve which is made from 4 control points (P_0 , P_1 , P_3 , and P_4). $P(t)$ is the final function of the curve in which $0 \leq t \leq 1$. A Bezier curve is a special case of B-splines curve i.e. the start and end point of the curve is coincident with the control points (Figure 24a).

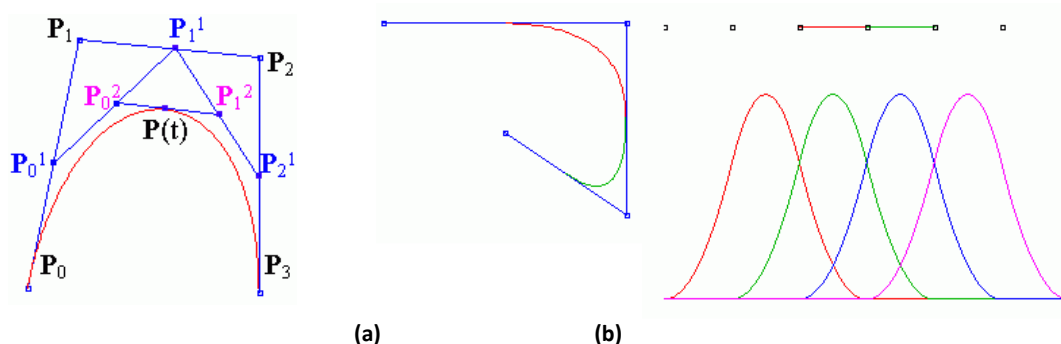


Figure 24. (a). A Bezier curve with its control points (b) B-splines curves created from 4 control points (left) and the basis functions used to create the curve (right). The polynomial degree is 2 and the knot vectors are equally spaced

In a B-splines curve, each control point is associated with a basis function (Figure 24b). The basis function is determined by the choice of the polynomial degree. Once the polynomial degree is determined, a set of points, known as the knot vectors is determined. The knot vectors determines

the span in which each of the basis function may exert its influence (Hearn and Baker, 1994). NURBS was essentially the generalisation of B-splines. In B-splines, each control point has the same weight, whereas in NURBS, different weights could be applied to each control point. This allows creation of curves that otherwise could not be created from B-splines or Bezier curves (Narayan et al., 2008).

The advantage of curved surface patches is their compact mathematical definition i.e. defining a surface without the need to store each of the interpolated points. For Bezier surfaces, this means that only control points need to be saved and additional knot vectors for B-splines curves. However, to create a complex shape, many patches are required and should be stitched (C0, C1 and C2 continuous) to avoid any cracks or gaps. Figure 25 shows C0, C1 and C2 continuity. C0 continuity means that two curves meet at the junction point while C1 continuity refers to a shared tangency between the two curves. C2 continuity means that the two curves have identical curvature at the junction point. Thus, a patch cannot be set up without regard to its neighbours. Because the surface can be expressed analytically, volume and surface area can be obtained. NURBS is considered to be the best solution because it possesses all advantages of Bezier and B-splines surfaces, while possessing additional advantages. One of the advantages is its ability to represent shapes easily which otherwise need B-splines surfaces with higher polynomial degree (Hearn and Baker, 1994). A further feature of parametric surfaces is the easy conversion into a polygon surface, but the same cannot be said of converting polygons into parametric surfaces. Some of the 3D body scanning technologies create parametric surfaces before it is finally converted into a higher number of polygon surfaces.

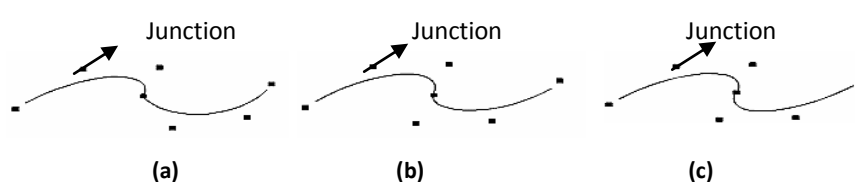


Figure 25. (a) C0 continuity, there is sharp point between two curves (b) C1 continuity. (c) C2 continuity

2.4 Joints movements in DHM

Joint movement in DHM is closely related with kinematics which deals with position, velocities, acceleration and disregards the underlying forces. Two types of kinematics which are mainly employed in DHM are forward kinematics and inverse kinematics. Forward and inverse kinematics are required to posture a DHM in an ergonomics application. Forward kinematics refers to the process of computing world space joint matrices based on specified Degree of Freedom (DOF) values whereas inverse kinematics refers to the opposite problem of computing a set of DOF values that position a joint at a desired world space goal (Hearn and Baker, 1994). The term “DOF values” refer to the amount of rotation or translation for each DOF of the corresponding joint while the term “DOF” refer to the motion ability of the corresponding joint.

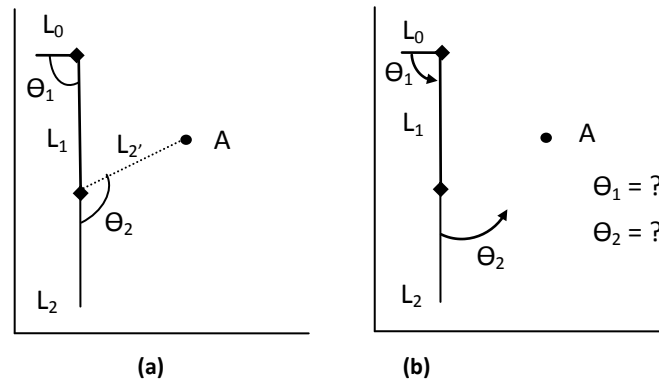


Figure 26. Forward and inverse kinematics illustrations

Figure 26 depicts both cases in a 2D world. Figure 26a shows the initial position of three segments L_0 , L_1 , and L_2 in which L_1 and L_2 has 1 DOF while L_0 is fixed. For the known θ_1 and θ_2 , which is the case for the forward kinematics, the end position of L_2 (L_2') can be calculated i.e. A. The case is more complex for the inverse kinematics, shown in Figure 26b. The end location (A) is known, but the required rotation to transform the segments L_1 and L_2 , so that L_2 touches A, are unknown. To determine the segments' position, the space for the segments rotation must be explored and the configuration in which the tip of L_2 segment is closest to A will be defined as the end configuration for the segments (Hearn and Baker, 1994).

```

HumanoidRoot : sacrum
sacroiliac : pelvis
|   l_hip : l_thigh
|   l_knee : l_calf
|   l_ankle : l_hindfoot
|   l_subtalar : l_midproximal
|   l_midtarsal : l_middistal
|   l_metatarsal : l_forefoot
|   r_hip : r_thigh
|   r_knee : r_calf
|   r_ankle : r_hindfoot
|   r_subtalar : r_midproximal
|   r_midtarsal : r_middistal
|   r_metatarsal : r_forefoot
v15 : 15

r_sternoclavicular : r_clavicle
r_acromioclavicular : r_scapula
r_shoulder : r_upperarm
r_elbow : r_forearm
r_wrist : r_hand
r_thumb1 : r_thumb_metacarpal
r_thumb2 : r_thumb_proximal
r_thumb3 : r_thumb_distal
r_index0 : r_index_metacarpal
r_index1 : r_index_proximal
r_index2 : r_index_middle
r_index3 : r_index_distal
r_middle0 : r_middle_metacarpal
r_middle1 : r_middle_proximal
r_middle2 : r_middle_middle

```

Figure 27. Skeletal hierarchy for legs-feet and shoulder-arms-a part of hands (adapted from <http://h-anim.org>, 2009)

To allow the application of forward or inverse kinematics, human joints are modelled as a joint hierarchy. ISO/IEC FCD 19774 – Humanoid animation (H-Anim), an international standard which specifies the structure and manipulation of a H-Anim figure i.e. articulated 3D representation that depicts animated characters, covers the issue in depth. A key feature from ISO/IEC FCD 19774 is the skeletal hierarchy which determines the relationship of different bones and body segments. Figure 27 shows the skeletal hierarchy for legs-feet and shoulder-arms-hands. Indentation of the skeletal hierarchy is to show that the indented joint or body segment is dependent on the previous joint or body segment. One joint is selected as the root and other joints are connected to it in a hierarchical manner. Any transformation that occurs on the root will affect all joints. There are parent and child relationships between indented joints directly above another in the skeletal hierarchy. Any

transformation to a parent will affect the child and its descendants. Translation and rotation are applied to the root while only rotation motion capability is allowed for any other joint. The rotation capability depends on the DOF of the corresponding joint. For example, the shoulder (glenohumeral) joint has 3 DOF (adduction/abduction, flexion/extension and internal/external rotation). To determine the location and orientation of a joint, an input of DOF values specifying the position and orientation relative to its parent joint is required. There is also constraint value, maximum and minimum value, for DOF values specified for each joint (Hearn and Baker, 1994).

To realise the modelling of DHM's joint movements, there were two important aspects that had to be understood i.e. (1) how the joint orientation and movements for DHM modelling were represented; (2) how the orientation of a joint relative to its parent affect its movement. Each of them is discussed in the following subsections.

2.4.1 Representing the orientation and movement of a joint

There are five different techniques to represent the joint movements for DHM modelling. These are: rotation matrix, fixed axis, Euler angles, axis angle and quaternion. Each technique will be explained in the following.

2.4.1.1 Rotation matrix

The rotation matrix in 3D world consists of 9 elements (see Figure 28). Each of its rows is a unit length and orthogonal to each other. The rotation matrix representation is unique. This means that for a given rotation matrix, there will be no other matrix rotation which can represent it without

performing a subsequent number of rotations. Thus, for example, a rotation matrix of $\begin{bmatrix} \frac{1}{\sqrt{2}} & \frac{1}{\sqrt{2}} \\ -\frac{1}{\sqrt{2}} & \frac{1}{\sqrt{2}} \end{bmatrix}$ in a 2D world can only be interpreted as a 45° rotation about Z axis in the anticlockwise direction.

$$R = \begin{pmatrix} u_x & u_y & u_z \\ v_x & v_y & v_z \\ w_x & w_y & w_z \end{pmatrix}$$

Figure 28. Rotation matrix

When subsequent rotations are represented using rotation matrices, a drift will occur due to rounding errors. For instance, given two sequences of 45° and 60° rotation about Z axis in a 2D world, the matrix that represents the overall rotation would be $= \begin{bmatrix} 0.7071 & 0.7071 \\ -0.7071 & 0.7071 \end{bmatrix} \times \begin{bmatrix} 0.5 & 0.8660 \\ -0.8660 & 0.5 \end{bmatrix} = \begin{bmatrix} -0.2588 & 0.9659 \\ -0.9659 & -0.2588 \end{bmatrix}$. As a result of the rounding error, the matrix may scale or shear and a special algorithm to re-orthogonalise the matrix is imperative. A rotation matrix is scaled or sheared when any of its matrix's elements squared sum from the same row or column is not equal to 1. Following the example above, the matrix that represents the

overall rotation was clearly scaled or sheared as the sum of matrix elements at the same column or row is not equal to 1. i.e. $(-0.2588)^2 + (-0.9659)^2 = 0.9999$.

Furthermore, interpolating positions between a starting and end point, defined in terms of

rotation matrices, yields unexpected results. Suppose the starting point is defined as $\begin{bmatrix} \frac{1}{\sqrt{2}} & \frac{1}{\sqrt{2}} \\ -\frac{1}{\sqrt{2}} & \frac{1}{\sqrt{2}} \end{bmatrix}$

and the end point is defined as $\begin{bmatrix} 0 & 1 \\ -1 & 0 \end{bmatrix}$ in a 2D world. A rotation matrix, such as $\begin{bmatrix} \frac{1}{3} & \frac{2\sqrt{2}}{3} \\ -\frac{2\sqrt{2}}{3} & \frac{1}{3} \end{bmatrix}$, is one of a number of possible positions between the starting point and end point rotation matrix. Listing some possible interpolation matrices, the result is depicted in Figure 29. From the figure, it is apparent that the result does not follow the expectation i.e. only half of the trajectory between the end point and starting point is able to be interpolated. Therefore, rotation matrices are unsuitable to be used in conditions in which position interpolation may take place (Scheider and Eberly, 2003).

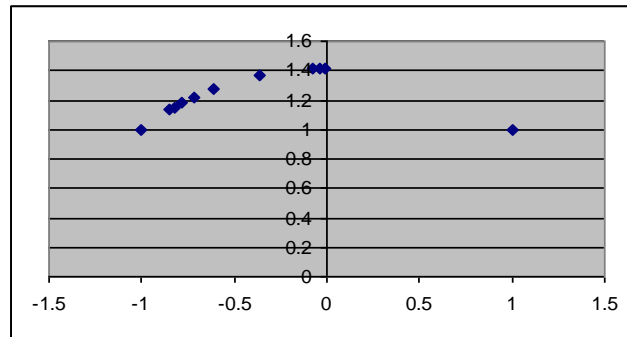


Figure 29. Results of interpolation from some possible rotation matrix interpolation between the starting point (the most left point) and the end point (the most right point)

2.4.1.2 Fixed axis

Fixed axis is an ordered triple of rotations $(\theta_x, \theta_y, \theta_z)$ about global axes. Attention must be paid to the order of rotation as similar angles but in a different order will result in a different end rotation. Interpolation is easily performed using fixed axis representation. However, contrary to the rotation matrix, a fixed axis representation is not uniquely defined. This means that an end position might be achieved by more than one set of rotations. For example, as shown in Figure 30, using the order of YXZ, both set of rotations of $(-45^\circ, 45^\circ, 90^\circ)$ and $(-45^\circ, 0, 45^\circ)$ will bring point $[1 \ 0 \ 0]$ to $[1, 1, 1]$.

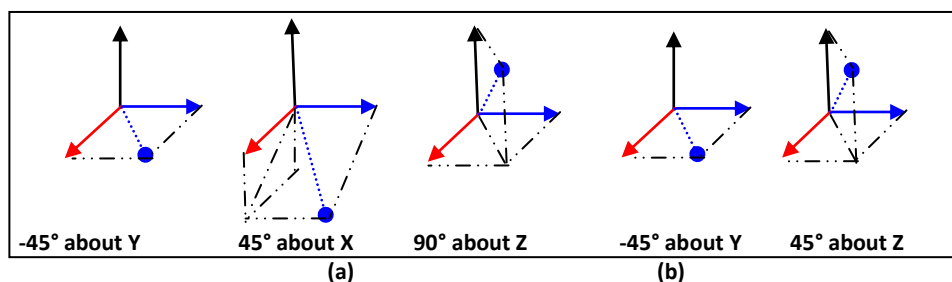


Figure 30. (a) Fixed angle rotation, YXZ order of $(-45^\circ, 45^\circ, 90^\circ)$. (b) angle rotation, YXZ order of $(-45^\circ, 0, 45^\circ)$

Because the rotations are carried out one at a time for each axis, a 'gimbal lock' effect may take place (see Figure 31). This takes place when the second rotation is 90° which causes the first and third axis of rotation to lie on the same direction and results in a loss of one DOF. One way to avoid this effect is to ensure that the second rotation is not equal to 90° (Hearn and Baker, 1994).

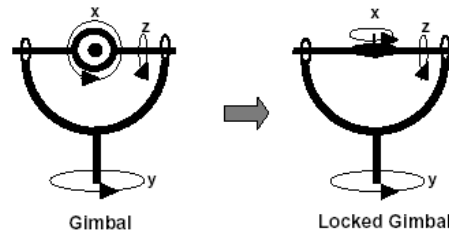


Figure 31. Gimbal lock effect

2.4.1.3 Euler angles

Euler angles are an ordered triple of rotations about local axes. The only difference between Euler angle and fixed angle is the axes to which the rotation is centred. In fact, Euler angle ordering is equivalent to reverse ordering in fixed angles and thus has the same problem as fixed angle. Another difference is the convention order for the rotation. For fixed axis rotations, since the rotation is based on the fixed angle, each axis should be present in the rotation order. Thus, the possible order is limited into 6 varieties i.e XYZ, XZY, YXZ, YZX, ZXY and ZYX. In contrast to the fixed axis rotation, the convention order for Euler angle is set according to the following rules: 1. the first axis can be of any axis, 2. the second axis can be of any axis except the first axis, 3. the third axis can be of any axis except the axis in number 2. Thus, a rotation order of ZXZ or ZYZ might be the choice, as well. As long as one convention/rotation order is constantly used throughout the process, there is no need to store the information about the convention in usage more than once (Hearn and Baker, 1994). Similar to the fixed angle, the order of rotation is of importance. In spite of its gimbal lock effect, Euler angles are commonly used as DOF input values for rotation.

2.4.1.4 Axis angle

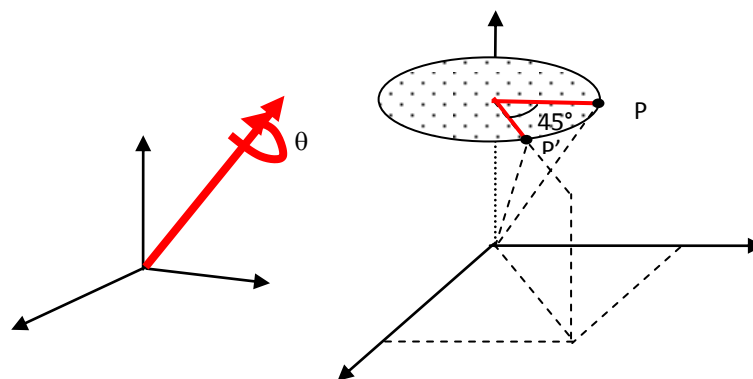


Figure 32. Axis angle representation

The left image in Figure 32 shows the components of axis angle i.e. an axis of rotation (a unit vector) and a rotation about it (θ). Interpolation may be employed on the axis of rotation and the rotation angle. For example, a rotation of P located at (1, 1, 0) about a vector $\vec{V} [0\ 1\ 0]$ with an angle of 45° will result in $P' \left(\frac{1}{\sqrt{2}}, 1, \frac{1}{\sqrt{2}} \right)$. The process is shown in the right image in Figure 32. This approach is free from gimbal lock but difficulties will be encountered in concatenating many axis rotations for the desired-axis-angle rotation (Hearn and Baker, 1994).

2.4.1.5 Quaternion

Quaternion employs axis angle principles (rotation axis and angle of rotation). It can be considered as adding an additional rotation angle to spherical coordinates (longitude, latitude and rotation angles) and brings in a smooth interpolation (Hearn and Baker, 1994). However, the notation is different since quaternions use complex number representation. The relation between axis angle and quaternion representation is in the following:

$$q = \cos(a/2) + i (x * \sin(a/2)) + j (y * \sin(a/2)) + k (z * \sin(a/2))$$

where:

a=angle of rotation.

x,y,z = vector representing axis of rotation.

In spite of its advantage being free from the gimbal lock effect, quaternion calculation is complex and the concept itself is difficult to grasp. Fortunately, the conversion of quaternion to and from Euler angle is feasible. However, it is much easier to convert Euler angle to quaternion than the other way around.

2.4.2 Effect of the relative orientation of a joint to its parent upon its movement

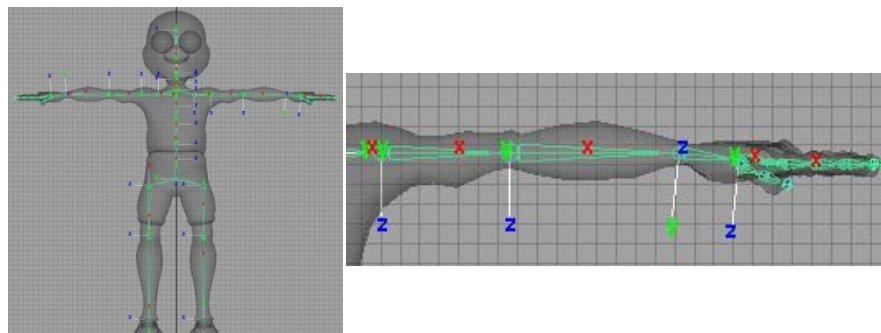


Figure 33. Illustration of the zero reference position and joints orientation (adapted from Centre for Digital Arts and Experimental Media - University of Washington, 2009)

In addition to a skeletal hierarchy, in order to animate a DHM, orientation for each joint is also required. The orientation of the joint provides a sense of direction to the corresponding bone. The

joint orientation is commonly established in a so called “zero reference position”. Figure 33 shows illustrations of joint orientation at zero reference position from a self created DHM and also a closer look of the arm joint orientation. Any joint movement will always be as based on the joint orientation of the zero reference position. For example, if we intend to flex the lower arm for a series of postures e.g. 135°, 90°, 60°, 120° etc.; for each posture, the flexion of the lower arm is always performed by rotating the lower arm from the zero reference position i.e. from a fully extended to 135°, from a fully extended to 90°, etc. The joint orientation shown in Figure 33 is based on a world coordinate system. A world coordinate system is the coordinate system which is used as the main reference to define locations of all objects for that particular 3D virtual setting.

Performing a joint movement requires 3D rotations in a world coordinate system and is complex as each bone has to be rotated on its own coordinate system with its own origin and axes. To illustrate the process, Figure 34 is used as an example. Using a rotation matrix to represent the joint movement, both bone 1 and bone 2 orientations are $\begin{pmatrix} \frac{\sqrt{2}}{2} & \frac{-\sqrt{2}}{2} \\ \frac{\sqrt{2}}{2} & \frac{\sqrt{2}}{2} \end{pmatrix}$ with an origin of (4,4) and (8,8), respectively.

If bone 1 undergoes a 30° anticlockwise rotation, its rotation cannot be performed at its current orientation and location. First, it has to be translated to (0,0,0) of the world coordinate system. Then, it has to be rotated so that both of its axes coincide with the world coordinate system axes, for this particular example the rotation is 45° anticlockwise, before the 30° anticlockwise rotation is performed. Next, the bone 1 has to be rotated 45° clockwise before it is translated to (4,4). All of the rotations could be expressed in a single 2x2 matrix by multiplying rotation matrices at each stage as shown in the following:

$$\text{bone}_1 * \begin{pmatrix} \frac{1}{\sqrt{2}} & \frac{1}{\sqrt{2}} \\ -\frac{1}{\sqrt{2}} & \frac{1}{\sqrt{2}} \end{pmatrix} \cdot \begin{pmatrix} \frac{\sqrt{3}}{2} & \frac{1}{2} \\ -\frac{1}{2} & \frac{\sqrt{3}}{2} \end{pmatrix} \cdot \begin{pmatrix} \frac{\sqrt{2}}{2} & \frac{-\sqrt{2}}{2} \\ \frac{\sqrt{2}}{2} & \frac{\sqrt{2}}{2} \end{pmatrix} = \text{bone}_1 * \begin{pmatrix} \frac{\sqrt{3}}{2} & \frac{1}{2} \\ -\frac{1}{2} & \frac{\sqrt{3}}{2} \end{pmatrix}$$

Since bone 2 is dependent on the bone 1, without performing the stages shown in Figure 35, the final matrix above could be used directly to rotate the bone 2.

$$\text{bone}_2 * \begin{pmatrix} \frac{1}{\sqrt{2}} & \frac{1}{\sqrt{2}} \\ -\frac{1}{\sqrt{2}} & \frac{1}{\sqrt{2}} \end{pmatrix} \cdot \begin{pmatrix} \frac{\sqrt{3}}{2} & \frac{1}{2} \\ -\frac{1}{2} & \frac{\sqrt{3}}{2} \end{pmatrix} \cdot \begin{pmatrix} \frac{\sqrt{2}}{2} & \frac{-\sqrt{2}}{2} \\ \frac{\sqrt{2}}{2} & \frac{\sqrt{2}}{2} \end{pmatrix} = \text{bone}_2 * \begin{pmatrix} \frac{\sqrt{3}}{2} & \frac{1}{2} \\ -\frac{1}{2} & \frac{\sqrt{3}}{2} \end{pmatrix}$$

However, if bone 2 rotates 30° anticlockwise while bone 1 remains at its position, the final matrix to rotate bone 2 will have to be defined by undergoing a similar sequence of processes shown in Figure 35. It is mentioned earlier that any joint movement will always be as based on the joint

orientation of the zero reference position. The reason for this is because it will avoid the need to perform step 2 and 4 every time the bone of the corresponding joint is rotated and shorten the process.

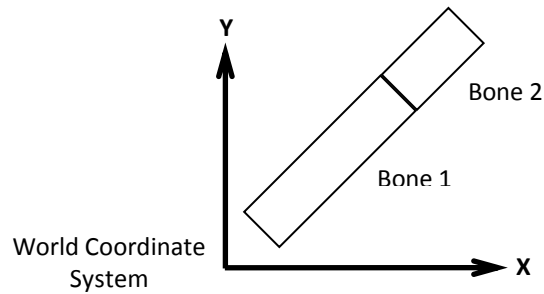


Figure 34. Case example to illustrate joint movement

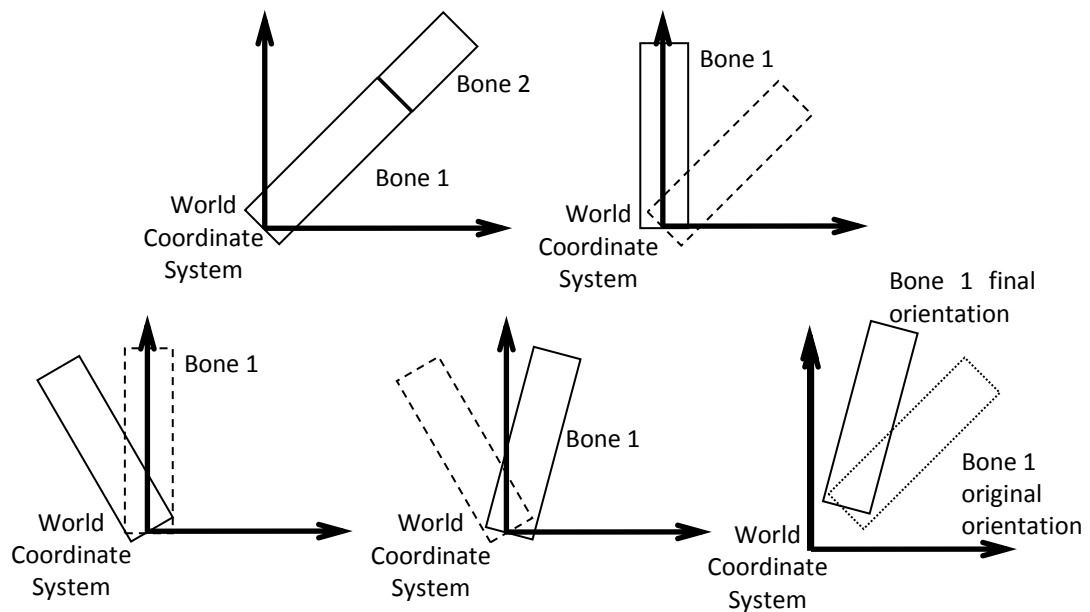


Figure 35. Steps in performing 30° rotations for bone 1: i) translate the bone to (0,0,0), ii) align the bone coordinate system with the world coordinate system by rotating it 45° anticlockwise, iii) perform the 30°, iv) return the bone coordinate system by rotating it 45° clockwise, and v) translate the bone to its original location

2.5 3D body scanning

This section elucidates types and mechanisms related to so called “body scanning” as well as current usage of 3D body scanners. There are two types of body scanner technologies. The first one is laser scanning which consists of the laser source, the optical system and the light sensor. Laser light sources project one or more thin stripes on the human body through its optical system. The laser intensity is low (eye-safe) to ensure its safety. The number of laser scanners and their movement across the object depend on the digitisation type. For a body scanner, more than one laser scanner, often located in pillars, are synchronously moved vertically to project the laser light across the body. Instead of vertical movement, a rotation of a single laser scanner is applied for a head scanner. Thus, a precise electric motor which governs the laser source/sensor is a necessity. In addition to this, the laser scanner needs more scanning time for a larger surface/object and is more

prone to movement artefacts (D'Appuzo, 2006). Movement artefacts occur when the body is moved due to breathing or body swaying and results in distorted body images.

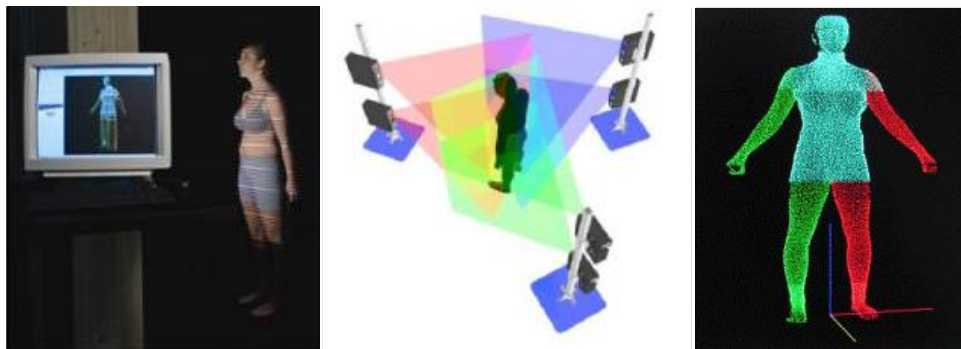


Figure 36. The left figure is projected light scanner (adapted from [TC]² 3D Body Scanner, TC), mid figure is projected light scanner with 6 light sources/sensors (adapted from Capturor, Inspeck) and the right figure is body points cloud (adapted from [TC]² 3D Body Scanner, 2010)

The second technology is the projection of light patterns. Instead of moving the light sources, stripes of light are projected on the object while a light sensor (digital camera) acquires the image. For a whole body image, from 6 up to 12 (4 angles and 3 different heights) light sources/sensors are required (Figure 36). Images of structured light patterns projected onto the front and the back of the object are acquired and, based on comparison of the distorted light patterns on the object and reference plane, the object shape is acquired. The light pattern is projected for each height level in turn and results in the prolongation of scanning time. Nevertheless, the scanning time of light patterns scanner is shorter in comparison to a laser body scanner. Another advantage of the projected light scanner is its lower cost due to less complexity and no concern about the health effect is raised, as only white light is involved. A shared disadvantage between the laser scanner and the light patterned projection is their inability to extract any data when the object surface is too bright/dark. This, in the end, may cause 'holes' in the surface of the scan. Body scanners produces range data i.e., discrete points set in 3D space which are sampled from any object in the real world (Istook and Hwang, 2001). These discrete points are called 'point clouds' (Figure 36). Originally, the output of the scanner is a point cloud consisting of many thousands of points, representing points on the object's surface. To form surfaces, these point clouds are processed further. The most common surface for the final outcome of the scanner is a polygon surface.

The development of body scanner technology has allowed accurate measurement as well visualisation of a person's body shape and type. According to Lerch et al. (2007), usage of body scanners can be categorised into four main areas: i) apparel, 2) ergonomics, 3) biomedical applications and 4) reverse engineering. They also specify possible applications for each main area, as shown in Figure 37. For ergonomics, they identified two possible applications of body scanning i.e. i) validation of product or work environment model and ii) body scan data in a sitting position to design seat in furniture, automotive and aircraft industries.

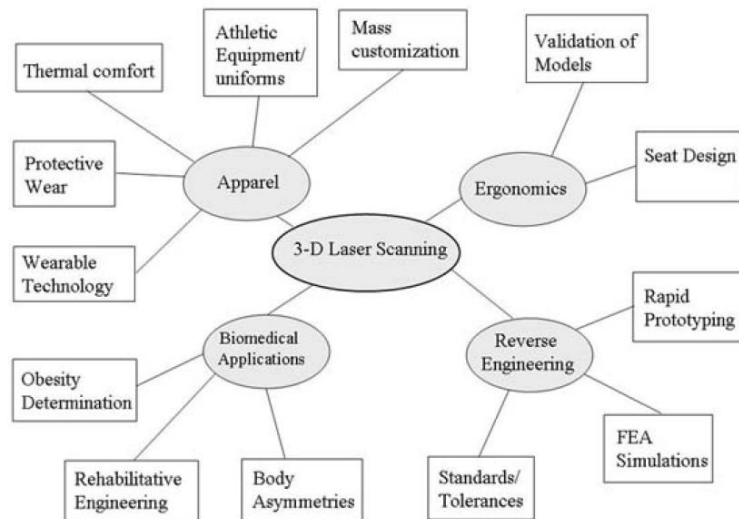


Figure 37. Main application areas for body scanning technology (adapted from Lerch et al. (2007))

An example of body scanning utilisation to accommodate seat design is a recent study by Reed and Parkinson (2008). They created a variability of torso shape in a sitting position through body scanning utilisation. They acquired torso shapes with various sizes and shapes and performed statistical analysis which allows them to create: 1) a new torso with various shape and size of torso based on certain characteristics e.g. Body Mass Index (BMI), sitting height, etc., and 2) modification on existing 3D data of torso. A similar study was also performed earlier by Allen et al. (2003) which enabled them to: 1) modify existing whole body data with regards to certain characteristics such as weight and height, and 2) create a whole body model by specifying height and weight. Figure 38 shows images from their study result

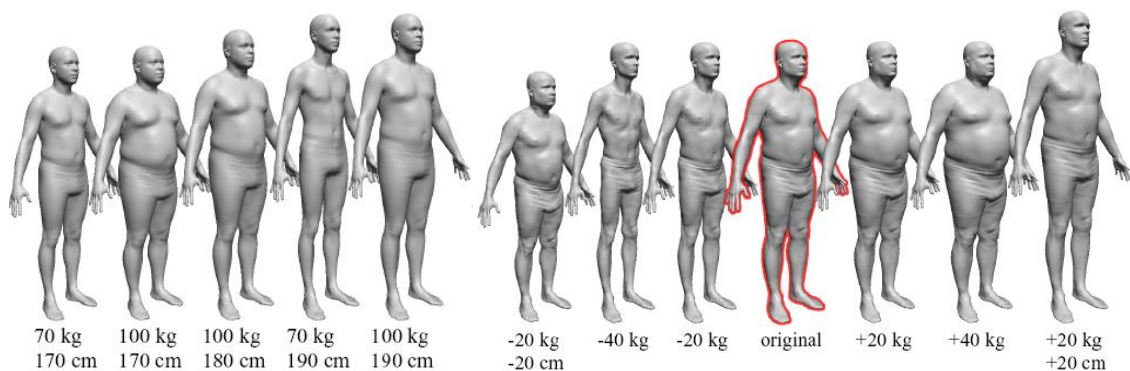


Figure 38. Left image shows new individuals created based on height and weight specification whereas the right image shows the modification of original whole body data by changing the weight and height (adapted from Allen et al. (2003))

2.6 Summary

The literature review was performed to fulfil the first objective of this research i.e. to review the state of the art of DHM in ergonomics modelling and body deformation. This objective was achieved by performing a literature review that was focused on DHM in ergonomics applications and existing

approaches to flesh deformation. Below is a summary of the findings, detailed discussion of the literature review findings is given in section 11.1.

From the review on DHM in ergonomics, several roles for DHM in ergonomics applications were identified. These were: (i) to evaluate the accommodation of a product or workplace; (ii) to assist in designing products which accommodate a large variety of people size and shape; and (iii) to function as a visualisation tool. In order to fulfil the above roles, the literature review suggested that accuracy, accommodation of different body types and sizes and realistic appearance of a DHM were important attributes of DHM in ergonomics modelling. From the study of existing DHMs in ergonomics applications; real time, limited or minimum user intervention and whole body modelling were also identified as common attributes of DHM in ergonomics modelling. These attributes could potentially become specifications of DHM to guide the development of flesh deformation modelling in ergonomics applications. These specifications essentially distinguish a DHM in ergonomics modelling from other types of DHM e.g. DHM for entertainment purposes,

The literature review revealed flesh deformation modelling as one of DHM characteristics and its important part in supporting the role of DHM as a visualisation tool. The literature review also identified five main categories of existing approaches to flesh deformation. These were anatomic, physical, geometric, example-based and sweep-based approaches. Some of these approaches were already adopted by existing DHM in ergonomics applications. However, further literature review on existing DHMs in ergonomics modelling demonstrated that existing DHMs in ergonomics applications still lacked realism. Despite the lack of realism, the literature review showed that current and future research in ergonomics applications were mostly focused on DHM's characteristics other than flesh deformation modelling. A combination of the above factors suggested that there was a research need to develop realistic flesh deformation modelling of DHM in ergonomics modelling. In addition to the two main findings above, the literature review revealed that characteristics of DHM in ergonomics modelling were driven by the DHM's roles in ergonomics modelling, as shown in section 2.1.2.

In addition to the review of the DHM in ergonomics applications and existing approaches of flesh deformation, a review on the basic theory on surface creation, DHM's joint movement and 3D body scan technology were also performed. From the literature review on these additional topics the following were explored: (1) four types of approaches to represent surfaces i.e. polygonal, subdivision, implicit and parametric surface; (2) four different techniques to represent joint movement i.e. rotation matrix, fixed axis, Euler angles, axis angles and quaternion; (3) how the relative orientation of a joint to its parent affected its movement; and (4) a brief review of 3D body scanning technology and how they have been used to study human body form. The first three of the

literature review's additional topics provided technical background that would likely be required for the actual development of the methodology to simulate body deformation due to joint movements.

As the first objective was achieved, this research would proceed to fulfil the second and third research objectives i.e. developing a set of specifications for DHM for ergonomics modelling and proposing a method to create flesh deformation at the elbow joint for ergonomics modelling, respectively. Findings from the literature review were followed by performing a user study which is described in the next chapter. The user study would complement the literature review's result and lead to the fulfilment of the second objective i.e. establishment of DHM specifications. The established DHM specifications would eventually be utilised to guide the fulfilment of the third objective i.e. development of the proposed FDM.

3 User Study

In chapter 2, a literature review was undertaken to satisfy the first objective of the research. The review provides knowledge about the state of the art in the use of DHM in ergonomics and body deformation. However it was also deemed necessary for this research to elicit the views of the end users of DHM for ergonomics simulation. This was performed through a user study. This chapter provides the background, methodology and results of the user study. The results of the user study together with the findings from the literature review will be the main driver in establishing a series of DHM specifications to address the second objective of this research.

The user study is driven predominantly from the findings of the literature review. The literature review suggests that flesh deformation modelling for DHM is one area of research that requires further investigation. This suggestion was based on the finding in section 2.1.2, which shows that a realistic outer surface simulation of the human skin surface is an important characteristic of DHM in ergonomics simulation. However, the literature review could not provide a link between the suggested need for this development and actual user needs for flesh deformation modelling e.g. is realistic flesh deformation modelling really a necessary DHM characteristic?; or do users expect to have realistic flesh deformation for ergonomics modelling in the future? Also, there is a lack of information on the scope of realistic surface simulation in the ergonomics field from a user's perspective e.g. What level of detail is required to be considered realistic?; or does flesh deformation at the joint affect DHM's realism? These two issues would be followed up through the user study and are established as the first two objectives of the user study.

The literature review also identified potential specifications for DHM in ergonomics modelling such as accuracy, realism, real time, and so on. Some of these potential specifications for DHM in ergonomics modelling appear to contradict each other. For instance, high accuracy and realism in flesh deformation modelling would likely require complex computation which could potentially increase the processing time and thus impact upon the real time ability of the system. This means that a trade-off between these contradicting potential DHM's specifications would likely be necessary. The users' views regarding any possible trade off would be investigated through the user study and is established as the third objective of the user study.

In addition to the flesh deformation modelling at the joints, flesh deformation could also be caused by an interaction between human skin and external objects/forces. Although flesh deformation modelling due to external objects/forces is not the focus of this research, knowledge of users' views on this area could provide an insight for further development of flesh deformation

modelling. Users' views on characteristics that constitute a good ergonomics application would also be explored through the user study. These two issues would be explored and is established as the fourth objective of the user study. The followings summarise the four objectives of the user study:

1. Users' views on the need for a realistic outer surface simulation of the human skin surface.
2. Users' views on what constitutes DHM's realism.
3. Users' views on the possible trade off of potential DHM's specifications.
4. User's view on the importance of flesh deformation due to contact with external objects/loads and characteristics that define the overall quality of ergonomics applications.

3.1 Methodology for the user study

This research proposed the use of a questionnaire for the user study. According to Stanton et al. (2005), questionnaires are a common method in ergonomics to acquire users' opinions and attitudes in order to probe their perception for an existing system. A questionnaire was chosen because it enables a flexible way to collect large amounts of specific data from a large population sample (Brace, 2008). Taking a questionnaire approach also has the benefit of being able to efficiently target a very geographically distributed audience. As the user study is aimed to seek users' views on DHM in ergonomics applications, the user would be expected to have had experience in using ergonomics applications. This means that the location of users with this experience would likely be dispersed. Therefore a questionnaire survey would be suitable as it could be used to target the users with this particular experience despite their dispersed locations.

An alternative approach would have been to use a telephone interview which also offers the ability to gather data from respondents without geographical limitation. However, a questionnaire survey would be more advantageous than a phone interview because during a phone interview a respondent is imposed to commit a certain time and date whereas a questionnaire allows respondents to fill it in their own time. Also, a questionnaire is less susceptible to interviewer and interviewee bias as the contact between a researcher and a respondent could be limited, especially for a mailed questionnaire. However, a questionnaire is not without disadvantages. According to Stanton et al. (2005), a questionnaire would likely yield a low response rate i.e. approximately 10% for a mailed questionnaire. They also argued that a questionnaire is prone to social desirability bias i.e. bias which is caused by the fact that participant is simply giving what the analyst wants. Brace (2008) also stated that a mailed questionnaire does not allow clarification for any inconsistency of a user's response. This study took into account these limitations by taking measures as described further in subsections 3.1.1 and 3.1.2.

The questionnaire for this research is loosely based on the recommended steps of questionnaire construction by Stanton et al. (2005) which includes: (1) defining study objectives; (2)

defining the population; (3) constructing the questionnaire; (4) piloting the questionnaire, (5) administering the questionnaire; (6) data analysis; and (7) follow up phase. The study objectives, which are aimed to identify what information is wanted from the questionnaire data that is gathered, were already described in the previous section. The definition of the population and how the questionnaire is administered will be outlined in section 3.1.1. The construction of the questionnaire as well as piloting of the questionnaire is described in section 3.1.2. Data analysis and results of the questionnaire are explained in section 3.2.

3.1.1 Sampling groups

Users of ergonomics CAD are becoming more diverse (Ruiter, 2000). However, the ergonomics CAD applications themselves set high demands on the users, such as knowledge in CAD and ergonomics, to avoid misinterpretation (Laitila, 2005). Taking these factors into consideration, two types of target population were then determined: firstly, experienced users with sound ergonomics knowledge and secondly, novel users with limited ergonomics knowledge. To represent the first population, registered ergonomics consultants, obtained from the Ergonomics Society webpage (2007), and an additional number of ergonomists known through personal contacts, were chosen. The Ergonomics Society webpage provided brief information regarding the types of ergonomics analysis which were performed for each registered consultant. However, some of the information is quite general and hence it was difficult to determine whether the corresponding consultant actually made use of ergonomics CAD or not. Therefore, it was decided to include the entire registered ergonomics consultant listing from the Ergonomics Society webpage into the sample group of the first population. The second group was represented by Industrial Design and Technology students at Loughborough University. The sample was selected due to the easy access as well as the sample's suitability in respect with the required criteria for the second target population. All Industrial Design and Technology students are taught core Ergonomics skills and are exposed to DHM use. However, since Loughborough University only had access to one DHM system, SAMMIE, it was recognised that the scope of the respondents' responses may be limited. For the first sample group, the questionnaire was distributed either by mail or electronic mail whereas for the second sample group, the questionnaire was distributed personally. To increase the return rate of the mailed questionnaire, a paid self-addressed envelope was enclosed in the mailed questionnaire. To increase the return rate of the second sample group i.e. Industrial Design and Technology students, the questionnaire was given to the lecturer of the class to distribute it to the students and to help raise its profile.

3.1.2 Questionnaire

The final questionnaire was divided into 6 sections. Prior to finalising the questionnaire, a pilot study was performed. The pilot study involved seeking advice from a more experienced questionnaire designer as well as administering the draft questionnaire to a potential user. Based on the input from the pilot study, the questionnaire was then modified and a final version was produced. The final version of the questionnaire included a combination of closed and open questions. Open questions were used to encourage respondents to explain their view and allow clarification of response. It was hoped that these measures would minimise the limitation of questionnaire surveys which was described by Brace (2008) i.e. it does not allow for clarification for any inconsistency in a user's response. The introduction of the questionnaire was also phrased such that the specific aim of the user study was not revealed. It was hoped that this would minimise the effect of social desirability bias as described by Stanton et al. (2005). The following shows the introduction of the questionnaire:

“The use of digital human modelling is a key component of ergonomics modelling. Several case studies reported the successful use of various digital human models to improve the physical ergonomics of different designs. Currently, the existing digital humans in various ergonomics applications are varied in terms of their realism, accuracy etc. This questionnaire is part of a PhD study which aims to investigate the usage of digital human models in ergonomics CAD software.”

The first section of the questionnaire is presented to gather the respondent's demographic data and experience in using ergonomics application. This was then followed by assessing the importance of a total of thirteen characteristics of DHM in the second section of the questionnaire. Some of the characteristics were adopted from Chaffin's (2005) findings. The respondents were also asked whether they have used or would like to have used the function related to the corresponding characteristic. This question was presented so that even if a certain characteristic is still not yet available from current ergonomics applications, users' desire for the characteristic could still be captured. This question aimed to explore users' views on how important flesh deformation modelling is in comparison to other characteristics. Table 2 shows the thirteen/attributes and their given definition in the questionnaire. An example of the given question to rate the importance is shown below. A complete version of the questionnaire is provided in appendix A (supplied in the accompanying CD).

Criteria	Description	Relevancy to previous experiences	
Natural and realistic looking postures/motion	How important is the visual accuracy of the postures and motions that the DHM adopts (e.g. reach).	<input type="checkbox"/> Essential <input type="checkbox"/> Important <input type="checkbox"/> Desirable <input type="checkbox"/> Unimportant	Have you used or would like to have used this function in any of your ergonomics analysis? <input type="checkbox"/> Used <input type="checkbox"/> Like to have used <input type="checkbox"/> Neither

Table 2. Thirteen characteristics which were presented in the questionnaire

Characteristic	Definition
Natural and realistic looking postures/motion	How important is the visual accuracy of the postures and motions that the DHM adopts (e.g. reach).
Realistic appearance	How important is a visually realistic flesh form for the DHM.
Level of details of realistic appearance	How important are realistic body details for the DHM (e.g. head, hands, feet, legs/arm, and torso).
Realistic and accurate joint flesh deformation	How important is visually realistic flesh deformation at the joint when the DHM posture changes.
DHM's flesh interaction with external forces	How important is the ability of the DHM's flesh to react to external loads e.g. flesh deformation of the buttocks/thigh in a sitting posture.
Shape flexibility	How important is the provision of data to be able to transform the DHM to represent any possible human body shape.
Size flexibility	How important is the provision of data to be able to transform the DHM to represent any possible human size.
Reach and fit analysis	How important is the ability to simulate whether a DHM fits i.e. adequate clearance, in a virtual environment set and is able to reach any specified object.
Postural/biomechanical analysis	How important is postural/biomechanical analysis to assess whether a particular design may result in injury related to musculoskeletal disorders.
Hand grip and strength	How important is the analysis on the fitness of hand tools in terms of comfort, efficiency and required strength of use.
Visual sight line	How important is the ability to show the DHM's field of vision.
Field of view on a mirror	How important is the ability to show the DHM's field of vision on a mirror.
Adding variety of clothing, helmets, etc.	How important is the ability to add clothing and accessories to assess their fitness and effects on motion restriction.

The third section of the questionnaire is aimed to explore users' views on the DHMs realism as well as contradicting DHM's specifications. In order to assess factors that affect DHM's realism, questions regarding the necessary level of detail (LOD) of DHM and unrealistic flesh deformation at the joint were given through the assistance of graphical illustrations of DHM. Closed and open questions were asked to find out respondents' willingness to compromise between accuracy and processing speed. Examples of the question for this section are shown below.



Unrealistic joint flesh deformation affects the overall level of DHM's realism.
☐ Strongly agree ☐ Agree ☐ Neutral ☐ Disagree ☐ Strongly Disagree

The more accurate and realistic a digital human model (whole body), the more likely it will take time to render/manipulate it. For ergonomics modelling applications, do you think that a waiting time would be inconvenient for you in the situation in which a real time interaction is required (e.g. manipulating the posture)?

☐ YES ☐ NO ☐ POSSIBLY

Please explain.

The fourth section questioned the respondents on their view towards the prospect of realistic DHM in the future and its role in ergonomics CAD. Two possible roles of realistic DHM i.e. aesthetics for presentation and visualisations, and accuracy for evaluations were also explored. The section ended with a final question concerning whether the respondents would favour ergonomics CAD applications with realistic DHM disregarding other issues. Examples of question from this section are shown below.

Do you think that more realistic looking DHMs will be part of the future trends of DHM's characteristics in ergonomics CAD software?

☐ YES ☐ NO ☐ POSSIBLY

Please explain.

Do you think that a realistic looking DHM would improve the accuracy of ergonomics analyses, e.g. reach and fit analysis?

☐ YES ☐ NO ☐ POSSIBLY

Please explain.

The fifth section investigated the value that users placed on the modelling of flesh deformation due to contact with external objects in the future and its role in improving ergonomic analysis accuracy. The last two questions focused on the scale of the flesh deformation due to contact with external objects application. Examples of the question are shown below.

Do you think that flesh deformation due to contact with external objects e.g. flesh deformation on the buttocks in a sitting posture, will be part of the future trends of DHM's characteristics in ergonomics CAD software?

☐ YES ☐ NO ☐ POSSIBLY

Please explain.

Is it important that the flesh deformation, due to contact with external objects, should be implemented for the whole body?

☐ YES ☐ NO

If your answer is YES, please explain.

If your answer is NO, which parts of the body are most important?

The questionnaire was finalised with a single open question about characteristics which defined the overall quality of ergonomics CAD software. This question was specially directed to respondents who used more than one ergonomics CAD application and hence were able to compare different packages of ergonomics CAD application.

3.2 User study result

This section will provide results of the user study. Questionnaires response rate and respondents background are provided, followed by the questionnaire results.

3.2.1 Response rate

Out of 60 distributed questionnaires, 15 responses were acquired for the first sample group (Group 1) i.e. ergonomists with experience in using ergonomics CAD application. In addition to this, another 5 responses were obtained from ergonomists with no experience in using ergonomics CAD application. The low return rate and 5 additional unexpected responses were owing to the lack of information concerning ergonomics CAD usage of the registered ergonomics consultancies from the Ergonomics Society webpage. In order to maximise data usage, the additional responses from ergonomists with no experience in using ergonomics CAD application would be analysed as a separate group (Group 2). For the novel users with limited ergonomic knowledge of ergonomics (Group 3), there were 7 responses out of 19 distributed questionnaires. The overall return rate of the questionnaire for this study (33% for expert users and 36% for novice users) and is still considerably higher than the 10% prediction by Stanton et al. (2005).

3.2.2 Respondents' backgrounds

The respondents' age for Group 1 ranged from 27-61 years old. Types of ergonomics CAD which were used by respondents are Jack, 3DMax, Poser, SAMMIE, ROBCAD/Man, eM-RAMSIS, 3DSSP and MannequinPro. The length of ergonomics CAD usage ranged from 2-3 weeks to 20 years. The respondents mainly used ergonomics CAD for reach and fit analysis, sight line analysis and

clearance/accessibility analysis. Other types of analysis were postural analysis, human strength analysis, and simulations of human motion. These findings were in line with Chaffin's (2001) findings. Additional types of ergonomics CAD usage were finger and hand studies and task analysis. It also appeared that ergonomics CAD were employed in various areas such as automotive, manufacturing, maintenance, education, etc.

The respondents' age for Group 2 ranged from 24 – 45 years old and 19-21 for Group 3. Group 3 used SAMMIE exclusively to perform reach and fit analysis, sight line analysis and postural analysis. Compared to the type of analysis of Group 1, group's 3 range of analysis was less varied, which was likely caused by the limited analysis demand within their course work. The duration of SAMMIE usage for group 3 respondents ranged from 10 hours to 10 months.

3.2.3 Questionnaires Result

The results are provided below in the order of the questions given in the questionnaire.

3.2.3.1 DHM characteristics importance level and their usage

In order to enable an importance level comparison among DHM characteristics, values were assigned towards the importance category i.e. essential = 3, important = 2, desirable = 1, unimportant = 0 for each characteristic. The level of importance for a particular characteristic was represented by the sum of these values (\sum importance) from all of the respondents. However, there were instances where respondents failed to rate the importance for one or more particular characteristics. To correct this discrepancy, a normalised response was used. A normalised response was the total values of the importance category (\sum importance) divided by the total number of respondents (\sum respondents) who responded for the corresponding characteristic. The responses for all groups are shown in Figure 39.

All groups agreed that (i) reach and fit analysis, (ii) visual sight line, (iii) size flexibility and (iv) shape flexibility were of importance. These findings were not surprising since these functionalities were required to perform basic ergonomics analysis. The importance of some functionality also seemed to depend on the level of expertise in ergonomics. For instance, in contrast with group 3, both group 1 and group 2, who had either expertise in ergonomics or professional ergonomics consultancy, perceived postural/biomechanical analysis as important. The same was also observable on natural and realistic looking postures/motion.

Despite concurring that natural and realistic looking postures/motion was important; all groups seemed to view that (i) realistic appearance, (ii) accurate/realistic joint flesh deformation, and (iii) level of details (LOD) of realistic appearance as less needed functionalities. A possible explanation for the contradictory finding was the dependency nature between the mentioned functionalities.

Realistic appearance, accurate/realistic joint flesh deformation and LOD of realistic appearance were all required to build a more realistic and accurate DHM which would make a natural and realistic looking postures/motion possible. However, once these functionalities were separated from their common goal, they lost their importance.

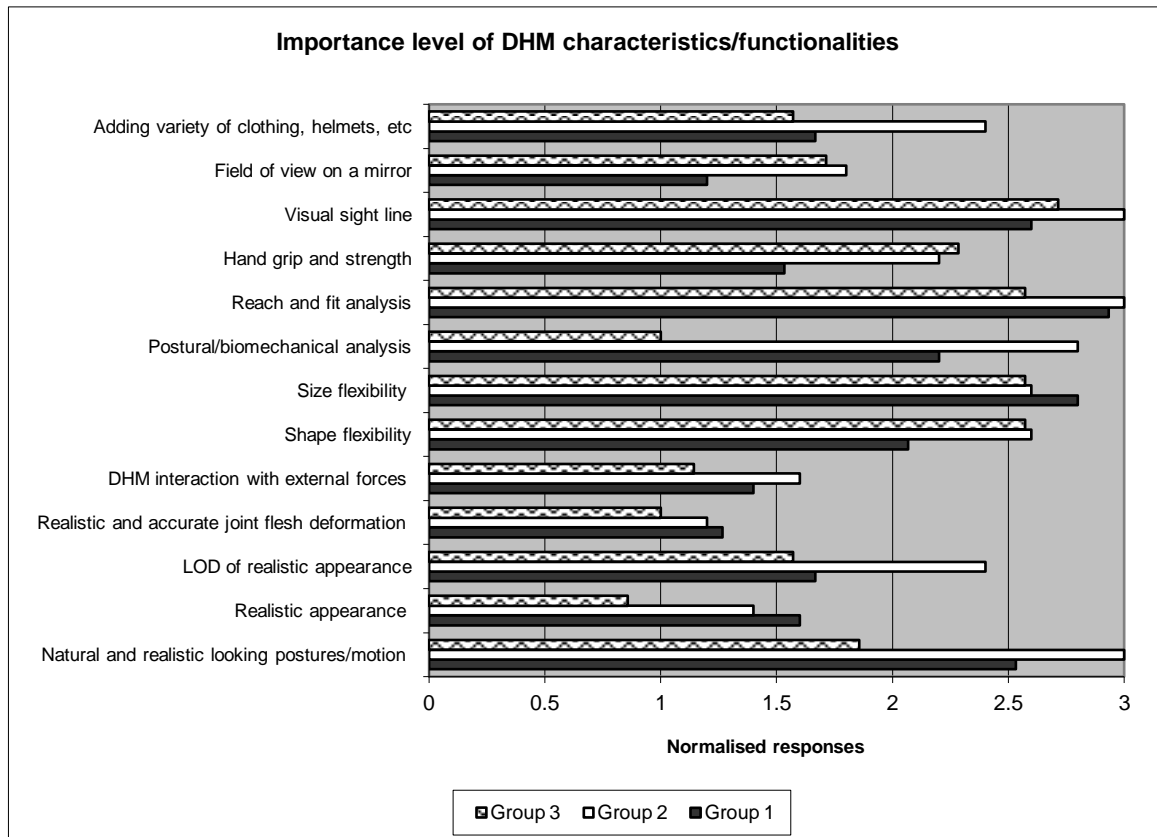


Figure 39. Importance level of DHM characteristics/functionalities for all groups

Regarding usage and desirability of DHM characteristics/functionalities, group 2 responses were excluded. This is because group 2 consisted of ergonomists who have no experience in using ergonomics CAD applications and therefore this particular question is irrelevant for them. The overall result of group 1 and group 3 on functionalities/characteristics usage was a reflection of their attitude on functionalities/characteristics importance. The types of usage for DHM were in agreement with other studies (Chaffin, 2005; Laitila, 2005). Figure 40 shows that: (i) reach and fit analysis, (ii) size flexibility, (iii) DHM posturing, (iv) visual sight line and (v) shape flexibility, were the most frequent usages of DHM in ergonomic CAD for both group 1 and group 3. Despite dissimilar respondents' access to ergonomics CAD, level of usage for functionalities/characteristics which were essential to perform ergonomics analysis was not affected. This suggests that, DHM functionalities/characteristics that were of paramount for basic ergonomics analysis, e.g. reach and fit analysis, were more accessible than others irrespective of the ergonomics CAD type. The overall result of group 1 and group 3 on functionalities/characteristics usage also suggested that respondents' attitude on functionalities/characteristics importance was a reflection of their

functionalities/characteristics usage. This was shown by the consensus of the overall results between the functionalities/characteristics importance and usage.

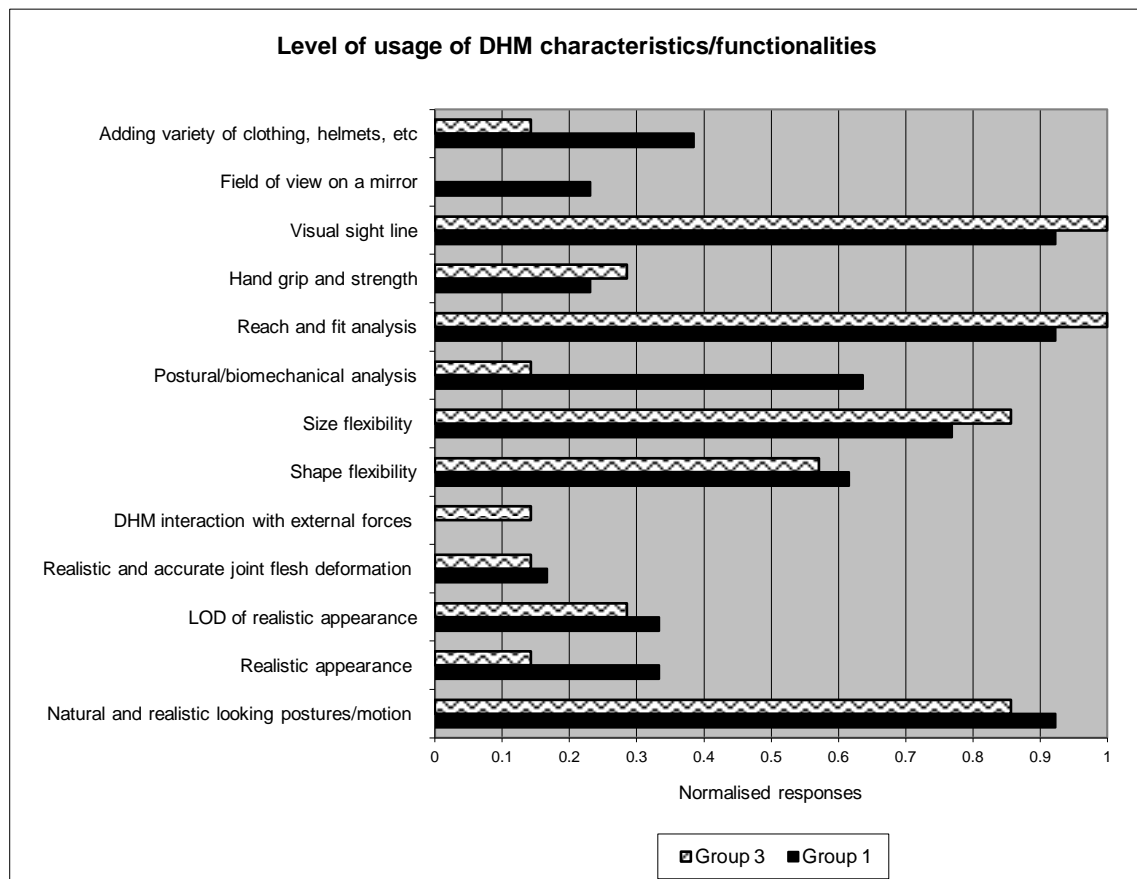


Figure 40. Usage of various DHM's characteristics

Respondents who did not have access to some of characteristics/functionalities were able to choose whether they would like to have used them or not. The result is shown in Figure 41. Hand grip and strength, DHM interaction with external forces, and adding variety of clothing, helmets etc. were desired by most respondents, respectively. The next functionalities, which were deemed to be desirable by the respondents, were realistic appearance, LOD of realistic appearance, and realistic/accurate joint flesh deformation. For both groups, their desire for most of the characteristics was more or less the same, except field of view on a mirror. The origin of this observable fact was more likely caused by the limited use of the functionality and the extent of respondents' experience in ergonomics. Group 1, as practicing ergonomists, might seldom encounter situations where field of view on a mirror was required. On the other hand, group 3, who were industrial design students might not have realised this. This result suggested that, as in the case of the DHM functionalities/characteristics' importance, desirability of DHM functionalities/characteristics is also dependent on the expertise and experience of respondents.

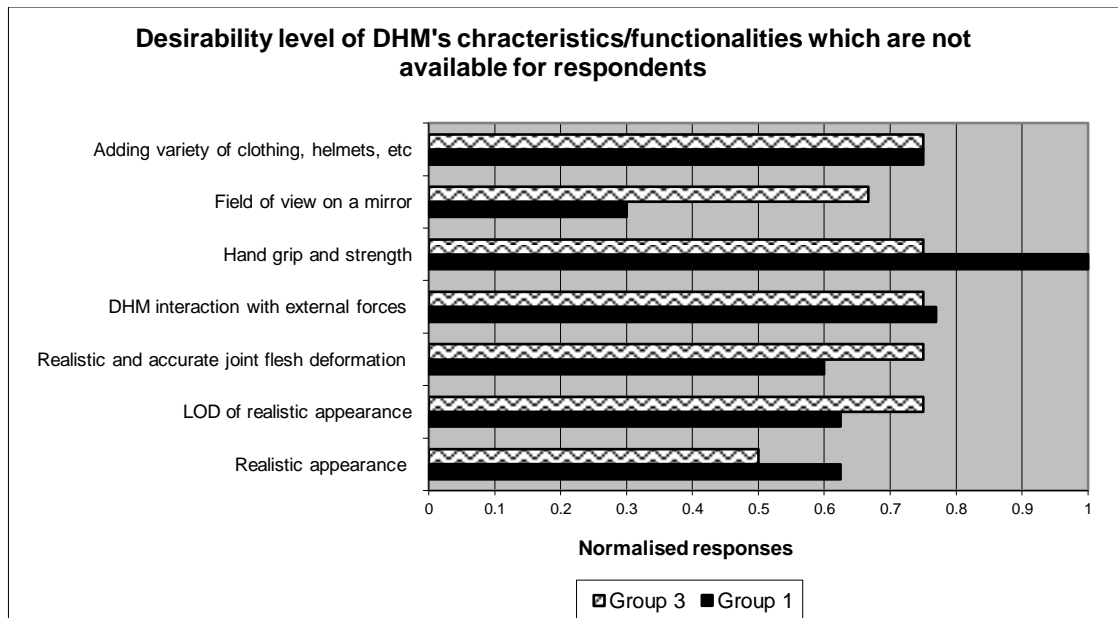


Figure 41. Respondents desire of various DHM's characteristics

3.2.3.2 Required level of detail for a realistic looking DHM

The respondents' opinion regarding required level of details (LOD) for a realistic looking DHM was inconclusive. Figure 42 shows that 60% of respondents agreed that uniform accuracy (level of detail) should be applied to represent a realistic DHM. However, 50% of respondents concurred that enhancing the details of certain body parts would be sufficient to produce the same effect (see Figure 43). The result showed that the respondents considered partially enhanced details would be more than adequate to produce DHM realism despite being aware that that a realistic DHM should ideally be represented by enhancing the details of the whole body. In addition to this, at the time when the questionnaire was conducted, most of the existing ergonomics CAD commonly employed partial LOD which might induce respondents' acceptability towards partial LOD. 68% of respondents agreed that unrealistic joint flesh deformation affected the overall DHM realism (see Figure 44).

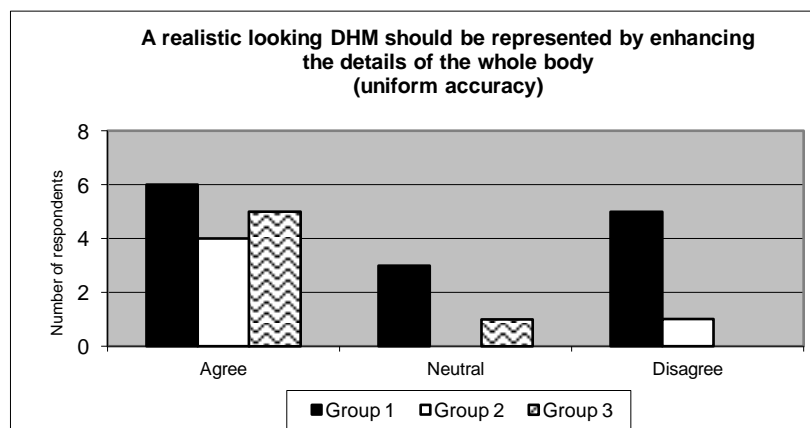


Figure 42. Respondents' response about the uniform accuracy/detail for DHM

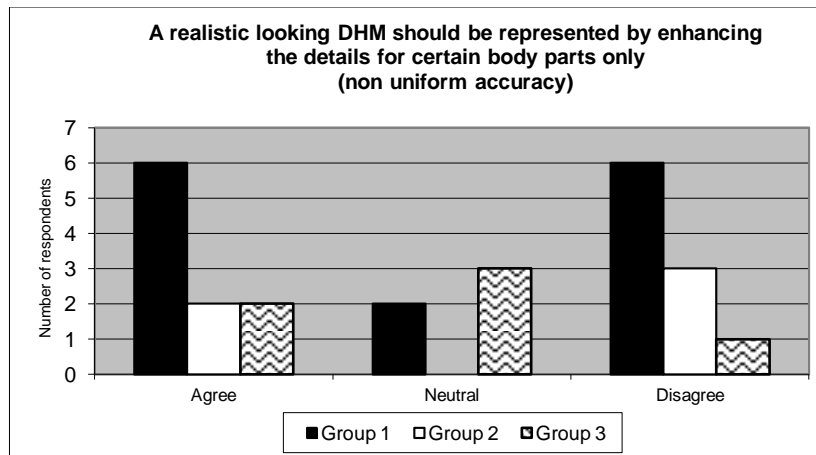


Figure 43. Respondents' responses about non-uniform accuracy/detail of DHM

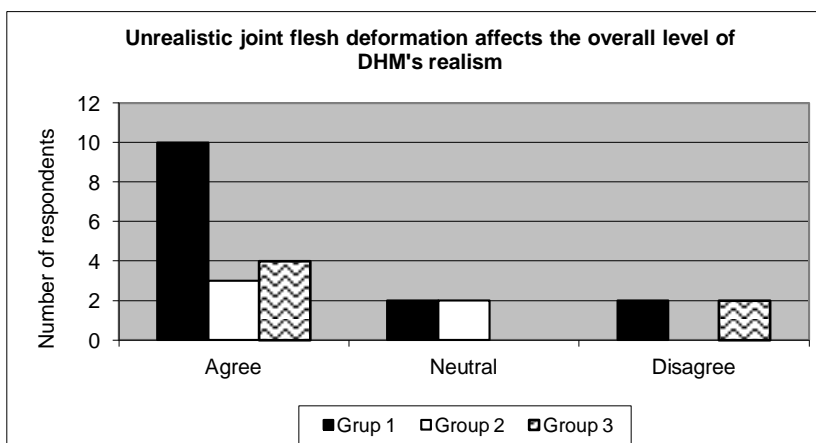


Figure 44. Respondents' response about the effect of unrealistic joint flesh

Regarding waiting time, 65% of the respondents agreed that it was inconvenient, as shown in Figure 45. Most of the respondents in group 1 stated that, as ergonomists, they needed to test various options in order to get an optimum solution in solving design problem. A similar view point was also demonstrated by group 3. Hence, time was quite a crucial issue and as a consequence 79% of the respondents were willing to make a trade between accuracy and realism (see Figure 46). Some of the respondents also suggested different DHM for analysis and presentation whereas others highlighted the need of a more detailed DHM's body parts even if they were less accurate e.g. hands and fingers.

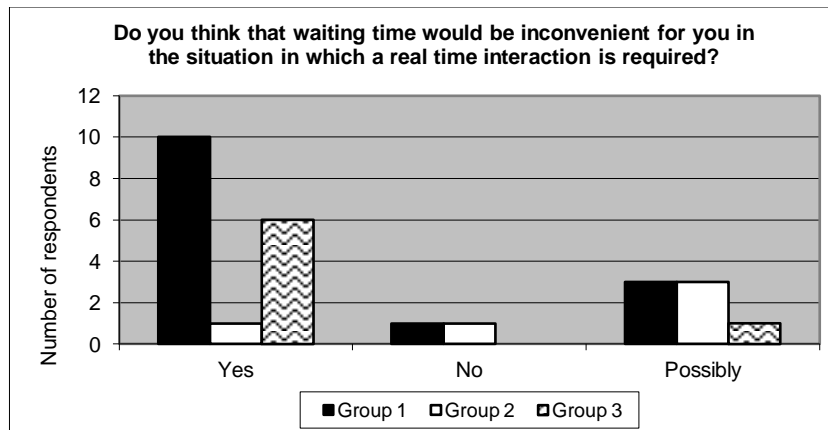


Figure 45. Respondents' responses about waiting time in which a real time interaction is required

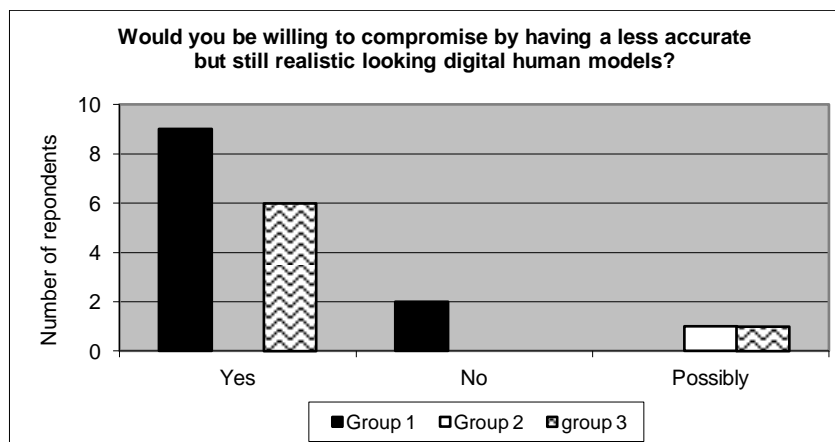


Figure 46. Respondents' willingness to trade some accuracy for real time interaction

3.2.3.3 Impact of realistic looking DHM

81% of the respondents perceived that realistic looking DHM would be part of the future trends of DHM characteristics in ergonomics CAD software (see Figure 47). Some of the respondents also highlighted the rapid advances of DHM in the gaming industry or other media and suggested adoption, where appropriate, to DHM in ergonomics CAD. On the question whether a realistic looking DHM would improve accuracy resulted in a diverse response (see Figure 48). This was shown by the high number of "possibly" responses and their added comments which pointed out that the increase in accuracy could only be possible if the realistic looking DHM was based on sound anthropometric and biomechanics principles. The careful approach of the respondents on this question showed respondents' ability to distinguish that a realistic appearance DHM did not necessarily equate to a more accurate DHM. Additional comments from respondents with the negative responses proved that respondents did not regard realistic looking but inaccurate DHM highly because there was no added value towards the ergonomics analysis outcome.

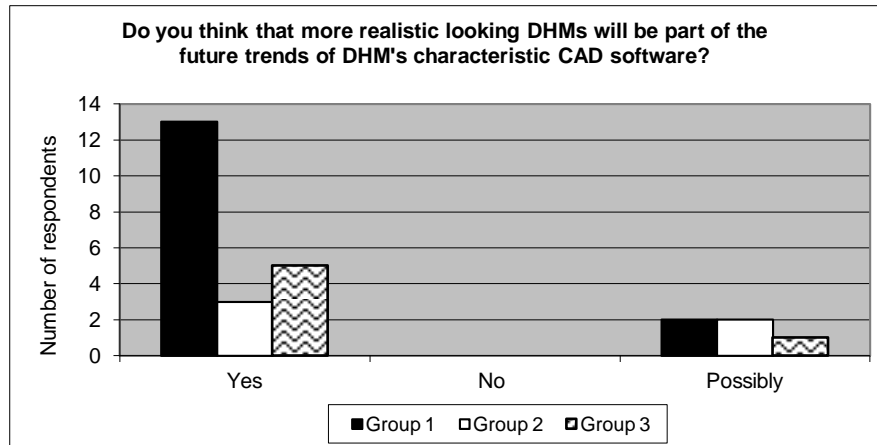


Figure 47. Respondents' view regarding the future trend of realistic DHM

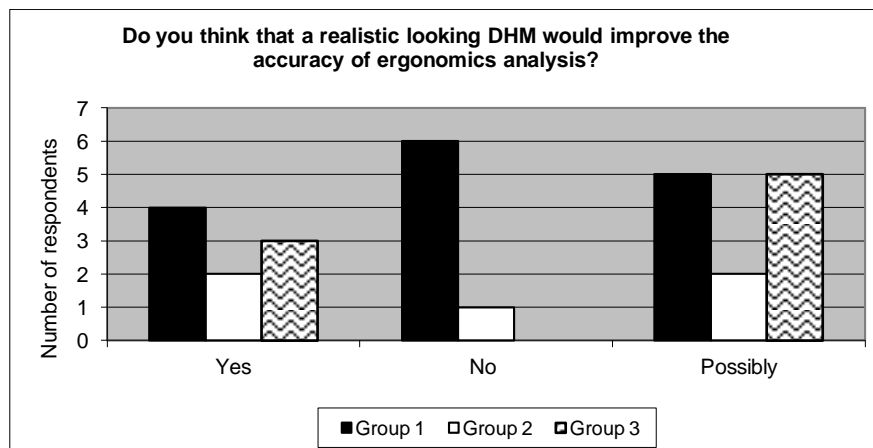


Figure 48. Effect of DHM realism on accuracy

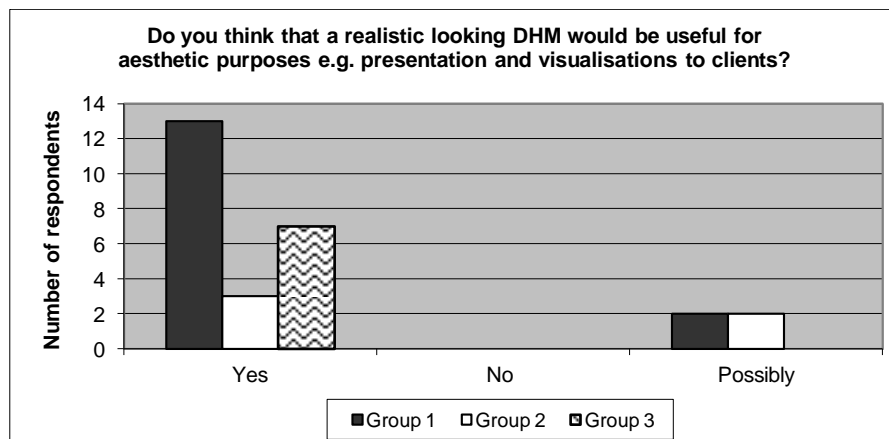


Figure 49. The use of realistic DHM for aesthetics purposes

For presentation and visualisations of ergonomics analysis results towards the clients, all groups favoured a realistic looking DHM (Figure 49). Based on the respondents of group 1 additional comments, clients tended to believe in the ergonomics analysis result and stay focus on the presented ergonomics issue when DHM were realistic. Some of them would perform the analysis

within common ergonomics CAD software and use other software package e.g. Poser, for presentation/visualisation in order to achieve a realistic DHM.

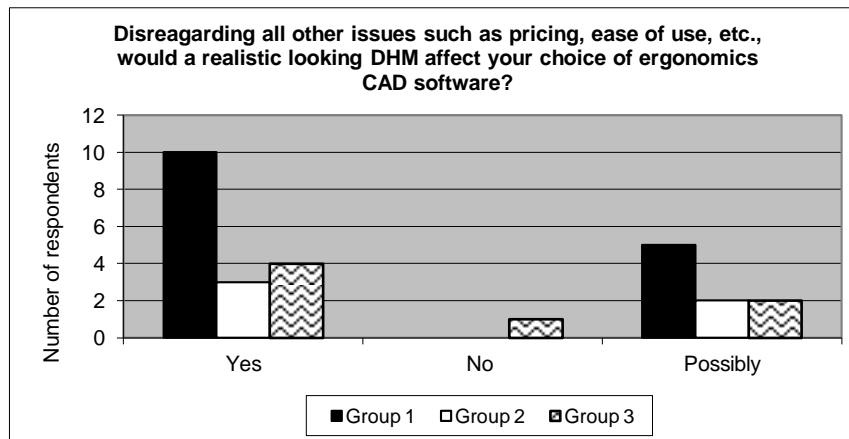


Figure 50. Effect of realistic DHM on ergonomics CAD choices disregarding other issues

Disregarding pricing, ease of use etc, most of the respondents agreed that realistic looking DHM affected their choice of ergonomics CAD software (see Figure 50). However, from the additional comments, it was also apparent that the realistic looking DHM had to have at least the same accuracy and functionality as their current ergonomics CAD which were required to perform essential ergonomics analysis. One of the comments was:

“Ease of use and speed, accuracy and flexibility are equally important if not more so.”

3.2.3.4 The importance of flesh deformation due to contact with external objects/loads

The respondents either assented or saw the possibility of integration of flesh deformation due to contact with external objects as part of the ergonomics CAD software in the future (see Figure 51).

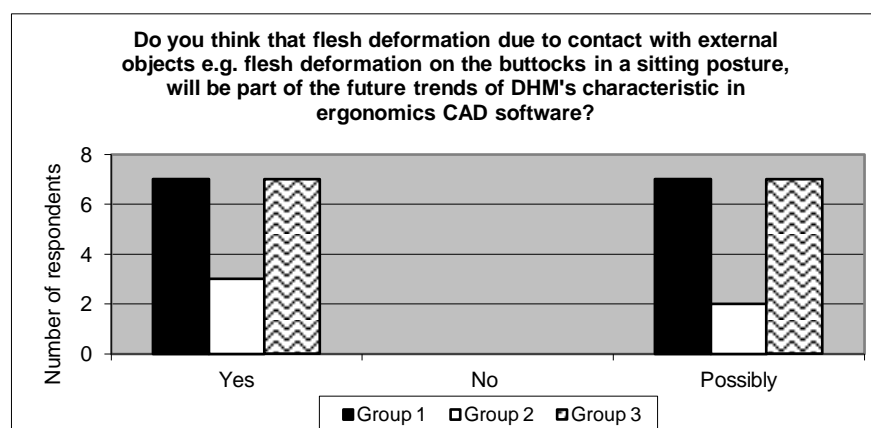


Figure 51. Flesh deformation due to contact with external sources and DHM future trend

Comments from respondents showed a positive outlook and hope towards flesh deformation with external objects/loads realisation. Overall, 88% of the respondents believed that the flesh deformation due to external forces would improve the accuracy of ergonomics analysis (see Figure

52). Respondents who disagreed seemed to doubt the beneficial effect in comparison with the arising complexity. One of the comments which opposed this view stated that:

“Ergonomics analysis is far too inaccurate for flesh deformation to make any difference to the result”.

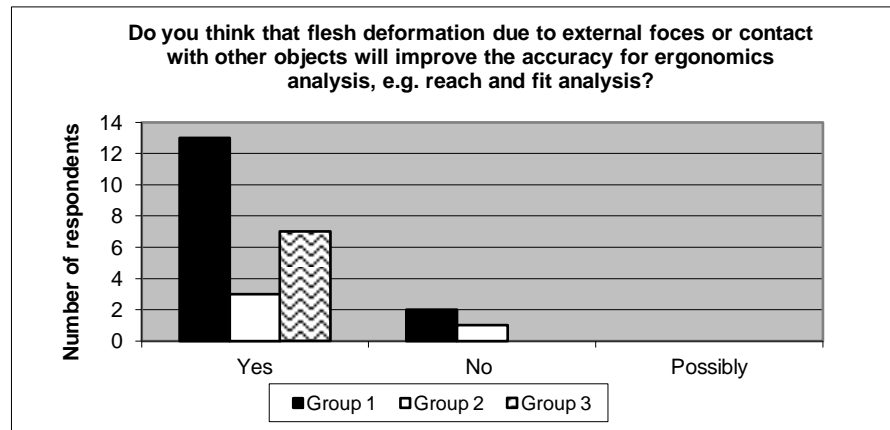


Figure 52. Effect of flesh deformation due to external forces on accuracy

86% of the respondents viewed that the flesh deformation should be accompanied by object deformation, as well (see Figure 53). The most common given examples of its application were seated DHM and its interaction with the seat. Other type of application example was motion restriction due to clothing and modelling DHM for cramped spaces.

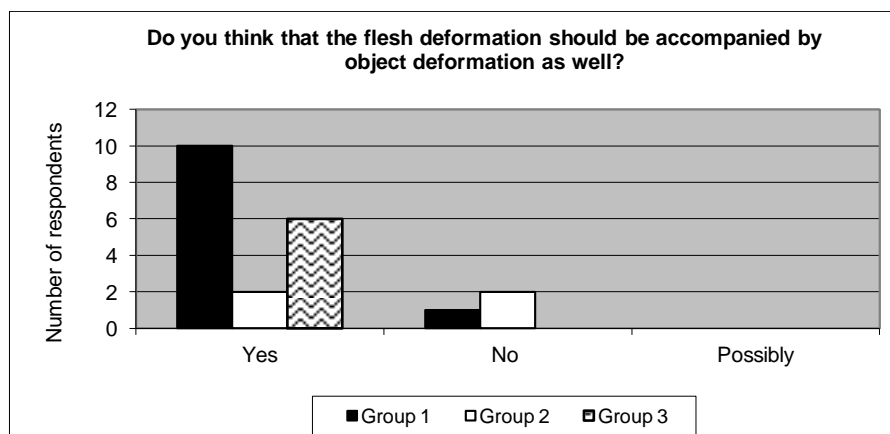


Figure 53. Flesh deformation and object deformation

Regarding whether flesh deformation due to contact with external objects should be implemented for the whole body, 73% of respondents preferred a whole body implementation (see Figure 54). Disregarding their preferences on the application scale of flesh deformation due to external forces, there were similar body parts which deemed as suitable i.e. buttocks and thigh.

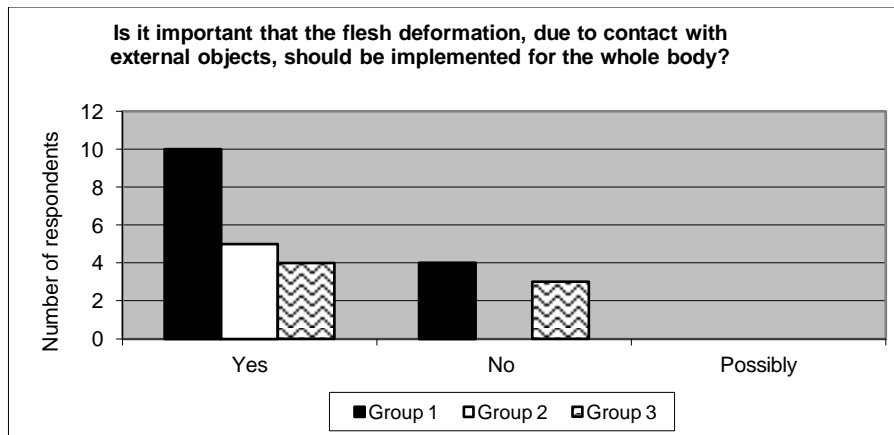


Figure 54. Whole body implementation of the flesh deformation due to external forces

3.2.3.5 Respondent perception of the characteristics that define the overall quality of ergonomics CAD software

This section was only applicable for ergonomists with experience in using ergonomics CAD because the respondents were required to have experience in using more than one ergonomics CAD. Based on the open question concerning characteristics affecting respondents' judgement about the overall quality of ergonomics CAD, respondents' answers were then categorised. The result was shown in Table 3. From the table, DHM realism/LOD characteristic was seen as important as DHM motion/posturing/joints. When a user is exposed to various ergonomics CAD with different level of realism but similar functionality, there is a possibility that realism would be seen as important characteristics to define the quality of an ergonomics CAD.

This was supported by a comment from respondent:

"Absolutely. I would never accept a software with worse looking DHM than we currently are using even if there were other good things with the software. Of course I wouldn't accept software that only had a good looking/realistic DHM but no useful functions etc."

Another characteristic which was seen to affect the overall quality of ergonomics CAD software was its analytical ability. Additional characteristics were usability, ability to customise DHM, compatibility, speed, reliable and recent anthropometry data sets, robustness and clothing allowances.

3.3 Summary

The user study was performed to follow up and confirm the findings from the literature review (see chapter 2). Results from both the literature review and user study would support the fulfilment of the second objective of the research i.e. establishment of DHM specifications for FDM in ergonomics modelling. Four objectives were established for the user study. These were: (1) users' views on the need for a realistic outer surface simulation of the human skin surface; (2) users' views on what constitutes DHM's realism; (3) users' views on the possible trade off of potential DHM's

specifications; and (4) user's view on the importance of flesh deformation due to contact with external objects/loads and characteristics that define the overall quality of ergonomics applications. To achieve these four objectives, a questionnaire was distributed to both experienced and less experience users of ergonomics modelling.

The result of user study revealed that experience and expertise of respondents affected how they judged the importance/desirability of DHM's characteristics. However, the effect is less apparent on how they viewed DHM's realism. Despite being seen as less important or urgent than other more fundamental characteristics such as reach and fit analysis for example, respondents did expect to see a more realistic DHM in the future. Respondents pointed out the importance of realistic flesh deformation in enhancing DHM realism but appeared less concerned about the level of detail of DHM. However, the user study's results also showed that what ergonomics CAD required was not only visually convincing DHM but also an accurate DHM which was based on the sound biomechanics and anthropometric principles. In principle, a visually realistic but anthropometrically inaccurate DHM was not preferred by the respondents as they saw no added value from it. Speed was of importance for all respondents. The results suggested that a realistic DHM should not hinder the ergonomists ability to explore different options for their analysis purposes in real time. Respondents, who have had experience in using more than ergonomics CAD application, agreed that a realistic looking DHM provided a more convincing ergonomics analysis presentation and visualisations to the clients. The user study also showed that a realistic looking DHM affected the overall quality of ergonomics CAD.

Lastly, the user study showed that flesh deformation due to external forces was also desired by ergonomists and seen to be part of future trend which then enabled a more accurate ergonomics analysis. From these findings, it could be proposed that the method to develop realistic and accurate flesh deformation around the joint should be: (i) based on sound biomechanics and anthropometric principles to support accuracy of the DHM's modelling, (ii) real time and (ii) realistic. The user study results support the earlier findings from the literature review which showed that these three aspects have the potential to be DHM specifications in ergonomics modelling. Together with the earlier findings from the literature review, the user study would be used to propose and establish DHM's specification in chapter 4.

Table 3. Characteristic that define overall quality of ergonomics CAD

Characteristics							Total
Usability	1	1	1				3
	Ease of use	Ease of learning/use	Usability				
Customising manikin	1	1	1				3
	Degree of user control over individual dimensions in order to construct custom manikins	Anthropometry data-base or how easy it is to create a manikin with a unique anthropometry characteristics	Anthropometric - ability to model as many body dimensions as possible accurately				
Anthro data set	1	1					2
	Usage of up to date anthro data sets	Provision of convincing references for sources of anthropometrics data.					
Compatibility	1	1	1				3
	Degree of compatibility with current CAD program import file formats	Ease of building workplace model/or loading externally built model	Ability to import from CAD products + optimise what is being looked at i.e. display + hide features, add + delete objects as well as humans				
Robustness	1						1
	Robustness						

Realism and LOD	1	1	1	1	1	1	6
	Realism	Also the detail discussed previously, such as hair and fingers.	Natural looks of the manikin	A good visual representation is important	How realistic the DHM looks (appearance)	Appearance-particularly head + hands for sights/controls	
Analysis	1	1	1	1	1		5
	Assessment package	Range of analyses available	Clear evidence of analytic capability is also needed (e.g. joints going out of constraints...)	Nice functions to manipulate the DHM (if you cant manipulate the DHM, it doesn't matter if it looks good)	Analysis tools - ability to perform vision/reach/comfort assessment		
Motion/posturing/joints	1	1	1	1	1	1	6
	The ability to create moving animations in Jack is definitely a benefit	Posturing of the manikins	Also ability to animate/demonstrate task action/motion sequences.	How realistic the DHM moves and looks while moving of manipulated position	How realistic the DHM can be moved (placement of joints, number of joints),	Joint limits/behaviour - ability to realistically manipulate the human within normal joints limits + hold limbs relative to objects	
Clothing allowances	1						1
	Allowances-for clothing Personal Protective Equipment (PPE) etc						

Functionality	1	1					2
	Functionality	Possibility to combine ergonomics and assembly simulation study (you often have to do a combination of both.					
Speed	1	1					2
	Speed (near real time is required) when e.g. manipulating a posture	Speed					

4 Methodology for FDM Development

To outline the proposed methodology for the research and the interrelation of the specific research activities, a flow chart of the research methodology is shown in Figure 55.

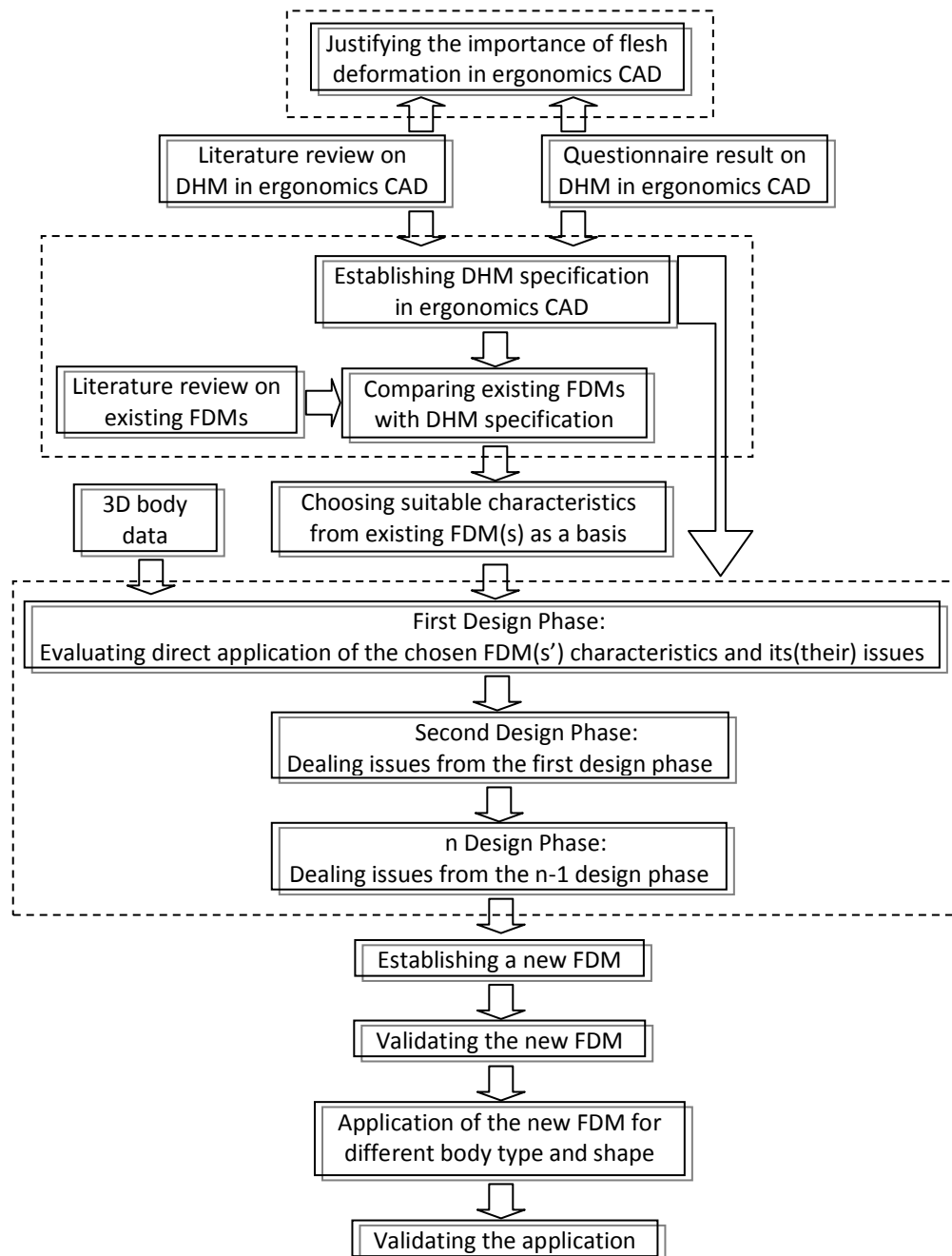


Figure 55. Flow chart of the research methodology

The first step in this research was to justify the importance of flesh deformation modelling in ergonomics CAD, which was achieved through undertaking the literature review and the user study i.e. questionnaire survey. The results of the user study (see chapter 3) and the literature review

(see section 2.1) highlighted the need to improve the realism in DHM in ergonomics CAD, essentially increasing the resemblance of DHMs to the real human form. The user study results also confirmed that developing a realistic flesh deformation around the joint was partly a way to augment DHM realism. In addition to this, the respondents also believed that as long as DHM realism was based on sound biomechanics and anthropometric principles, a higher level of accuracy would be achieved. This finding served to justify the importance of flesh deformation modelling for DHM in ergonomics CAD which was the first objective of the research.

Once the importance of flesh deformation in ergonomics CAD was confirmed, the proposed next step was to verify the necessity of a new flesh deformation method for DHM in ergonomics CAD. The proposed method to verify this was by performing a comparison between existing FDMs and a set of specifications, which satisfied the requirements for DHM flesh deformation for ergonomics CAD. Section 2.2 in the literature review listed and explained briefly each of the existing FDMs. The following subsection in this chapter will attempt to establish a DHM specification for flesh deformation at the joint derived from both the literature review and the user study results. These specifications were then employed to evaluate the existing FDMs. The outcome of this process was expected to serve as a rationale for the need of a new FDM as well as identifying the extent to which existing FDMs' characteristics matched the specifications for flesh deformation at the joint.

Identifying existing FDMs that suited DHM specifications for flesh deformation was important because this research proposed the use of existing FDMs with suitable characteristics as a basis for further development. Basing a new FDM on an existing method(s) was deemed to be more advantageous than creating a completely new FDM. Basing a new FDM on an existing method(s) would enhance the success rate of the new FDM development as the existing FDM(s) had been proven to deliver, at least partially, elements that would address the specification. Furthermore, it would also shorten the time to develop a new FDM and enable an exploration of its application in an ergonomics CAD context.

The flow chart shows that the design of the FDM consisted of several stages. The exact number of these was not known at the beginning of the study as the number of iterations was difficult to predict. However, at that stage, it was already clear that the first design phase would be a further evaluation of the existing chosen FDM(s). This evaluation addressed any required modification to suit the 3D body data usage and DHM flesh deformation specifications. DHM specifications, whenever appropriate, were used to guide the decision making throughout the new FDM design phase. Once the design phase was completed, a review of the new FDM took place. The review purpose was mainly to investigate the new FDM ability to fulfil the DHM specifications for the flesh

deformation at the joint. The review outcome was used as a basis for suggesting further works in the future studies.

The next stage of the research was the application the new FDM to accommodate different body size and shape. The ability of the new FDM to accommodate different body size and shape was considered to be important as this feature is one of the important roles of DHM in ergonomics (see section 2.1.1). The last part of the research was a validation of the application, which then provides guidance and directions for future studies.

4.1 DHM specifications

Badler (1997) argued that the characteristics of DHM vary and depend on application. He addressed two examples in which human size, capabilities, joints and strength limits are essential to applications for design evaluation whereas real time behaviour is more essential for games, training and military simulations. His suggestion implied that a set of DHM specifications for ergonomics applications would be beneficial to guide the development of flesh deformation modelling in ergonomics applications.

This section proposes a set of DHM specifications for flesh deformation modelling in ergonomics applications. As shown in Figure 55, the literature review conducted in chapter 2 and the user study results in chapter 3 were used to produce a set of specifications to drive the development of DHM flesh deformation for ergonomics CAD. The proposed specifications, which satisfy DHM flesh deformation requirements for ergonomics CAD modelling, are addressed in the subsections below.

4.1.1 Accuracy

The first and foremost of these specifications is accuracy, which refers to the ability in producing the geometry of human form and shape precisely. This specification was identified from the literature review in section 2.1.1 regarding DHM's roles in ergonomics applications. The literature review revealed that one of the DHM roles in ergonomics CAD modelling is to evaluate the fitness of the product and eliminate or reduce the necessity of physical mock-ups and testing with real human subjects. This role could only be achieved by representing human body forms and functions as accurately as possible. Findings from the user study also demonstrated how DHM accuracy in ergonomics CAD modelling was judged to be of importance by the respondents (see section 3.2.3.3).

This research adopts the accuracy definition given by CEN (2007). According to CEN (2007), DHM accuracy is defined as the precision with which a DHM system reproduces the size, shape, posture, angles, movement paths and other geometric characteristics of the individual from whom

the measurements were taken. With respect to flesh deformation model of DHM at the elbow joint, this means that the method should be able to reproduce the size, shape and geometry of the flesh deformation of a person to be modelled.

4.1.2 Realism

The next specification is the realism of the DHM which refers to the resemblance of the DHM to a real human body form. This specification was identified from the literature review in section 2.1.1 regarding the roles of DHM in ergonomics application. The literature review revealed that to support DHM's role as a visualisation tool, realism is required. The literature review also showed that despite few studies assessing the importance of DHM realism, a demand for a realistic DHM was present. In addition to this, the result of the user study revealed that respondents preferred a realistic DHM over an unrealistic one as long as realism did not affect DHM accuracy and its processing time (see section 3.2.3.2 and 3.2.3.3). Users also acknowledged that a realistic DHM would help to convey or share ergonomics analysis results to the clients because an accurate and realistic DHM would result in a more convincing ergonomics analysis presentation and visualisations to the clients. A realistic DHM would also likely keep the attention of the clients towards the analysis itself rather than on any lack of realism in the DHM. Vugt et al. (2007) also identified that when someone is accustomed to a high level of realism, they would show less engagement when exposed to a less realistic DHM. Currently, some of the respondents had to use another application package, for instance 3ds MAX or Poser, to create a realistic DHM exclusively for the presentation. Hence, the user study findings supported the view of Lämkuil et al. (2007) in which they argued that the demand for a more human-like virtual human was present.

Oxford dictionary defines "realism" as:

"The quality or fact of representing a person or thing in a way that is accurate and true to life".

Research in the field of interaction between users and DHM commonly categorise realism into two: (i) behaviour realism; and (ii) form realism (Vugt et al., 2007). Behaviour realism concerns facial expression, motion, gestures, conversation, intelligence, and so on. Form realism concerns the outer or visual appearance e.g. cartoon-like, fantasy creature, etc. In this research, the term "realism" specifically refers to form realism. Realism is not the same as accuracy. Realism refers to the visual appearance of DHM whereas accuracy refers to the geometry precision of DHM. Accurate flesh deformation would likely result in realistic DHM but not necessarily vice versa. For instance, given a box with a size of 3x3x3 cm, a 3D image, which is created based on this geometry, will represent the box accurately and realistically. However, if the 3D image creation ignores the size, e.g. using the size of 2x2x2, the 3D image of the box will still be realistic and yet inaccurate.

4.1.3 Whole body modelling

Based on the literature review, all of the existing DHMs offer whole body modelling, which signified that this was the norm for DHM in ergonomics (see section 2.1.3). Whole body modelling is crucial to perform most ergonomics analyses. This is probably because the existing DHM was partly designed to accommodate anthropometric related assessment on product and workspace. In a complex assessment on product and workspace, there is a strong likelihood that more than one anthropometric dimensions (multivariate dimensions) would be utilised and likely require whole body modelling. For instance, reach and fit analysis and visual sight line, the two most common ergonomics analyses (see section 3.4.1), would require whole body modelling. It would be impossible to simulate a visual sight line without taking into account the posture of the torso in the sitting position or the combination of postures between the torso and lower limbs in a standing position. The same thing also applies for reach and fit analysis. Therefore, ability to model the whole body is proposed as the next DHM specification.

4.1.4 Real time

The fourth specification for DHM is its suitability for real time processing. This specification was identified in the literature review in section 2.1.3 regarding existing DHMs for ergonomics applications. This specification was also identified from the user study. Respondents of the user study highlighted the importance of real time processing which would enable them to explore alternatives and seek an optimum solution for any ergonomics design problem in an expedient manner. In addition to this, the respondents also viewed longer waiting times as an inconvenience (see section 3.2.3.2).

According to Badler (1997), the processing time for digital human modelling could range from a “real time” to offline. Oxford dictionary (2010) defines “real time” as the following:

“...relating to a system in which input data is processed within milliseconds so that it is available virtually immediately as feedback to the process from which it is coming...”

Applying this definition into flesh deformation modelling, “real time” could be translated as an ability to generate flesh deformation immediately as soon as a user changes the DHM’s posture.

The real time specification is closely linked to accuracy, realism and whole body modelling. As shown by the literature review on existing flesh deformation (see section 2.2.1), accurate anatomic representation of flesh deformation demanded high computational processes which lead to the increasing processing time for DHM. As a result, a compromise was made by creating a model specifically for a particular body part (see section 2.2.1), offline simulation (see section 2.2.2), or simplifying the flesh deformation process (see section 2.2.3, 2.2.4 and 2.2.5). Whole body modelling

and high realism DHM could also result in a lengthy processing time which contradicted the real time nature of ergonomics simulation as highlighted in the user study. However, as whole body modelling needs to be satisfied, a trade-off between “accuracy”, realism, and “real time” would need to be made. The user study also revealed that respondents would not mind trading realism to accuracy in order to maintain the real time specification.

4.1.5 Accommodation of different body sizes and types

The literature review underlined that the most common use of DHM is to assist in the design of products which can accommodate a large variety of people size and shape (see section 2.1.1). The user study results supported this by demonstrating that the respondents viewed shape/size flexibility and reach/fit analysis as important DHM functionalities (see section 3.2.3.1). This finding was to be expected as these functionalities were required to perform basic ergonomics analysis. The alteration of anthropometric features is generally needed to study workspaces, evaluate posture, understand fit, and so on. To alter anthropometric features, the user typically specifies nationality, gender, or age, of the DHM depending on the data availability of the ergonomics simulation. The user could also specify certain anthropometric dimensions of the DHM which are then used to predict the rest of anthropometric dimensions which are needed to create a 3D model (e.g. proportional human models where all limbs are sized to match a stature percentile measurement). The ability to model different body sizes and shapes in ergonomics simulation is crucial. This is to ensure that product or work place would be suitable for a variety of target users. As a result, all elements of DHM, including flesh deformation at the joint, should reflect this. Thus, a flesh deformation method should be applicable to accommodate different body sizes and shapes. Therefore, the fifth specification of DHM is to support (maintain) the ability to accommodate different body sizes and types.

4.1.6 Minimum user intervention

As explained in section 2.1.3, ergonomics applications, to some extent, allow the user to specify or modify the features of the DHM. The modifiable features are mainly aimed at accommodating simulation of DHM with different body size, shape and posture by determining the nationality and percentile of the DHM. The user intervention in ergonomics simulation is generally limited to alteration of DHM’s posture, DHM’s anthropometric features, and type of ergonomics analysis. Typically, the user does not have any access to alter the range of joint movements as these parameters are based on scientific study and additional data is extremely limited. However systems such as HADRIAN provided additional joint range of motion data that can be employed in DHM systems such as SAMMIE to model the capabilities of other populations such as those who are older

or who have disabilities (Marshall et al., 2004). The user is also not normally expected to have to correct model errors, to define acceptable postures to drive flesh deformation, or address unrealistic results while altering the DHM's postures e.g. collapsing joints, lack of muscle bulging, etc. This particular feature sets the difference between DHM for ergonomic simulation and entertainment. In entertainment, the user is expected to produce realistic flesh deformation through manipulation of the DHM's geometry directly.

4.2 Comparing DHM specifications and existing FDM

The list of DHM specifications above capture fundamental characteristics which are seen as essential, or at least highly desirable, for DHM flesh deformation in ergonomics CAD. Any improvement which is aimed at DHM flesh deformation should take these specifications into account. Based on the literature review of the existing FDMs, each of the methods was compared with the DHM specifications to gauge its suitability to improve flesh deformation method.

4.2.1 Anatomical approach

The anatomical approach, see section 2.2.1, provides extremely high accuracy and realism. However, the compromise to this accuracy is the likelihood of issues with real time processing due to its extensive computational level. Other problems which could arise are its feasibility for whole body application, due to its nature of depicting human body parts as accurately as possible i.e. accurate representation of muscle, bone, tendons, etc. With such a high level of detail, a whole body application would demand a more extensive computational level which in turn might result in a much slower processing time. The anatomical approach is largely based upon 3D finite element meshing which would require a careful mesh arrangement as well as assigning material properties. To accommodate different body sizes and shapes, there is a strong likelihood that both of these parameters would have to be adjusted manually and hence restricts the anatomical approach's ability to accommodate different body sizes/shapes automatically. However, as the anatomical approach represents the body parts accurately, the likelihood that user intervention is required to modify or correct its appearance is small.

4.2.2 Physical approach

The physical approach ranges from using a spring and mass system to a simplified shape of muscle with volume preservation to simulate flesh deformation (see section 2.2.2). Although the complexity is less in comparison with the anatomic approach, as some simplification is applied for this approach, in terms of computational demand level and complexity, the physical approach is unlikely to be significantly different from the anatomical approach. Performing interaction in the mass and spring system or deforming simplified muscles while preserving the volume demands

complex calculation, especially if the process has to be performed in a large scale, e.g. whole body modelling. Therefore, similar shortcomings and advantages as those of the anatomical approach would also apply.

4.2.3 Geometrical approach

The geometrical approach is popular, commonly used for animation packages such as 3ds Max (Autodesk, 2009), due to its cheap computational cost. However, the geometrical approach is not without its drawbacks. A significant problem concerns realism and accuracy. As highlighted in the literature review, the lack of muscle bulging/swelling and collapsing joints in extreme positions are limitations of the approach. So user intervention was needed to correct and adjust the parameter values assigned to the area around the joint. Another problem with the geometrical approach is its inability to accommodate different body types and sizes automatically. The geometrical approach is based on assigning certain parameters, so called weights, to the mesh/vertices around the joint. In most cases, the parameters could be established automatically and refined manually whenever it is necessary. However, there is a strong likelihood that these refined parameters would not be suitable for other mesh/vertex data. Therefore, accommodating different body sizes and types would likely require constant manual adjustment to the parameters.

4.2.4 Shape by example approach

The shape by example approach, which showed a relatively realistic end result, was characterised by making use of a set of examples which are usually obtained from a single person e.g. an elbow in different flexion range, a knee in different flexion range, and extracting a common feature from the examples to predict flesh deformation for a new posture, either by interpolation or approximation. The literature review suggests that no user intervention is required to achieve realistic flesh deformation. However, the feature established from a set of examples could only be applied for that that particular set of examples. This characteristic is a major drawback when it comes to accommodating different body types and sizes.

4.2.5 Sweep blend approach

The sweep blend approach, initiated by Shen et al. (1994), used cross sections along the bone to create the body surface (see the left image in Figure 17). Instead of creating the usual polygon surface, the approach results in a NURBS surface which can be converted subsequently into a polygon surface. Since this approach is based on altering the geometry of shape i.e. discounting the actual process which causes muscle and skin deformation, the realism level is at the same level as that of the geometrical approach. Flesh deformation around the joint is performed through deforming the cross section and rearranging their orientation so that no intersections between cross

sections occur (see the middle image in Figure 17). To mimic muscle bulges, a sine function and cross section scaling are applied. The approach is suitable for real time application and can accommodate different body sizes and shapes. This was because the human body model largely depends on the cross sections which can be modified easily to reflect the individual. The cross section is created from a certain number of sampled points and it can be scaled to cater for different body sizes (see the right image in Figure 17).

4.2.6 Discussion

To ease the comparison between existing flesh deformation methods and DHM flesh deformation specifications, existing FDMs were assessed and scored using three values i.e. -1, 0 and 1. Value 1 represents the ability of an existing FDM to satisfy a particular DHM flesh deformation specification without any modification. Value 0 represents a limited or unproven ability of an existing FDM to satisfy a particular DHM flesh deformation specification and / or a need for further modification of the existing FDM to satisfy the DHM flesh deformation specification. Value -1 suggests the existing FDM's inability to satisfy a particular DHM flesh deformation specification even with further modification.

This research assumed that DHM flesh deformation specifications are of equal importance i.e. equal weighting. This assumption is not necessarily true because there is a possibility that each of DHM flesh deformation specifications has a different level of importance in different applications. The results of the user study highlighted that users were willing to trade one characteristic for another and so some form of weighting must exist. However, any weightings were discounted at this stage as they were likely to be highly context sensitive and this approach also served to simplify the comparison process. Furthermore, equal weighting excluded the need for a further study to establish the actual weight of each specification and thus maintain the focus on the core of this research, the design of a new FDM.

Using the above values, a table which summarises the suitability of existing FDMs was created (see Table 4). The result shows that the Shen et al. (1994) method i.e. sweep blend approach appeared to have a potential for further development to suit DHM flesh deformation specifications in Ergonomics CAD or comply with these specifications. However, as can be seen from the table the Shen et al. (1994) method was not without its disadvantages. The large number of '0's' indicated significant further development was required or there were a number of unknowns regarding its suitability. Whilst the overall values in the comparison table appear close what the Shen et al. (1994) method offers that others do not is that all of the other approaches have at least one '-1' value that indicates that there will be always one specification that will be unable to be met.

Table 4. Quantification of comparison between existing FDMs and DHM specification for flesh deformation

		DHM flesh deformation specifications						Total
		Accuracy	Real Time	Realism	Automatic accommodation of body sizes and types	Whole body modelling	Minimum user intervention	
Existing FDM	Anatomical	1	-1	1	-1	-1	1	0
	Physical	1	0	1	-1	-1	1	1
	Geometrical	0	1	0	-1	1	0	1
	Shape by example	0	0	0	-1	1	1	1
	Shen et al. (1994) – Sweep blend approach	0	1	0	0	1	0	2

In addition there are a number of specific features of the Shen et al. (1994) approach that would require careful examination. A common plane, a plane which is created from all of the bones involved for that particular joint, was required to form cross section planes. Figure 17b illustrates a joint in which two bones, shown in bold lines, are involved e.g. the knee or the elbow. Once a common plane is created from these two bones, the cross sections' orientation can be drawn on this plane (shown in thin line in Figure 17b). A cross section plane is a plane that goes through one of the thin lines shown in Figure 17b, and is perpendicular with respect to the common plane. The need to base the cross section plane creation onto the common plane between two bones would impose limitations on its applicability to a more complex joint i.e. the shoulder joint. The reason is because it is impossible to create a plane from more than two vectors, which in this case are the bones. The method resolves this issue by simplifying the joints i.e. in situations of more than two bones; the bone with least impact would be omitted during the flesh deformation. For instance, the shoulder joint consists of three bones i.e. the clavicle (collarbone), the scapula (shoulder blade), and the humerus (upper arm bone). In this example, the clavicle could be omitted and hence enable the creation of the common plane from the scapula and humerus.

Taking into account the advantages (see section 4.2.5) and disadvantages of the Shen et al. (1994) method, their method was chosen as a basis for the proposed FDM. The following bullet points outline the rationale behind this judgement and areas that needed further investigation:

- The Shen et al. (1994) approach was suitable for real time application because there was only a limited number of data i.e. sampled points to represent cross sections, to be handled for flesh deformation of a particular body part whereas other approaches would require a massive number of polygon coordinates for the corresponding body part.

- Shen et al. (1994) showed that their method could be used to produce DHMs to mimic the effect of different body weight by simply scaling the cross sections i.e. size alteration. Thus, the usage of cross sections to guide the surface creation presented a possibility to accommodate various body type and size. However, simply scaling the same cross sections would not result in an accurate modelling of various body types and sizes as there is a strong possibility that the shape of the cross sections shape alteration is also required. Therefore, the proposed FDM will try to address their method limitation by not only altering the size of the cross sections but also by altering the shape of the cross sections.
- The Shen et al. (1994) approach demonstrated the ability to extract cross sections from a 3D human model. The 3D human model was created manually and used polygons to create its surface. Because their 3D human model is created manually, its accuracy and realism would be inferior compared to 3D body data which is captured automatically from a real person. Fortunately, as the 3D body data is also constructed from polygons, their method presents the possibility of 3D body data integration from a body scanning system. Therefore, the proposed FDM will attempt to address a lack of accuracy and realism of human body shape and form presentation by introducing 3D body data.
- The Shen et al. (1994) method was suitable for whole body modelling as it had been shown in their study.
- The Shen et al. (1994) method shows that the flesh deformation could be achieved automatically without user intervention by applying the sine function and cross section scaling to mimic muscle bulges. Thus, their method possesses an ability to achieve minimum user intervention in generating flesh deformation. However, both the sine function and cross section scaling are rough approximations of flesh deformation as their values are determined from purely an aesthetic (realism) aspect of DHM flesh deformation. In addition to this, a set of sine function values and cross section scaling factors for a particular DHM are not necessarily applicable for other DHMs. Therefore, the proposed FDM will try to address these limitations.

Further investigation will be explained in chapter 5, which constitutes the first design phase of the new FDM development.

4.3 Summary

In this chapter, the methodology of the research was outlined. The role of the literature review, which was performed in chapter 2 and the user study, which was performed in chapter 3, were highlighted. As explained in the methodology of the research, both the literature review and user study drove the establishment of DHM specifications. Six DHM specifications were established.

These were: accuracy, realisms, whole body modelling, real time (modelling), accommodation of different body types and sizes, and minimum user intervention. These signified attributes that were relevant and suitable for DHM modelling in ergonomics applications. This research proposed the utilisation of these specifications to guide the development of the proposed FDM and ensure its suitability for DHM modelling. The establishment of the DHM specifications also indicated that the second objective of the research i.e. to establish DHM specification for DHM modelling in ergonomics application was achieved.

In accordance to the research methodology, the DHM specifications were used to evaluate existing FDMs which had been previously reviewed in the literature review. The aim of the evaluation was to seek an appropriate existing FDM that had a potential to suit DHM modelling in ergonomics applications. This step was necessary because this research intended to base the new FDM from an existing FDM, as opposed to create a completely new FDM. The evaluation showed that the Shen et al. (1994) method had the potential to suit DHM modelling in ergonomics applications. Based on this result, this research proposed the modification of their method as a basis to create the new FDM, which would be addressed from chapter 5 onward, and suggested the beginning of the process to answer the third research question i.e. to develop FDM that was suitable for DHM modelling in ergonomics CAD.

5 First Design Phase

Based on the discussion in section 4.2.6, it was established that the Shen et al. (1994) method would be used as a basis for the proposed FDM. Also, from section 1.4 and 2.6, it was revealed that this research intended to utilise 3D scan data as a part of the proposed FDM. As the Shen et al. (1994) method is originally aimed for a self-created 3D model; an evaluation was required to identify issues that would arise due to the utilisation of 3D scan data in this research. Therefore, the first design phases evaluated the direct application of this FDM (without undue modification) on 3D scan data and identified issues that affected its application to this research. Whilst direct application of the Shen et al. (1994) method is not directly related to this research, the output was perceived to be directly suited to supporting the needs for the development of the FDM. The first design phase is shown in Figure 56. Figure 56 also shows where the first design phase is located, relative to the previous and next stages of the research. The output from this phase was intended to be an evaluation of the Shen et al. (1994) method together with a list of issues to be addressed in subsequent design phases.

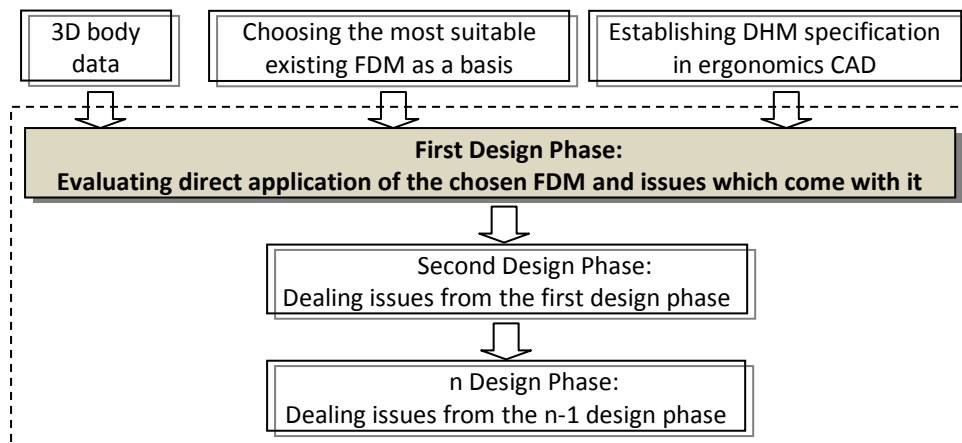


Figure 56. First design phase

5.1 First design phase strategy

The fundamental difference between this research and the Shen et al. (1994) method is the type of data used to develop the model. Shen et al. (1994) used a self-created body model (essentially fictional or idealised data) whereas this research proposed the use of actual 3D body data, which is usually produced by a 3D body scanner. As stated in section 1.4 and section 2.6, this research intended to utilise 3D body data. The utilisation of 3D body data in this research was proposed to address a number of the DHM specifications i.e. realism and accuracy determined earlier in section 4.1. Robinette et al. (2004) argued that employing three-dimensional anthropometry from 3D body scans removed much of the guesswork in characterizing human size,

shape, posture and motion. Furthermore, it is believed that 3D body data will enable capturing body images of people with different body sizes and shape easily. This will significantly reduce the effort required to generate body models of different shapes and sizes, which would be a limitation of self created models. A light patterned projection body scanner from [TC]² called NX-12, was used in this research. [TC]² is an American based company that was founded in 1979 and specialises in providing advanced technologies and digital solutions for apparel and clothing industries ([TC]², 2011). This scanner was chosen as it has a number of advantages compared to laser based scanners as discussed in Section 2.6 and one was also available in the Design School at Loughborough University. The [TC]² NX-12 has a total of 16 sensors with 4 view angles, which are pre-installed at 4 heights in the provided booth (1.8 m height x 1.2 m width x 0.7 m depth), and is able to provide 400 body measurements. It has 3 mm circumferential accuracy with data density between 600,000 – 1 million cloud points ([TC]², 2011). The [TC]² NX-12 creates a body mesh automatically along with its landmarks (only for torso), joint location approximation and body sizes for apparels. In order to assess the Shen et al. (1994) method, a number of stages of data capture and analysis would need to be performed using 3D geometry from the body scanner. Figure 57 shows the strategy for the first design phase. The first step in the first design phase was 3D data capture which involves acquiring and extracting 3D body data. The outcome from this step was then used to analyse the application of the Shen et al. (1994) method to a 3D body data, which covered three major issues i.e. bone location, cross section and region for flesh deformation application.

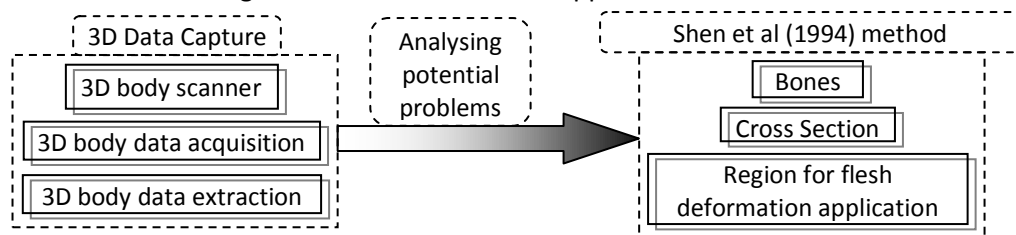


Figure 57. Strategy for the first design phase

5.2 3D data capture

The [TC]² NX-12 produces a 3D whole body model (see right figure in Figure 58) from a scanned human form (see left figure in Figure 58). As mentioned previously, the [TC]² NX-12 projects a light pattern (structure white light) onto the body. The light pattern distortion due to the body curvature allows recreation of the body curvature in the scanning system. To properly capture the light pattern distortion, a certain level of contrast between the body and the light pattern is crucial. For instance, wearing white apparel will omit the pattern as the white light will not be distinguishable from the white apparel. The same also applies with wearing black apparel. The [TC]² NX-12 is only able to produce a 3D whole body data from the original scan or “raw data” when the raw data is judged to be sufficiently recognisable to create 3D whole body. For example if during the scanning

process, the whole neck and a large part of the shoulder is occluded by hair, the [TC]² NX-12 will not be able to generate 3D whole body data. To capture 3D scan data of a person using [TC]² NX-12, he/she needs to be still during the scanning. Slight movements, especially in the upper limbs, would cause distortion on the generated 3D scan data.

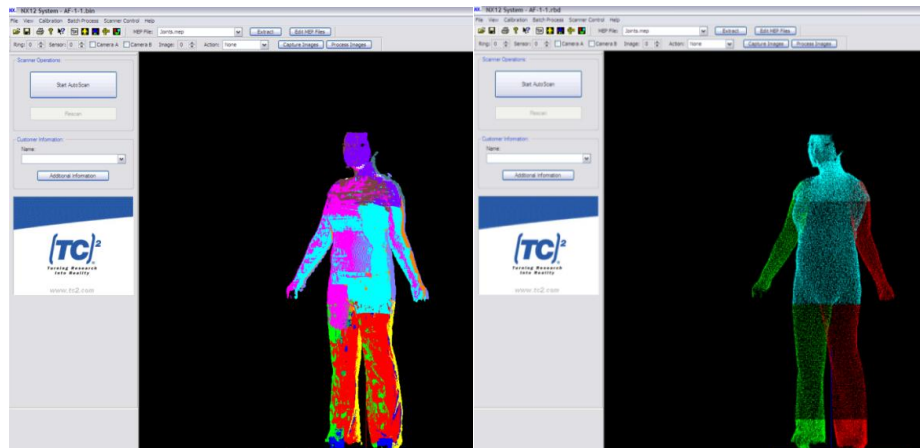


Figure 58. Raw data of 3D whole body data and final output of 3D body data from [TC]² NX-12

The 3D body data essentially consists of a “point cloud”, thousands of points, which can then be transformed by the [TC]² NX-12 into polygon faces (facets) automatically. While transforming the points cloud into polygon faces, the [TC]² NX-12 divides the whole body scan data into 5 body parts i.e. torso, left arm, right arm, left leg and right leg. The polygon faces for each body part are written to a virtual reality modelling language (vrml) file (*.wrl). A vrml is a text file format to describe three-dimensional interactive worlds and objects and is designed particularly to suit World Wide Web (www). A vrml file typically contains information such as vertices and edges of 3D polygons of an object, its surface color, its textures, etc (Ranjan, 2006). Subsequent manual editing of the vrml file in a word processor application allows the relevant body data (upper and lower arm) to be extracted. The [TC]² NX-12 also allows joint extraction from the 3D whole body data as shown in Figure 59.

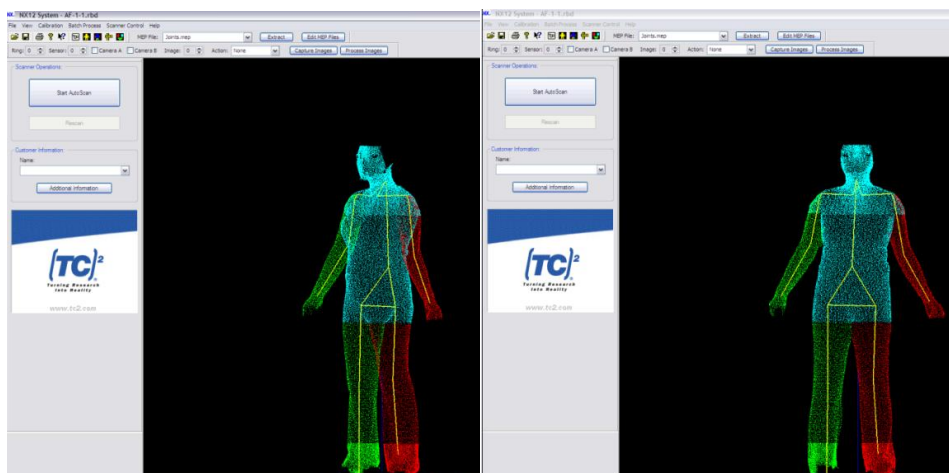


Figure 59. Joint extraction from 3D whole body with [TC]² NX-12

The coordinates for joint locations are saved into a “.joint” text file which can again be opened with a word processor application to extract relevant joint coordinates i.e. shoulder, elbow and wrist joint. A CAD software package called Pro-Engineer Wildfire 4.0 (PTC, 2011) was used to study the 3D scanned arm data along with its joint locations. Figure 60 shows a 3D scanned arm and its joint location. Using the joint locations, the upper arm and lower arm “bones” could be created by connecting the shoulder joint to the elbow joint and the elbow joint to the wrist joint, respectively (see the rightmost figure in Figure 60). From this point forward, the term “bone” is used to signify a 3D line that is created by connecting two joints. The method to determine the joint locations is a trade secret of the [TC]² NX-12 body scanner software and, as such, its reliability cannot be ascertained within the scope of this thesis.



Figure 60. A 3D scanned arm with its joint location in Pro-Engineer Wildfire 4.0 and bones which are created from them

5.3 Analysis of 3D data capture integration into the Shen et al. (1994) method

The next step for the first design phase was to analyze the application of this 3D body data into the Shen et al. (1994) method. As shown in Figure 57, the analysis comprised of three parts i.e. bones, cross section generation and level of flesh deformation application. During this stage, simplification was avoided wherever possible. This was based upon the assumption that applying simplifications at this early stage would lead to reduced accuracy as the method develops, which is undesirable in this research.

5.3.1 Bones

Through the use of the automatic capture of joint locations from the 3D scan data, a carrying angle could be observed, as shown in Figure 62. A carrying angle is created by the longitudinal axis of the lower arm bone and the plane perpendicular to the flexion/extension axis. It is caused by the tilt in the flexion/extension axis at the humerus - ulna joint and the angulations of the ulna itself (see Figure 61). The carrying angle tends to be larger in females than males and the range is about 10-20 degrees. Typically the angle decreases as the arm is flexed (Van Roy et al., 2005). In order to

achieve more accuracy, this research would attempt to include the carrying angle into the proposed FDM. This is in contrast to the method of Shen et al. (1994) which omitted the carrying angle because they specified the location of the bones manually (from their own created body models) and hence location of the bones were not necessarily anatomically correct.

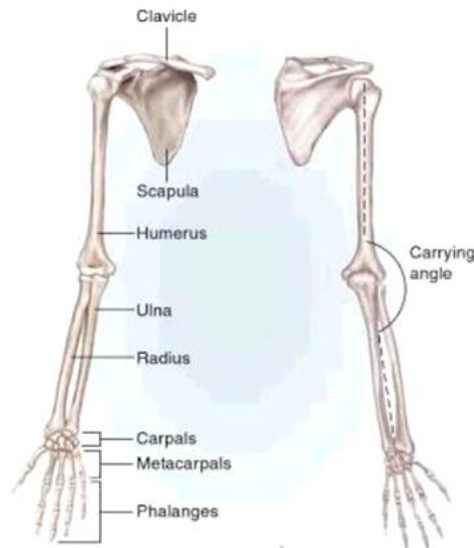


Figure 61. Anatomy of the upper and lower arm and the carrying angle which is created from ulna and humerus (adapted from Watkins (2010))

In Shen et al. (1994), the upper and lower arm bones were used to create a common plane e.g. in the case of the elbow, a plane which contains both upper and lower arm. The role of the common plane is to assist in creating the planes on which cross sections would be located. By ignoring the carrying angle, the common plane orientation would be constant. This is because the angle between the longitudinal axis of the lower arm and the plane perpendicular to the flexion/extension axis stays the same throughout the flexion-extension of the lower arm. On the contrary, the decision to include the carrying angle means that the common plane orientation has to be recalculated throughout the flexion-extension of the lower arm. Fortunately, the common plane could easily be recalculated (using a cross product of vectors) and would less likely affect the processing time of the proposed FDM.

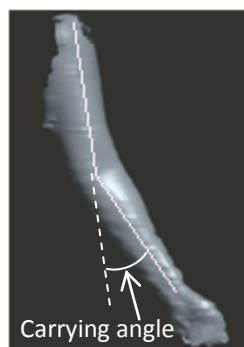


Figure 62. 3D arm data from a 3D body scanner preserves the carrying angle

5.3.2 Cross Sections

The use of cross sections, which form the main core of the Shen et al. (1994) method, requires consideration of several underlying aspects i.e. acquiring cross sections, location and number of cross sections, cross section planes, an optimum sampling number of cross sections and cross section deformation. Each of these is discussed in context of 3D body data in the following subsections.

5.3.2.1 Acquiring cross sections

Shen et al. (1994) acquired each cross section by using a number of rays, originating at the bone, which intersect the polygon surface from their own created human body model. The intersection points were then used to create a cross section. A mini study was performed to validate the suitability of their approach for acquiring cross sections from 3D body data. A fully extended 3D scanned arm, captured from the [TC]² NX-12, was used in this study. Following their approach, acquiring a cross section was done by intersecting the scanned arm surface with rays which were located on a plane and originated from a chosen point along the skeleton bone/segment. There was no restriction applied to the plane's orientation and location as the purpose of this mini study was purely to confirm Shen et al. (1994) cross section acquisition approach. Figure 63 shows that the rays are located on a plane and originate from a point along the upper arm bone. Once these rays are intersected with the facets of the 3D scanned arm, the sampled points are obtained and used to create the cross section for that particular location and orientation.

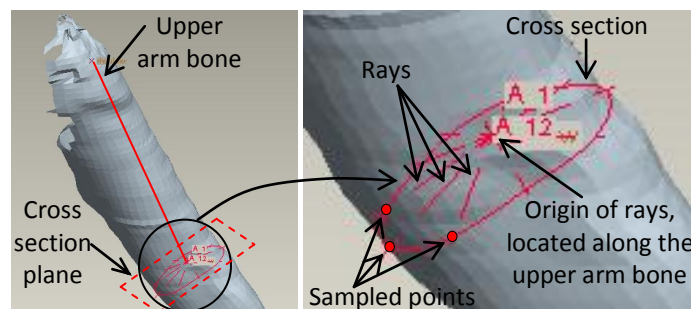


Figure 63. Rays, originating from a point along the upper arm segments, were intersected with the scanned arm surface (facets)

The vrml file from the [TC]² NX-12 provides the vertex coordinates and their connectivity relationship. The left figure in Figure 64 shows a facet of a 3D scanned arm with its three vertices being connected. However, to perform cross section acquisition, the normal vector of each facet is required (see Figure 64b). Pro-Engineer Wildfire 4.0 was utilised by re-saving the 3D scanned arm as a VRML file which allowed automatic provision of normal vectors. Alternatively, the 3D scanned arm could also be saved as an STL (STereoLithography) file which also provides lists of unit normal vector and vertices of polygons (Gibson et al, 2010).



Figure 64. (a) A facet of a 3D scanned arm polygonal surface. (b) A facet with its normal vector

The normal vector of each facet could be calculated manually if Pro-Engineer is not available. The following pseudo code described the steps to obtain the normal vector of each facet.

```

Read vertex connectivity relationship
Count the number of facets ( $n$ )
For  $i = 1 \dots n$ 
    Extract vertex coordinates for the  $i$  facet ( $v_i^{c1}, v_i^{c2}, v_i^{c3}$ )
    Calculate the unit vector for  $\overrightarrow{v_i^{c1}v_i^{c2}}$ 
    Calculate the unit vector for  $\overrightarrow{v_i^{c1}v_i^{c3}}$ 
    Calculate the normal vector (cross product between  $\overrightarrow{v_i^{c1}v_i^{c2}}$  and  $\overrightarrow{v_i^{c1}v_i^{c3}}$ )
    Save the normal vector for the  $i$  facet
End

```

In Matlab 7.0, a numerical computing tool that allows computation, programming and visualisation (The MathWorks, 2011), each ray was tested against the normal vector of each facet. If the ray is not perpendicular to the normal vector of the corresponding facet i.e. the ray is not parallel with the facet, a further check is performed to learn where the intersection will occur. This check is required because the ray is expressed as an infinite line equation in 3D even though it is actually a vector with a certain direction. Figure 65 illustrates how intersecting a ray with the facets from the 3D scanned arm result in 2 intersection points.

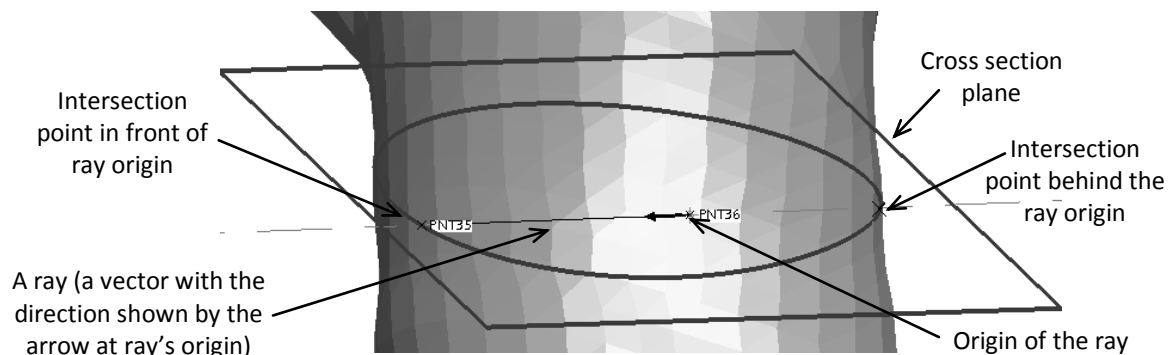


Figure 65. Illustration which shows that for each ray, two intersection points could be acquired i.e. intersection point in front of and behind the ray origin; only the intersection point in front of the ray origin is used

The process is shown in the following pseudo code:

```

For i = 1 ... number of rays
    While intersection point is not found
        For j = 1 ... number of polygon
            Check if i ray vector is perpendicular to the normal of the j facet
            If false
                Check if the intersection is located in front of the ray origin
                If true
                    Calculate intersection point
                    Check if the intersection point is located inside the j polygon
                    If true
                        Save the intersection point
                    If false
                        Go to j+1 polygon
                If false
                    Go to j+1 polygon
            If true
                Go to j+1 polygon
        End
    End
    Go to i+1 ray
End

```

The procedure shown in the pseudo code above was tested on the fully extended 3D scanned arm. The purpose of this test is to confirm the functionality of the algorithm above. Firstly, the number of the rays had to be determined. Any set number of rays could be used as any chosen number of rays will not affect the outcome of the test. For this purpose, 16 rays, which originated from a point along the upper arm bone, were created and used to determine sampled points i.e. intersection points with the facets. The pseudo code was successful in obtaining a set of sampled points from the aforementioned 3D scanned arm, as shown in Figure 66. These sampled points could then be used further to create a cross section through the use of spline function (see section 2.3). Thus, the result of the mini study shows that the Shen et al. (1994) cross sections acquisition approach is applicable for 3D scan data.

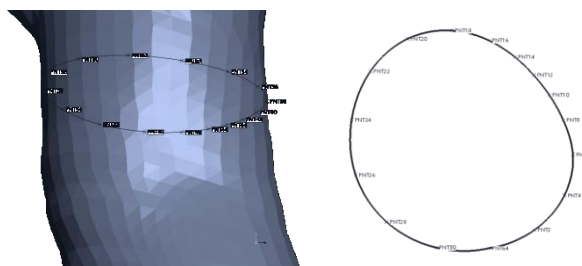


Figure 66. Obtaining intersection points by employing the pseudo code to create a cross section with the spline function

5.3.2.2 Location and number of cross sections

The Shen et al. (1994) method located the cross sections at a uniform distance from each other (see Figure 67). The distance between the cross sections is arranged so that no intersection between cross sections occurs at any time during flexion-extension movements.

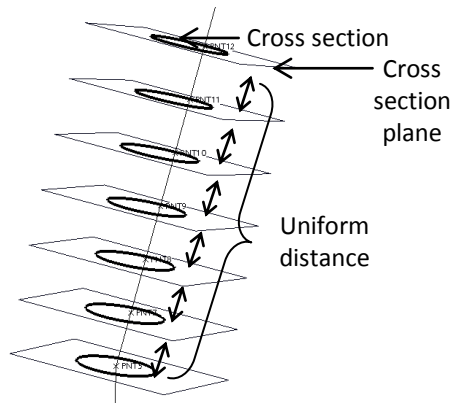


Figure 67. Uniform distance between cross sections

The proposed method in this research aimed to achieve a real time solution and yet accommodate different body types and sizes, therefore it was desirable to minimise the number of cross sections. Unlike acquiring cross sections in the previous subsection, determining the location and number of cross sections is far more complex. At this stage, the need to optimise the number and location of cross sections was identified. However, an in-depth study to determine an optimum number of cross sections and the locations for them was carried on later in this research.

5.3.2.3 Cross section planes

Each of the cross sections in Shen et al. (1994) method is placed on a plane. The plane orientation of a cross section largely depends on its location i.e. whether it is a cross section along a bone or a cross section at the joint. Details for each case and their suitability with 3D scan data are discussed separately below.

For a cross section that is located along a bone, its plane's orientation is determined by the orientation of the planes at both ends of the bone. For example, in the left image in Figure 68 the orientation of a cross section's plane at i (N_i) depends on the plane's orientation of cross sections at N_u and N_0 . Shen et al. (1994) described the plane orientation at N_i as: $\frac{\angle N_u N_0}{n+1} \times i$, where n is the number of cross sections between N_u and N_0 and i is the angle between the orientation of planes at N_u and N_0 . This equation demonstrates that the orientation of cross section planes which are located in between the two end planes is determined by the linear interpolation of the angle between the two end planes. For instance, in the case shown in the right image in Figure 68, if there are 9 cross sections in between the two end planes and the angle difference between the end plane 0 and end plane 1 is 30° , the interpolation angle between two adjacent cross sections would be 3° .

(calculated by dividing the angle over the number of cross sections plus 1). Figure 68 illustrates the final orientation of the cross section planes. As this approach did not show any potential conflict with the utilisation of 3D scan data and DHM specifications, it had the potential to be incorporated in the proposed FDM.

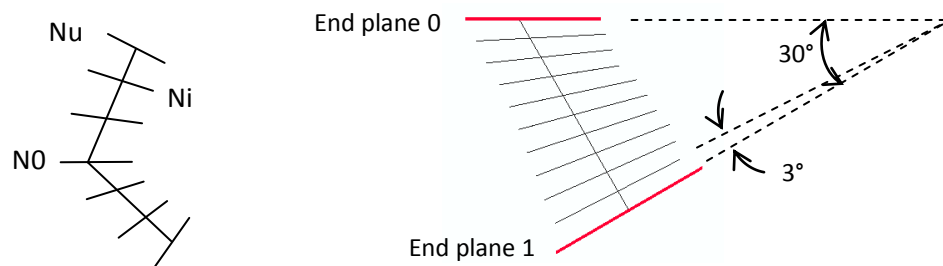


Figure 68. Illustration of the interpolated planes for cross sections along a bone

For a cross section that is located at the joint i.e. a meeting point between two bones, its plane orientation is determined by the two bones e.g. the upper and lower arm bones for a cross sections at the elbow joint. The plane orientation at the joint is the average of the angle between the two bones. Shen et al. (1994) called this plane orientation the “bijective plane”. Figure 69 shows the plane orientation at the elbow (end plane 0). No suggestion was found in their research with regards to whether the concept of bijective plane was based on observation of actual flesh deformation or not. However, there was a possibility that their concept of bijective plane was not based on accurate representation of flesh deformation since their method was aimed mostly to create a realistic, but not necessarily accurate, flesh deformation. As this research intended to achieve both accuracy and realism, a mini study was performed to validate and gauge the suitability of Shen et al. (1994) bijective plane concept. If the bijective plane concept for the elbow plane orientation is true, then the ratio of the upper arm-elbow angle (α) and arm angle (2α) would remain constant i.e. 0.5, throughout the range of the arm movement (see Figure 69).

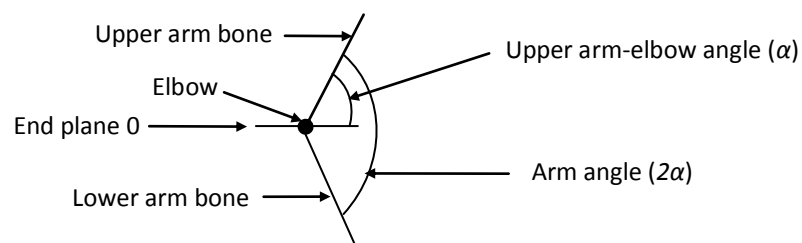


Figure 69. Illustration of the bijective plane at the elbow and end planes at the wrist and shoulder

To investigate whether this ratio remained constant, this mini study required a methodology concerning how to determine the actual elbow plane orientation. A visual observation shows that a crease is developed at the anterior of the elbow as the elbow flexes. Figure 70 shows a set of photographs of the crease development. This crease becomes more prominent as the arm reaches

maximum flexion. Based on this visual observation, it was assumed that the crease at the anterior of the elbow was a possible identifier of the orientation of the cross section at the elbow. Together with the elbow joint, the crease at the anterior of the elbow was used to create the elbow plane orientation.

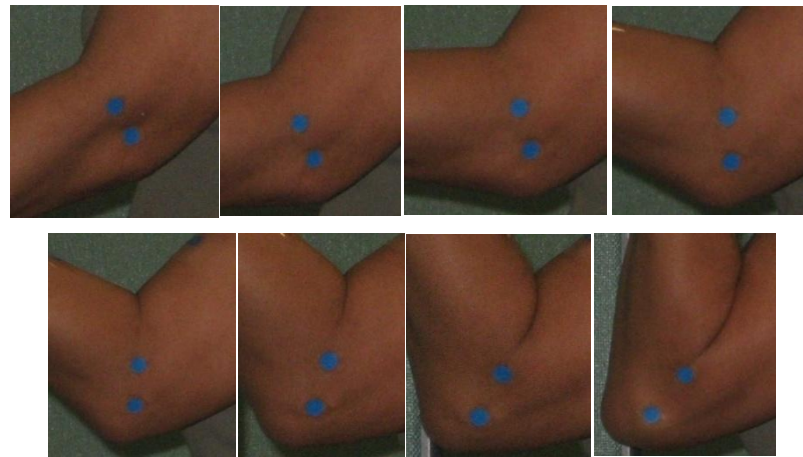


Figure 70. Creases development as the arm flexes

Ideally, a study should attempt to include as many participants as possible to provide an accurate representation of the population of interest. However, considering the fact that this study was a mini study which served to direct the core of the research, a limited number of participants was deemed to be sufficient. Although the participant number was limited, the participant choice attempted to represent different body sizes and shapes. Nonetheless, a limited number of participants meant that the mini study results might not be directly applicable to represent the population of interest.

Five participants, three males and two females, took part in the mini study. All of the participants were of Asian race and represents different body sizes/shapes with a height range of 143–180 cm and a weight range of 45–73.9 kg. The participants were asked to perform a series of extension-flexion movements and a series of photographs of their arms were taken. The photographs were taken from the side of the body (Figure 71). This extension-flexion movement was guided by a board in an attempt to constrain both the upper and lower arm parallel to the board at all times. The camera was also parallel to the board and set to maximum zoom. This approach was taken to minimize parallax effects on the photograph. Joints were identified via manipulation and markers were attached on the joint locations i.e. the shoulder, elbow and wrist, prior to the photograph shots. The photographs were then analysed in Pro-Engineer WildFire 4.0, as shown in Figure 72a. Based on the markers, the upper and lower arm bones are drawn and the angle between these two bones is measured ($\text{arm}_{\text{angle}}$). Next, the line which determines the plane orientation at the elbow, similar to that of “end plane 0” in Figure 69, is drawn according to the

elbow crease methodology established earlier. Once this line is drawn, the angle between this line and upper arm is obtained (upper arm-elbow_{angle}). Examples of elbow plane orientation in different arm postures are shown in Figure 72b.

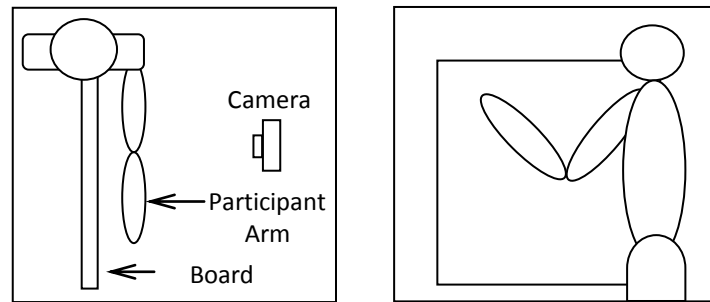


Figure 71. Experimental setting for the mini study (top view, side view)

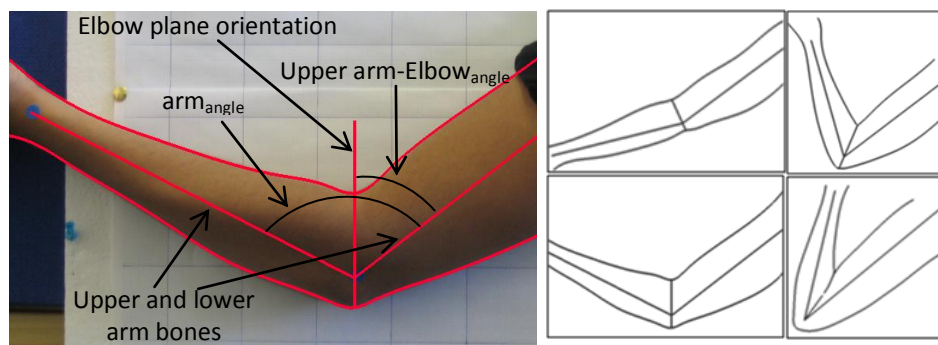


Figure 72. (a). Photograph analysis shows the arm bones, elbow line, upper arm-elbow_{angle} and arm_{angle} (b). Elbow plane orientation for different arm postures

A ratio between upper arm-elbow_{angle} and arm_{angle} was then calculated to show the relationship between upper arm-elbow_{angle} and arm_{angle}. As was discussed earlier, if the Shen et al. (1994) bijective plane concept is not a mere simplification, the ratio between upper arm-elbow_{angle} and arm_{angle} will remain constant i.e. 0.5, for all arm angles. Figure 73 shows the ratio between upper arm-elbow_{angle} and arm_{angle} for five participants. It shows that the elbow plane orientation does not follow the bijective plane concept i.e. that it is constantly located at the angle which is the average value between the upper arm and the lower arm angle. In fact, Figure 73 shows that the elbow orientation plane would get closer to the upper arm as the arm approaches maximum flexion, which is also shown in the bottom right figure of Figure 72b. Thus, based on the underlying assumption of elbow plane orientation determination, the bijective plane concept in the Shen et al. (1994) method is an over simplification. As this research aimed to achieve flesh deformation at the elbow with accurately, the bijective plane was not adopted and the relationship which was found in this mini study would be employed. Figure 73 also shows high degree of correlation in the ratio progression between the participants which addresses some of the potential concerns with the small sample.

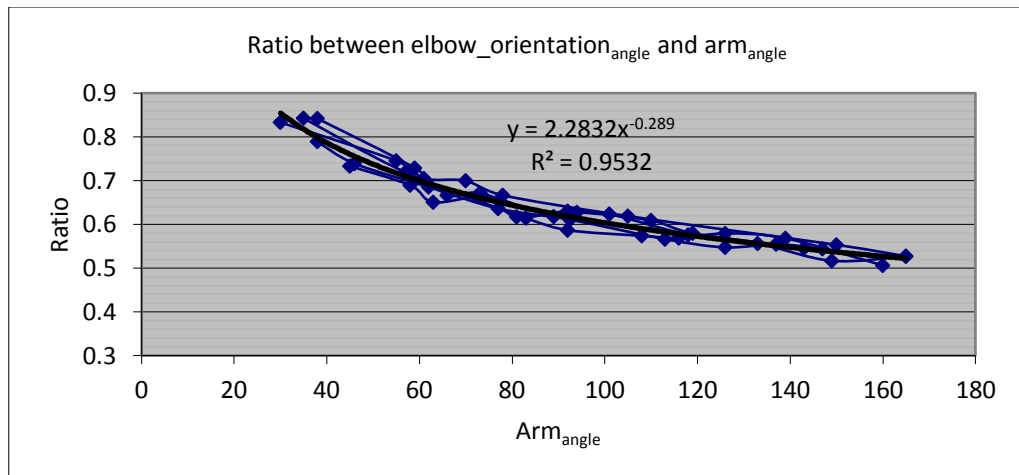


Figure 73. The relationship between elbow line_{angle} and arm_{angle} shows that the ratio changes as the arm flexes

5.3.2.4 Optimum sampling number of cross sections

Each cross section was represented by a number of points through which a B-spline curve was passed. Shen et al. (1994) did not specify clearly the number of sampling points to create a cross section. However, even if they had specified the number of sampling points, there is still a possibility that it would not be appropriate as their method utilises their own created body model whereas in this research 3D body data will be used. Therefore, the sampling number of points to create the cross section needed to be investigated in this research. The sampling number investigation should take into account relevant DHM specifications i.e. accuracy and speed. The sampling number should be kept to a minimum in order to achieve a real time flesh deformation at the joint and yet keeping the information lost to a minimum as well. Thus, the aim was to determine an optimum number of points which balanced the speed and accuracy. As with the number and locations of cross sections, the need to investigate this issue was acknowledged and would be addressed in the subsequent design phase.

5.3.2.5 Cross section deformation

In Shen et al. (1994), each cross section was deformed based on the concept that no intersection was allowed between cross sections by adjusting the orientation of the cross section planes (see the mid and rightmost figures in Figure 74).

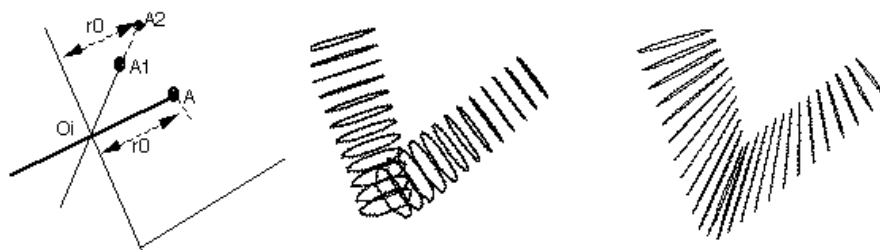


Figure 74. Cross section deformation in Shen et al. (1994) (adopted from Shen et al. (1994))

An additional process is introduced to avoid volume squashing by introducing a scale factor for sampling points at the corresponding cross sections. The scale factor will ensure that the sampling points' distances to the bone are kept constant. For instance, the original distance of point A, a point which belongs to a cross section, from the bone is r_0 . As the arm flexes, the cross section plane changes its orientation and causes rotation of the point A to A1. Because point A1's distance to bone is less than r_0 , the A point is then moved to A2 (see the leftmost figure in Figure 74). Although the scaling factor could stop the arm volume from squashing, the scale factor would not necessarily be able to represent the changes of the flesh deformation, especially at the elbow area, accurately. Therefore, Shen et al. (1994) introduced an additional "swell" function i.e. a sine function, which is used on the scaling factor where the region on the anterior part of the upper and lower arm should swell (see the rightmost figure in Figure 74). As no swell function is applied on the posterior of the lower and upper arm the profile for this form would retain its shape throughout the extension-flexion movements.



Figure 75. Flesh deformation changes at the posterior of the upper arm as the arm was flexed

To find out whether this was another simplification by their method, a set of photographs, the same set of as those from the mini study for cross section planes (5.3.2.3), were used. Figure 75 illustrates the outline of the elbow from the photograph set which shows that the posterior of the lower and upper arm indeed changes during flexion of the elbow. Therefore, based on the observation result and the fact that the Shen et al. (1994) cross sections adjustment is largely based on a crude approximation of actual flesh deformation at the elbow, this research would not apply their method in deforming the cross sections.

As their approach was not chosen to deform the flesh around the elbow, another alternative to govern this element of the flesh deformation was required. In section 4.2, where existing flesh deformation methods were compared with the DHM specification, one of the strengths of the "shape by example" approach is its ability to produce flesh deformation without user intervention. The key for the shape by example approach is providing a set of posture examples which could then be used to produce a new posture through interpolation of the examples. The example set consists

of the initial state, end state and any state in between these two extreme states. This principle could be applied to deform the cross sections by providing examples of cross sections in various postures. Other approaches, such as the anatomic and physical approaches achieve flesh deformation by contracting and relaxing muscles under the skin. This is a totally different approach in comparison to the proposed FDM where the flesh deformation is achieved by adjusting and deforming the shape of the cross sections. Hence, they would not be suitable as an alternative method to govern flesh deformation. The decision to drive flesh deformation by the adjustment of the cross sections' shape through example interpolation means that this research would need to establish a set of cross section examples. This issue would be addressed in the subsequent design phase.

5.3.2.6 Region for flesh deformation application

As described in section 5.3.2.5, Shen et al. (1994) method used a combination of cross sections' scaling and a sine function to simulate flesh deformation. The scaling and sine function were applied on the area of the arm where flesh deformation was required to create a realistic flesh deformation. Their research did not specify this area. It was probable that, as their method is aimed to achieve a realistic flesh deformation, this area was determined intuitively. Thus, this area was not necessarily representing the true area in which flesh deformation occurred. As this research aimed to achieve accuracy and realism modelling, their approach would not be suitable for this research. This decision resulted in the need to resolve the next issue i.e. determining the extent of the flesh deformation area at the elbow. This introduced two research questions:

- Does the whole upper and lower arm deform during extension-flexion of the arm?
- What area of the elbow deforms the most?

Thus, this research would need to establish the boundaries of the flesh deformation at the elbow. This formed a further issue to be explored at the next design phase.

5.4 Summary

Evaluation of the Shen et al. (1994) method revealed that their approach has significant merit in establishing a FDM that meets the requirements of the DHM specification outlined earlier. The evaluation also revealed that the limitations of their method need to be addressed through a series of modifications and development studies. There were various reasons that prompted the need for further modifications and studies. These reasons were as the following: (i) the introduction of the 3D scan data; (ii) some issues were not sufficiently detailed enough in the Shen et al. (1994) method; and (iii) some issues required adjustments in order to satisfy the DHM specifications for flesh deformation. Issues which had been investigated could be categorised into three major parts

i.e. bones, cross section generation and region for flesh deformation application. The following bullet points summarise and provide a brief outline of the evaluation outcome for each issue:

- Determining the carrying angle

The Shen et al. (1994) method omits the carrying angle whereas this research aims to preserve it in order to avoid simplification at this early stage. Thus, an investigation on how to integrate the carrying angle into the new FDM was required.

- Determining a set of examples to govern the flesh deformation

This arises as the Shen et al. (1994) approach in deforming cross sections is unsuitable, as shown in section 5.3.2.5. Hence, the new FDM endeavoured to apply interpolation which required capturing a set of suitable examples of the elbow in different postures.

- Determining cross section properties

As with Shen et al. (1994), cross sections are the core of the new FDM. The first issue which needed to be dealt with was how to acquire the cross sections. This issue had to be established first as it was impossible to deal with other cross section properties without having the cross section to begin with. The next step was to deal with cross section planes, cross section deformation, and the optimum sampling number of the cross sections.

- Determining boundaries of the flesh deformation application at the elbow

The Shen et al. (1994) method applied flesh deformation at the elbow intuitively and was not necessarily based on the true region where flesh deformation occurred. This approach suited their aim i.e. creating a realistic flesh deformation. However, as this research required accuracy and realism, an investigation to determining the boundaries of elbow deformation i.e. the extent of the elbow area which undergoes flesh deformation and needs to be modelled, was required.

These issues were explored in the second design phase.

6 Second Design Phase

The second design phase is the actual phase where the proposed FDM was built. The DHM specifications were used to assist the decision making process to ensure that the proposed FDM was suitable for ergonomics CAD, as shown in Figure 76. Relevant DHM specification(s) were considered in resolving each issue.

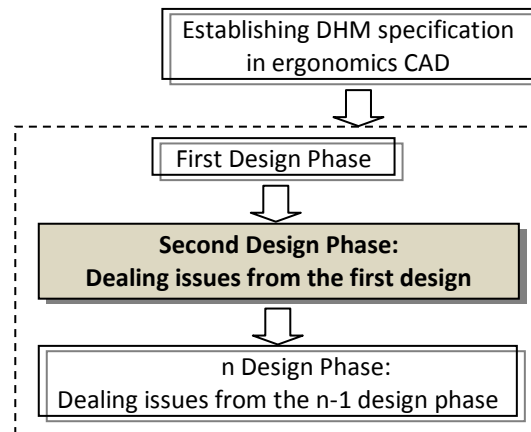


Figure 76. Second phase, relatives to other stages in the research

The first design phase revealed 4 issues which had to be dealt with in the second design phase. These four issues were: i) determining the carrying angle; ii) determining a set of examples to govern the flesh deformation; iii) determining cross section properties; and iv) determining the boundaries of the application of flesh deformation at the elbow (see section 5.4). Figure 77 shows details of the strategy to explore these issues. The strategy shows the order of how these issues were approached and the relationship between them.

The carrying angle determined how the upper and lower arm bones moved with respect to each other and would be addressed first as it is independent from other issues. The next issue to be examined was determining boundaries of the local deformation at the elbow. This had to be established early because it determined the area from which the cross sections should be obtained. It was essentially setting the limits of the flesh deformation modelling at the elbow.

The last two major issues to be examined were determining cross section properties and a set of examples to govern the flesh deformation. The first design phase highlighted the idea that a set of examples would be used to govern the flesh deformation. Setting examples to govern the flesh deformation had to be resolved before determining cross section properties because it ensured that the cross section properties were determined based on a suitable choice of arm postures. The set of examples were essentially cross sections which would be used as references to create a new cross section through interpolation. There were two sub issues to deal with in setting up examples to

govern the flesh deformation i.e. defining postures to derive the cross section examples and establishing a method to obtain the cross section examples from the pre-determined postures. Providing that the 3D scan data could be used to acquire cross sections, this chapter would not discuss the method to obtain the cross section examples from the pre-determined postures as the Shen et al. (1994) method had been established as a suitable approach in section 5.3.2.1.

As the cross section is the core of the proposed FDM, this issue dominated most of the second phase design. The choice of number, location, and orientation of the cross sections were largely dependent on the plane on which the cross section was situated. Once the cross section properties were established, an optimum number of cross sections would be determined. The final step of the second design phase was to perform interpolation of the cross sections.

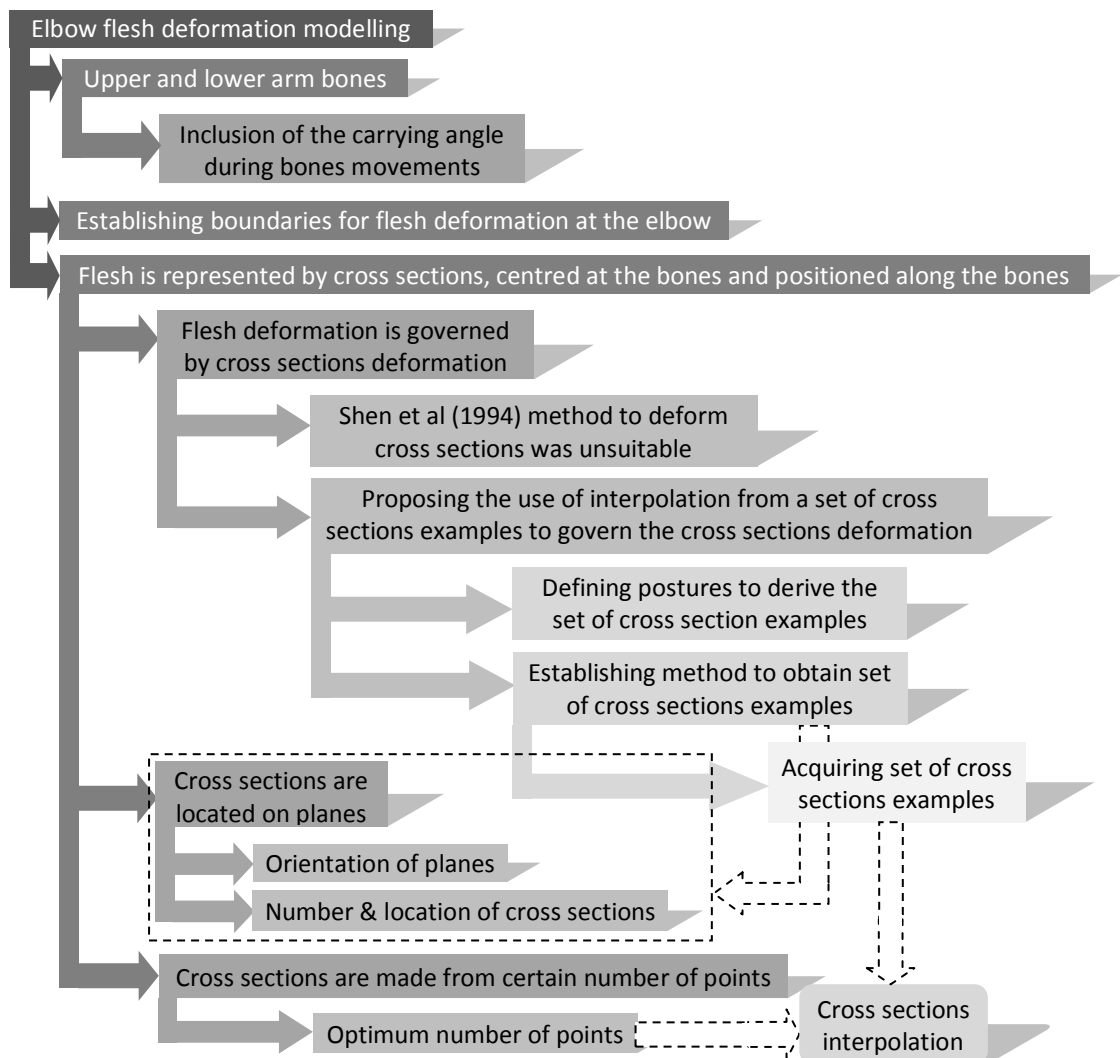


Figure 77. Strategy for second design phase

In addition to providing details of the strategy to explore issues from the first design phase, Figure 77 also implicitly outlines the proposed FDM. The strategy revealed that the proposed FDM was based on deforming cross sections to simulate flesh deformation. The cross section

deformation was led by interpolation from a set of cross sections examples which was acquired from chosen arm postures. The cross sections, created from an optimum number of points, were located on planes which were centred on either the upper or lower arm bones. The movement of the upper and lower arm bones would take the carrying angle into consideration and thus replicated this characteristic in the flesh deformation.

6.1 Determining the carrying angle

In section 5.3.1, which looked into the bones for the elbow, it was found that the automatic joint location from the [TC]² NX-12 preserved the carrying angle of a fully extended 3D scanned arm. In line with the endeavour to achieve accurate DHM flesh deformation, it was decided that the carrying angle would be incorporated into the proposed FDM. Firstly, a mini literature study was performed to establish facts regarding the carrying angle. Based on the information from the mini literature study, a strategy to determine the carrying angle would be developed and followed accordingly.

6.1.1 A mini literature study on the carrying angle

Recalling some of the information already outlined in the section 5.3.1, the carrying angle is created by the longitudinal axis of the forearm and the plane perpendicular to the flexion/extension axis. The carrying angle of the elbow can be measured with a protractor goniometer or X-ray images and is measured while the arm is fully extended and the wrist is in supination (Van Roy et al., 2005). Van Roy et al. (2005) also pointed out considerable differences in reported carrying angle values as a result of different measuring methods. They briefly described various means of measuring the angle which are quoted in the following:

“(a) the longitudinal axes of the arm and the forearm, (b) the longitudinal axes of the humerus and the ulna, determined on X ray, (c) the longitudinal axes of the humerus and the ulna determined on X rays by means of the construction of two midpoints at both the distal humerus and the proximal ulna, (d) the medial tangential lines to the humerus and the ulna, determined on X rays, (e) the longitudinal axis of the ulna and a perpendicular line to the transepicondylar line, and (f) the longitudinal axis of the ulna and a line perpendicular to the axis of the elbow flexion.”

This finding suggested that, in order to measure a carrying angle, this research needed to decide which measuring methods should be used.

A study by Khare et al. (1999) reported that the carrying angle is affected by the length of the lower arm bone. A shorter lower arm bone results in a greater carrying angle. Assuming that the length of the lower arm bone is proportional to body height, the shorter the person, the greater the

carrying angle. Van Roy et al. (2005), Zampagni et al. (2006) and Zampagni et al. (2008) supported earlier findings regarding the carrying angle differences between females and males. Their studies suggested that the carrying angle is larger in females than males. These findings suggested that a carrying angle is specific for each individual as it depends on individual's body size and gender. Thus, in order to represent a carrying angle accurately, this research needed to capture the carrying angle for each individual of whom a flesh deformation at the elbow was to be modelled.

Several studies, such as Goto et al. (2004), Paraskevas et al. (2004), Van Roy et al. (2005), Zampagni et al. (2006) and Zampagni et al. (2008), also confirmed earlier findings in which the carrying angle presents a linear variation during the flexion-extension movement. To capture the linear decrement of the carrying angle during the flexion-extension movements, a specific and complex measurement set up is required. For instance, Zampagni et al. (2006) used a VICON Motion System 460 optoelectronic system whereas Van Roy et al. (2005) added sensors to the goniometer and devised software that tracked the sensors orientation and movement. In another study, Goto et al. (2004) combined the use of MRI and a special posture device. These findings suggested that, although linear decrement of the carrying angle during the flexion-extension movement was measurable, it required a complex measurement set up. This research needed to consider whether to pursue this complex measurement set up or to propose an alternative approach for representation of the carrying angle's linear decrement.

6.1.2 The strategy to determine the carrying angle

The literature review has shown that the carrying angle decreases linearly as the arm flexes. As it had been described briefly in the literature review, supplying this information requires a complex and comprehensive measurement. Performing this measurement would certainly provide more accurate information which addresses one of the DHM requirements i.e. accuracy. Although it is possible to perform this measurement, this research would not perform a complex and comprehensive measurement to depict the carrying angle behaviour during the flexion-extension movements. The proposition was that an in-depth and complex measurement of the carrying angle's linear decrement was disproportionate to the main aims of the research, especially considering the limited resources of this research. Therefore, an alternative approach to represent the carrying angle's linear decrement would be proposed. To support the alternative approach, available data from the carrying angle studies discussed above would be used, in particular Van Roy et al. (2005) who reported their study results in detail.

The literature review has shown that each individual has a specific value of carrying angle. This suggested that carrying angle measurement was required to represent each individual accurately. The literature review also demonstrated that there were various measuring methods to capture the

carrying angle, ranging from simple ones to complex ones. This suggested that, as this research had options to choose from the range of measurements, given a single 3D scan data of a fully extended and pronated arm from an individual, there was a possibility for its carrying angle information extraction. Thus, based on this consideration, this research would perform the carrying angle measurement for fully extended and supinated arm. Figure 78 illustrates the strategy to determine the carrying angle which eventually led to the carrying angle integration into the upper and lower arm bones movement.

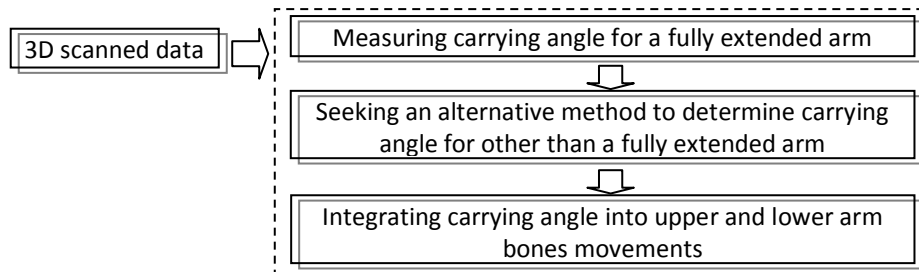


Figure 78. Detail steps on carrying angle determination

6.1.3 Determining the carrying angle for a fully extended and pronated arm

The previous subsection highlighted the reason why the carrying angle would only be captured from the fully extended arm. This section outlines how carrying angle from a 3D scan of fully extended arm would be measured. There were two important issues to be addressed i.e. (1) which measuring method to be adopted and gathering information on how to perform the adopted method; and (2) how to adjust the adopted method to suit the nature of 3D scanned arm. The first issue was related with the finding of the mini literature review in section 6.1.1 which showed that the carrying angle could be measured in various ways. In this research, the carrying angle measurement for a fully extended arm would be performed by measuring the angle between the longitudinal axes of the arm and the forearm i.e. the upper arm bone and the lower arm bones. This approach was chosen because the axes of the arm and forearm could be extracted easily from 3D scanned arm, as explained in section 5.2 which showed that the automatic provision of joint location by the 3D scanner allows the upper and lower arm bones to be created. Also, the method of measurement chosen was less complex in comparison to other methods that were described by Van Roy et al. (2005) in section 6.1.1. Golden et al. (2008) described the manual measurement of a carrying angle as the following:

“The goniometer was placed on the anterior surface of the upper limb and was aligned with the ulna distally, the goniometer's hinge with the cubital fossa, and the humerus proximally.”

The manual measurement technique implied that the measurement of carrying angle should be performed on the anterior surface of the arm. The manual measurement also implied that the projection of the upper and lower arm bones on the anterior surface of the arm was used to measure a carrying angle. These two requirements could easily be determined by performing visual and tactile observations on the arm. However, as these types of observations were either restricted to be performed on a 3D scanned arm, adjustments were required to suit the nature of 3D scanned arm. As the projection of the upper and lower arm bones on the surface of 3D scanned arm would be complex, the bones would be projected on a 3D plane instead. Thus, a plane that approximated the relevant anterior surface of the arm was established. To mimic the anterior surface of the arm, the 3D plane was defined as a 3D plane that was perpendicular to the orthogonal side view of an arm with a neutral (0°) flexion and medial-lateral rotation of the shoulder. This requirement was easily fulfilled as a person to be scanned with the [TC]² NX-12 should adopt a neutral (0°) flexion and medial-lateral rotation of the shoulder.

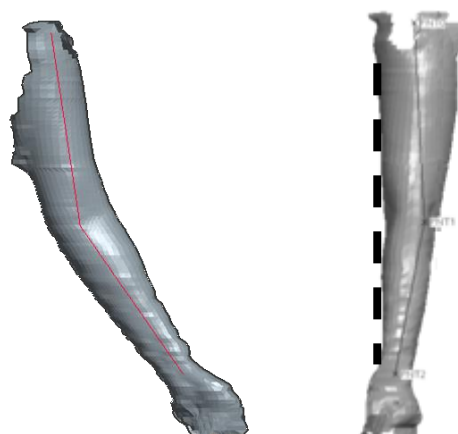


Figure 79. A 3D arm data from a 3D body scanner preserves the carrying angle

To investigate the proposed approach, a participant was scanned with the [TC]² NX-12 while her arm was fully extended arm and wrist was supinated. The orthogonal front view of a 3D scanned arm data along with its joints are shown in the left image in Figure 79 whereas the orthogonal side view of the 3D scanned arm is shown in the right image. As described above, the 3D plane was defined as a 3D plane that was perpendicular to the orthogonal side view of a 3D scanned arm. The right image in Figure 79 shows the orientation of the 3D plane that is perpendicular to the orthogonal side view and illustrates how it approximated the anterior surface of the 3D scanned arm.

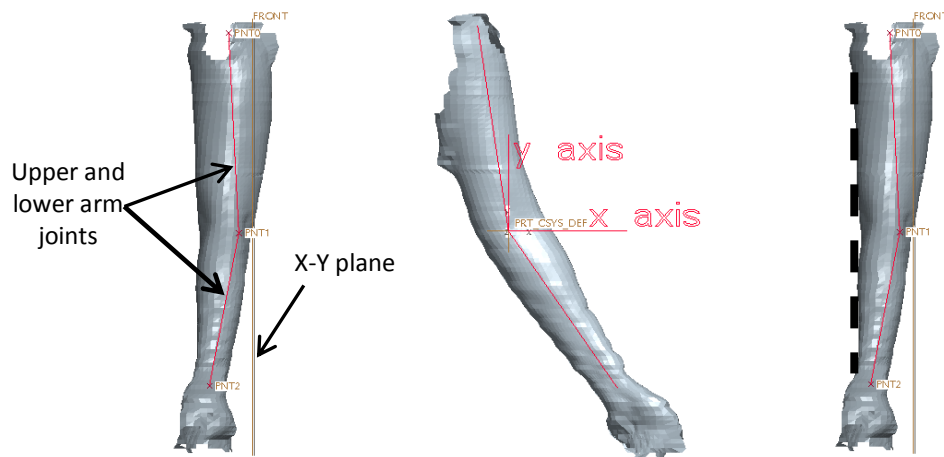


Figure 80. X-Y plane for carrying angle measurement and X-Y axis with respect to the arm

The 3D plane that was perpendicular to the side view of the 3D scanned arm was essentially the X-Y plane of the 3D CAD coordinate system. Figure 80 shows the X-Y plane and X-Y axis with respect to the 3D scanned arm. To enable the carrying angle measurement, the upper and lower arm bones were projected on the X-Y plane. Figure 81 shows the projection results and how the carrying angle was measured.

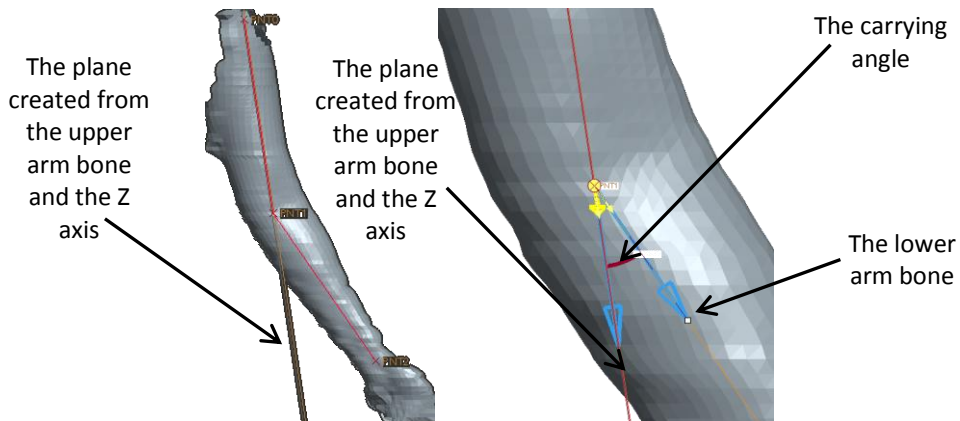


Figure 81. The carrying angle is measured from an additional plane and the lower arm bone

6.1.4 Determining the carrying angle for a posture other than a fully extended and pronated arm

The decision to limit the carrying angle measurement only for a fully extended arm prompted the need to seek an alternative way to determine the carrying angle for other arm postures. An alternative way was proposed by utilising existing data which was available through other studies to approximate the carrying angle for other postures. While undertaking the mini literature reviews in section 6.1.1, one of the studies i.e. Van Roy et al. (2005) reported their study result in detail.

Table 5. Van Roy et al. (2005) data

Carrying angle	Female	Male
Full extension	Minimum = 11.9, maximum = 21	Minimum = 4.2, maximum = 15.1
Full flexion	Minimum = -0.7, maximum = 3.9	Minimum = -1.1, maximum 5.8

From the measurements of 10 female and 10 male participants, they reported the following data. For females, the minimum carrying angle for a full extension was 11.9° with a range of 9.1°, whereas the minimum carrying angle for a full flexion was -0.7° with a range of 4.6°. For males, the minimum carrying angle for a full extension was 4.2° with a range of 10.9°, whereas the minimum carrying angle for a full flexion was -1.1° with a range of 5.8°. Table 5 summarises the results. Utilising these data, together with the knowledge that the carrying angle varies linearly from extension to flexion a carrying angle approximation was devised.

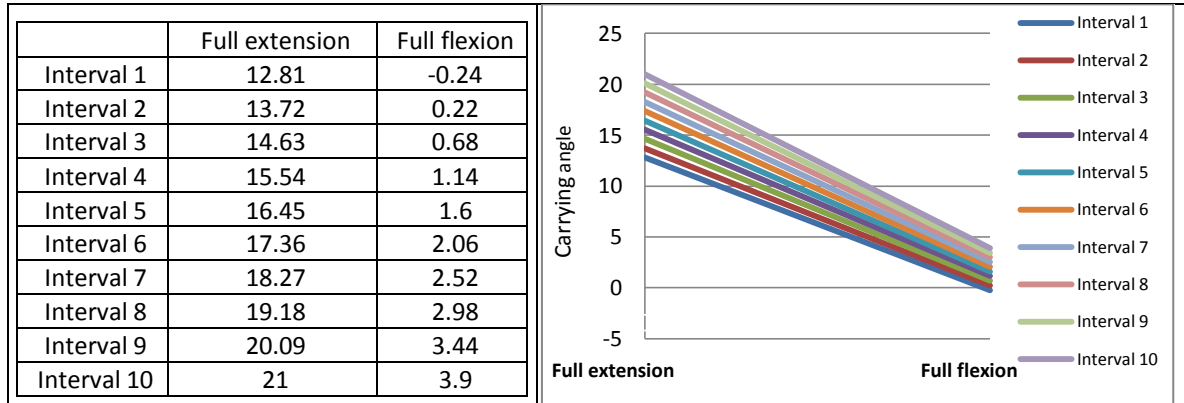


Figure 82. Illustration of the second and the third assumptions

The carrying angle approximation was based on three assumptions. The first assumption was that the full extension carrying angle from the 3D scanned arm fell into the range of the table above. The second assumption was that if the range of the full extension and flexion carrying angle were divided into a similar number of intervals, the intervals from these two ranges could be mapped linearly. For instance, in the case of females, if the full extension carrying angle was divided into 10 intervals, the full flexion carrying angle was also divided into 10 intervals and each interval was mapped onto the corresponding interval, i.e. one to one mapping. An illustration of one to one mapping from this example is shown in the left figure in Figure 82. The third assumption was that the linear variation during the extension-flexion movements could be represented by the one to one mapping described in the second assumption. The right figure in Figure 82 shows the results of the linear variation during the extension-flexion movements based on one to one mapping.

Based on these assumptions, the full extension carrying angle from the 3D scanned arm was used to determine its location in the full extension range from Table 5. This location was then used to determine its corresponding location in the full flexion range from Table 5. The following equation summarises this concept:

$$\text{ratio} = \text{abs}[(3\text{D carrying angle} - \text{min carrying angle max extension}) / \text{range of carrying angle extension}];$$

$$\text{carrying angle max flex} = \text{ratio} * \text{range of carrying angle max flex} + \text{min of carrying angle max flex};$$

A case example illustrates how the carrying angle approximation works. Firstly, the gender of the person from whom the 3D scanned arm has to be known. Next, the carrying angle and the arm

angle have to be acquired from the 3D scanned arm while the arm is fully extended and pronated. For this case example, the gender is female, the carrying angle is 20° and the arm angle of a fully extended arm is 160°. The equation above and the values from Table 5 could be used to determine the carrying angle when the arm is flexed to 140° as follows:

$$ratio = abs\left(\frac{(20 - 11.9)}{(21 - 11.9)}\right) = abs\left(\frac{8.9}{9.1}\right) = 0.978$$

$$carrying\ angle\ for\ maximum\ flexion = 0.978 \times (3.9 - (-0.7)) + (-0.7) = 3.7988$$

$$carrying\ angle\ for\ 140^\circ = \frac{(140 - arm\ angle\ at\ maximum\ flexion)}{(160 - arm\ angle\ at\ maximum\ flexion)} \times (20 - 3.7988) + 3.7988$$

6.1.5 Integrating carrying angle into upper and lower arm bone movements

To integrate the carrying angle, the zero reference position of the arms (see section 2.5) was used due to its simplicity. By adopting the zero reference position, the lower and upper arm bones were located in a straight line and have identical joint orientations. The orientation for the upper and lower arm bones is shown in Figure 83.

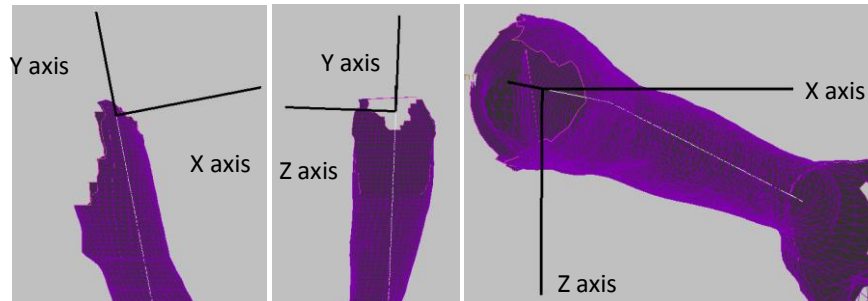


Figure 83. The upper arm bone orientation. The lower arm bone orientation would be identical as that of the upper arm bone orientation

When the arm is fully extended, shown in Figure 84, there is already a certain degree of flexion and carrying angle for the lower arm bone with respect to the upper arm bone. As a consequence, the use of zero reference position resulted in the need to express the orientation of the lower arm bone as two rotations from the zero reference position. The first rotation represented the lower arm flexion whereas the second rotation integrated the carrying angle into the lower arm movement. The theory outlined in section 2.5 regarding rotation in 3D was used to perform the lower arm movement.

Knowing the lower arm bone orientation (see Figure 83) and that the lower arm movement consisted of two rotations (see Figure 84), the lower arm bone movement process could be performed. The step by step process is shown in the Figure 85.

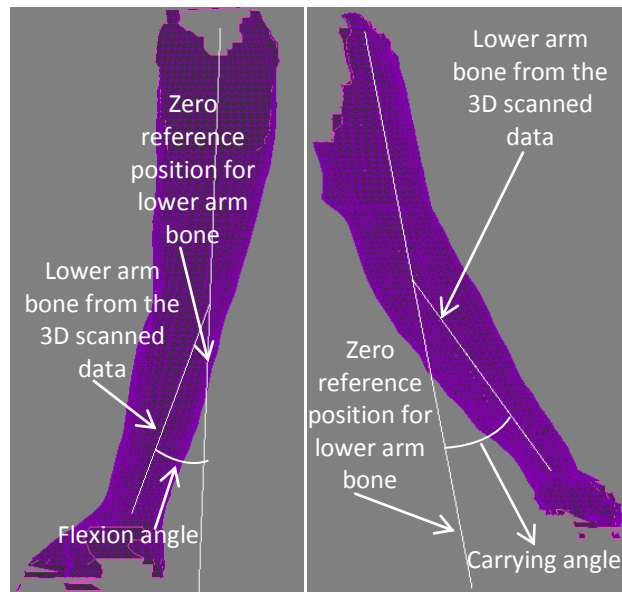


Figure 84. Adoption of zero reference position causes the lower and upper arm bones being located on a straight line. As the consequences, there is a certain degree of flexion and carrying angle even for a fully extended arm

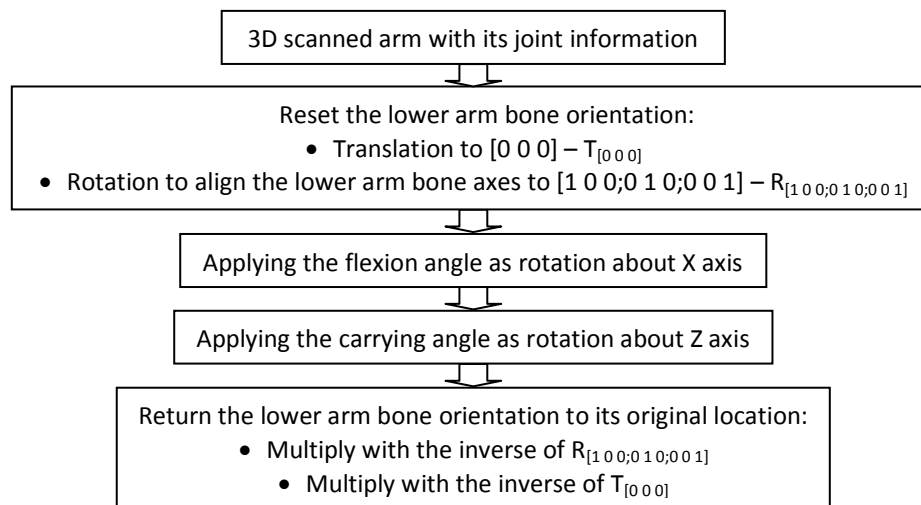


Figure 85. Step by step process for the lower arm bone movements

The application of the flexion angle and the carrying angle could be performed at once by employing the Euler angle concept (see section 2.4.3). Euler angles were chosen in this research as they were commonly used and relatively less complex in comparison to the quaternion alternative. The use of Euler angles allowed the creation of a rotation matrix which represented the overall rotations without having to perform the rotations one by one. However, the Euler angle concept required a determination of the rotation order. From the Figure 85, it is clear that the order was XZY i.e. rotation about X axis, followed by rotation about Z axis and then rotation about Y axis. The flexion angle and the carrying angle were the rotations about X axis and Z axis, respectively, whereas the rotation about Y axis was 0°. The following equation, based on the Euler angle concept, was used to create the rotation matrix ($R_{\text{lower arm}}$) which represented the overall movement of the lower arm:

$$R_{lower arm} = \begin{bmatrix} \cos(\beta) & -\cos(\alpha) \times \sin(\beta) & \sin(\alpha) \times \sin(\beta) \\ \sin(\beta) \times \cos(\gamma) & \cos(\alpha) \times \cos(\beta) \times \cos(\gamma) - \sin(\alpha) \times \sin(\gamma) & -\cos(\beta) \times \cos(\gamma) \times \sin(\alpha) - \cos(\alpha) \times \sin(\gamma) \\ \sin(\beta) \times \sin(\gamma) & \cos(\gamma) \times \sin(\alpha) + \cos(\alpha) \times \cos(\beta) \times \sin(\gamma) & \cos(\alpha) \times \cos(\gamma) - \cos(\beta) \times \sin(\alpha) \times \sin(\gamma) \end{bmatrix}$$

where: α = flexion angle, β = the carrying angle, $\gamma = 0^\circ$

6.2 Determining the boundaries of the region for flesh deformation at the elbow

The next issue to be dealt with in the second design phase was determining the boundaries of region for flesh deformation at the elbow. The need to determine the boundaries of the elbow flesh deformation area was outlined in section 5.3.2.6. The flow charts in Figure 86 shows the proposed strategy to resolve this issue.

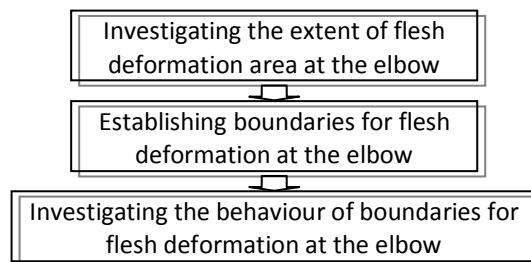


Figure 86. The proposed strategy to determine the region for flesh deformation at the elbow

6.2.1 Investigating the flesh deformation area at the elbow and establishing boundaries for flesh deformation at the elbow

The first step to determine the boundaries of the flesh deformation at the elbow was to investigate the flesh deformation area at the elbow. This investigation aimed to answer the two research questions in section 5.3.2.6 i.e. (i) Do the whole upper and lower arm deform during extension-flexion of the arm?; and (ii) What area of the elbow deforms the most?. Once these two research questions were answered, the boundaries of application of flesh deformation at the elbow and its behaviour would be established in the subsequent two subsections.

To answer the two questions above, a mini study which investigated the extent of flesh deformation at the elbow was undertaken. Through this mini study, it was hoped that the scale of the arm deformation could be established. The mini study was performed by observing the arm in various postures and studying the changes that occurred. The observation was mainly a visual observation. To visually observe the arm in various postures and study the changes that occurred, arms in various postures were compared and area differences between them highlighted. The visual observation was performed for both the upper and lower arms. For the visual observation, the same set of photographs from the first design phase (see 5.3.2.3) was re-used again. The photographs were outlined in Pro-Engineer Wildfire 4.0 to accentuate the arm shapes. Firstly, a comparison was

performed for the upper arm. For this purpose, the photographs were arranged so that the upper arm overlapped. An example of the results is shown in the Figure 87. The area difference of the upper arm between various postures suggested that the area difference was predominantly located in the posterior and anterior part of the upper arm as well as around the elbow.

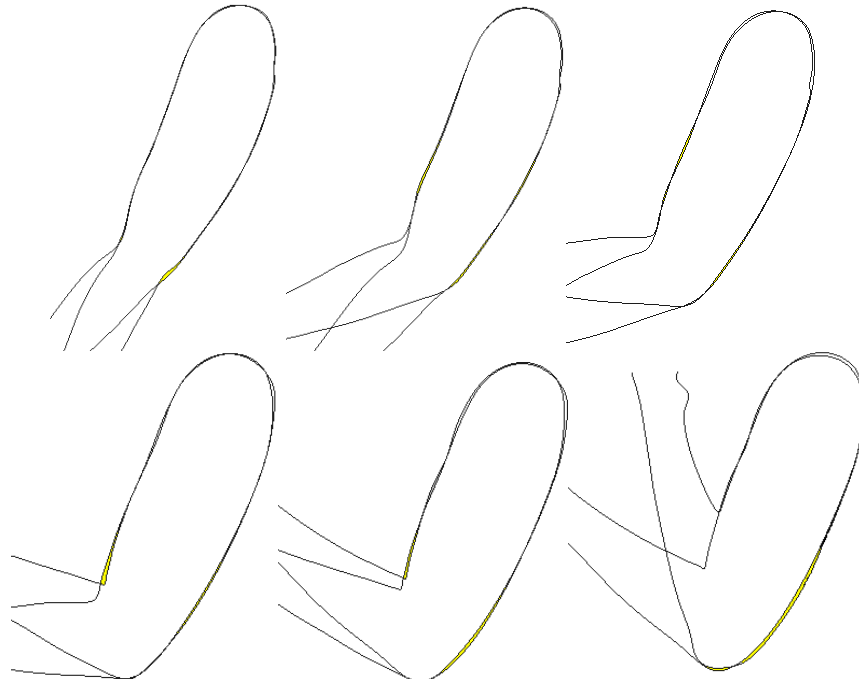


Figure 87. Upper arm outline comparison for various postures

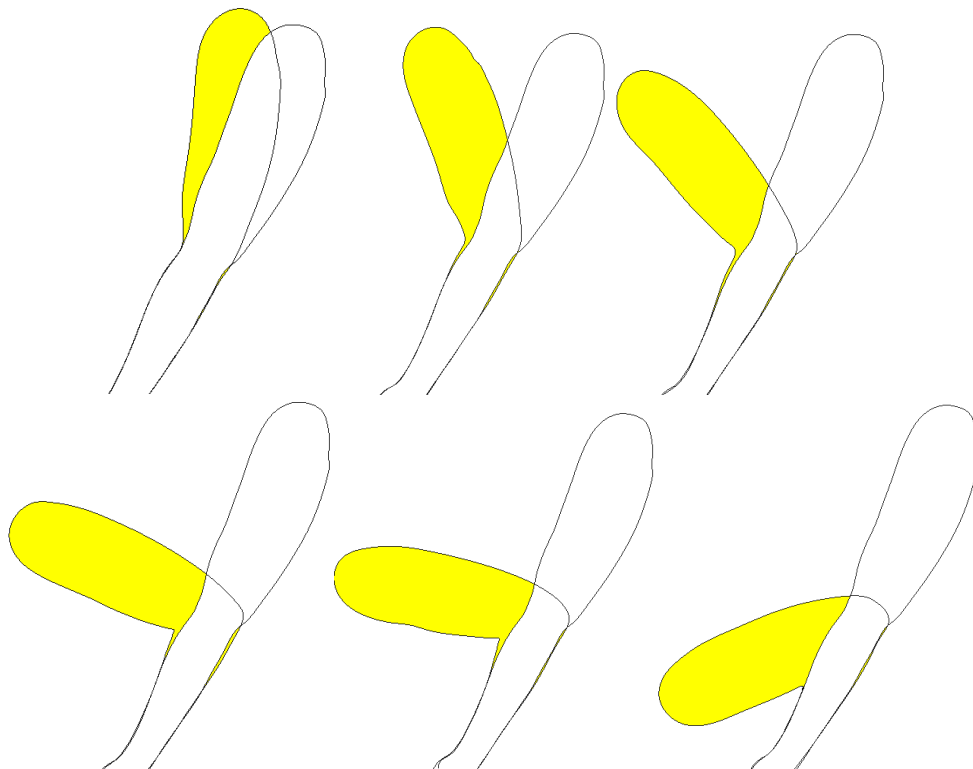


Figure 88. Lower arm outline comparison for various postures

Next, a comparison was performed to study the flesh deformation area difference for the lower arm. For this purpose, rotations were performed to the photographs so that the lower arm

overlapped. Lower arm overlapping at different postures allowed the area difference observation. The hand was used as the reference for the lower arm overlapping. An example of the results is shown in Figure 88. Similar to the upper arm, the area difference of the lower arm between various postures was predominantly located in the posterior and anterior part of the lower arm as well as around the elbow.

The outline comparison for both upper and lower arm revealed that both upper and lower arms did not deform uniformly during extension-flexion of the arm. The biggest flesh deformation was evident in close proximity to the elbow. The deformation area difference also became more prominent as the arm flexed. Both observations suggested that the area difference for both upper and lower arm was limited to a certain part of the upper and lower arm and was demonstrated clearly while the arm assumed maximum flexion. Figure 89 shows noticeable area difference up to the point where the upper and lower arm met. Based on the result of the observation, the flesh deformation area for the elbow was then defined as the area bounded by where the upper and lower arm met during maximum flexion. For simplicity, this flesh deformation area for the elbow would be referred to as “flesh deformation area (FDA)” throughout the thesis.

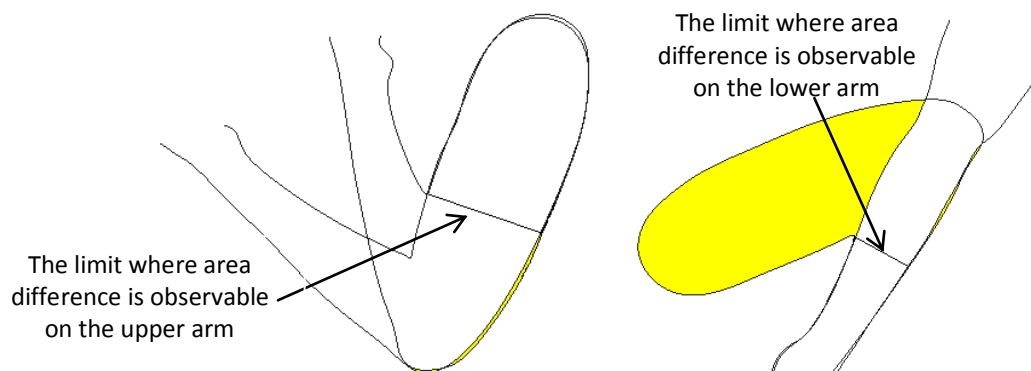


Figure 89. The area difference for the upper and lower arm during maximum flexion

6.2.2 Studying the boundaries for flesh deformation at the elbow

Referring to the flow charts in Figure 86, once the boundaries for the flesh deformation were determined, the next step was to study its behaviour. For this purpose, a new set of photographs from the same participants in the first design phase were obtained by utilising the method described in section 5.3.2.3. The only difference was that additional markers were attached on the participants' skin to signify the FDA. The participant was asked to assume a full flexion and the area where the upper arm met the lower arm was marked (see Figure 90). By attaching additional markers, the behaviour of the boundaries during extension-flexion movements could then be observed.

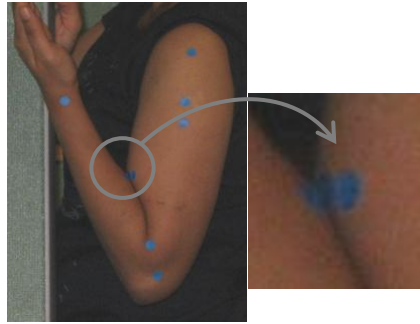


Figure 90. Attaching markers to signify flesh deformation area

Figure 91 shows the outline of the arm through extension-flexion movements from one of the participants. The result showed that the boundaries for flesh deformation area did not remain constant for both upper and lower arm. As the arm flexed, the boundary for upper arm flesh deformation moved towards the shoulder while the boundary for the lower arm moved towards the wrist. Thus, the FDA and its boundaries were a function of the arm extension-flexion angle.

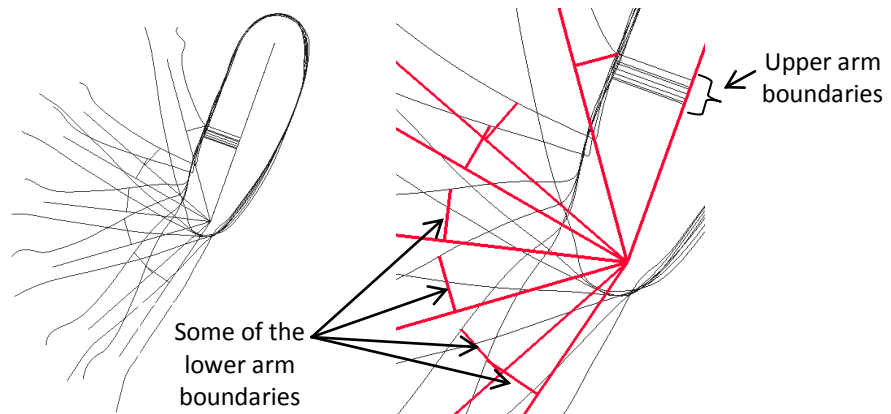


Figure 91. The boundaries movement during extension-flexion movements

To investigate further the relationship between FDA and the arm angle during extension-flexion, the distances of the boundaries to the elbow joint and arm angle were measured and recorded. Figure 92 shows an example of how the lower arm boundary distance and the upper arm boundary distance were measured. This measurement was performed for each subject photograph and its value was recorded together with its corresponding arm angle.

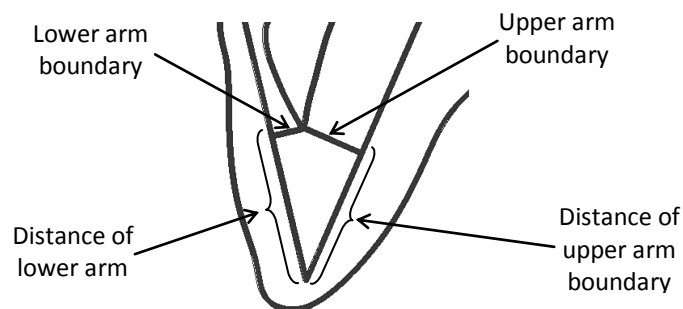


Figure 92. An example of how distances of the lower arm boundary and upper arm boundary are being measured

Figure 93 shows the relationship between the upper arm boundary and the arm angle whereas Figure 94 shows the effect of the arm angle on the lower arm boundaries. The graphs confirmed that as the arm flexed, the distance to the elbow for the two boundaries increased. The graphs also suggested that the relationship between upper arm boundaries and the arm angle was linear whereas the relationship between the lower arm boundaries and the arm angle was largely linear. Knowing the relationship between the lower/upper arm boundaries and the arm angle was really useful and could be used in the later stage. For instance, given the information of the upper/lower arm boundary of a fully extended arm, the relationship could be utilised to predict the upper/lower arm boundaries movement for any other posture.

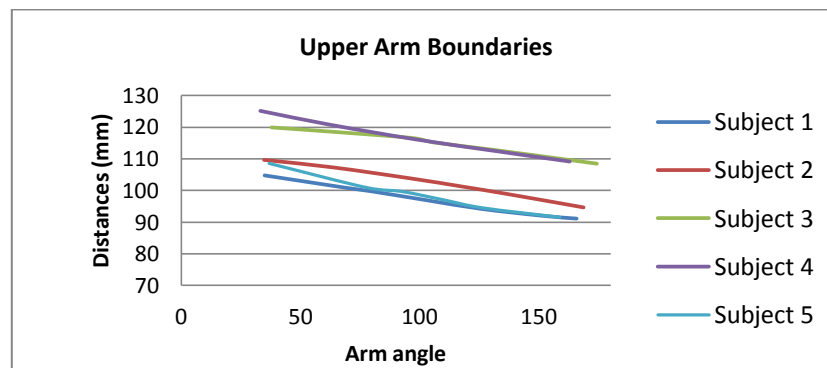


Figure 93. Relationship between upper arm boundaries and arm angle

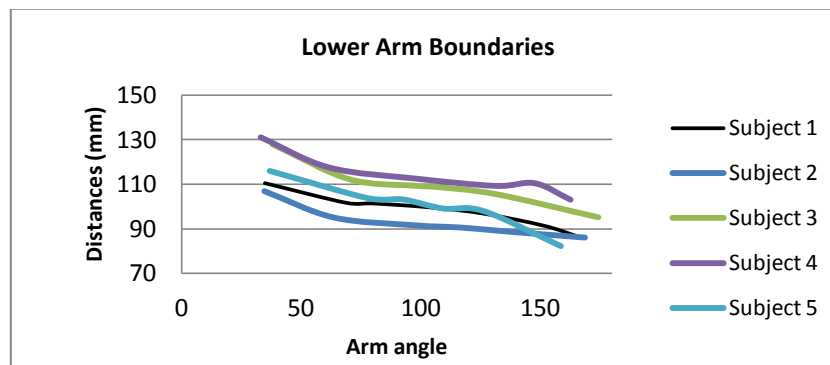


Figure 94. Relationship between lower arm boundaries and arm angles

6.3 Determining a set of posture examples to govern the flesh deformation

The next issue for the second design phase was to determine a set of posture examples. From the set of posture examples, cross section examples could be extracted and used to govern the flesh deformation, as discussed in the first design phase (see section 5.3.2.5) and reiterated in the beginning of this chapter. At the end of this section, the arm postures, from which the cross section examples could be acquired, are established. Figure 95 shows the strategy to establish a set of posture examples to govern the flesh deformation.

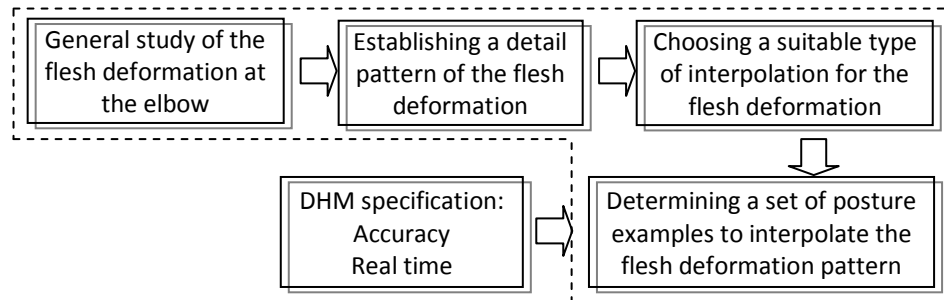


Figure 95. Flow chart which shows steps in determining a set of examples to govern flesh deformation

6.3.1 General study of the flesh deformation at the elbow

As this research intended to integrate 3D body scan data into the proposed FDM (see section 5), the 3D scanner was the first option to study the flesh deformation. Another reason for employing 3D scan data was that it would enable investigation of the flesh deformation in 3D. For this study, one participant was enlisted to gain a basic understanding of the use of the 3D body scanner for this purpose. While being scanned, the participant was asked to assume various arm postures, ranging from full extension to full flexion. The result is shown in Figure 96 and it was apparent that the 3D body scanner was only able to produce a reasonable 3D scanned arm within a limited flexion angle. The bottom figures of Figure 96 demonstrate the 3D scanner failure to produce a complete 3D scanned arm for a $\approx 90^\circ$ flexion. The reason for this was down to the inability of the 12 cameras of the 3D body scanner to fully capture the image of the arm from different perspectives. When the arm was flexed near to or more than 90° , part of the arm would be occluded or became unclear and hence affected the overall quality of the camera images and the 3D scanned arm outcome.

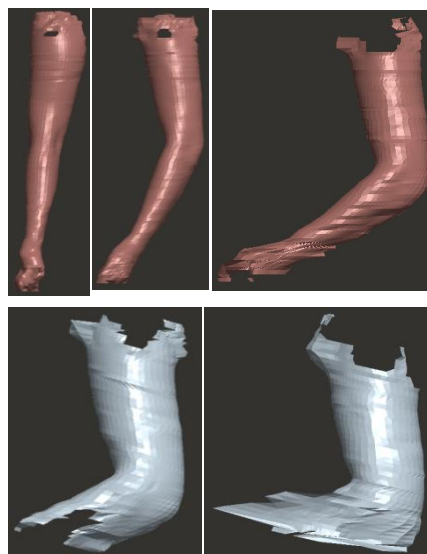


Figure 96. Result of the 3D body scanner for arms with $\pm 90^\circ$ flexion

As it was impossible to use 3D scanned arm to directly study flesh deformation, the five participants' photographs from the first design phase (see 5.3.2.3) were re-used. However, using the photographs meant that flesh deformation was investigated in 2D instead of 3D. Investigating elbow

flesh deformation in 2D limited the investigation to the side view, as other views would likely fail to assist in providing more information. Photographs from the anterior would have a problem with capturing flesh deformation of the lower arm when the arm angle approached 90° flexion whereas the top view photographs would also likely be affected by perspective distortion. The use of side view photographs might result in a less accurate outcome which eventually might affect the accuracy of the proposed FDM. It is acknowledged that this decision was a compromise of what this research intended to achieve.

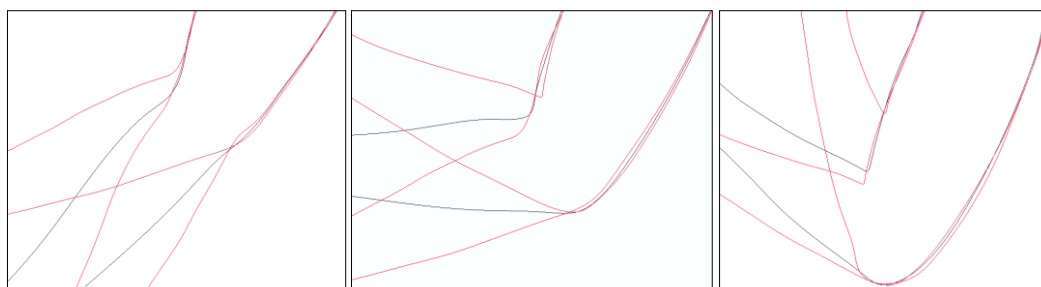


Figure 97. Flesh deformation at different stages: (a) between neutral- $\approx 135^\circ$ (b) between $\approx 135^\circ$ - $\approx 90^\circ$ and (c) between $\approx 90^\circ$ -maximum flexion

Referring to Figure 95, the first step to determine a set of posture examples was a general study of the flesh deformation at the elbow. The general study of the elbow was needed to investigate how the flesh at the elbow deformed from one posture to another. The nature of the flesh deformation e.g. gradual, random, etc., would be observed visually. For the purpose of the general study, the upper and lower arm in each photograph was outlined in Pro-Engineer WildFire 4.0, similar to section 5.3.2.3 and section 6.2.1. Figure 97 shows photograph outlines from one of the subjects. In this research, a fully extended arm was represented with an arm angle that was closer to 180° and a fully flexed arm was represented with an arm angle that was closer 0°. The photograph outlines show that the posterior of the elbow changed subtly until it reached an angle of $\approx 135^\circ$. As the arm flexed, the elbow began to protrude outward gradually. The changes in between $\approx 135^\circ$ and $\approx 90^\circ$ also happened gradually. The posterior of the upper arm changed at a much faster rate than that in between the full extension and $\approx 135^\circ$ flexion. The elbow area also protruded but at much slower rate than in between full extension and $\approx 135^\circ$ flexion and also followed by inward changes of the upper arm anterior. Creases started to develop as the flexion went $\geq \approx 90^\circ$ towards maximum flexion. The posterior of the upper arm near to the elbow joint continued to grow gradually whereas the anterior of the arm remained the same. The general study showed that the flesh deformation changes were directly affected by the arm angle. The study also revealed that the flesh deformation changes occurred in a subtle and gradual manner. The subtle and gradual changes meant that the flesh deformation changes were either linear or non-linear.

6.3.2 Establishing a detail pattern of the flesh deformation

Referring to the strategy shown in Figure 95, the next step was to investigate the flesh deformation change in more detail. The aim of the investigation was to establish the true relationship between the flesh deformation changes and the arm angle. This aim could be achieved by knowing the exact pattern of the flesh deformation changes by means of the quantification of the flesh deformation changes against the arm angle. Following this reasoning, a mini study to quantify the flesh deformation changes against the arm angle was performed. For this mini study, the same photographs and outlines from section 6.2.2 were reused. The proposed method for the quantification of the flesh deformation changes is to track the movement of points on the arm outline by measuring their distances to the bones for various arm angles. Figure 98 shows an illustration of the proposed method where the movement of point A is tracked for three different arm postures and its distance towards to the upper arm bone is measured i.e. D1, D2 and D3.

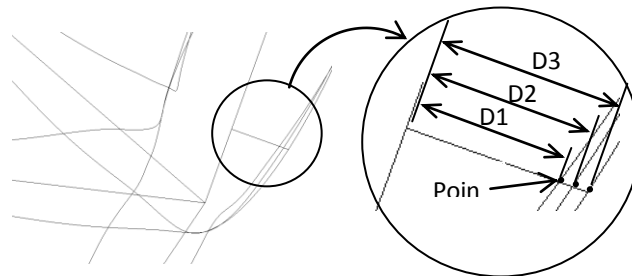


Figure 98. The proposed method to quantify the flesh deformation changes

The tracking of the points' movements was limited to a chosen area, so called "the quantification area". The quantification area was driven by the FDA. Section 6.2.1 has defined the FDA as the area where the upper and lower arm met during maximum flexion. Section 6.2.2 found that the minimum FDA occurred while the arm was fully extended and gradually grew as the arm flexed. This meant that the FDA of a fully extended arm was the base component of the FDA i.e. always present throughout the whole range of extension-flexion of the arm. Based on the above reasoning, this mini study used the FDA of a fully extended arm to guide the determination of the area of interest for the quantification. Figure 99 shows how the FDA of a fully extended arm was used to set the quantification area for any other postures.

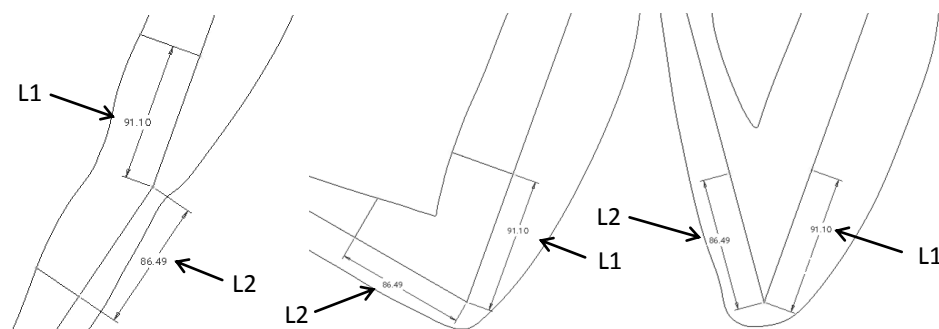


Figure 99. Usage of a fully extended arm FDA as a reference to determine the quantification area for other arm postures

The quantification also required the determination of tracked locations and their number. The tracked locations and their number were chosen such that they could capture the flesh deformation changes within the quantification area. Ten tracked locations were used and distributed within the quantification area, which was divided into three smaller areas i.e. the upper arm, the elbow and the lower arm. Using ten tracked locations means that if there is n number of arm postures there will be $10n$ locations to be collected for each subject and $50n$ locations in total to be analysed. Four of the tracked locations were allocated at the upper arm area and divided the area into three equal sections. Another two of the tracked locations were positioned at the elbow and partitioned the area into three equal sections. The remainder of the tracked locations separated the lower arm area into three equal sections. By dividing the quantification area into three parts and positioning the tracked locations at each part, it was hoped that the tracked locations could capture the flesh deformation changes accurately despite its small number. Figure 100 shows the distribution of the 10 tracked locations. A plot of the arm angles and tracked location distances on each of this area was expected to depict the exact pattern of the flesh deformation changes. To ease data analysis, an average of tracked locations' distances for each posture was calculated for every subject and area. For example, in the case of the upper arm area where there are 4 tracked locations ($D_1 \dots 4$) and n number of arm postures ($P_1 \dots n$), the tracked locations' average distance for each posture ($D^{P_1 \dots n}$) are calculated as follows:

$$D^{P_1} = \frac{\sum [D_1^{P_1} + D_2^{P_1} + \dots + D_4^{P_1}]}{4}$$

$$D^{P_n} = \frac{\sum [D_1^{P_n} + D_2^{P_n} + \dots + D_4^{P_n}]}{4}$$

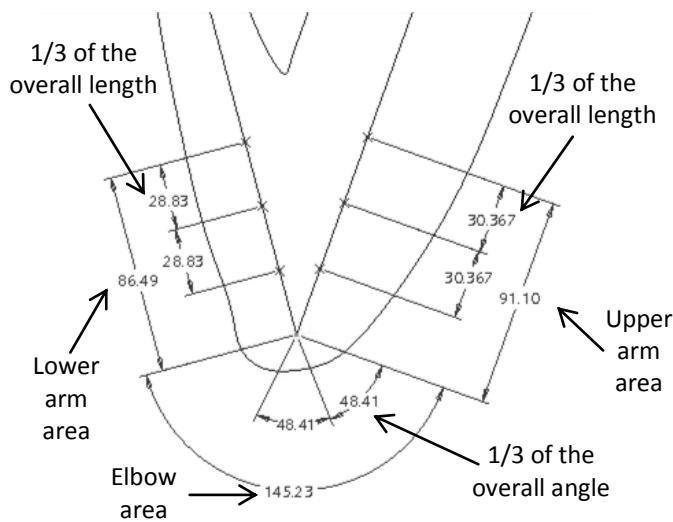


Figure 100. An illustration of the distribution of the 10 tracked locations on the arm outline while the arm is fully flexed

Figure 101 shows the result of the quantification. From the graphs, it was clear that the flesh deformation changed in a non-linear manner with respect to the arm angle for all of the

quantification area i.e. upper arm, elbow and lower arm. Non-linear regressions, which were the best fit for the data pattern, confirmed further the non-linear relationship between the flesh deformation changes and arm angles. The quantification result also showed that the relationship between the flesh deformation and the arm angle could be represented with two degree polynomial functions, despite their low R^2 values. The low R^2 values for all of the non-linear regressions were mainly caused by the wide spread of the data points. The wide spread of the data points was mainly caused by the direct use of the tracked locations distances from participants with different body size/shape. For instance, as shown in Figure 101, there is a substantial difference between subject 1 (42 kg in weight and 143 cm tall) and subject 5 (73 kg and 166 cm respectively). The greater the variation of the arm sizes from one participant to another, the greater the spread of the tracked location. Nonetheless, despite their low R^2 values, the non-linear regression lines highlighted the pattern of the flesh deformation changes. Therefore, they would be utilised to assist in choosing a suitable type of interpolation to interpolate the flesh deformation changes pattern.

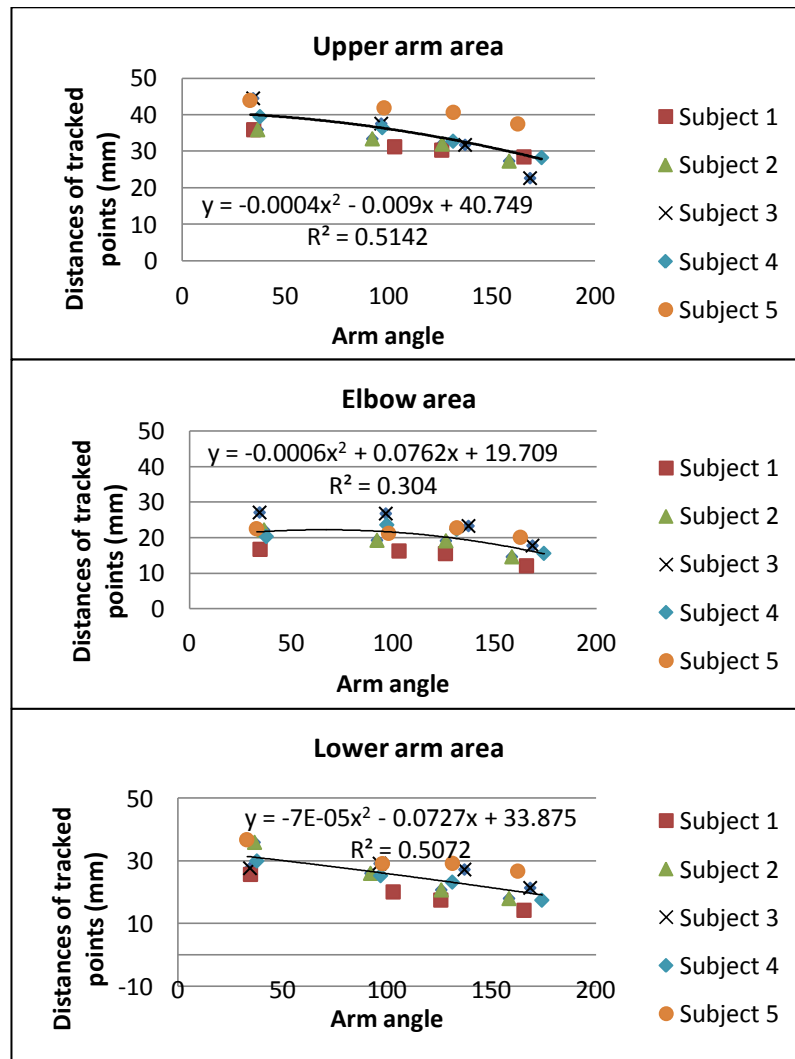


Figure 101. Result of the flesh deformation changes quantification and non-linear regression lines for all of the quantification areas from the five subjects

6.3.3 Choosing a suitable type of interpolation and determining a set of posture examples to interpolate the flesh deformation pattern

Referring to the strategy shown in Figure 95, the next step was to choose a suitable type of interpolation. The chosen type of interpolation would affect the determination of the set of posture examples. As it was shown in Figure 101, the relationship between the flesh deformation changes and the arm angle could be represented with a two degree polynomial function. This research endeavoured to apply linear interpolation to represent the non-linear behaviour of the flesh deformation changes. The linear interpolation was chosen because it was simpler than non-linear interpolation and was preferred as it would be more appropriate for real time processing, which was one of DHM specifications.

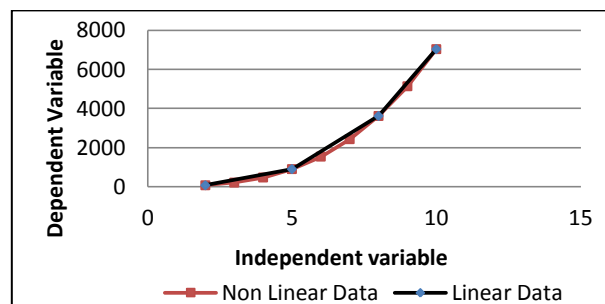


Figure 102. Using linear interpolation to interpolate non-linear data

After determining an appropriate method of interpolation, an appropriate set of posture examples was determined. In this case, determining an appropriate set of posture examples was essentially deciding where and how the linear interpolation would be located to represent the non-linear nature of the flesh deformation changes. To interpolate non-linear data, several linear interpolations could be used by dividing the data range into smaller sections so that even if linear interpolation was applied, it would still be able to represent the data, as shown in Figure 102. In the case shown in Figure 102, the dependent variable could be predicted by creating three linear interpolations i.e. a linear interpolation between 2 - 5, 5 - 8 and 8 - 10. Naturally a higher number of linear interpolation sections would lead to a higher accuracy. However, this would also mean more data to be processed or stored and so limit some of the advantage of using linear interpolation. Therefore, a minimum number of linear interpolations would be preferred in this research. Simply setting a minimum number of linear interpolations without considering the nature of the non-linear interpolation to be represented resulted in inaccuracy, which was undesirable. A high degree of curvature likely prompted the need for a higher number of linear interpolations to represent the data and vice versa. Observation of the regression lines of the flesh deformation changes revealed their low degree of curvature tendency (see Figure 101). Thus it was decided that the flesh

deformation changes would be approximated with 3 linear interpolation sections, similar to the case example shown in Figure 102.

Given that 3 linear interpolation sections were used to approximate the regression lines, two locations needed to be determined. The two locations represented two arm angles between the two extremes of arm angles i.e. full extension and full flexion. These two chosen arm angles should be located such that the non-linear part of the flesh deformation changes could be approximated with a minimum error. Another aspect which had to be considered in choosing the two arm angles was practicality. Any participant, from whom the cross sections examples were obtained, would have to assume these two arm angles. Arranging the participant to assume 121.8° during cross section extraction, although possible, was impractical. Therefore, this research limited the values of these two arm angles into integer values only. Another related issue with practicality was the level of the angle distinction. For instance, distinguishing 121° and 122° would be impractical as the angle difference was too small to be incorporated into participant arm posture. For this research, based on the experience of working with participants in the mini study, 5° was chosen as the level of the angle distinction.

```

Obtain the regression line for the required quantification area (f)
For  $x_i = \text{round}(\alpha_{full\ extension}) : -5 : \text{round}(\alpha_{full\ flexion})$ 
    Calculate  $y_i = f(\alpha_{full\ extension} \dots x_i)$ 
    Determine line equation ( $f_{full\ extension-i}$ ) between ( $\alpha_{full\ extension}, f(\alpha_{full\ extension})$ ) and ( $x_i, y_i$ )
    Calculate  $y_{full\ extension-i} = f_{full\ extension-i}(\alpha_{full\ extension} \dots x_i)$ 
    Calculate error ( $\epsilon_{full\ extension-i}$ ) =  $y_{full\ extension-i} - y_i$ 
For  $x_j = (x_i - 10) : -5 : \text{round}(\alpha_{full\ flexion})$ 
    Calculate  $y_{i-j} = f(x_i \dots x_j)$ 
    Determine line equation ( $f_{i-j}$ ) between ( $x_i, y_i$ ) and ( $x_j, y_j$ )
    Calculate  $y_{i-j} = f_{i-j}(x_i \dots x_j)$ 
    Calculate error ( $\epsilon_{i-j}$ ) =  $y_{i-j} - y_{ij}$ 
    Calculate  $y_j = f(x_j \dots \alpha_{full\ flexion})$ 
    Determine line equation ( $f_{j-full\ flexion}$ ) between ( $x_j, y_j$ ) and ( $\alpha_{full\ flexion}, f(\alpha_{full\ flexion})$ )
    Calculate  $y_{j-full\ flexion} = f_{j-full\ flexion}(x_j \dots \alpha_{full\ flexion})$ 
    Calculate error ( $\epsilon_{j-full\ flexion}$ ) =  $y_{j-full\ flexion} - y_j$ 
End
End

```

Keeping in mind those aspects above, Matlab 7.0 was used to seek the two arm angles with a minimum overall error level for the quantification areas. The regression lines from the quantification result were used to determine the two arm angles. For each possible pair of arm angles, the error level was calculated. The error level was defined as the total distance difference between the regression lines and the linear interpolations from the possible pair. This process is shown in the pseudo code above. The application of the pseudo code showed that 135° and 90° were the two arm angles with the least error i.e. 6.2492 mm, 6.2492 mm and 0.7291mm for the

upper arm, lower arm and the elbow area, respectively. With respect to this result, 135° and 90° flexion were chosen.

A series of studies in this subsection resulted in the determination of 4 postures i.e. fully extended, 135°, 90° and fully flexed as the set of posture examples. These example postures divided the non-linear flesh deformation changes into 3 sections i.e. fully extended-135°, 135°-90° and 90°-fully flexed, in an attempt to represent its non-linearity. For the purposes of simplicity, the set of examples will be referred to as “key postures” throughout the thesis.

6.4 Establishing a method to acquire the cross sections from the key postures

The previous subsection established key postures to govern the flesh deformation. Knowing the key postures meant that a method to acquire the cross sections from these key postures could be developed. The previous subsections also revealed that the 3D body scanner i.e. [TC]² NX-12 was not be able to acquire 3D scanned arm postures $\geq 90^\circ$. Therefore, although section 5.3.2.1 showed that cross sections could be easily extracted from the 3D scanned arm, an alternative way to capture the arm shape of the key postures was still required. A strategy to establish the method to acquire the cross sections from the key postures is shown in Figure 103.

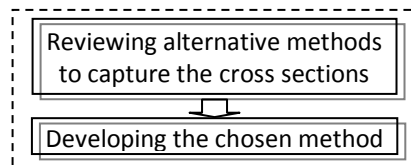


Figure 103. A strategy to establish the method to acquire cross sections from the key posture

6.4.1 Reviewing alternative methods to capture cross sections

To incorporate the concept of key postures into the proposed FDM, a method to obtain the cross sections for key postures was required. The 3D body scanner limitation imposed the necessity to seek for alternatives ways as introduced earlier. It should be kept in mind that any method to be pursued would affect other issues for the cross sections. Several methods were considered:

- Handheld Laser scanner

A handheld laser scanner is a portable device to acquire the 3D shape of objects which consists of a laser projector and cameras (Lieu and Sorby, 2009). The laser scanner is swept onto any surface in a similar way as using a paint spray. The images generated by each sweep are automatically stitched together to create a complete surface which is immediately available on the provided software. Handheld laser scanners offer flexibility as they enable capturing of any area of interest (Winkelbach et al., 2006). This method was deemed to be the most suitable approach to acquire the 3D shape of the arm in different postures accurately. However,

obtaining cross sections from the 3D shape of the arm required joint location determination; therefore a manual positioning of the corresponding joints would need to be performed. Another way to get around this demand would be to draw the required cross sections on the arm and follow the drawn cross sections with the handheld laser scanner. Although it was simple, this process would likely require a considerable amount of time from any participant involved for data collection. Also, the participant would have to keep their arm still throughout the manual scanning process as slight movements would affect the scanning result (Burdea and Coiffet, 2003). Thus, despite its prospect for simplicity and higher accuracy, this approach was not pursued any further, mainly due to the unavailability of the device.

- 3D motion capture

3D motion capture is commonly used to represent the joint location for motion studies or any other field where a natural and realistic joint movement is required. The most common 3D motion capture is an optical method where markers attached to a certain joint would be tracked. Some of the available 3D motion capture systems use either reflective markers or infra red emitters. Occlusions of the markers might take place as the person moves; however the missing data could be recovered through estimation of their missing points. The usage of 3D motion capture would likely enable capturing points in a 3D environment accurately (Menache, 2011). To acquire a cross section, similar to the handheld laser scanner, a cross section line could be drawn on the skin and markers could then be attached on it. With the available 3D Motion Capture i.e. Vicon, a trial was performed to investigate the possibility to use the markers to capture points' locations which covered a certain area. However, as was expected, occlusion took place and it was proved to be difficult to attach the markers onto the arm without causing any compression to the flesh. Therefore, despite the availability of the device, this device was not utilised to obtain cross sections.

- MRI

MRI is a medical imaging technique based on detection of hydrogen atoms in matter and their behaviour under strong magnetic fields. MRI provides an optional approach in providing cross-sectional images of soft tissues in detail without exposing a person to potentially harmful X-rays as would be the case with Computed Tomography (CT). MRI provides cross sectional images of organs, bones and tissues along the length of the body which could then be used to reconstruct three-dimensional data describing individual organs, bones and tissues accurately (Seager and Slabaugh, 2011). However, due to its high cost, MRI accessibility was considerably limited i.e. usually only found in hospital or medical related research facilities. In addition to this, as MRI is considered a clinical diagnostic procedure, ethical issues would have to be addressed and an

ethical clearance would have to be acquired prior to obtaining MRI scan(s) from each and every participant (Lo, 2010). Based on these considerations, this approach was not chosen.

- Circling wire and photographs

The next method to be considered was simultaneous use of circling the wire around the arm and photographs. The idea was to circle the wire around the arm at the key postures, followed by taking photographs of the arm from the sagittal and frontal planes while assuming the key posture angles. By digitising the shaped wire, cross sections could be recreated and positioned further to match the photographs. This approach was considered to be economical and simple compared to previous approaches. Furthermore, the time to gather the data from anyone involved for data collection might be quicker than other previous approaches. However, this approach was not without drawbacks either. First of all, using the wire to capture the arm cross section presented a difficulty in avoiding compressing the flesh. Also, there would be a significant amount of data processing once the data collection was completed. Although this approach would likely be able to recreate the arm at key posture by utilising the photographs to assist digitised cross sections' placement and orientation, the joint location information would not be readily available. Thus, an additional method to incorporate joint location information would likely be required.

Based on the advantages and disadvantages of several methods above, the last method i.e. synchronous use of a circling wire and photographs was chosen. This method was simple and easily accessible which gave it a strong advantage in comparison with other methods.

6.4.2 Developing the chosen method to capture cross sections

The development of a circling wire and photographs method mainly involved two things i.e. taking the photographs and capturing cross sections. Photographs acquisition would be discussed first in this subsection, followed by capturing cross sections. The setting of the first approach is shown in Figure 104. This method was essentially similar to that in section 5.3.2.3, in which an attempt to validate the bijective method of Shen et al. (1994) was performed. Two cameras were used synchronously to acquire photographs of side and front views. A sitting position was chosen to avoid participant fatigue. While being seated, a study participant moved the arm from extension to flexion. A partition board was used to guide the alignment of the arm extension-flexion movement in order to minimise the effect of parallax between the arms and one of the cameras i.e. the camera to capture the side view photographs.

An example of the result from the setting of the first approach is shown in Figure 105. The fact that the photographs were taken while the study participant sat imposed a limitation on the shoulder angle which also played a role in upper arm obstruction by the lower arm. Except for the

first two images in Figure 105, the lower arm could be observed significantly obstructing the upper arm on all of the images. Obstruction of the upper arm by the lower arm resulted in difficulty in cross section placement and orientation which was undesirable. Therefore, a second approach for the setting was developed.



Figure 104. The first proposed setting to acquire side view photographs



Figure 105. Results of the first setting of the side view photographs

For the second approach of the setting, instead of sitting, the participant would stand. In addition to this, a handlebar was provided. The base of the handle had to touch the partition board. The handle bar and the standing position allowed a participant to adjust their position such that the upper and lower arms were aligned with the partition board to minimise the parallax effect. The second approach of the setting is shown in Figure 106. A reference was attached to the partition board to assist the scaling of the photograph of the arm side view, shown in the right most figure of Figure 106. Prior to taking photographs of the arm, markers were attached to the skin in the following locations: on the shoulder (side and front), on the mid of the arm (side), on the elbow (mid, side and front) and on the wrist (side, front and back). While assuming arm maximum flexion, a marker was attached to the area where the upper arm meets the lower arm to signify its FDA. The introduction of a handle bar and standing position produced an improvement in avoiding upper arm obstruction.

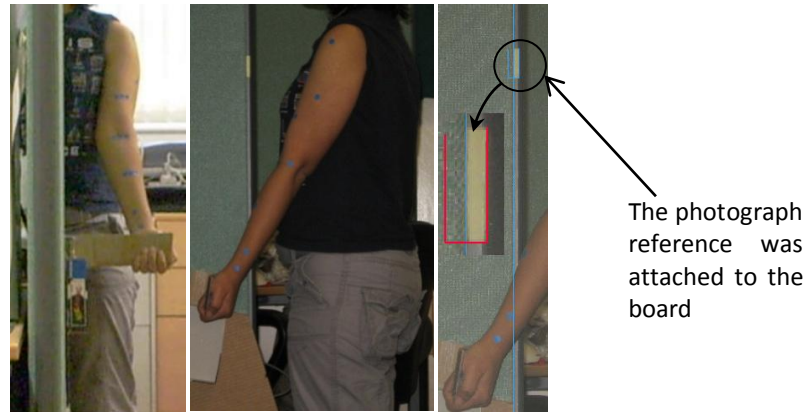


Figure 106. Second setting to obtain photographs of front and side view of the arm

Capturing the cross sections was simply performed by using a wire which was flexible and yet had an ability to maintain the shape of the cross sections. Once the cross section was captured, the cross section shaped wires were then traced manually and digitised. The manual tracing was performed by placing the wires onto a piece of paper and tracing them manually. The digitisation was performed by firstly scanning the paper with a digital flat-bed scanner and then saved as JPEG image files. These files were then traced automatically with CorelTrace and the results were converted into .dxf. Pro-Engineer Wildfire 4.0 was then utilized to read these files and recreate the cross sections.

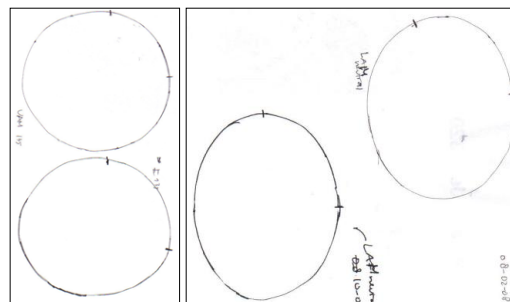


Figure 107. Variation in cross sections capture result

While reviewing possible methods to capture the cross sections in section 6.4.1, the drawback of wire usage to capture the cross sections i.e. difficulty to avoid flesh compression, was identified. Although it was difficult to avoid flesh compression, a simple measure was performed to minimise it. The simple measure was essentially checking the tightness of the wire once it was circled around the arm and adjusting it if necessary. To test the measurement method, a repeated attempt to capture the same cross sections was performed on a participant. Two cross sections were obtained for each of mid upper arm and mid of lower arm. The wires were circled perpendicularly with respect to the arm in order to capture cross sections that are perpendicular to the arm. The four cross sections were then traced and digitised. Figure 107 shows the variation on the cross section which demonstrated that cross sections variations still occurred although care was taken to avoid flesh compression. Nonetheless, despite the cross sections variations, their overall shapes were still in accordance with each other. Based on the test, it was also evident that, while obtaining the cross

sections, it was necessary that markers were drawn on the wire to indicate its orientation (e.g. mid lateral and mid anterior). The absence of the markers resulted in confusion on the wire orientation once the cross section shaped wire was taken off from the arm. Another matter which became clear during the test was the need to ensure that the circled wire was aligned appropriately with respect to the arm. This was relatively straightforward for cross sections that were perpendicular to the arm. However, accurately capturing cross sections that were not perpendicular to the arm could be difficult. The Shen et al. (1994) approach required the cross sections to be located on a plane that constantly changed its angle with respect to the upper/lower arm bone. This meant that using the wire to capture the cross section would hinder the application of their approach and limit the cross sections' plane orientation for the upper and lower arm onto a perpendicular plane.

6.5 Determining cross section planes' orientation

Because of the nature of the chosen method to capture the cross sections, the orientation of the cross section planes for cross sections that were located along a bone would be directly affected by it. As described in section 5.3.2.3, Shen et al. (1994) used interpolated orientation for cross section's planes that were located along a bone. However, capturing the cross sections with wire and adopting interpolated orientation of cross section planes on both the upper and lower arm would be complicated, as discussed in section 6.4.2. Therefore, the cross section planes which were located along the upper/lower arm bone would be kept perpendicular with respect to the upper/lower arm bone. In contrast, the cross section planes at the elbow would be dependent on the arm angle and adopted the relationship between arm angle and the elbow plane orientation which was described in section 5.3.2.3.

6.6 Determining number of cross sections and their location

The decision concerning the number of cross sections and their location was affected by the previous decisions in the design phase and the relevant DHMs specification for the flesh deformation, as shown in Figure 108. The previous decisions in the design phase, which influenced this stage included: the FDA concept, the chosen method to acquire the cross sections, and the orientation of the cross section planes. Each of these had to be considered before a mini study regarding the number of cross sections and their location could be performed.

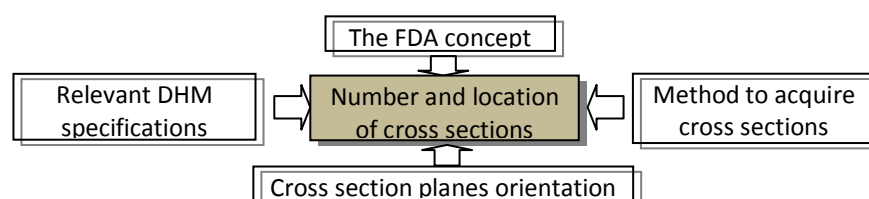


Figure 108. Factors which affect the decision concerning the number and location of cross sections

Based on this rationale, a strategy to resolve the issue concerning the number of cross sections and their locations was developed. The strategy is shown in Figure 109. First, a review regarding relevant factors to decide the number and location, shown in Figure 108, would be performed. It was hoped that the review would provide a clear direction for the mini study.

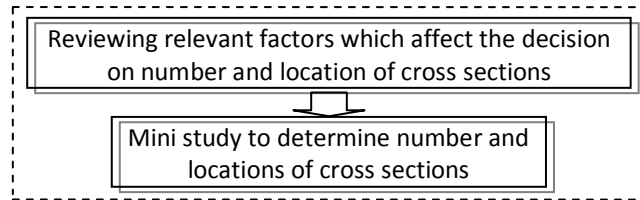


Figure 109. Strategy to determine the cross sections' number and location

6.6.1 Reviewing relevant factors to the determination of cross sections' number and location

The first factor to be considered was the flesh deformation area concept. The introduction of the FDA concept implied the need for cross sections at both ends to signify the boundaries i.e. the upper arm and lower arm boundary. Therefore, two cross sections should be placed at the upper and lower arm boundaries. For future reference, cross sections at these locations would be referred as Upper Arm Far (UAF) and Lower Arm Far (LAF).

The result of mini study in section 6.2.2 showed that the upper and lower arm boundaries moved further from the elbow joint as the arm flexes. Further observation of the movement of these boundaries showed that as the arm flexed, the anterior surface area of the arm became smaller and the posterior surface area increased. Figure 110 shows an illustration of the anterior and posterior surface area changes for different arm postures. While the arm was fully extended, the anterior surface area and posterior surface area was approximately the same. As the arm was flexed, the anterior markers on both upper and lower arm moved closer to the elbow crease and resulted in a smaller anterior surface area. Thus, the continual decrement of the anterior surface area during extension-flexion arm movement should be taken into account while determining the number and location of the cross sections.

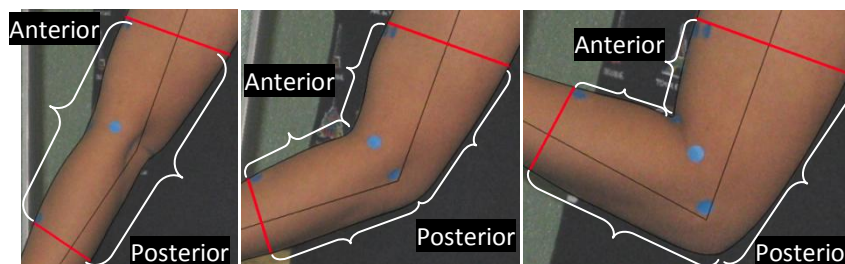


Figure 110. Growth of posterior area as the arm flexes

At the end of section 6.4.2, it was established that the cross sections would be acquired manually. To acquire cross sections manually, a location identifier was used e.g. the markers on the

boundaries of the flesh deformation area (see Figure 90 on page 105) for UAF and LAF cross sections. Location identifiers would also be required for cross sections which would be determined in the next subsection. The proposed location identifiers for these cross sections were the anterior elbow crease and the markers on the boundaries of the flesh deformation area. They were chosen as they could easily be identified. Cross sections which would be determined in the next subsection would always be bounded by these two location identifiers. Figure 111 shows the bounded area for cross sections in the upper and lower arms which were determined with the assistance of the chosen location identifiers above. The graphs from the mini study in section 6.2.2, which depicted the upper and lower arm boundary movement, showed that the FDA varied between subjects and arm postures. As the location identifier was driven by these boundaries, this meant that the bounded area shown in Figure 111 also varied. To accommodate this, the location of cross sections which were bounded by this area should be expressed as a relative length between the locations identifiers e.g. for a cross section that was located at the middle of the upper arm bounded area, its location was expressed as 50% of the distance between the upper arm boundary and the elbow crease.

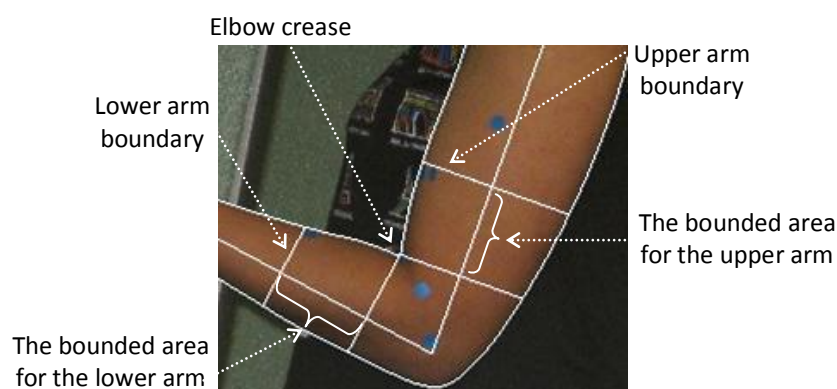


Figure 111. Illustration of the bounded area for the cross sections

The second factor which affected the determination of the number and location of the cross sections was the orientation of the cross section planes. In section 6.5, the orientation of the cross section planes was determined to be perpendicular with respect to the upper/lower arm bone, except at the elbow. The validation of the bijective plane concept for the elbow plane orientation in section 5.3.2.3 implied that a cross section would be located at the elbow joint. The mini study also implied that the cross section plane at the elbow joint would not be perpendicular. This cross section would be referred to as Elbow (E) from this point onward.

As a consequence of employing perpendicular planes for other cross sections, the area just before/after the elbow cross section would not be covered even if two cross sections were located as close as possible to the elbow joint. Figure 112 shows the gap at the elbow joint which increases as the arm approaches maximum flexion. The figure shows that irrespective of the number of cross

sections, there is still an area that is not covered as the arm flexes. To overcome this, creating additional cross sections in this area would likely be imperative to fill in the gap. The additional cross sections would require enough space in order to avoid intersection between them. Intersection between these cross sections would result in distortion during surface creation. Therefore, the determination of the number and location of the cross sections should ensure that enough space was reserved for the additional cross sections at the elbow joint.

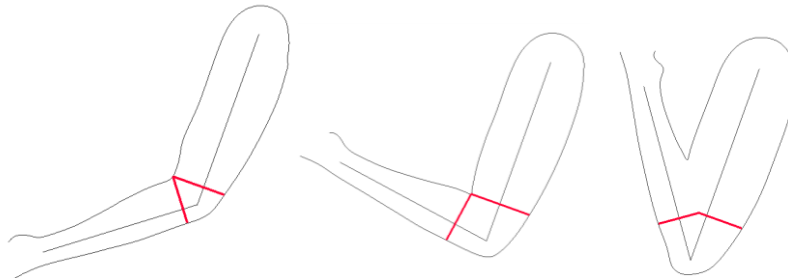


Figure 112. Gaps at the elbow joint which are caused by orientation of the cross section planes

The next factor which affected the cross sections' number and location determination was the chosen method for the cross sections acquisition. As the chosen method required physical measurement i.e. circling the wire to capture the cross sections of the arm, the time required to obtain the cross sections should be considered. This study aimed to accommodate FDM for different body sizes and shapes, thus, there was a possibility that physical measurements had to be performed on a wide range of study participants. Therefore, without losing much information of the arm shape, the lesser the number of the cross sections, the better it would be. Limiting the number of cross sections would also mean that there was less data to manipulate to perform flesh deformation and reduce the processing time. This was particularly relevant with one of the DHM specification i.e. real time.

To summarise, the review above has highlighted several points to be considered while determining the number and locations of cross sections:

1. The existence of UAF, LAF and E as part of the cross sections' location and number
2. Limiting the number of cross sections without losing too much information
3. Cross sections plane were perpendicular, except the cross section at the elbow
4. Cross sections would be placed in between the two identifiers i.e. (i) the upper arm boundary and the elbow crease for the upper arm and (ii) the lower arm boundary and the elbow crease for the lower arm.
5. Expressing the location of the cross section as a fraction (percentage) of the area bounded by the location identifiers.
6. The need to leave enough space to create additional cross sections at the elbow joint

6.6.2 Mini study to determine number and locations of cross sections

Before a mini study could be performed, a decision regarding whether there would be a distinction between the upper and lower arm in terms of the number cross sections and their locations, would be required. The cross sections which were obtained from testing the cross section acquisition method showed that the upper and lower arms were of similar shapes i.e. ellipsoidal shapes (see section 6.4.2, Figure 107 page 118). As there were no major shape differences between them, there was no evidence to support the distinction of the number and location of the cross sections between them. Therefore, similar number and location of cross sections would be applied for both the upper and lower arms. Setting a similar number and location of cross sections was also more advantageous as it would reduce the number of combinations to be explored and hence significantly simplify the problem. Keeping a similar number and location of the cross sections meant that if a cross section was added at a fraction (see point 5 in section 6.6.1) of the area bounded by the location identifiers for the upper arm (see point 4 in section 6.6.1), another cross section was also added at a similar fraction of the area bounded by the location identifiers for the lower arm. Figure 113 illustrates this example in which a pair of cross sections at 50% of the bounded area of the upper and lower arm is added.

Taking into account the decision above, a mini study to investigate the effect of number and location of cross sections on surface creation was proposed. The study was performed by visually observing the surfaces that were created from different combination of the number and location of the cross sections. To create different combinations, cross sections were inserted at different locations within the bounded area (see point 4 in section 6.6.1) and placed on perpendicular planes with respect to the arm bones (see point 3 in section 6.6.1). The surface was created from inserted cross section(s) and the existing cross sections (see point 1 in section 6.6.1).

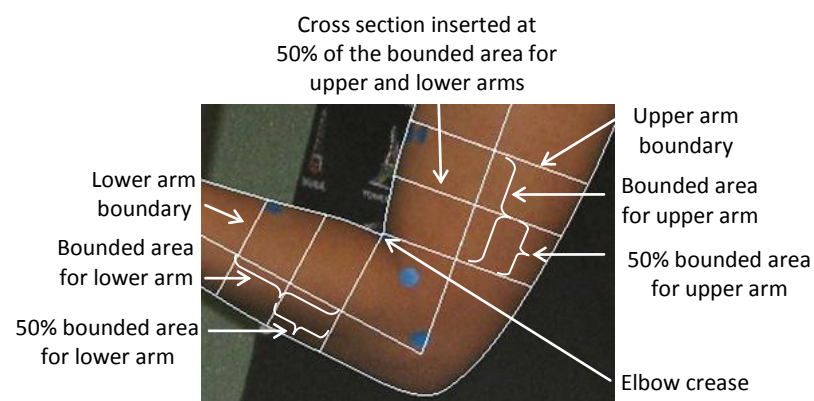


Figure 113. Insertion of cross sections at 50% of the upper and lower arm FDA length onto the pre-determined cross sections' location i.e. UAF, E, and LAF

For this study, the set of photographs from one participant in section 6.2.2 was re-used. However, only photographs of the fully extended and flexed arm were utilised. Using these two

photographs was considered to be sufficient as they represented the extreme state of the arm movements. For each photograph (see Figure 113), the location of the upper and lower bones were determined using the method in 5.3.2.3. Next, perpendicular planes with respect to the bones were drawn to mark the location identifiers. The distance between the identifiers at each bounded area was used to guide the cross section insertion.

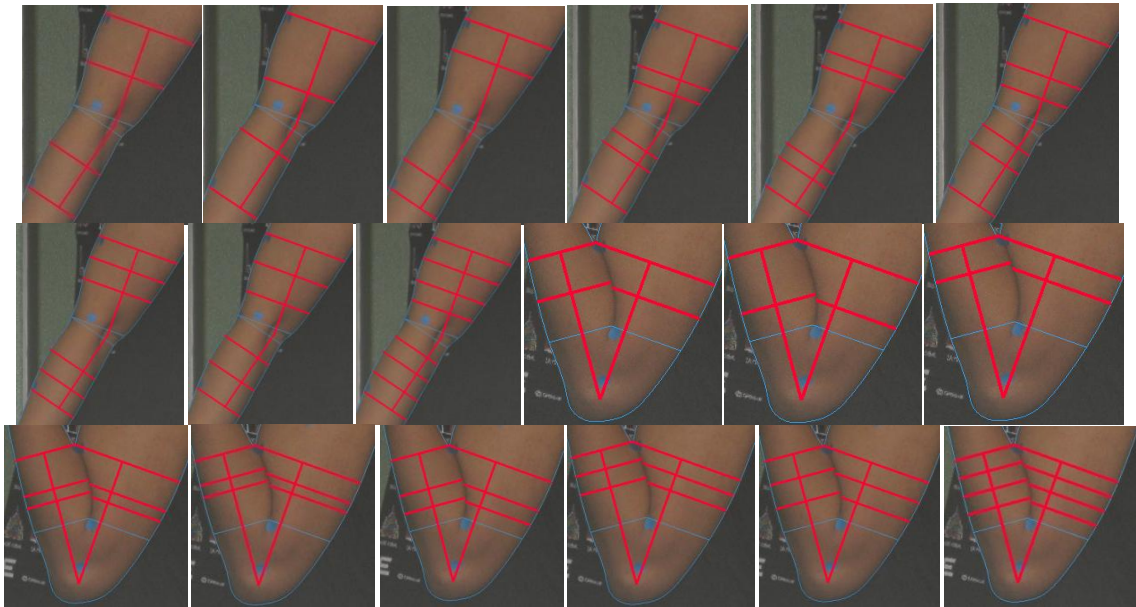


Figure 114. Locations for the inserted cross sections for both upper and lower arms are 50%, 33.33%, 66.66%, [33.33%-50%], [50%-66.66%], [25%-50%], [50%-75%], [33.33%-66.66%] and [35%-75%], from right to left

To reduce the complexity in the mini study, two types of simplification were introduced. Firstly, simple circle shapes were used to represent the cross section. At this stage, using circle cross sections was deemed to be sufficient and was more practical than collecting the real cross sections. The second simplification was introduced to limit the possible combination of the insertion location of the cross sections and avoid testing a vast number of combinations. To limit the possible combination, a set of combinations of locations and number of cross sections were determined. Referring to the point 5 in section 6.6.1, the set of combinations was expressed in the fraction of the bounded area. The chosen combinations were 50%, 33.33%, 66.66%, [33.33%-50%], [50%-66.66%], [25%-50%], [50%-75%], [33.33%-66.66%] and [35%-75%]. The chosen combination was shown in Figure 114 for the fully extended and flexed arms.

Figure 115 shows the surface created from the chosen combinations. The result suggested that uniform distribution of cross section resulted in a more predictable shape outline. If each cross section location could be likened as a point and the surface created as a line, placing the points uniformly would give the same level of control over the overall shape of the line. This was because the surface created from a series of cross sections was affected by the distance between the cross sections. In addition to this, adding more cross sections uniformly also increased the ability of the final 3D shape to follow the outline of the arm. However, it should be remembered that more cross

sections might require longer time for cross sections' acquisition and analysis. It would also mean that, as cross sections' acquisition had to be performed with smaller spaces in-between them, the cross section acquisition became complex.

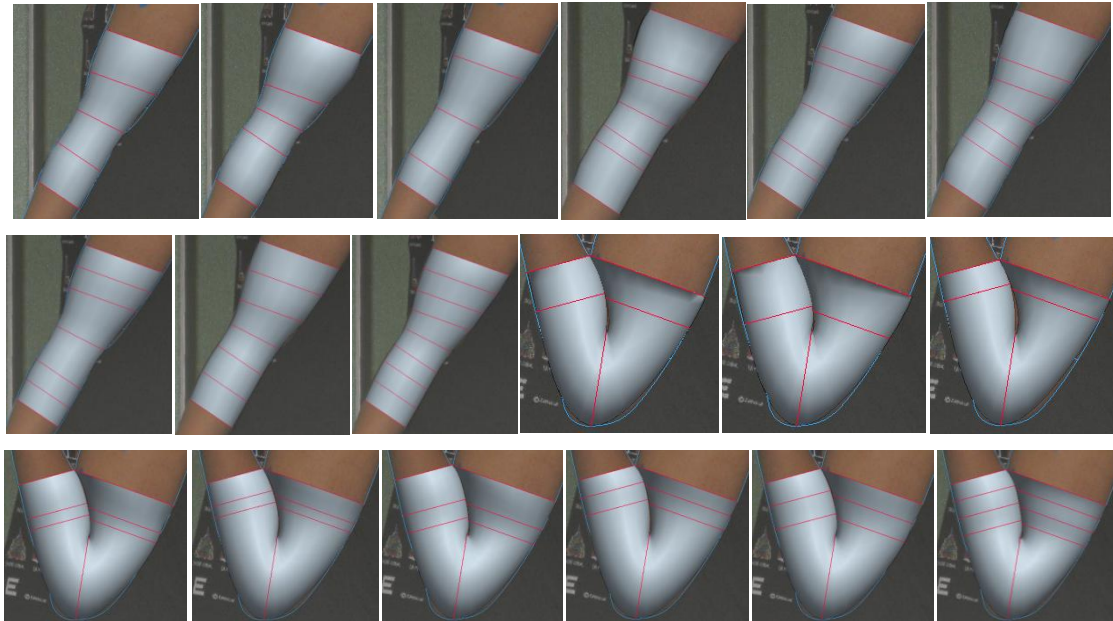


Figure 115. Effect of cross section's location to 3D shape using simplified cross sections

The space available for required additional cross section at the elbow was shown by the area between the closest cross section to the elbow (red line) and the blue line. From the figure, it was clear that positioning cross section on 33.33% of the FDA at both upper and lower arm limited the available space for additional cross section at the elbow. Figure 114 shows that 50% of the upper and lower arm FDA gave the best advantage as it ensured that there was enough space to create additional cross sections at the elbow joint (see point 6 in section 6.6.1). Inserting the perpendicular cross section too close to the UAF/LAF would leave bigger space around the elbow joint whereas the opposite would leave too small space for the creation of the additional cross sections at the elbow.

Based on the result of the mini study, it was decided that a cross section would be positioned in between both the Upper Arm Far-Elbow (UAF-E) and Lower Arm Far- Elbow (LAF-E) regions. The cross section would be positioned at the mid point of the UAF-E and LAF-E regions. These two cross sections would be named as Upper Arm Mid (UAM) and Lower Arm Mid (LAM). Locating the UAM and LAM at the middle of the UAF-E and LAF-E regions assisted in producing a more predictable shape by applying a uniform distribution of cross sections and yet maintaining a low number of cross sections (see point 1 in 6.6.1). It also ensured that enough space was reserved for additional cross sections to fill the gap at the elbow. Altogether, twenty physical measurements by using the wire would have to be performed and processed in order to model the flesh deformation at the elbow. From this point forward UAF, UAM, E, LAM and LAF would be referred as “five key cross sections”.

6.7 Optimum number of sampling points for cross sections

As described in section 5.3.2.4, determining an optimum number of sampling points to represent a cross section was essential as it would support two of DHM specifications i.e. accuracy and real time. From this point forward, points that were required to represent the shape of a cross section would be referred as “sample points”. Too few sample points would result in inaccurate representation of the corresponding cross section whereas too many sample points might result in higher computation demand as there were more data to handle. Thus, a mini study was performed to establish the optimum number of sample points. To determine the optimum number of sample points, the error level of different sampling point numbers was investigated.

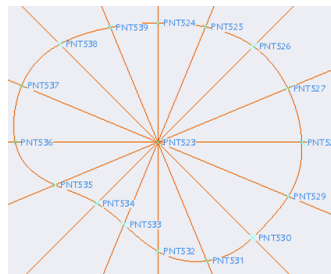


Figure 116. An illustration of sampling 16 points from the elbow cross sections

For this mini study, elbow cross sections at 4 key postures were gathered from three participants, of Asian origin, with different body types i.e. endomorph, ectomorph and mesomorph. Elbow cross sections were used because they had more shape complexity in comparison to UAF, UAM, LAM and LAF. To obtain the elbow cross sections, wires were circled at the elbow joint. The images of the wire, representing the shape of the elbow cross sections, were digitised using the scanner. The digitised images were then traced automatically and converted into .dxf files with CorelTrace. Pro-Engineer Wildfire 4.0 was subsequently utilized to read these files and sample points along the cross sections. The sampling points were sampled through intersecting the cross sections with a number of vectors centred at the cross section's centre. Figure 116 shows an example of how 16 sampling points were acquired. Various sampling point numbers were utilised to recreate the elbow cross sections. A comparison was made to compare them with the original corresponding elbow cross sections and the error level was calculated.

The results are shown in: Figure 117, Figure 118, and Figure 119. The maximum distance represented the highest Euclidean distance error of the recreated cross sections with respect to their original shape. The area difference represented the area difference between the recreated cross sections with respect to their original shape. As it had been expected, the higher the number of sample points, the lower the error in distance and area and thus the closer the recreated cross sections to their original shape. The graphs also show that, initially, the error level declines sharply and is then followed by a more level decline. This meant that the advantage of adding number

points only produced much effect on the error level up to a certain point. Based on the graphs, 16 sample points were chosen to be the optimum number points. In all of the graphs, the 16 sample points were located at the portion where the error level began to level out which meant that the gain of adding more sample points was less substantial

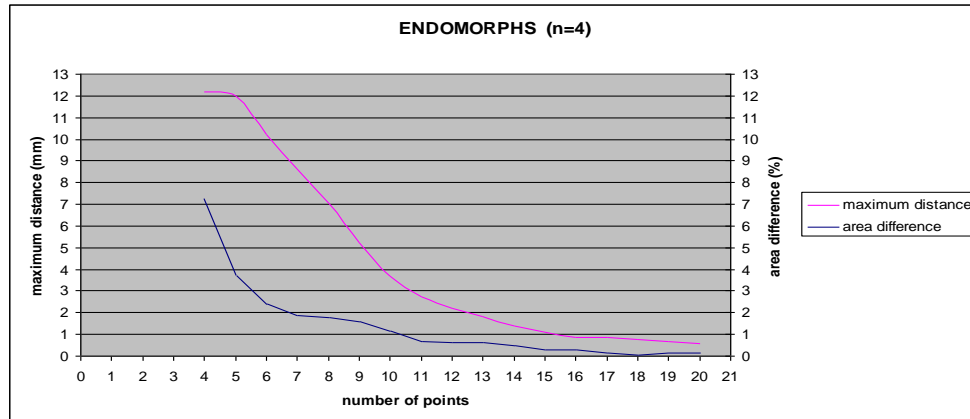


Figure 117. Effect of sample points number on the error level of the cross sections for endomorphs body type

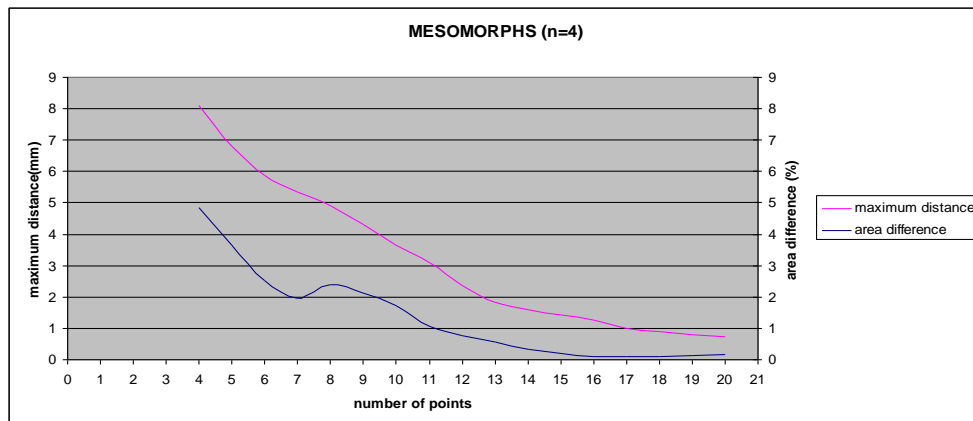


Figure 118. Effect of sample points number on the error level of the cross sections for mesomorphs body type

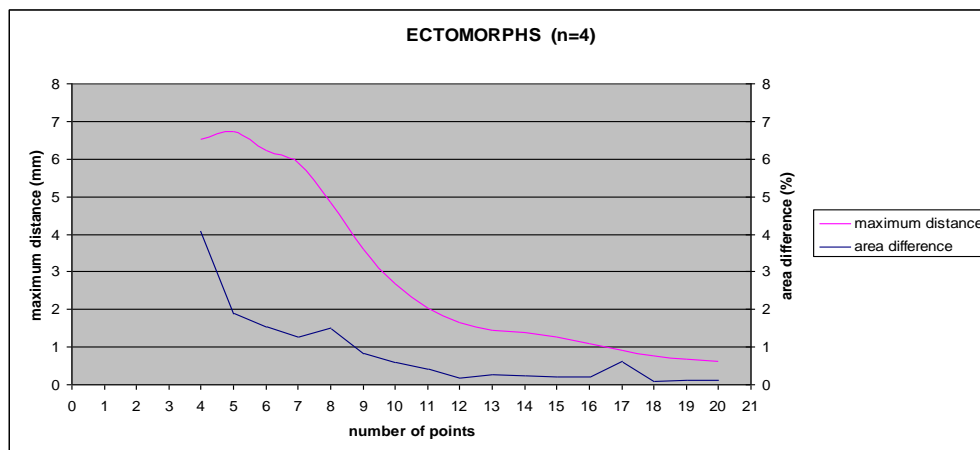


Figure 119. Effect of sample points number on the error level of the cross sections for ectomorph body type

6.8 Summary

The second design phase was succesful in resolving four issues which had been specified in the first design phase. The results for each issue are as follows:

- (i) *Determining the carrying angle.* Measurement of the carrying angle would only be performed for a fully extended arm whereas the decrement of carrying angle would be approximated from the measured carrying angle of a fully extended arm with the support of existing data from Van Roy et al. (2005).
- (ii) *Determining the boundaries of the application of flesh deformation at the elbow.* Two boundaries, so called “upper and lower arm boundaries”, were established to limit the application of flesh deformation at the elbow. They were defined as the meeting point of the upper and lower arm during maximum flexion. The area bounded by these two boundaries was called the flesh deformation area (FDA).
- (iii) *Determining a set of examples to govern the flesh deformation.* Four arm postures, referred to as key postures, were chosen as examples to govern the flesh deformation. The four key postures were: a fully extended arm, a 135° flexed arm, a 90° flexed arm and a fully flexed arm.
- (iv) *Determining cross section properties.* Sixteen sample points were chosen to represent every cross section. The plane of a cross section that was located along the upper or lower arm bones would be perpendicular to the upper or lower arm bones. The plane of a cross section that was located at the elbow would follow the regression equation that captured the relationship between the elbow plane’s orientation and arm angle as described in section 5.3.2.3. There were five key cross sections which had to be obtained for each key posture. These were: (1) UAF (upper arm far), which was located at the upper arm boundary; (2) UAM (upper arm middle), which was located at 50% of the distance between the upper arm boundary and the anterior elbow crease; (3) E (elbow), which was located at the elbow joint; (4) LAM (lower arm middle), which was located at 50% of the distance between the lower arm boundary and the anterior elbow crease; and (5) LAF (lower arm far), which was located the lower arm boundary. A combination of circling wire around the arm and side-front view photographs would be used to acquire the five cross sections above for each key posture.

The second design phase also identified issues that required further investigation which arose entirely from the inability to utilise 3D scan data to acquire five key cross sections from two of the key postures i.e. 90° and maximum flexion. As a result, as described in section 6.4.2, a combination of the circling wire around an arm and photographs was proposed as an alternative approach to acquire five cross sections for each key posture. The alternative approach affected the course of the design phases in two ways:

- (i) *The need to determine a method to integrate joint information into the result of the adopted approach.* The adopted approach allowed the arm shape recreation but without any notion about the location of the joints. As the flesh deformation was partly driven by the bones movement, which were defined by the location of the joints, knowing the locations of the joints was imperative. As this was not anticipated from the earlier design phase, the integration method would need to be established in the third design phase. The proposed integration method would likely involve the utilisation of the joint information from the 3D scan data.
- (ii) *The need to create additional cross sections at the elbow.* The alternative approach, a combination of wire usage and photographs, imposed limitations on the possible plane orientation i.e. perpendicular with respect to the upper or lower arm bones, for cross sections that were located along the upper and lower arm bone. As described in section 6.6, this then resulted in an area that would not be covered as the arm flexes. Thus, a method to provide additional cross sections for this area would be required.

The second design phase also showed that as some of the issues were related to each other, their final solution was influenced or affected by the chosen solution in the previous stages. For instance, the determination of the key posture was affected by the chosen boundaries of the elbow flesh deformation i.e. FDA. Another example was how the chosen method to capture the cross sections affected the final outcome on cross section plane orientation, number and location. The second design phase also showed that relevant DHM specifications assisted the decision making to resolve most of the issues. For instance, to satisfy the accuracy and real time specifications, the search for an optimum number of sample points to represent a cross section was performed. A similar example of an effort to satisfy the accuracy and real time specifications was the search of optimum number of key postures to represent the non-linear behaviour of flesh deformation at the elbow. The overall design process from the second design phase demonstrated clearly the complexity of the process to develop the proposed FDM.

Following the results of the second design phase, the third design phase would address the identified two issues above. In addition to this, the concept concerning the utilisation of interpolation to govern the flesh deformation would also be finalised in the subsequent design phase.

7 Third Design Phase

The third design phase was aimed at resolving issues which were identified in the second design phase. These issues were: (i) integrating joint information from the 3D scanned arm into the chosen method to obtain the cross sections, (ii) creating additional cross sections to fill the gap at the elbow joint and (iii) performing interpolation to govern the flesh deformation. The first two issues arose as a result of the chosen method to acquire five cross sections for each key posture i.e. a combination of wire usage and a set of photographs. Relevant DHM specification(s) would be considered in resolving each issue. Figure 120 shows the relationship between the first two issues to be addressed in the third design phase and their relationship with the previous design phases. The strategy to resolve each issue and the final outcome are discussed in each section.

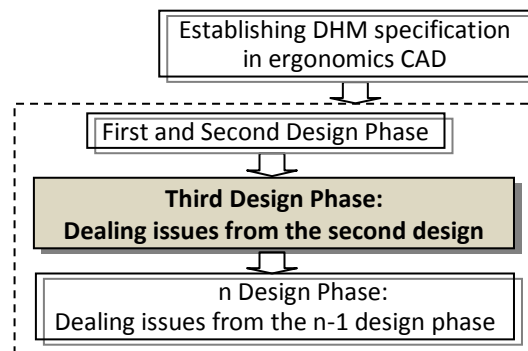


Figure 120. Third design phase, relatives to other stages in the research

7.1 Integrating joint information and digitised cross sections

The first issue to resolve was to investigate how to integrate joint locations from a 3D scanned arm i.e. a shoulder, elbow and wrist joints with digitised five key cross sections i.e. UAF, UAM, E, LAM and LAF. As described in chapter 6, the chosen approach to obtain cross sections for the four key postures i.e. full extension, 135° flexion, 90° flexion and maximum flexion; only gave an ability to recreate the surface of an arm i.e. by arranging them along the lower/upper arm bones. However, flesh deformation due to joint movements could only be modelled when the relationship between five key cross sections and relevant joint locations was established for all key postures. Thus, to allow flesh deformation modelling, an integration of digitised five key cross sections with joint locations was required for each key posture. From this point forward, the digitised five key cross sections of a key posture would be referred to as “*digitised cross sections*” whereas five key cross sections which were a result of interpolation of digitised cross sections would be referred to as “*interpolated cross sections*”. The term “*five key cross sections*” would refer to be both i.e. “*digitised cross sections*” and “*interpolated cross sections*”

Joint locations of a 3D scan data were proposed to be utilised because they provide a readily available 3D coordinates of joint locations. This decision was also in line with the intention of this research to maximise the utilisation of 3D scan data, where appropriate, as described in chapter 1. However, utilisation of a 3D scan data and/or its joint locations also presented a limitation i.e. they were dependent on the [TC]² NX-12 body scanner's abilities to provide 3D scanned arms for required key postures and robust joint locations. Effects of this limitation would be reviewed in section 7.1.1. The outcome of the review was then used as the foundation of the proposed strategy for integration of joint information and digitised cross sections.

7.1.1 The strategy to integrate joint information and digitised cross sections

In order to propose a strategy that supports the utilisation of joint locations' 3D scan data from [TC]² NX-12 3D body scanner, there were two aspects to be considered. These were: (1) [TC]² NX-12's ability to provide 3D scanned arm; and (2) [TC]² NX-12's ability to provide robust joint locations. Each of the aspects is discussed in the following:

1. **[TC]² NX-12 3D body scanner's ability to provide 3D scanned arm.** Based on the studies in section 6.3, four key postures i.e. a full extension, 135° flexion, 90° flexion and maximum flexion, were proposed to guide the flesh deformation. For each key posture, its digitised cross sections required integration with joint locations that were corresponding with the arm angle of the key posture e.g. digitised cross sections of 90° flexion would require joint locations of 90° flexion. However, the studies in section 6.3.1 showed that [TC]² NX-12 only produced a 3D scanned arm for an arm angle that was $\geq 90^\circ$. Thus, the 3D body scanner only provided joint locations for two of the key postures i.e. a full extension and 135° flexion. Assuming that the joint locations of these two key postures could be used, it meant that a different integration approach would be required for 90° and maximum flexion of which 3D scanned arms were not available. Thus, two stages of integration would be required: (1) integration of digitised cross sections and joint locations where joint locations of a 3D scanned arm were available; and (2) integration of digitised cross sections and joint locations where joint locations of a 3D scanned arm were **not** available.

Figure 121 shows the proposed approach for each stage. The proposed approach for the first stage was based on associating joint locations and digitised cross sections by using the side and front view photographs of an arm. In section 6.4.2, which described the cross sections acquisition method, capturing the arm cross sections was also accompanied by taking photographs of an arm from the side and front which were at 90° with respect to each other. Assuming that these photographs and a 3D scanned arm shared exactly the

same arm posture, the 3D scanned arm could be positioned to match the photographs. Since the 3D scanned arm provided joint locations, a direct link between photographs and joint locations could be established. This direct link provided a means to integrate joint locations and digitised cross sections because the photographs were required to arrange the placement of digitised cross sections. For the second phase, the proposed approach adopted the approach from the mini study in section 6.2.2. In section 6.2.2, the photographs of the arms were arranged such that flesh deformation changes could be observed from one posture to another by overlapping the upper arm from the photographs. Adopting this approach enabled incorporation of the set of photographs that were embedded with the joint information i.e. the outcome from the first stage, onto the photographs that were without joint information. As the proposed approach only provided general guideline, details of each stage would have to be established. The details of each stage contained a protocol that needed to be followed to integrate joint locations and digitised cross sections.

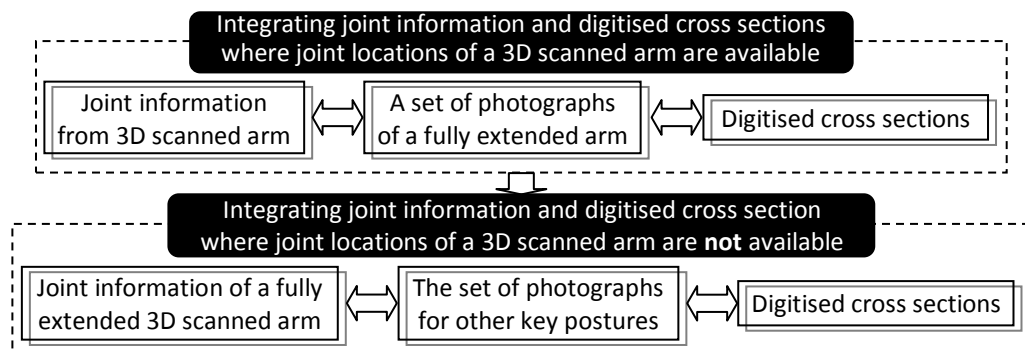


Figure 121. Two stages of joints information and digitise cross sections integration

2. **[TC]² NX-12 3D body scanner's ability to provide robust joint location.** [TC]² NX-12 is mainly aimed at extracting body measurements for either clothing purposes in which the arm remains fully extended i.e. the first key posture. Thus, it is highly probable that the body scanner ability could produce a robust joint location for this posture. However, it was not known whether the robustness was applicable for joint location at 135° flexion. Thus, a mini study would be required. The outcome of the mini study determined whether joints location of a 3D scanned arm at 135° flexion could be used as part of the integration process or not.

Based on the review of the two aspects above, a strategy to address the integration of joint locations and digitised cross sections was proposed. Figure 122 shows the proposed strategy which consisted of three phases. Each phase is discussed in the following subsections.

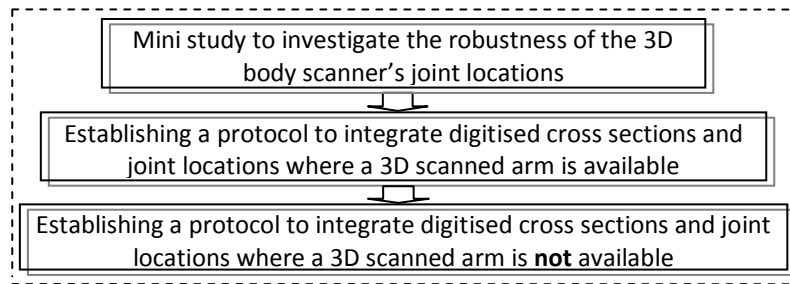


Figure 122. The proposed strategy to integrate digitised cross sections and joint locations

7.1.2 Mini study to investigate the robustness of the 3D body scanner's joint locations

Following the proposed strategy shown in Figure 122, a mini study concerning the robustness of joint information from the 3D body scanner ([TC]² NX-12) was performed. The aim of the mini study was to investigate the robustness of the 3D body scanner's joint information, especially for joint locations at 135°. This research defined the robustness of the 3D body scanner's joint information as ability of the 3D body scanner to produce joint information with a considerably small variation. Variation of the lower and upper arm bones' length was proposed to measure the robustness. Given the same arm and posture to be scanned for a number of times, it was argued that the length of the lower and upper arm bone should be more or less constant as there were no changes on the object to be scanned. Variation of the arm's lengths could be identified from its standard deviation value. The smaller the variation of the lower/upper arm length, the smaller the standard deviation. Smaller standard deviation indicated the robustness of joint information extraction. Using this rationale, to investigate the robustness of the 3D body scanner joint extraction, the standard deviation of the upper and lower arm bones was calculated.

For the mini study, a participant was required to be scanned while assuming a full extension and 135° flexion. A total of 12 3D scanned arm data were collected, 6 for a fully extended arm (data set 1) and another 6 for 135° flexion (data set 2). The processing of 3D scanned arm data and the upper and lower arm bone determination followed the approach described in section 5.2. Table 6 shows data for each group and its corresponding standard deviation value. The result shows that a fully extended arm was more likely to produce a smaller variation in the upper and lower arm bones length. Based on the mini study result, it was apparent that the joint location given by the 3D body scanner showed a tendency to be less reliable when the arm was no longer in a full extension. The reason for this might be down to the aim of the 3D body scanner itself which focused on measuring anthropometric features while a person assumed a posture in which the arm remained fully extended. Based on the mini study result, it was decided that only joint locations from a 3D scan of a fully extended arm would be utilised in the integration of digitised cross sections and joint

locations. This decision was in line with one of the DHM specifications i.e. accuracy. This decision also implied that the method to integrate digitised cross sections and joint locations where a 3D scanned arm was available would only be applicable for a fully extended arm.

Table 6. Variations of upper and lower arm bone length from the 3D scanned arms

	Fully extended arm		135° flexion	
	Upper arm bone length (mm)	Lower arm bone length (mm)	Upper arm bone length (mm)	Lower arm bone length (mm)
	224.258	208.773	218.675	205.612
	220.092	213.174	209.865	209.865
	212.3858	214.781	228.508	209.912
	210.282	206.1402	186.712	186.712
	216.1435	203.2949	154.293	213.448
	220.2363	202.6917	155.783	207.235
Standard deviation	6.542705	3.96987	32.01387	9.567587

7.1.3 A protocol for integration of a 3D scan of a fully extended arm with its joint information and digitised cross sections

Following the proposed strategy shown in Figure 122 (section 7.1), a protocol on utilising side-front view photographs to integrate joint locations and digitised cross sections was required. The proposed protocol, shown in Figure 123, implied that data acquisition and pre-processing were required before the integration could take place. This data acquisition and pre-processing were mostly identified from the earlier design phases i.e. section 5.2, 6.2.2 and 6.4.2.

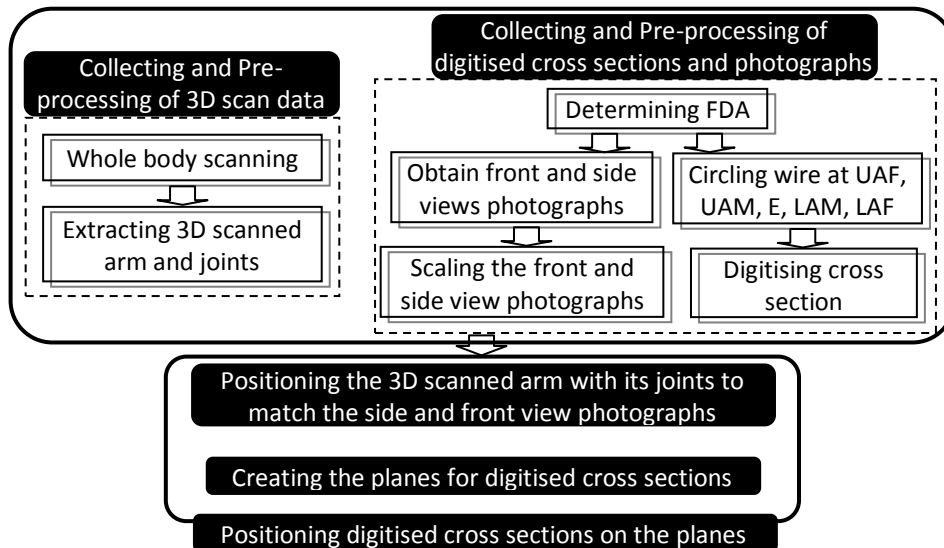


Figure 123. The proposed protocol to integrate joint locations of 3D scanned arm and digitised cross sections

To assess the feasibility of the proposed protocol, each step of the protocol was followed and applied on participant data. A 3D scan of a fully extended arm and cross sections (UAF, UAM, E, LAM and LAF) of a fully extended arm data was collected from the same participant in the mini study in section 6.4.2. In addition to this, the participant's eight photographs i.e. 4 front and 4 side views photographs, which depicted four key postures, which were already obtained during the mini study

in section 6.4.2, were also used. For this subsection, only the front and side views photographs of a fully extended arm were required. Each step of the protocol is outlined as follows:

1. **Collecting and pre-processing of 3D scan data.** Following the carrying angle requirement (see section 6.1.2), the participant's arm was scanned while assuming a fully extended posture and pronated hand. Data pre-processing for the 3D scan data in section 5.2 was followed to extract the 3D scanned arm and its relevant joint information.
2. **Collecting and pre-processing of digitised cross sections and photographs.** The side-view photographs were captured simultaneously by two cameras. A reference was attached to the partition board to assist the scaling of the photograph of the arm side view. Prior to taking photographs of the arm, markers were attached to the skin on the shoulder (side and front), the mid of the arm (side), the elbow (mid, side and front) and on the wrist (side, front and back) and the FDA (the area where the upper and lower arms meet while the arm is maximally flexed). Complete details of how to obtain the side-front view photographs were given in section 6.4.2.



Figure 124. Scaling the front view photograph to match the size of the arm of the front view photograph

Following the proposed protocol's diagram in the Figure 123, the front and side views photographs had to be scaled. Scaling the front and side view photographs was aimed to ensure that both photographs were consistent in representing the arm dimension. The reference, which could be used to scale the photograph, only existed in the side view photograph. As the size of the reference was known, the side view photograph was scaled so that the reference size matched to its real life size. Assuming that the length of the arm in the side and front view photographs were the same, the length of the arm in the side view photograph could be used to scale the front view photograph. Using Pro-Engineer WildFire 4.0, the side view photograph of the fully extended arm was scaled using the reference within the photograph. A rotation of the photograph was also used if the digital camera was slightly tilted during data collection. To scale the front view photograph, firstly,

the size of the arm in the side view photograph was measured (L_1) and this was then used to scale the arm length's in the front view photographs so that its arm size (L_2) matched the size of the arm in the side view photograph (see Figure 124).

Cross sections were acquired by circling the wire at UAF, UAM, E, LAM and LAF while the participant extended the arm fully. Referring to sections 5.3.2.3 and 6.6.2, the location of each cross section was defined as: (i) at the upper boundary of FDA for UAF, (ii) at the lower boundary of FDA for LAF, (iii) at the elbow joint and the crease of the anterior elbow for E, (iv) at the mid point between the crease of the anterior elbow and the upper boundary of FDA for UAM, and (v) at the mid point between the crease of the anterior elbow and the lower boundary of FDA for LAM. Figure 125 shows an illustration of the wires used to capture the cross sections at the five different locations. The wires, taking after the shapes of the cross sections, were traced manually and then digitised using a flat-bed scanner as previously described in section 6.4.2. The digitised images were then traced automatically and converted into .dxf files with CorelTrace. Pro-Engineer Wildfire 4.0 was then utilized to read these files and recreate the cross sections. The final outcome of this process was B-spline curves of cross sections.

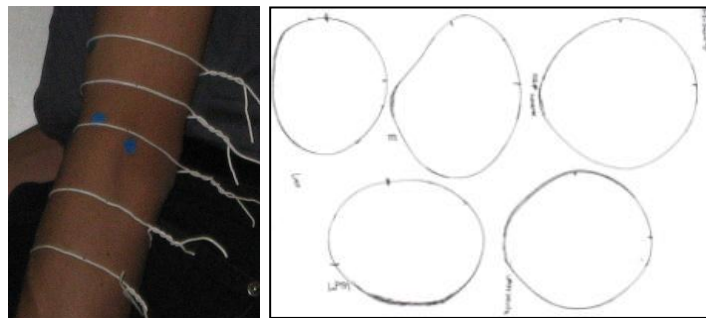


Figure 125. Using the wires to capture the cross sections at five locations while the arm is fully extended and the digitised cross sections

3. ***Positioning the 3D scanned arm with its joints to match the side and front view photographs.*** To position the 3D scan of a fully extended arm with its joint location so that it matched the side and front view photographs, Pro-Engineer Wildfire 4.0 was utilised. Pro-Engineer Wildfire 4.0 provided warp feature which allowed transformation i.e. rotation and translation, of any object in its virtual 3D environment. This feature was used to transform the 3D scanned arm with its joints to match the side and front view photographs. The 3D scanned arm and its joints were positioned and orientated manually so that it was as close a match to the photograph as possible (see Figure 126). Visual judgement was used to define the best fit.

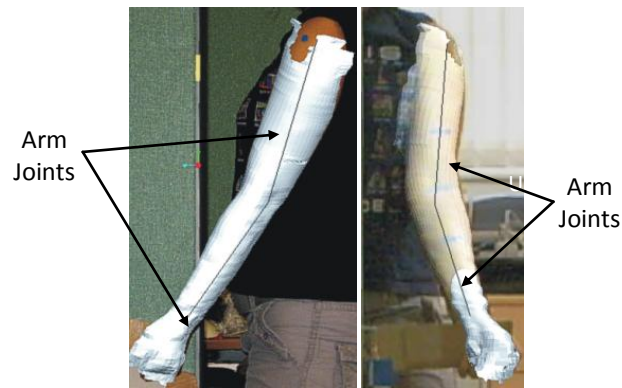


Figure 126. Embedding joints from 3d scanned arm onto the photographs

4. **Creating the planes for digitised cross sections.** Using the FDA markers within the photographs and the embedded joints from the 3D scanned arm, the orientation and location of four digitised cross sections' planes, i.e. UAF, UAM, LAM and LAF were determined (Figure 127). Referring to section 6.5, except the E cross section, the rest of the cross sections were placed on the planes which were perpendicular to the upper/lower arm bones.

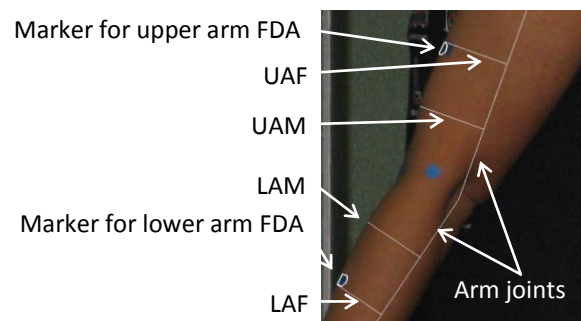


Figure 127. Locations of UAF, UAM, LAM and LAF on the side view photograph of a fully extended arm

A special procedure was required for the placement of the E cross section. The E cross section was placed on a plane that was created from two components: (i) the elbow plane line that passed through the elbow joint and crease of the anterior arm and (ii) the common plane of the upper and lower arm bones. The line that passed through the elbow joint and crease of the anterior arm was created in accordance with the finding in section 5.3.2.3 whereas the common plane concept was briefly explained in 5.3.1. Firstly, using the upper and lower arm bones, a common plane was created (UA-LA, Figure 128a). Then on this plane, with the assistance of the photograph, the elbow plane line (E line) which passed through the elbow was drawn (Figure 128b). The elbow plane was defined by creating a new plane which was perpendicular to the UA-LA plane and passed through the E line (Figure 128c).

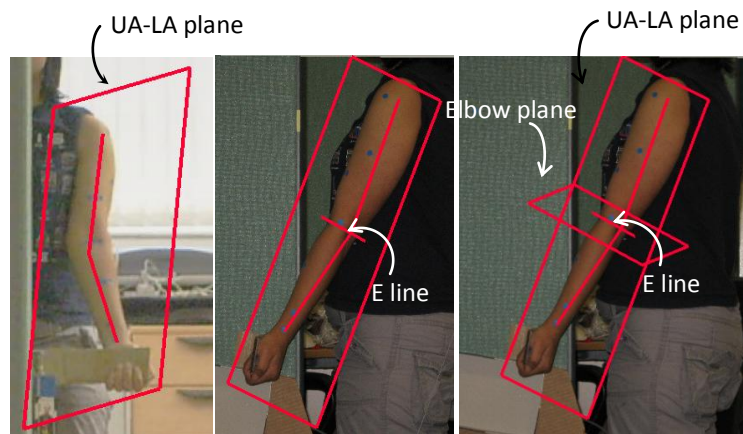


Figure 128. a) Creating common plane from upper and lower arm bone; b) Creating E line, which passed through elbow and crease of the anterior elbow, on the common plane; c) Creating the elbow plane which passed through E line and perpendicular with respect to the common plane

5. **Positioning digitised cross sections on the planes.** Once the joint information and planes of digitised cross sections were embedded onto the photographs, the digitised cross sections of a fully extended arm could be added. Each of the digitised cross sections was located on its corresponding plane and orientated manually with the assistance of the side and front view photographs. The final result, shown in Figure 129, demonstrated that proposed protocol succeeded to integrate joint locations of a 3D scan of a fully extended arm and digitised cross section.

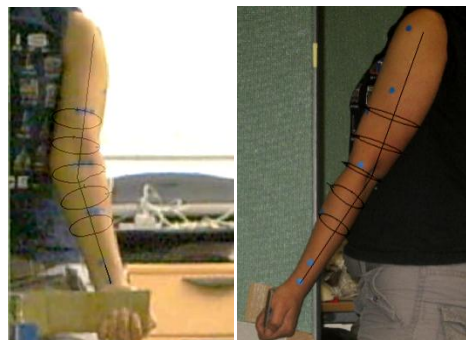


Figure 129. Five cross sections were manually located and orientated

7.1.4 A protocol for integration of joint information and digitised cross sections where a 3D scanned arm was not available

Following the strategy shown in section 7.1, a detail protocol to integrate joint locations and digitised cross sections for key posture other than a fully extended arm was proposed. Section 7.1 described how the proposed approach was based on the mini study's method in section 6.2.2. In section 6.2.2, the photographs of the arms were arranged such that flesh deformation changes could be observed from one posture to another. This arrangement was based on the assumption that the extension-flexion of the lower arm could be performed without any required movement from the upper arm. Thus, the upper arm would remain constant i.e. the same posture, throughout flexion-

extension movement. This meant that the upper arm could be used to guide the placement and orientation of the photographs of the other key postures. This assumption also implied that the upper arm bone of the other key postures would be the same as that of the fully extended arm. To determine the lower arm bone, the arm markers within the photographs were used. As described in section 6.4.2, prior to taking the photographs of the arm, markers were attached to the skin in various locations, including the wrist i.e. on the side, front and back. Using two of these photographs' markers, e.g. side and front, the location of the wrist joint could be approximated. The proposed protocol is shown in Figure 130.

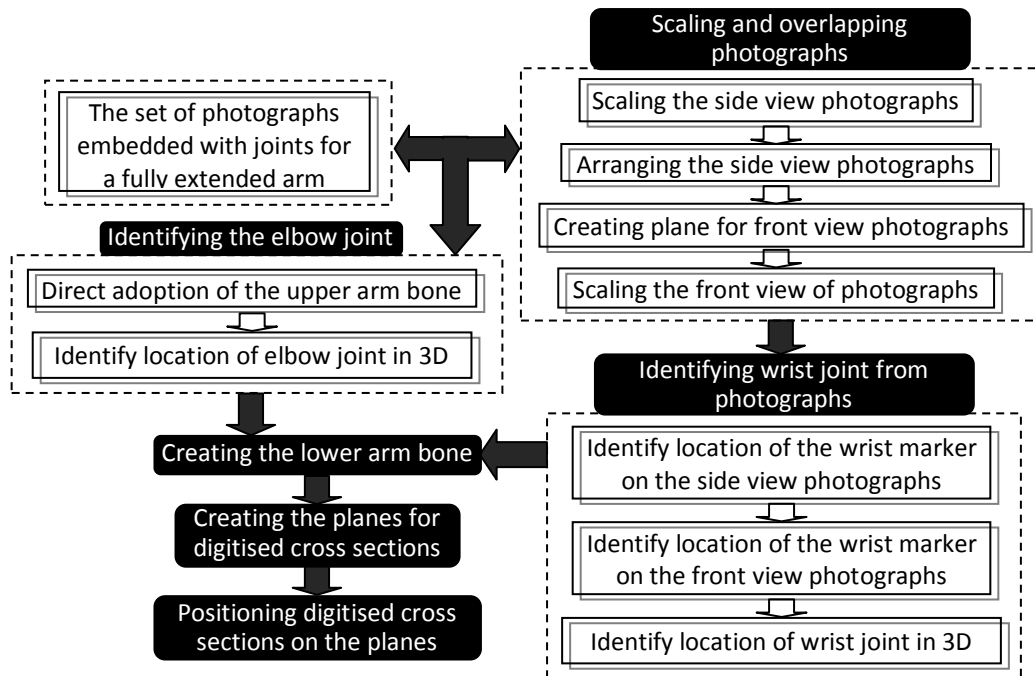


Figure 130. The proposed procedure to extend the joint information of a fully extended arm to other key postures

To investigate the feasibility of the proposed protocol, each step of the protocol was followed and applied on the participant's data that has been collected in section 7.1.2. The protocol for integration of digitised cross sections and joint locations is detailed as follows:

1. **Scaling and overlapping photographs.** The scaling of side view photographs for the three key postures i.e. 135°, 90° and maximum flexion followed the protocol described in point 2 in section 7.1.3. After size adjustment, the side view photographs of the other key posture photographs were overlapped with the side view photographs of a fully extended arm. Adopting the method described in section 6.2.2, upper arm was used to guide the placement and orientation of the photographs of the three key postures. The results are shown in Figure 131.

The partition board's edge of the side view photograph indicated how to position the front view photograph i.e. its location and orientation, with respect to the side view photographs.

A close observation of Figure 131 shows that the side view photographs of the three key

postures had to be rotated (α_1 , α_2 , α_3) in order to ensure that their upper arm overlapped with that of the fully extended arm. As a result, the location and orientation of the front view photographs were also changed.

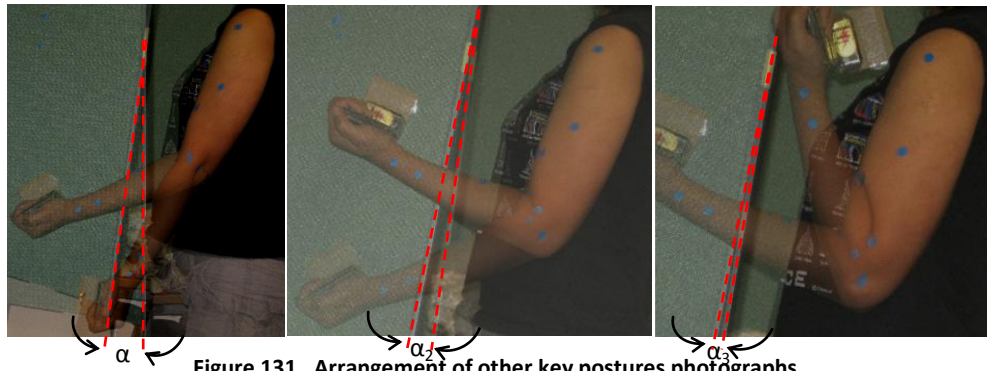


Figure 131. Arrangement of other key postures photographs

Figure 132a showed how the partition board's edge was used to assist creating the plane for the front view photograph. This was then followed by scaling the front view photograph which was described in point 2 in section 7.1.3. The final result is shown in Figure 132b.

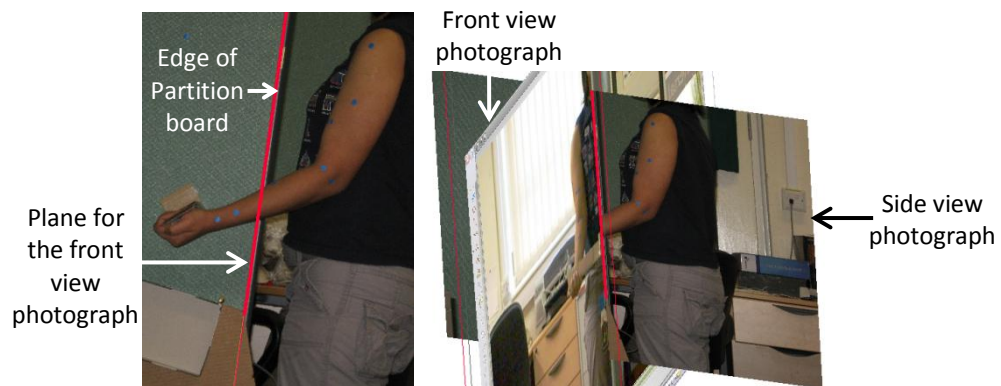


Figure 132. (a) The board in the side view photograph was used to create the plane for the front view photograph. (b) The front view and side view photograph after rescaling

2. **Identifying the wrist joints from photographs.** To determine the wrist joint location of the three key postures, both of the side and front view photographs were used. First, the wrist marker in the side view photograph was identified. A plane which was parallel with respect to the front view photograph plane (FV_{plane}) was created on the wrist marker. Next, a second plane which went through both of the elbow joint and the wrist marker was created. Figure 133a shows both planes. The last plane was created using the front view photograph. The wrist marker location on the front view photograph was identified and a plane parallel to the side view photograph plane (SV_{plane}) was created (see Figure 133b). The wrist joint was the intersection of the three planes.

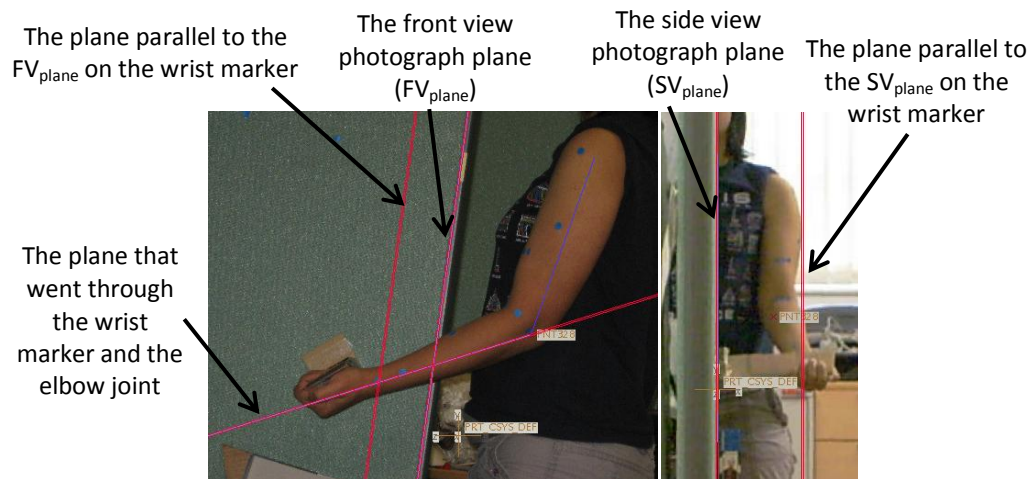


Figure 133. Left image: creating two planes on the side view photograph. Right image: creating a plane on the front view photograph

3. **Identifying the elbow joints.** The next step was to identify the location of the elbow joint. As a result of overlapping all of the upper arms in the side view photographs, the upper arm bone i.e. shoulder and elbow joints of the fully extended arm was adopted directly for the three key postures.
4. **Creating the lower arm bones.** The lower arm bones of the three key postures were created by connecting the elbow and wrist joints. Figure 134 shows the upper and lower arm bones for all key postures.

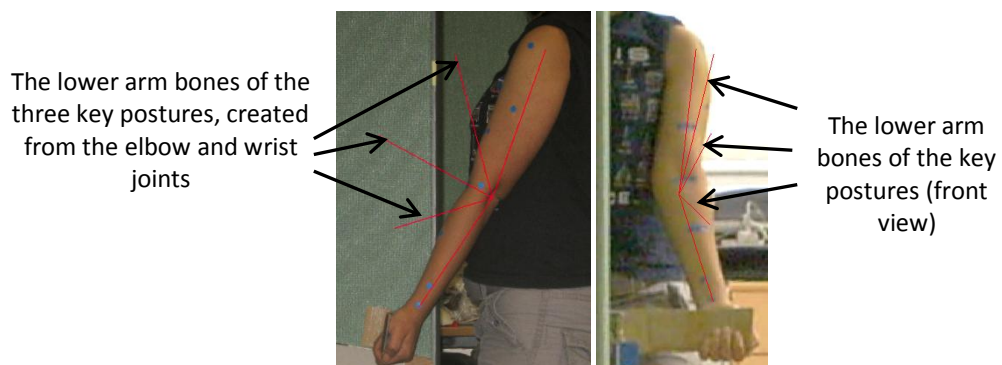


Figure 134. Extending joint location of a fully extended arm into other key postures

5. **Creating the planes for digitised cross sections.** The approach was similar to that described in point 4 in section 7.1.3. Figure 135 shows the locations and plane orientation of the cross sections of UAF, UAM, LAM, and LAF which were determined for the three key postures by using the markers.

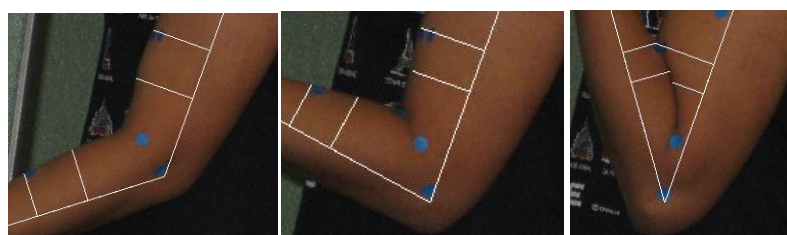


Figure 135. Locating UAM and LAM for all key postures

6. **Positioning digitised cross sections on the planes.** Point 5 in section 7.1.3 described the protocol to position digitised cross sections on planes. Figure 136 shows an example of the final result of the integration between joint locations and digitised cross sections for 135° flexion.

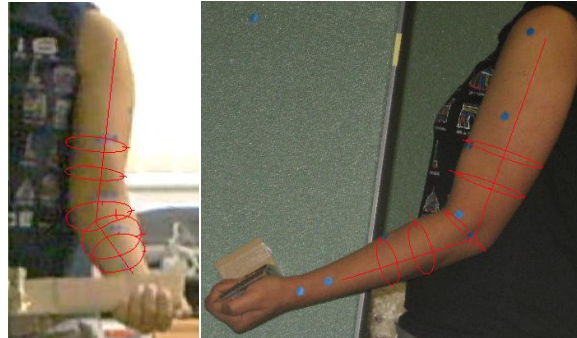


Figure 136. Final result of the integration between joint locations and digitised cross sections for 135° flexion

7.1.5 Discussion

As described in section 7.1.1 and 7.1.2, the protocols to integrate joint information and digitised cross sections were based on consideration and partial investigation of two relevant aspects i.e. [TC]² NX-12's ability to provide 3D scanned arm and [TC]² NX-12's ability to provide robust joint locations. The protocols focused on the utilisation of [TC]² NX-12 3D body scanner as it provided readily available 3D coordinates of joint locations. Two stages of protocols were proposed i.e. (1) A protocol to integrate joint information of a 3D scan of a fully extended arm with digitised cross sections; and (2) A protocol to integrate joint information and digitised cross sections for 135°, 90° and maximum flexion.



Figure 137. Vitus Smart LC (Human Solutions, 2011) 3D laser scanner

The first protocol, described in detail in section 7.1.3, involved manually matching a 3D scan of a fully extended arm and its joint information to side-front view photographs. This, in turn, allowed the integration of joint information and digitised cross sections because the photographs were also used to assist positioning digitised cross sections. At the end of section 7.1.3, it was shown that the

proposed protocol to integrate joint locations of a fully extended 3D scanned arm and digitised cross section was successful. It is acknowledged that the accuracy level of the integration result could be compromised by the manual adjustments involved in the protocol because they were likely affected by intra and inter-observer effects. For future studies, the level of manual adjustment could be minimised by taking side-front view photographs and 3D scan data of arms simultaneously. This could be achieved by utilising a laser body scanner instead of a light-patterned body scanner. A light-patterned body scanner required a specific environment setting i.e. a closed cubicle with black wall due to its sensitivity to colour contrast which, in return, inhibited the possibility to obtain side-front view photographs and a 3D scanned arm simultaneously. In contrast, a laser body scanner, such as Vitus Smart LC (shown in Figure 137) would not require a closed cubicle with black wall which meant that side view and front photographs could be acquired simultaneously while a participant was being scanned.

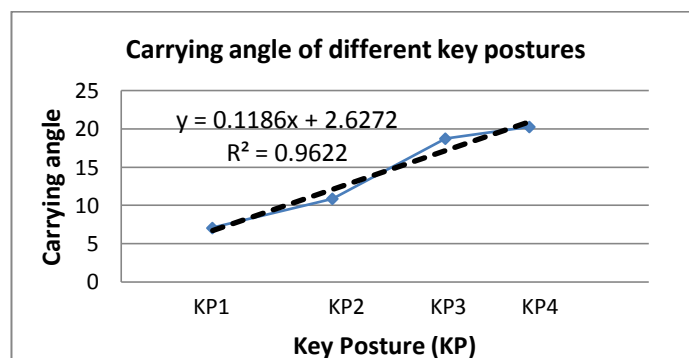


Figure 138. The carrying angle of different key posture from Figure 134

The second protocol, described in detail in section 7.1.4, involved the use of markers on the side-front view photographs and joint information of a 3D scan of a fully extended arm. The joint information of a 3D scan of a fully extended arm provided joint information for the upper arm i.e. shoulder and elbow, whereas the markers of side-front view photographs provided joint information for lower arm i.e. wrist. At the end of section 7.1.4, it was shown that the proposed protocol to integrate joint locations and digitised cross section for postures other than a fully extended arm was successful. A close observation on Figure 134 showed that the second protocol unexpectedly produced a side effect of enabling measurement of the carrying angle for other key postures. This presented an opportunity to investigate the ability of the second protocol in capturing the behaviour of carrying angle as the arm flexion took place. In section 6.1.1, it was found that carrying angle decreased linearly as the arm flexed. Adopting the carrying angle measurement method in section 6.1.3, the carrying angles in Figure 134 were measured. The result, shown in Figure 138, demonstrated that the carrying angle decreased more or less linearly as the arm flexed, which was in accordance with the finding in section 6.1.1. As the carrying angle measurement was based on joint locations (shoulder, elbow and wrist joint), this suggested that the second proposed protocol

approximated the joint locations with sufficient accuracy. Thus, given side-front views photographs and a 3D scan of a fully extended arm, linear decrement of the carrying angle could be obtained. This unexpected finding provided an option to represent the linear decrement of the carrying angle in addition to the proposed method which was described in section 6.1.4. It also suggested that the proposed method was in accordance with one of DHM's specifications i.e. accuracy. For future studies, the carrying angle's result of the proposed protocol could be compared with that of manual measurement.

7.2 Generating the additional cross sections

The second issue to be resolved was to establish a method to generate additional cross sections from five key cross sections. As described in section 6.6, due to planes orientation of UAF, UAM, LAM and LAF i.e. perpendicular with respect to the upper/lower arm, a gap was created at the elbow joint area. This gap could potentially reduce the detail at the elbow joint area and subsequently affect the quality of the flesh surface. To avoid this, creation of additional cross sections at the elbow was required. From this point forward, additional cross sections at the elbow would be referred to as "additional cross sections". As obtaining additional cross sections through the wire was not an option, the reasons being described in section 6.4.2; an alternative method was proposed.

This research proposed utilisation of five key cross sections. The proposed method was inspired by how a surface could be sampled to provide some points. Applying this principle in this research, a certain number of points could be sampled from a surface created from five key cross sections. These points could subsequently be used to generate additional cross sections. Figure 139 shows the strategy of the proposed method to generate additional cross sections. The first phase of the strategy was performed to gather information regarding surface creation and how it could be used to provide a certain number of points to generate additional cross sections. The outcome of this phase was then used to provide general outline of the method which was subsequently detailed in the third phase.

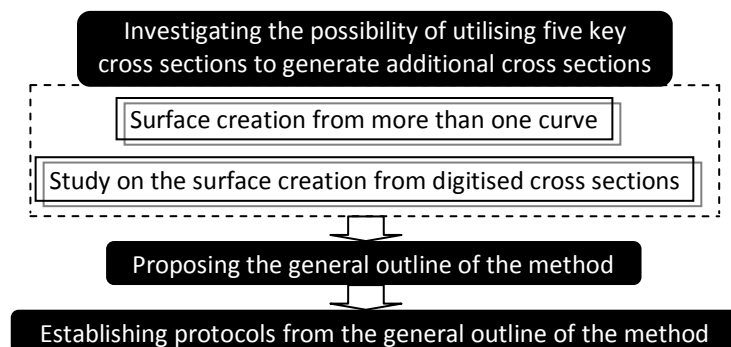


Figure 139. The strategy to create additional cross sections from digitised cross section or their interpolation

7.2.1 Investigating the possibility of utilising five key cross sections to generate additional cross sections

Following the strategy shown in Figure 139, investigations concerning the possibility of utilising five key cross sections to generate additional cross sections were performed. The investigations took form as two studies which looked into how surfaces are created from more than one curve and how these principles could be adopted to a surface created from five key cross sections. In each of the studies, important factors would be identified. These important factors would then be used to outline the proposed method in generating additional cross sections in section 7.2.2.

7.2.1.1 Surface creation from more than one curve

This section studied how a surface is created from underlying curves. A 3D surface could be created providing there is more than one line/curve that could be used to guide the surface creation. To represent a 3D surface, a finite number of points on the surface are calculated. The calculation of these points could be seen as sampling at different locations along the finite number of “surface lines” which connect the corresponding lines/curves. Figure 140 shows the illustration of a simple surface creation from two lines i.e. A and B. A finite number of surface lines (x_i) that connect the lines A and B are created. By sampling at different locations (p_i) along the finite number of surface lines (x_i), the surface could be represented. This principle could be applied to generate the additional cross sections at the elbow by obtaining points from “surface lines” of the digitised cross sections’ surface.

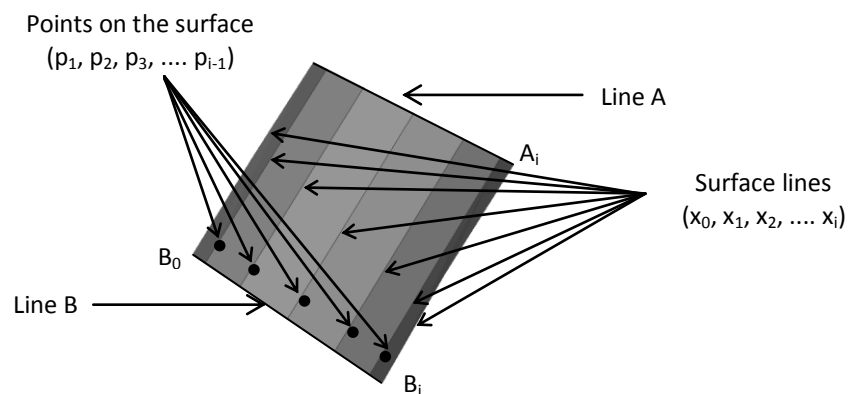


Figure 140. Surface creation from two lines (A and B); a finite number of surface lines (x_i) which connects the line A and B were formed. Sampling at different locations along the surface lines allows the surface creation

To apply the principle, “surface lines” had to be created from the digitised cross sections’ surface and a number of points had to be obtained from them. Creation of surface lines would require an establishment regarding the number of surface lines which reflected the number of points that were required to create each of the additional cross section. In section 6.7, it was found that the optimum number of points to represent a cross section was 16. Assuming that this finding was also applicable for an additional cross section, the number of surface lines was suggested to be

16. Obtaining a number of points from surface lines would require an establishment regarding the location and number of additional cross sections to be created. In section 6.6, it was found that uniform placement of cross sections resulted in a more predictable shape outline. Taking into account this finding, additional cross sections were suggested to be located at 1/3 and 2/3 of the LAM-E and UAM-E.

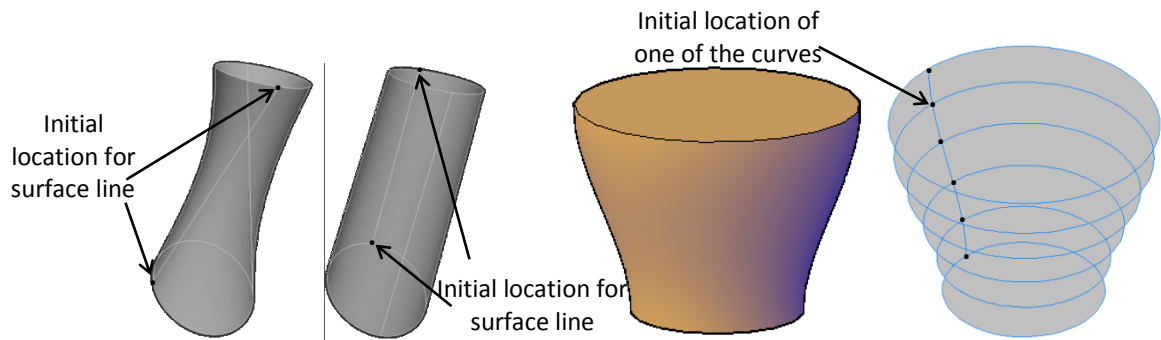


Figure 141. Initial location of surface creation and its effect

Figure 140 shows that to create x_i finite number of surface lines, both line A and B are divided into i sections. The figure also reflects that the creation of x_i begins at the initial point of both lines i.e. A_0 and B_0 and ends at the end of both lines A_i and B_i . As A and B are mere straight lines, it is easy to determine where x_i should be initiated i.e. the initial point of A and B. However, if A and B are 3D closed curves e.g. circles, the location where x_i is initiated would affect the final surface, as shown in the first two images in Figure 141. For a surface that was created from more than two curves, the initial points of all curves had to be located on the same plane in order to avoid the effect illustrated in the first image in Figure 141. An example of this is shown in the last two images in Figure 141. As the existing digitised cross sections were closed curves, this meant that “initial location” would need to be determined prior to the creation of a finite number of surface lines (x_i). Also, to avoid the effect illustrated in the first image in Figure 141, the initial locations of the digitised cross sections had to be located on the same plane. To fulfil this condition, the initial locations were decided to be obtained from an intersection between all of the digitised cross sections and a plane. The common plane i.e. a plane created from the upper and lower arm was suggested to be used as it always intersected all of the digitised cross sections.

7.2.1.2 Study on the surface creation from digitised cross section

This study investigated the surface creation from digitised cross sections. The aim of the study was to identify important factors that might affect the adoption of points from surface lines to create additional cross sections. The study was performed by performing visual observation on the surfaces of all key postures which were created from their digitised cross sections. The same data as that in 7.1 was used and surfaces were created for each key posture in Pro-Engineer WildFire 4.0.

The surface creation result is shown in Figure 142 in which bold lines represent the correct shape of the elbow deformation.

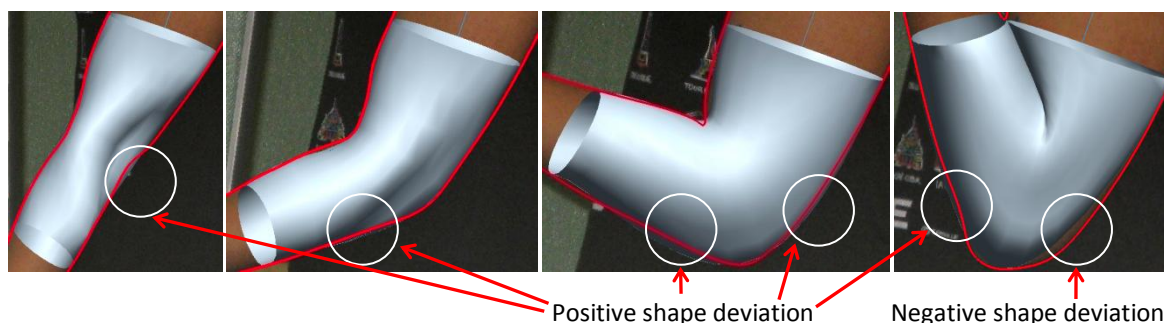
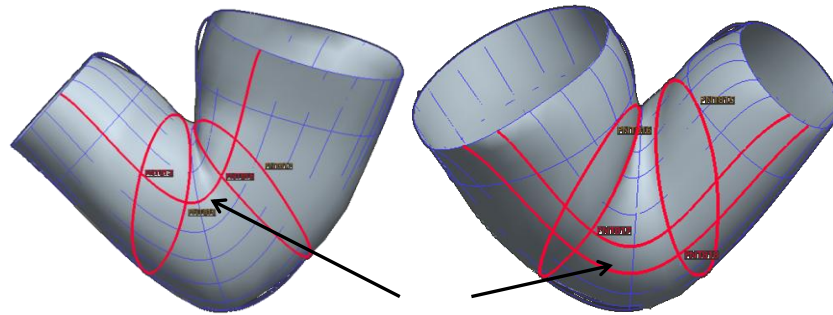


Figure 142. Positive and negative shape deviation of the surface creation result (bold line shows the correct shape of the elbow deformation)

The surface creation result demonstrated that the surface deviation of the arm was more likely to occur at the posterior part of the elbow. This meant that some of the surface lines in this part of the elbow would also likely inherit the shape deviation as they were derived from an already deviated shape. Inclusion of these surface lines would likely result in the recurrence of shape deviation on the additional cross sections at the elbow. Thus, usage of surface lines that inherited the shape deviation should be avoided. Therefore, a procedure to exclude them was required. A closer observation on Figure 142 shows that as the arm flexes, the posterior shape deviation is intensified, especially around the elbow. As the arm flexes towards 90°, the posterior shape deviation is positive with respect to the correct shape of the flesh deformation. Positive shape deviation means that the shape deviation is larger than the actual shape of the flesh deformation. In contrast, as the arm approaches maximum flexion, the posterior shape deviation becomes a mix of positive and negative with respect to the correct shape of the flesh deformation. Thus, the exclusion of surface lines could not be based on only positive deviation detection as there was a mix of positive and negative shape deviation. Another option for surface lines exclusion was by completely excluding the posterior part of the surface lines while retaining the anterior surface lines. This would be a simple solution as the need to detect negative and positive shape deviation could be avoided. The maximum width of the arm was suggested to be the boundary to separate the anterior and posterior surface lines. This suggestion was made to ensure that the surface lines retained information regarding the maximum width of the arm as this information was crucial in one of ergonomics assessments i.e. fit analysis. However, the maximum width of the arm would likely vary from one location to another. This meant that the surface lines which determine the maximum width of the arm were not necessarily the same from one location to another. Figure 143 shows an illustration where the maximum width of the arm at two locations is determined by a dissimilar set of surface lines. Therefore, for each additional cross section, the surface lines exclusion that was based on maximum width of the arm was suggested to be assessed individually.



Points that determined the maximum arm width for location 1

Figure 143. Surface lines which determine the maximum width of the arm at one location would be different from another location

However, exclusion of surface lines at the posterior part of the elbow would also result in the lack of constraints to drive the additional cross sections at the elbow so that it followed the shape of the posterior part of the elbow. The first two images in Figure 144 illustrated this situation. In Figure 144a, surface lines that inherit the shape deviation are identified. In Figure 144b, as these surface lines are omitted, the lack of constraints to produce additional cross sections at the elbow is shown. Thus, exclusion of surface line(s) at the posterior part of the elbow required an establishment of a new parameter to replace them. The posterior profile of the elbow from the side view photographs was suggested as the new parameter. This new parameter, so called the “profile”, is shown as the bold line in the last image in Figure 144.

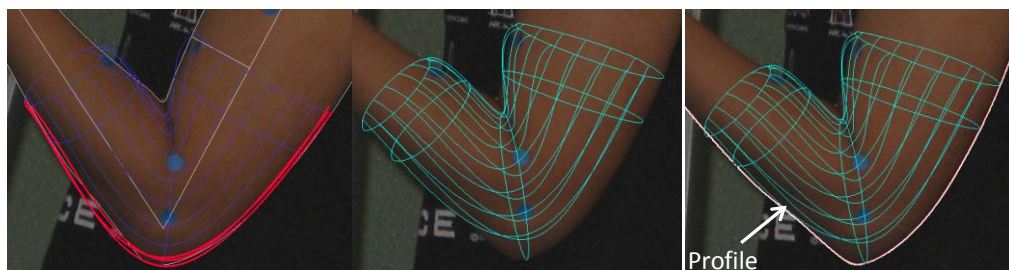


Figure 144. (a) Some surface lines which cause deviation at the posterior of the elbow, shown with bold red lines (b) Another parameter is required to guide the additional cross section creation, even after the surface lines which caused arm shape deviation is discarded (c) Profile, the new parameter to assist creating the additional cross sections

Since the FDM was limited to the flesh deformation area, the profile was also limited to flesh deformation area. The profile would ensure that the additional cross sections complied with the arm shape. The profile could be created from the mapping of the prominent points along the arm surface onto the side view. When a 3D object was photographed, it was essentially being projected onto a 2D plane and the outline that was obtained from the photograph was produced by prominent points along the surface. To incorporate the profile into the remaining surface lines i.e. surface lines at the anterior part of the arm, it had to be placed on a plane. Placing the profile on a plane would allow sampling the profile at the locations of the additional cross section around the elbow and assist the additional cross sections at the elbow to follow the arm shape. The prominent points of the cross sections, which were used to create the 3D objects, could be utilised to guide creation of a plane. However, these prominent points did not necessarily lay on the same plane, as shown in

Figure 145, and would result in the need of limiting the number of the prominent points that could be used to create a plane. To create a plane, only three prominent points could be used. As there were five digitised cross sections i.e. UAF-UAM-E-LAM-LAF, there were also five prominent points to choose. The prominent points from UAF, E and LAF were suggested to create the plane for the profile because they represented the flesh deformation area fully. From these three prominent points, two vectors i.e. UAF-E and LAF-E could be created and used to create the plane for the profile.

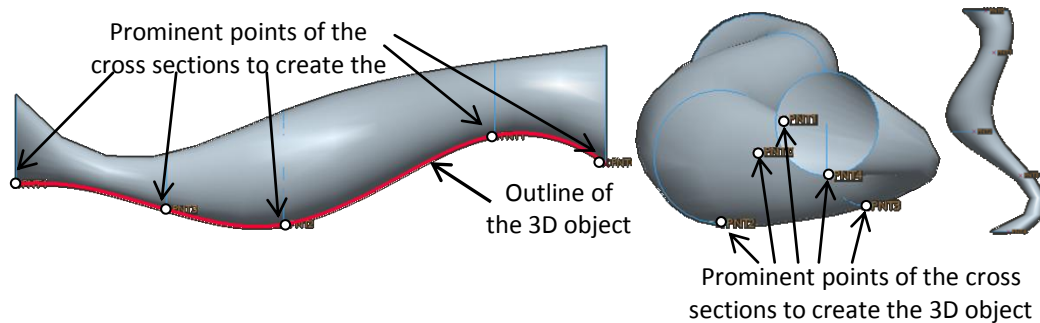


Figure 145. Illustration to show that an outline obtained from side view (bold line) is not necessarily produced by prominent points which lay at the same plane (side, front and top view, respectively)

7.2.2 Proposing the general outline of the method to create additional cross sections

Section 7.2.1 identified important stages which had to be considered to create additional cross sections from five key cross sections. These were: surface lines creation, surface line(s) exclusion and incorporation of a profile to replace the excluded surface line(s). Section 7.2.1 also provided suggestions for each stage i.e. the number of surface lines, using maximum arm width to exclude surface lines and /required points for each additional cross section. Based on the identified stages and suggestion for each stage, the general outline of the method was proposed. This is shown in Figure 146.

The figure indicates that the proposed method would be applicable for five key cross sections i.e. digitised and interpolated cross sections. The figure also implies that integration of joint information and digitised cross sections, as described in section 7.1, had to be completed before additional cross sections could be created from digitised cross sections. Likewise, the interpolation process, which will be described in section 7.3, had to be completed before additional cross sections could be created from interpolated cross sections. Once the required five key cross sections were provided, 16 surface lines and a profile would be created. Points were then obtained from the surface lines and profile at four locations i.e. 1/3 and 2/3 of UAM-E and LAM-E sections. After exclusion some of these points i.e. points that could cause shape deviation as described in section 7.2.1.2, four additional cross sections were then created and eventually integrated with the

corresponding five key cross sections. The protocol of each step in the proposed method is detailed in section 7.2.3

The proposed method had the advantage in maximising data utilisation and minimising further need of data collection. However, using the digitised cross sections or their interpolation to create additional cross sections also meant that the quality of the digitised cross sections or their interpolation would directly affect the quality of the additional cross sections. This could potentially be the limitation of the proposed method if the quality of the digitised cross sections or their interpolation was poor. To minimise this potential limitation, measures which were introduced in section 6.4.2 to reduce the error to capture the digitised cross sections could be followed.

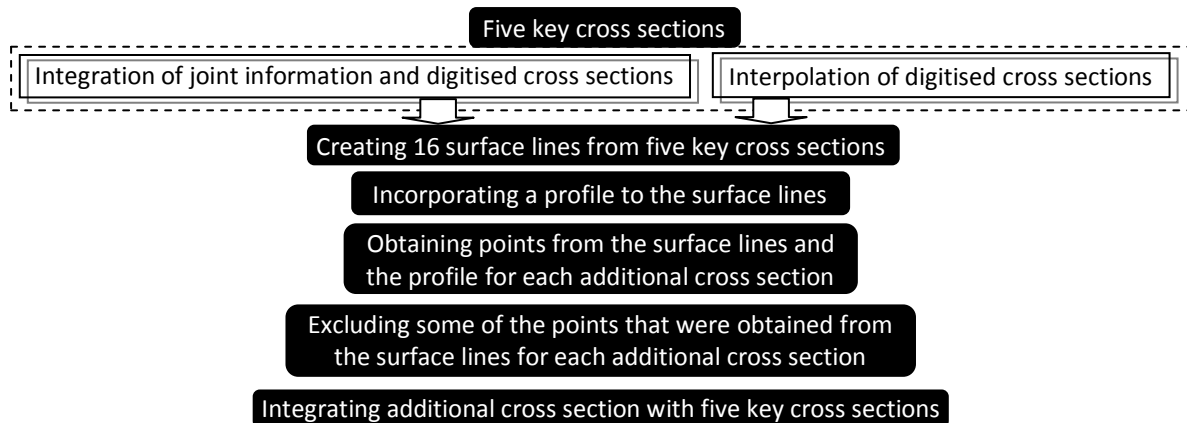


Figure 146. The proposed method to create additional cross sections

7.2.3 Establishing protocols from the general outline of the method

Following the strategy shown in Figure 139 (section 7.2), details on the proposed methods of additional cross sections' creation were required. For each step of the proposed method, a protocol was proposed and established. The protocol was mainly based on the suggestion given in section 7.2.1. To assess the feasibility of the proposed protocol, using Pro-Engineer WildFire 4.0, each step of the protocol was followed and applied on the digitised cross sections of the same participant from section 7.1.

7.2.3.1 A protocol to create 16 surface lines from five key cross sections

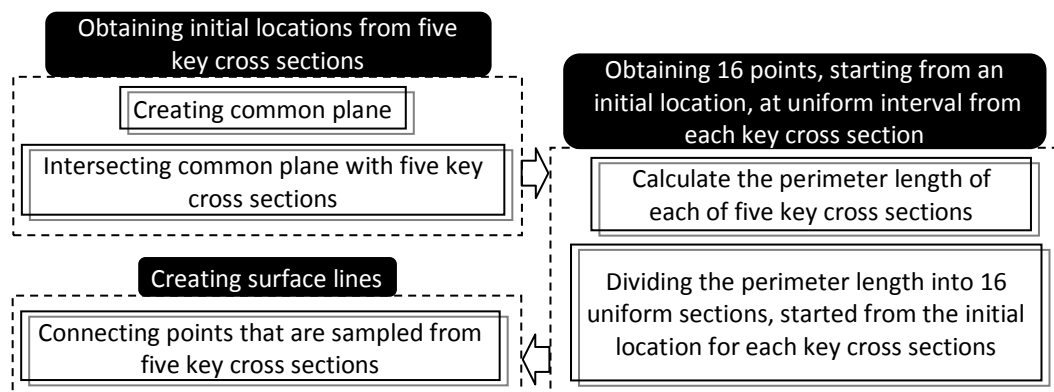


Figure 147. The protocol for surface lines creation

Figure 147 shows the protocol for surface lines creation which consisted of three main stages. Details of the protocol's each stage was explained in the following:

1. **Obtaining initial locations from five key cross sections.** The initial location of the surface lines was determined by firstly creating the common plane i.e. the plane created from upper and lower arm bones. The left figure in *Figure 148* shows the common plane which was created from the upper and lower arm bones. The next step was to intersect the common plane with five key cross sections. Using the common plane guaranteed that the initial point would intersect these cross sections. The intersection of a key cross section and the common plane would result in two intersection points i.e. the anterior and posterior intersection point. Although either of these points could be used as the initial location of the surface lines, the anterior intersection was chosen as the initial location. This decision was made to avoid the clutter in the posterior part of the elbow once a profile was established. The right figure in *Figure 148* shows the initial location of surface lines of the five key cross sections.

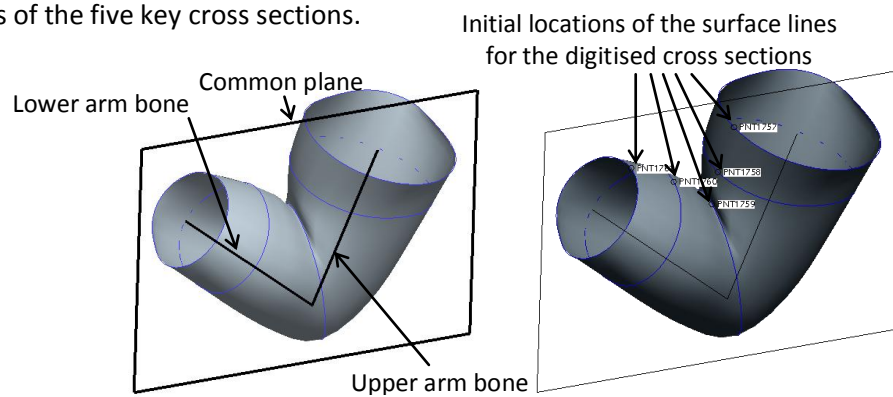


Figure 148. The common plane and the initial locations of the surface lines

2. **Obtaining 16 points, starting from an initial location, at uniform interval from each key cross section.** For each key cross section, the perimeter was calculated. Then, starting from the initial location, the perimeter for each key cross section was divided into 16 equal intervals. At the end of this step, the coordinates of the initial location and the 15 points that marked the interval was recorded for each key cross section e.g. for UAF = $[p_{initial}^{UAF}, p_{initial+1}^{UAF}, \dots, p_{initial+15}^{UAF}]$. Figure 149 illustrates the 16 points from UAF.

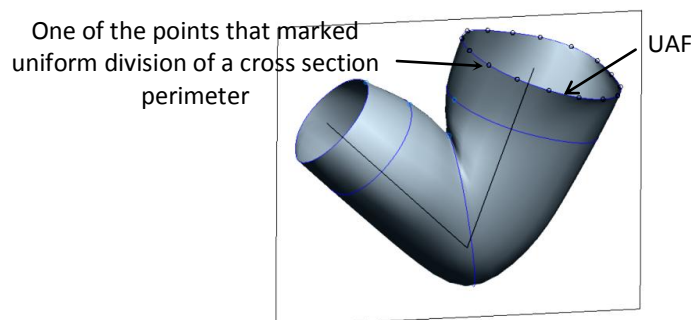


Figure 149. The 16 points from UAF showed uniform division of its perimeter

3. **Creating surface lines.** Creating surface lines was performed by connecting the corresponding 16 points between each key cross section, started from the initial location of the surface e.g. for a surface line at the initial location ($\text{surface_line}_{\text{initial}}$) = $[p_{\text{initial}}^{\text{UAF}}, p_{\text{initial}}^{\text{UAM}}, p_{\text{initial}}^{\text{E}}, p_{\text{initial}}^{\text{LAM}}, p_{\text{initial}}^{\text{LAF}}]$. Figure 150 shows an example a surface line that was created from all of the initial locations of the five key cross sections.

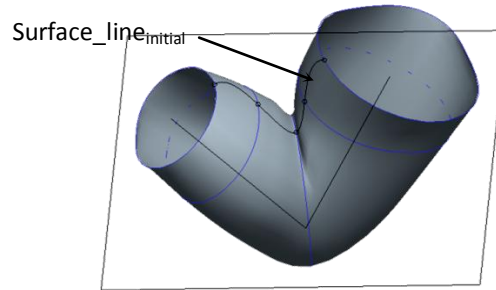


Figure 150. Creating a surface line at the initial location

Figure 150 suggested that the protocol was successful in creating surface lines. To accommodate automatic creation of surface lines, the protocol described above was used as a basis to develop an algorithm to create the surface lines. The algorithm is shown in the following pseudo code.

For each of cross section

Find the intersection between the bone with the cross section plane (p_{bone})
Find the line equation that intersect the cross section plane with the common plane
Use the line equation to calculate a point that is x distance from p_{bone} (p_{common})
Transform the sampling points, p_{bone} , p_{common} into the local coordinate system
Create Bspline curve from the sampling points of the cross section
Change the Bspline curve of the cross sections into Bezier curve
Calculate the anterior intersection point (p_{initial}) between Bezier curve and $\overrightarrow{p_{\text{bone}} p_{\text{common}}}$
Calculate the perimeter of Bezier curve (start from p_{initial})
Divide the perimeter into 16 sections
Calculate the points which divide the perimeter into 16 sections

End

7.2.3.2 A protocol to incorporate a profile to the surface lines

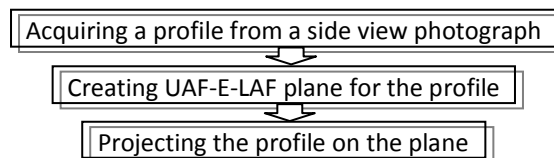


Figure 151. The protocol to incorporate a profile to the surface lines

Figure 151 shows the protocol to incorporate a profile to the surface lines which consisted of three stages. Details of the proposal's each stage is described in the following:

1. **Acquiring a profile from a side view photograph.** The profile was acquired from the side view photographs which had been arranged and overlapped in section 7.1. Using Pro-Engineer WildFire 4.0, the outline of the posterior part of the elbow was traced manually.

The outcome of the manual tracing was a digitised profile i.e. B-spline curves on the plane of the side view photographs i.e. Y-Z plane, similar to that shown in the last image in Figure 144.

2. **Creating a plane for the profile.** Following the suggestion in section 7.2.1.2, a plane was created from the prominent points of UAF, E and LAF. Using the side view perspective, the prominent points of UAF, E and LAF were identified. Figure 152 shows the plane that was created from the prominent points of UAF, E and LAF.

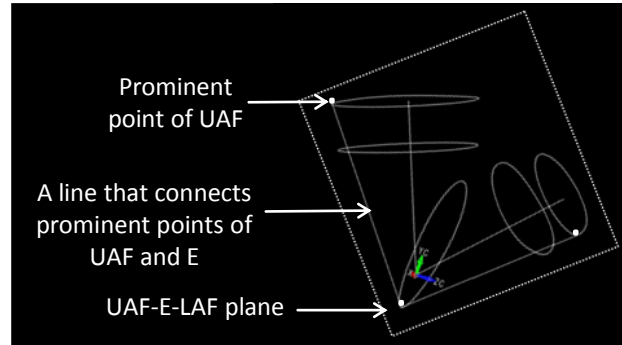


Figure 152. Creating a plane for the profile by using prominent points of UAF, E and LAF

3. **Projecting the profile onto the plane.** To project the profile from the side view plane onto the plane which was created from prominent points of UAF, E, LAF; a series of rays (vectors) along the profile was created. These rays were perpendicular with respect to the side view plane (see Figure 153a). The intersection between these rays and the UAF-E-LAF plane would be used to recreate the profile on the UAF-E-LAF plane (see Figure 153b).

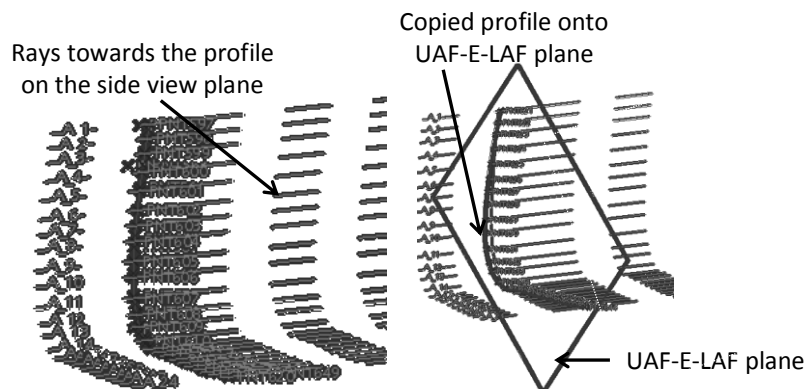


Figure 153. Left hand image: rays were created from points on the profile that were located on the side view plane; middle image: intersection between the rays and UAF-E-LAF plane

Figure 154 shows the profile (red line) and the surface lines (white lines) which were created from the five key cross sections. Figure 154 shows that the proposed protocol was successful in incorporating a profile to the surface lines. The following pseudo code describes the algorithm to project the profile from the side view plane onto the UAF-E-LAF plane.

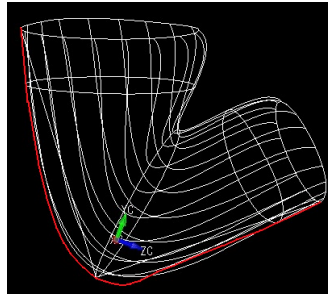


Figure 154. The final result of incorporating a profile to the surface lines

```

Obtain n points from the profile
For  $n_{1..n}$ 
    Create line equations ( $L_{1..n}$ ) perpendicular towards the profile on the side view plane for n points
End
Create plane equation for UAF-E-LAF plane
For  $L_{1..n}$ 
    Intersect  $L_i$  UAF-E-LAF plane
End
Create the new profile
  
```

7.2.3.3 A protocol to obtain additional cross sections' points from surface lines and a profile

Figure 155 shows the protocol to obtain additional cross sections' points from surface lines and a profile which consisted of two stages.

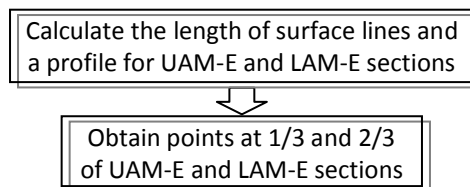


Figure 155. The protocol to obtain points for additional cross sections at the elbow

Details of the proposal's each stage is described in the following:

1. Calculate the length of surface lines and a profile for LAM-E and UAM-E section.

The first step to obtain points for additional cross sections was to measure the length of surface lines and a profile at LAM-E and UAM-E section. Figure 156 shows part of surface lines that were located between LAM-E and UAM-E section.

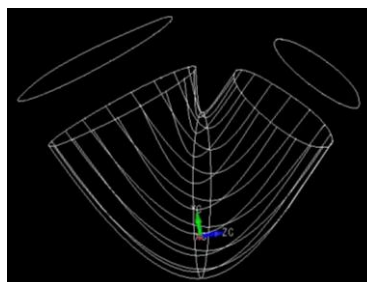


Figure 156. Part of the surface lines which were located at LAM-E and UAM-E sections

2. Obtain points at 1/3 and 2/3 of LAM-E and UAM-E section. Once the length of surface lines and the profile at LAM-E and UAM-E section were acquired, the location of points that were located at 1/3 and 2/3 of these sections were determined. For each of additional cross section, 17 points were acquired i.e. 16 points from the surface lines and 1 point from the profile. As these points were sampled based on the lengths of the curves, these points did not lie on the same plane. This was a feature that distinguished the additional cross sections from the digitised cross sections. Figure 157 shows an example of points that were sampled from surface lines at 1/3 of the UAM-E section.

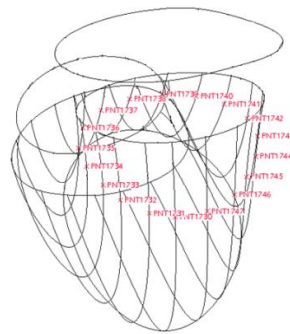


Figure 157. Obtaining points at 1/3 of surface lines of UAM-E section

Figure 157 shows that the proposed protocol was successful in obtaining points from surface lines. The following pseudo code describes the automatic process to obtain points from surface lines and profile in detail.

```

Obtain 16 surface lines (see pseudo code on subsection 7.2.3.1 )
Copy the profile onto UAF-E-LAF plane (see pseudo code on subsection 7.2.3.2)
For each of surface line and the profile
    Create Bspline curve
    Convert Bspline curve into Bezier curve
    Calculate and index the curve length
End
For each of additional cross section
    For each of surface line and the profile
        Obtain points at 1/3 and 2/3 of UAM-E
        Obtain points at 1/3 and 2/3 of E-LAM
    End

```

7.2.3.4 A protocol to exclude some of the points that were obtained from the surface lines

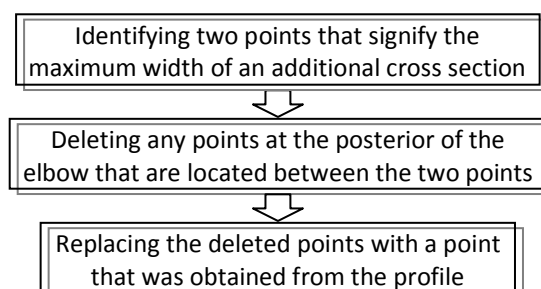


Figure 158. The protocol to obtain points for additional cross sections at the elbow

Figure 158 shows the protocol to obtain points for additional cross sections at the elbow which consisted of three stages. Details of the proposal's each stage is described in the following:

1. **Identifying two points that signify the maximum width of an additional cross section.** The first step to exclude points that were obtained from the surface lines was to identify two points that signify the maximum width of an additional cross section. A point with maximum width was identified as a point with the largest positive and negative x coordinate values. Figure 159 shows two points that signified the maximum width of the arm for an additional cross section at 1/3 of UAM-E section.

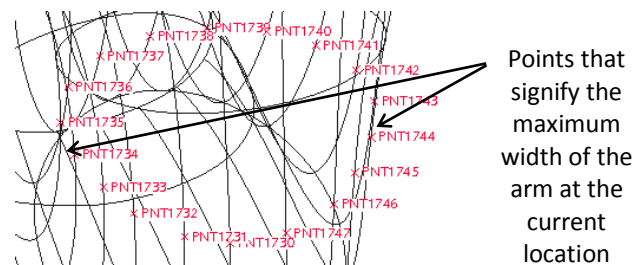


Figure 159. Choosing 2 points which determine the maximum width of the arm of additional cross section's

2. **Deleting any points at the posterior of the elbow that are located between the two points which had been identified in step 1.** Once the two points that signify the maximum width of an additional cross section was identified, the next step was to delete any points at the posterior of the elbow between the two points which had been identified in step 1. Figure 160 shows the remaining points after excluding the described points.

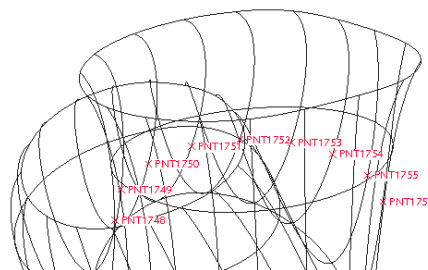


Figure 160. Discarding the posterior points using the two chosen two points determined in Figure 159

3. **Replacing the deleted points with a point that was obtained from the profile.** The last step was to replace the deleted points with a point that was obtained from the profile. Once this step was performed, the four additional cross sections could be created, as shown in Figure 161.

Figure 161 demonstrates that the proposed protocol was successful in creating additional cross sections by firstly excluding points that could result in shape deviation. The following pseudo code shows the surface line exclusion method. As this method assumed that the 16 points were already acquired, the pseudo code started directly from determining points with the maximum width.

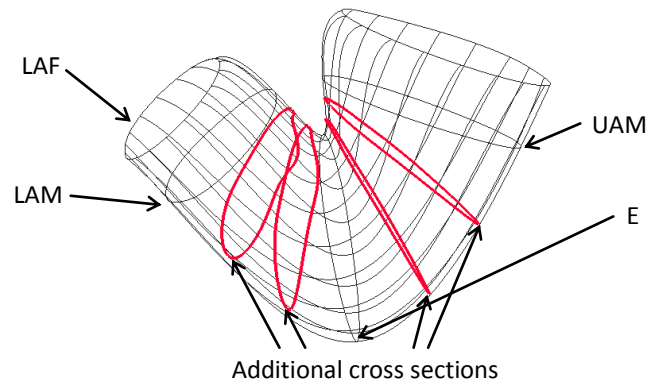


Figure 161. An example of additional cross sections, which were created in Pro-Engineer, based on the output of the algorithm in Matlab 7.0

For each of additional cross section

Obtain 16 points from surface lines (see section 7.2.3.3)
 Assign number (1 to 16) to these 16 point (number 1 is assigned for the initial location of surface line)
 Find the point with the largest and smallest x value
 Find the number for these points e.g. point 6 and point 12
 Delete the points with numbers that are located between these two points e.g. point 7, 8, 9, 10, 11

End

Insert the point from the profile

7.2.3.5 A protocol to integrate additional cross sections with five key cross sections

As described in section 7.2.1.1, to avoid surface distortion, surface creation from more than one curve required all of the curves' initial locations to be located on the same plane. This condition also applied to a surface that was created from additional cross sections and five key cross sections. Thus, this protocol was required to ensure that the condition was fulfilled and surface distortion was avoided.

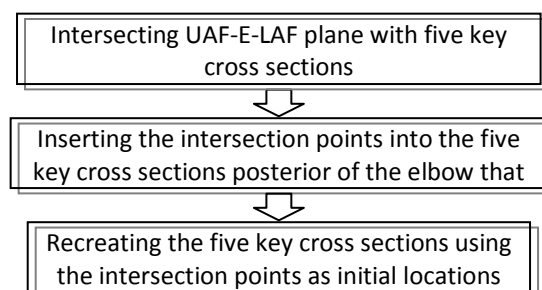


Figure 162. A protocol to integrate additional cross sections with five key cross sections

The protocol, shown in Figure 162, bore similarity to that in section 7.2.3.1 where a plane was utilised to assist creation of initial locations. The UAF-E-LAF plane was chosen to be used for two main reasons. Firstly, some of additional cross sections' points were already located on the UAF-E-LAF plane i.e. additional cross sections' points that were obtained from a profile. Thus, utilising UAF-E-LAF plane reduced the amount of computation required. Secondly, the intersection between key cross section and UAF-E-LAF plane was essentially a 2D problem i.e. intersection between a 2D line

(the result of intersection between UAF-E-LAF and the key cross section's plane) and a closed curve (the key cross section). Thus, utilising UAF-E-LAF plane reduced the complexity of the required computation. Once the intersection points between UAF-E-LAF plane and five key cross sections were found, these points would have to be inserted into the five key cross sections and used to recreate them. Once this process was completed, a surface that comprised of the five key cross sections and additional cross sections could be created. The following pseudo code describes the necessary steps to integrate the digitised and additional cross sections. An algorithm that was based on the pseudo code above was created in Matlab 7.0.

For each of the digitised cross section

Create Bspline curve from the sampling points of the cross section
 Change the Bspline curve of the cross sections into Bezier curve
 Find the intersection between the UAF-E-LAF plane with the Bezier curve
 Insert the intersection into the sampling points of the cross section
 Arrange the sampling points of the cross section

End

Figure 163 shows an example of the final result of integration between additional cross sections and five key cross sections for one of the key postures. As cross sections were created from initial locations that were located on the same plane i.e. UAF-E-LAF plane, the final surface was free from effect described in section 7.2.1.1. The figure demonstrated that the protocol to integrate additional cross sections and five key cross sections achieved what it was aimed for. Figure 163 also implied that the overall proposed method and protocols to create additional cross sections were feasible.

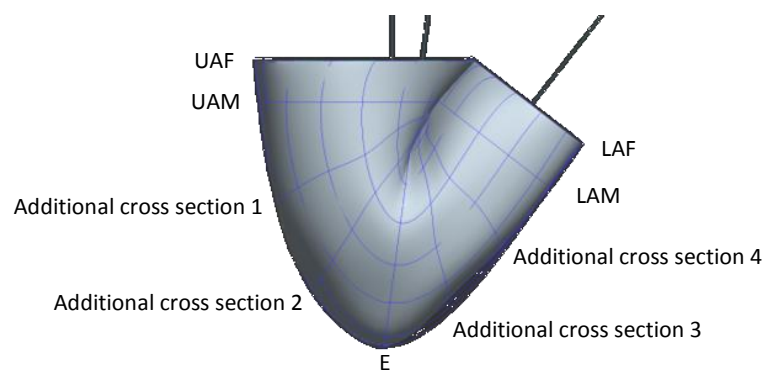


Figure 163. Arm surface that is created from both the digitised and additional cross sections

7.3 Interpolation to govern the flesh deformation

The final issue to be resolved in the third design phase was performing interpolation to govern the flesh deformation. This issue was related with the previous finding in section 5.3.2.5 which suggested the unsuitability of Shen et al. (1994) method in driving flesh deformation for ergonomics application. This finding prompted this research to propose the use of interpolation from a set of examples. The use of interpolation implied that data collection were only required for the examples

set. To derive a new data, interpolation method had to be established and subsequently applied to the examples set. In this research, the set of examples was essentially a pre-determined arm posture which represented different stages of flesh deformation. Given that each of the pre-determined arm posture within the set had information which was required to create flesh deformation; the set could be interpolated to derive information which was required to create flesh deformation for a new arm posture.

There were five elements of mandatory information that were required to model flesh deformation of the elbow. These were: (1) carrying angle; (2) the shape of five key cross sections; (3) the locations of five key cross sections with respect to the joint locations; (4) the orientation of five cross sections' planes with respect to the upper/lower arm bones; and (5) a profile to assist creation of additional cross sections. These elements were mostly available for the example set i.e. key postures, but not for other arm postures. This section aimed to provide a means to derive the five elements for other arm postures from the key postures' information. For each element, interpolation method had to be established.

Figure 164 shows the strategy to resolve the issue of interpolation to govern flesh deformation. The first step was to review each element of the mandatory information. The review was aimed to identify related previous studies and findings; and formed the basis of the proposed interpolation method for each element. Detail of the proposed interpolation method for each element would then be addressed in the protocol establishment.

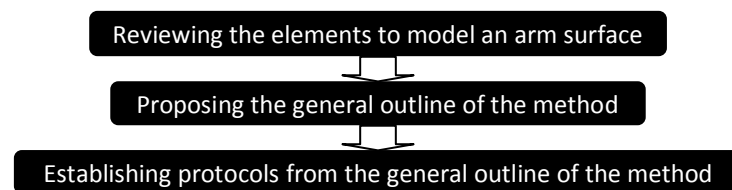


Figure 164. The strategy to resolve the issue of interpolation to govern the flesh deformation

7.3.1 Reviewing the elements to model an arm surface

To produce flesh deformation of the elbow, five elements of mandatory information were required. This subsection reviewed each of the mandatory elements by identifying related previous studies or findings. The review of each element is detailed in the following:

- (i) **Carrying angle.** The carrying angle was identified in section 5.3.1 and was studied in details in section 6.1. The results of the study in section 6.1 demonstrated that as the arm flexed, the carrying angle decreased linearly. This suggested that given the carrying angles of a fully extended and flexed arm were known; the carrying angle for any arm posture in between these two extremes could be predicted. The study also found that as the arm flexed, the complexity to measure the carrying angle increased. This finding

prompted this research to propose the utilisation of the carrying angle from a 3D scan of a fully extended arm as a basis to predict the carrying angle of a fully flexed arm (see section 6.1.3 and 6.1.4). However, in section 7.1.4, it was found that the integration of joint locations and digitised cross sections resulted in a by-product i.e. an ability to measure the carrying angle for each key posture. This finding suggested that the by-product provided an opportunity to obtain the carrying angle of a fully flexed arm directly i.e. without the need to perform prediction as described in the proposed approach in section 6.1.3 and 6.1.4.

(ii) ***The shape of five key cross sections.*** The concept of cross sections' usage to create surface and flesh deformation was explored in chapter 5. In section 5.3.2.5, this research proposed an interpolation from a set of cross sections that represented different stages of flesh deformation at the elbow. The interpolation concept was investigated further in section 6.3 and the result showed that flesh deformation could be approximated by linear interpolation from four key postures i.e. full extension, 135°, 90° and maximum flexion were established. Data collections, as described in section 5.2 and section 6.4, provided the shape of digitised cross sections i.e. five key cross sections of the key postures. As described above, digitised cross sections represented different stages of flesh deformation. To perform linear interpolation on the digitised cross sections, their shape had to be expressed numerically. In section 6.3.2, a mini study to investigate detail pattern of flesh deformation was performed by quantifying the shape changes of the posterior outline of the elbow. The quantification was introduced to express different shapes of the posterior outline of the elbow numerically. This finding suggested that a similar quantification approach could also be applied to obtain the shape of five key cross sections from the digitised cross sections.

(iii) ***The locations of five key cross sections with respect to the joint locations.*** The locations of five key cross sections were addressed in section 5.3.2.2 and 6.6. In section 6.6.1, it was established that: (1) UAF and UAM were located in between the upper arm boundary and the elbow crease; (ii) LAM and LAF were located in between the lower arm boundary and the elbow crease; and (iii) E was located at the elbow joint. Because the upper and lower arm boundaries changed throughout the flexion-extension of the elbow, as described in section 6.2, the locations of UAF, UAM, LAM and LAF would also changed. By following the protocol in section 7.1.3 and 7.1.4, the locations of UAF, UAM, LAM and LAF for the four key postures could be obtained. This indicated that an approach to acquire the locations of UAF, UAM, LAM and LAF for arm postures other

than the key postures was required. In section 6.2, a study that was performed to investigate the extent of flesh deformation showed that the upper and lower arm boundaries movement was more or less linear. This meant that, given the locations of UAF, UAM, LAM and LAF for each key posture were known, the locations of UAF, UAM, LAM and LAF for any arm posture could be derived by linear interpolation. Thus, this presented the ability to acquire the locations of UAF, UAM, LAM and LAF for arm postures other than the key postures.

- (iv) ***The orientations of five key cross sections' planes with respect to the upper/lower arm bones.*** The orientations of five key cross sections' planes were addressed in section 5.3.2.3 and 6.5. Their plane orientations were divided into two categories. The first category was the plane orientations of UAF, UAM, LAM and LAF which remained constant i.e. they were always perpendicular with respect to the upper/lower arm bones. Because these plane orientations remained constant throughout extension-flexion of the elbow, this indicated that there was no need to perform interpolation on them. The second category was the plane orientation of E which changed according to the arm angle. In section 5.3.2.3, the plane orientation of E was indicated by the elbow joint and the crease at the anterior of the elbow which could be determined from a side view photograph. As side view photographs were only available for key postures, an approach to determine the plane orientation of E for other arm postures was required. Fortunately, the study that was performed in section 5.3.2.3 showed that there was a strong relationship between the arm angle and the plane orientation of E. This presented a possibility to determine the plane orientation of E through the established relationship.
- (v) ***A profile to assist the creation of additional cross sections.*** In section 6.6, the need of additional cross sections to create and realise flesh deformation at the elbow was identified. In section 7.2.1.2, a profile that was created from side view photographs was proposed to assist the creation of additional cross sections. As side view photographs were only available for key postures, this indicated that an approach to create profiles for arm postures other than key postures was required. In section 6.3.2, an investigation on the pattern of flesh deformation at the elbow was performed by investigation shape changes of the posterior outline of the elbow. As the posterior outline of the elbow was essentially a profile, the result of the study was also relevant for a profile. The study revealed that linear interpolation from four key postures could be used to approximate the flesh deformation. This suggested that a profile for an arm

posture other than key postures could be derived through linear interpolation. As linear interpolation required numerical expression of a profile, the quantification approach, similar to that described in section 6.3.2 would be required.

Based on the review of mandatory elements above, the general outline of the interpolation method for each element was proposed (see Figure 165). As shown in the figure, corresponding elements of the four key postures were required to create a profile and five key cross sections' shape and locations for an arm posture other than the key postures. In contrast, to create the carrying angle of an arm posture other than the key postures, only carrying angles of a full extension and flexions were required. Lastly, to create E's planes orientation for an arm posture other than key postures, the regression which was described in section 5.3.2.3 would be utilised.

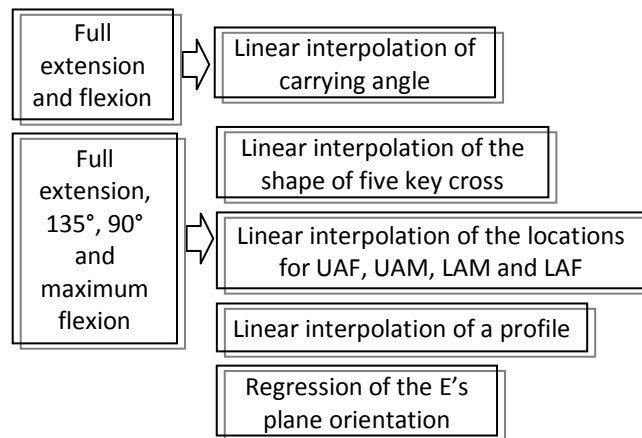


Figure 165. The proposed interpolation methods

7.3.2 Establishing protocols for the proposed interpolation methods

This section was aimed to provide protocols for the proposed interpolation methods which were described in section 7.3.1.

7.3.2.1 A protocol to interpolate carrying angle

Figure 166 shows the protocol to interpolate carrying angle. Firstly, carrying angles of full extension and flexion had to be obtained. The required steps were described elsewhere in section 6.1.3 and 7.1. Once these angles were acquired, a carrying angle for an arm posture could be determined by linear interpolation.

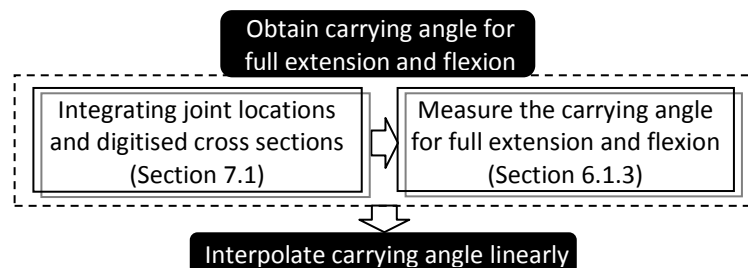


Figure 166. Protocol to interpolate carrying angle

For instance, given that the arm angle of a full extension ($arm_angle_{full\ extension}$) was 150° and the arm angle of a full flexion ($arm_angle_{full\ flexion}$) was 30° . If the carrying angle for a full extension ($carrying_{full\ extension}$) was 20° and the carrying angle for a full flexion ($carrying_{full\ flexion}$) was 10° , respectively; a carrying angle at 120° ($carrying_{120^\circ}$) was calculated as:

$$carrying_{full\ flexion} + \frac{120 - arm_angle_{full\ flexion}}{arm_angle_{full\ extension} - arm_angle_{full\ flexion}} \times (carrying_{full\ extension} - carrying_{full\ flexion})$$

$$= 10^\circ + \frac{120^\circ - 30^\circ}{150^\circ - 30^\circ} \times (20^\circ - 10^\circ) = 17.5^\circ$$

7.3.2.2 A protocol to interpolate digitised cross sections

Figure 167 shows the protocol to interpolate digitised cross sections. The protocol was preceded by the integration of joint locations and digitised cross section which was described in section 7.1. This was because the first step of the protocol required bone point which could only be obtained after the integration of joint locations and digitised cross sections was completed. To investigate the feasibility of the protocol, data from the participant in section 7.1 was used.

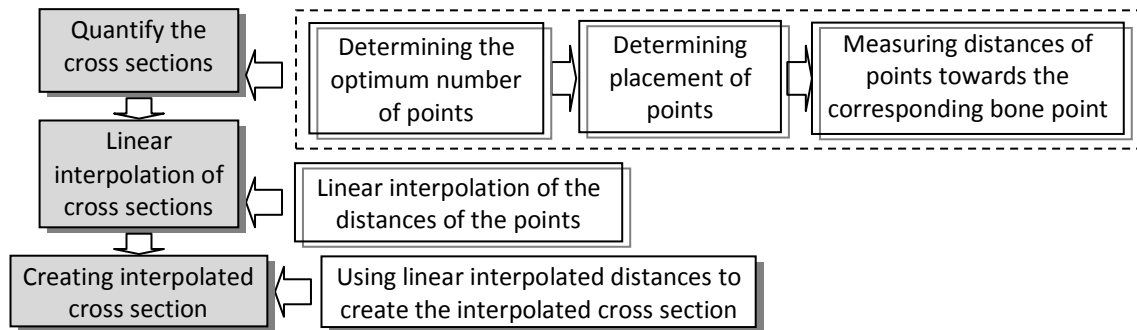


Figure 167. The proposed protocol for cross section interpolation

Detail of each stage of the protocol is described below:

- 1. Quantify digitised key cross sections.** As described in section 7.3.1, the shape of UAF, UAM, E, LAM and LAF needed to be quantified first. The aim of cross section shape quantification was to express the shape of the cross section numerically so that linear interpolation could be performed. The shape quantification of the cross section, which was applied on each cross section, adopted similar principles as that in section 6.3. Points were selected at the cross section perimeter and their distances towards the corresponding “bone point” of the cross section were measured. The corresponding “bone point” for each cross section is essentially the intersection point between the plane of that cross section and the arm bone that goes through the plane. Figure 168 depicts how the bone points are determined for some of the cross sections.

To initiate the quantification, the number of the points that would be tracked and measured had to be determined first. 16 points were chosen as the number of points for

tracking and distance measurement. This decision was based on the result from the section 5.3.2.4 which showed that 16 points were the optimum number of cross section sample points. The next step was to determine the 16 points on the perimeter of the cross section. To maintain the consistency of how to acquire the points for all of the cross sections, the point would always be acquired starting at the intersection between the cross section and a plane that is created from the bone point and the X-Z plane. This point would be referred to as the “initial point”. Figure 169 shows the plane and the initial point.

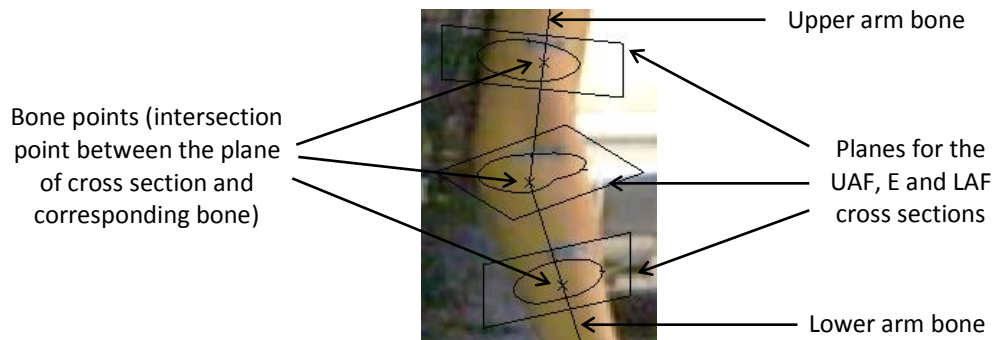


Figure 168. Determining the bone points for some of the cross sections

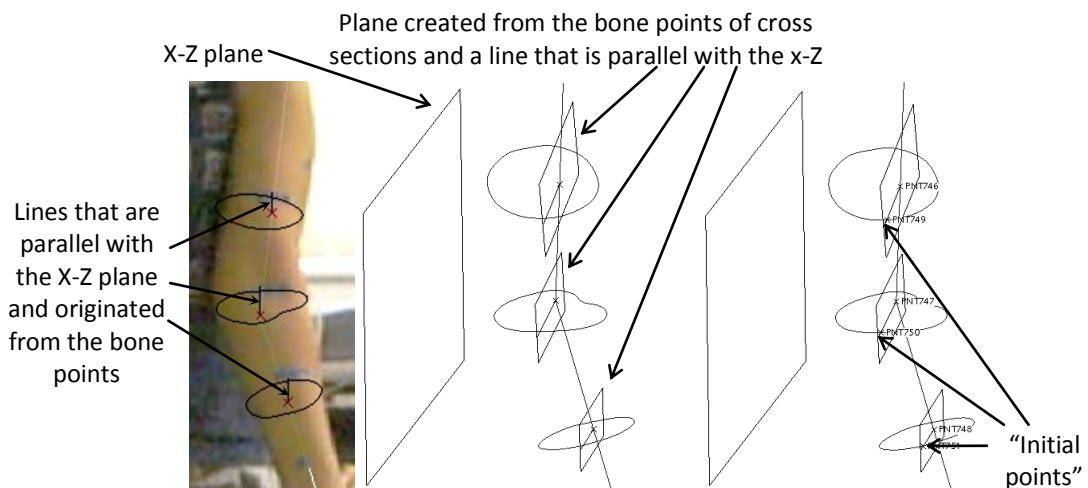


Figure 169. Creating planes to determine the initial locations for two cross sections

Once the initial point was obtained, further processing was performed in 2D as this would simplify the acquisition of the additional points. To determine the other 15 points, 15 rays (vectors) were created using the initial point as the reference. The intersections of these rays with the cross section determined the location of the other 15 points. The 15 rays originated from the bone point of the cross section, followed a clockwise direction and divided the cross sections into 15 equal sections i.e. each ray was separated by 24° .

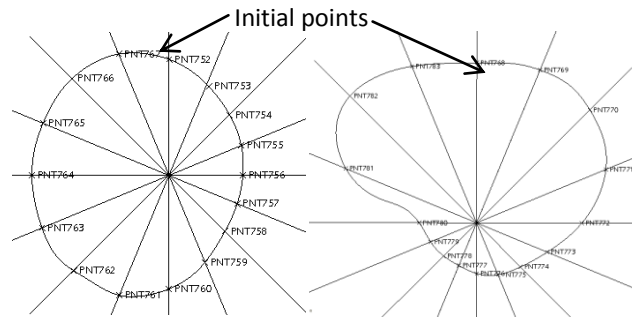


Figure 170. Creating 15 rays of vectors that were originated from the bone point of the cross section in a clockwise direction

Figure 170 shows the 15 rays, the bone point of the cross section and the initial points for two different cross sections. The last step of the first stage was to measure and record the distance of the points from the bone point. All of these processes were performed manually in Pro-Engineer WildFire 4.

2. **Linear interpolation of five key cross sections.** The proposed second stage of the cross section interpolation was the linear interpolation itself. The four key postures divided the range of the arm movement into three segments i.e. maximum extension-135°, 135°-90° and 90°-maximum flexion. This meant that for each cross section, there were three segments of linear interpolation. For example, for UAF, there would be linear interpolation between $UAF_{\text{maximum extension}} - UAF_{135^\circ}$, $UAF_{135^\circ} - UAF_{90^\circ}$, $UAF_{90^\circ} - UAF_{\text{maximum flexion}}$. To create a cross section at x° arm flexion, the distance of each location from the corresponding set of cross section was linearly interpolated using the formulae:

$$\Delta d_n = \frac{(x - PAS_{\text{lower bound angle}})}{(PAS_{\text{upper bound angle}} - PAS_{\text{lower bound angle}})} \times (d_n^{\text{PAS upper bound}} - d_n^{\text{PAS lower bound}})$$

$$d_n = \Delta d_n + d_n^{\text{PAS lower bound}}$$

Where:

- x = angle of which the cross section interpolation is performed
- $PAS_{\text{upper bound angle}}$ = the upper bound angle for the key posture interval
- $PAS_{\text{lower bound angle}}$ = the lower bound angle for the key posture interval
- $d_n^{\text{PAS upper bound}}$ = the distance of the n sample point for the upper bound of the key posture interval
- $d_n^{\text{PAS lower bound}}$ = the distance of the n sample point for the lower bound of the key posture interval
- d_n = the interpolated distance of the n sample point

For instance, to create the E cross section at 120°, the formulae above could be used to interpolate the distance of locations between E_{90° and E_{135° (see Table 7). The first two columns show the distance of each location for E_{90° and E_{135° . The third column shows the application of the equation above whereas the last column shows the final distance.

Table 7. Linear interpolation for distance of location in E_{120}°

E_{135}° (mm)	E_{90}° (mm)		E_{120}° (mm)
31.3821	38.2413	$=((120-90)/(135-90))*(31.3821-38.2413)+38.2413$	33.66853
32.8505	36.8258	$=((120-90)/(135-90))*(32.8505-36.8258)+36.8258$	34.1756
35.6375	35.9686	$=((120-90)/(135-90))*(35.6375-35.9686)+35.9686$	35.74786
37.0860	35.5575	$=((120-90)/(135-90))*(37.0860-35.5575)+35.5575$	36.57652
37.9789	35.6548	$=((120-90)/(135-90))*(37.9789-35.6548)+35.6548$	37.20425
37.2212	35.9394	$=((120-90)/(135-90))*(37.2212-35.9394)+35.9394$	36.7939
35.4629	35.4845	$=((120-90)/(135-90))*(35.4629-35.4845)+35.4845$	35.47011
33.7627	37.9057	$=((120-90)/(135-90))*(33.7627-37.9057)+37.9057$	35.14366
28.6880	38.2172	$=((120-90)/(135-90))*(28.6880-38.2172)+38.2172$	31.86443
23.3859	33.0447	$=((120-90)/(135-90))*(23.3859-33.0447)+33.0447$	26.60549
22.7405	30.6997	$=((120-90)/(135-90))*(22.7405-30.6997)+30.6997$	25.39354
29.3843	32.1252	$=((120-90)/(135-90))*(29.3843-32.1252)+32.1252$	30.29792
37.5985	34.8986	$=((120-90)/(135-90))*(37.5985-34.8986)+34.8986$	36.69855
38.8693	37.7343	$=((120-90)/(135-90))*(38.8693-37.7343)+37.7343$	38.491
36.5062	39.7502	$=((120-90)/(135-90))*(36.5062-39.7502)+39.75029$	37.58754
32.6774	39.7126	$=((120-90)/(135-90))*(32.6774-39.7126)+39.7126$	35.02249

3. Creating interpolated cross sections. The proposed final stage was to create the interpolated cross section. To create the interpolated cross section, vectors that originated from the bone point were created as before. The vector length corresponded with the linear interpolation result. The ends of the vectors form the points from which the interpolated cross section was then constructed. Figure 171 shows the result of the E cross section at 120° and the cross section comparison between E_{120}° , E_{90}° and E_{135}° .

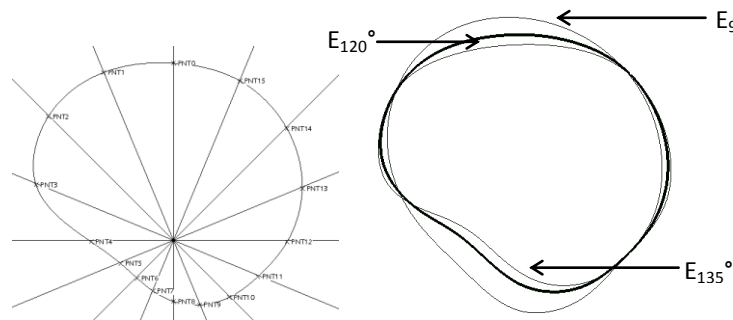


Figure 171. E cross section at 120° and comparing it with E_{90}° and E_{135}°

Figure 171 demonstrated that the protocol was successful in generating interpolated cross section from digitised cross sections.

7.3.2.3 A protocol to interpolate locations' of UAF, UAM, LAM and LAF

As described in section 7.3.1, the locations of UAF, UAM, LAM and LAF planes changed linearly with respect to the arm angle. This suggested that if the location UAF, UAM, LAM and LAF of the key posture were known, the location of UAF_{int} , UAM_{int} , LAM_{int} and LAF_{int} for any arm angle (arm_angle_{int})

could be calculated through a linear interpolation. Figure 172 shows the protocol to interpolate the location of UAF, UAM, LAM and LAF for a given arm angle.

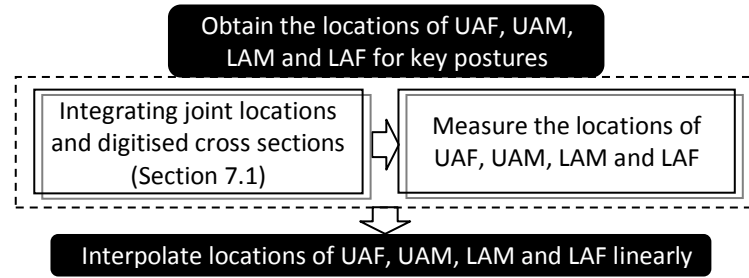


Figure 172. The protocol to interpolate the locations of UAF, UAM, LAM and LAF for a given arm angle

The following equation could be used to calculate the UAF_{int} , UAM_{int} , LAM_{int} and LAF_{int} .

$$\begin{aligned}
 & \text{If } key_posture_{angle_1} \leq arm_angle_{int} \leq key_posture_{angle_2} \text{ then} \\
 UAF_{int} &= \frac{arm_angle_{int} - key_posture_{angle_1}}{key_posture_{angle_2} - key_posture_{angle_1}} \times (UAF_{key_posture_{angle_2}} - UAF_{key_posture_{angle_1}}) \\
 & \quad + UAF_{key_posture_{angle_1}}
 \end{aligned}$$

For example, if UAF_{90° and UAF_{135° are 100 mm and 90 mm, respectively. To find out the UAF_{int} at 120° could be calculated as follows:

$$UAF_{int} = \frac{120 - 90}{135 - 90} \times (90 - 100) + 100 = 93.3 \text{ mm}$$

7.3.2.4 A protocol to interpolate plane of E

As described in section 7.3.1, the E plane's interpolation utilised the results of the mini study in section 5.3.2.3 where the relationship between the arm angle and the orientation plane of E was established. The orientation plane of E (the upper arm-elbow_{angle}) was expressed as the angle between the elbow orientation line and the upper arm bone. As shown in Figure 173, the relationship between the orientation plane of E and the arm angle could be represented by a linear equation: $y = 0.5136x - 5.6974$. y is the angle between the elbow orientation line and upper arm whereas x is the arm angle.

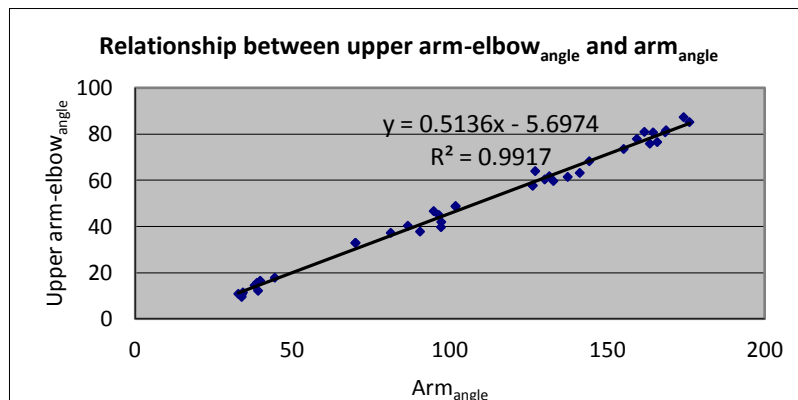


Figure 173. Relationship between arm_{angle} and upper arm-elbow_{angle}

For instance, given an arm angle of 127° , by inputting this value into the linear equation above, the elbow plane orientation angle would be 59.5° . The elbow orientation plane could then be drawn based on the knowledge that the elbow orientation angle is the angle between the elbow orientation plane and arm angle. Figure 174 shows the prediction result of the elbow orientation plane for an arm angle of 127° . Once the elbow plane orientation was established, the elbow plane could be created. The method to create the actual elbow plane from the elbow plane orientation was described in detail in section 7.1.3.

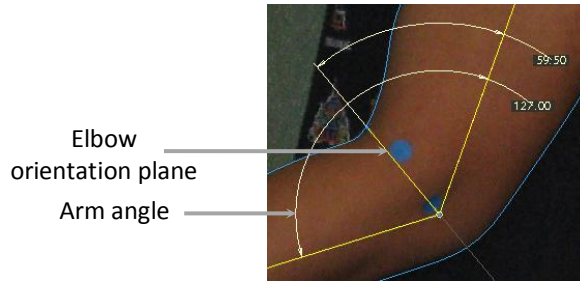


Figure 174. Predicting the elbow orientation plane by using the linear equation that relates the angle between upper arm-elbow_{angle} and arm_{angle}

7.3.2.5 A protocol to interpolate profiles

As described in section 7.3.1, the interpolation of profiles adopted the shape quantification principle from section 6.3.2 which enabled shapes comparison. This principle was also adopted in section 7.3.2.2 where it was used to interpolate five key cross sections. Therefore, the proposed protocol to interpolate profiles was similar to the protocol of five key cross sections' interpolation. However, unlike the cross section interpolation, the proposed quantification would be performed by measuring the distances of the quantification locations towards to the bones. Figure 175 shows the proposed protocol to interpolate profiles. As shown in the figure, the overall steps to interpolate profiles resembled those of five key cross sections' interpolation. Similar to the protocol to interpolate five key cross sections, the proposed protocol to interpolate profiles was also preceded by integration of joints locations and cross sections which was described in section 7.1. To investigate the feasibility of the proposed protocol, data from the same participant in section 7.1 was utilised.

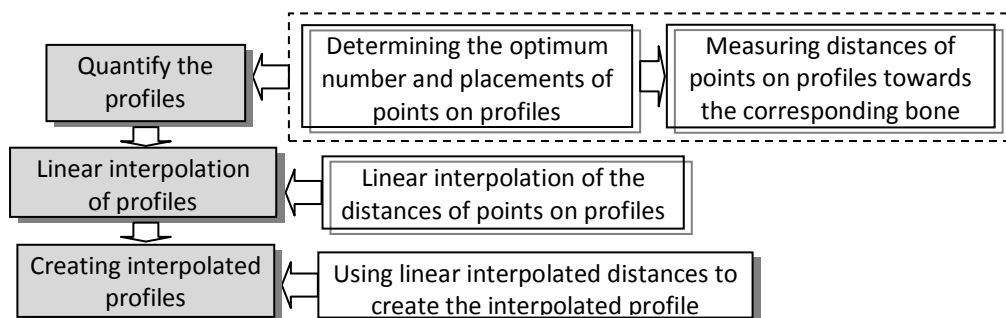


Figure 175. The proposed protocol to interpolate profiles

Details of each step were described in the following:

1. **Quantify the profiles.** In order to provide accurate quantification of the profiles' shapes, the optimum number and placement of points to quantify the shape had to be determined. Since none of the previous studies addressed this, a preliminary study was required. This would be addressed in the "1.1. Mini study to determine the optimum number and placements of points on profiles". Once the optimum number and placement of points along the profile was established, the actual profile quantification and interpolation would take place. This was addressed in the 1.2

1.1. Mini study to determine the optimum number and placements of points on profiles

The proposed method for the mini study was to compare the error level of the of the profile representation produced from different combinations of the number and placement of the points. The combination which produced the least error would signify the optimum number and placement of the points. The mini study used the same participants from the mini study in section 6.3. As there were four profiles for each participant, i.e. one from each of the key posture, there were 20 profiles to be analyzed. For each participant, profiles of the arm key postures were tracked and drawn manually in Pro-Engineer. Each profile was divided into 4 segments by utilizing locations of the digitised cross sections i.e. UAF-UAM, UAM-E, E-LAM and LAM-LAF. Four points were assigned to mark these segments. The aforementioned segment division was applied to ease the comparison on the number and placement of the points. Figure 176a shows the segment and the corresponding four points that marked them.

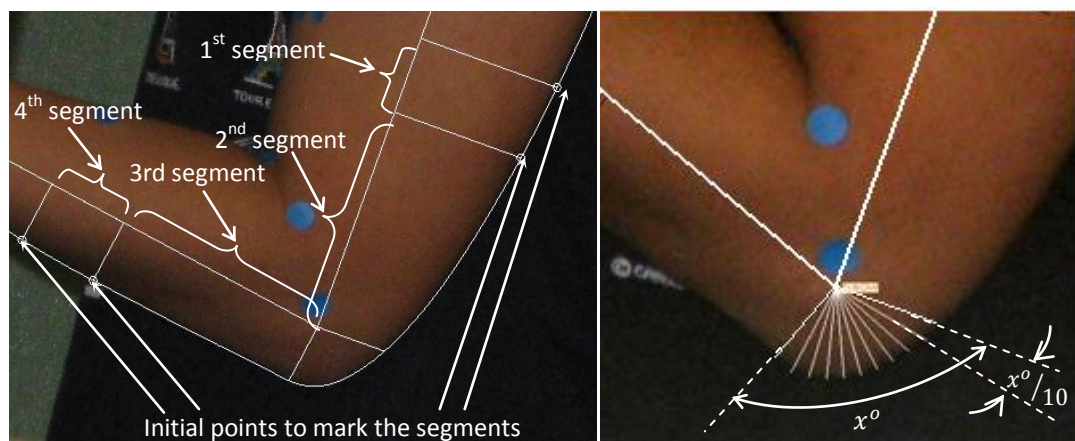


Figure 176. (a). Initial points were assigned to mark the segments i.e. UAF-UAM, UAM-E, E-LAM, LAM-LAF (b). A closer look of initial points at the elbow

To reduce the complexity of the problem, a fixed number of points were assigned at the elbow joint area i.e. the area marked by perpendicular lines of the upper and lower arm. These points divided the elbow joint area uniformly. 9 points were assigned at the elbow

joint because this number of points was deemed to be sufficient to capture the detail of the elbow joint area. It is acknowledged that this decision was a simplification of the ideal approach to determine the optimum number and placement of points to represent the profile. Figure 176 b shows the location of the 9 points at the elbow joint. All of these 13 points would constantly be used during the comparison process. Figure 177 shows the location of the 13 points on one of the key postures from one of the participants.

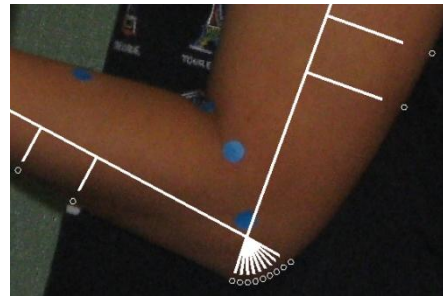


Figure 177. The 15 locations of the profile that would be used during the comparison process

The search for the optimum number and placement of points was done sequentially. This meant that the optimum number and placement of points in the first segment would have to be completed before assessing different combination of points in the second segment and so on. For each segment, a different number and placement of points were added. As the segment length was different for each key posture and participant, the placement of the points was expressed as the percentage of the segment length. For each combination, together with the previous 13 points, a profile was created. The distance deviation (in mm) between the created and original profile was then measured. A larger distance deviation showed a larger error and vice versa. The combination that exhibited the least error would be chosen. This procedure was applied for every key posture for all participants. Figure 178 shows an example of a combination of points that was being assessed for a particular posture. The figure also shows the comparison between the created profile and the original profile.

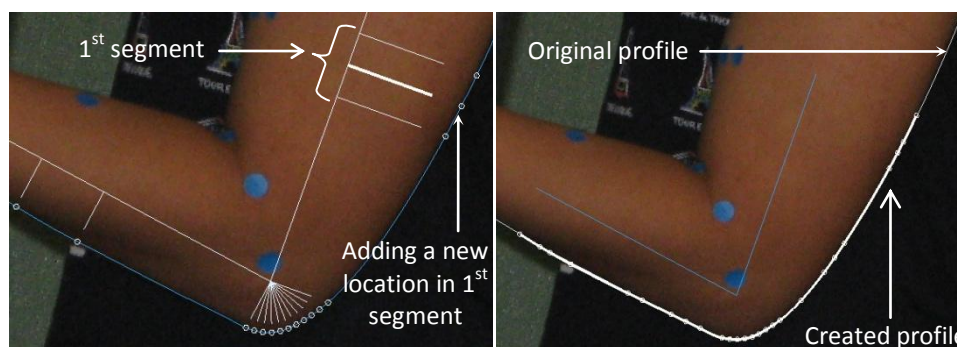


Figure 178. (a)An example of adding a location in a segment while searching for the optimum number and placement of points on the profile. (b) The created profile was shown together with the original profile

An algorithm was developed in Matlab 7.0 to automate the search for the optimum number and placement of points on the profile from the 20 profiles. The pseudo code from the algorithm is shown below.

```

For k = 1 .. 4 segments
  Iterate = 1
  While iterate = 1
    For i = 1...n participant
      For j = 1 .. 4 profile of key postures
        Read the profile data
        Read the joint data
        Determine the 13 locations
        Determine the distance of the 13 locations
        Determine the distance of the 13 locations
        For l = 0.1:0.1:0.9
          If l  $\approx$  the 13 locations then
            Insert l into the 13 locations
            Determine the placement of the l location
            Create ray for the l location
            Intersect rays with the jth profile
            Calculate the error for each l location
          End
          Sum the error for all of key postures for each l location
        End
        Sum the error for all of participant for each l location
        Determine the location with the minimum error for the kth segment
        Insert the location with the minimum error into the 13 locations
        If the new sum error is not significantly changed (0.5) then go to the next segment
      End
    End
  End
  Save the final locations

```

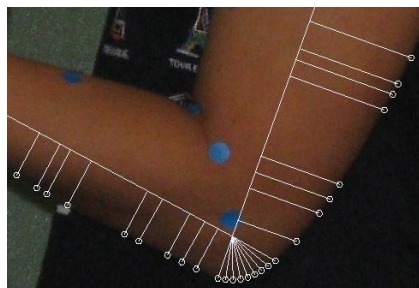


Figure 179. Final sampling points of 1st segment to the 4th segment

The output of the algorithm showed that the optimum number of points were 26. The placement of the points as suggested by the algorithm was as the following:

- Segment 1 (UAF-UAM): [50% 70%]
- Segment 2 (UAM-E): [50% 60% 90% 70%]

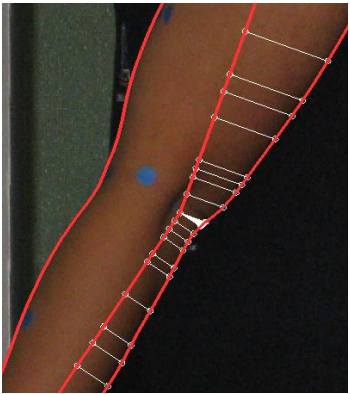
- Segment 3 (E-LAM): [10% 20% 30% 50% 60%]
- Segment 4 (LAM-LAF): [40% 60%]

Figure 179 shows the optimum number and placement of points on a profile for the profile interpolation.

1.2. Utilising the optimum number and placement of points on a profile to quantify the profile

Once the optimum number and placement of points on a profile was established, it could be used to quantify the profile. Table 8 shows the quantification's result for a fully extended arm from the data of the same participant in section 7.1.

Table 8. An example of quantification result for the profile of a fully extended arm

Distances of the optimum number and placement points on the profile	
Segment 1 [41.5; 36.6; 34.4; 30.7] mm	
Segment 2 [24.3; 23; 21.7; 18.3] mm	
The elbow segment [12.8; 12.6; 12.2; 12; 11.9; 11.7; 11.6; 11.5] mm	
Segment 3 [10.9; 10.8; 11.1; 12.2; 12.7] mm	
Segment 4 [14.2; 15.7; 16.8; 17.4] mm	

- Linear interpolation of profiles.** The linear interpolation for the profile was principally similar as that of the five key cross sections' interpolation. Firstly, the distances of the points on a profile towards the bone were calculated for each of the key posture. Once the distances were established for all of the key postures, a profile for any posture could be calculated by means of a linear interpolation as described in the example in subsection 7.3.2.2. An algorithm was created to perform the linear interpolation for the profile. The pseudo code of the algorithm is shown below.

```

Choose the participant
Input an angle for the profile interpolation (profileint)
If full extension < angle < 135° then
    Read the profile data for full extension and 135°
    Read the joint data for full extension and 135°
If 135° < angle < 90° then
    Read the profile data for 135° and 90°
    Read the joint data for 135° and 90°
For each profile
    Create rays for the locations file
  
```

```

For each ray
    Intersect ray with both profile data
    Calculate distance of the intersection towards the bone
End
End
For each distance of the locations
    Apply linear interpolation equation
End

```

- 3. Creating interpolated profile.** Once the interpolated distance of the optimum points were calculated, the interpolated profile could be created (drawn). The approach to create the interpolated profile was also similar in principle to the approach in the subsection 7.3.2.2. Rays (vectors) that are located at the optimum points and originated from the bones were created. The vector length for each point would be matched with the linear interpolation result. Figure 180 shows examples of the profile interpolation's result for arm angles 105° and 68°, respectively.

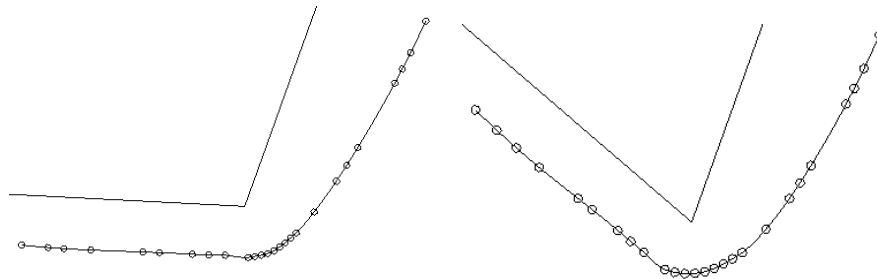


Figure 180. Examples of the profile interpolation results

Figure 180 demonstrates that the proposed protocol was successful in generating interpolated profiles from the key postures' profiles.

8 Review of the Proposed FDM

In the proposed methodology for the research (see Chapter 4), once the design phases succeeded in establishing the proposed FDM, the next step was to review the proposed FDM. Figure 181 shows where the review of the proposed FDM was located with respect to the other stages of the research. The review aimed to confirm that the proposed FDM has achieved what it was initially developed for. The proposed FDM would be compared to the set of DHM specifications which were used to guide its development. These specifications include: (i) accuracy; (ii) real time; (iii) realism; (iv) accommodation of different body sizes and types; (v) whole body modelling and (vi) minimum user intervention. At the end of chapter 7, it was also indicated that a feasibility testing would also be performed in this chapter so that the feasibility of the proposed FDM was ascertained. The integral feasibility test would be carried out first in section 8.1 and then followed by the review of proposed FDM in section 8.2. A general outline of the proposed FDM and the results of its review were published in Hermawati and Marshall (2008).

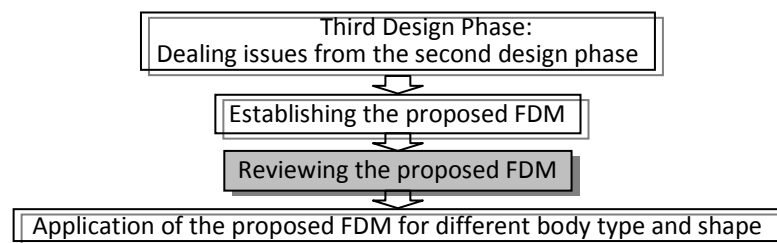


Figure 181. The relationship of the proposed FDM's review with the previous and next stages of the research

8.1 Feasibility testing of the proposed FDM

This section aims to explain details of the feasibility testing which included the proposed methodology of the feasibility testing and results.

8.1.1 Methodology of the proposed FDM's feasibility testing

The concept of the proposed FDM that had been proposed throughout the design phase needed to be integrated so that the feasibility of the proposed FDM was ascertained. To accommodate this, this research proposed creation of software programme embedded with relevant principles and protocols of the proposed FDM and applied it on participants' data. Through the application of the software programme to participants' data, problems that might occur due to the interaction between the proposed principles and protocols could be identified. The software programme would be developed in Matlab 7.0 and five participants who had been recruited during FDM development would be involved. Figure 182 shows processes that were proposed to perform the feasibility testing. There were five main processes to perform the feasibility testing i.e. data

collection, data preparation, software programming, evaluation of programming results and modification. Each of the process would be covered in the following subsections.

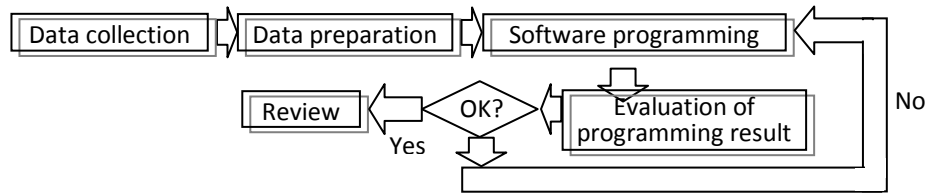


Figure 182. Detail processes to create the programming to review some of the FDM specifications

8.1.2 Data collection

As described in the methodology subsection 8.1.1, five participants were involved. Details of the participant were shown in Table 9 . For each participant, the following data were collected: (i) five key cross sections for each key posture; (ii) 3D scan of a fully extended arm; (iii) side and view photographs. All of these data had been collected for one participant during the study in section 7.1. Therefore, data collection was only performed for the remaining participants. To collect five key cross sections, 3D scan data and photographs, existing methods which were outlined in section 6.4.2 and 7.1 were followed.

Table 9. Detail of the five participants who were involved to review the accuracy and realism of the proposed FDM

	Participant 1	Participant 2	Participant 3	Participant 4	Participant 5
Gender	Female	Male	Male	Male	Female
Height (cm)	143	180	166	166	152
Weight (kg)	46	64.5	65.2	73.9	59.3

8.1.3 Data preparation

Data preparation aimed to pre-process the collected data that were required to generate the flesh deformation for every participant. This included the parameterisation of the digitised cross sections, the location of the cross sections and profile for every key posture. In addition to this, for each participant, data preparation also extracted the angular range of the arm movement and the joint coordinates of both a fully flexed-extended arm. Relevant methods which had been established in section 6.6.2, 6.7, 7.1.3, 7.1.4 and 7.3.2.3 were applied to parameterise the digitised cross sections for each key posture. The result of the parameterisation would be employed to drive the interpolation of the cross sections for postures other than the key posture.

Figure 183 shows the steps to parameterise the digitised cross sections. Any related equipment and software that were used to carry out the steps were also included in the figure. As shown in Figure 183, the bone point of the cross section was utilised for the parameterisation of the cross section, which followed the proposed concept in section 7.3.2.3. The advantage of this parameterisation approach is that the result of the parameterisation could be used to interpolate cross sections directly by means of linear interpolation. Table 10 shows an example of the result

from parameterisation of the digital cross sections which was taken from participant 1 for a fully extended and 90° flexion key posture. The result shows distances between sampling points and bone point for each key cross section. Complete results of digital cross sections' parameterisation can be found in appendix B (supplied in the accompanying CD).

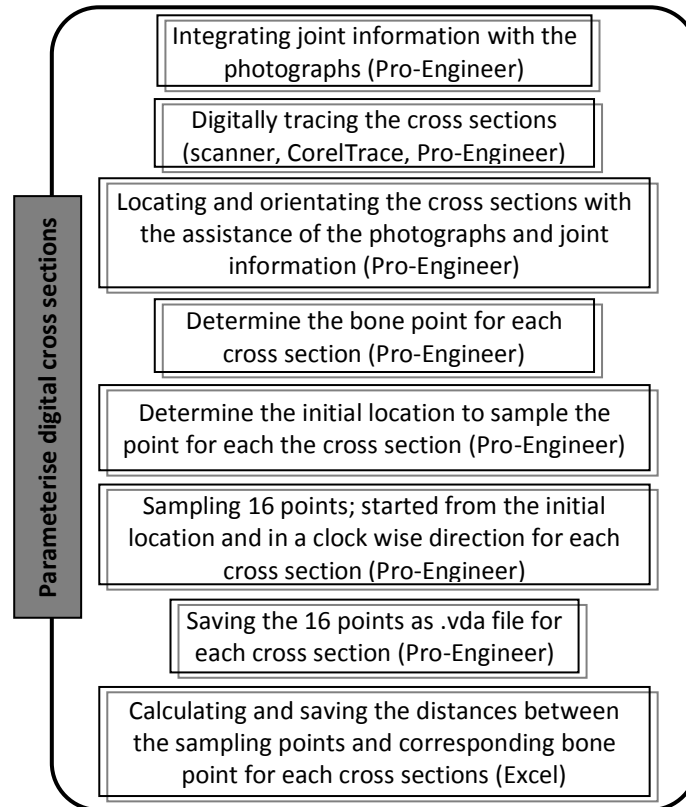


Figure 183. Steps to parameterise the digital cross sections

Table 10. Example of the result of digital cross sections' parameterisation

	(mm)										
	UAF	UAM	E	LAM	LAF		UAF	UAM	E	LAM	LAF
Fully extended	39.7154	41.2875	44.62	42.0297	34.3305	90° flexion	40.3491	37.6659	57.2572	36.4078	28.8716
	33.9399	37.0616	48.0327	41.7791	34.5099		36.0085	32.2186	57.8872	36.114	27.7352
	29.4883	33.3088	51.2481	40.7105	33.4782		32.2153	27.8222	50.774	35.2096	26.8613
	26.731	29.7848	34.5509	37.0408	30.5295		29.8631	25.5166	38.0641	33.0122	25.7545
	25.3811	26.8229	13.892	30.3813	27.382		29.0194	25.0054	25.6809	29.9346	24.2421
	25.2076	25.3112	11.7233	22.2474	23.8166		29.7647	26.2266	19.7682	26.6115	22.5491
	27.314	25.4402	10.9445	17.0385	20.2086		32.3967	29.1746	17.9214	23.6982	21.1411
	32.1157	27.0038	10.9	14.4143	17.6908		36.9657	33.7985	18.2496	21.8918	20.1999
	38.7242	29.4506	11.5229	13.5779	16.8414		42.6922	39.5885	19.213	21.5903	20.2184
	43.6067	32.121	12.7987	14.3253	17.9275		49.1513	44.878	19.752	23.0728	22.1903
	45.8406	35.098	14.7846	16.9886	21.951		53.0046	46.8721	20.673	27.1012	27.0977
	46.9719	38.6388	17.6634	22.6756	29.1497		51.3404	45.6484	22.7042	33.761	33.0137
	46.138	41.9485	26.1339	32.6742	33.7936		48.0071	44.5738	28.2907	39.3247	36.4587
	46.3881	44.2248	38.7016	39.9103	35.4225		45.2468	44.0044	36.616	40.9956	36.7437
	46.5397	44.437	46.2143	42.7898	35.6591		43.8441	43.1718	44.7847	39.436	34.3366
	44.6527	43.5382	46.4185	42.753	34.8819		43.0144	41.2405	52.2676	37.1271	30.84

Section 6.2.2, 7.1.3 and 7.1.4 were used as a basis to parameterise the locations of the cross sections. The parameterisation is required to provide information regarding the location of the UAF, UAM, LAM and LAF for each key posture. By knowing this information and applying the method in

section 7.3.2.3, the location of the UAF, UAM, LAM and LAF for posture other than key posture could be calculated. Details of the steps are shown in Figure 184. Table 11 shows the complete result of the location of five key cross sections for all key postures and participants.

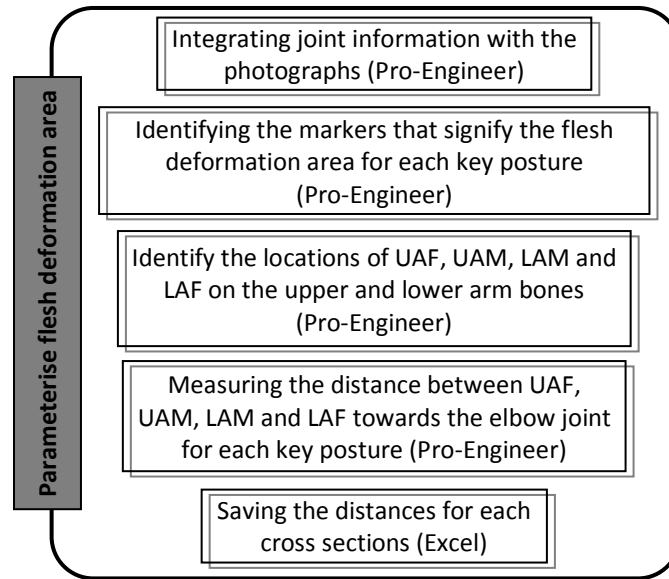


Figure 184. Steps to parameterise the flesh deformation area

Table 11. Results of cross sections location towards the elbow joint for all key postures and participants

		(mm)				
		UAF	UAM	E	LAM	LAF
Participant 1	<i>fully extension</i>	90.9002	47.3279	0	44.8489	89.8831
	<i>135°</i>	93.8135	57.987	0	58.2492	96.6611
	<i>90°</i>	97.3546	71.0772	0	69.8328	98.4946
	<i>maximum flexion</i>	102.4564	82.4979	0	87.6483	107.8786
Participant 2	<i>fully extension</i>	95.1999	47.5762	0	43.9595	87.2079
	<i>135°</i>	99.3647	59.3607	0	49.305	89.5805
	<i>90°</i>	104.3686	75.9438	0	63.8007	92.2678
	<i>maximum flexion</i>	110.3223	95.2321	0	95.8696	110.0567
Participant 3	<i>fully extension</i>	109.2034	54.6499	0	47.4841	93.1262
	<i>135°</i>	113.6644	69.9581	0	64.191	107.0805
	<i>90°</i>	117.4842	85.3169	0	74.7727	108.3353
	<i>maximum flexion</i>	120.8744	95.6805	0	103.5241	128.8079
Participant 4	<i>fully extension</i>	107.2576	55.8144	0	54.2057	90.5622
	<i>135°</i>	109.5941	75.4285	0	61.2377	109.0946
	<i>90°</i>	113.4357	87.5727	0	82.1031	114.5424
	<i>maximum flexion</i>	119.2298	88.5949	0	99.5949	130.2075
Participant 5	<i>fully extension</i>	97.0519	41.4731	0	56.379	89.6357
	<i>135°</i>	102.0999	55.484	0	65.6358	98.1357
	<i>90°</i>	102.971	70.8482	0	87.8894	107.3357
	<i>maximum flexion</i>	104.0598	80.9211	0	89.6241	109.392

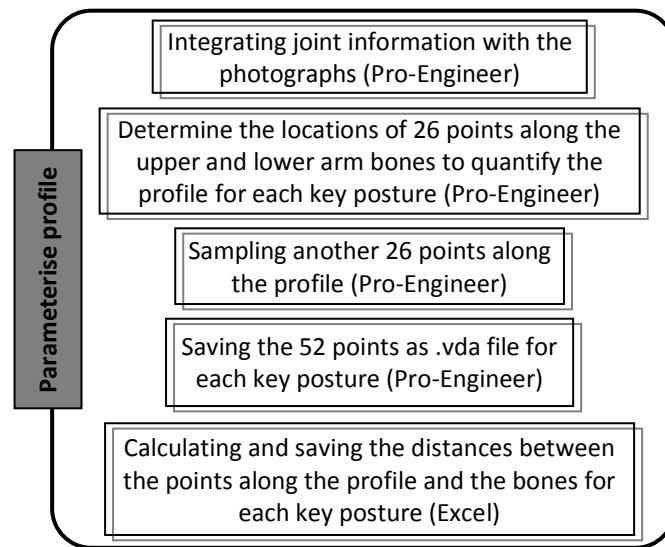


Figure 185. Steps to parameterise the profile

Sections 7.2.3.2 and 7.3.2.5 were used to guide the parameterisation of the profile. The result of the parameterisation would be utilised to generate a profile for postures other than key postures. Details of the steps are shown in Figure 185. Table 12 shows an example of distance between the points along the profile and the bones for participant 1's key postures. Complete result of distances of points along the profile and bones for all participants could be found in appendix C (supplied in the accompanying CD).

Table 12. Distances of points along the profile and bones for all participant 1's key postures

	(mm)			
	Full extension	135°	90°	Maximum flexion
Participant 1	41.3508	42.7562	45.6706	48.3861
	36.3665	39.8202	44.0215	47.6969
	34.0656	38.4611	43.2618	47.3259
	30.3415	36.181	42.0219	46.6715
	23.3626	28.8322	34.8878	38.975
	21.9174	27.2649	33.1402	36.794
	20.2941	25.7042	31.1591	34.3621
	15.8753	22.4369	26.1574	28.4375
	12.6816	19.4375	21.3125	20.4025
	12.5028	18.7901	20.2956	17.7345
	12.3365	18.2698	19.7462	16.1019
	12.1817	17.8391	19.5204	15.4062
	12.0475	17.5024	19.3828	15.4682
	11.9279	17.2818	19.1056	16.1816
	11.8178	17.138	18.753	17.4136
	11.7168	17.0985	18.5139	18.8579
	11.634	17.1694	18.5795	20.2558
	10.8753	17.8593	19.9339	21.779
	10.7782	18.0419	20.4601	21.5041
	11.0159	18.098	20.7708	21.9637
	11.9958	18.3348	21.2173	23.8414
	12.5151	18.5512	21.4437	24.4663
	14.0124	19.5805	22.4911	24.7461
	15.2742	20.2477	22.4698	24.5451
	16.2466	20.4727	22.2663	24.4271
	17.3844	20.4126	21.6077	24.1718

The information on the angular range of the arm movement determined the boundaries for the possible arm postures. To extract the information regarding the angular range of the arm movement, the angle between the upper and lower arm bones were measured while the arm was fully extended and flexed. This information was extracted from the integrated joint information and the photographs. The measurement was performed in Pro-Engineer and the information from each participant was saved in Excel. Table 13 shows the angular range of arm movement for all participants.

Table 13. The angular range of the arm movement for all participants

	Participant 1	Participant 2	Participant 3	Participant 4	Participant 5
Full extension	154.707	160.1598	164.7665	155.2131	150.248
Maximum flexion	34.5607	33.691	37.747	39.286	45.655

In order to create the flesh deformation in a 3D setting, the coordinates of the joints were required. The joint coordinates of a fully extended arm would be used to create the local coordinate system for the upper arm bone and lower arm bone. Local coordinate systems were crucial to create an arm movement and flesh deformation around the elbow in a 3D setting. The coordinates of the joints could also be used to determine the carrying angle, following the method discussed in 6.1.3. In order to allow linear interpolation of the carrying angle for any arm angle, the carrying angles of a fully extended and flexed arm had to be known. Therefore, joint coordinates for these two key postures had to be provided. To obtain the joint coordinates of a fully flexed and extended arm for each participant, the steps shown in Figure 186 were followed. Table 14 shows the complete result of joints coordinates for fully extended and flexed arms for all participants.

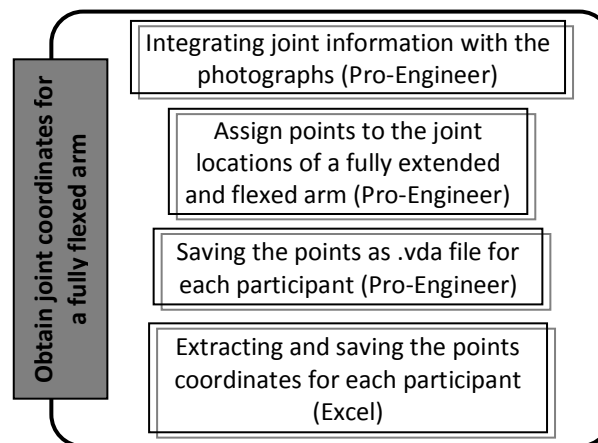


Figure 186. Steps to obtain the coordinates of the joint location for a fully flexed arm

Table 14. Complete results of joint coordinates for fully extended and flexed arms (in mm units)

	Shoulder			Elbow			Wrist		
	X	Y	Z	X	Y	Z	X	Y	Z
Participant 1	24.3339	209.7823	-75.437	0	0	0	51.5522	-161.591	108.6192
	12.0348	209.7823	-75.437				38.0889	188.4515	48.9475
Participant 2	31.5228	272.2523	-91.2034	0	0	0	43.954	-214.91	123.2795
	31.5228	272.2523	-91.2034				32.8377	238.8627	65.7937
Participant 3	33.9435	247.1501	-113.693	0	0	0	29.2191	-205.096	120.5697
	33.9435	247.1501	-113.693				27.3351	231.5103	54.812
Participant 4	39.8175	236.8335	-125.292	0	0	0	45.3295	-169.66	159.9927
	39.8175	236.8335	-125.292				47.3675	228.1717	48.1656
Participant 5	0.5036	208.19	-121.035	0	0	0	92.2444	-139.17	157.5896
	0.5036	208.19	-121.035				38.2503	203.9085	51.2244

8.1.4 Software programming (phase 1)

Once the data preparation was completed, the next step was to perform programming. As proposed in section 8.1.1, the programming was based on the principles or protocols which had been established during the development of the proposed FDM. The programming was performed in Matlab 7.0. The following were the key principles and protocols that were used in the programming:

1. Carrying angle calculation for a fully extended and flexed arm (section 6.1.3). Using the joint coordinates from the data preparation as an input, this algorithm would calculate the carrying angle from a fully extended and flexed arm. The output of this algorithm was used to perform linear interpolation on the carrying angle for postures other than a fully extended or flexed arm (see page 100 in section 6.1.4). The carrying angle contributed to create the lower arm bone movement as described in section 6.1.5.
2. Linear interpolation of the five key cross sections (section 7.3.2.2). This algorithm aimed to produce an interpolation of five key cross sections for postures other than the key postures. The input of this algorithm came from the result of the digitised cross sections' parameterisation. The algorithm followed the equation on page 165 in section 7.3.2.2 and produced the interpolated five key cross sections in 2D. These 2D five key cross sections would then be transformed into a 3D setting. The 3D transformation of the five key cross sections allowed the creation of the surface lines, which were necessary for creation of the additional cross sections.
3. Linear interpolation of the planes for UAF, UAM, LAM and LAF (section 7.3.2.3). This algorithm determined the location of the planes for interpolated UAF, UAM, LAM and LAF. The input of the algorithm came from the parameterisation of the cross sections' location. This input was used in the equation in section 7.3.2.3 to determine the planes' location along the lower and upper arm bones. The algorithm also provided the local coordinate system for each plane. Once the location and local coordinate system of the

planes was determined, the 2D cross sections of UAF, UAM, LAM and LAF (see number 2) were then transformed onto these planes.

4. Linear interpolation of the elbow's plane (section 7.3.2.3). This algorithm was required to interpolate the location of the elbow's plane for any required arm posture. The input of the algorithm was the angle and joint coordinates of the arm posture. The angle of the arm would be used to determine the orientation of the elbow plane, as described in section 7.3.2.3. The orientation of the elbow plane and the common plane, which was calculated from the joint coordinates, were then used to create the elbow plane. This was then followed by transforming the interpolated E cross section (see number 2) onto the plane.
5. Linear interpolation of the profile (section 7.3.2.5). This algorithm was responsible for generating a profile for postures other than the key postures. The input of this algorithm was the result of the key postures' profile parameterisation. The interpolated profile was established in a similar manner with the interpolation of cross sections. The output of this algorithm would be placed on the UAF-E-LAF plane (see page 153 in section 7.2.3.2) and used as part of the inputs to create the additional cross sections at the elbow (see section 7.2.3.3).
6. Creation of additional cross sections at the elbow (see section 7.2). The algorithm to create additional cross sections would be applicable for any arm posture. The input of this algorithm was: (1) the five key cross sections, (2) the profile, (3) the joint coordinates, and (4) the local coordinate system for upper and lower arm bones. Following the method described in section 7.2, 16 surface lines were created from the five key cross sections. Sampling at 1/3 and 2/3 between UAM-E and LAM-E would be performed on the profile and the surface lines. The individual exclusion of the surface lines that was established in section 7.2.3.2 would be followed strictly. The outcomes of these processes were points which were then used to create the additional cross sections at the elbow.
7. Integrating the additional cross sections at the elbow and the five key cross sections (see section 7.2.3.5). This algorithm was proposed to ensure that curves of the five key cross sections and the additional cross sections at the elbow were all initiated from points that were located on the same plane. This condition had to be met to avoid surface distortion for the flesh deformation (see section 7.2 , page 145-146).

During the programming development, it was found that point number 7 was unnecessary. This was because the curves for five key cross sections and additional cross sections at the elbow were

already initiated from points that were located on the same plane at the end of the point number 6. The final outcome of the programming was the coordinates of five key cross sections and additional cross sections at the elbow. The pseudo code of the complete programming is shown in the following.

```

Choose the participant
Input an arm angle for the flesh deformation at the elbow ( $\alpha$ )

Extract information from joint coordinates of a fully extended and flexed arm
Calculate the carrying angle for a fully extended arm
Calculate the carrying angle for a fully flexed arm
Perform linear interpolation of carrying angle for  $\alpha$  ( $carrying\_angle_\alpha$ )
Create the local coordinates system for a fully extended arm ( $CS_{upper\ arm}^{full\ extension}$  and  $CS_{lower\ arm}^{full\ extension}$ )
Rotate the  $CS_{lower\ arm}^{full\ extension}$  to  $\alpha$  with and  $carrying\_angle_\alpha$ 

Determine the two corresponding key postures for  $\alpha$ 
Extract information of the five key cross sections for the corresponding key postures
Perform linear interpolation of the five key cross sections (2D)

Extract the location of UAF-UAM, LAM and LAF from the corresponding key postures
Perform linear interpolation for the location of UAF, UAM, LAM and LAF
Create the local coordinates system for the planes of UAF, UAM, LAM and LAF
Transform the UAF, UAM, LAM and LAF cross sections to their planes

Determine the elbow interpolation plane from  $\alpha$ 
Calculate the local coordinates system for the elbow plane
Transform the E cross section to its plane

Extract the profiles of the corresponding key postures
Perform linear interpolation for the profile ( $profile_\alpha$ )
Determine the coordinates of the prominent points from UAF, E and LAM cross sections
Create the plane ( $plane_{UAF-E-LAF}$ ) from the above prominent points
Copy the profile to the  $plane_{UAF-E-LAF}$ 

Determine initial location of the surface lines
Create the surface lines
Sample 16 points ( $point_{surface\ lines\ 1..16}^{additional\ cross\ section\ 1..4}$ ) from the surface lines for the additional cross section (at 1/3, 2/3 between UAM-E and E-LAM)
Determine points with the maximum width ( $maximum\_width_{max\_left}^n$  and  $maximum\_width_{max\_right}^n$ ) for each of additional cross section
Use the  $maximum\_width_{max\_left}^n$  and  $maximum\_width_{max\_right}^n$  to delete  $point_{surface\ lines\ 1..16}^{additional\ cross\ section\ 1..4}$  at the posterior of each of the additional cross section.
Sample 4 points ( $point_{1..4}^{profile}$ ) from the  $profile_\alpha$ 
Combine the remaining of  $point_{surface\ lines\ 1..16}^{additional\ cross\ section\ 1..4}$  and  $point_{1..4}^{profile}$ 

```

8.1.5 Evaluation of programming results (phase 1)

As described in section 8.1.1, once the software programme was created, it was evaluated by testing it on the data of the five participants. The results from the evaluation would be used as feedback for further modifications to the software programme. To evaluate the software

programme, it was utilised to predict the flesh deformation for three different angles for all of the participants. The proposed angles were 145°, 110° and 60°. Each of these angles represented the interval of the key posture i.e. a full extension-135°, 135°-90°, and 90°-maximum flexion, respectively. For each angle and every participant, the outcome of the programming would be visualised in Pro-Engineer Wildfire 4.0. The test revealed three potential problems. Detail discussion of each of the problems and solutions to overcome them were explained in the following:

1. *Some of the five key cross sections do not coincide with the profile for all key posture intervals*

The test result showed cases where gaps between the five key cross sections and the profile were present on the Y-Z plane, as shown in Figure 187. Figure 187 shows how UAF, UAM, LAM and LAF do not coincide with the profile. The incorrect placement of the five key cross sections occurred on all participants and, although was observable on all tested arm angles, was mostly evident on the arm posture in the range of 90°-maximum flexion.

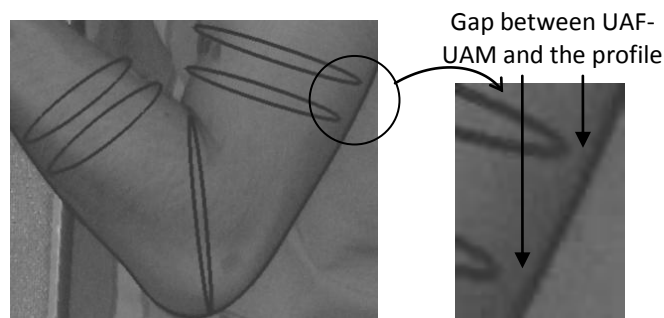


Figure 187. Misplacement of the five key cross sections for 60° flexion

This phenomenon occurred because the cross section and profiles of the key postures were acquired separately. Although efforts were made to ensure that the arm angles of key postures i.e. full extension, 135°, 90° and maximum flexion, were exactly the same for both acquisition processes, there was likely to be some subtle angle variation. As the key postures were used to derive the cross sections and profiles for other arm angles, the angle variation manifested as unsynchronised placement between the five key cross sections and profiles for other arm angles. As the arm angle progressed towards maximum flexion, the effect of angle variation accumulated. This also explained why the gap between the five key cross sections and profiles was largest for the third key posture interval i.e. 90°-maximum flexion.

The presence of gaps between these key cross sections and the profile would yield distortion in the subsequent creation of surface lines and additional cross sections at the elbow. This could then lead to shape distortion on the resulting arm surface. Thus, it was important to ensure that the five key cross sections coincided with the profile before

subsequent processes began. The offered solution to this problem was to adjust the placement of five key cross sections to match the profile. The reason why this solution was chosen as opposed to adjusting the profile to match the cross sections was related to the function of a profile itself. A profile essentially held detailed information regarding the location of cross sections with respect to each other. Its role was also to ensure that additional cross sections could produce a detailed flesh deformation at the elbow. While a key cross section held detail information about the size and shape of the surface cross section at that point, it did not necessarily hold information of where it should be located with respect to other key cross sections. Thus, the proposed approach was to modify the five key cross sections location to match the profile which essentially acted as a guide in this regard. The gap between the five key cross sections and its profile was another area likely to benefit from advances in 3D body scanning technology to enable extraction of both key cross sections and profiles for all key postures. The proposed solution would be applied on the programming (phase 2).

2. *Incorrect prediction of UAF, UAM, LAM and LAF for arm posture in the range of 90°-maximum flexion*

Incorrect prediction of UAF, UAM, LAM and LAF were observable on the Y-Z plane (the same plane as the side view photograph) for arm postures in the range of 90°-maximum flexion. Figure 188 shows an example of incorrect prediction of UAF, UAM and LAM for a 60° arm flexion.

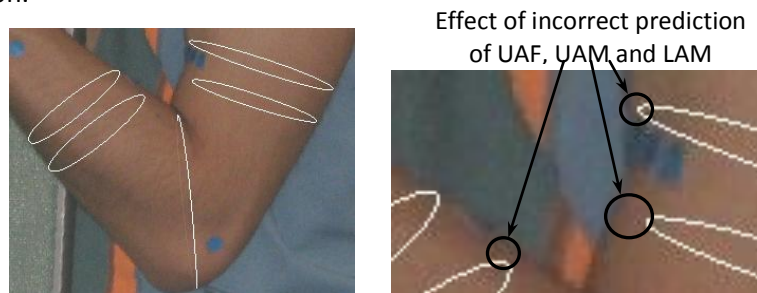


Figure 188. Predicted UAF, UAM and LAM, for arm posture in the range of 90°-maximum flexion, are compared to the side view photograph

The incorrect prediction was caused by the incorrect assumption which stated that UAF, UAM, LAM and LAF could be predicted through linear interpolation for this particular key posture interval. The assumption did not reflect the real phenomenon in which cross sections of UAF, UAM, LAM and LAF would likely remain the same until the arm flexion reached a state where the anterior flesh of the upper and lower arm met. As the anterior flesh of upper and lower arm met, flesh compression would occur. First, UAM and LAM would meet and then followed by changes of their cross sections' shape as the arm flexed further and flesh compression took place. Once the flesh compression occurred, the

dimension of UAM and LAM on the Y-Z plane (side view) would decrease but its dimension on X-Y plane (front view) would increase. The effect of flesh compression as the arm flexed also applied for UAF and LAF although UAM and LAM were the most affected. Thus, the assumption of how UAF, UAM, LAM and LAF deformed linearly throughout the whole range of arm movement was not applicable for arm postures in the range of 90°-maximum flexion, especially in the Y-Z plane i.e. the same plane as the side view photographs.

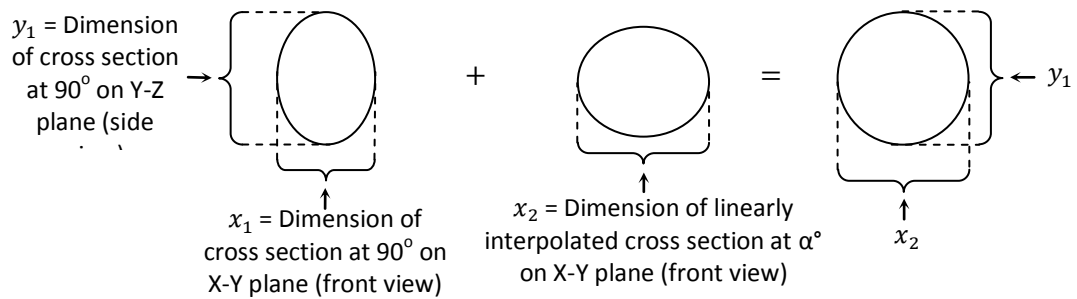


Figure 189. The proposed suggestion to solve the incorrect prediction of UAF, UAM, LAM and LAF for arm posture between 90°-maximum flexion

Taking into consideration this phenomenon, the proposed suggestion was to maintain the size of UAF-LAF and UAM-LAM on Y-Z plane (side view) for arm angles that fell into the range of 90° ≤ arm angle < maximum flexion. In addition to this, the dimensions of UAF, UAM, LAM and LAF of the 90° key posture were also adjusted on X-Y plane i.e. the plane of the front view photograph, to match the X-Y dimension of the interpolated cross sections. Figure 189 shows an illustration of the proposed solution. The solution was based on the assumption that until the flesh compression took place, the dimension of UAF, UAM, LAM and LAF on Y-Z plane (the side view photograph) remained similar to those of the 90° key posture whereas their size on the X-Y plane (the front view photograph) would change slightly. The adjustment involved scaling the UAF, UAM, LAM and LAF at 90° so that their size on X-Y plane matched to the interpolated UAF, UAM, LAM and LAF (see Figure 189). Figure 190 shows how the UAF, UAM, LAM and LAF of a 60° arm flexion were in accordance with the arm shape of the side view photograph by applying the proposed solution. The proposed solution would be applied on the programming (phase 2).

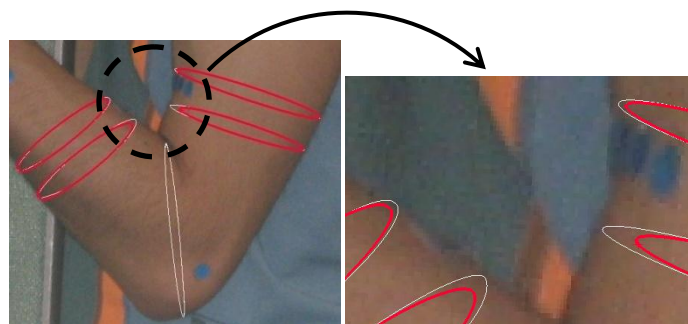


Figure 190. Adjusting UAF, UAM, LAM and LAF (white line) after interpolating them (red line)

3. Failure of the surface lines exclusion algorithm to capture the maximum width of the arm for arm postures in the range of full extension-135°

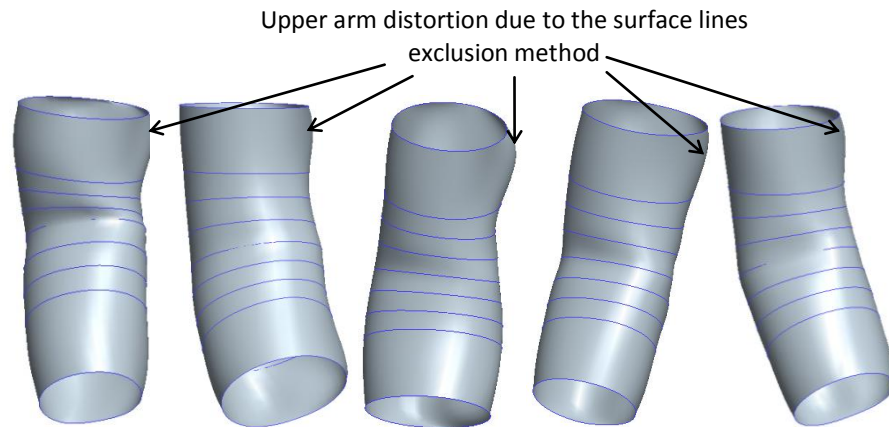


Figure 191. Upper arm distortion for an arm angle between a full extension-135° for all participants

A partial distortion at the upper arm was observable for an arm angle between a full extension-135°. This tendency was found on all participants as shown in the Figure 191. Based on the observation, this distortion was caused by the failure of the surface lines exclusion algorithm to capture the maximum width of the arm for arm postures in the range of a full extension-135°, shown in Figure 192. The cross section with the dashed line was generated from the application of the surface lines exclusion. On the contrary, the cross section with the solid line was generated by keeping most of the surface lines and resulted in preserving the maximum width of the arm.

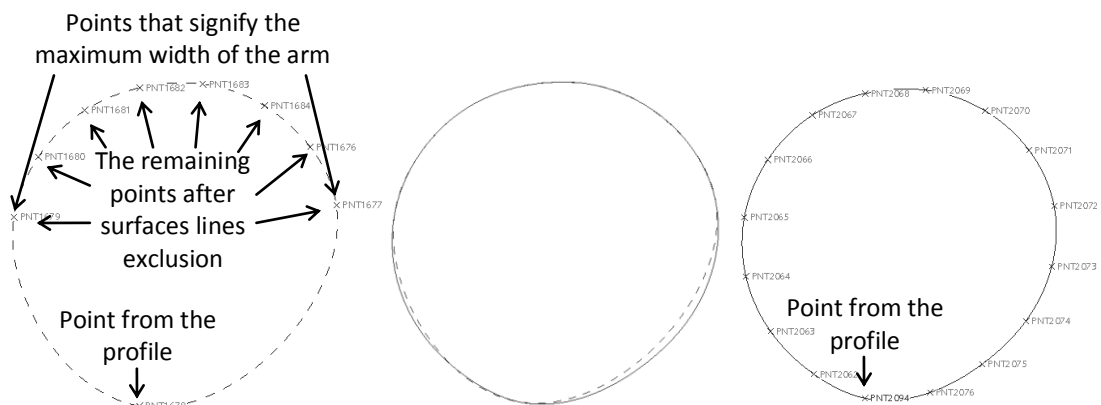


Figure 192. The cross sections which are resulted from the surface lines exclusion algorithm (dashed line) and a single exclusion of the surface lines (solid line)

Current surface lines exclusion discarded all points at the posterior part of the arm once the boundaries i.e. two points that determined the maximum width of the arm, were identified. The leftmost image in Figure 192 illustrates that only 8 points at the anterior part of the arm remained after surface lines exclusion. However, due to the nature of the curve creation, this resulted in lack of control at the side of the cross sections, as shown in the middle image in Figure 192. This finding suggested the need for modification on the

surface lines exclusion for the arm angle between a full extended arm and a 135° flexion. The proposed modification was by supplying another set of points after identifying points that signified the maximum width of the arm.

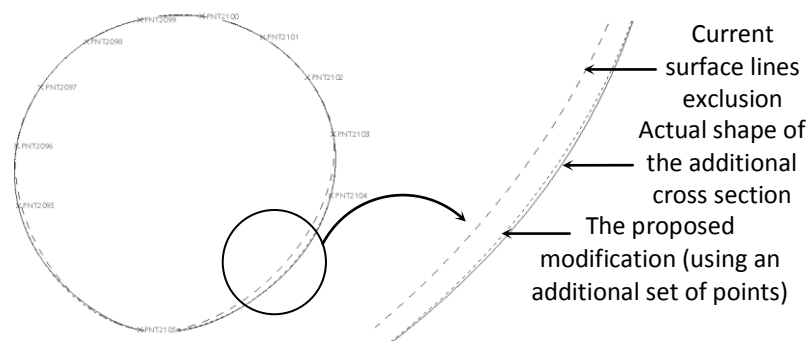


Figure 193. The cross section which is created with an additional set of points is able to mimic the actual shape of the additional cross section, compare to the current method of surface lines exclusion

Figure 193 shows the actual shape of the additional cross section compared to the cross sections which were created based on the current surface line exclusion method and the proposed modification. The result seemed to suggest that the proposed modification followed the actual shape of the additional cross section better. The proposed modification would be integrated into the programming in phase 2.

8.1.6 Software programming (phase 2)

The three suggested modifications above were adopted in the developed programming (phase 2). For the first suggestion i.e. translating the five key cross sections so that they coincide with the profile, the magnitude of translation had to be determined. In order to determine this, the gap between the cross sections and the profile had to be calculated. The gap for each cross section was determined by the 2D distance, on the Y-Z plane, between the point which determined the maximum width of the cross section (*maximum_width*) and the profile. Although there were two points that determined the maximum width for each of the cross sections, only one point, the one closer to the profile, would be utilised. Figure 194 shows an example of *maximum_width* for UAF and UAM.

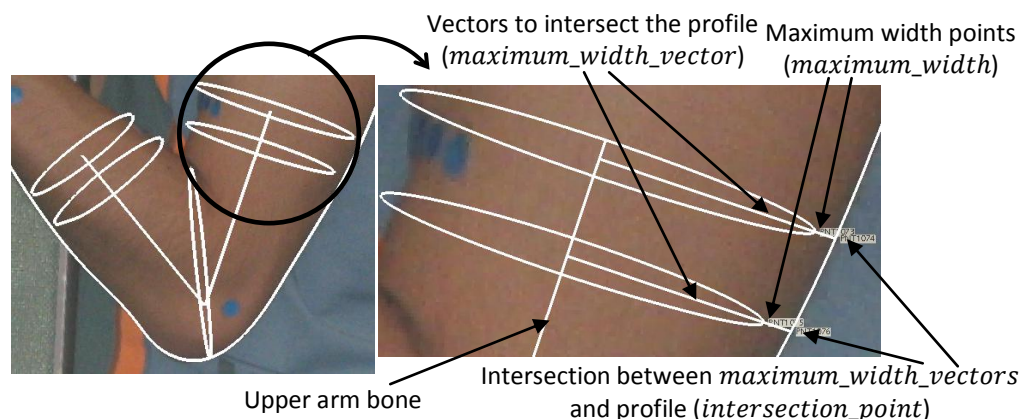


Figure 194. Processes to translate the UAF and UAM cross sections

To calculate the distance of these points to the profile, three steps were performed. First, vectors (*maximum_width_vector*), which passed through *maximum_width* and either perpendicular to upper arm bone (for UAM and UAF)/lower arm bone (LAM and LAF) or passed through the elbow joint (for E), were created. Next, the *maximum_width_vector* was intersected with the profile to obtain *intersection_point*. The last step was to measure the distance between *intersection_point* and *maximum_width*. An algorithm that followed this process was created in Matlab 7.0 and the pseudo code of the algorithm is shown below. This algorithm would be added after the interpolation of the five key cross sections.

<p>For each of five key cross sections</p> <p>Create the B-spline curve from the sampled point of the cross section</p> <p>Determine the point which determine the maximum width of the cross section at Y-Z plane (<i>maximum_width</i>)</p> <p>Create five vectors (<i>maximum_width_vectors</i>) on Y-Z plane that pass through <i>maximum_width</i> and are either \perp to the upper arm bone (for UAF and UAM)/lower arm bone (for LAM and LAF) or pass through the elbow joint (for E)</p> <p>Intersect the (<i>maximum_width_vectors</i>) with the profile and obtain <i>intersection_point</i></p> <p>Calculate distance between <i>maximum_width</i> and <i>intersection_point</i></p> <p>Translate the cross sections</p> <p>End</p>
--

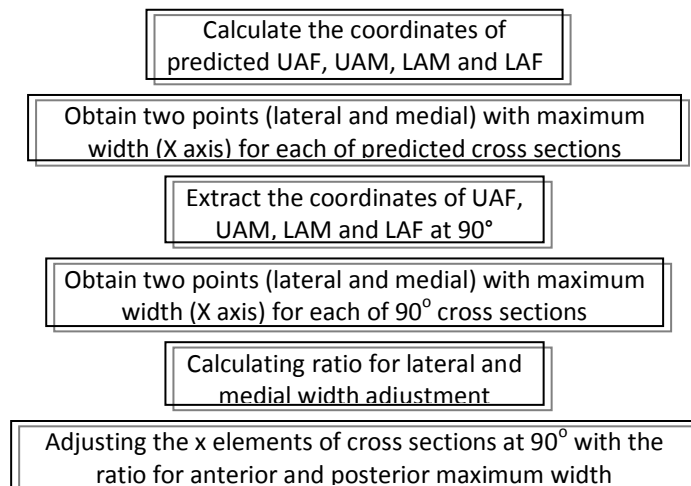


Figure 195. Steps to adjust the UAF, UAM, LAM and LAF for the arm posture between 90°-maximum flexion

The next modification to the programming was related to the suggested modification for UAF, UAM, LAM and LAF at 90°-maximum flexion arm posture. Figure 195 shows the steps that were required to perform the modification. These steps were performed in a 2D setting and would be added within the process of cross sections' interpolation. As shown, in Figure 195, coordinates of UAF, UAM, LAM and LAF for both predicted arm angle and 90° flexion had to be extracted. Figure 196 shows an example of the UAM cross section at 60° and 90°. Following the steps shown in Figure 195, the maximum x elements from the coordinates of interpolated UAM at 60° and 90° were obtained. Figure 196 shows the corresponding maximum x elements for both cross sections. These

values were then used to adjust the UAM at 90°. The final adjusted UAM at 90° was then used to represent the final UAM at 60°. The final result is shown in the right image (solid line) in Figure 196. Without applying this modification to UAM at 60°, the situation described in point 2 at section 8.1.5 would occur.

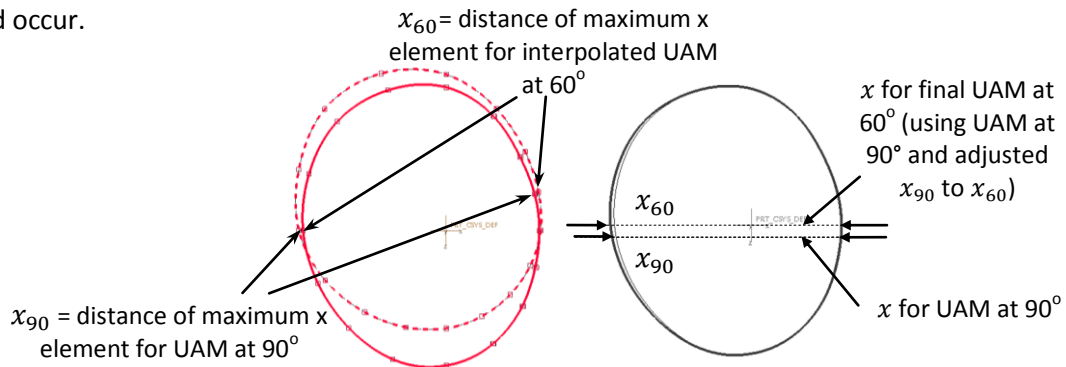


Figure 196. Left image is UAM at 60° (dashed line) and UAM at 90° (solid line). Right image is UAM at 90° after lateral and medial width adjustment (solid line) compared to UAM at 90° before adjustment (thin line)

The following shows the pseudo code of the created algorithm following the process above. This algorithm would be added after interpolating the cross sections and before the five key cross sections takes place.

For UAF, UAM, LAM and LAF (between 90°-maximum flexion)

- Calculate the coordinates for the interpolated angle
- Calculate the coordinates for the 90° flexion
- Obtain the maximum x elements for interpolated angle
- Obtain the maximum x element for 90° flexion
- Calculate the first ratio (lateral)
- Adjust the coordinates for the 90° flexion (lateral)
- Calculate the second ratio (medial)
- Adjust the coordinates for the 90° flexion (medial)

End

In accordance with the proposed modification for point 3 in section 8.1.5, an algorithm for the surface lines exclusion for the arm range between the full extended arm and 135° flexion was created in Matlab 7.0. This algorithm was added onto the existing programming which had been shown in section 8.1.4. The following pseudo code details the steps in the proposed modification of surface lines exclusion.

For each additional cross section

- Obtain 16 points from surface lines
- Assign number (1 to 16) to these 16 point (number 1 is assigned for the initial location of surface line)
- Find the point with the largest and smallest x value
- Find the number for these points e.g. point 6 and point 12
- Include the first posterior points after these two points e.g. point 7 and point 11
- Delete the points with numbers that are located between these two points e.g. point 8, 9, 10

End

8.1.7 Evaluation of programming results (phase 2)

This subsection outlines the output of the modified programming from the previous subsection. Three tests were performed to evaluate the three proposed solutions from section 8.1.5. The first test was aimed to evaluate the proposed solution to ensure that five key cross sections coincided with the profile for all key posture intervals. Following the evaluation of the first phase, the modified programming was tested with the same three arm angles i.e. 145°, 110° and 60°, which represented the three intervals of the key postures. With respect to the cross section translation, the proposed modification was successful in ensuring that the five key cross sections coincided with the profile. Figure 197 demonstrates this in which examples of three different postures from three different participants are shown.

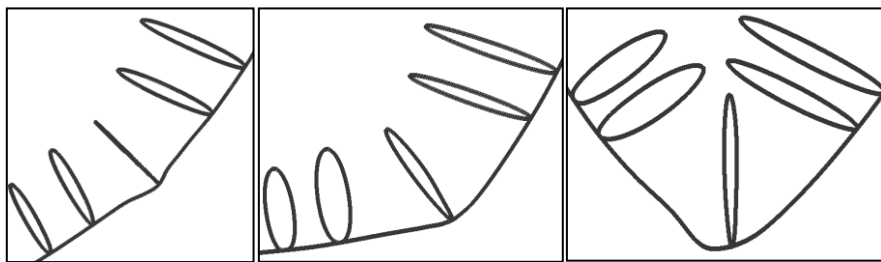


Figure 197. Result of the five key cross sections translation, which shows that they coincide with the corresponding profile

The second test was performed to evaluate the proposed solution which was aimed to overcome the incorrect prediction of UAF, UAM, LAM and LAF for arm posture in the range of 90°-maximum flexion. For the second test, the modified programming was run to predict UAF, UAM, LAM and LAF at 60° which was one of the arm angles used in the first evaluation. Figure 198 shows the result of the modification on three participants. The result demonstrated that, for the arm angle in the range of 90°-maximum flexion, the proposed modification was able to generate UAF, UAM, LAM and LAF that were in accordance with the corresponding profile.

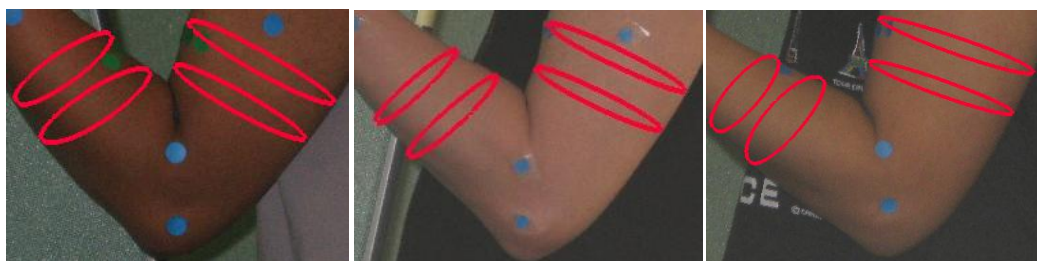


Figure 198. Results of the proposed modification for UAF, UAM, LAM and LAF for arm angle between 90°-maximum flexion

In comparison with the real phenomenon, the proposed suggestion was a mere simplification which would result in a reduced accuracy level. However, as the anterior part of the elbow during flexion was not a particularly functional area for most ergonomics applications, a reduced accuracy level for this part of the elbow was deemed to be acceptable in this research. A perfect solution

would be to determine the average angle of where UAM-LAM would undergo flesh compression. The arm angle at which UAM-LAM would undergo flesh compression would likely depend on the body type e.g. for an endomorph, the UAM-LAM would undergo flesh compression at an earlier arm angle than for an ectomorph due to the corpulence of the upper and lower arm. Figure 199 illustrated how, for similar arm angles, the corpulence of the upper and lower affected the extent of flesh compression at the anterior part of the elbow. Thus, it was suggested that the arm angle of which the flesh compression begun was determined for each body type. As achieving this solution would require a considerable amount of data collection and analysis, this solution could be explored further in future studies.



Figure 199. Effect of body type to the arm angle

The third test was aimed to evaluate the proposed solution which was aimed to overcome the failure of the surface lines exclusion algorithm to capture the maximum width of the arm for arm postures in the range of full extension-135°. Because the modification was only aimed for the arm range between a full extension and 135°, the test would only be performed for this range by utilising the modified programming to predict the flesh deformation for arm angles with > 135° flexion. This was then followed by comparing the results with those of the original programming. Figure 200 shows the comparison result.

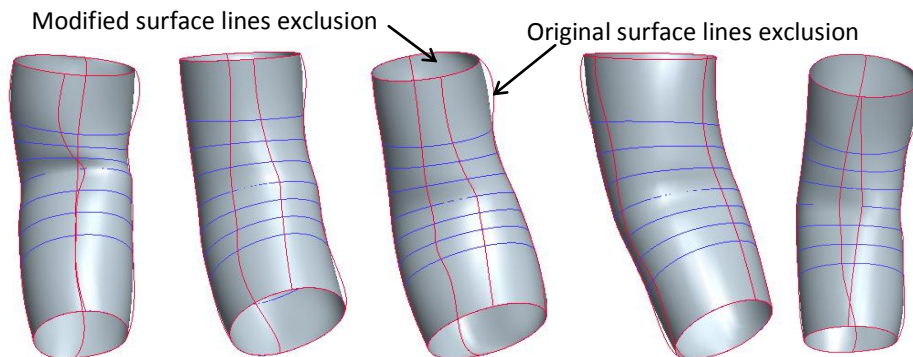


Figure 200. Comparing the result between the original (transparent surface) and modified (solid surface) surface lines exclusion's programming for a 145° flexion

The results showed that the partial distortion at the upper arm could be reduced by applying the proposed solution. Although this approach provided a practical solution to the problem, this approach was also a simplified solution. To provide a more accurate solution, a mini study could be performed to determine the optimum number of set points which had to be included after identifying the points which signified the maximum width of the arm. The mini study should be

performed by using cross sections from different body types and sizes to ensure that the optimum number of set points was applicable for all body types and sizes. Considering the resources that would be required, this approach could be explored in further studies.

The overall results of the second evaluation seemed to suggest that the proposed solutions, which were integrated into the second phase of the software programming in section 8.1.6, were successful in solving the three issues which were identified in section 8.1.5. This also indicated that the concept of the proposed FDM was finalised and effort could be focused on reviewing the proposed FDM against the DHM specifications which were established in section 4.1. This would be addressed in the next section of this chapter.

8.2 Methodology of proposed FDM's review

To determine whether the proposed FDM fulfilled the DHM specifications or not, the review should ideally bring forth a measurable or quantifiable result. For some of the specifications this would mean integrating the proposed FDM into an existing DHM of an ergonomics CAD system. Integrating the proposed FDM into an existing ergonomics CAD system would allow its performance to be measured as part of the overall DHM. Specifications which would require this were whole body modelling and real time modelling.

For other specifications, i.e. accommodation of different body sizes and types, further research work would be required in order to demonstrate the ability of the proposed FDM to comply with it. The flesh deformation of the proposed FDM was based on the provision of the basic elements i.e. five key cross sections, profile and flesh deformation area for each key posture as well as the carrying angle. All of these elements demanded a direct and comprehensive data acquisition from participants. This meant that at this stage, the ability of the proposed FDM to accommodate different body sizes and shapes was limited to those participants whose basic elements had been obtained previously. Therefore, to show that the proposed FDM could accommodate different body sizes and types without rigorous data acquisition, further research work was needed as shown in Figure 181. On the contrary, the conformation of the proposed FDM to other specifications, such as realism, accuracy, and minimum user intervention, could be assessed without the need to integrate it with an existing system or further research work.

Thus, three different approaches of review were required to address the scope of the specifications. The proposed approaches are detailed below:

1. Specifications that did not require the integration of the proposed FDM into an existing ergonomics CAD system (accuracy, realism and minimum user intervention).

Qualitative assessment was proposed to be applied to review the FDM against the realism and minimum user intervention specifications; and quantitative assessment for the

accuracy specification. The qualitative and quantitative assessment would be based on the implementation of the proposed FDM on the five participants which were recruited during the proposed FDM development. The implementation of the proposed FDM would attempt to synthesise a posture that was not explicitly captured from a participant i.e. any arm postures except the four key postures. The implementation would in the end demonstrate the proposed FDM's ability to generate accurate and realistic flesh deformation with a minimum user intervention for any arm postures.

In order to facilitate the implementation of the proposed FDM, numerical computing (a software programme) would be required. The functions of the software programme were as the following:

- i. To ensure that all of the decisions from the design phases of the proposed FDM could be performed easily in a computer numerical environment.
- ii. To ensure that all of the decisions and existing algorithms from the design phases of the proposed FDM were compatible in a computer numerical environment.
- iii. To allow automatic generation of the flesh deformation for any arm posture from the basic elements of the flesh deformation.

The software programme which was developed in section 8.1 was proposed to be utilised as it satisfied the three functions above.

2. Specifications that required further research work (accommodation of different body sizes and shapes).

It had been mentioned previously how the proposed FDM ability to accommodate different body sizes and shapes was limited by the necessity to provide the flesh deformation elements through rigorous data acquisition. Thus, a concept that allowed the application of the proposed FDM with a minimum data acquisition from new participants would be required. To develop this concept, further research work would have to be done. The concept development would likely demand an in-depth research and hence, instead of performing it at this stage, it would be performed separately and take place after this initial review. Review for this particular specification would be performed at the end of the further research work.

3. Specifications that required the integration of the proposed FDM into an existing ergonomics CAD system (real time modelling and whole body modelling).

This research proposed a “retrospective analysis” approach which was essentially a pragmatic review of the perceived efficacy of the proposed FDM. A retrospective analysis would attempt to analyse and identify retrospectively the stages of the proposed FDM's

development process in which the corresponding specifications were used to guide the decision making. Although this approach would provide neither a quantitative nor qualitative output, it could demonstrate how the corresponding specifications were ingrained into the proposed FDM's development process. This approach was based on the assumption that had the proposed FDM been integrated with an existing ergonomics CAD, the outcome would satisfy the corresponding specifications because the development of the proposed FDM had been guided constantly by them.

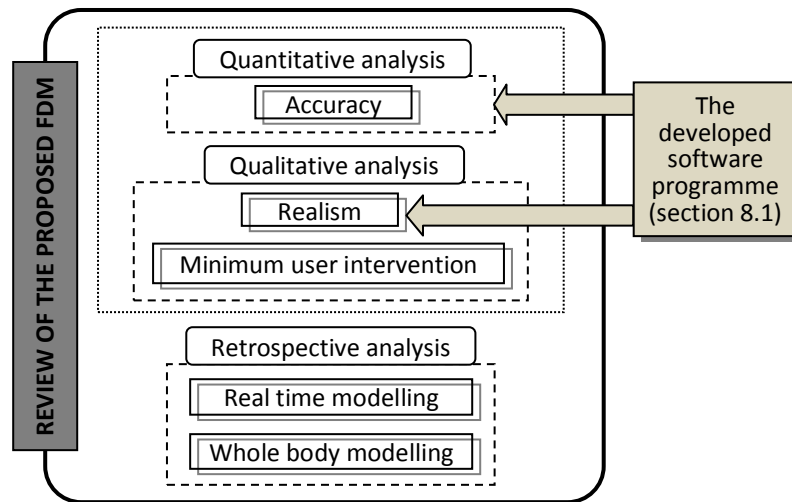


Figure 201. The review process of the proposed FDM for the current chapter

Based on the explanation above, except for the accommodation of different body sizes and shapes specification, the review of the proposed FDM would be performed against all of the DHM specifications. It was also clear that the review for these specifications was distinguished into two categories i.e. retrospective analysis and qualitative/quantitative analysis. Figure 201 shows the complete process of the review. For each of the DHM specification's review shown in Figure 201, details of its methodology and result are outlined in the following subsections.

8.2.1 Review of the proposed FDM's accuracy

As had been suggested in section 8.2, the review of the proposed FDM's accuracy could be started once the programming development was completed. The review was aimed to measure the level of accuracy of the proposed FDM. In order to achieve this, a methodology was proposed (see Figure 202). The methodology involved a comparison of the output of the proposed FDM and the original data. Interpolated five key cross sections and profiles were chosen to represent the output of the proposed FDM because they determined the overall shape of the flesh deformation at the elbow. Corresponding to the chosen proposed output of FDM, the original data consisted of 3D scan data and side view photographs. Offset measurement i.e. Euclidean distances, would be applied to measure the difference between the output of the proposed FDM and the original data. The offset measurement output would then be analysed to determine the average error of the proposed FDM.

Figure 202 shows that the comparison between the proposed FDM and original data would be performed for each interval of the key postures. For each interval of the key postures i.e. full extension-135°, 135°-90° and 90°-maximum flexion, an arm posture would be chosen for the comparison. Five participants that took part during the development of the proposed FDM would be involved again. Thus, there would be six comparisons to be performed for each participant.

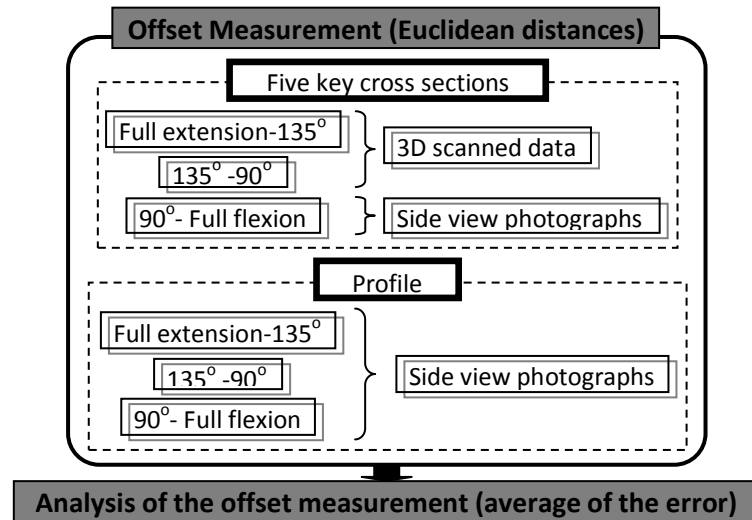


Figure 202. Proposed methodology for validating the accuracy of the proposed FDM

For the offset measurement of five key cross sections, two types of original data were used i.e. 3D scan data and side view photographs. Ideally, the 3D scan data should be utilised for the comparison. However, as had been explained in section 6.3, 3D scan data could only be obtained for limited arm angles i.e. >90°. Thus, for the interval of key postures within 90°-maximum flexion, side view photographs for the profile comparison would be used. For the first two intervals of key postures i.e. full extension-135° and 135°-90°, two 3D scan data would be acquired from each participant. As it would be impractical asking the participant to hold and flex the arm at a certain arm angle during 3D scanning, the participant was liberated to assume any arm angle as long as it was within the boundary of the key posture interval. To maintain the consistency with the side view photographs and manual measurements of the five key cross sections, the arm was scanned with a pronated wrist and only the left arm of the 3D scanned arms would be utilised for review.

For the offset measurement of profile, side view photographs were used. In section 6.4.2, in addition to capturing the side view photographs of key postures, side view photographs of arm postures that were in between the key postures were also captured for each participant. These side view photographs would be used for the comparison. Variation of the arm angles, which existed for each key posture interval in these side view photographs, would allow reviewing the proposed FDM's accuracy for a wider range of arm angles. Detailed steps and analysis of the offset

measurements for five key cross sections and profile are outlined in the subsections 8.2.1.1 and 8.2.1.2.

8.2.1.1 Comparison of five key cross sections

This subsection addressed detailed steps and results of five key cross sections comparison between the proposed FDM's output and original data. A method similar to that in section 5.3.2.1 was proposed for the offset measurement between the five key cross sections and the 3D scanned arm. This method involved creating rays, which originated from the centre of each cross section and passed through the sampled points of the cross section, and intersected the rays with the 3D scanned arm. Distance differences between the intersection points ($d_{3D_data}^n$) and the corresponding sampled points (d_{FDM}^n) determined the error level of the proposed FDM with respect to the corresponding 3D scanned arm. Figure 203 shows an illustration of the proposed method.

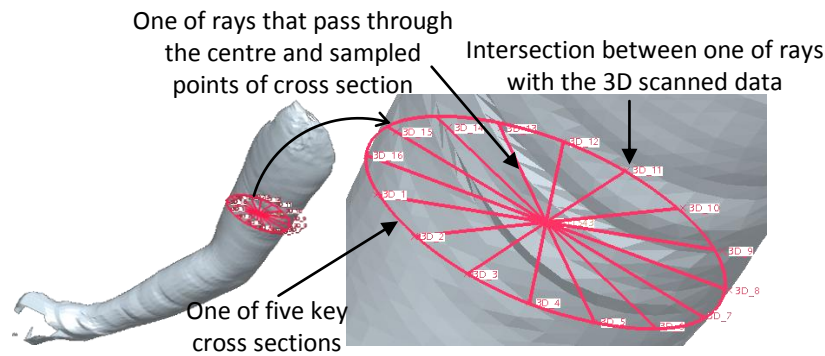


Figure 203. Proposed method to measure the offset for between the five key cross sections and 3D scan data

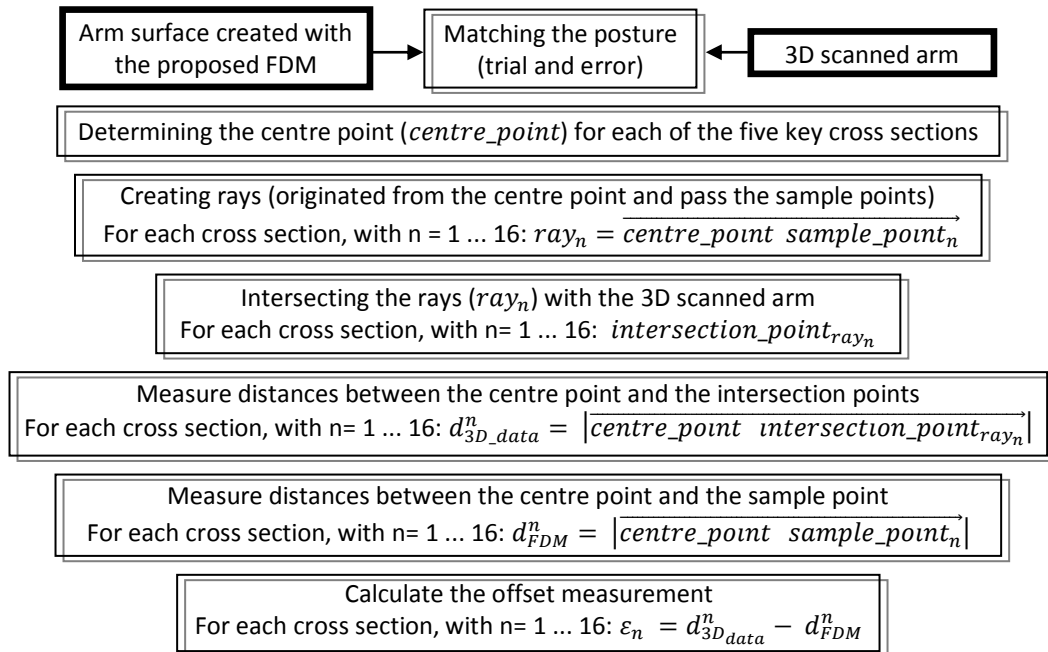


Figure 204. Details of the proposed steps to measure the offset of the five key cross sections between 3D scanned arm and the proposed FDM

Detail of steps in the proposed method is shown in Figure 204. The first step of the proposed method involved performing trial and error to match the arm surface created with the proposed

FDM to the 3D scanned arm. This trial and error was needed because the proposed FDM could not directly predict the arm angle of the 3D scanned arm and thus estimation of the arm angle had to be performed. The trial and error was performed in Pro-Engineer WildFire 4.0 and visual observation was used to judge the best fit of the matching between the proposed FDM and the 3D scan data.

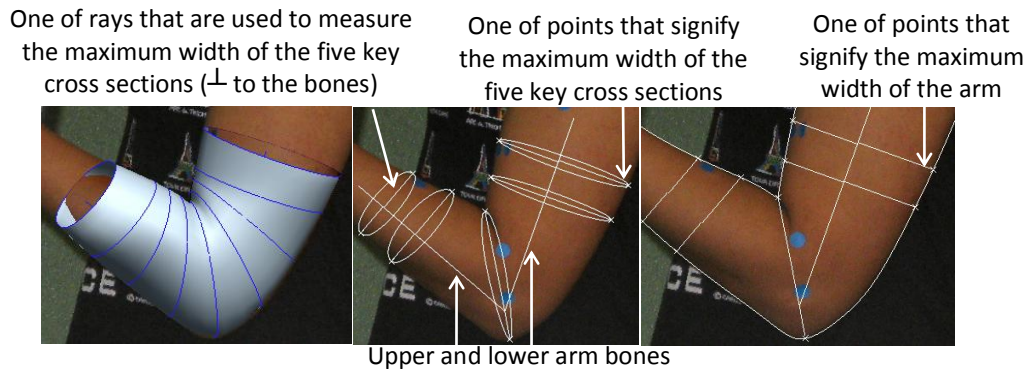


Figure 205. The offset measurement between the five key cross sections and the side view photographs

The offset measurement between the five key cross sections and the side view photographs would employ a similar quantification method to section 7.3.2.5. The maximum width of the five key cross sections would be compared with the set of photographs. Firstly, curves which outlined the shape of arm on the set of photographs would be created. This would then be followed by generating a set of rays that passed through the maximum width of the arm. The intersection of these rays with the curves would be used to calculate the Euclidean distance difference. Figure 205 shows illustration of the proposed method whereas Figure 206 shows detail steps of the proposed method for the offset measurement between the five key cross sections and the side view photographs.

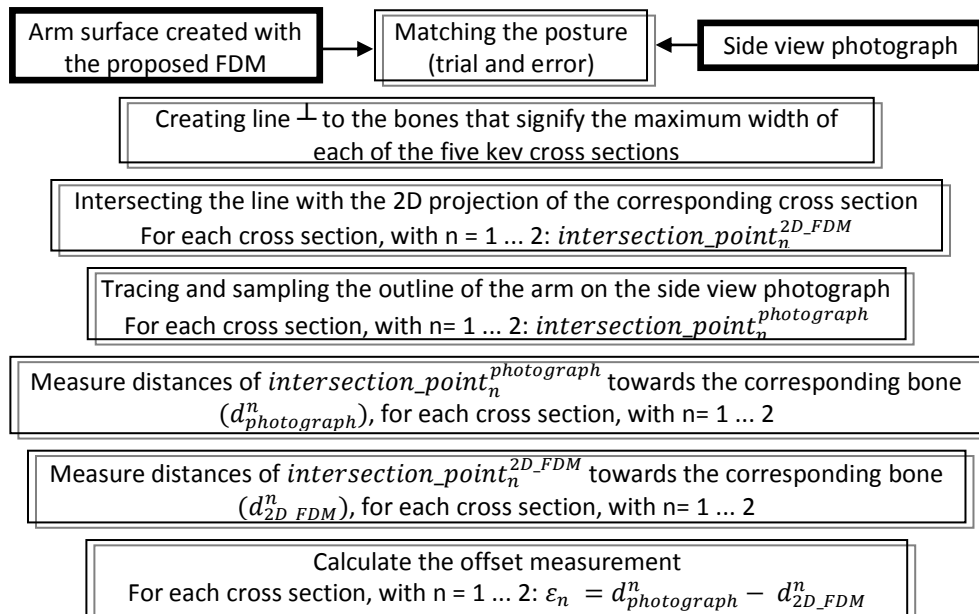


Figure 206. Detail of steps for the offset measurement between the five key cross sections and the side view photograph

To review the five key cross sections, Matlab 7.0 and Pro-Engineer Wildfire 4.0 were used. Matlab 7.0 generated the coordinates for the five key cross sections by running the software programme which was created for the feasibility testing in section 8.1. These coordinates, together with 3D scanned arm (for angles in the range of full extension-135° and 135°-90°) or side view photographs (for angles in the range 90°-maximum flexion) were then visualised in Pro-Engineer Wildfire 4.0. An algorithm was created to compare the five key cross sections of the proposed FDM and 3D scanned arm. The algorithm was based on the process shown in Figure 204. However, the offset calculation between the five key cross sections of the proposed FDM and the side view photograph was performed manually in Pro-Engineer Wildfire 4.0 as there were only a limited set of offset calculation which could be performed easily in Pro-Engineer Wildfire 4.0. Table 15 shows the result of five key cross sections offset measurement for each participant and the average error of all participants. The result suggested that the average of total error was less than 3 mm.

Table 15. Average of total error of the proposed FDM

	Full extension – 135°	135°-90°	90°-maximum flexion
Participant 1	1.97 mm	1.58 mm	0.56 mm
Participant 2	3.07 mm	2.42 mm	1.40 mm
Participant 3	2.07 mm	2.63 mm	1.55 mm
Participant 4	1.92 mm	2.71 mm	1.29 mm
Participant 5	3.74 mm	2.79 mm	1.67 mm
Average error (ϵ)	2.55 mm	2.43 mm	1.29 mm

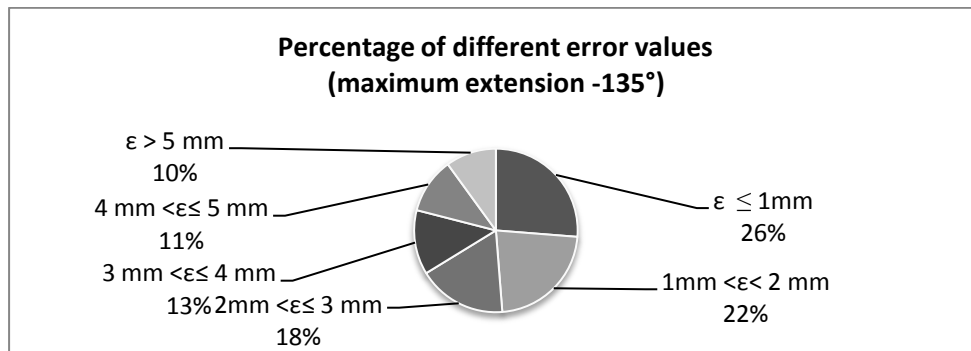


Figure 207. Proportion of different error level for the first interval of key postures i.e. maximum extension-135°

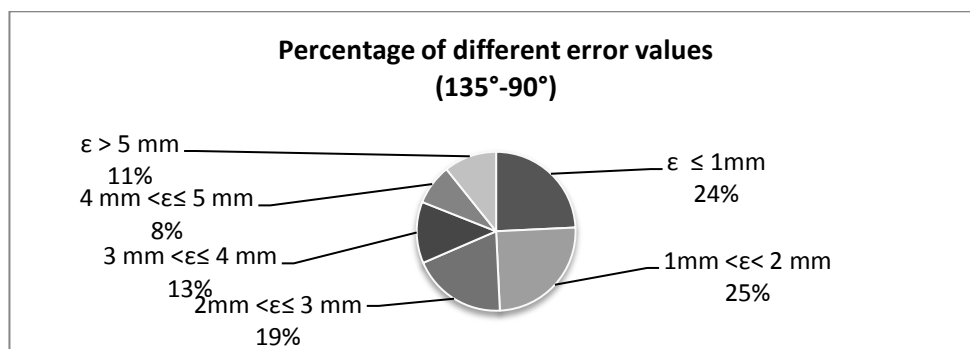


Figure 208. Proportion of different error level for the second interval of key postures i.e. 135°-90°

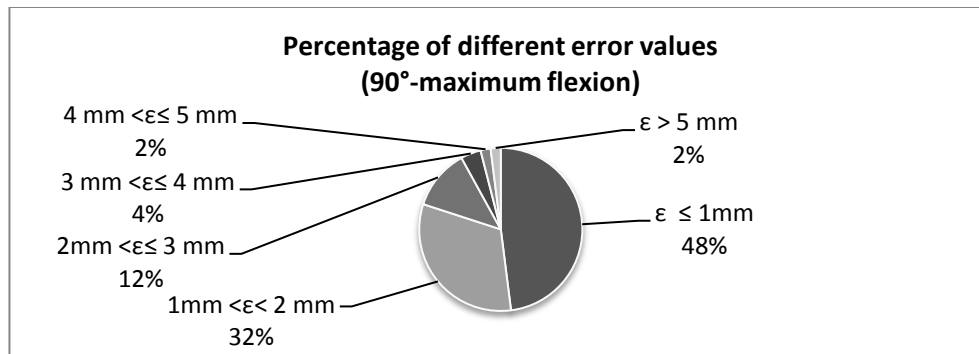


Figure 209. Proportion of different error level for the third interval of key postures i.e. 90°-maximum flexion

The proportion of the error level for each key posture interval is shown in Figure 207, Figure 208 and Figure 209. These figures show that error of less than 3 mm dominated the error proportion with 66%, 68% and 92% for the first, second and third interval of the key postures.

8.2.1.2 Comparison of profiles

This subsection outlines detailed steps and results of the comparison between profiles of the proposed FDM's output and original data. As discussed at the end of section 8.2.1, the offset measurement utilised the existing side view photographs from five participants which had been involved during the development of the proposed FDM. For each participant, three side view photographs were chosen to represent each interval of the key postures i.e. between full extension-135°, 135°-90° and 90°-maximum flexion. The offset measurement for the profile would be based on the method in section 7.3.2.5. The proposed method would utilise the profile's optimum number of points to quantify the original data. The result of original data's quantification would then be used to calculate the Euclidean distance difference between the profile of the proposed FDM and the original data. Figure 210 shows illustration of the proposed method.

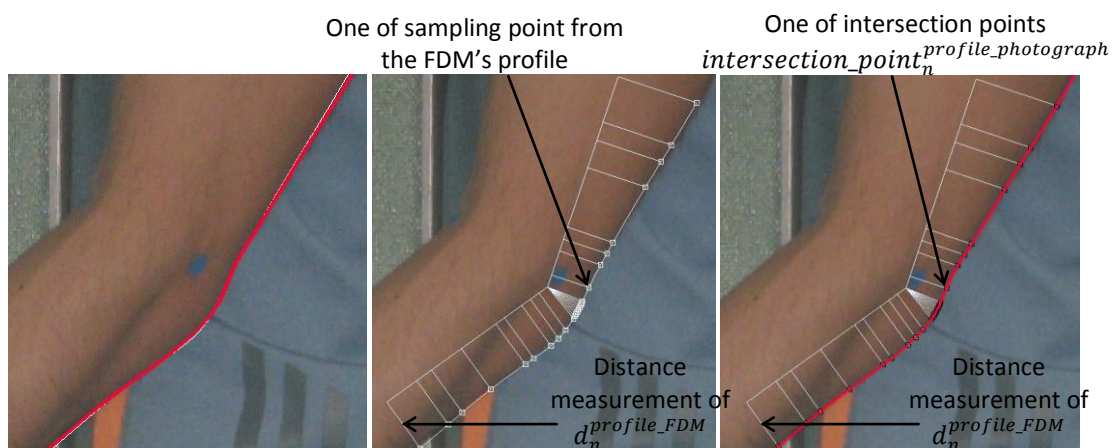


Figure 210. The offset measurement between profile of the proposed FDM (thin line) and profile of the side view photograph (bold line)

Figure 211 shows the proposed details steps of the offset measurement for the profile, which would be employed on the output of proposed FDM and the side view photograph. Following the

steps shown in Figure 211, an algorithm was created to perform the offset measurement on the profile automatically. The algorithm was created in Matlab 7.0. The offset measurement for each participant is shown Table 16. The result showed that the average error was ≈ 1 mm for all participants with various arm angles.

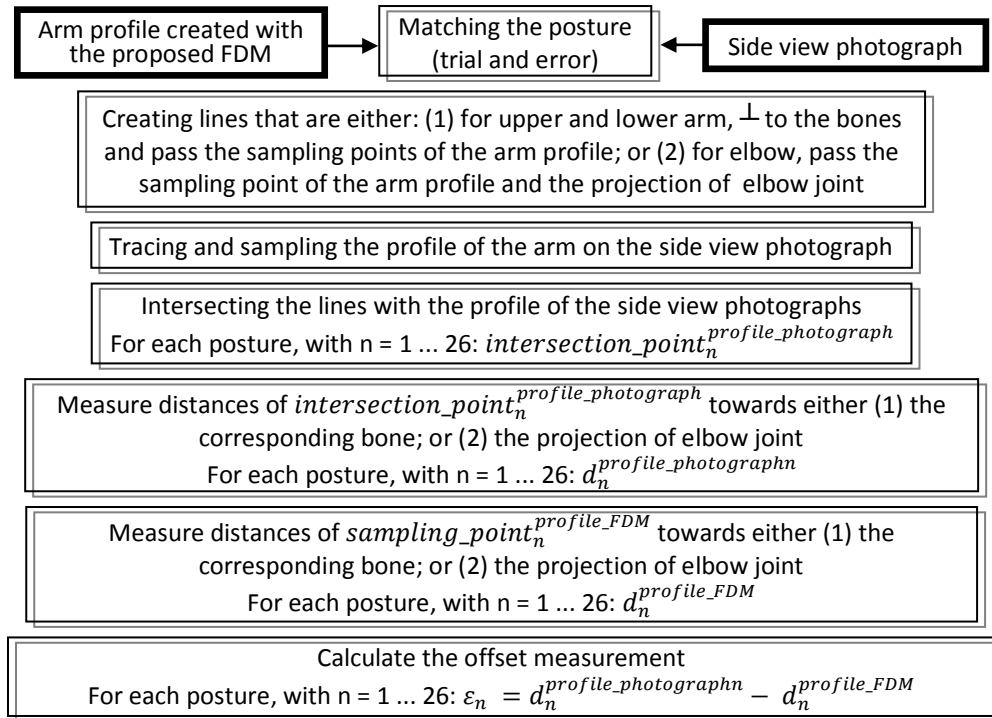


Figure 211. The proposed offset measurement for the profile

Table 16. Average error of the offset measurement for the profile interpolation

	Full extension – 135°	135°-90°	90°-maximum flexion
Participant 1	0.45 mm	0.58 mm	0.66 mm
Participant 2	0.46 mm	0.64 mm	0.37 mm
Participant 3	0.78 mm	0.51 mm	1.02 mm
Participant 4	0.9037 mm	0.80 mm	1.03 mm
Participant 5	1.12 mm	0.59 mm	0.31 mm
Average error (ε)	0.74 mm	0.62 mm	0.68 mm

8.2.1.3 Discussion of the review of the proposed FDM's accuracy

The average error level of the proposed FDM was determined by offset measurement of five key cross sections and profiles. This combination of offset measurements was applied to ensure that the error level of the overall surface created from the proposed FDM could be determined. However, as shown from detailed steps in Figure 203, Figure 205 and Figure 210, the error level determination was limited to finite sampling locations. This limitation was addressed through the qualitative assessment that was proposed to review the realism of the proposed FDM and would be described in detail in section 8.2.2. The review result on accuracy showed that the average error level of all participants for both five key cross sections and profiles were less than 3 mm. As the flesh deformation was a 3D object simulation, the 3 mm error level should be interpreted with care.

This was because a 3 mm error could mean that the surface level was elevated or reduced by up to 3 mm. This demonstrated further how the qualitative assessment of the realism review could complement the results of the accuracy review.

There were two sources which contributed to the overall error level of the proposed FDM. The first one was an internal error which was caused by the proposed FDM missed depicting some of the details at the elbow area. This was potentially a result of compromises which had to be made throughout the FDM's design phases in order to balance the various needs of DHM specifications e.g. the need to produce an accurate flesh deformation had to be balanced with the need to produce a real time flesh deformation. The internal error might also be a result of an error accumulation from the further processing of some of the proposed FDM's elements because they were obtained from various methods i.e. 3D scan data to obtain joint locations, circling the wire around the arm to obtain cross sections, and side view photographs to obtain profiles. This could likely be minimised by utilising 3D scan data, provided that the 3D scanning technology was able to provide 3D scan arms for the whole range of extension-flexion of the elbow.

The second source of the proposed FDM's overall error level was external error which was caused by a poor quality of 3D scanned arms that were used to review the accuracy of the proposed FDM (see section 8.2.2 for poor quality of 3D scanned arms). Poor quality of a 3D scanned arm could be caused by slight movement or occlusion of the crotch area of the arm (see Figure 145 for an example of poor quality 3D scanned arm). Some efforts that were made to minimise poor quality of 3D scanned arm are: (i) calibration prior obtaining 3D scanned arm; (ii) providing modification of the handheld to steady the arm; (iii) reviewing the result of 3D scanned arm once it was taken and politely request participants to be scanned again if the result is unsatisfactory; and (iv) specifically instruct participants to wear non-white or black apparel as well as removing the apparel for the upper body if they wish

In terms of accuracy, this research did not specify the accuracy value which had to be accomplished. The reason behind this was because to the extent of this research's knowledge, there was no specified value of accuracy for existing FDM or DHM modelling in ergonomics simulation. Currently, there were two existing standards on DHM for ergonomics simulation i.e. BS EN ISO 15536-1:2008 and BS EN ISO 15536-2:2007. Both standards, as stated in BS EN ISO 15536-1:2008, establish:

“... general requirements for the design and development of computer manikins, body templates and manikin systems. It addresses their anthropometric and biomechanical properties, taking into account their usability and restrictions for structural complexity and functional versatility, and is also intended as a guide for the selection of manikins

and manikin systems and for the evaluation of their accuracy and usability for the specified use.”

A close review on both standards did not explicitly reveal a numerical value of either required accuracy or inaccuracy for DHM. As a result, it was difficult to justify the definite cut off for level accuracy e.g. if an error level reached x then it was not accurate. For evaluation of product design or work space where tolerance value of error level was higher than 3 mm e.g. between 0.5-1 cm, the proposed FDM would likely be sufficiently accurate. However, for a critical safety modelling where flesh deformation was of paramount parameter, a 3 mm error level might not be sufficient.

8.2.2 Review of the proposed FDM's realism

The review of the proposed FDM's accuracy showed that the proposed FDM was able to produce flesh deformation with a considerably low level of error. However, the review of the proposed FDM's accuracy was performed with limitation i.e. it only analysed the error on a finite number of points on the 3D surface. Hence, it could not truly reflect the ability of the FDM to represent the 3D surface and the review result of the FDM's accuracy could not simply be extended onto the review of the proposed FDM's realism. Therefore, visual observation was performed to review the proposed FDM's realisms which referred to the resemblance of the DHM to a real human body form, as explained in section 4.1.2. The visual observation result also complemented the review result of the proposed FDM's accuracy, as discussed earlier in section 8.2.1.3.

Similar to the review of the proposed FDM's accuracy, review for this section would be performed for each interval of the key postures. The proposed approach to review this DHM specification was by comparing the flesh deformation from the proposed FDM with the 3D scanned arm when it was available (full extension-135° and 135°-90°) and side view photographs when 3D scanned arm was not available (90°-maximum flexion). The comparison would be performed by visually observing the flesh deformation for the five participants. The same data of 3D scanned arms and side view photographs that had been chosen to review the five key cross sections (see section 8.2.1.1) would be re-used. Because the process of matching the proposed FDM to either the 3D scanned arm or side view photographs had been performed in section 8.2.1.1, the visual observation on the proposed FDM could be started directly. The result of visual observation for the first two intervals of key postures and the last key posture interval was given in section 8.2.2.1 and section 8.2.2.2, respectively. This subsection was concluded with discussion of the visual observation results in section 8.2.2.3.

8.2.2.1 Visual observation to compare the flesh deformation from the proposed FDM with the 3D scanned arm (full extension-135° and 135°-90°)

The visual observation for arm postures between full extension-135° on five participants showed that the proposed FDM could capture details of the arm, particularly at the elbow area. This was shown by examples (participant 1 and 3) in Figure 212 in which the indentation at posterior of the elbow area, which was captured by 3D scanned arm, was replicated by the proposed FDM. Images in Figure 213, which were taken from participant 2 and 5, demonstrate further the ability of the proposed FDM to capture details at the anterior of the elbow area. An ability to capture this level of detail could assist in providing higher realism to the flesh deformation. Figure 213 also demonstrates cases of poor quality 3D scanned arms which were referred earlier in section 8.2.1.3.

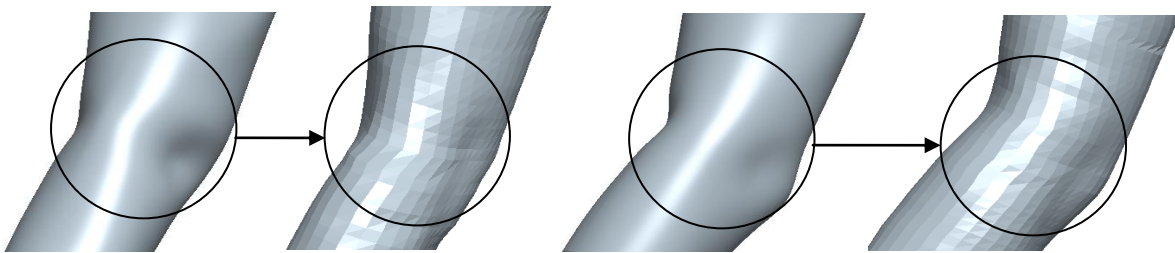


Figure 212. The proposed FDM was able to capture details at the elbow i.e. indentation at the posterior of the elbow area, which is highlighted by the solid lined circles

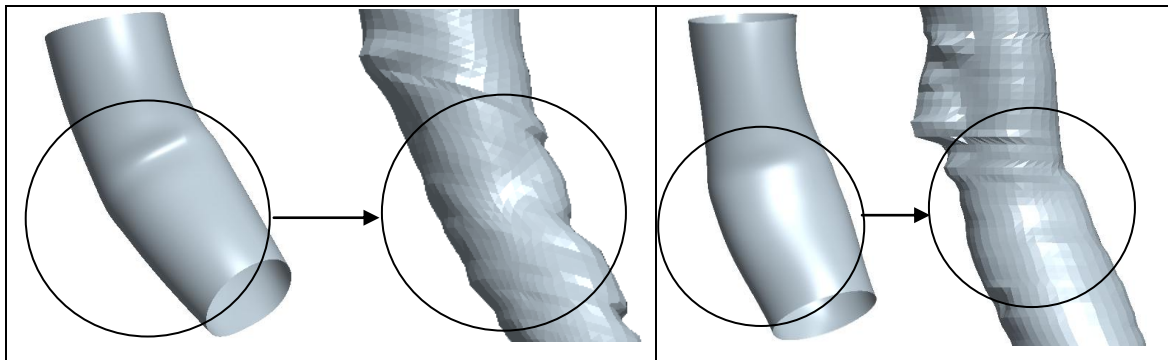


Figure 213. Visual observation shows the ability of the proposed FDM to capture details at anterior of the elbow area i.e. the area where the crease starts to develop as the arm flexes, which is highlighted by solid lined circles

However, as shown in Figure 214, it was also found that the proposed FDM produced a less realistic result for participant 4. The figure shows that although indentation at the posterior of the elbow was present, there appeared to be a smoothing effect at the area identified by the circles. This was likely caused by an inaccuracy of cross section measurement for LAM. This smoothing effect would likely be observable in the next interval of the key postures i.e. between 135°-90°. This was because the interpolation for the second interval was partly based on the five key cross sections from the previous interval i.e. five key cross sections at 135°. Therefore, it was more likely that the proposed FDM of the second interval would have similar realism level to that in the first interval.

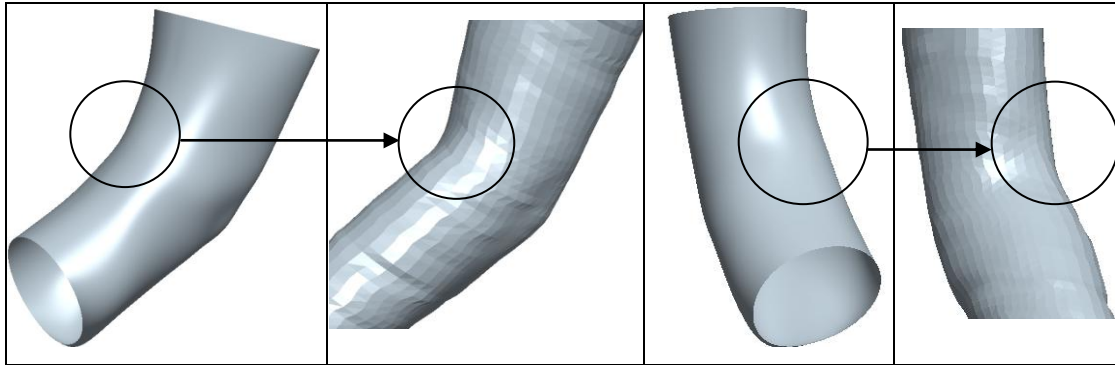


Figure 214. The effect of inaccurate manual measurement of the five key cross sections to the final result of the proposed FDM on both the anterior and posterior of the elbow area (highlighted by solid lined circles)

The visual observation on the second interval of the key postures i.e. between 135°-90° showed that the proposed FDM retained its ability to capture the details at posterior of the elbow, as highlighted by the dashed lines in Figure 215.

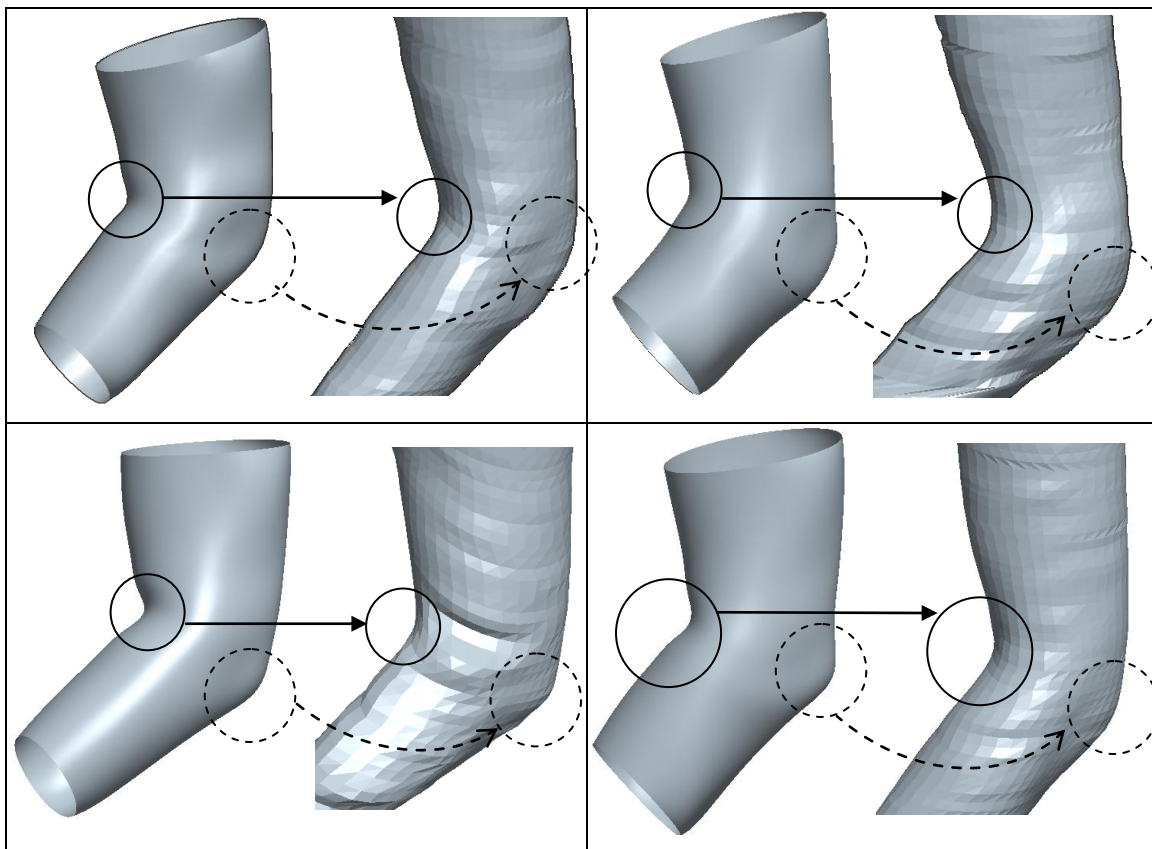


Figure 215. Visual observation on the arm postures between 135°-90°. Solid lined circles highlight the anterior of the elbow area whereas the dashed lined circles highlighted the posterior of the elbow area

It was also apparent from right lower images in Figure 215 that the proposed FDM captured slightly more detail compared to the 3D scanned arm, due to the usage of the profile. For the anterior of the elbow area, the proposed FDM showed slight discontinuities as highlighted by circle with solid lines in Figure 215. As expected, a less realistic result, shown in Figure 216, was also found

for the same participant as that in the first interval of the key postures. This suggested that capturing the shape of a cross section accurately was of importance.

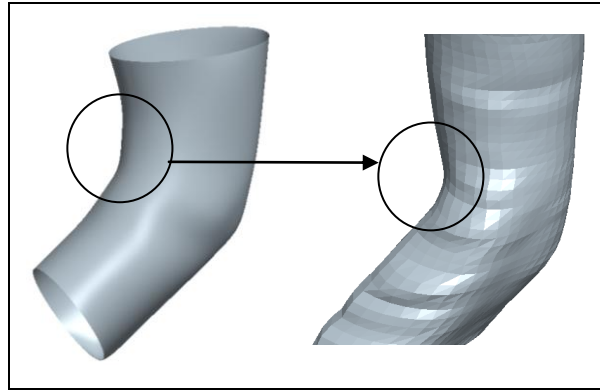


Figure 216. Less realistic result, highlighted by the solid lined circles, due to the inaccurate five key cross sections which were obtained through manual measurement

Additional images, which were taken from different views, are shown in Figure 217 up to Figure 221 for the result of the proposed FDM for arm postures of full extension-135° and Figure 222 up to Figure 226 for the result of the proposed FDM for arm postures of 135°-90°. The images, accompanied by the 3D scan image, demonstrate further the extent of realism of the proposed FDM.

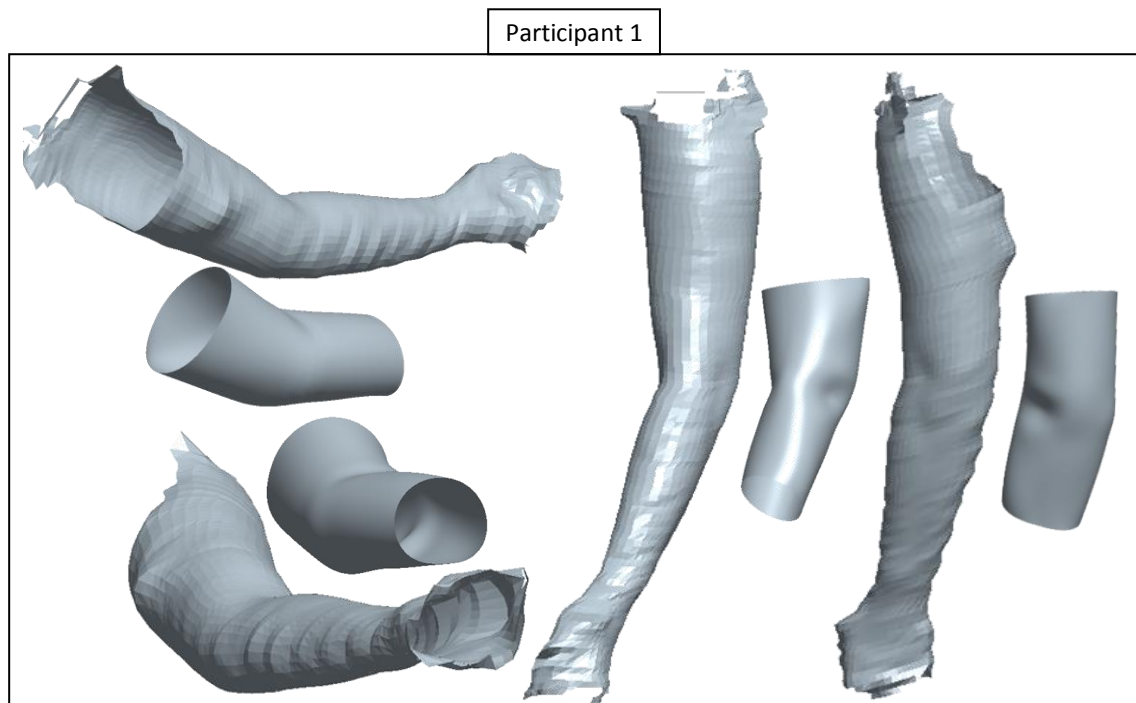


Figure 217. Images of the proposed FDM for an arm posture between a fully extended arm-135° for participant 1

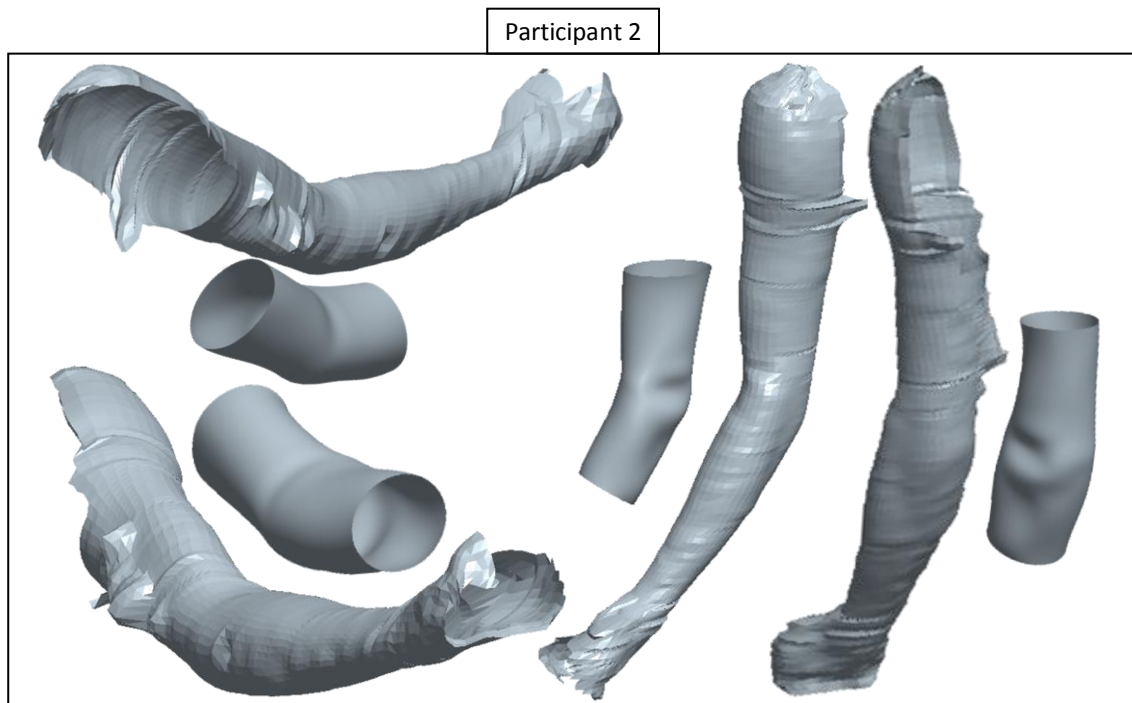


Figure 218. Images of the proposed FDM for an arm posture between a fully extended arm-135° for participant 2

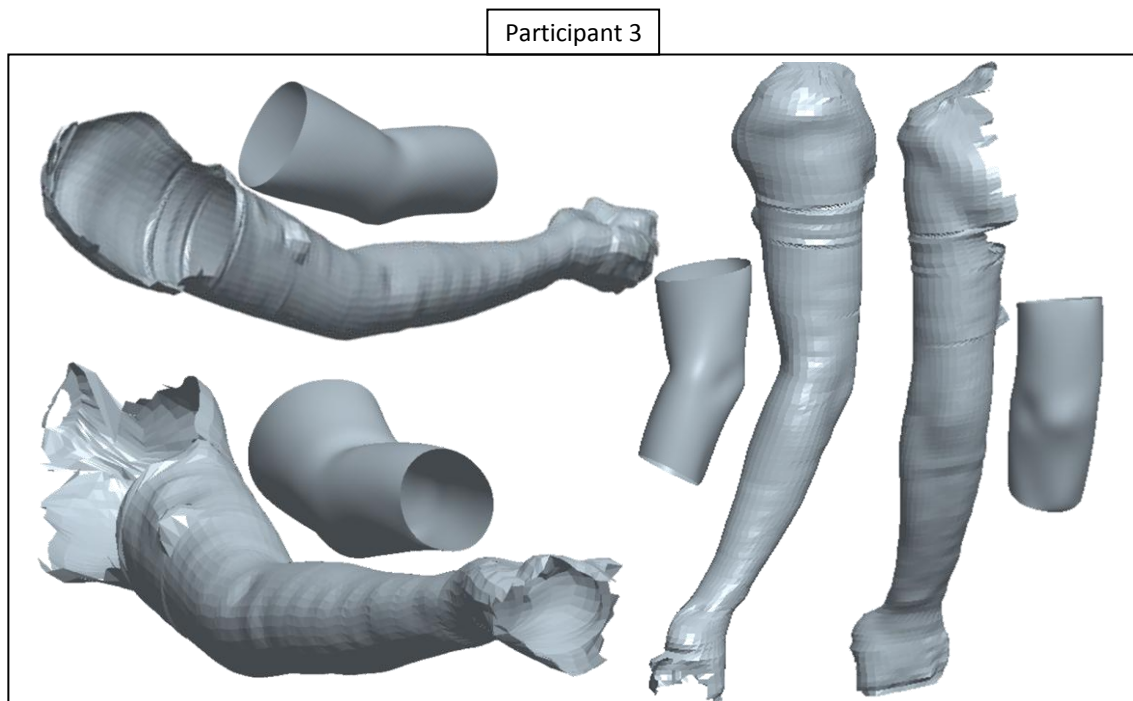


Figure 219. Images of the proposed FDM for an arm posture between a fully extended arm-135° for participant 3

Participant 4

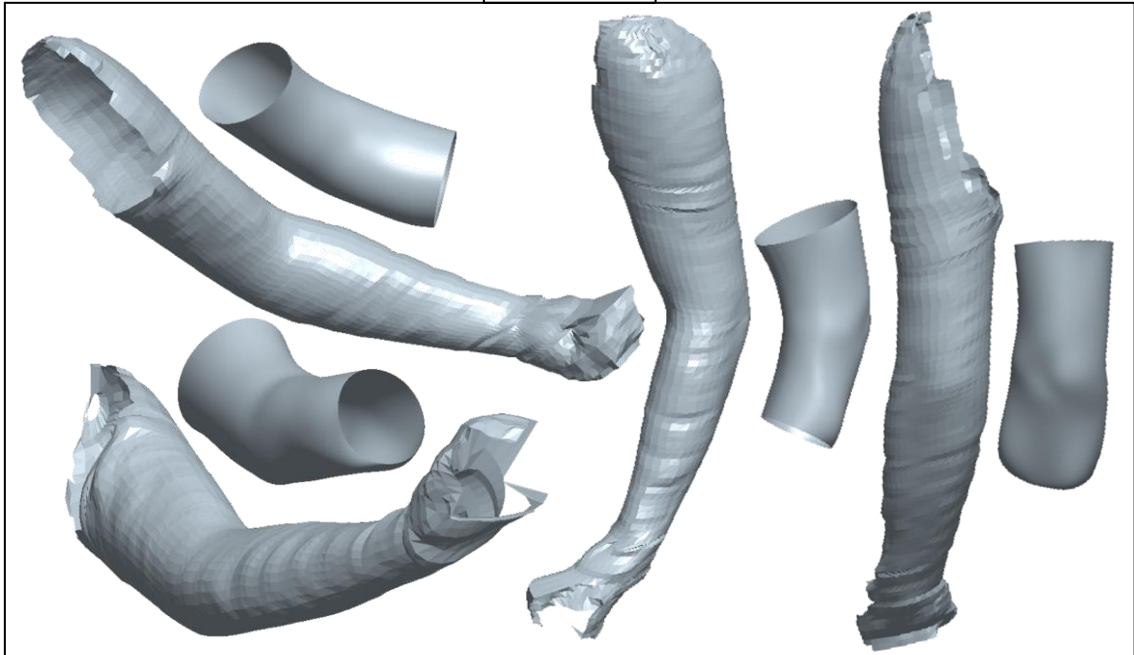


Figure 220. Images of the proposed FDM for an arm posture between a fully extended arm-135° for participant 4

Participant 5

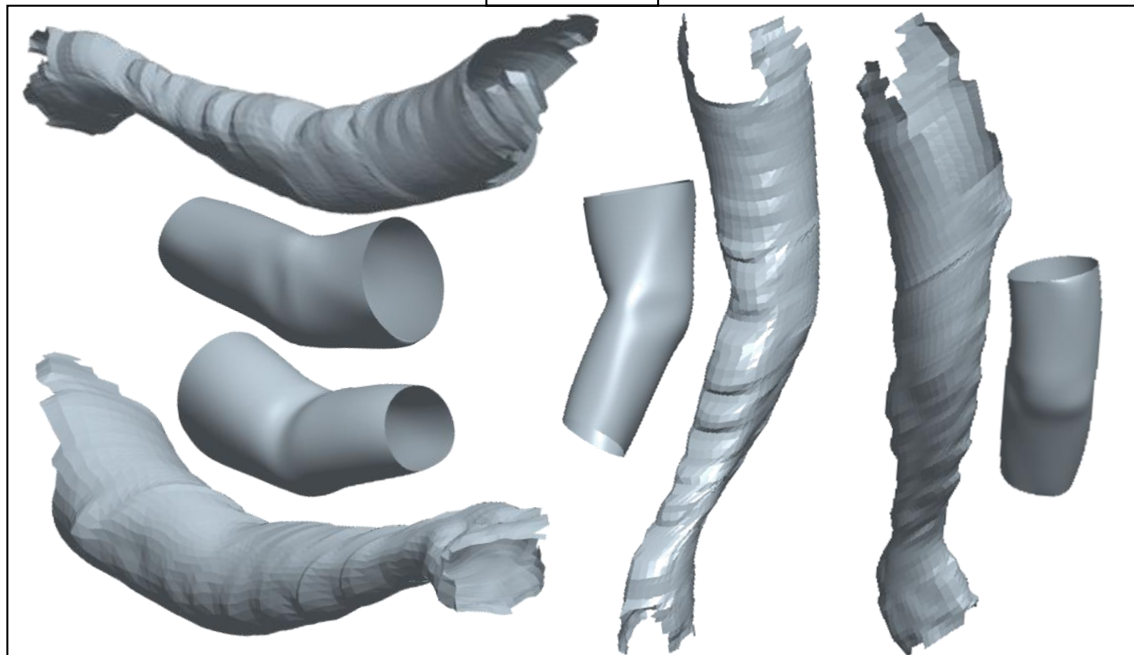


Figure 221. Images of the proposed FDM for an arm posture between a fully extended arm-135° for participant 5

Participant 1

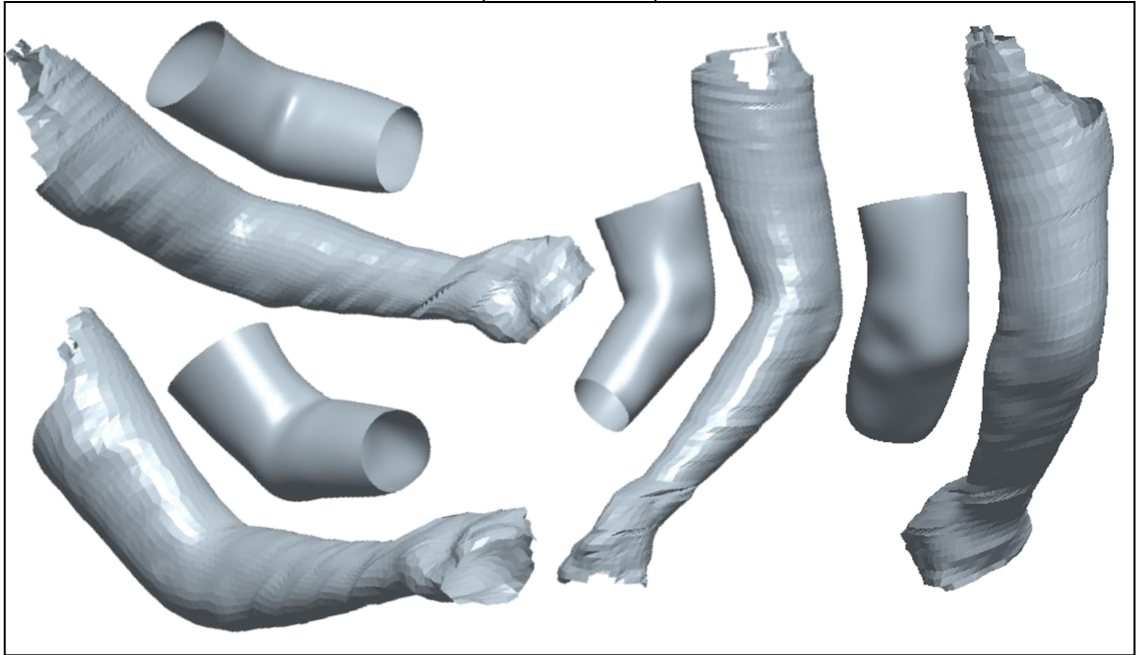


Figure 222. Images of the proposed FDM for an arm posture between 135°-90° for participant 1

Participant 2

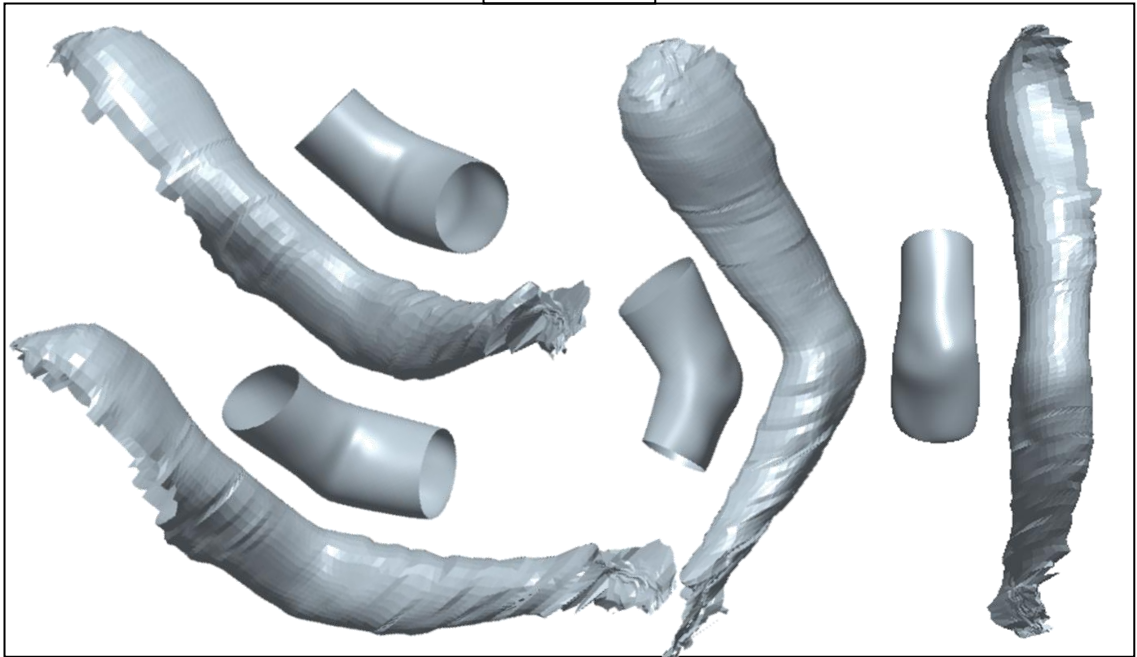


Figure 223. Images of the proposed FDM for an arm posture between 135°-90° for participant 2

Participant 3

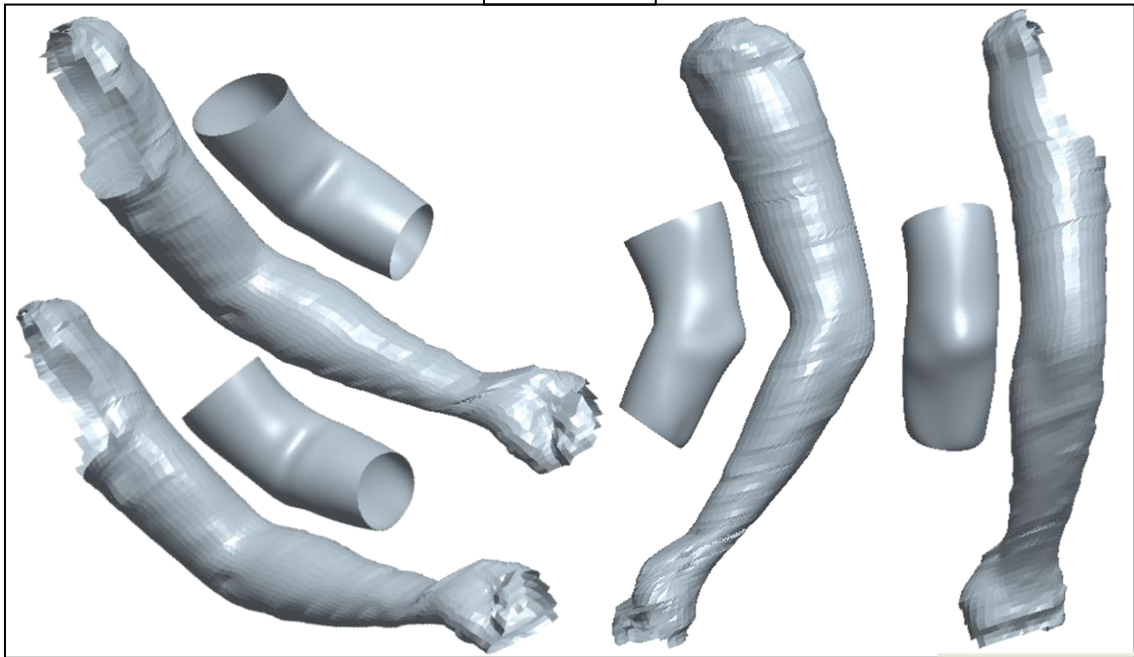


Figure 224. . Images of the proposed FDM for an arm posture between 135° - 90° for participant 3

Participant 4

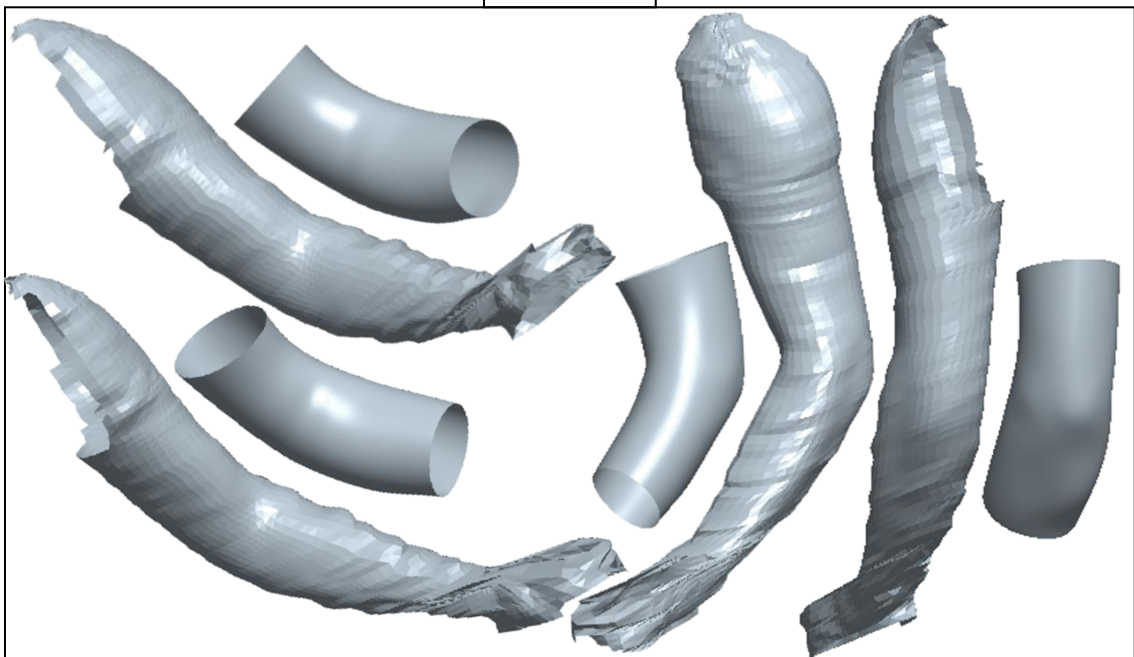


Figure 225. Images of the proposed FDM for an arm posture between 135° - 90° for participant 4

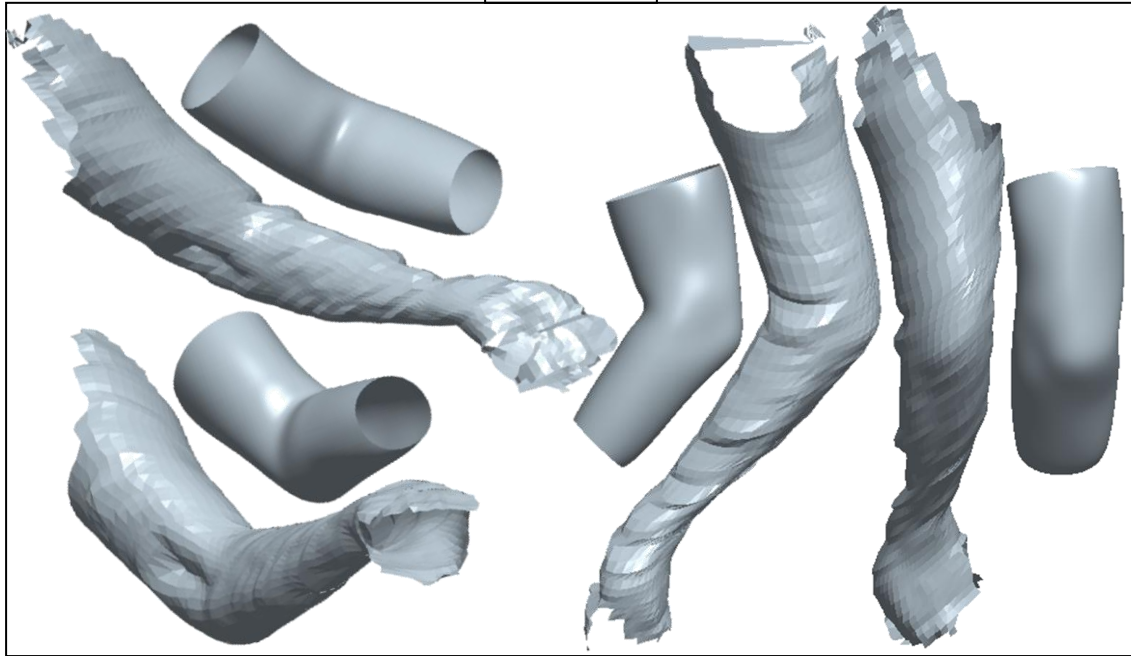


Figure 226. Images of the proposed FDM for an arm posture between 135°-90° for participant 5

The images from different views of full extension-135° and 135°-90° flexion show that the proposed FDM conformed to the overall shape of the arm. Also, generally the proposed FDM had the ability to capture details around the elbow e.g. indentation at the posterior of the elbow, crease at the anterior of the elbow; which increased the resemblance of the proposed FDM to the real arm. It was also apparent from the images that the lower arm seemed to move naturally with respect to the upper arm which was possibly the result of integrating the carrying angle into the arm movement.

8.2.2.2 Visual observation to compare the flesh deformation from the proposed FDM with side view photograph (90°-maximum flexion)

The visual observation for arm postures between 90°-maximum flexion showed a mixed result regarding its level of realism on the posterior and anterior of the elbow area. For the posterior of the elbow area, the proposed FDM ability to capture the details appeared to be dependent on the complexity of the profile of the arm posture. This was shown by the images in Figure 227. The three top images in Figure 227 show that the proposed FDM, shown as thin white line, were able to depict the posterior of the elbow area when the profile, shown as solid black line, at the elbow was a simple curve. However, as the profile at the posterior of the elbow became complex, as shown in the two lower images, the proposed FDM failed to follow the profile closely.

The proposed FDM's ability to represent the details at the anterior of the elbow area also showed a similar mixed result. Figure 228 shows the result of the visual observation. The top three images show the circumstances where the proposed FDM were able to follow the anterior of the

elbow area closely. The lower two images show the opposite. The circles in these two images highlight the area where the proposed FDM (thin white line) failed to follow closely the anterior of the elbow (bold black line).



Figure 227. The ability of the proposed FDM (thin white line) to capture details at the posterior of the elbow area depends on how complex the profile (bold black line) is at that area

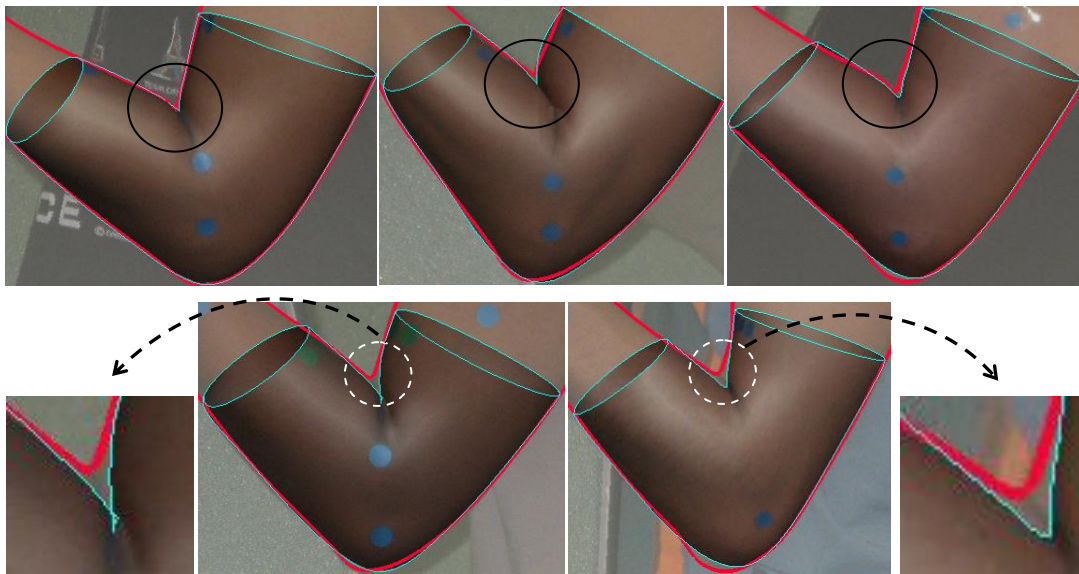


Figure 228. A mixed result of the proposed FDM (thin white line) regarding its ability to capture details at the anterior of the elbow area (bold black line)

Figure 229 shows images of different views from the proposed FDM's results for arm postures in the range of 90°-maximum flexion. Similar to the results of the proposed FDM for full extension-135° flexion and 135°-90° flexion, the images demonstrate that the proposed FDM had an ability to conform to the overall shape of the arm and at the same time captured details of flesh deformation at the elbow area.

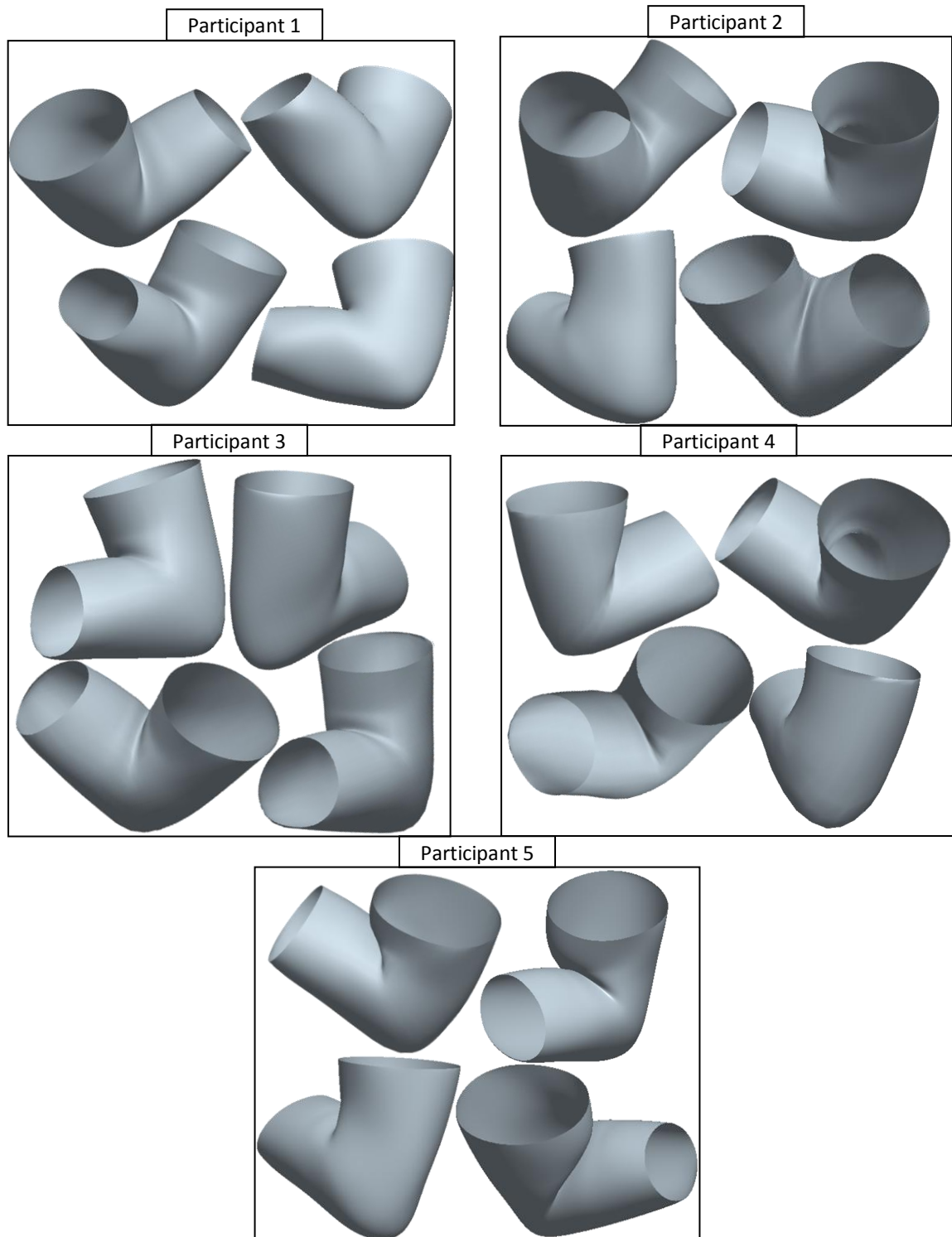


Figure 229. Images of the proposed FDM for arm postures between 90° - maximum flexion for the five participants

8.2.2.3 Discussion on the review of the proposed FDM's realism

The visual observation revealed that the proposed FDM captured slightly more detail in comparison to the 3D scanned arm for arm postures in the first two key posture intervals i.e. full extension-135° and 135°-90° flexion. The ability of the proposed FDM to capture more detail than the 3D scanned arm was likely due to the usage of a profile. A profile, which was created from a side

view photograph, allowed capturing the shape of the elbow in detail. As the final surface of proposed FDM was created based on this profile, the output of the proposed FDM would also show these details. In contrast to this, the 3D scan data was created from a cloud of points which then went through a set of processes such as noise reduction, smoothing, etc. Thus, even though 3D body scanning technologies synthesised images from different view angle, there was the likelihood that some detail would be lost during these processes. This finding suggested that using a profile which was obtained from side view photograph was beneficial for the proposed FDM.

The visual observation also revealed that there was apparent discontinuation at the anterior area of the elbow (see Figure 215). This discontinuation was likely caused by a sudden change of orientation and close anterior proximity between UAM, E, LAM and additional cross sections as the arm flexed. As a result, the NURBS algorithm failed to produce surface continuation in the anterior area of the elbow. This also explained why the discontinuation was more observable in the second interval of the key postures (135°-90° flexion) than in the first interval of the key postures (full extension-135° flexion).

The visual observation showed that there was a mixed outcome regarding the proposed FDM's realism on the posterior and anterior of the elbow area for arm postures between 90°-maximum flexion. It was apparent from the images in Figure 227 that as the shape of posterior area of the elbow became complex, the proposed FDM failed to create a surface that followed it closely. It was thought that this was caused by the limited number of additional cross sections at the elbow area. However, simply adding more additional cross sections at the elbow area might encourage a discontinuation effect at the anterior area of the elbow. Further study was probably required to determine the balance between the two. For arm postures between 90°-maximum flexion, it was also demonstrated that the proposed FDM failed to follow the anterior area of the elbow closely for some of the participants (see the two lower images in Figure 227). This failure was likely caused by the offset distance between the predicted elbow plane orientation (see section 7.3.1) and the point where the upper and lower arm meet during the arm flexion. The prediction of elbow plane orientation was based on the early study in the first design phase (see section 5.3.2.3) where the relationship between elbow plane orientation and arm angle were established by means of a set of side view photographs of various arm angles. As participants that were involved in this study were the same as those involved in the review of the FDM, variation between individuals could be ruled out as a cause. A possible cause was dissimilar assignments of joints location i.e. shoulder, elbow and wrist joints. In section 5.3.2.3, in order to calculate the arm angle and orientation of the elbow plane, joints locations were approximated. This approximation might not be the same as those produced by a 3D scanned arm which was used to derive the joint locations. In other words, there

was incompatibility between joints assignment on the side view photograph and 3D scanned arm. Again, this problem could likely be remedied when 3D scan technologies could be used to derive the relationship between arm angle and elbow plane orientation.

The overall result of realism seemed to show that the proposed FDM could produce a more detailed flesh deformation around the elbow. It is acknowledged that this research approach to justify the level of realism was rather limited as the level of realism was judged solely by the researcher. Thus, for a future research, survey which involved novice and expert users of ergonomics modelling could be performed to assess the result of the proposed FDM. The survey could utilise Likert scales to compare the flesh deformation results of the proposed FDM to original data (photographs, 3D scan, etc.) or flesh deformation of existing approaches (linear blend skinning, example based, etc.).

8.2.3 Review of the proposed FDM for minimum user intervention

In order to review whether the proposed FDM conformed to the minimum user intervention specification, a qualitative approach was used. The qualitative approach was based on the definition of “minimum user intervention specification” which was described in section 4.1.6. Important criteria from the definition would be extracted and then used to justify whether the proposed FDM could fulfil them or not. The extraction of criteria and justification of the proposed FDM are outlined in section 8.2.3.1 and discussion of the result is given in section 8.2.3.2.

8.2.3.1 Results of the proposed FDM's review for minimum user intervention

Based on the description given in section 4.1.6, there were two main criteria: (i) user intervention was limited to specifying or modifying the DHM feature to accommodate different postures, body size, body shapes, etc; and (ii) no direct modification of any parameter was allowed should unrealistic flesh deformation occur. Following the proposed review method above, these two criteria would be utilised to assess the proposed FDM. For the first criteria i.e. to assess if the proposed FDM allowed the user to specify different body shapes/sizes and posture, the software programme which was developed in section 8.1 and based on the proposed FDM principle, was used.

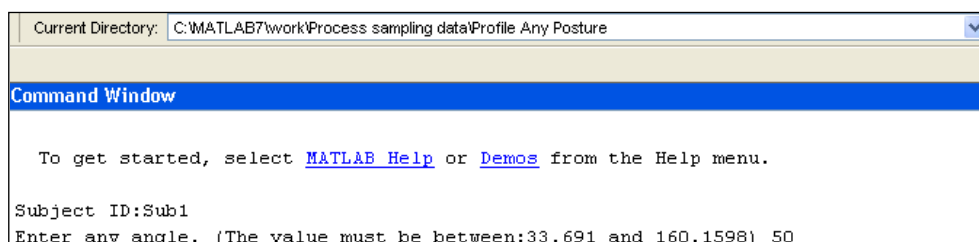


Figure 230. The programming from section 8.4 demonstrates that the proposed FDM allow a user to specify body type/size i.e. choosing the subject and arm angle

As shown in Figure 230, in order to generate flesh deformation, the software programme allowed the user to specify the participant and an arm angle. The user was allowed to input any angle within the range of full extension and maximum flexion, 160.1598° and 33.691° respectively, determined from the data collection for this particular participant. The software programme then produced coordinates of the five key cross sections and additional cross sections at the elbow area for that particular participant, shown partially in Figure 231. This demonstrated the proposed FDM's conformation to the first criteria.

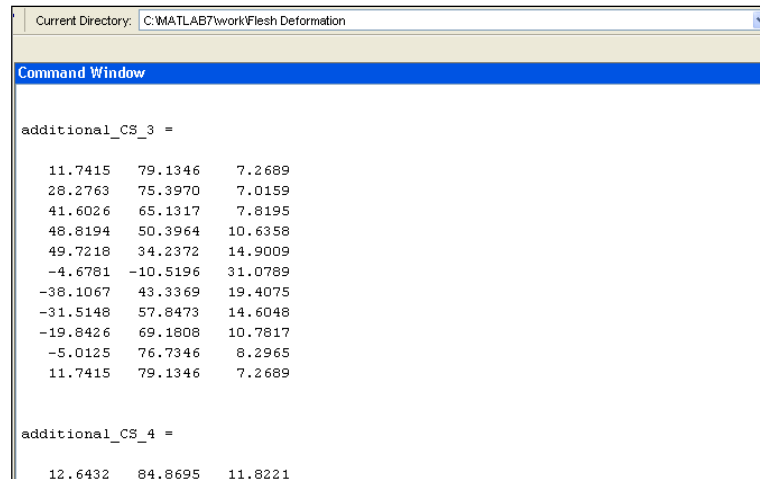


Figure 231. The output of the programming that was developed in section 8.4 is coordinates of five key cross sections and additional cross sections for the specified participant and arm angle

For the second criteria, the software programme output was used to justify the conformation of the proposed FDM. The software programme output was the coordinates of the five key cross sections and additional cross sections at the elbow. These coordinates, were then used directly to create the surface of the arm in Pro-Engineer (see Figure 232). This suggested that the user simply did not have any access to modify any parameter to correct the flesh deformation. This showed that the proposed FDM complied with the second criteria of the minimum user intervention specification.

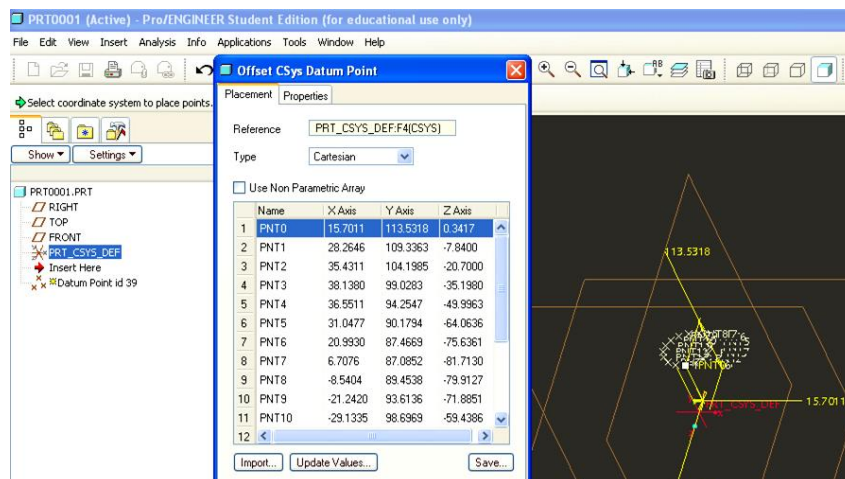


Figure 232. Using the output of the programming as input in Pro-Engineer to visualise the result

8.2.3.2 Discussion of the proposed FDM's review for minimum user intervention

The result of qualitative assessment suggested that criteria, which were extracted from the definition of minimum user intervention in section 4.1.6, could be satisfied by the proposed FDM. Currently, to generate coordinates of five key cross sections and additional cross sections flesh deformation surface for any arm angle, a user was required to enter the arm angle manually. This was not likely required when the proposed FDM became a part of a fully functioned ergonomics application. In a fully functioned ergonomics application, a change of a joint angle was likely prompted by either forward or inverse kinematics which was described in section 2.4. Also, currently, the coordinates' values of five key cross sections and additional cross sections would need to be transferred into Pro-Engineering to create the final surface of the elbow. This was not likely required in a fully functioned ergonomics application as the coordinates' values would be utilised directly to create the elbow surface. Nonetheless, the qualitative assessment showed that the proposed FDM did not expect a user to tweak or having to correct the elbow surface.

8.2.4 Review of the proposed FDM against the real time modelling specification

As shown in Figure 201, a retrospective analysis was used to review the proposed FDM against the real time modelling specification. As it was already explained in the methodology section, the retrospective analysis involved analysing and identifying the stages of the proposed FDM's design process which demonstrated how a particular specification was ingrained into the design of the proposed FDM. To ensure that a real time modelling could be achieved, there were two factors that had to be focused on i.e. (i) the amount of data that had to be handled in real time; and (ii) the type of data processing that had to be handled in a real time. As reducing the amount of data to be handled in real time would decrease the amount of processing in real time, limiting the amount of data that had to be handled could arguably support real time modelling. Also, as simple type of data processing would likely decrease the processing time, opting for simple type of data processing could potentially support real time modelling. Thus, by analysing and identifying stages of the proposed FDM that supported these two factors, the conformability of the proposed FDM to the real time modelling specification could be suggested. Section 8.2.4.1 outlines the analysis and identification of stages of the proposed FDM for each factor whereas section 8.2.4.2 provides discussion of the review.

8.2.4.1 Results of the proposed FDM's review for real time modelling specification

In relation to limiting the number of data to be handled in a real time, several approaches had been employed for the proposed FDM, as listed below:

1. Identifying the optimum number of the cross sections

The process of searching for the optimum number of the cross sections was introduced in section 5.3.2.2 (see page 84). The search for an optimum number of cross sections would allow the minimisation of data handling and yet maintain the information as much as possible. The actual process took place in the section 6.6.2.

2. Identifying the optimum number of sample points to create the cross sections

The cross sections, which were essentially curves, would need a number of points to create them. This was the reason why the sampling points were required. Identifying an optimum number of sample points was important as it would minimise the data handling and information lost as it had been stated in section 5.3.2.4. The search was performed in section 6.7.

3. Identifying optimum number and placement of points on the profile to create the profile

The profile, which was used to create the additional cross sections at the elbow, was a curve and needed a number of points to create it. Similar to the two previous elements, searching for the optimum number and placement of points on the profile would limit the amount of data handling without losing information. The search was performed in section 7.2.3.2.

Table 17 shows the amount of data to be utilised for real time processing i.e. key postures' data, whereas Table 18 shows the amount of data which was generated during real time processing to create a flesh deformation at a given arm angle. The amount of data and processing time would have been increased had more key postures, cross sections number and sample points been used. In addition to reducing the number of data to be processed in real time, as suggested earlier in section 8.2.4, another way to decrease the real time processing was by opting for a simple type of processing. This was shown by the fact that the proposed FDM opted for a linear interpolation to interpolate the profile and five key cross sections' shapes and locations. A mini study in section 6.3, which aimed to investigate the extent of flesh deformation, found that the flesh deformation could be represented by interpolating the key posture linearly. In this section, it was clearly stated that the linear interpolation was chosen to conform to the real time specification. This principle was then employed further to govern the flesh deformation, as described in section 7.3.2.3, 7.3.2.2 and 7.3.2.5. On the contrary, Shen et al. (1994) method utilised collision detection to deform the shape of cross sections, especially those located at anterior of the elbow, in order to avoid intersection between cross sections at the upper and lower arm as the arm flexed. As suggested by its name, collision detection was essentially a special algorithm aimed to detect collision between 3D objects. Ericson (2005) suggested that poor design of collision detection could easily become a bottleneck especially for 3D surface creation that required a large percentage of it. Eberly (2007) also stated that performing collision detection was a complex task as the collision detection system must handle

different situation each time. This suggested, in contrast to the proposed FDM, the Shen et al. (1994) potentially required a more complex processing type which could result in the increase of processing time.

Table 17. Amount of data to be processed in real time to generate flesh deformation at the elbow

Data	Used for real time processing?	Amount of data
Coordinates of sample points for five key cross sections	Y	3 (X, Y, Z) x 16 points x 5 cross sections x 4 key postures = 960 (X, Y, Z)
Coordinates of sample points for the key postures' profile	Y	3 (X, Y, Z) x 26 points x 4 key postures = 312 (X, Y, Z)
Carrying angle	Y	2 (maximum and minimum angle)
Flesh deformation area	Y	4 (UAF, UAM, LAM and LAF) x 4 key postures = 16
Joint coordinates	Y	3 (X, Y, Z)
Total		1293 data points

Table 18. Amount of data processing in real time to generate flesh deformation at the elbow

Real time data processing	Amount of data involved in real time processing
Calculating carrying angle	2 (maximum and minimum angle)
Calculating flesh deformation area	4 (UAF, UAM, LAM and LAF) x 2 key postures = 16
Calculating joint coordinates	3 (X, Y, Z) x 3 joints (shoulder, elbow, wrist) = 9 (X, Y, Z)
Generating interpolated five key cross sections	Linear interpolation from two key postures: 2D (X, Y) x 16 points x 2 key postures = 64 (X, Y)
Generating interpolated profiles	Linear interpolation from two key postures: 2 x 2D (X, Y) x 26 points = 104 (X, Y)
Transforming the five key cross sections into 3D	3D (X, Y, Z) x 16 points x 5 key cross sections = 270 (X, Y, Z)
Transforming the profiles into 3D	3D (X, Y, Z) x 26 points = 78 (X, Y, Z)
Generating surface lines for additional cross sections at the elbow	3D (X, Y, Z) x 16 points x 5 key cross sections = 270 (X, Y, Z)
Sampling the surface lines to create additional cross sections at the elbow	3(X, Y, Z) x 16 surface lines x 4 additional cross section at the elbow = 192 (X, Y, Z)
Sampling the profile to create additional cross sections at the elbow	3(X, Y, Z) x 4 additional cross section at the elbow = 12 (X, Y, Z)
Total	1015 data points

Based on the retrospective analysis above, it was evident that the real time specification was fully integrated into the proposed FDM. Throughout the development process of the process FDM, decisions on elements or processes to create the flesh deformation were aimed to either minimise the amount of data to be handled or the complexity of data processing.

8.2.4.2 Discussion of the proposed FDM's review for real time modelling

The retrospective analysis for real time modeling was focused on two factors i.e. the amount of data and complexity of processing that had to be handled in real time. These two factors governed the ability for real time modelling to be achieved as they had a direct effect upon the length of processing time. Optimising the number of data to be handled as well as simplification of the processing was likely to affect the overall level of accuracy. The results of retrospective analysis

demonstrated that efforts were made in this research to minimise the amount of data and complexity of processing to be handled in real time.

With hindsight, this research had optimised the amount of data and processing simplification whenever it was appropriate. Also, this research has used appropriate methods to determine the optimum amount of data i.e. supported by data analysis. With regards to the ability of the proposed FDM to accommodate real time modeling, the retrospective analysis seemed to suggest that the proposed FDM had a pragmatic potential to suit real time modeling. To confirm this finding, integration of the proposed FDM with existing ergonomics simulation was suggested for future research. However, further work on applying the proposed FDM on other joints e.g. hip, knee, etc., would need to be performed prior integrating the proposed FDM with existing ergonomics simulation.

8.2.5 Review of the proposed FDM against the whole body modelling specification

A retrospective analysis was used to review the proposed FDM against the whole body modelling specification. Reducing the level of complexity of the flesh deformation modelling would greatly assist the application of flesh deformation for the whole body modelling. This had been emphasised in section 4.2 where the comparisons between existing FDM approaches and the DHM specifications were done. The comparison showed that some of the existing FDM were not suitable for whole body modelling because of their level of complexity. The comparison also identified that the Shen et al. (1994) was suitable for a whole body modelling and was confirmed by their success in modelling the whole body. The usage of cross sections simplified the simulation of the flesh deformation whose otherwise demanded complex computation and processing. In section 4.2.6, ability to model the whole body was one of the reasons why the Shen et al. (1994) method was chosen as a basis for the proposed FDM.

Table 19. Differences between the proposed FDM and Shen et al. (1994) method

The proposed FDM for elbow joint	Shen et al. (1994) for elbow joint
Introducing carrying angle	Carrying angle is absent
Orientation of cross sections remains the same, apart from the one at the joint	Orientation of cross sections changes as the joint moves
Cross section shapes changes as the elbow moves (a product of linear interpolation of key postures' cross sections)	Cross section shape remains the same as the elbow moves
Profile is used to refine flesh deformation at the posterior of the elbow	A function is used to simulate muscle bulge at the anterior area of the elbow
Flesh deformation is contained within flesh deformation area	Flesh deformation is not contained within a specific area

As the proposed FDM was based on the concept that was put forward by Shen et al. (1994) i.e. deforming cross sections to simulate the flesh deformation, it could be assumed that the proposed FDM could be applied for the whole body modelling. Hence, it could further be assumed hypothetically that had the proposed FDM been integrated with an existing ergonomics CAD, the proposed FDM could also be utilised to perform a whole body modelling. Despite fundamental differences between the proposed FDM and Shen et al. (1994) method (see Table 19), both methods still relied on manipulating cross sections to create flesh deformation.

9 Application of the Proposed FDM for Different Body Types and Sizes

Currently, the proposed FDM or “the new FDM” could only produce flesh deformation for an individual of whom the required elements to produce flesh deformation were provided, such as five key cross sections, profiles, etc. However, the provision of these elements required rigorous measurement, data collection as well as extensive data processing. This suggested that the new FDM’s ability to produce flesh deformation was limited. Thus, this particular stage of research aimed to resolve this limitation by proposing a method that minimised the amount of data required and then used this data to synthesize flesh deformation at the elbow. In addition to resolving the aforementioned limitation, the proposed method also aimed to provide a means to review the ability of the new FDM in accommodating different body types and sizes (see section 8.2). Figure 233 shows the relationship of this particular stage of research (the application of the new FDM to different body types and sizes) with respect to the previous stages of research, which established and reviewed the new FDM (i.e. chapters 5-7 and 8, respectively). This chapter explains the details of the proposed method, which will be referred to as “the framework” from this point forward.

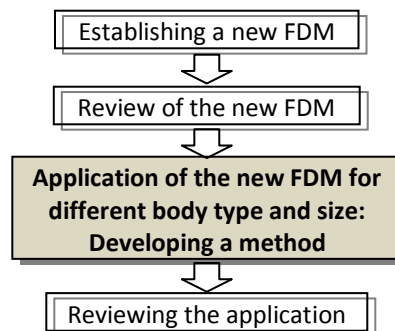


Figure 233. The application of the new FDM with respect to other activities in the research

9.1 Strategy to apply the new FDM for different body types and sizes

The strategy to create the framework is shown in Figure 234. This strategy was similar to the methodology which had been adopted to develop the new FDM. First, a general outline of the framework was proposed.

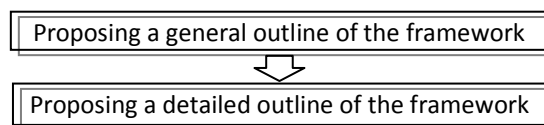


Figure 234. Methodology to create the application of the new FDM

The general outline of the framework identified anticipated components and their relationship with each other. As the general outline of the framework was an initial anticipation, there was a

possibility that some changes would take place at later stages. Based on the general outline of the framework, details of the framework were then proposed. The details of the framework would be established in several stages. It was anticipated that this process would be iterative and testing would occur during development as development progresses, forming a series of rolling improvements.

9.2 The general outline of the framework

As had been mentioned in this chapter's introduction, the framework aimed to minimise the amount of data required and then to use this data to synthesize the required elements for flesh deformation at the elbow, such as five key cross sections, profiles, etc. To achieve this, an already existing approach to model different body sizes and shapes/types in ergonomics application, the so called "database approach", was partly adopted. The approach involves the utilisation of a 2D anthropometry database. The term "2D anthropometry" refers to the anthropometry measurement using two dimensions. The database, which stores 2D anthropometry measurements of different body sizes and types, is used to synthesise 2D anthropometry measurements for the DHM based on a limited number of inputs. The limited number of inputs is entered by the user. The inputs are essentially aspects that affect 2D anthropometric measurements and include nationality, gender, body size (percentile) and body type (ectomorph, endomorph, etc.). The inputs are then used to extract and synthesise relevant information from the 2D anthropometry database, resulting in creation of a DHM with particular size and type.

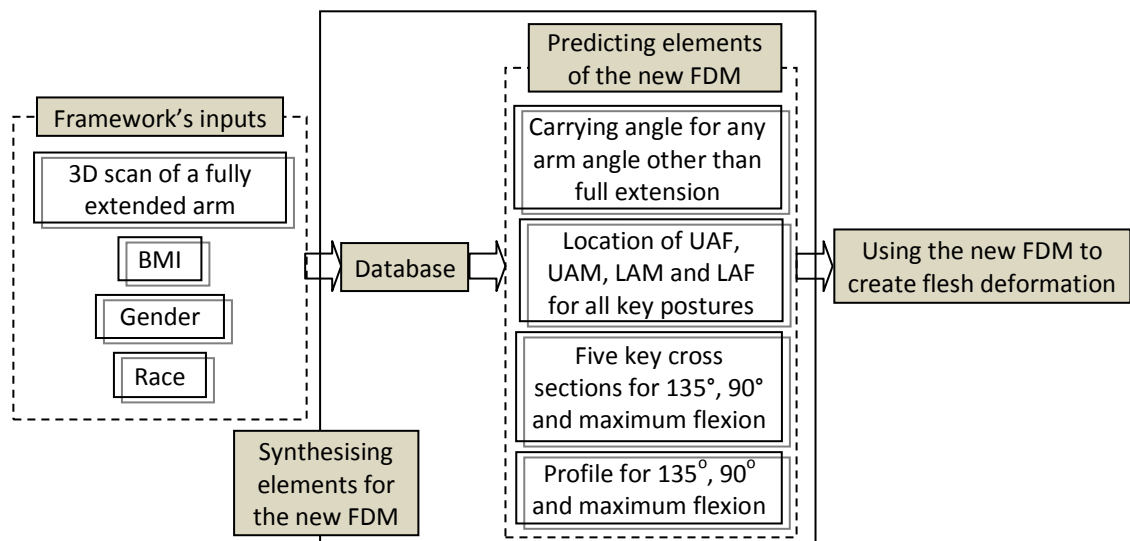


Figure 235. Relationship between the inputs, database, prediction of the elements for flesh deformation and the new FDM

The proposed framework would adopt similar inputs as that of the database approach i.e. body size, body type, gender and nationality. This decision was based on the assumption that the flesh deformation at the elbow was also influenced by these four types of inputs. A user was required to

key-in these four types of inputs. Similar to the database approach, these four types of inputs were also used to extract relevant data from the database and synthesise elements required for the new FDM. Figure 235 shows details of the framework's inputs i.e. 3D scan of a fully extended arm, BMI, gender and race. To represent a body size, a 3D scanned arm was chosen because it could simultaneously supply information regarding the length, profile and circumferential size/shape at different locations of an arm. Although this research suggested the use of a 3D scanned arm, any 3D arm with readily available joint information could also be used. To comply with the need of a limited number of inputs, only a 3D scan of a fully extended arm was proposed to be used.

To represent a body type, BMI was chosen. BMI is a commonly used index that is used to classify whether an adult was underweight, overweight, obese or of normal weight. BMI is obtained by dividing the weight (in kilograms) with the square of the height (in meters). BMI was chosen because of its ease to be obtained and measured. However, BMI also has its own drawbacks. As it is only based on weight and height, BMI could not distinguish between weight associated with fat (endomorph body type) and weight associated with muscle (mesomorph body type). It is acknowledged that choosing BMI was less than ideal and might result in a less accurate depiction of a body type.

In the 2D anthropometry database, the term nationality referred to the country of where the anthropometry data was taken from. This meant that the data categorisation was made at the level of country origin which was a more refined approach in data categorisation compared to simply using racial categorisation. However, categorising the data based on nationality also required an extensive data collection, which was beyond the purpose this particular part of research. Therefore, for the framework, the data categorisation would not be based on nationality and instead would be based upon the race type.

Figure 235 shows that the synthesis process of the proposed framework involved using a limited number of inputs to extract relevant data or information from the database. The extracted data or information was then used to predict the required FDM elements for flesh deformation at the elbow. To create flesh deformation using the new FDM, elements such as: (i) five key cross sections of key postures, (ii) profile of key postures, (iii) location of UAF, UAM, LAM and LAF for key postures and (iv) the carrying angle, were required. Some of these elements were already available from the 3D scanned arm i.e. five key cross sections of a fully extended arm, profile of a fully extended arm, and carrying angle of a fully extended arm. Thus, as shown in Figure 235, only elements of FDM that were not available had to be synthesised by the proposed framework. FDM elements that had to be synthesised were: (i) location of UAF, UAM, LAM and LAF for each key posture; (ii) five key cross

sections at 135°, 90° and maximum flexion; (iii) profiles at 135°, 90° and maximum flexion; and (iv) the carrying angle for any arm angle other than a fully extended arm.

9.3 Stages to detail the general outline of the framework

Since the general outline of the framework was established, the development stages to detail the general outline of the framework could be identified. The complete stages of framework development are shown in Figure 236.

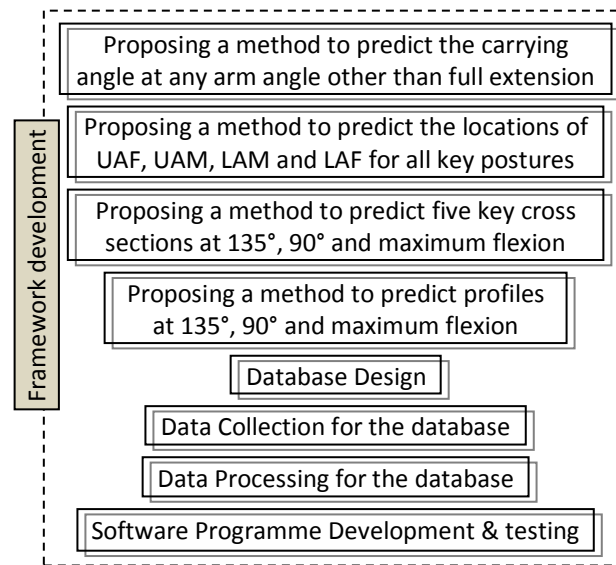


Figure 236. Stages in framework development

The first stage was to propose prediction methods for FDM elements that had to be synthesised. These were: (i) predicting the locations of UAF, UAM, LAM and LAF for all key postures; (ii) predicting five key cross sections at 135°, 90° and maximum flexion; (iii) predicting profile at 135°, 90° and maximum flexion; and (iv) predicting carrying angle for maximum flexion. To support the establishment of the prediction methods, whenever it was required, the existing data from the five participants which were involved in the development of the new FDM (see section 5.3.2.3) were used. It was believed that the small number of participants should pose no drawback because the proposed prediction method would eventually be tested during the software programming. Table 20 shows detailed characteristics of the five existing participants. The arm length was obtained from 3D scan data and was measured from acromion (shoulder) to wrist.

Table 20. Characteristics of five existing participants which were involved in the development of the new FDM

	Participant 1	Participant 2	Participant 3	Participant 4	Participant 5
Gender	Female	Male	Male	Male	Female
Height (cm)	143	180	166	166	152
Weight (kg)	46	64.5	65.2	73.9	59.3
BMI	22.5	19.9	23.7	26.8	25.7
Arm Length (mm)	425.7	540.5	513.85	508.4	470.4

The next stage of the framework development was the database design in which the structure and content of the database were established. Based on the proposed predictions methods, the structure and the required type of data for the database were identified. Upon the establishment of the database design, data collection and data processing for the database were performed. This was then followed by software programming which integrated the limited number of inputs, database and the new FDM to create flesh deformation for different body sizes and types. The software programmes were essentially the ultimate output of the framework. Testing would also take place during the software programmes' development to ensure that the developed framework and software programmes functioned properly. Any modification that was required would be adopted. Each stage of the framework development is discussed separately in the following sections.

9.4 Predicting the carrying angle at a full flexion

As explained in section 6.1.1, the carrying angle changed as the arm flexed. The changes of the carrying angle were described as a linear reduction of the carrying angle of a fully extended arm. This linear behaviour presented a possibility to predict the carrying angle for any arm angle in between a fully extended and flexed arm provided that the carrying angles at a fully extended arm and at a fully flexed arm were known. However, the joint information of a 3D scan of a fully extended arm only provided access to the carrying angle of a fully extended arm. Thus, a method to predict the carrying angle of a fully flexed arm was needed to ultimately determine the carrying angle at any required arm angle. Section 6.1.4 has already addressed this issue by proposing an approximation method which combined the use of the 3D scan of a fully extended arm and existing data from Van Roy et al. (2005), which is shown in Table 21. Details of the procedure to determine the carrying angle for any arm angle other than a fully extended arm is shown in Figure 237.

Table 21. Data from Van Roy et al. (2005) which was used to assist the prediction of the carrying angle for full flexion

Carrying angle	Female	Male
Full extension	Minimum = 11.9, maximum = 21	Minimum = 4.2, maximum = 15.1
Full flexion	Minimum = -0.7, maximum = 3.9	Minimum = -1.1, maximum 5.8

As shown in Figure 237, the proposed approximation method required the knowledge of the gender from whom the 3D scanned arm was acquired. Gender information was required because, as shown in Table 21, the carrying angle range was different for male and female. The proposed approximation method also required the carrying angle and the arm angle of the 3D scan of a fully extended arm. The method to obtain the carrying angle from a 3D scan of a fully extended arm could be found in section 6.1.3. Once all of this information was obtained, the carrying angle for maximum flexion was determined by the following equations:

$$\text{ratio} = \text{abs}[(3\text{D carrying angle} - \text{min carrying angle full extension}) / \text{range of carrying angle extension}];$$

carrying angle max flexion = ratio* range of carrying angle max flexion + min of carrying angle max flexion;

Once the carrying angle of a fully extended and flexed arm were known, the carrying angle of any arm angle in between these two arm postures was determined through the following equation:

$$\text{carrying angle at } x^\circ = \frac{(\text{carrying angle}^{\text{full flexion}} - \text{carrying angle}^{\text{full extension}})}{\text{angle}^{\text{full flexion}} - \text{angle}^{\text{full extension}}} \times (x - \text{angle}^{\text{full extension}})$$

The above equation suggested that the arm angle at a full or maximum flexion was required. Since this information was not available from the inputs, this research proposed an alternative approach to provide the angle of maximum flexion. The proposed alternative approach was to provide a constant value for the maximum flexion's angle. The proposed value was 35° as it was demonstrated to be the average values for maximum flexion at the elbow joint (Luttgens and Hamilton, 1997).

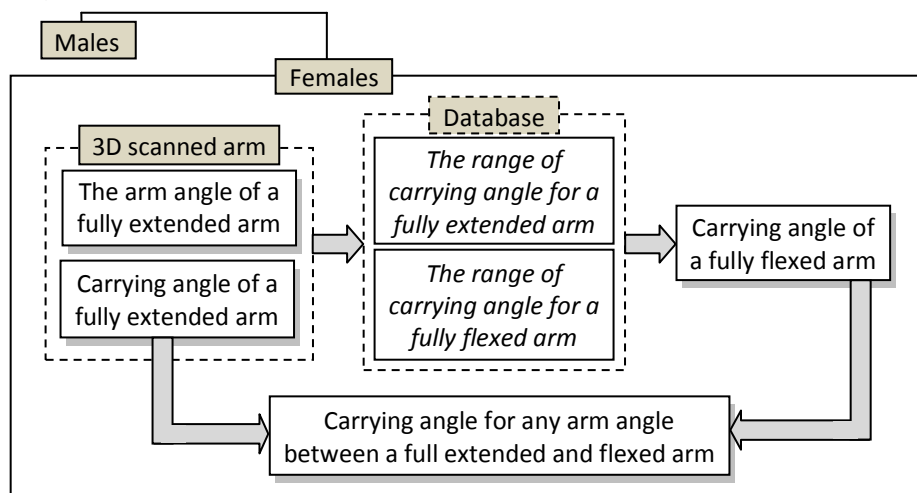


Figure 237. The prediction method to determine the carrying angle for an arm posture other than a fully extended arm

9.5 Predicting the locations of UAF, UAM, LAM and LAF for all key postures

In order to propose the method to predict the location for UAF, UAM, LAM and LAF, the strategy shown in Figure 238 was followed. The first stage of the strategy was to establish issues for the study. The issues for the study were focused to elucidate the relationship between the inputs and the locations of UAF, UAM, LAM and LAF. As described in section 9.2, the general outline of the framework made assumptions that the inputs i.e. body size, body type, gender and race, affected the elements of FDM, including UAF's, UAM's, LAM's and LAF's locations. Thus, the first four issues of the study would be focused on these areas. Another focus for the study was how the locations of one key cross section related with another. An understanding of existing relationship(s) between the locations of one key cross section with another would likely allow a more thorough and accurate

decision regarding the final prediction method. Based on the reasoning above, 7 issues with regard to the locations of UAF, UAM, LAM and LAF were established. These were:

1. The effect of body size i.e. arm length and the location of UAF, UAM, LAM and LAF
2. The effect of body type i.e. BMI and the location of UAF, UAM, LAM and LAF
3. The effect of gender on the location of UAF, UAM, LAM and LAF
4. The effect of race on the location of UAF, UAM, LAM and LAF
5. The relationship between UAF and LAF
6. The relationship between the location of UAF and UAM
7. The relationship between the location of LAM and LAF

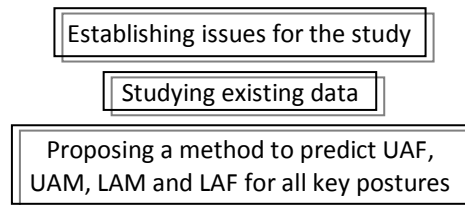


Figure 238. Strategy to produce a method to predict UAF, UAM, LAM and LAF location for all key postures

The existing five participants' data, which was already described in section 9.3, was utilised to study each of the issues above. Upon completion of the study, key findings of the study would be identified and used to form suggestions that guided the proposed method to predict UAF, UAM, LAM and LAF location for all key postures. Section 9.5.1 outlines the strategy and result of the study for each issue whereas section 9.5.2 outlines the proposed method to predict UAF's, UAM's, LAM's and LAF's locations for all key postures.

9.5.1 Study on the locations of UAF, UAM, LAM and LAF

In order to provide further information on the first four of the issues above i.e. the effect of body size, body type, race and gender on the locations of UAF, UAM, LAM and LAF; two graphs from section 6.2.2 were used. The graphs depicted the movement of the upper and lower arm boundaries of the five participants' flesh deformation area (FDA) as the arm flexed. Since UAF's, UAM's, LAM's and LAF's locations were basically bounded by the upper and lower arm boundaries of the flesh deformation area; the graphs enabled an overview of the overall locations of these key cross sections. Figure 239 and Figure 240 show the two graphs.

To observe the effect of body size on the location of the four key cross sections, the upper and lower and lower arm boundaries of the FDA from participant 1, whose arm length was the shortest, was compared with the other 4 participants. Both graphs demonstrated that participant 1 had the smallest FDA compared to the rest of participants. This result suggested that the increment of arm length was generally followed by the increment of FDA. To observe the effect of body size on the

four key cross sections' location, the upper and lower arm boundaries of the FDA from participant 4, whose BMI or weight was the highest, was compared with the other 4 participants. Both graphs demonstrated that participant 4 exhibited the largest value of FDA's boundaries. This result suggested that an increment in BMI was generally followed by an increment in FDA.

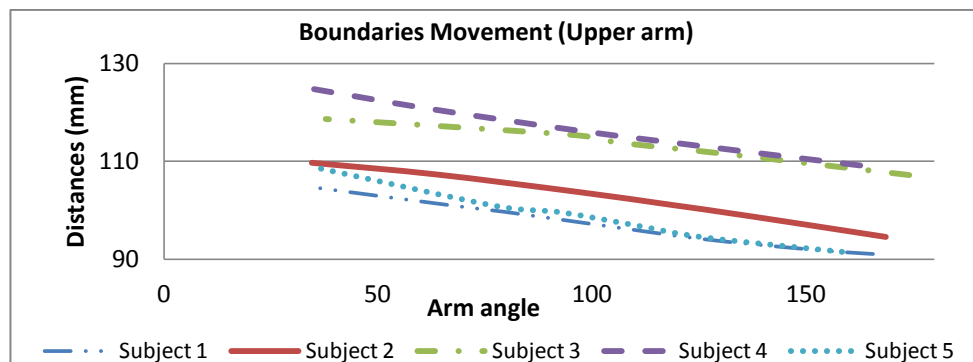


Figure 239. FDA for the upper arm, from a fully extended arm to a fully flexed arm, for five participants with various body size and type

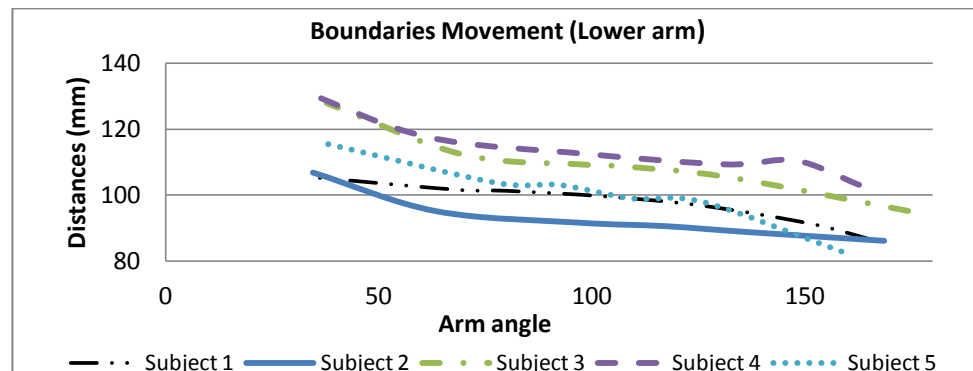


Figure 240. The relationship between body size and type with respect of FDA for the lower arm also yields a similar result as that of the upper arm

Due to the limited number of participants, the effect of gender and race on the locations of UAM, UAF, LAM and LAF could not be observed from the existing data. This limitation also applied to the remaining FDM elements to be predicted i.e. five key cross sections and profiles. Thus, the study suggested the use of relevant research findings to infer the effect of race and gender. With regards to gender, Malina et al. (2004) suggested that there was muscle to fat ratio difference between males and females. There was a strong likelihood that this difference affected flesh deformation and would ultimately impact on the new FDM's elements, especially those that were closely related with flesh deformation. As the locations of UAF, UAM, LAM and LAF, the shape of five key cross sections, and the shape of profiles were closely related with the flesh deformation; it was inferred that these elements were affected by gender. With regards to race, Walker (1993) suggested that different race would exhibit different body size and proportions. As different body sizes were shown to affect the FDA, it could be inferred that race had an effect on UAF's, UAM's, LAM's and LAF's locations. Provided that body sizes were shown to affect the remaining elements of

FDM to be predicted i.e. the shape of five key cross sections and the shape of profiles; this inference was also applicable to them. As both inferences were applicable to the remaining FDM elements to be predicted, to avoid repetition, issues regarding the effect of gender and race on these FDM elements would not be put forward and discussed in the subsequent sections i.e. section 9.6 and 9.7.

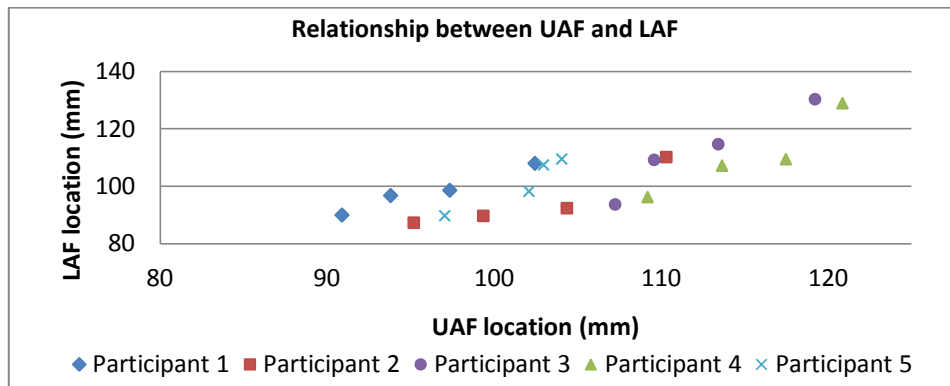


Figure 241. Relationship between UAF and LAF

To study the remaining issues, existing data from section 8.1.3 (see Table 11) were utilised. The existing data consisted of detail locations of UAF, UAM, LAM and LAF for all key postures. As this data provided comprehensive information on these four key cross sections' location, it provided an opportunity to study the relationship of UAF-LAF, UAF-UAM and LAM-LAF in detail. To investigate the relationship between the locations of UAF and LAF, a general observation on the relationship between UAF and LAF was required. This was achieved by charting the locations of UAF and LAF for all key postures of the five participants. The result was shown in Figure 241. The graphs clearly demonstrate that, for all participants, an increase in the location of UAF is also followed by an increase in the location of LAF. This behaviour suggested that there was a dependency between the locations of UAF and LAF. The graphs also demonstrate that UAF's and LAF's location at 135° and 90° flexion were bounded by UAF's and LAF's location at full extension and full flexion. This suggests that UAF's and LAF's location at 135° and 90° were dependent on UAF's and LAF's location at full extension and flexion.

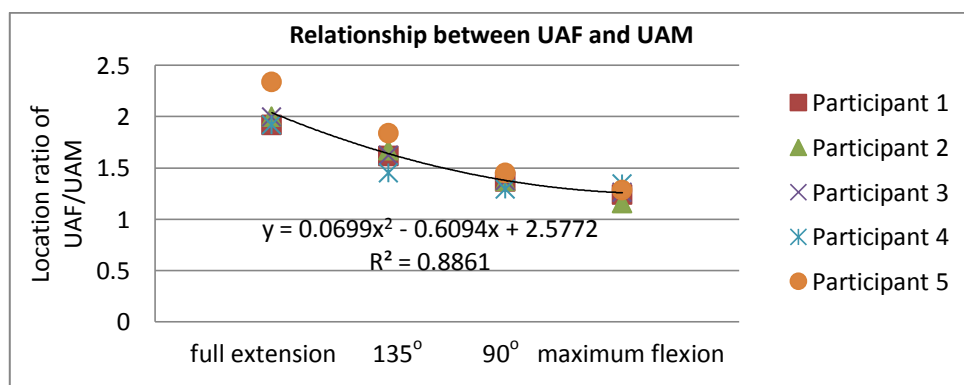


Figure 242. Relationship between UAF and UAM

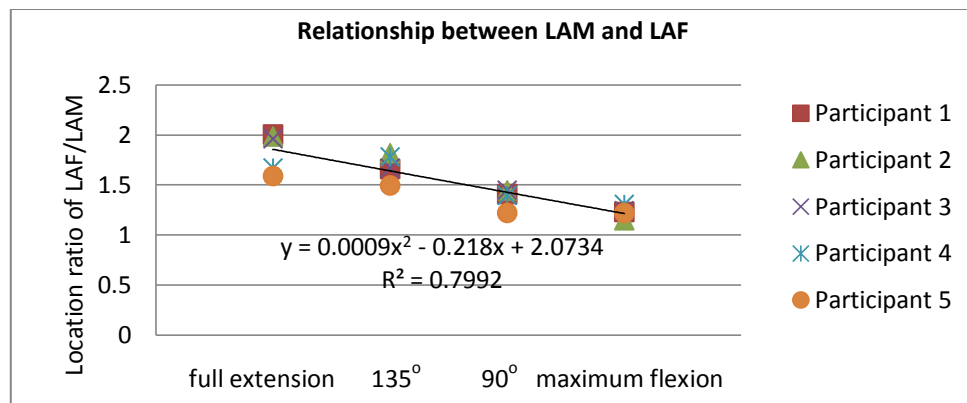


Figure 243. Relationship between LAM and LAF

To study the relationship between UAF and UAM, a ratio between the location of UAF and UAM was charted for all key postures of the five participants. A similar approach was also employed to study the relationship between LAM and LAF. Using the ratio was deemed to be suitable as it reflected the relative changes of UAF and UAM with respect to each other; and likewise for LAM and LAF. Figure 242 and Figure 243 show the graphs that depict the location ratio between UAF-UAM and the location ratio between LAF-LAM, respectively. The graphs suggest that the relationship between the location of UAF and UAM was non-linear and so was the relationship between the location of LAM and LAF.

From the studies about UAF's, UAM's, LAM's and LAF's locations; several key findings were identified. The following numbered bullet points outline the findings of the study and analyse their implication upon the prediction method:

1. The effect of gender and race

Whilst not directly investigated, the study inferred that gender and race had an effect on UAF's, UAM's, LAM's and LAF's locations. To account for the effect of gender and race, it was suggested that the prediction for UAF's, UAM's, LAM's and LAF's locations was performed separately for each gender and race.

2. The effect of BMI and body size

The study showed that BMI and body size affected the locations of UAF and LAF. To account for the effect of BMI and body size, it was suggested that UAF's and LAF's locations was predicted based on the relationship between BMI, body size and the locations of UAF and LAF, respectively. This key finding also implied that the database should include individuals that represented a range of BMI and body size for each gender and race.

3. The relationship between the location of UAF and the location of LAF

There were two key findings concerning the relationship between the locations of UAF and LAF. As shown shortly, both findings were closely related to the finding of the study concerning the effect of BMI and body size effect.

The first key finding showed that there was dependency between the locations of UAF and LAF. Having this dependency meant that if one of the locations was known, the other could be predicted. For instance, if UAF's location for a key posture was known, LAF's location for that key posture could be predicted from the location of UAF. The dependency between UAF's and LAF's locations constrained the suggestion which was drawn from the study on the effect of BMI and body size i.e. predicting the UAF's and LAF's locations based on their relationship with BMI and body size. This was because simply predicting *both* of UAF's and LAF's locations based on their relationship with BMI and body size meant that the dependency between UAF's and LAF's locations was not recognised. This potentially affected the outcome of the prediction. Thus, to account for the dependency between UAF and LAF, it was suggested that the relationship between body size, body type and the locations of UAF and LAF was used to predict *either UAF or LAF* but *not both*. Adopting this suggestion provided an opportunity to predict either UAF's or LAF's locations based on the relationship between the locations of UAF and LAF.

The second key finding showed that the locations of UAF and LAF for 135° and 90° flexion were dependent on the locations of UAF and LAF for full extension and flexion. In other words, this finding demonstrated that UAF's locations of different key postures were related and likewise for LAF's locations. Having this dependency meant that the locations of UAF and LAF for 135° and 90° flexion could be predicted if the locations of UAF and LAF for a full extension and flexion were known. This dependency also constrained the suggestion which was drawn from the study on the effect of BMI and body size i.e. predicting the locations of UAF and LAF based on their relationship with BMI and body size. Solely predicting UAF's locations for all key postures based on their relationship with BMI and body size potentially resulted in a failure to acknowledge the relationship between UAF's locations of different key postures; and likewise for LAF's locations. This potentially affected the end result of the prediction. Therefore, to account for the relationship between UAF's locations of different key postures and between LAF's locations of different key postures, it was suggested that the relationship between body size, body type and the locations of UAF and LAF was used *only* to predict the locations of UAF or LAF for *a full flexion and extension*. Adopting this suggestion presented an opportunity to predict UAF's and LAF's locations at 135° and 90° flexion based on the relationship of UAF's locations and LAF's of different key postures, respectively.

4. The relationship between the locations of UAF or LAF and the locations of UAM or LAM, respectively

The study showed that there was relationship between the location of UAF or LAF and the location of UAM or LAM, respectively. To account for the relationship between the locations of UAF and LAF and the locations of UAM or LAM, it was suggested that the prediction of UAM's or LAM's locations was based on this relationship.

The analysis of the study's key findings above concluded this subsection. In the next section (section 9.5.2), guided by the suggestions that were drawn from the analysis of the study's key findings, the prediction method of UAF's, UAM's, LAM's and LAF's locations for all key postures was proposed.

9.5.2 Proposing a method to predict the location of UAF, UAM, LAM and LAF for all key postures

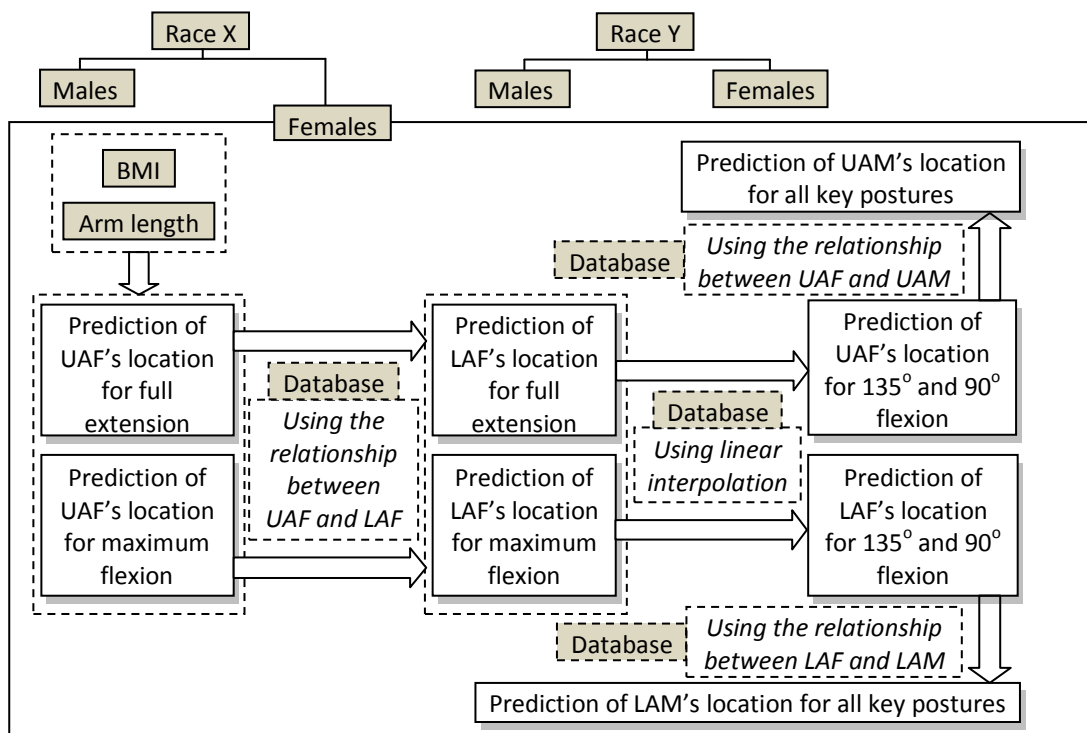


Figure 244. The proposed prediction method to determine the location of UAF, UAM, LAM and LAF

As described earlier, the proposed method to predict UAF's, UAM's, LAM's and LAF's locations was based on the suggestions which were formed from the key findings of the study in section 9.5.1. The proposed method, shown in Figure 244, demonstrated that the prediction of UAF's, UAM's, LAM's and LAF's locations was performed separately for each race and gender. This approach, driven by the suggestion that was drawn from the first key finding in section 9.5.1, ensured that the effect of gender and race was accounted for and ultimately improved the accuracy of the prediction result. Figure 244 also demonstrates that UAF's and LAF's locations were predicted prior to UAM's and LAM's locations. Details of the prediction method for UAF's and LAF's locations and UAM's and LAM's locations are discussed below.

9.5.2.1 *Predicting the locations of UAF and LAF for all key postures*

To predict the locations of UAF and LAF for all key postures, two suggestions from the study regarding the relationship between UAF's and LAF's locations in section 9.5.1 were followed. The two suggestions were: 1) using the relationship between body size, body type and the locations of UAF and LAF to predict *either UAF or LAF* but *not* both; and 2) using the relationship between body size, body type and the locations of UAF and LAF to predict the locations of UAF or LAF for *full flexion* and *extension*. As described in section 9.5.1, both suggestions acted as constraints for the suggestion drawn from the finding concerning the effect of BMI and body size i.e. predicting UAF's and LAF's locations based on their relationship with BMI and body size.

Following the two suggestions above, this research proposed a three stage prediction method for UAF's and LAF's locations, as shown in Figure 244. These were:

i) *Predicting the location of UAF for full extension and full flexion based on body size and type.*

This stage conformed to the first and second suggestion described in the first paragraph of this section. The locations of UAF were chosen to be predicted from its relationship with body size and type as the study showed that UAF's locations followed a more predictable pattern with respect to body size and type than the locations of LAF (see Figure 239 and Figure 240). To account for the effect of race and gender, the relationships between body size, type and the location of UAF had to be established separately for each gender and race.

ii) *Predicting the location of LAF for full extension and full flexion based on the location of UAF.* This stage conformed to the first and second suggestion described in the first paragraph of this section. To account for the effect of race and gender, the relationships between the locations of UAF and LAF for full extension and flexion had to be established separately for each gender and race.

iii) *Predicting the location of UAF and LAF for 135° and 90° flexion based on the location of UAF and LAF for full extension and flexion.* This stage conformed to the second suggestion described in the first paragraph of this section. To account for the effect of race and gender, the relationships between the locations of UAF/ LAF at 135° and 90° flexion and the locations of UAF/LAF at full extension and flexion had to be established separately for each gender and race.

9.5.2.2 *Predicting the locations of UAM and LAM for all key postures*

To predict UAM's and LAM's locations for all key postures; there was only one suggestion which was followed. The suggestion was derived from the key finding of the study in section 9.5.1 which investigated the relationship of UAF-UAM and LAM-LAF. Following the suggestion, the relationship

of UAF-UAM and LAF-LAM was used to predict the location of UAM or LAM from the location of UAF or LAF, respectively. To incorporate the effect of race and gender, the relationship for UAF-UAM and LAF-LAM had to be established for each gender and race.

9.6 Predicting five key cross sections at 135°, 90° and maximum flexion

As described in the general outline of the framework in section 9.2, a 3D scanned arm, one of the previously identified inputs, provided five key cross sections of a fully extended arm. To assist the synthesis of 3D scan data's key cross sections, additional data were required i.e. five key cross sections of individuals at four key postures. The additional data were required because the synthesis of key cross sections involved creating different shape cross sections for the required key postures. As shown in Figure 245, five key cross sections went through shape changes from one key posture to another. The database would store this additional data.

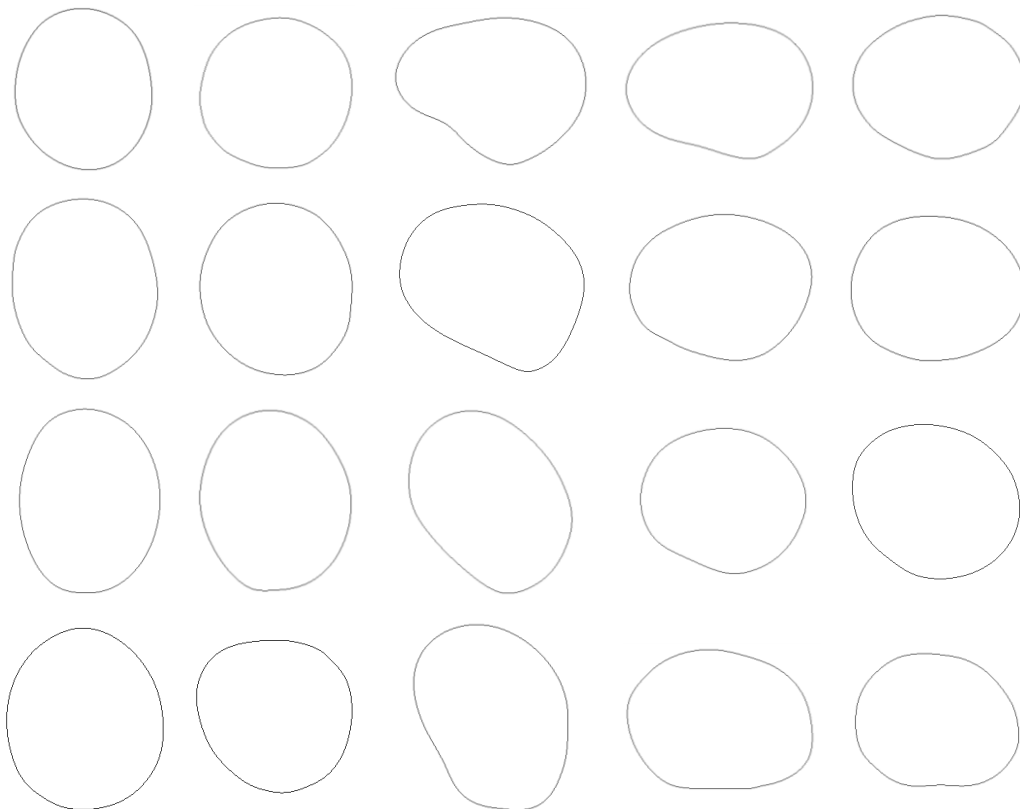


Figure 245. Five key cross sections from different key postures, top row: a fully extended arm, bottom row: a fully flexed arm

Given the five key cross sections of the 3D scan of a fully extended arm, a closest match of the 3D scan of a fully extended arm could be identified from the database. The closest match was essentially data of an individual in the database with similar characteristics (body size, body type, gender and race) to the 3D scanned arm. In line with the general outline of the framework

described in section 9.2, once the closest match was identified, the closest match's key cross sections at 135°, 90° and maximum flexion from the database were extracted and used to assist the synthesis of key cross sections. The ultimate output of the synthesis was coordinates of the five key cross sections at 135°, 90° and maximum flexion, which were required by the new FDM.

Figure 246 shows the strategy used to propose a method to predict five key cross sections at 135°, 90° and maximum flexion. This strategy was similar to the strategy in section 9.5 which was utilised to propose a method for the prediction of UAF's, UAM's, LAM's and LAF's locations. The first step of the strategy was to establish issues for the study. Similar to section 9.5, some of the issues of the study were also focused to explain the relationship between the inputs (gender, race, body size and BMI) and the relevant FDM's element (five key cross sections). However, as described in section 9.5.1, the proposed inference regarding the effect of gender/race on the FDM's elements was applicable for all of the FDM's elements to be predicted. Therefore, this section will only focus the study on two of the inputs i.e. body size and body type.

As suggested in the first paragraph of this section, the database was required to store additional data i.e. five key cross sections of individuals at four key postures. Thus, the issue concerning the required amount of data to represent five key cross sections in the database was also studied. Another focus of the study was the relationship between shape changes among five key cross sections of various key postures. An understanding of existing relationship(s) between the locations of one key cross section with another would likely allow a more thorough and accurate decision regarding the final prediction method. Thus, in total, there were 5 issues which needed to be studied to predict five key cross sections for 135°, 90° and maximum flexion. These were:

1. The effect of BMI on five key cross sections
2. The effect of body size on five key cross sections
3. The amount of data to be stored for every individual in the database
4. The shape changes of each key cross sections from one key posture to another
5. The relationship between key cross sections from one key posture to another

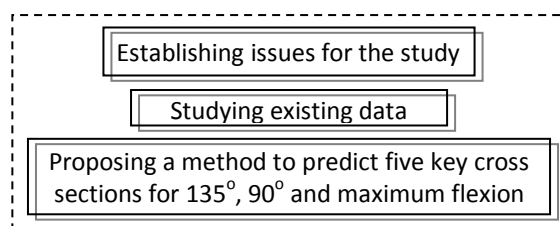


Figure 246. Strategy to develop a prediction method of five key cross sections for 135°, 90° and maximum flexion

The existing five participants' data, which was already described in section 9.3, was utilised to study each of the issues above. Upon completion of the study, key findings of the study would be identified and used to form suggestions that guided the proposed method to predict UAF, UAM,

LAM and LAF location for all key postures. Section 9.6.1 outlines the strategy and result of the study for each issue whereas section 9.6.2 outlines the proposed method to predict five key cross sections at 135°, 90° and maximum flexion.

9.6.1 Study on five key cross sections of all key postures

To study the five key cross sections for all key postures, existing data from section 8.1.3, which was the result of the integration of digitised cross sections, joint information and the photographs set, was used. The existing data consisted of 2D form of the five key cross sections for each key posture of participants. As the existing five key cross sections were already in 2D form, comparison in a 2D environment could easily be performed with the help of Pro-Engineer WildFire 4.0. The study would be carried out by visually observing these cross sections to address each of the established issues.

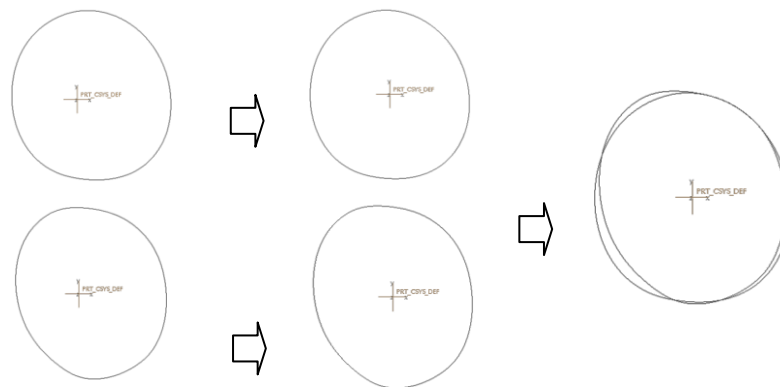


Figure 247. Utilising the centre of both key cross sections to overlay them

To investigate whether the five key cross sections were affected by BMI or not, data from participants 3 and 4 were compared. From existing data of participants, only data from these two participants were used for the investigation. This was because they were the only participants with similar height, but of different weight. The comparison was performed by overlaying each of the participants' five key cross sections in Pro-Engineer WildFire 4.0. Figure 247 shows how overlaying of the 2D key cross sections in Pro-Engineer WildFire 4.0 were performed by determining the centre of each key cross section and using them to overlap the two key cross sections.

Using the overlaying method shown in Figure 247, the comparison of key cross sections between participant 3 and 4 was performed for each key posture e.g. participant 3's UAF at 135° flexion was overlaid with participant 4's UAF at 135° flexion. Figure 248 shows examples of the comparison result for the five key cross sections from different key postures. The comparison result clearly demonstrated that cross sections of participant 4 (dashed line), whose higher BMI, were bigger compared to those of participant 3 (solid line). This result suggested that BMI affected five key cross sections.

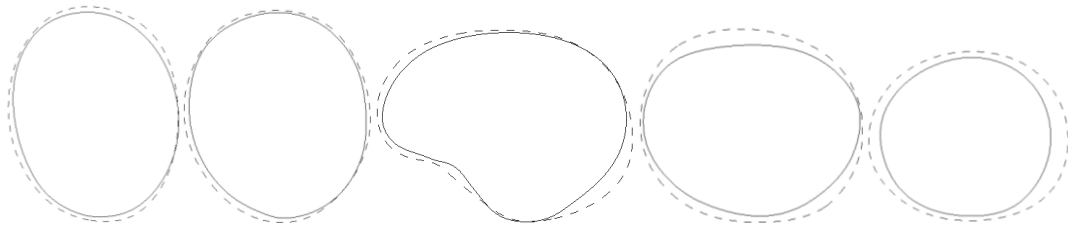


Figure 248. Examples of the comparison results of five key cross sections between participant 3 (dashed line) and participant 4 (solid line) of which participant 3 has higher BMI than the other participant

To investigate whether the five key cross sections were affected by body size, the data of participant 1 was compared to the data of the rest of the participants. Participant 1 was chosen because of her body size (height and arm length) was the smallest compared to the rest of participants. The method shown in Figure 247 was utilised to create overlay of key cross sections from different key postures e.g. participant 1's UAF of 135° flexion was overlaid with the remaining participants' UAF of 135°. Figure 249 shows an example of the comparison result of UAF, UAM, E, LAM and LAF for different key postures. The result shows that participant 1 generally had the smallest cross sections in comparison with other participants' cross sections. This result suggested that body size affected the five key cross sections.

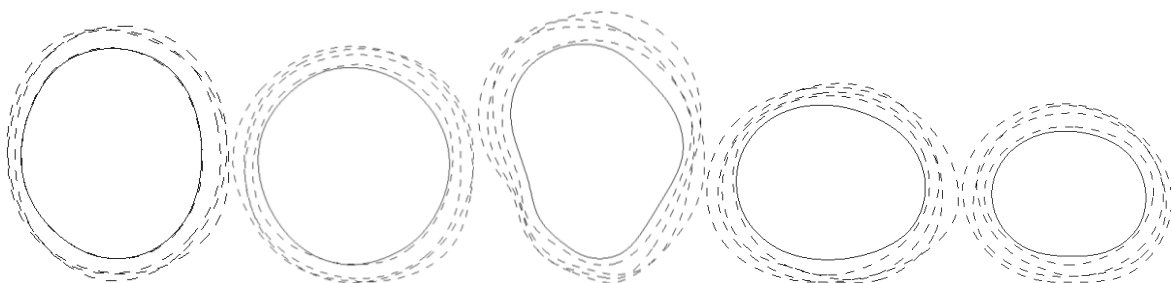


Figure 249. Examples of the comparison result of five key cross sections comparison between participant 1 (solid lines) and the rest of participants (dashed line) which shows that participant 1, with the least body size, generally has smaller cross sections

The next issue to be studied was the amount of data to be stored for every individual in the database. As there were 16 sample points for each cross section and there were five key cross sections for each key posture, 80 sample points had to be stored for each key posture. Thus, if there was N number of individuals and 4 key postures for each individual, the total amount of sample points to be stored would be $N \times 4 \times 80$ or $N \times 320$. A high number of data did not only need larger storage capacity but would also be slower to be processed or analysed. This suggested that a method to reduce the number of data would likely be required.

The next issue to be studied was how the shape of each of the five key cross sections changed from one key posture to another. As described in section 9.6, an understanding of how their shape changes would help in proposing the method for the prediction of the five key cross sections. For the study, the shape changes of the five key cross sections from one key posture to another from each participant were visually observed. To allow the visual observation, five overlays were created

for each participant. Each overlay captured the changes of a key cross section at different key postures. For example, the 5 overlays that were created for participant 1 would be: (i) UAF overlay which consisted of $UAF_{full_extension}$, UAF_{135} , UAF_{90} , and $UAF_{maximum_flexion}$; (ii) UAM overlay which consisted of $UAM_{full_extension}$, UAM_{135} , UAM_{90} and $UAM_{maximum_flexion}$; (iii) E overlay which consisted of $E_{full_extension}$, E_{135} , E_{90} and $E_{maximum_flexion}$; (iv) LAM overlay which consisted of $LAM_{full_extension}$, LAM_{135} , LAM_{90} and $LAM_{maximum_flexion}$; and (v) LAF overlay which consisted of $LAF_{full_extension}$, LAF_{135} , LAF_{90} and $LAF_{maximum_flexion}$. The shape changes of UAF, UAM, LAM and LAF are be discussed first, followed by the discussion on the shape changes of E:

1. *The shape changes of UAF, UAM, LAM and LAF.* Figure 250 showed the overlays of UAF, UAM, LAM and LAF for all participants across different key postures.

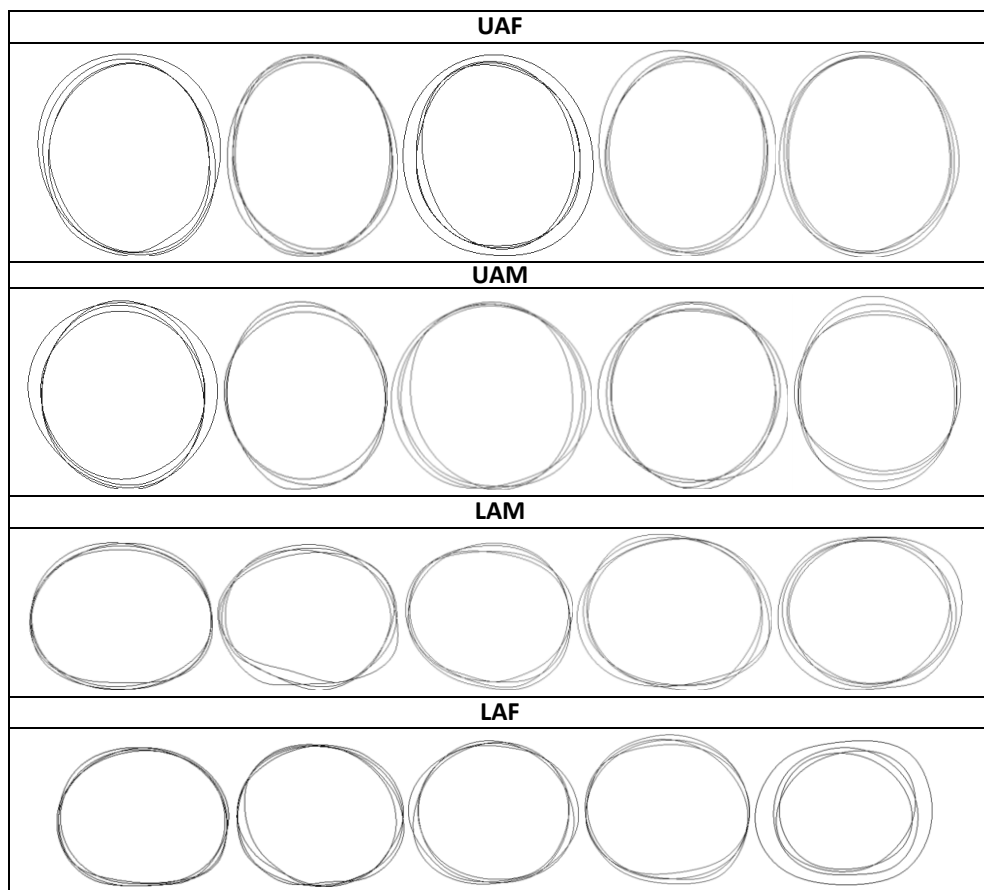


Figure 250. Images of UAF, UAM, LAM and LAF from different key postures for participant 1 to participant 5

The figure demonstrated that, for each participant, the sizes of UAF, UAM, LAM and LAF changed from one key posture. The size of cross sections in anterior-posterior and lateral-medial direction increased as the arm flexed towards 90° flexion. In contrast, from 90° to maximum flexion, the size of cross sections' sizes in anterior-posterior decreased as the compression of the flesh at the upper and lower arm occurred. However, the size of reduction in this direction was compensated by the increment of the cross sections' size in lateral-medial direction. This behaviour has been identified in section 8.1.5 where the feasibility testing of

the new FDM was performed. The figure also demonstrated that, for each participant, despite the size changes, the shape of UAF, UAM, LAM and LAF generally remains similar from one key posture to another i.e. ellipsoids. However, as shown from the figure below, shape variations on UAF, UAM, LAM and LAF did occur and resulted in cross sections that were not completely concentric.

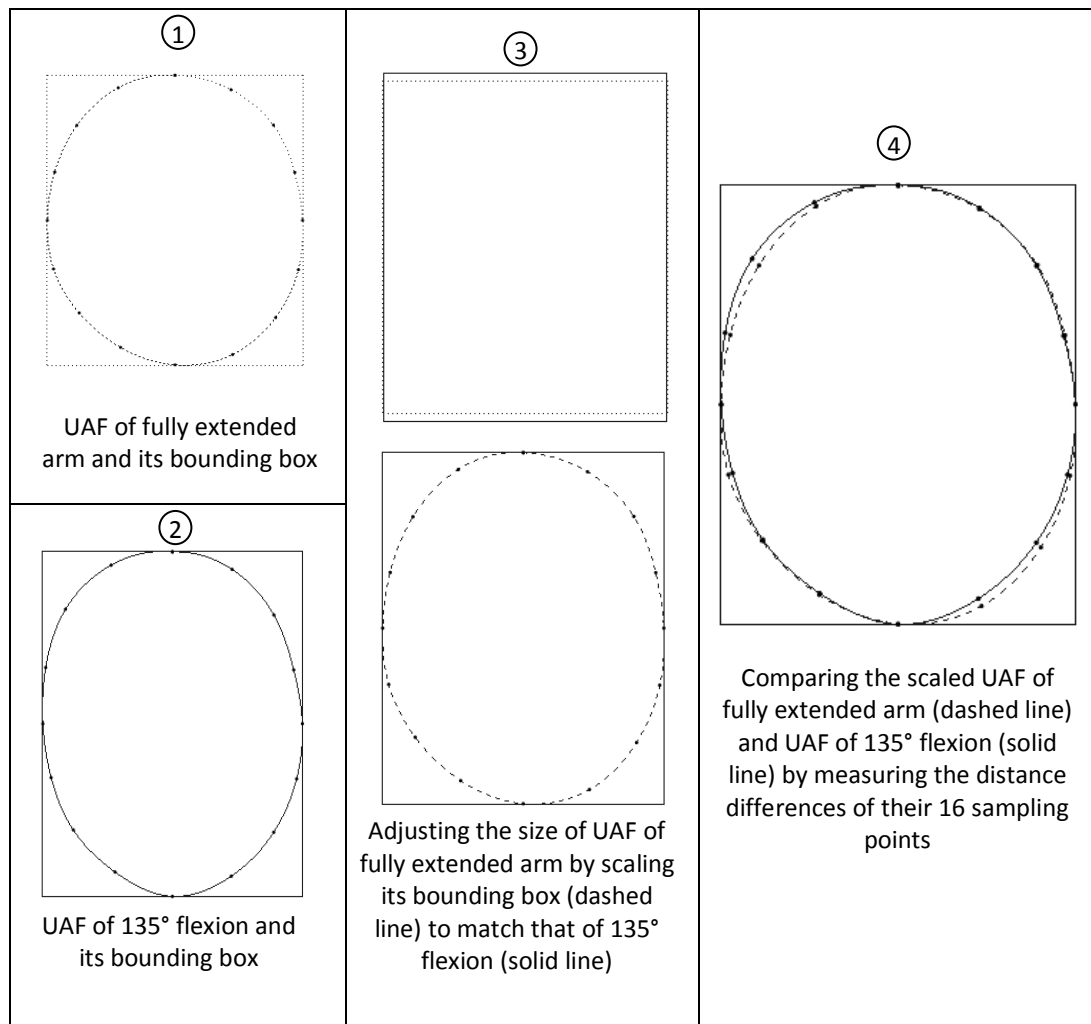


Figure 251. Steps to scale cross section of a fully extended arm to match the size of those from other key postures

A small investigation was performed to study the level of shape variation further. The investigation was performed by creating a bounding box for each cross section and scaling the bounding box for fully extended arm's cross sections such that they were the same size as the bounding box of other key posture's cross section. Figure 251 illustrates the process. The outcome of the process was the distance differences of the sampling points between the scaled cross section of fully extended arm and the cross section of other key postures. The distance difference of the sampling points reflected the shape variations of cross sections across different key postures. This process was performed for each cross section and participant. Distance differences for each cross section and participant was then averaged. A

simple algorithm was created in Matlab 7.0 to perform the scaling procedure and calculate the averaged error. The result of the investigation was shown in Table 22. The result showed that the mean error between a scaled cross section of a fully extended arm and those from other key postures was less than 1.5 mm with a range of average error: 0.5347-1.4864. This suggested that, although shape variations on UAF, UAM, LAM and LAF did occur, the shape of cross sections from one key posture to another generally remained the same and could be approximated with a scaled cross section of a fully extended arm.

Table 22. Mean error between scaled cross section of a fully extended arm and those from other key postures

	Average of distance differences of sampling points (mm)				
	Participant 1	Participant 2	Participant 3	Participant 4	Participant 5
UAF	0.666	0.8537	0.6846	1.1605	0.6003
UAM	1.0393	0.6332	0.9458	0.9484	0.834
LAM	1.4195	0.5651	1.3009	1.4775	0.7918
LAF	1.4864	0.6169	0.8017	0.5347	1.0708

2. *The shape changes of E.* Figure 252 showed the overlays of E from participant 1 to participant 5. The figure showed that there was an apparent shape change of E as the arm assumes one key posture to another. In addition to the shape changes, there was also size change, especially in the vertical direction (anterior-posterior of the elbow). This means that simply scaling E of fully extended arm to predict E of other key posture would not be possible.

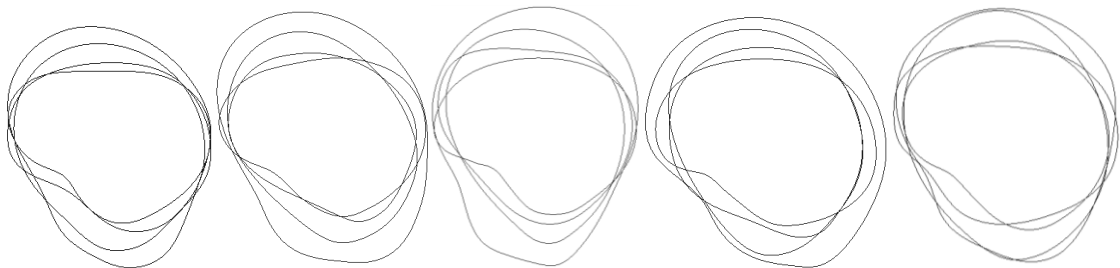


Figure 252. Images of E from different key postures for participant 1 to participant 5 shows apparent shape changes from one key posture to another

The last issue to be investigated was the relationship between key cross sections from one key posture to another. To investigate this issue, the five key cross sections were overlaid for each key posture and participant. For example, for participant 1, there will be 4 overlays: (i) full extension overlay which consists of $UAF_{full_extension}$, $UAM_{full_extension}$, $E_{full_extension}$, $LAM_{full_extension}$ and $LAF_{full_extension}$; (ii) 135° overlay which consists of UAF_{135} , UAM_{135} , E_{135} , LAM_{135} and LAF_{135} ; (iii) 90° overlay which consists of UAF_{90} , UAM_{90} , E_{90} , LAM_{90} , LAF_{90} ; and (iv) maximum flexion overlay which consists of $UAF_{maximum_flexion}$, $UAM_{maximum_flexion}$, $E_{maximum_flexion}$, $LAM_{maximum_flexion}$, $LAF_{maximum_flexion}$. Figure 253 shows an example of the overlay results from participant 1. The visual observation shows that there is dependency between UAF and UAM as well as between LAM and LAF. For all key postures, the size of UAM is always smaller compared to the UAF and so is LAM compared to LAF. Also, there is a

similarity in terms of the general shape between UAM and UAF and between LAM and LAF. The prediction for the five key cross sections should take into account this dependency.

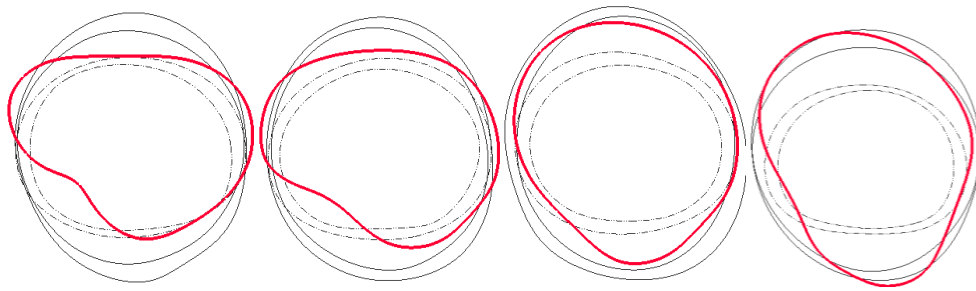


Figure 253. Overlays result from participant 1, which shows that there is dependency for UAM-UAF and LAM-LAF

From the studies about the five key cross sections from all key postures, several key findings were identified. The following numbered bullet points outline key findings of the study and analyse their implication upon the prediction method:

1. The effect of BMI

The results of the study showed that BMI affected the five key cross sections. This finding suggested that the database should include cross sections from individuals with different BMI in order to improve the output for the closest match search which ultimately affected the outcome of the prediction result.

2. The effect of body size

The results of the study showed that body size affected the five key cross sections. Based on this finding, a similar suggestion was also proposed i.e. inclusion of cross sections from individuals with different body sizes.

3. The amount of data to be stored for every individual in the database

The study identified the extent of the possible data size to store cross sections in the database i.e. $N \times 320$ where N was the number of individuals in the database. This clearly demonstrated that the size of data would expand rapidly as the number of individuals in the database increased. By storing a higher number of cross sections that covered a wide range of body type, body size, gender and race in the database, the database would be able to provide a better closest match and was likely to increase the accuracy of cross sections prediction. However, large amounts of data would also demand bigger storage and more processing time to deal with which in turn affected the real time modelling ability of the framework. To balance the need of accuracy and real time modelling, the cross sections should be stored effectively by ensuring that only information that were required for cross sections predictions were stored in the database. Also, whenever it was appropriate, a method to compress the number of data to be stored should be performed.

4. The shape changes of each key cross sections from one key posture to another

The study demonstrated two key findings. The first finding was related to the shape changes of UAF, UAM, LAM and LAF cross sections whereas the second finding was related to the shape changes for E cross section.

With regard to the shape changes of UAF, UAM, LAM and LAF, the study showed that cross sections' vertical (anterior-posterior) and horizontal (lateral-medial) dimensional changed from one key posture to another. The results of the study also showed that the shape of UAF, UAM, LAM and LAF of various key postures generally remained similar and could be approximated with a scaling of cross section of a fully extended arm. These findings suggested that prediction of UAF, UAM, LAM and LAF for 135°, 90° and maximum flexion could be performed by simply resizing the vertical and horizontal dimension of UAF, UAM, LAM and LAF of full extension. It is acknowledged that simply resizing the vertical and horizontal dimension might not truly represent the shape changes of UAF, UAM, LAM and LAF across different key postures, as shown by the level of average error in Table 22. However, as resizing vertical and horizontal dimension involved a simple algorithm, it would be quicker to process. In addition to this, the resizing process would only require the database to store the vertical and horizontal dimension of a cross section, as opposed to storing 16 sample points of a cross section. Thus, both of the required algorithm and data promoted the real time modelling ability of the framework.

With regard to the shape changes of E, the study showed that there was an apparent complex shape change of E from one key posture to another. The complex shape change meant that the prediction approach for UAF, UAM, LAM and LAF i.e. resizing the initial input, would not be suitable. The study also showed that, despite the complex shape change, E's shape for each key posture for the five participants still followed a common shape. As there was a common shape of E for each key posture across different participant, an output of an interpolation would likely result in a more predictable and desirable shape. Thus, this finding suggested that given two closest matches of E of a fully extended arm, the E at 135°, 90°, and maximum flexion could be derived through an interpolation from the closest matches.

5. The relationship between key cross sections from one key posture to another

The study showed that there was dependency between UAF and UAM as well as between LAM and LAF. This finding addressed the fifth issue which concerned the relationship between key cross sections from one key posture to another.

In section 9.2, where the proposed framework was outlined, it was implied that the prediction of the cross sections at 135°, 90° and maximum flexion would be based on synthesising the information from the closest match of cross sections at a fully extended

arm. Having the dependency between UAF and UAM meant that if data from individual x^{th} was used as the closest match for UAF, data from the same individual should also be used as the closest match for UAM. The same was also applicable for the dependency between LAF and LAM. Thus, the dependency between UAF and UAM suggested that the closest match search for UAF and UAM should be performed subsequently to ensure that that same closest match was obtained for UAF and UAM; and likewise for LAF and LAM. If the search for the closest match was performed separately for UAF and UAM, there was a possibility that the closest match for UAF and UAM was of different individual e.g. individual x^{th} for UAF and individual y^{th} for UAM. If the closest match for UAF and UAM was of different individual, it meant that the dependency between UAF and UAM was no longer accommodated and could yield inaccurate prediction result as the synthesis of each cross section was driven by data from different individual.

The analysis of the study's key findings above concluded this subsection. In the next section (section 9.6.2), guided by the suggestion that were drawn from the analysis of the study's key findings, the prediction method of five key cross sections at 135°, 90° and maximum flexion was proposed.

9.6.2 Proposing a method to predict five key cross sections at 135°, 90° and maximum flexion

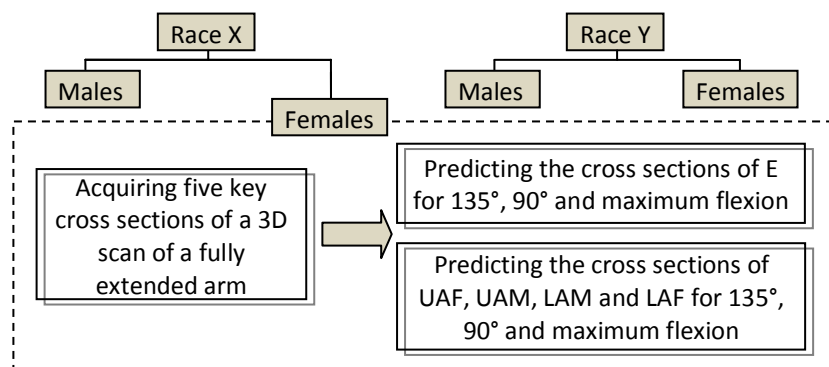


Figure 254. General outline of the proposed method to predict the five key cross sections

Figure 254 shows the general outline of the proposed method to predict the five key cross sections at 135°, 90° and maximum flexion. It indicated that the prediction method was performed separately for each race and gender. This approach was taken to ensure that the inference established in section 9.5.1 regarding the effect of race and gender on the predicted elements of FDM was taken into account. Figure 254 also shows that the 3D scanned arm's five key cross sections were required for the prediction method. To comply with the new FDM, the five key cross sections of a 3D scan of a fully extended arm had to be represented as distances between bone point and sampling points (see section 8.1.3). To obtain sampling points from the 3D scan data, an

existing algorithm in section 5.3.2.1 was followed. Figure 255 illustrates the procedures of the existing algorithm where *a number of* rays that originated from *the location of the cross section (bone point)* and located on *the plane of the cross section* were intersected with the 3D scan surface, starting from *the initial location*. The procedures of the existing algorithm implied that it consisted of four important aspects i.e. the number of rays, the location of the cross section, the plane of the cross section, and the initial location. The following provide an overview of these aspects for the five key cross sections:

- i) *The number of rays.* 16 rays would be created to acquire 16 sample points for each key cross section. This number of rays was chosen to match the requirement of the new FDM.
- ii) *The locations of the key cross sections.* The locations of key cross sections of a 3D scanned arm data could only be provided through performing the prediction method in section 9.5.2. Thus, this indicated that the prediction of the locations of UAF, UAM, LAM and LAF had to be completed prior to the prediction of five key cross sections.
- iii) *The plane orientations of the key cross sections.* Section 7.3.1 provided guidance concerning the plane orientation of the five key cross sections. The plane of UAF, UAM, LAM and LAF were perpendicular to the upper or lower arm whereas the plane of E was dependent on the angle of the upper and lower arm.
- iv) *The initial location for sampling points.* Section 7.3.2.2 provided guidance concerning the initial location of the 16 sampling points. The initial location was essentially the intersection between the cross section and a plane that was created from the bone point and the X-Z plane. Section 7.3.2.2 also showed that the sampling for each key cross section was performed in a clock wise direction.

By incorporating the aspect details into the existing algorithm, sample points for the five key cross sections of the 3D scan of a fully extended arm could be acquired. For each key cross section the Euclidean distances of the sample points towards the corresponding bone point could be calculated. This step also concluded the process to acquire the five key cross sections of the 3D scan data and was subsequently followed by prediction of five key cross sections at 135°, 90° and maximum flexion.

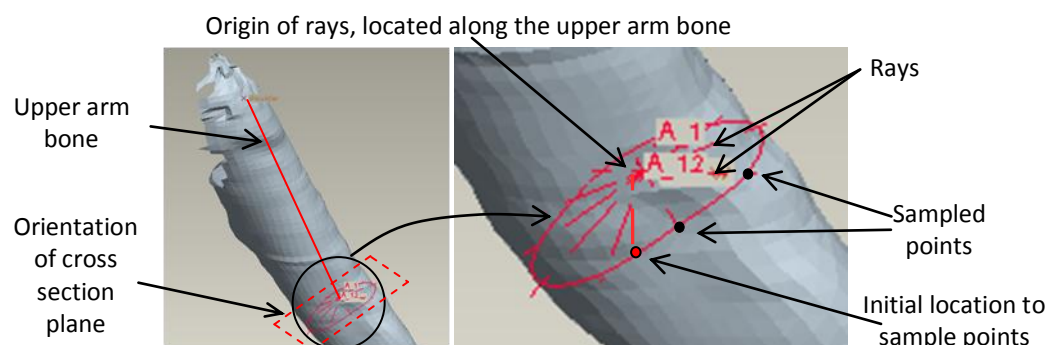


Figure 255. Procedures of the algorithm from section 5.3.2.1 to acquire key cross sections of 3D scanned arm

As shown in Figure 254, the prediction for the five key cross sections was categorised into two parts. The first part of the method was applicable for UAF-UAM and LAM-LAF whereas the second part of the method was applicable for E. This division was driven by the key findings of the fourth issue of the study which demonstrated that, while the shape of E was quite complex, the shape of UAF, UAM, LAM and LAF generally resembled ellipsoids which could be approximated by the resizing vertical and horizontal dimension of a cross section. Details of each method are outlined in the following.

9.6.2.1 Predicting UAF, UAM, LAM and LAF key cross sections at 135°, 90° and maximum flexion

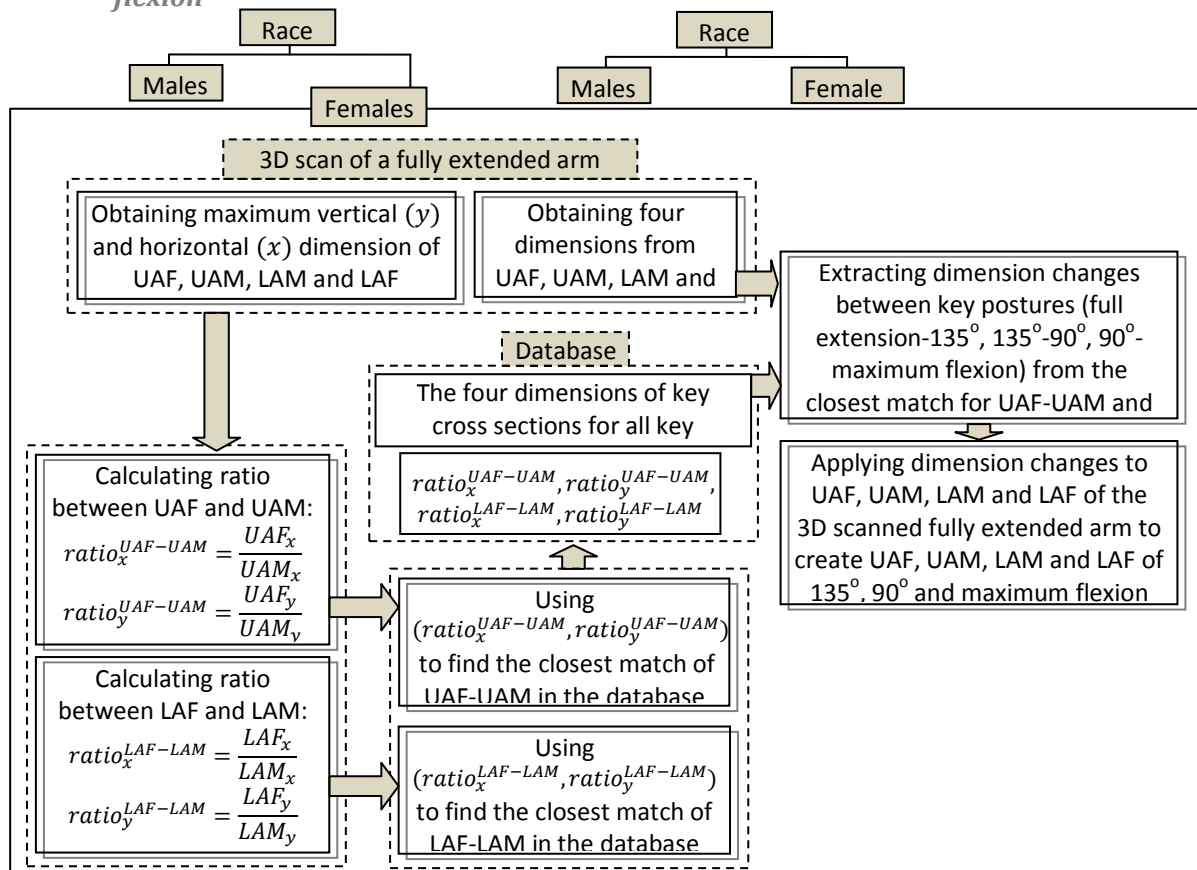


Figure 256. Proposed method to predict cross sections of UAF, UAM, LAM and LAF for 135°, 90° and maximum flexion

As suggested by the heading, the first part of the method was applicable to predict the UAF, UAM, LAM and LAF key cross sections at 135°, 90° and maximum flexion. The prediction method for the cross sections of UAF, UAM, LAM and LAF adopted the suggestions that were based on the key findings from the fourth and fifth issue of the study in section 9.6.1. The two suggestions were: i) simultaneous search of closest match for UAF and UAM to ensure that the same closest match was obtained for UAF and UAM; and likewise for LAF and LAM; ii) predicting UAF, UAM, LAM and LAF for 135°, 90° and maximum flexion by resizing the vertical and horizontal dimension of UAF, UAM, LAM

and LAF of a 3D scanned arm. Figure 256 showed the proposed method which accommodated the two suggestions above.

The prediction method was essentially divided into two main stages i.e. 1) finding the closest match for UAF, UAM, LAM and LAF of a 3D scanned arm and 2) resizing the dimensions of a 3D scanned arm's key cross sections to predict the cross sections of UAF, UAM, LAM and LAF at 135°, 90° and maximum flexion. Each stage of the proposed method is discussed in detail in the following:

1. Finding the closest match for UAF, UAM, LAM and LAF of a 3D scanned arm. The first stage was governed by the suggestion that was based on the key finding of the fifth issue of the study in section 9.6.1 i.e. simultaneous search of the closest match for UAF and UAM to ensure that the same closest match was obtained for UAF and UAM; and likewise for LAM-LAF. To allow the simultaneous search, this research proposed the use of the dimension ratio of UAF-UAM and/or LAF-LAM as a means to capture their relationship which was subsequently used to search for the closest match of UAF-UAM and/or LAF-LAM simultaneously. Figure 256 shows the steps of how the ratio was used to find the closest match. Detail of the steps involved is discussed in the following:

i) *Obtaining maximum vertical and horizontal dimensions from UAF, UAM, LAM and LAF.* The measurement of the maximum vertical and horizontal dimensions of UAF, UAM, LAM and LAF were performed in a 2D environment. This was proposed to reduce the complexity of the overall prediction process. The existing method in section 7.3.2.2, where distances of sampling points were multiplied to the unit vectors in 2D, was applied to allow a 2D measurement of a cross section. The unit vector directions and coordinates values are shown in Figure 257. The combination between: (i) the method to sample cross sections from 3D scan data; and (ii) the method to recreate the cross sections in 2D environment, determined 2D cross sections orientation.

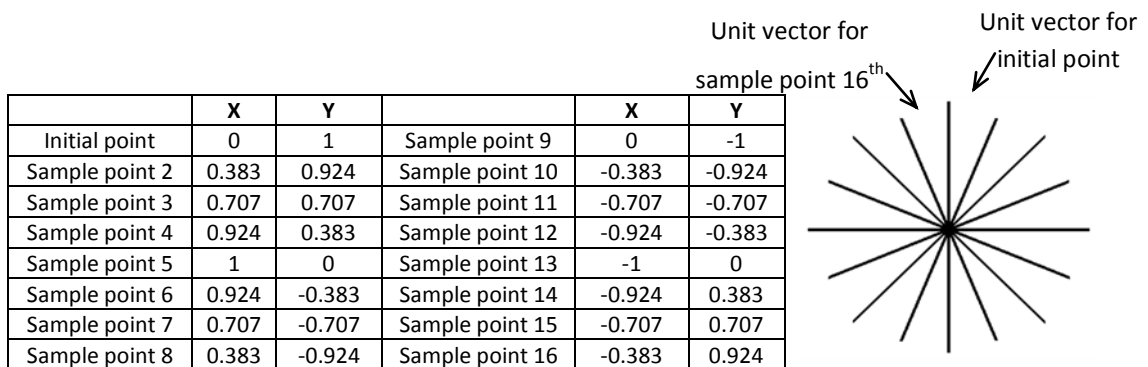


Figure 257. Unit vector directions and coordinates to recreate cross sections of 3D scanned arm

Once the cross sections of UAF, UAM, LAM and LAF were transformed into a 2D environment, its maximum vertical and horizontal dimension were measured. The

measurement was performed by creating a bounding box around each 2D cross section. As the bounding box was essentially created from the maximum vertical and horizontal dimension of the 2D cross section, its orientation is clearly dependent on the 2D cross section. Examples of key cross sections' maximum vertical and horizontal dimension are shown in Figure 258.

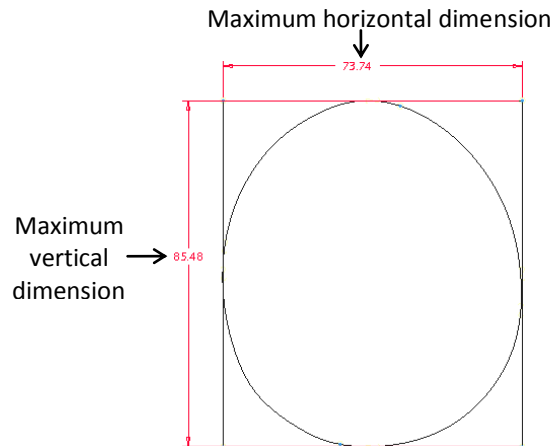


Figure 258. Example of the utilisation of bounding boxes to measure the maximum vertical and horizontal dimension for UAF_{full extension} from participant 2

- ii) *Calculating the ratio for UAF-UAM and/or LAF-LAM.* The next step was to calculate the ratio values for UAF-UAM ($ratio_x^{UAF-UAM}$ and $ratio_y^{UAF-UAM}$) and LAF-LAM ($ratio_x^{LAF-LAM}$ and $ratio_y^{LAF-LAM}$). Figure 256 shows how the ratio was calculated for UAF-UAM and LAF-LAM.
- iii) *Using the ratio to find the closest match.* Once the ratio values of UAF-UAM and LAM-LAF of the 3D scan of a fully extended arm were calculated, they were utilised to identify the closest match in the database. The closest match was essentially the data from an individual with the most resemblance to the 3D scanned arm's five key cross sections. Since the ratio values of UAF-UAM and LAM-LAF was used to find the closest match, this indicated that the database also had to store ratio values of a fully extended arm for every individual in the database i.e. (1) $ratio_x^{UAF-UAM}$ and $ratio_y^{UAF-UAM}$ for UAF-UAM; (2) $ratio_x^{LAF-LAM}$ and $ratio_y^{LAF-LAM}$ for LAF-LAM. As the database was categorised based on race and gender, this also suggested that the ratio values would also have to be provided for each race and gender.

To identify the closest match in the database, the ratio values, of both the database and 3D scanned arm, would be treated as Cartesian coordinates so that they could be charted in a 2D coordinate system. For instance, if the 3D scanned arm has $ratio_x^{UAF-UAM} = 0.97$ and $ratio_y^{UAF-UAM} = 1.18$, the 3D scanned arm's Cartesian coordinates for the UAF-UAM ratio would be: (0.97, 1.18). By treating ratio values of the database and 3D scanned arm as

Cartesian coordinates, the closest match could be determined by identifying data in the database with the smallest Euclidean distance to the Cartesian coordinate of the 3D scanned arm. For instance, if the Cartesian coordinates for UAF-UAM in the database are as the following: [(0.99, 1.15), (0.96, 1.09), (0.95, 1.17), (0.94, 1.13), (0.94, 1.11)], the closest match for the previous example would be (0.95, 1.17), as shown in Figure 259.

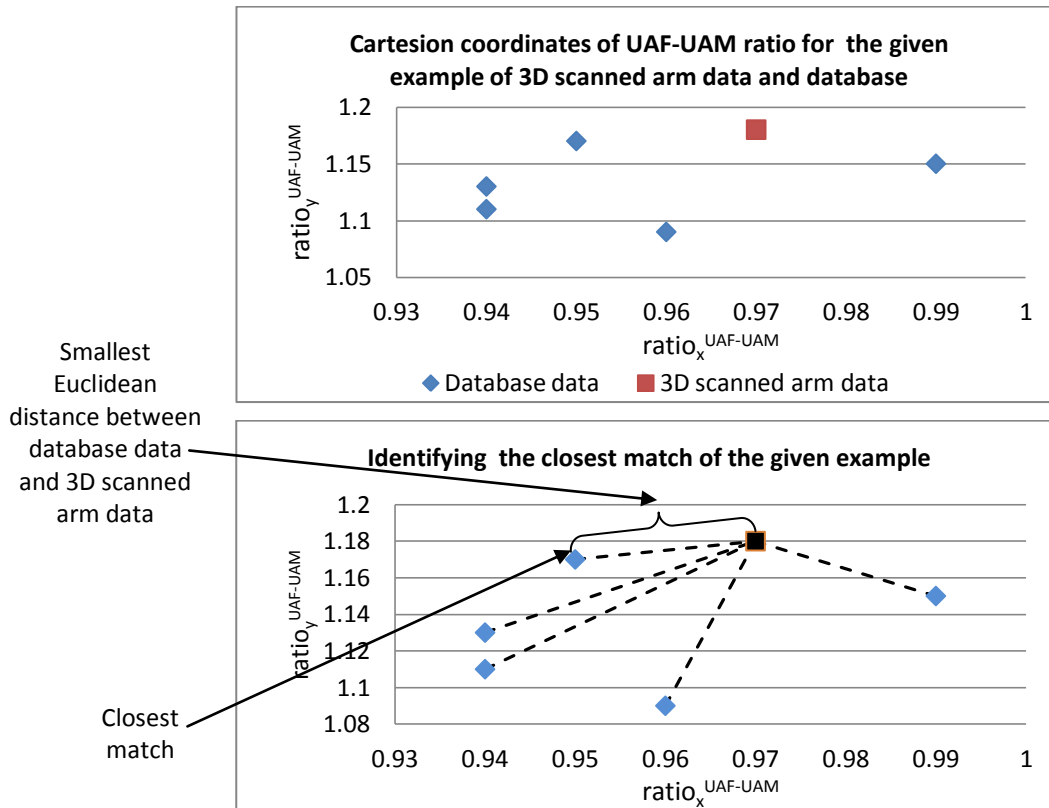


Figure 259. Example of Cartesian coordinates depiction for ratio of UAF-UAM for 3D scanned arm and database data. The identification of closest match is performed by measuring the Euclidean distance of the 3D scanner arm towards each database and choosing the database data with the smallest Euclidean distance

2. Resizing the dimensions of a 3D scanned arm's key cross sections to predict the cross sections of UAF, UAM, LAM and LAF at 135°, 90° and maximum flexion. The second stage was governed by the suggestion that was based on one of the key findings of the fourth issue of the study in section 9.6.1 i.e. predicting UAF, UAM, LAM and LAF for 135°, 90° and maximum flexion by resizing the vertical and horizontal dimension of UAF, UAM, LAM and LAF of a 3D scanned arm. The resizing of key cross sections adopted the same principle that was used in the investigation of key cross sections' shape variation in section 9.6.1, where UAF, UAM, LAM and LAF were adjusted in the vertical dimension (anterior-posterior direction) and horizontal dimension (medial-lateral direction). This principle was adopted because it provided more flexibility in resizing the dimensions of a 3D scanned arm's UAF, UAM, LAM and LAF.

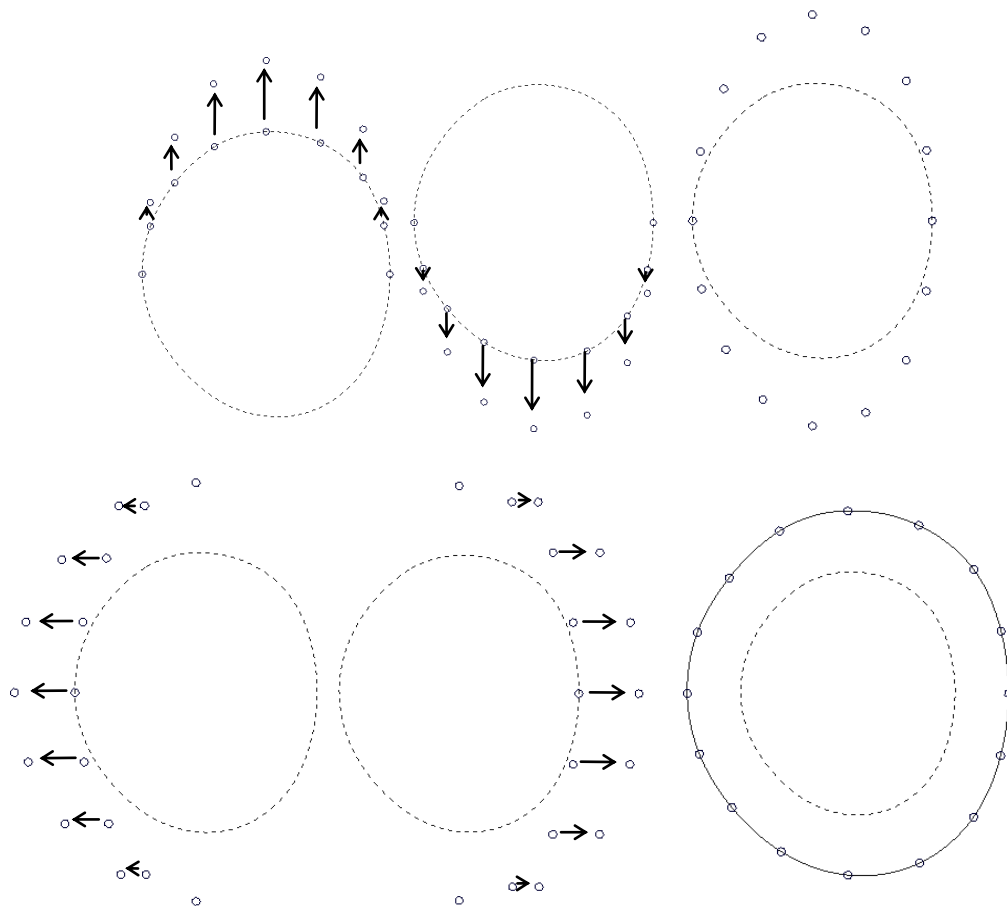


Figure 260. Top images: the anterior-posterior resizing for vertical dimension; bottom first two images: the medial-lateral resizing for horizontal dimension; bottom rightmost image: the final outcome of the four ways dimensional resizing

Figure 260 illustrates the approach. The first two images at the top show the anterior-posterior resizing for the vertical dimension whereas the first two images at the bottom show the dorsal-ventral resizing for horizontal dimension. The adoption of the approach implied that sampling points should be sampled from the centre of a key cross section instead of the bone point. This could easily be achieved by determining the centre of a key cross section (the centre of the bounding box of the key cross section) and finding the intersections between the key cross section and 16 unit vector (see Figure 257) that originated from the centre of the key cross section.

Figure 256 shows steps to resize key cross sections of a 3D scanned arm. Detail of each step is discussed in the following:

- i) *Measuring the dimensions of key cross sections from the closest match and a 3D scan data in detail.* The first step to resize key cross sections was to measure the dimensions of the key cross sections from the closest match and 3D scan data in detail. Four dimensions, shown in Figure 261 were measured for each key cross section. The four dimensions of a key cross section consisted of anterior, posterior, dorsal and ventral

dimensions of its bounding box. For instance, the four dimension of UAF at 135° consisted of $UAF_{y_1}^{135^\circ}$ (anterior), $UAF_{y_2}^{135^\circ}$ (posterior), $UAF_{x_1}^{135^\circ}$ (medial) and $UAF_{x_2}^{135^\circ}$ (lateral).

For each key cross section, there were 16 dimensions that were measured from the closest match and 4 dimensions that were measured from a 3D scanned arm data. For example, for UAF, the dimensions that were obtained from the closest match were:

$UAF_{y_1}^{full\ extension}$, $UAF_{y_1}^{135^\circ}$, $UAF_{y_1}^{90^\circ}$, $UAF_{y_1}^{maximum\ flexion}$, $UAF_{y_2}^{full\ extension}$, $UAF_{y_2}^{135^\circ}$, $UAF_{y_2}^{90^\circ}$, $UAF_{y_2}^{maximum\ flexion}$, $UAF_{x_1}^{full\ extension}$, $UAF_{x_1}^{135^\circ}$, $UAF_{x_1}^{90^\circ}$, $UAF_{x_1}^{maximum\ flexion}$, $UAF_{x_2}^{full\ extension}$, $UAF_{x_2}^{135^\circ}$, $UAF_{x_2}^{90^\circ}$, $UAF_{x_2}^{maximum\ flexion}$; whereas the dimensions that were obtained from the 3D scanner arm data were $UAF_{y_1}^{full\ extension^{3D\ scanned\ arm}}$, $UAF_{y_2}^{full\ extension^{3D\ scanned\ arm}}$, $UAF_{x_1}^{full\ extension^{3D\ scanned\ arm}}$ and $UAF_{x_2}^{full\ extension^{3D\ scanned\ arm}}$.

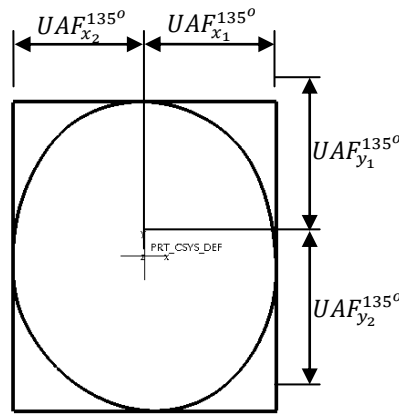


Figure 261. Example of the four dimensions of a key cross section's bounding box

- ii) *Extracting dimension changes.* Once the entire set of dimensions was obtained for UAF, UAM, LAM and LAF of 3D scan data and closest match, the “dimension changes” of UAF, UAM, LAM and LAF was established. The dimension changes were expressed as ratios of the new dimension value of 3D scanned arm to the original dimension value of 3D scanned arm. The new dimension value of the 3D scanned arm was defined as a sum of the dimension differences (between closest match's other key postures and closest match's fully extended arm) and the original dimension value of 3D scanned arm. For each key cross section, there were four dimension changes. For instance, dimension changes of UAF for 90° flexion would be:

$$ratio_UAF_{x_1}^{full\ extension-90^\circ} = \frac{(UAF_{x_1}^{90^\circ} - UAF_{x_1}^{full\ extension}) + UAF_{x_1}^{full\ flexion^{3D\ scanned\ arm}}}{UAF_{x_1}^{full\ flexion^{3D\ scanned\ arm}}}$$

$$ratio_UAF_{x_2}^{full\ extension-90^\circ} = \frac{(UAF_{x_2}^{90^\circ} - UAF_{x_2}^{full\ extension}) + UAF_{x_2}^{full\ flexion^{3D\ scanned\ arm}}}{UAF_{x_2}^{full\ flexion^{3D\ scanned\ arm}}}$$

$$ratio_UAF_{y_1}^{full\ extension-90^{\circ}} = \frac{(UAF_{y_1}^{90^{\circ}} - UAF_{y_1}^{full\ extension}) + UAF_{y_1}^{full\ flexion^{3D\ scanned\ arm}}}{UAF_{y_1}^{full\ flexion^{3D\ scanned\ arm}}}$$

$$ratio_UAF_{y_2}^{full\ extension-90^{\circ}} = \frac{(UAF_{y_2}^{90^{\circ}} - UAF_{y_2}^{full\ extension}) + UAF_{y_2}^{full\ flexion^{3D\ scanned\ arm}}}{UAF_{y_2}^{full\ flexion^{3D\ scanned\ arm}}}$$

Dimension changes were calculated for UAF, UAM, LAM and LAF of the predicted key postures i.e. 135°, 90°, and fully flexed arm.

iii) *Applying dimension changes to UAF, UAM, LAM and LAF of 3D scanned arm.* Dimension changes were then used to resize UAF, UAM, LAM and LAF of a 3D scanned arm. Horizontal dimension changes were used to resize the horizontal dimensions of the cross sections of 3D scan data and likewise for vertical dimension changes. Figure 262 illustrates this process. To resize horizontal dimensions, dimension changes were multiplied to x element of sampling points' coordinates of 3D scanned arm, with the exceptions of initial point and sample point 9. To resize vertical dimensions, dimension changes were multiplied to y element of sampling points' coordinates of 3D scanned arm, with the exception of sample point 5 and 13. x elements of sample points' coordinates that were enclosed with solid lines were subject to be scaled using horizontal dimension changes. y elements of sample points' coordinates that were enclosed in dashed lines were subject to be scaled using vertical dimension changes. This principle was the same as that depicted in Figure 260.

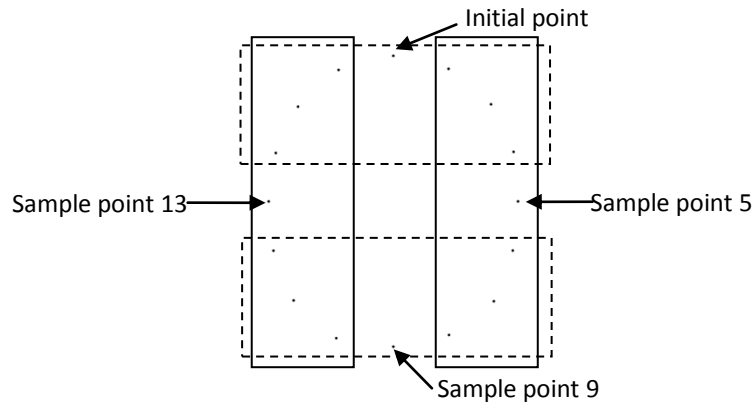


Figure 262. Initial point and sample point 9 remain constant during the scaling of horizontal dimensions, whereas sample point 5 and 13 remained constant during the scaling resizing of vertical dimension

For instance, to predict UAF at 90°, $ratio_UAF_{x_1}^{full\ extension-90^{\circ}}$ and $ratio_UAF_{x_2}^{full\ extension-90^{\circ}}$ would be used to resize $UAF_{x_1}^{full\ flexion^{3D\ scanned\ arm}}$ and $UAF_{x_2}^{full\ flexion^{3D\ scanned\ arm}}$; whereas $ratio_UAF_{y_1}^{135^{\circ}-90^{\circ}}$ and $ratio_UAF_{y_1}^{135^{\circ}-90^{\circ}}$ were applied to $UAF_{y_1}^{full\ flexion^{3D\ scanned\ arm}}$ and $UAF_{y_2}^{full\ flexion^{3D\ scanned\ arm}}$.

$$UAF_{x_{sample\ point\ 2..sample\ point\ 8}}^{90^{\circ}predicted} = UAF_{x_{sample\ point\ 2..sample\ point\ 8}}^{full\ flexion^{3D\ scanned\ arm}} \times ratio_{UAF_{x_1}}^{full\ extension-90^{\circ}}$$

$$UAF_{x_{sample\ point\ 10..sample\ point\ 15}}^{90^{\circ}predicted} = UAF_{x_{sample\ point\ 10..sample\ point\ 15}}^{full\ flexion^{3D\ scanned\ arm}} \times ratio_{UAF_{x_2}}^{full\ extension-90^{\circ}}$$

$$UAF_{Y_{\text{sample point 14}} \dots \text{sample point 4}}^{90^\circ \text{predicted}} = UAF_{Y_{\text{sample point 14}} \dots \text{sample point 4}}^{\text{full flexion}^{3D \text{ scanned arm}}} \times \text{ratio}_{UAF_{Y_1}}^{\text{full extension}-90^\circ}$$

$$UAF_{Y_{\text{sample point 6}} \dots \text{sample point 12}}^{90^\circ \text{predicted}} = UAF_{Y_{\text{sample point 6}} \dots \text{sample point 12}}^{\text{full flexion}^{3D \text{ scanned arm}}} \times \text{ratio}_{UAF_{Y_2}}^{\text{full extension}-90^\circ}$$

9.6.2.2 Predicting E key cross sections at 135°, 90° and maximum flexion

The second part of the key cross section prediction method was to predict E at 135°, 90° and maximum flexion. The prediction method for the E cross sections was based on the suggestion that were drawn from one of the key findings in the fourth issue of the study in section 9.6.1. The suggested approach involved predicting E by performing interpolation of two closest matches from the database. To accommodate the real time modelling specification, linear interpolation was chosen due to its simplicity. To realise this approach, the shape of E from all individuals in the database had to be stored. As had been described in the key finding from the third issue of the study in section 9.6.1, the amount of data to be stored would be $N \times 320$ for each individual in the database. With this amount of data, even if storage capacity was of no concern, data analysis and processing would likely become a problem when the number of individuals in the database increased. Following the suggestion given in the second important finding from the section 9.6.1, this research proposed data compression.

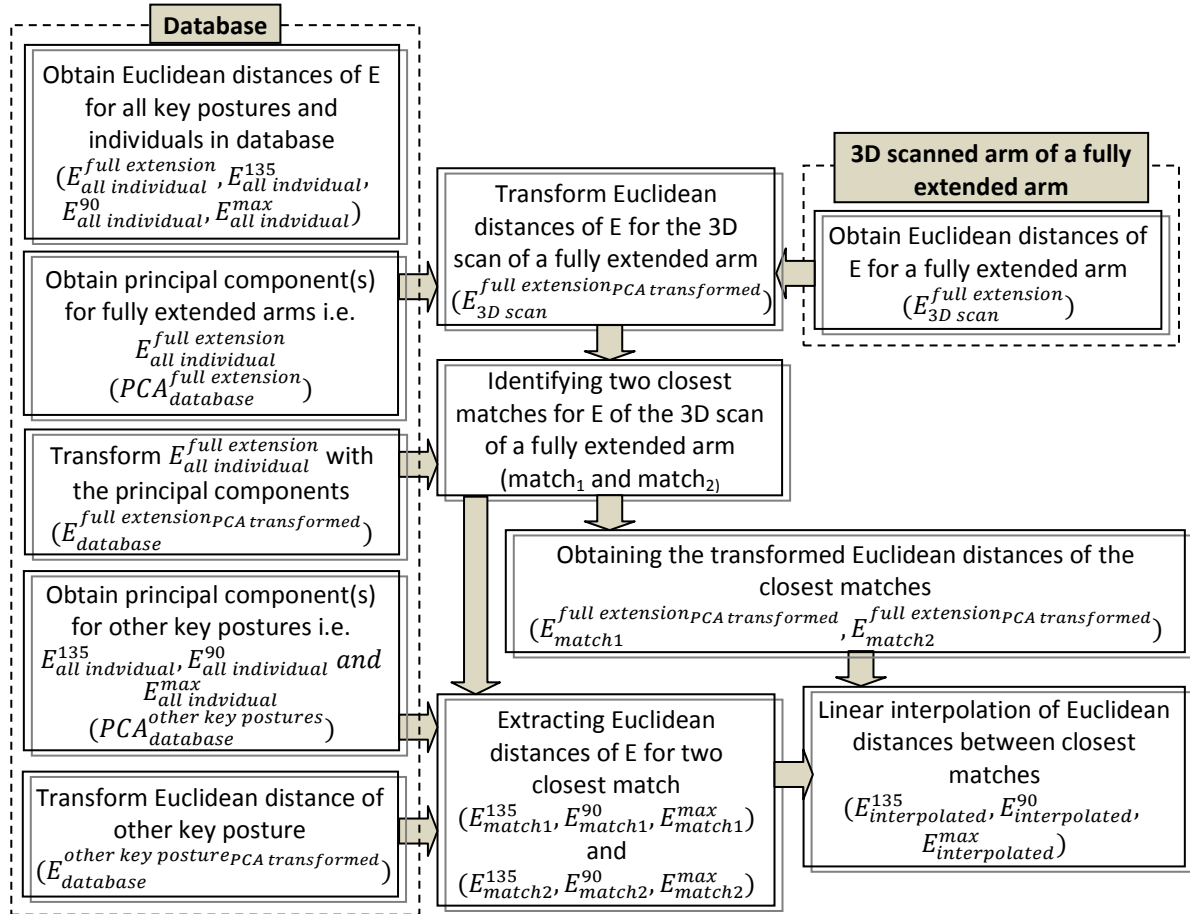


Figure 263. The proposed prediction method for E utilised the database and the 3d scan of a fully extended arm

A mathematical procedure called Principal Component Analysis (PCA) was proposed. PCA is a procedure of transforming correlated variables into a smaller number of uncorrelated variables. Principal Component Analysis was used to reduce the number of data while at the same time maintain the variation within the data set. PCA creates and ranks a new set of variables, so called “Principal Components”, which represent and weighs the variation within the original data set (Jolliffe, 2002). Once the principal components were established, the original data could be transformed and their number could be reduced and hence minimise the amount of data to be stored and analysed. The original data could be re-obtained by using the Principal Components to re-transform the transformed value. Reduction in the number of data was achieved by choosing a limited number of principal components that represented major variation within the data and discarding remaining principal components. Thus, extreme reduction in the data could be achieved by usage of only a small number of the principal components and vice versa. However, using a smaller number of the principal components also meant that some of the detail would be lost, especially when the variation within the dataset is large. To anticipate this, this research introduced a 90% limit. The 90% limit meant that the number of principal components chosen should be able to depict 90% of the variation within the dataset. By applying PCA onto the original data, subsequent processes such as finding the closest match for E would be simpler because the number of data is reduced. Further information and procedure details of PCA could be found further in Jolliffe (2002).

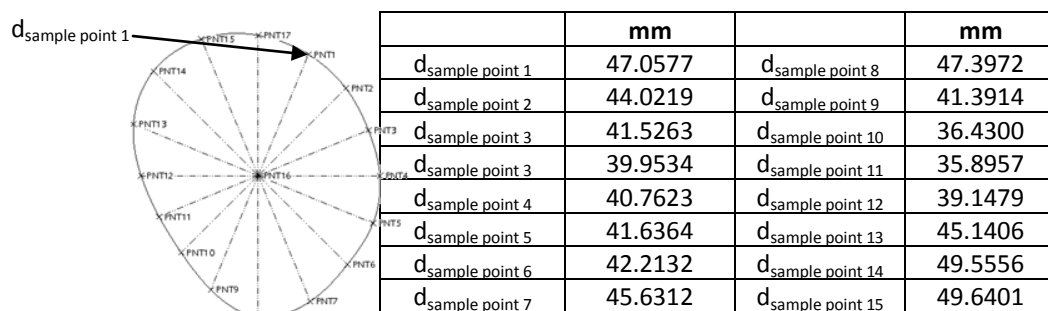


Figure 264. Expressing the 16 sample points as distances towards the centre of E's bounding box

Figure 263 shows details of the proposed method to predict E. As shown in Figure 263, prior to the application of the proposed prediction method, the 16 sample points of E for both data from individuals in the database and from the 3D scanned arm would have to be expressed as Euclidean distances towards the centre of E. Expressing the cross sections in Euclidean distances allowed the application of PCA. Figure 264 shows an example of Euclidean distances of the 16 sample points towards the centre of E^{90} 's bounding box ($E_{individual\ 1}^{90}$).

Once the Euclidean distances of the 16 sampling points were obtained, the next step was to reduce the number of Euclidean distances of the 3D scanned arm's E by transforming them through principal components ($E_{3D\ scan}^{full\ extension_{PCA\ transformed}}$). The transformation was also performed to the

entire E of a fully extended arm in the database ($E_{database}^{full\ extension\ PCA\ transformed}$). As there were 16 Euclidean distances for each E and n individuals for each gender and race, there were 16 variables and 16n data which needed to be transformed. Once the principal components of fully extended arms from data from individuals in the database were calculated and chosen, they were then used to transform the E of the 3D scan of a fully extended arm ($E_{3D\ scan}^{full\ extension\ PCA\ transformed}$). Figure 266 shows an example of the transformed values by utilising principal components which represented 90% of the 16 Euclidean distances of E of fully extended arms from participant 1 to participant 4 (shown in Figure 265). As shown in Figure 266, the 16 Euclidean distances were simplified into 1 value as there is only one principal component being chosen.

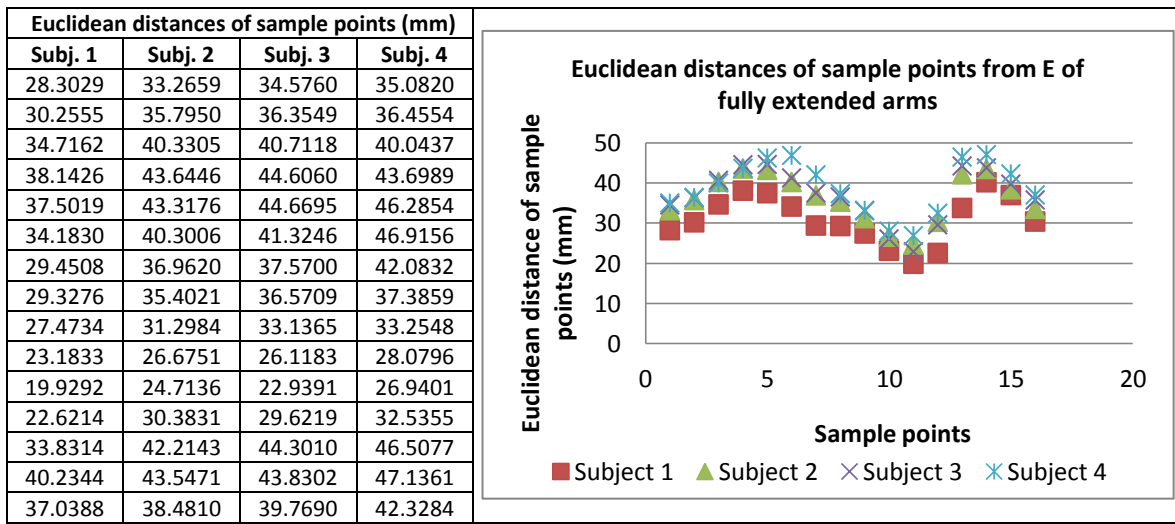


Figure 265. Euclidean distances of E of fully extended arms from participant 1 to participant 4

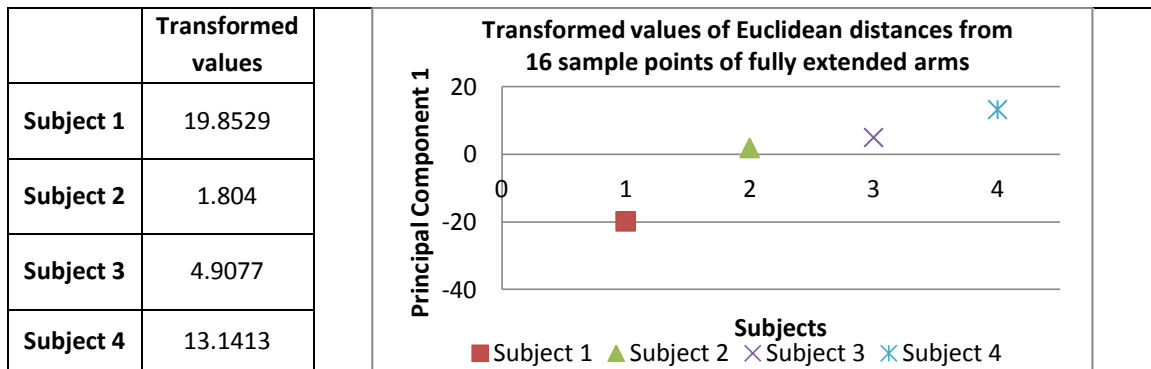


Figure 266. Principal component which represent 90% of variation among the Eulclidean distances from participant 1 to participant 4

By performing the above steps, E of both the database and 3D scanned arm data could be compared easily. The comparison would result in the identification of two closest matches for E ($match_1, match_2$). The steps to identify the two closest matches were similar to those described in Figure 261. In addition to identifying the two closest matches, the Euclidean distances between E of the 3D scanned arm and the two closest matches would also be noted

$(d_{match1}^{3D\ scan}, d_{match2}^{3D\ scan})$. As shown in Figure 263, Euclidean distances of E for full extension, 135°, 90° and maximum flexion were extracted from the individuals who were the closest matches i.e. $E_{match\ 1}^{135}$, $E_{match\ 1}^{90}$ and $E_{match\ 1}^{max}$ for $match_1$; and $E_{match\ 2}^{135}$, $E_{match\ 2}^{90}$ and $E_{match\ 2}^{max}$ for $match_2$. Also, the ratio of the transformed Euclidean distances of 3D scanned arm ($E_{3D\ scan}^{full\ extension\ PCA\ transformed}$) with respect to the transformed Euclidean distances of two closest matches ($E_{match\ 1}^{full\ extension\ PCA\ transformed}$ and $E_{match\ 2}^{full\ extension\ PCA\ transformed}$) would be calculated. The ratio was calculated by following the equation below:

$$ratio = \frac{(E_{3D\ scan}^{full\ extension\ PCA\ transformed} - E_{match\ 1}^{full\ extension\ PCA\ transformed})}{(E_{match\ 2}^{full\ extension\ PCA\ transformed} - E_{match\ 1}^{full\ extension\ PCA\ transformed})}$$

The ratio was then used to perform linear interpolation on the Euclidean distances of the two closest matches. For each Euclidean distance and each key posture, the following equation was applied:

$$\begin{aligned} d_i^{135\ prediction} &= ratio * (d_i^{135\ match2} - d_i^{135\ match1}) + d_i^{135\ match1} \\ d_i^{90\ prediction} &= ratio * (d_i^{90\ match2} - d_i^{90\ match1}) + d_i^{90\ match1} \\ d_i^{max\ prediction} &= ratio * (d_i^{max\ match2} - d_i^{max\ match1}) + d_i^{max\ match1} \end{aligned}$$

The interpolated Euclidean distances were then used to create the predicted E of 135°, 90° and maximum flexion.

9.7 Predicting profiles at 135°, 90° and maximum flexion

The synthesis process for five key cross section and profiles were essentially similar. The reason behind this similarity was the fact that both, based on the limited information from 3D scan data, had to create different shapes of either cross sections or profiles for the required key postures. Thus, the synthesis process for a profile also required additional data i.e. profiles of individuals at four key postures, to be stored in the database. Given the profile of the 3D scan of a fully extended arm, a closest match of the 3D scan of a fully extended arm could be identified from the database. Once the closest match was identified, the closest match's profiles at 135°, 90° and maximum flexion from the database were extracted and used to assist the synthesis of 3D scan data's profiles.

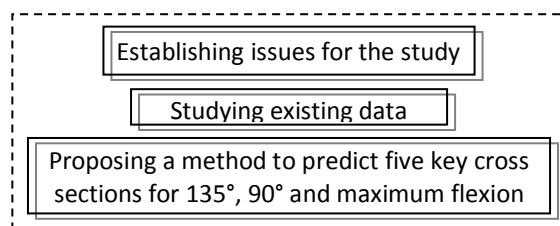


Figure 267. Strategy to develop a prediction method of five key cross sections for 135°, 90° and maximum flexion

Figure 267 shows the strategy which was used to propose a method to predict profiles at 135°, 90° and maximum flexion. This strategy was similar to the strategies in section 9.5 and 9.6, which were utilised to propose the prediction method for key cross sections' locations and shapes. The first step of the strategy, as shown in Figure 267, was to establish issues for the study. There were 7 issues which needed to be studied to predict profiles at 135°, 90° and maximum flexion. These were:

1. *The extent to which profiles should be predicted (e.g. whole profile, FDA only).* By studying this issue, the prediction method could be optimised through focusing the effort only for the part of profile which was essential for the new FDM.
2. *Profiles compatibility between a 3D scanned arm and the new FDM.* It was of importance that this issue was investigated as the profile of the 3D scan data was used to identify the closest match from the database which stored profiles that were acquired based on the new FDM's existing approach i.e. using side view photographs.
3. *Current approach of the new FDM to represent profiles.* Studying this issue helped ensure the compatibility between profiles of 3D scan data and the database.
4. *The amount of data to store profiles.*
5. *The shape variation of profiles from one person to another and from one key posture to another.* An understanding on this issue would allow a more thorough and accurate decision regarding the final prediction method.
6. *The effect of BMI on the shape of profiles.*
7. *The effect of body size on the shape of profiles.*

Similar to the section 9.5 and 9.6, the existing five participants' data, which was already described in section 9.3, was utilised to study each of the issues above. Also, upon completion of the study, key findings of the study would be identified and used to form suggestions that guided the proposed method to predict profiles at 135°, 90° and maximum flexion. Section 9.7.1 outlines the strategy and result of the study for each issue whereas section 9.7.2 outlines the proposed method to predict profiles at 135°, 90° and maximum flexion.

9.7.1 Study on profiles of all key postures

The first issue of the study concerned the extent to which a profile should be predicted. Referring back to the new FDM, it was shown that the profile at the flesh deformation area (FDA) was the part of the profile which was required by the new FDM (see Figure 268). This suggested that the predicted profile at 135°, 90° and maximum flexion should encompass the FDA. Thus, limiting the prediction of a profile only for the FDA might seem to be the best option. However, this also meant that the profile prediction was based upon the result of the FDA prediction i.e. the prediction of the UAF and LAF locations in section 9.5.2. Although this was possible, any inaccuracies in the

FDA prediction would have an impact on the profile prediction and result in accumulation of error. Based on this reasoning, the FDA was not suggested as a parameter to limit the extent to which a profile should be predicted.

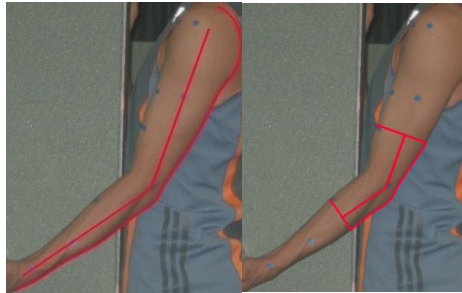


Figure 268. The whole extent of profile compares to the actual profile that is used in the new FDM

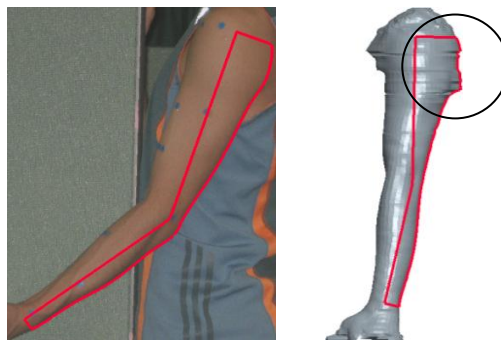


Figure 269. Using the whole length of upper and lower arm as the limit of the profile would eliminate the effect of FDA on the profile (left image, bold lines). However, the profile of the 3D scanned arm is prone to distortion especially around the shoulder area (right image, bold lines)

Another possible parameter candidate to limit the extent of the profile was the shoulder and the wrist i.e. the whole length of the upper and lower arm, as shown in the left image in Figure 269. However, the existing results of the 3D scanned arm from the five participants, which were obtained in section 8.1.2, suggested that there was considerable amount of distortion to the profile area especially around the shoulder, as shown in the right image in Figure 269. Similar to the prediction of the five key cross sections, the 3D scan would be used as a source to find the closest match in the database. Thus, if the profile of the 3D scanned arm was distorted, it was likely that this would lead to an incorrect identification of the closest match.

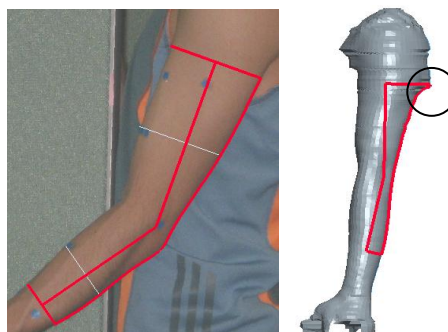


Figure 270. Using 2/3 of the upper and lower arm length as the limit of the profile would minimise the distortion of the 3D scanned arm's profile around the shoulder and yet ensure that profile for the flesh deformation area is included

A compromise between the two previous options was 2/3 of the upper and lower arm length, as shown in Figure 270. Using 2/3 of the upper and lower arm length meant that the distortion of the profile at the shoulder could be minimised (see right image in Figure 270) and yet it would ensure that the profile would include the FDA (see left image in Figure 270). A brief analysis on the FDA of the five participant showed that FDA was always less than 2/3 of the upper and lower arm length for any key posture. As shown in Table 23, the ratio between the UAF location or LAF location with upper arm length or lower arm length, respectively, was always less than 0.66 i.e. 2/3 of the upper and lower arm length. This suggested that using 2/3 of the upper and lower arm length was a potential parameter to limit the extent to which a profile should be predicted.

Table 23. FDA, which determines the location of UAF and LAF, is always less than 2/3 of the upper and upper arm length for all participant and key postures

	UAF location (mm)	LAF location (mm)	Upper arm length (mm)	Lower arm length (mm)	UAF location/Upper arm length	LAF location/Lower arm length
Participant 1	90.9002	89.8831	224.258	208.77276	0.405337602	0.430530784
	93.8135	96.6611			0.418328443	0.462996706
	97.3546	98.4946			0.434118738	0.471778982
	102.4564	107.8786			0.456868428	0.516727375
Participant 2	95.1999	87.2079	288.848	273.0775	0.329584764	0.319352199
	99.3647	89.5805			0.34400342	0.328040575
	104.3686	92.2678			0.361327065	0.337881371
	110.3223	110.0567			0.381938944	0.403023684
Participant 3	109.2034	93.1262	274.156	245.1163	0.398325771	0.37992659
	113.6644	107.0805			0.414597528	0.436855892
	117.4842	108.3353			0.428530472	0.441975095
	120.8744	128.8079			0.440896424	0.52549708
Participant 4	107.2576	90.5622	272.805	241.9534	0.393165814	0.374296042
	109.5941	109.0946			0.40173054	0.450890957
	113.4357	114.5424			0.415812393	0.473406863
	119.2298	130.2075			0.437051374	0.538151148
Participant 5	97.0519	89.6357	240.817	217.6163	0.403011	0.411897914
	102.0999	98.1357			0.423973141	0.450957488
	102.971	107.3357			0.427590162	0.493233733
	104.0598	109.392			0.432111396	0.502682933

The second issue of the study concerned the compatibility between the profile of the new FDM and a 3D scanned arm. As described briefly in section 9.7.1, the profile of the new FDM was acquired following the method in 7.3.2.5 which required side view photographs of key postures. The side view photograph was essentially a 2D projection of an arm to the side view plane and required the arm to be in a certain orientation with respect to this plane. Thus, a different orientation of the arm with respect to the side view plane would generate a different shape of profile. To ensure the compatibility between a profile from a 3D scanned arm and a profile from a side view photograph, the 3D scanned arm should also adopt the same orientation as that of the side view photograph. Figure 271 showed that the orientation of a 3D scanned arm with respect to the side view plane was not the same as that of the side view photograph. This suggested that the profile of a 3D scanned

arm was not automatically compatible with the profile of the new FDM and further effort was required ensure each other's compatibility.

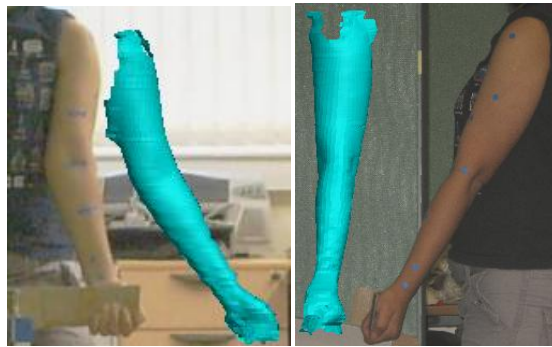


Figure 271. The orientation of the 3D scanned arm is not the same as that in the side view and front view photograph which would result in compatibility

The third issue to be studied concerned the current approach of the new FDM to represent profiles. Section 7.3.2.5, which described the method to obtain and represent a profile for the new FDM, was revisited to study this issue. As described in section 7.3.2.5, through a process so called “quantification”, each profile was represented as distances between a finite number of points on the profile and the bones, as shown in Figure 272. The number and placement of points on the profile was determined through optimisation to ensure that they could represent profiles from different key postures and individuals with the least error. To ensure the compatibility with the current approach of the new FDM, the existing method to represent a profile should be adopted. Also, in conjunction with the suggestion given from the first study, only 2/3 of the upper and lower arm profile would need to be represented as distances between points on the profile and the bones.

Distance between one of the points
on the profile and the bone

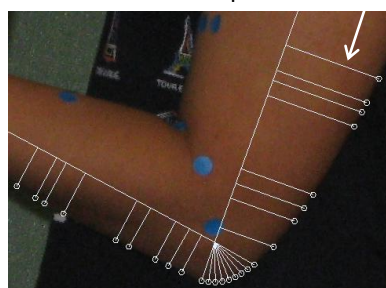


Figure 272. Optimum number and placement of points on the profile for the five participants' data

The fourth issue of the study concerned the amount of data to be stored. If the optimum number and placement of points was found to be x and the total number of individuals in the database was n , the amount of profile data to be stored for all key postures would be: $x_{distance} \times n \times 4$. This meant that the amount of profile data to be stored would increase as the number of individuals in the database increased, even with a constant number of points on the profile. As described in section 9.6.1, an increase in the number of data could have adverse impact on the

ability of the framework to accommodate the real time modelling specification. Therefore, the amount of data to be stored should be reduced.

To study the fifth issue i.e. shape variation of profiles from one person to another and from one key posture to another, visual observation was performed on two areas. Discussion for each observation is given in the following:

i. Visual observation of variation of the profiles for each key posture among the participants.

Adopting the suggestion from the first issue of the study, 2/3 of the upper and lower arm length was used as the limit of the extent of the profiles. For the visual observation, all of the profiles were arranged such that the upper arm bones were aligned. This process was performed for each key posture on all participants. Figure 273 shows two profiles of a fully flexed arm before and after the alignment. As shown in Figure 273, the alignment of the upper arm bones resulted in the alignment of the lower arm provided the arm angle of both profiles were similar.

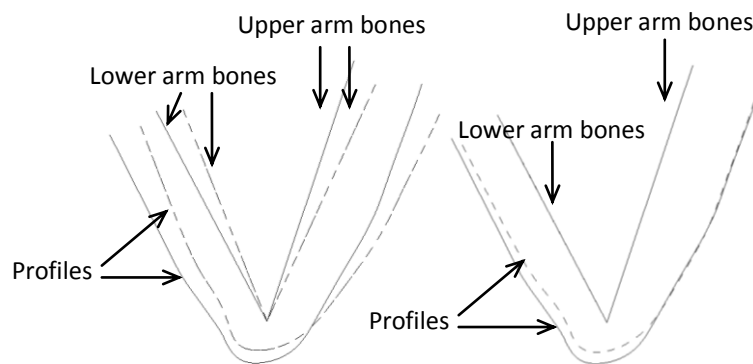


Figure 273. The profile of a fully flexed arm from participant 2 and participant 3 before and after the upper arm alignment took place

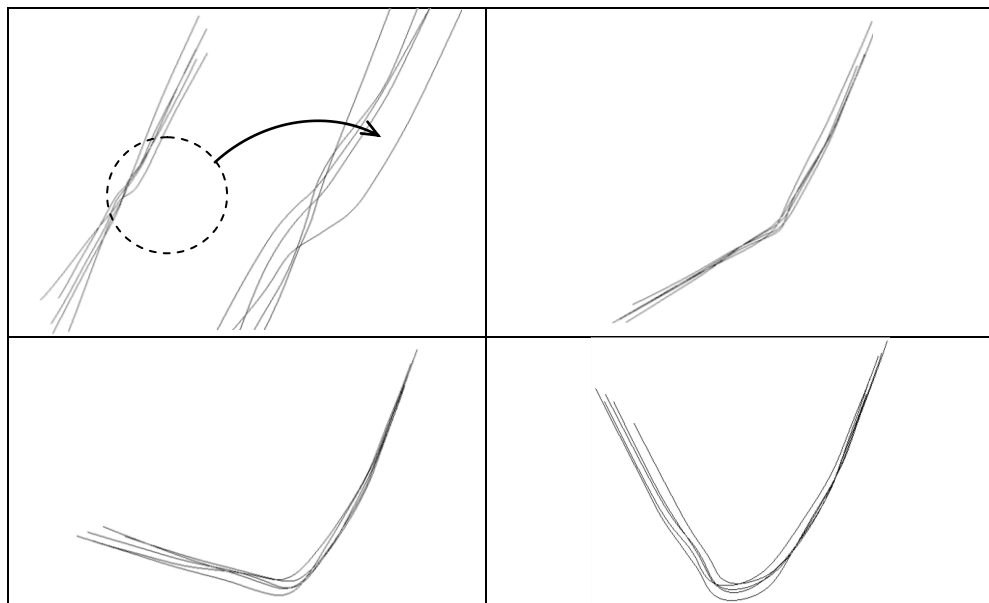


Figure 274. Images of profiles of four key postures from five participants show that although variation occurs, a general pattern or shape is also apparent for each key posture

The complete result of the profile comparison, shown in Figure 274, suggested that, for all key postures, the degrees of inclination of the upper and lower arm profiles varied among participants. Figure 275 shows a clear example of inclination difference on the upper and lower arm profile from two participants for profiles at 135°. The upper and lower arm profile inclination difference was likely caused by two factors i.e. arm angle and arm size difference. The effect of the first factor i.e. arm angle difference was apparent on the lower arm profiles of fully extended and flexed arms where arm angles of fully extended and flexed arm angle varied from one person to another. For instance, the arm angle of full extension and flexion for participant 1 were 154.7° and 34.6°, respectively, whereas the arm angles for participant 2 were 160.2° and 33.7° (see Table 6 in section 8.1.3 for complete data of arm angle values from the five participants). The top left and bottom right images in Figure 274, which depict profiles of all participants for fully extended and flexed arms, demonstrate how different angles for full extension and flexion resulted in different degrees of inclination of the lower arm profiles.

The second factor that caused different degrees of inclination of the arm profile was arm size difference. Arm size difference mainly occurred due to the differences in body size and body type. The effect of the arm size difference on the inclination was apparent for both upper and lower arm profiles. A good example of the arm size effect is shown by the images in Figure 275 which demonstrated the presence of inclination difference despite similar arm angles (135°).

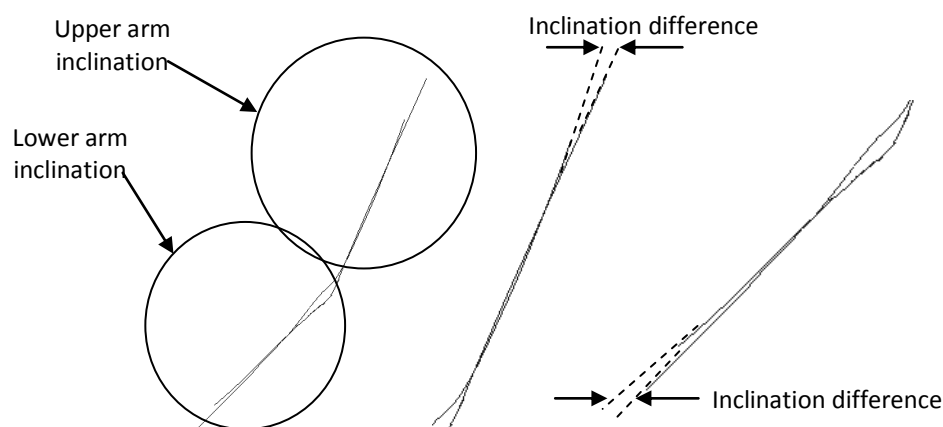


Figure 275. Images show how inclination of profiles from two participants is different for profiles at 135°. Middle image shows inclination difference for upper arm whereas the image at the most right shows the inclination difference for the lower arm

- ii. *Visual observation of how the profile changed from one key posture to another for each participant.* The complete results of how the profile changed as the arm flexed are shown in Figure 276.

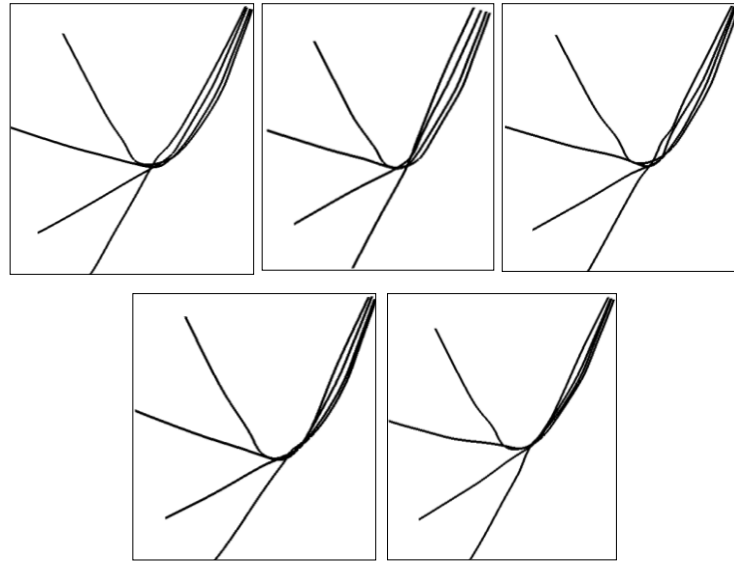


Figure 276. Images show how the profile changes from one key posture to another for all participants

For all of the participants, the results showed that the inclination of the upper arm's profile changed gradually as the arm flexed. The result also showed that the gradual inclination was dependent on the upper arm inclination of the fully extended arm as none of the upper arm inclination at 135°, 90° and maximum flexion intersected the upper arm inclination of the fully extended arm.

The sixth issue of the study concerned the effect of body size on the profile. To study the effect of body size on profiles, a profile of participant 1, who had the smallest body size, was compared to the rest of the participants and visually observed. The result is shown in Figure 277 with the bold line indicating the profiles of participant 1. The result demonstrated that the profile of participant 1 was the shortest in comparison to the rest of participants. This suggested that body size affected profiles. The result also showed that the profile for the 90° and maximum flexion of participant 1 seemed to be the scaled version of other participants' profiles.

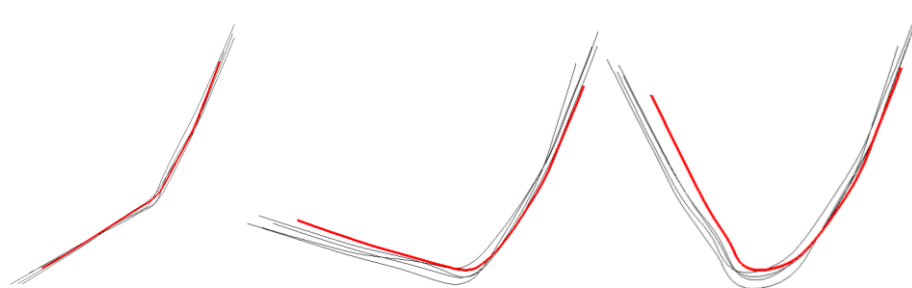


Figure 277. Comparison between the profiles of participant 1 (bold lines) and the rest of the participants for 135°, 90° and maximum flexion (left to right)

The last issue of the study concerned the effect of BMI on profiles. To study the effect of BMI on profiles, profiles from participants 3 and 4, who had similar height but different weight, were compared and visually observed. The result, as shown in Figure 278, demonstrated that there was difference between them. The difference could be observed on the profiles of a fully extended, 135°

and 90° flexion arm. Participant 3, who had lower BMI, showed more details i.e. curvature in the elbow area compared to participant 4 who had higher BMI. Although the difference existed, it was observable mainly at the elbow area.

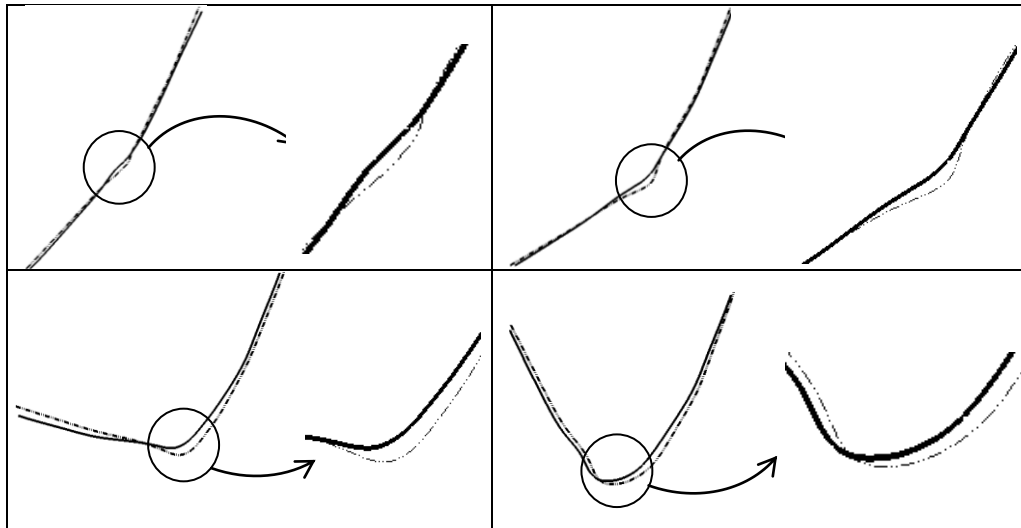


Figure 278. Profile comparison between participant 3 (dash line) and participant 4 (solid lines) for all key postures

From the studies about the profiles from all key postures, several key findings were identified. The following numbered bullet points outline key findings of the study and analyse their implication upon the prediction method:

1. The extent to which profiles should be predicted

The study revealed that a profile should at least encompass the flesh deformation area in order to comply with the requirements of the new FDM. The study suggested the use of up to 2/3 of the length of upper and lower arm profile to limit the extent to which a profile should be predicted. The adoption of this limit meant that the optimum number and placement of points of the profile had to be re-established as previously they had only been established for the FDA exclusively. Thus, the optimum number and placement of points were re-established by adopting the approach previously described in section 7.3.2.5 which determines the points with the least error in representing the profiles from all of the participants and all key postures. Once the optimum number and placement of points on a profile was established, they could be used to represent profiles of the framework (database and 3D scan data) as distances between these points and the bones.

2. Profiles compatibility between a 3D scanned arm and the new FDM

The study showed that a profile of a 3D scanned arm was not automatically compatible with the new FDM's profile. The incompatibility was a result of orientation difference between the 3D scanned arm and the arm of the side view photograph with respect to the side view plane. It was important that profile compatibility was met between the two as it would ensure the closest match of the profile of a 3D scanned arm was correctly identified from

the database. Thus, a re-orientation of the 3D scanned arm to match the arm's orientation of the side view photographs was suggested to ensure the compatibility between the profile of a 3D scanned arm and the new FDM profile.

To accommodate the re-orientation of a 3D scanned arm, a "template" concept was suggested. The template assisted positioning and orientating a 3D scanned arm so that it mimicked the arm posture of the side view photographs from which a profile for the database was obtained. In addition to this, the template concept was also useful to maintain the consistency in sampling the points for the cross sections. The reorientation of the 3D scanned arm would likely involve translation and rotation. To aid the reorientation, the template could include joint information of an arm that matched the arm's orientation of the side view photographs of the new FDM. The template's joint information would guide the translation and the rotation of the 3D scanned arm so that its upper arm joint location coincided with that of the template. Since the carrying and arm angle of a fully extended arm varied from one person to another, the lower arm joint could not be used to help the reorientation of the 3D scan data. However, solely overlapping the upper arm bone did not guarantee that the lateral-medial orientation between the template and a 3D scanned arm was the same. Thus, it was suggested the template should also include cross sections to refine the lateral-medial orientation of the 3D scan data.

3. Current approach of the new FDM to represent a profile

The study showed that distances between points on a profile and its bones were used to represent a profile in the new FDM. As described earlier in the key finding's analysis of the first issue of the study, the same approach of the profile representation as that of the new FDM was suggested for the framework to ensure the suitability with the new FDM. Representing a profile as distances between points on the profile and its bones also presented a possibility to predict profiles at 135°, 90° and maximum flexion through the modification of distances between points on the profile of the 3D scan of a fully extended arm and its bones. This could be achieved by establishing how distances of points on the closest match's profiles toward the bones changed from one key posture to another and subsequently applied these changes to distances between points on the profile of the 3D scan of a fully extended arm and its bones. Table 24 shows a case example to illustrate this possibility.

Table 24. Distances for the case example, where the distances of 135° of the 3D scanned arm is predicted by direct application of $d_{135}^{CM}-d_{max\ extension}^{CM}$ (closest match data) to is $d_{max\ extension}^{3D}$ (3D scan data)

$d_{max\ extension}^{CM}$	d_{135}^{CM}	$\Delta = d_{135}^{CM}-d_{max\ extension}^{CM}$	$d_{max\ extension}^{3D}$	$d_{135}^{predicted} = \Delta + d_{max\ extension}^{3D}$
39.3813	42.5854	3.2041	41.0328	44.2369
34.6141	40.1714	5.5573	34.5872	40.1445
32.7791	39.1111	6.332	32.2756	38.6076
30.4379	37.4562	7.0183	29.497	36.5153
28.2235	31.5079	3.2844	25.1253	28.4097
27.7933	30.0453	2.252	24.022	26.274
27.1796	28.5808	1.4012	22.7178	24.119
24.8252	25.4329	0.6077	18.1292	18.7369
21.9588	22.8955	0.9367	14.7893	15.726
21.5356	22.4296	0.894	14.5972	15.4912
21.1446	22.0811	0.9365	14.4284	15.3649
20.7836	21.8415	1.0579	14.2732	15.3311
20.4547	21.6562	1.2015	14.1309	15.3324
20.1574	21.5701	1.4127	14.0111	15.4238
19.8908	21.5457	1.6549	13.9117	15.5666
19.6646	21.6046	1.94	13.8232	15.7632
19.4587	21.731	2.2723	13.7452	16.0175
18.8455	22.4773	3.6318	13.342	16.9738
19.5997	22.322	2.7223	13.8934	16.6157
20.2229	21.9234	1.7005	15.3891	17.0896
20.2485	21.753	1.5045	18.8532	20.3577
20.3709	22.0237	1.6528	19.8711	21.5239
21.5448	23.9174	2.3726	22.5102	24.8828
23.4278	25.0209	1.5931	25.6806	27.2737
24.1241	25.205	1.0809	27.1624	28.2433
24.1775	24.7967	0.6192	28.9528	29.572

Given the distances of points on closest match's profiles towards their bones ($d_{max\ extension}^{CM}$ and d_{135}^{CM}) and the distances of points on the profile of 3D scan of a fully extended arm towards its bones ($d_{max\ extension}^{3D}$) were known; the distance changes of the closest match ($d_{135}^{CM}-d_{max\ extension}^{CM}$) could be extracted to predict the profile at 135° flexion by simply adding it into $d_{max\ extension}^{3D}$.

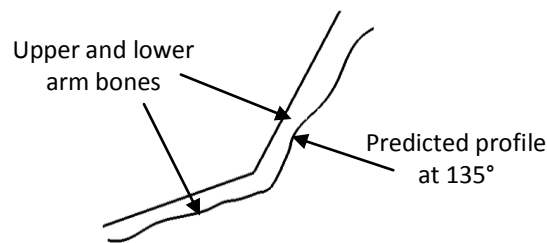


Figure 279. Result of profile prediction at 135° by direct application of distance changes i.e. $d_{135}^{CM}-d_{max\ extension}^{CM}$ to the profile of the 3D scan data i.e. $d_{max\ extension}^{3D}$

However, as shown in Figure 279, the predicted profile at 135° flexion did not produce a satisfying result. The distortion of the prediction result was due to the assumption that the profile of a fully extended 3D scanned arm ($d_{max\ extension}^{3D}$) has exactly the same arm size and arm angle as the profile of the closest match's fully extended arm ($d_{max\ extension}^{CM}$). Since this was not the case i.e. $d_{max\ extension}^{3D} - d_{max\ extension}^{CM} = \Delta$, the distortion took place. Although finding an exact match of a fully extended arm's profile from an individual was achievable, it

would be impractical as it would mean that an exact profile match for every possible individual had to be stored in the database. Thus, it was suggested that, instead of utilising the modification of the profile of a fully extended 3D scanned arm, the prediction for profiles at 135°, 90° and maximum flexion should be based on modification of the closest match's profile.

4. The amount of data to store a profile

The decision to use distances requires identification of an optimum number and placement of points on the profile was closely related to the fourth issue of the study i.e. the amount of data to be stored. The study found that for x number of points on a profile, n individuals in the database and 4 profiles for each individual, there will be $x \times n \times 4$ distances to be stored. This finding demonstrated that the size of data would expand rapidly as the number of individuals in the database increased. To avoid the effect of large amounts of data on the real time modelling ability of the framework, a reduction in the number of data were needed. To fulfil this need, Principle Component Analysis was suggested to be utilised. Principal Component Analysis was already proposed as part of the prediction method for E key cross sections at 135°, 90°, and maximum flexion in section 9.6.2. Principle Component Analysis reduced the number of data for key cross sections' (from x number of data to y number of data, where $x > y$) and assisted closest match identification. The suggestion to use Principle Component Analysis was based on the consideration that the approaches to represent a profile and E key cross section were similar i.e. using Euclidean distances between points on a profile/key cross section and reference point(s).

5. The shape variation of profiles from one person to another and from one key posture to another

The fifth issue of the study demonstrated that the inclination of the upper and lower arm profile varied from one person to another for all key postures. The study revealed that the inclination of the upper arm profile was dependent on the arm size, arm angle and the upper arm profile's inclination of a fully extended arm. The study also revealed that the inclination of the lower arm profile was dependent on the arm size and arm angle. Having these findings meant that the inclination of the closest match's profile could be modified to incorporate the effect of arm size and angle on the 3D scan data's profile. The modified closest match's profile could then be used as the predicted profiles at 135°, 90° and maximum flexion. Thus, this research suggested modification of profile inclination as a means to provide profile prediction at 135°, 90° and maximum flexion. The adjustment of the closest match's profile inclination would likely involved rotating it to match the

inclination of the 3D scan data's profile. As the inclination differences between upper and lower arm were not likely to be same, the adjustment of the closest match's profile inclination for the upper and lower arm should be performed separately. To accommodate separate profile inclination's adjustment between the upper and lower arm profile, a cut point was required. As the profiles were represented with distances between sampling points along the profile and the bones, the suggested cut point was the sampling point at the middle of the E region which divided the E region into two equal areas.

Figure 280 shows the E region, the cut point for the upper and lower arm profiles and 9 sampling vectors to acquire 9 points on the profile. Having this cut point; the inclination of the upper or lower arm could then be expressed as the gradient between the cut point and the distal point on the profile of the upper or lower arm.

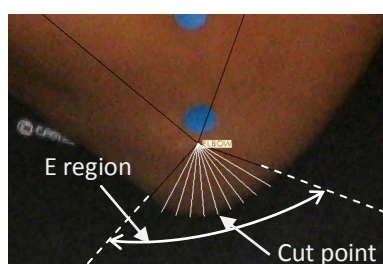


Figure 280. The cut point for upper and lower arm profiles is located at the middle of E region

6. The effect of body size

The study for this issue had identified the effect of body size on profiles. The study showed that the length of profile was linear with a change in body size. Thus, in addition to suggesting modification of the closest match's profile inclination as a means to predict profiles at 135°, 90° and maximum flexion, this research also suggested modification of the closest match's profile length i.e. scaling as additional means. Also, to incorporate the effect of body size on the profiles, the database should consist of profiles of individuals with different body sizes.

7. The effect of BMI

The study for this issue had identified the effect of BMI on profiles. The study of BMI on the profiles showed the presence of variation for the profiles of the same key posture across the five participants. To incorporate this, profiles of individuals with different body size should be collected for the database. BMI was also suggested to be used as one of possible parameter to find the closest match for the profile of the 3D scanned arm.

The analysis of the study's key findings above concluded this subsection. In the next section (section 9.7.2), guided by the suggestion that were drawn from the analysis of the study's key findings, the prediction method of the profiles at 135°, 90° and maximum flexion was proposed.

9.7.2 Proposing a method to predict profiles at 135°, 90° and maximum flexion

This section outlines the proposed method to predict the profiles at 135°, 90° and maximum flexion. The general outline of the proposed method, shown in Figure 281, depicts how the prediction of the profiles was performed separately for each race and gender. This approach was driven by the inference that was established in section 9.5.1 regarding the effect of race and gender on the predicted elements of FDM. Figure 281 also shows how the proposed method consisted of three main stages. These were: i) obtaining the profile of a 3D scanned arm; ii) finding closest match for the profile of a 3D scanned arm; and iii) predicting the profiles at 135°, 90° and maximum flexion. Details for each stage are discussed in the following.

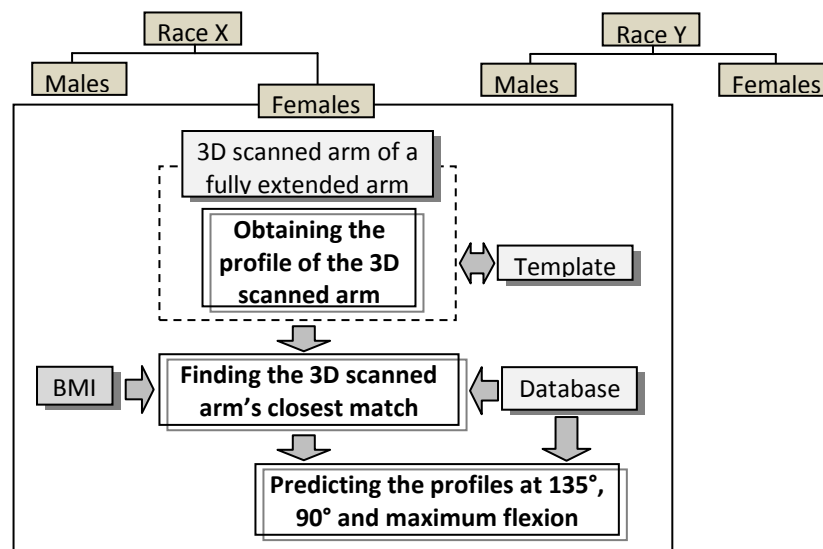


Figure 281. The general outline of the proposed method to predict the profiles at 135°, 90° and maximum flexion

9.7.2.1 Obtaining the profile of a 3D scanned arm

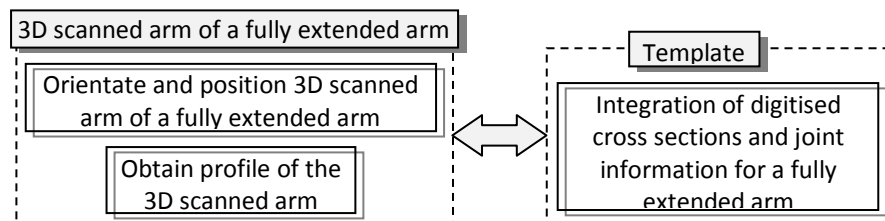


Figure 282. The template concept was introduced as a procedure to obtain the profile of a 3D scanned arm that is compatible to the database's profiles

Figure 282 illustrates the procedure for the first stage i.e. obtaining the profile of a 3D scanned arm. The first stage was related to the suggestion that was proposed based on the key finding of the third issue of the study in section 9.7.1. The key finding revealed that the profile of a 3D scanned arm and the database were incompatible unless the profile of the 3D scanned arm was obtained from the same orientation view as that of the database. The template concept was suggested as a means to obtain the profile of a 3D scanned arm that was compatible with the new FDM's profile.

The template essentially represented the orientation from which the profile of the database was obtained. Thus, the function of the template was to aid the re-orientation of the 3D scanned arm such that it had the same orientation as the arm in the new FDM.

As suggested in section 9.7.1, a template should consist of cross sections and joint information. Furthermore, a template should reflect the orientation of the arm to acquire profiles for the database. The result of the integration between the digitised cross sections and the 3D scan's joint information for a fully extended arm (see section 7.1.3) matched the suggested condition and hence would be utilised. The integration result from any participant could be used as a template. However, for this research, data from participant 1 would be used as a template as the participant had given her consent and agreed to volunteer if any more data or measurement was required.

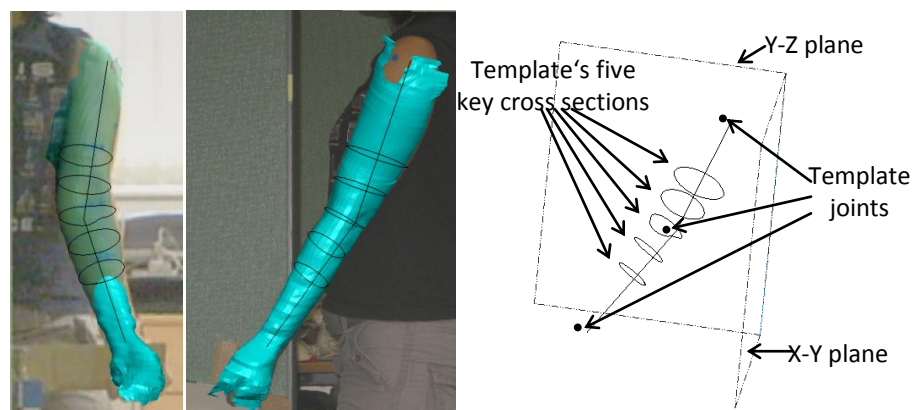


Figure 283. The integration between the digitised cross sections and joint information of the 3D scanned arm for participant 1. The result of the integration is shown in the rightmost image

The first two images in Figure 283 show the integration between the digitised cross sections and the 3D scan's joint information for a fully extended arm of participant 1. The output of this process, which is shown in the rightmost image of Figure 283, was used as the template. As shown in the rightmost image, the template consisted of five key cross sections and the joint information i.e. coordinates of shoulder, elbow and wrist joints.

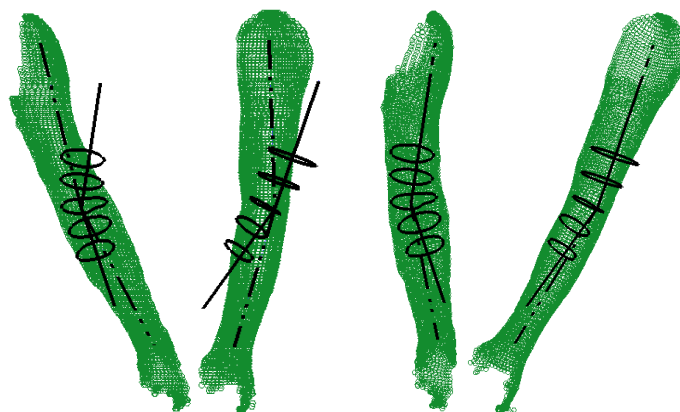


Figure 284. Translation and rotation of a 3D scanned arm so that its elbow joint and upper arm (dashed lines) coincide with the template's elbow joint and upper arm (solid lines)

As suggested in section 9.7.1, the re-orientation of the 3D scanned arm involved translation and rotation. To accommodate both translation and rotation, the template's joint information and cross sections were used. The translation would ensure that the elbow joint of the 3D scanned arm and the template coincided. The first two images (front and side views) in Figure 284 show the result of the translation where the elbow joint of a 3D scanned arm (dashed lines) and the template (solid lines) coincides. The next step was to perform rotation on the upper arm bone of the 3D scanned arm so that it coincided with the upper arm bone of the template. The last two images in Figure 284 show the side and front views of the rotation result. As shown in these images, the upper arm bone (the shoulder and elbow joints) of the 3D scanned arm coincided (dashed lines) with the upper arm bone of the template (solid lines). However, as suggested in section 9.7.1, this did not necessarily mean that their lateral –medial upper arm orientation was similar. Thus, a refinement for lateral-medial rotation of the upper arm of a 3D scan was required.

The elbow's cross sections of the template and the 3D scanned arm were suggested to be used in refining the 3D scanned arm's lateral –medial orientation. The elbow cross section was chosen because it had distinctive shape which would enable easier identification of the medial-lateral orientation of the arm. The left image in Figure 285 shows an example of elbow cross sections from the template (solid line) and a 3D scanned arm (dashed line) before refinement. The proposed refinement method utilised flat areas characteristic of the anterior of the elbow cross section. The flat area was defined as the area at the anterior part of the elbow where the curvature was minimal. This characteristic was observed by revisiting visual observation results on five key cross sections from the five participants in section 9.7.1 and 9.6.1. The elbow cross sections for fully extended arms from five participants showed that, although there was shape variation, their shape shared similar characteristics such as bulges at the posterior of the elbow and flat areas at the anterior of the elbow, as shown in the right image in Figure 285.

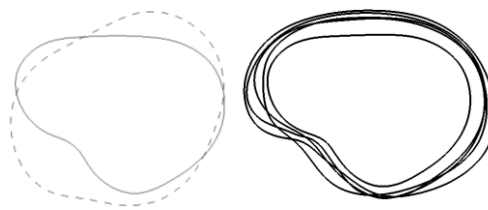
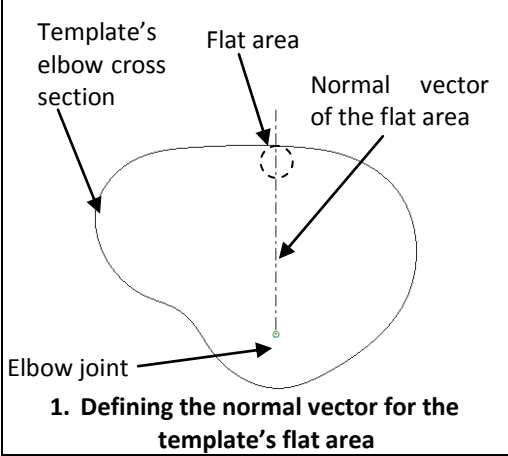
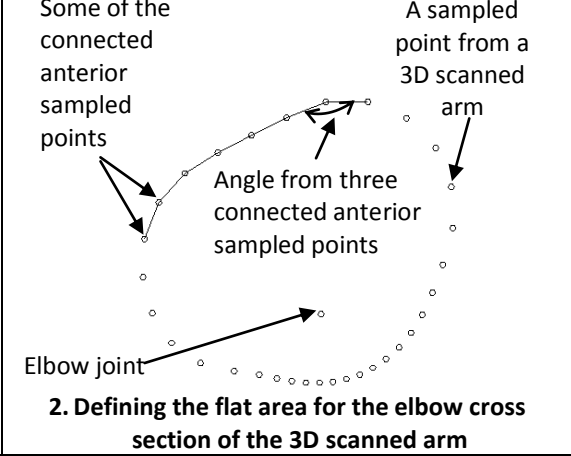
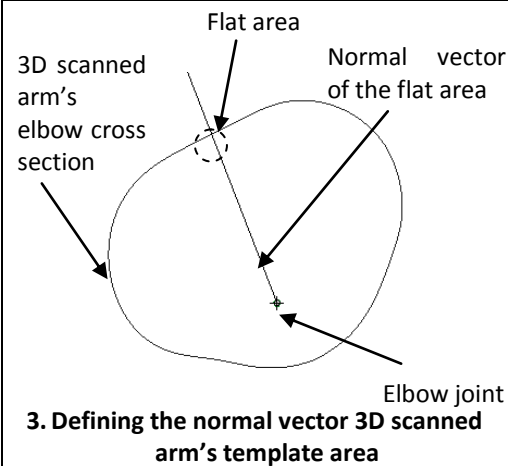
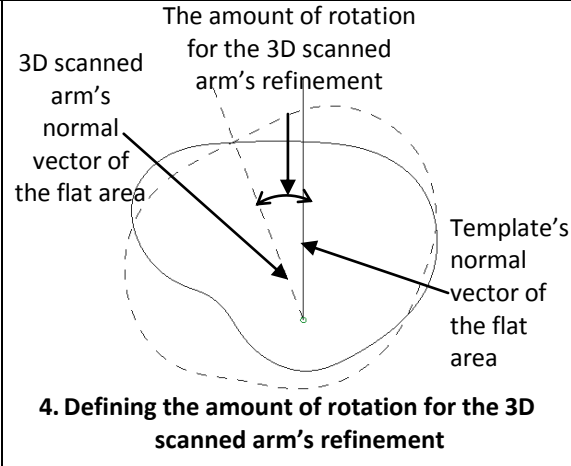
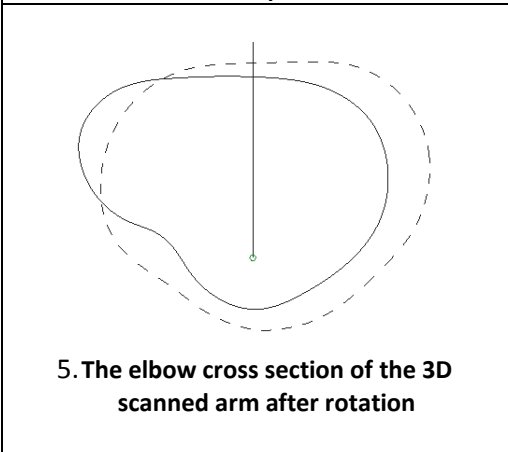
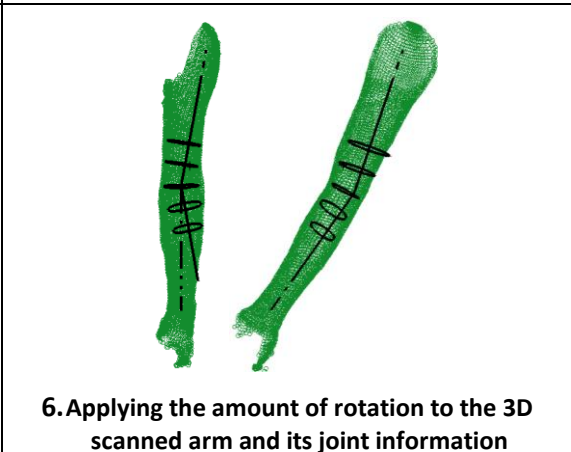


Figure 285. Left image shows an example of elbows from the template (solid line) and 3D scanned arm (dashed line) prior the refinement. Right image shows prominent characteristics of elbow cross sections from the five participants

Images in Table 25 illustrate the proposed steps to refine the lateral-medial orientation of a 3D scan's upper arm. As shown in these images, the refinement of lateral-medial orientation of the 3D scanned arm would be performed by rotating the 3D scanned arm so that the flat area of its elbow cross section matches to that of the template. The flat area of the elbow cross sections for the template could be defined manually, whereas an algorithm would be developed for the 3D scanned

arm. The flat area for the 3D scanned arm could be determined by calculating the angle between three adjacent anterior points that are sampled on the elbow cross sections. The set of points with the lowest angle would be chosen to represent the flat areas and a normal vector would be created from the first and last point from the set of points. This normal vector would then be rotated to match the normal vector of the template's flat area. The last image in Table 25 illustrates the final result of the proposed refinement.

Table 25. The proposed step by step process to perform refinement of lateral-medial orientation of the 3D scanned arm

 <p>Template's elbow cross section</p> <p>Flat area</p> <p>Normal vector of the flat area</p> <p>Elbow joint</p> <p>1. Defining the normal vector for the template's flat area</p>	 <p>Some of the connected anterior sampled points</p> <p>Angle from three connected anterior sampled points</p> <p>A sampled point from a 3D scanned arm</p> <p>Elbow joint</p> <p>2. Defining the flat area for the elbow cross section of the 3D scanned arm</p>
 <p>3D scanned arm's elbow cross section</p> <p>Flat area</p> <p>Normal vector of the flat area</p> <p>Elbow joint</p> <p>3. Defining the normal vector 3D scanned arm's template area</p>	 <p>The amount of rotation for the 3D scanned arm's refinement</p> <p>3D scanned arm's normal vector of the flat area</p> <p>Template's normal vector of the flat area</p> <p>4. Defining the amount of rotation for the 3D scanned arm's refinement</p>
 <p>5. The elbow cross section of the 3D scanned arm after rotation</p>	 <p>6. Applying the amount of rotation to the 3D scanned arm and its joint information</p>

9.7.2.2 Finding closest match for the profile of a 3D scanned arm

Figure 286 illustrates the procedure for the second stage i.e. finding the closest match for the profile of a 3D scanned arm. The second stage was driven by several suggestions in section 9.7.1. One of them was the suggestion that was drawn from the key finding of the third issue i.e. using distances between a number of points on the profile and the bones. As shown in Figure 286, the optimum number and placement of points was used to quantify or represent the framework's profiles as distances between the points on the profiles with corresponding bone points. Another suggestion that was drawn from the key finding of the fourth issue of the study was also followed i.e. using PCA to reduce the number of data to be stored and handled in the database. As shown in Figure 286, PCA was used to store the profile data in the database and to assist the process to identify the closest match. The last suggestion that affected the procedure to find the closest match was that from the sixth issue of the study i.e. using BMI as one of the possible parameters to identify a closest match. As clearly shown in Figure 286, in addition to finding the closest match based on the shape similarity of profiles between the 3D scanned arm and the database, BMI was also utilised.

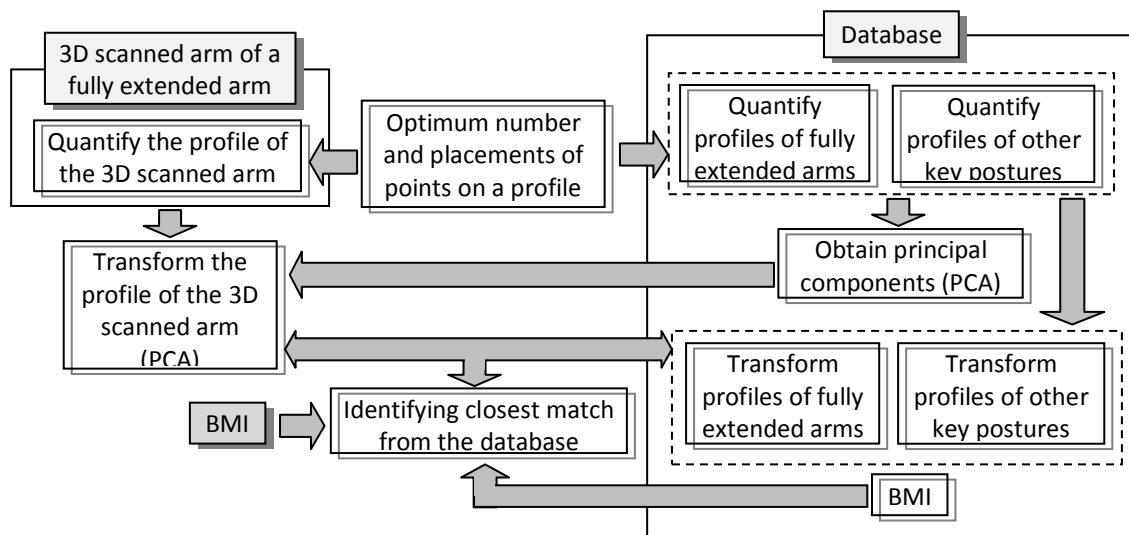


Figure 286. The procedures to find the closest match for a 3D scanned arm

As described above, the proposed method required an optimum number and placement of points on the profile. As had been identified in the study in section 9.7.1, these optimum points were essential to represent the shape of a profile. To determine these optimum points, profiles from individuals were required. The determination of the optimum points would utilise profiles from all individuals and follow the suggestion that was drawn from the key finding of the first issue i.e. applying an existing approach which was described in section 7.3.2.5. Once the optimum points were identified, they were then used to quantify or represent profiles from all individuals as distances between points on the profiles and their corresponding bones.

However, as described in the first paragraph of this section, instead of simply storing these distances as they were, Principal Component Analysis (PCA) was performed on the quantification results. The application of PCA was distinguished into two parts i.e. PCA of the quantification result of fully extended arms ($PCA_{full\ extension}^{database}$) and PCA of the quantification result of other key posture ($PCA_{other\ key\ postures}^{database}$). Once the principal components for each PCA process were obtained, quantification data of the profiles was then transformed into a smaller number of data ($d_{full\ extension\ PCA\ transformed}^{database}$, $d_{other\ key\ posture\ PCA\ transformed}^{database}$). Similar to the application of PCA for cross section prediction, the 90% rule would be used to determine the number of principal components i.e. the number of the transformed data. The distinction between a profile of a fully extended arm and other key postures was applied because only transformed data of fully extended arms in the database would be compared to the transformed quantification data of the 3D scanned arm.

The closest match identification, as shown in Figure 286, were determined based on two things i.e. shape of the profile and BMI. To account for the profile shape, the profile of a 3D scan of a fully extended arm would be transformed using the principal component of the fully extended arms ($PCA_{full\ extension}^{database}$). Once the transformed value ($d_{full\ extension\ PCA\ transformed}^{3D\ scan}$) was obtained, it would be compared to the transformed value of fully extended arms in the database ($d_{full\ extension\ PCA\ transformed}^{database}$). The comparison would be performed by measuring the distance of $d_{full\ extension\ PCA\ transformed}^{3D\ scan}$ to the data for each individual in the database e.g. $d_{full\ extension\ PCA\ transformed}^{database_1}$ for individual 1, $d_{full\ extension\ PCA\ transformed}^{database_2}$ for individual 2, etc. To account for the effect of BMI, the BMI difference between individuals in the database and the individual with the 3D scan were used. To integrate the effect of both profile shape and BMI, the following equation would be used. The closest match was defined as data with the least Δ value.

$$\Delta_n = d_{full\ extension\ PCA\ transformed}^{3D\ scan} - d_{full\ extension\ PCA\ transformed}^{database_n} + BMI^{3D\ scan} - BMI^{database_n}$$

9.7.2.3 Creating the profiles at 135°, 90° and maximum flexion

The third stage of the proposed method was the actual creation of profiles at 135°, 90° and maximum flexion for the 3D scanned arm. Based on the findings from the fifth and sixth issue of the study in section 9.7.1, it was identified that the prediction method should be based on the modification of the closest match's profile inclination. This was taken into account by proposing the steps shown in Figure 287. As shown in Figure 287, a predicted 135° profile was essentially a rotated and scaled version of the closest match's 135° profile. The rotation and scaling of the 135° profile ensured that the profile of the closest match matched the arm size and inclination of the 3D scanned

arm. The predicted 135° profile was then used to predict the 90° and maximum flexion profiles. The usage of a rotated and scaled 135° profile as a basis to predict 90° and maximum flexion profiles meant that they automatically matched the arm size and inclination of 3D scanned arm.

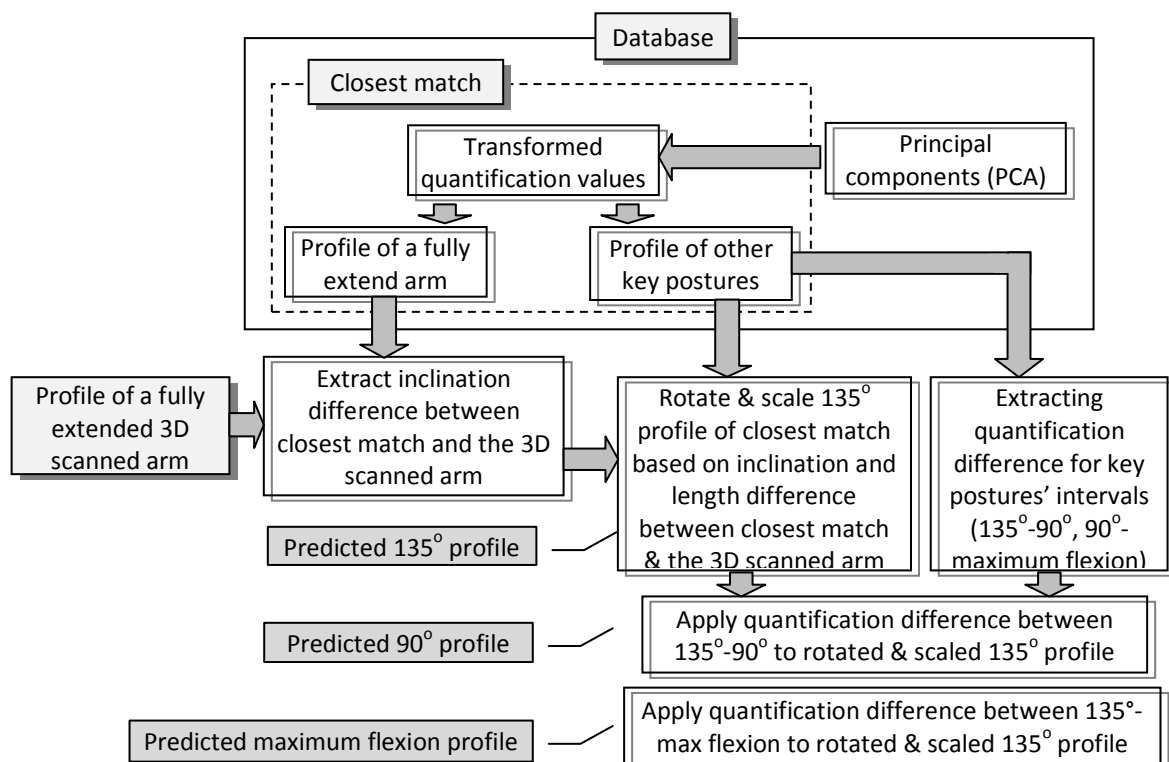


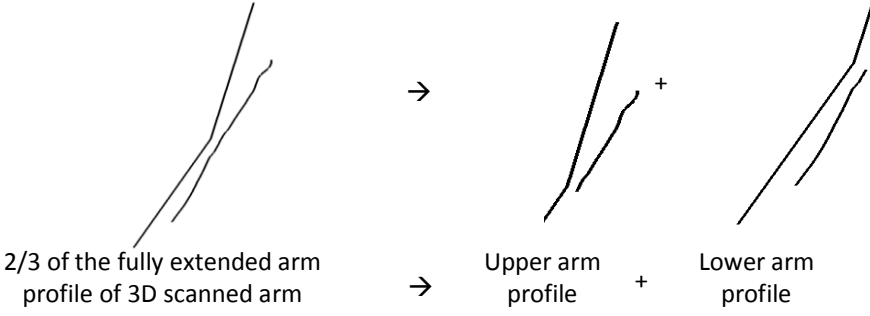
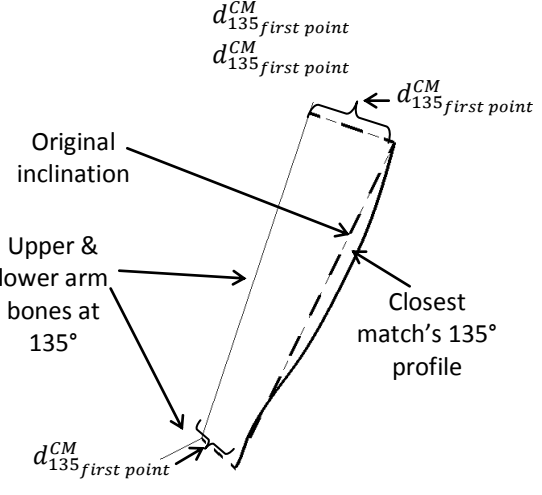
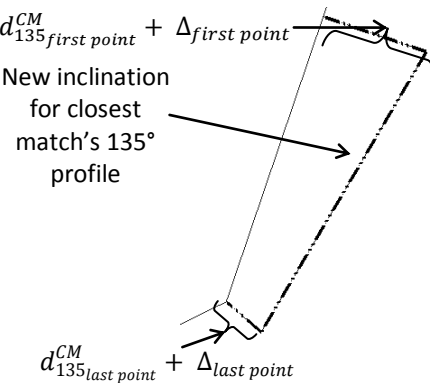
Figure 287. The procedures for predicting profiles of 3D scanned arm at 135°, 90° and maximum flexion

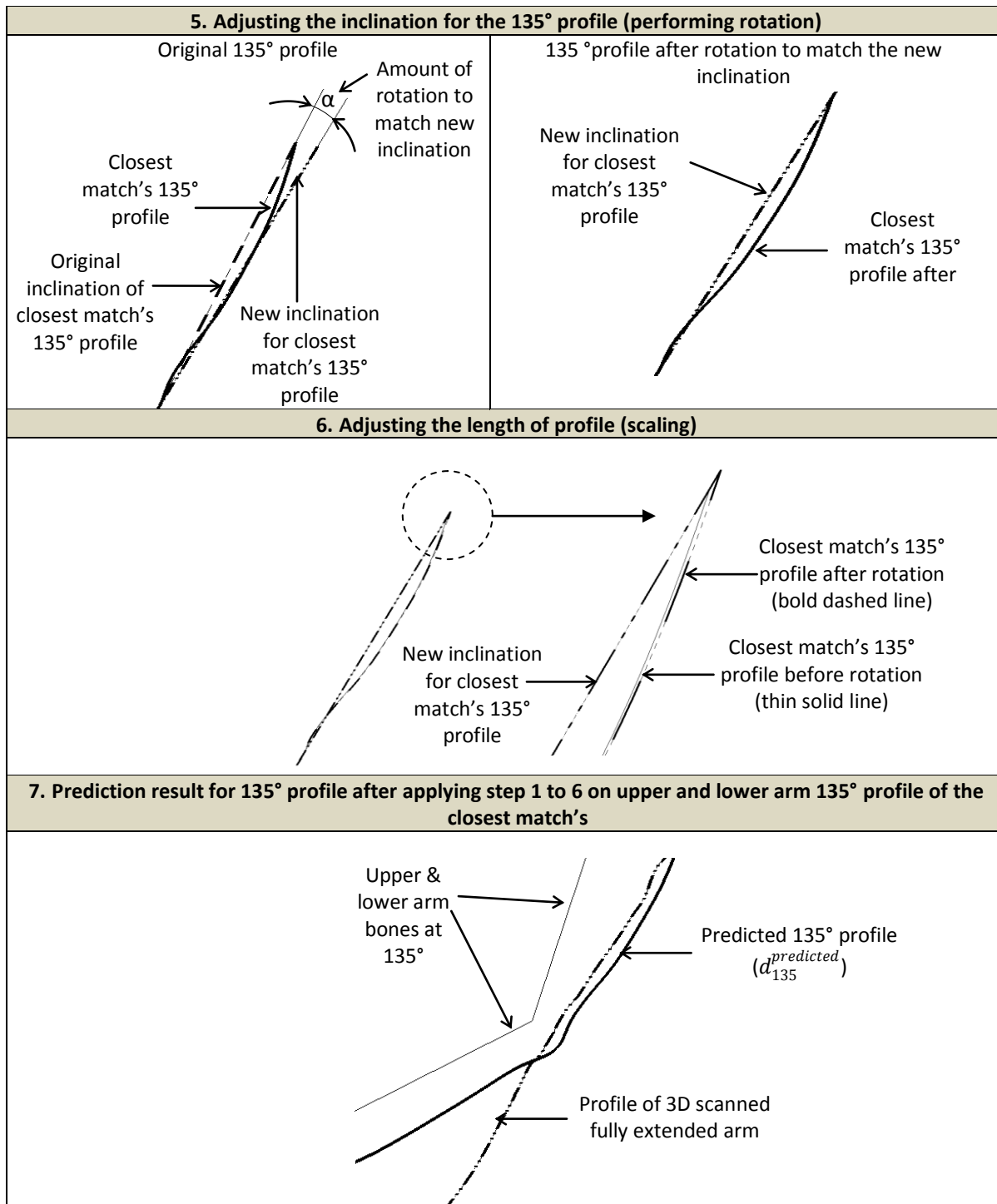
Table 26 shows the proposed detailed steps of rotating and scaling the closest match's 135° profile. Table 26 only depicts the process for the upper arm because the proposed steps are the same for upper and lower arm profiles. As shown in Table 26, in accordance to the suggestion drawn from the key finding of the first issue of the study, only 2/3 of the 3D scanned arm profile was used. The first step of the proposed prediction method for the 135° profile was to separate the upper and lower arm of the 3D scanned arm profile by utilising the suggested cut point in section 9.7.1 (see the analysis of key finding of the fifth issue of the study). Next, measures to accommodate inclination difference, hence accommodating arm width difference, was performed.

Steps 2 to 5 were aimed to accommodate inclination differences between the 3D scanned arm and the closest match data by means of rotation. Step 2 was aimed to obtain distances between the bones and the first and last points of the fully extended arm's profiles of both the 3D scan and the closest match data. The distances of the first and last points of the upper/lower arm profile were used to define inclination of the arm profile. They were chosen because they enclose the whole component of upper/lower arm profile. In step 3, the first and last point's distance differences between the 3D scan and the closest match data were calculated. The result was then used in step 4, where it was used to create the new inclination for the 135° closest match's profile. In step 5, an

angle between the original and new inclination of 135° closest match's profile was measured. This was then used to rotate the 135° closest match's profile. Step 5 concluded the measures to accommodate arm width differences between the 3D scan and the closest match data. The output of steps 2 to 5 was then scaled to accommodate arm length differences between the 3D scan and the closest match data. Once the same process i.e. step 2 to 6, was applied to the lower arm profile, the predicted 135° profile ($d_{135}^{predicted}$) was complete.

Table 26. Steps to predict 135° profile through scaling and readjustment of the closest match 135°

1. Separating the upper and lower arm profile of 3D scanned arm	
 <p>2/3 of the fully extended arm profile of 3D scanned arm → Upper arm profile + Lower arm profile</p>	
2. Acquiring distances of the first and last points for fully extended arm profiles of closest match and 3D scanned arm	
Acquiring distances from the first and last points from 3D scanned profile ($d_{full\ extension\ first\ point}^{3D\ scan}, d_{full\ extension\ last\ point}^{3D\ scan}$)	Acquiring distances from the first and last points from closest match ($d_{full\ extension\ first\ point}^{CM}, d_{full\ extension\ last\ point}^{CM}$)
3. Find distance difference for the first and last points	
$\Delta_{first\ point} = d_{full\ extension\ first\ point}^{3D\ scan} - d_{full\ extension\ first\ point}^{CM}$ $\Delta_{last\ point} = d_{full\ extension\ last\ point}^{3D\ scan} - d_{full\ extension\ last\ point}^{CM}$	
4. Determining new inclination for closest match's 135° profile	
 <p>Original inclination</p> <p>Upper & lower arm bones at 135°</p> <p>Closest match's 135° profile</p> <p>$d_{135\ first\ point}^{CM}$</p> <p>$d_{135\ last\ point}^{CM}$</p>	<p>New inclination (dashed-dotted line) is created from:</p> $d_{135\ first\ point}^{CM} + \Delta_{first\ point}$ $d_{135\ last\ point}^{CM} + \Delta_{last\ point}$  <p>New inclination for closest match's 135° profile</p> <p>$d_{135\ first\ point}^{CM} + \Delta_{first\ point}$</p> <p>$d_{135\ last\ point}^{CM} + \Delta_{last\ point}$</p>



Once the prediction for 135° profile was complete, the predicted 135° profile ($d_{135}^{predicted}$) was used as a basis to predict the 90° ($d_{90}^{predicted}$) and maximum flexion ($d_{maximum\ flexion}^{predicted}$) profiles. As shown in Figure 287, the distance difference between the original 135° closest match's profile (d_{135}^{CM}) and 90° closest match's profile (d_{90}^{CM}) were utilised to predict the 90° profile. A similar process was also performed for the prediction of the maximum flexion profile. The equation below illustrates the process:

$$\Delta_{135-90} = d_{90}^{CM} - d_{135}^{CM}$$

$$d_{90}^{predicted} = \Delta_{135-90} + d_{135}^{predicted}$$

$$\Delta_{135-maximum\ flexion} = d_{maximum\ flexion}^{CM} - d_{135}^{CM}$$

$$d_{maximum\ flexion}^{predicted} = \Delta_{135-maximum\ flexion} + d_{135}^{predicted}$$

9.8 Database Design

The proposed prediction methods for the FDM, which were addressed in sections 9.4, 9.5, 9.6 and 9.7, guided the decisions on the database design. As described in section 9.3, the database design involved determining the structure and contents of the database. The structure of the database referred to how the database categorised its data. This research proposed gender and race as attributes to categorise the data in the database. This decision was made to take into account the effect of race and gender, as required by the proposed prediction methods in section 9.4, 9.5, 9.6 and 9.7. Thus for each x data from a particular race; these data should be categorised further into two groups i.e. x_1 for males and x_2 for females.

The proposed prediction methods in section 9.4, 9.5, 9.6 and 9.7 indicated that the following data was required as the contents of the database:

1. *The range of carrying angle for a fully extended and flexed arm for each gender.*

These data, shown in Table 21, were required to accommodate the prediction method for carrying angle at maximum flexion (see section 9.4).

2. *BMI from all individuals in the database.*

BMI was required to identify the closest match for the profile prediction (see section 9.7.2.3).

3. *A mathematical equation that captured the relationship between BMI, the length of upper arm and UAF's locations of fully extended and flexed arms for each gender and race.*

This mathematical equation was required to predict the locations of UAF of fully extended and flexed arms based on the BMI and the arm length of a 3D scan data (see section 9.5.2.1).

4. *A mathematical equation that captures the relationship between UAF and LAF, for fully extended and flexed arms, for each gender and race.*

This mathematical equation was required to predict the location of LAF of fully extended and flexed arms when UAF's locations at fully extended and flexed arms were already known (see section 9.5.2.1).

5. *A mathematical equation that captured the relationship of UAF and LAF from a fully extended arm to fully flexed arms for each gender and race.*

This mathematical equation was required to predict the location of UAF and LAF at 135° and 90° flexion when UAF's and LAF's locations at fully extended and flexed arms were already known (see section 9.5.2.1).

6. *A mathematical equation that captures the relationship of UAF's- UAM's locations and LAF's-LAM's locations for each gender and race.*

This mathematical equation was required to predict the location of UAM and LAM when UAF's and LAF's location were known, respectively (see section 9.5.2.2).

7. *Ratio values of maximum vertical and horizontal dimensions of UAF-UAF and LAF-LAM cross sections for fully extended arms from all individuals in the database.*

The ratio values were required to find simultaneous closest matches for UAF-UAM and LAF-LAM cross sections of a 3D scan data (see section 9.6.2.1).

8. *The four vertical and horizontal dimensions of UAF, UAM, LAM and LAF cross sections for each key posture from all individuals in the database.*

These dimensions were required to resize the dimensions of a 3D scanned arm's UAF, UAM, LAM and LAF in order to predict its UAF, UAM, LAM and LAF cross sections at 135°, 90° and maximum flexion (see section 9.6.2.1).

9. *Transformed values of E cross sections of fully extended arms from all individuals in the database.*

The transformed values were required to assist identification of the closest matches for E cross section' of a 3D scan data (see section 9.6.2.2).

10. *Transformed values of E cross sections of 135°, 90° and fully flexed arms from all individuals in the database.*

These transformed values were required to predict E cross sections at 135°, 90° and maximum flexion once the closest matches of a 3D scan data's E cross section were identified (see section 9.6.2.2).

11. *Transformed values of fully extended arms' profiles from all individuals in the database.*

The transformed values were required to identify the closest match of a 3D scan data's profile (see section 9.7.2.2).

12. *Transformed values of 135°, 90°, and fully flexed arms' profiles from all individuals in the database.*

The transformed values were required to predict profiles at 135°, 90°, and fully flexed arms for a 3D scan data (see section 9.7.2.3).

From the list above it is clear that, except for the first item of the database contents, data collection was required for the remaining items of the database contents. Data collection for these database items is addressed in the next section.

9.9 Data collection for the database

The following list outlines what and how data were collected for the database. Procedures already established for the development of the FDM were used wherever possible:

1. *Height and weight.* Height and weight of participants were collected for the database item number 2 - BMI.
2. *Five key cross sections for all key postures.* Five key cross sections for all key postures were collected for database item numbers 7, 8, 9 and 10. To obtain these key cross sections, the procedure in section 6.4.2 was followed. The procedure involved circling wires around the arm to capture the shapes of cross sections at five locations (see section 6.6.2 for details about these five locations); and followed by tracing and digitising the shapes of the wires to obtain the five key cross sections.
3. *Side and front view photographs for all key postures.* The side and front view photographs were collected for database item numbers 3, 4, 5, 6, 11 and 12. The procedure in section 6.4.2 was followed to obtain side and front view photographs for all key postures. The procedure involved attaching markers on selected areas (on the shoulder-side and front; on the mid of the arm-side; on the elbow-mid, side and front; on the wrist-side, front and back; and the area where the upper arm meets the lower arm during maximum flexion-side and front) and obtaining simultaneous images of the side and front view of arms while assuming the four key postures.
4. *3D scan of a fully extended arm and its joint information.* A 3D scan of a fully extended arm and its joint information were collected for database item numbers 3 to 10 (see section 9.8). The guideline in section 7.1.3 was followed to capture the 3D scan of fully extended arms. The guideline essentially required the arm to be fully extended and the hand to be pronated while being scanned in the [TC]² NX-12 body scanner.

Once detailed information on what data to be collected was established, the decision regarding who these data should be collected from was made. As discussed in the database design in section 9.8, the database's structure was proposed to accommodate the effect of race and gender. The sample was thus chosen to balance gender, however it would be impractical to try to address all possible races. Thus, it was decided to focus on two races (Asian and Caucasian) to allow validation of the specification to accommodate different races within the FDM. Asian and Caucasian races were chosen mainly for pragmatic reasons, due to the availability of participants. Also, this choice of

races allowed data from the five participants, who were involved in the FDM development, to be re-used as they were of Asian origin. Six participants were chosen to represent each gender and race i.e. Asian male, Asian female, Caucasian male and Caucasian female resulting in a total of 24 participants. The five participants used in the development of the new FDM were also used for the database. Out of the 24 participants, one of the participant's data (an Asian male) was later discovered to be unsuitable for the database. This was because the 3D scan data of the fully extended arm was heavily distorted. The distortion resulted in incorrect joint information, and further efforts to re-obtain 3D scanned data was not possible as the participant withdrew from the data collection. As this discovery was late on in the development of the database it was decided to work with the 23 remaining sets of complete data.

Table 27. BMI classification (adapted from WHO (1995, 2000) and WHO Expert Consultation (2004))

Classification	BMI	
	Caucasian	Asian
Underweight	<18.5	<18.5
Normal range	18.5 – 24.99	18.5 – 22.99
Overweight	≥25	≥23
Obese	≥30	≥27.5

Table 28. Participant's height, weight, BMI and arm length

Asian male				Asian female			
Height (cm)	Weight (kg)	BMI	Arm Length (mm)	Height (cm)	Weight (kg)	BMI	Arm Length (mm)
166	73.9	26.8	514	156	86	35.3	475
166	65.2	23.7	519	152	59.3	25.7	470
162	55.6	21.2	509	143	46	22.5	425
177	65.1	20.8	568	165	56.5	20.7	517
180	64.5	19.9	561	156	50	20.5	483
Caucasian male				158	47.4	18.9	495
				Caucasian female			
Height (cm)	Weight (kg)	BMI	Arm Length (mm)	Height (cm)	Weight (kg)	BMI	Arm Length (mm)
172	94.4	31.9	559	164	100	37.2	506
177	96.1	30.7	558	174	87.5	28.9	520
182	82.6	24.9	583	171	72.7	24.9	526
178	73	23	578	164	56.9	21.1	494
186	75	21.7	600	168	58.8	20.8	511
188	73	20.6	586	148	41.5	18.9	464

As discussed in section 9.2, this research utilised BMI to represent different body types. According to WHO (1995, 2000), the BMI value could be used to identify whether someone was underweight, normal weight, overweight, or obese. The international cut point for each category is shown in the second column in Table 27. For Asian and Pacific populations, a slightly lower cut point of BMI classifications was introduced (WHO Expert Consultation, 2004). These values were shown in the third column in Table 27. Using cut points from the BMI classification, efforts were made to recruit participants with BMIs that cover the range of BMI classification. However, due to the difficulty in recruiting participants who represented the underweight category, it was deemed to be

sufficient to replace the underweight category with the lower range of normal weight. BMIs of the recruited participants for each gender and race are listed in Table 28. As shown, the range of BMI is 19.9 - 26.8 for Asian males (group 1); 18.9 - 35.3 for Asian females (group 2); 20.6 - 31.9 for Caucasian males (group 3); and 18.9 - 37.2 for Caucasian females (group 4).

In addition to representing gender and race, participants were chosen so that they could represent variation in body size and shape. This approach was in line with the suggestions that were drawn from the key findings of the studies in section 9.5, 9.6 and 9.7. In these sections, high variation of different body size and shape of individuals was suggested for the database as it enabled provision of best closest match(es) possible for the 3D scan data. However, with such a small number of participants, it is acknowledged that it was impossible to fully capture body size and shape variation that existed for each gender and race. It is also acknowledged that this could ultimately affect the effectiveness of the database to predict elements of FDM for a wide range of body size and shape. However, with the extent of data collection, pre-processing and analysis involved, 6 participants' data within each group were deemed to be sufficient for this PhD. Table 28 shows arm length for all participants to reflect the variety of body sizes from the participants. The range of arm length for group 1 was 509-568 mm; 425-517 for group 2; 558-600 for group 3; and 464-526 for group 4. A comparison of the arm length's range with available anthropometrical data was performed to show how the range of each group represented the population. The result, accompanied by the arm length anthropometric data, is shown in Table 29. The comparison result showed that for both Caucasian male and female groups, the range of the arm length was quite limited i.e. 8.5-48 percentile and 0.6-33 percentile, respectively. It is acknowledged that a limited range means that the database ability to predict accurately would also be limited.

Table 29. Comparing anthropometrical data of arm lengths for Asian i.e. Sri Lankan and Caucasian i.e. United Kingdom (adopted from Peebles and Norris, 1998) to the arm length's range from each group

Nationality	Gender	Mean \pm SD (mm)	Percentile	
			5 th	95 th
Sri Lanka	Female	496 \pm 29.71	450	542
	Male	532 \pm 27.22	486	573
UK	Female	538.3 \pm 29.2	490.2	586.4
	Male	601.7 \pm 31.9	549.2	654.2

Asian male		Asian female	
Arm length (mm)	Percentile	Arm length (mm)	Percentile
509	20.1	425	0.8
568	90.7	517	76.1
Caucasian male		Caucasian female	
Arm length (mm)	Percentile	Arm length (mm)	Percentile
558	8.5	464	0.6
600	48	526	33.7

Figure 288, Figure 289 and Figure 290 show examples of the data collection's result from some participants. Figure 288, Figure 289 and Figure 290 show side-front view photographs, 3D scan data and digitised cross sections, respectively. Further data processing was required to these data before they could be utilised to provide the required database item numbers 3 to 12. Data processing for these data is addressed in detail in section 9.10.



Figure 288. Examples of side-front view photographs from participants for the database

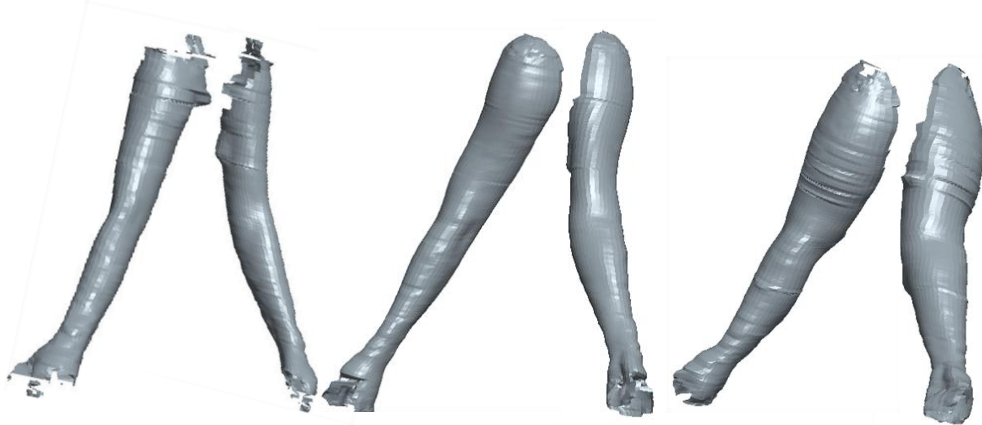


Figure 289. Examples of 3D scan data from participants for the database

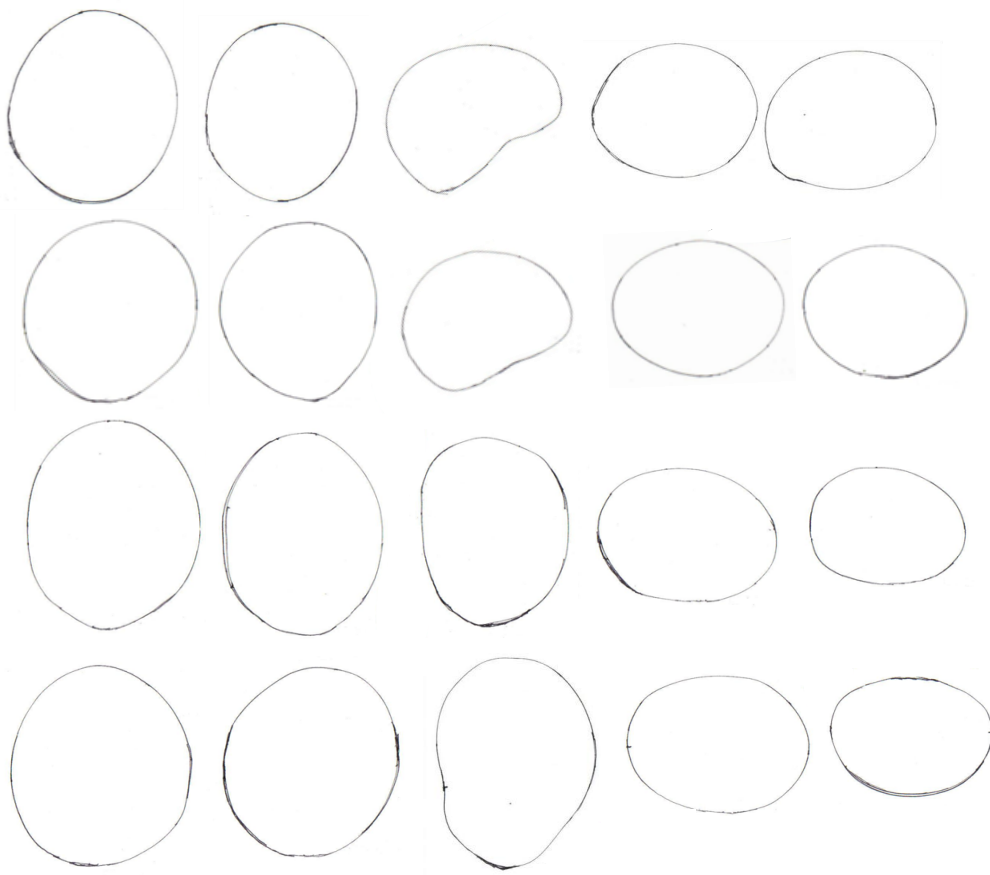


Figure 290. Examples of the results of manually tracing the shapes of wires that were circled around the arms

9.10 Data processing for the database

In essence, the data processing was aimed to manipulate the raw data, which were acquired from data collection in section 9.9, in order to provide database items described in section 9.8. As shown in section 9.9, four types of data were collected i.e. height and weight; five key cross sections of all key postures; side-front view photographs of all key postures; and 3D scan of a fully extended arm with its joint information. Height and weight, which were collected to provide BMI values (database item number 2), could directly be used to determine BMI values by dividing the weight (in kilograms) with the square of the height (in meters). In contrast, five key cross sections of all key postures, side-front view photographs of all key postures and 3D scan of a fully extended arm with its joint information required substantial amount of data processing before they could be used to determine database item number 3 to 12. Database item number 3 to 6 linked with the locations of UAF, UAM, LAM and LAF cross sections; whereas database item number 7 to 10 and database item number 11 to 12 related to five key cross sections and profiles, respectively. Each of these would be addressed in the followings subsections.

9.10.1 Data processing for database items that were linked to the locations of UAF, UAM, LAM and LAF

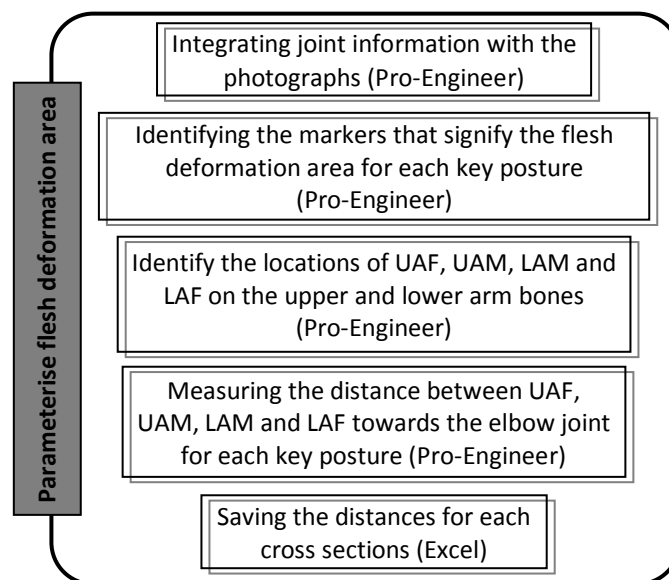


Figure 291. Existing procedure which was adopted to obtain the locations of UAF, UAM, LAM and LAF

Database items that were linked to the locations of UAF, UAM, LAM and LAF were database item numbers 3 to 6. For these database items the locations of UAF, UAM, LAM and LAF were required. To provide these locations, an existing procedure in section 8.1.3 was followed. As shown in Figure 291, the procedure involved integrating joint information from the 3D scan data with side-front view photographs to identify and measure the locations of key cross sections. The application

of the procedure did not only yield UAF's locations at fully extended and flexed arms; it also gave UAF's, UAM's, LAM's and LAF's locations for all key postures. Thus application of these procedures also automatically provided the required locations of cross sections for database item numbers 4, 5 and 6 (section 9.10.1.2, 9.10.1.3 and 9.10.1.4 respectively). Once the locations of UAF, UAM, LAM and LAF were obtained, database item number 3 to 6 could be determined.

9.10.1.1 Database item number 3: A mathematical equation that captured the relationship between BMI, upper arm lengths and UAF's locations of fully extended and flexed arms

To capture the relationship between BMI, arm length and the location of UAF mathematically, a method to represent a relationship between a dependent variable and more than two independent variables was required. Multiple regression was deemed to be suitable as it was: (1) able to represent a function with more than two independent variables and (2) suitable for real time processing. The method allows for processing of, for example, a measured quantity y for several values of parameters x_1 and x_2 . A multivariate model of the data would be $y = a_0 + a_1x_1 + a_2x_2$. Multiple regression then solves for unknown coefficients i.e. a_0 , a_1 and a_2 , by performing a least squares fit. Table 30 shows BMI, upper arm length and the location of UAF for fully extended arms for each gender and race; whereas Table 31 shows BMI, upper arm length and location of UAF for fully flexed arms for each gender and race. Using the data shown in Table 30 and Table 31, multiple regressions for UAF's locations of fully extended and flexed arms were established in MATLAB. The multiple regressions basically expressed the location of UAF of fully extended arms or fully flexed arms (dependent variables) as a function of two independent variables i.e. BMI and arm length.

Table 30. UAF location at fully extended arm, BMI, and upper arm length for participant in each gender and race group

Asian female (fully extended)			Asian male (fully extended)		
Arm length (mm)	UAF location (mm)	BMI	Arm length (mm)	UAF location (mm)	BMI
239.718	119.859	35.34	272.805	107.2576	26.82
240.8168	97.0519	25.67	276.3234	109.2034	23.66
280.695	105.653	20.75	264.1288	92.41515	21.19
279.3168	81.07447	20.55	307.4616	107.318	20.78
220.0922	90.9002	22.49	288.8478	95.1999	19.91
241.9262	97.19507	18.99			
Caucasian Female (fully extended)			Caucasian Male (fully extended)		
Arm length (mm)	UAF location (mm)	BMI	Arm length (mm)	UAF location (mm)	BMI
270.7646	145.5903	37.18	248.0116	146.5713	31.91
274.707	136.836	28.9	298.9604	137.8653	30.67
277.2412	117.726	24.86	317.9522	120.1857	24.94
254.7648	72.71687	21.16	311.2934	79.95387	23.04
267.3338	98.56543	20.83	315.152	75.38987	21.68
241.832	94.2562	18.95	307.9072	92.24	20.658

Table 31. UAF location at fully flexed arm, BMI, and upper arm length for participant in each gender and race group

Asian female (fully flexed)			Asian male (fully flexed)		
Arm length (mm)	UAF location (mm)	BMI	Arm length (mm)	UAF location (mm)	BMI
239.718	137.2571	35.34	268.9646	119.2298	26.82
240.8168	104.0598	25.67	274.156	120.8744	23.66
279.2132	102.4564	20.75	264.1288	102.4564	21.19
279.3168	125.76	20.55	296.126	114.91	20.78
219.4252	102.4564	22.49	286.2324	110.3223	19.91
241.9262	106.283	18.99	264.1288	102.4564	21.19
Caucasian Female (fully flexed)			Caucasian Male (fully flexed)		
Arm length (mm)	UAF location (mm)	BMI	Arm length (mm)	UAF location (mm)	BMI
271.681	160.1916	37.18	291.2292	170.9569	31.91
308.91	149.8923	28.9	303.2544	154.2114	30.67
278.4758	128.2736	24.86	328.245	136.345	24.94
259.1684	112.0552	21.16	314.2246	104.5001	23.04
267.3338	107.8101	20.83	317.6422	109.5311	21.68
241.832	95.47859	18.95	315.7044	113.4664	20.658

Table 32 and Table 33 show the multiple regression results. The results shown include the coefficients of the least square fits i.e. a_0 , a_1 and a_2 , and the R^2 values of the multiple regressions. The coefficients, which were stored in the database, could be used to predict the locations of UAF of fully extended or flexed arms with the multivariate model of:

$$\text{location of UAF} = a_0 + a_1 \text{arm_length} + a_2 \text{BMI}$$

Table 32. Result of multiple regressions for UAF's location at fully *extended* arms

Asian Female				Asian Male			
a_0	a_1	a_2	R^2	a_0	a_1	a_2	R^2
44.2895	0.0543	1.7002	0.567	-52.9078	0.3443	2.5870	0.789
Caucasian Female				Caucasian Male			
a_0	a_1	a_2	R^2	a_0	a_1	a_2	R^2
-97.9438	0.5089	2.9359	0.454	-55.5056	0.0325	6.0609	0.852

Table 33. Result of multiple regressions for UAF's location at fully *flexed* arms

Asian Female				Asian Male			
a_0	a_1	a_2	R^2	a_0	a_1	a_2	R^2
-0.3496	0.2614	2.0035	0.638	-64.0459	0.4173	2.7422	0.8
Caucasian Female				Caucasian Male			
a_0	a_1	a_2	R^2	a_0	a_1	a_2	R^2
-48.4401	0.3679	2.9342	0.99	-73.9276	0.1865	5.7801	0.902

9.10.1.2 Database item number 4: A mathematical equation that captured the relationship between the location of UAF and LAF at fully extended and flexed arms

To depict the relationship between UAF's and LAF's locations of fully extended and flexed arms, UAF's and LAF's locations were charted against each other. Table 34 shows the location of UAF and LAF of *fully extended arms*. This table was used to capture the relationship between the location of UAF and LAF of fully extended arms for each gender and race. Table 35 shows the location of UAF

and LAF of *fully flexed arms* and was used to obtain the relationship between the location of UAF and LAF of fully flexed arms for each gender and race. A quick observation on these two tables revealed that as the arm flexed the location of LAF generally became farther than the locations of UAF.

Table 34. UAF and LAF locations of fully extended arms from all groups

Asian Female (fully extended arm)						
Participant	1	2	3	4	5	6
UAF location (mm)	119.859	97.0519	90.9002	110.84	90.9002	97.1314
LAF location (mm)	114.41	89.6357	89.8831	106.63	89.8831	97.8771
Asian Male (fully extended arm)						
Participant	1	2	3	4	5	
UAF location (mm)	107.2576	109.2034	87.9142	105.65	95.1999	
LAF location (mm)	90.5622	93.1262	71.8421	99.442	87.2079	
Caucasian Female (fully extended arm)						
Participant	1	2	3	4	5	6
UAF location (mm)	147.055	139.868	118.408	100.514	94.4472	73.2993
LAF location (mm)	136.276	141.641	117.161	115.279	93.6163	72.979
Caucasian Male						
Participant	1	2	3	4	5	6
UAF location (mm)	148.484	138.896	122.601	85.589	81.8481	78.018
LAF location (mm)	145.936	122.148	112.774	81	72.7302	62.3155

Table 35. Data for establishing the relationship between the location of UAF and LAF for fully flexed arms

Asian Female (Fully flexed arm)						
Participant	1	2	3	4	5	6
UAF location (mm)	137.25714	104.0598	102.4564	125.76	102.4564	106.283
LAF location (mm)	146.086	109.392	107.8786	129.34	107.8786	115.727
Asian Male (Fully flexed arm)						
Participant	1	2	3	4	5	
UAF location (mm)	119.2298	120.8744	102.4564	114.91	110.3223	
LAF location (mm)	130.2075	128.8079	111.627	119.15	110.0567	
Caucasian Female (Fully flexed arm)						
Participant	1	2	3	4	5	6
UAF location (mm)	160.1916	149.8923	128.2736	112.0552	107.8101	95.47859
LAF location (mm)	169.209	159.019	133.261	118.011	112.337	113.269
Caucasian Male (Fully flexed arm)						
Participant	1	2	3	4	5	6
UAF location (mm)	170.9569	154.2114	136.345	104.5001	109.5311	113.4664
LAF location (mm)	185.302	147.578	141.808	118.68	110.839	108.769

Figure 292 and Figure 293 show the graphs that chart the UAF's and LAF's locations for fully extended and fully flexed arms, respectively, for each gender and race. To represent the relationship between UAF's and LAF's locations mathematically, linear regression was fitted to the data. The linear regression was chosen due to its simplicity, which suggested its suitability for a real time application. The graphs of both figures show that the relationship between the locations of

UAF and LAF could be expressed linearly with at least 75% reliability. The linear equations shown in both figures would be stored in the database. As described in section 9.5.1, these equations were used to predict the locations of LAF once the locations of UAF of fully extended and flexed arms were known. The coefficients of all of the linear regressions were then stored in the database.

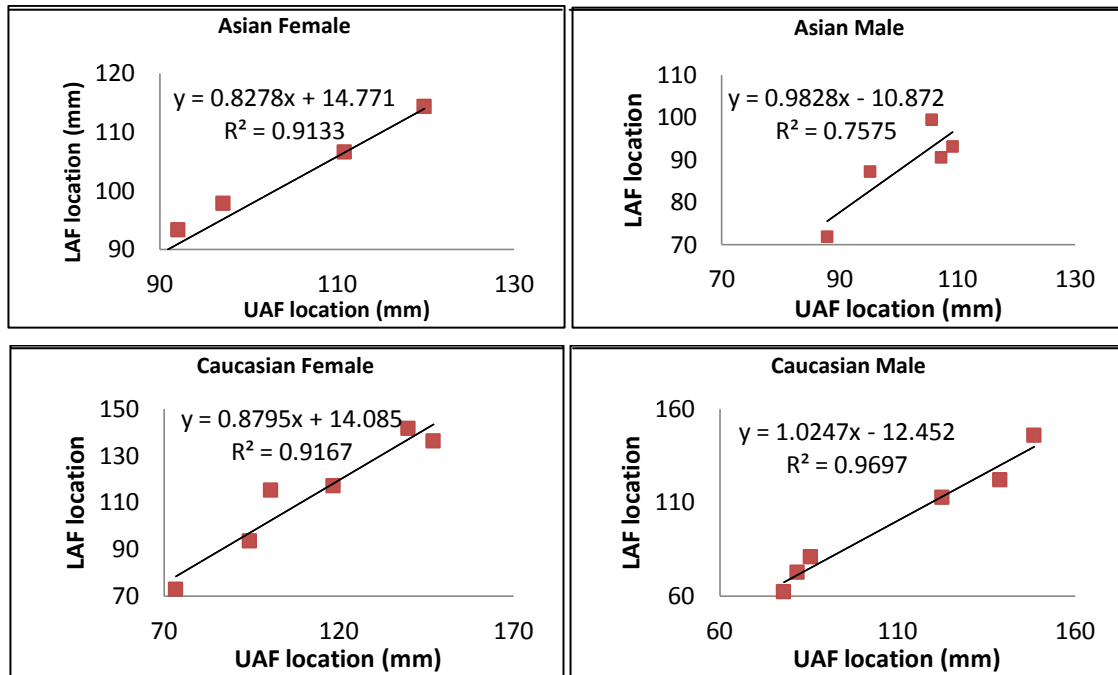


Figure 292. Relationships between the location of UAF and LAF for fully extended arm for all groups

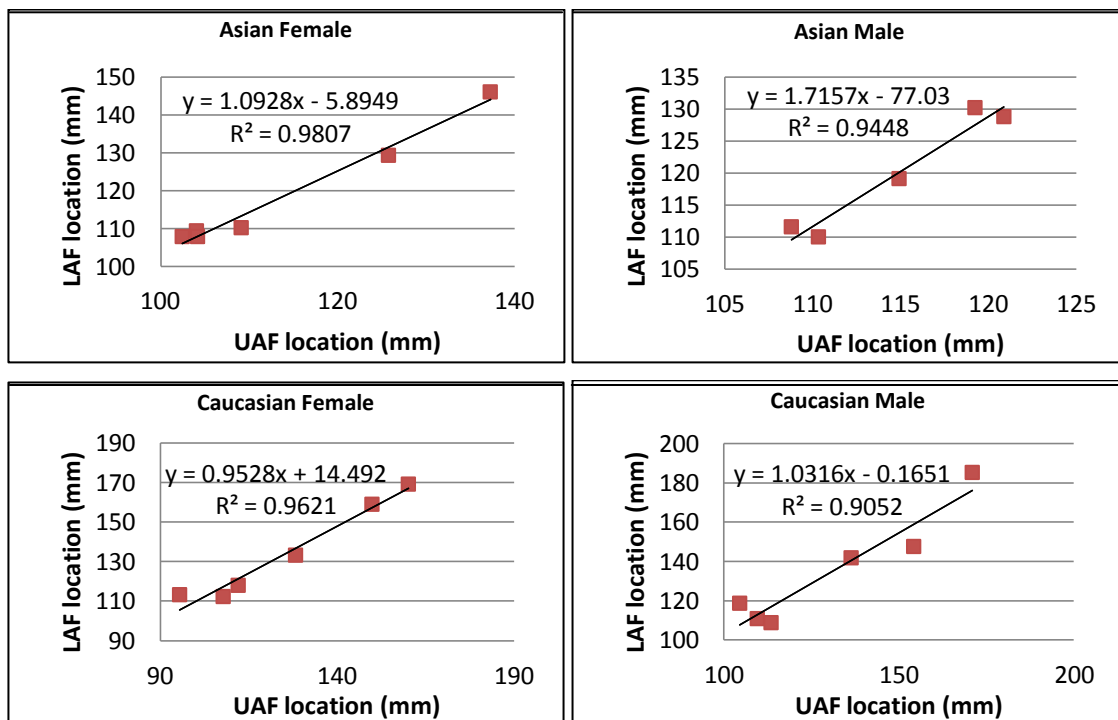


Figure 293. Relationships between locations of UAF and LAF for fully flexed arms for all groups

9.10.1.3 Database item number 5: A mathematical equation that captured the relationship of UAF and LAF from a fully extended arm to a fully flexed arm

Table 36 shows UAF's and LAF's locations for all key postures for each race and gender which were used to establish the relationship of UAF and LAF during movement from a fully extended arm to a fully flexed arm.

Table 36. Data to establish relationship between UAF and LAF from fully extended to fully flexed arm

Asian Female		Participant					
		1	2	3	4	5	6
UAF location (mm)	Fully extended	119.859	97.0519	90.9002	110.84	89.4768	97.1314
	135°	124.379	99.02	93.67342	113.86	94.02086	100.106
	90°	126.99244	101.328	97.40878	117.08	99.18339	103.361
	Fully flexed	137.25714	104.06	102.4564	125.76	104.1836	106.283
LAF location (mm)	Fully extended	114.41	89.6357	89.8831	106.63	89.8792	97.8771
	135°	121.7736	94.8641	94.49962	110.51	94.70712	102.931
	90°	130.58538	100.771	101.6673	119.18	100.613	107.75
	Fully flexed	146.086	109.392	107.8786	129.34	107.881	115.727
Asian Male		Participant					
		1	2	3	4	5	
UAF location (mm)	Fully extended	107.2576	109.203	87.9142	105.65	95.1999	
	135°	109.88906	113.604	92.02789	108.82	99.39894	
	90°	113.19831	117.446	95.9882	112.31	104.3873	
	Fully flexed	119.2298	120.874	102.4564	114.91	110.3223	
LAF location (mm)	Fully extended	90.5622	93.1262	71.8421	99.442	87.2079	
	135°	102.76788	104.262	79.36494	104.54	92.40755	
	90°	112.50711	113.225	88.48786	112.55	99.104	
	Fully flexed	130.2075	128.808	111.627	119.15	110.0567	
Caucasian Female		Participant					
		1	2	3	4	5	6
UAF location (mm)	Fully extended	147.055	139.868	118.408	73.299	100.514	94.4472
	135°	148.85642	140.661	120.064	80.137	102.7831	97.7457
	90°	152.31703	147.004	123.2407	88.231	106.3104	102.266
	Fully flexed	160.56562	149.892	128.2736	95.479	112.0552	107.81
LAF location (mm)	Fully extended	136.276	141.641	117.161	72.979	115.279	93.6163
	135°	141.41517	145.38	119.8105	82.558	115.9119	98.5529
	90°	153.07437	151.218	128.0458	97.42	116.7029	103.87
	Fully flexed	169.209	159.019	133.261	113.27	118.011	112.337
Caucasian Male		Participant					
		1	2	3	4	5	6
UAF location (mm)	Fully extended	148.484	138.896	122.601	81.848	78.018	85.589
	135°	153.61404	142.723	125.3586	89.916	82.55418	90.214
	90°	159.88546	148.391	128.9503	99.814	94.54268	96.9037
	Fully flexed	170.95686	154.211	136.345	109.53	113.4664	104.5
LAF location (mm)	Fully extended	145.936	122.148	112.774	72.73	62.3155	81
	135°	152.69236	126.145	116.8987	81.782	69.35945	90.454
	90°	168.2854	138.246	130.4218	95.828	86.17522	103.548
	Fully flexed	185.302	147.578	141.808	110.84	108.796	118.68

To establish the relationship the locations of UAF were charted against the arm angles. A similar procedure was also performed to establish the relationship of LAF's locations from a fully extended to a fully flexed arm. The results are shown in Figure 294, for UAF locations, and in Figure 295, for LAF location.

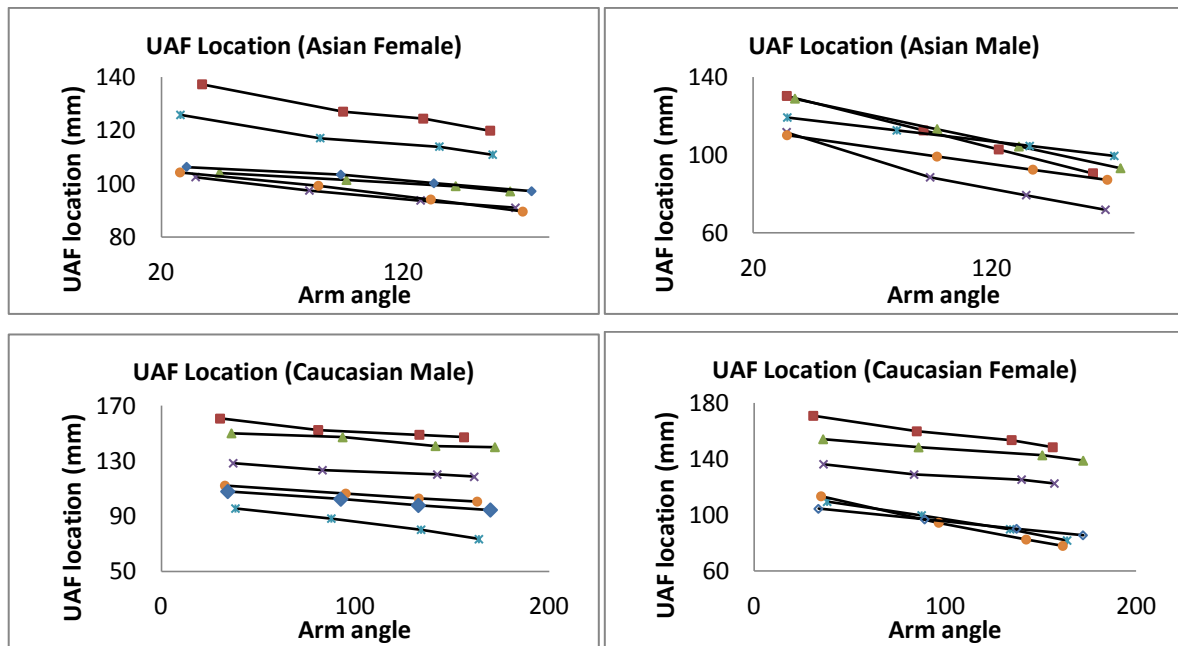


Figure 294. UAF locations are charted for each key posture and each participant in the groups

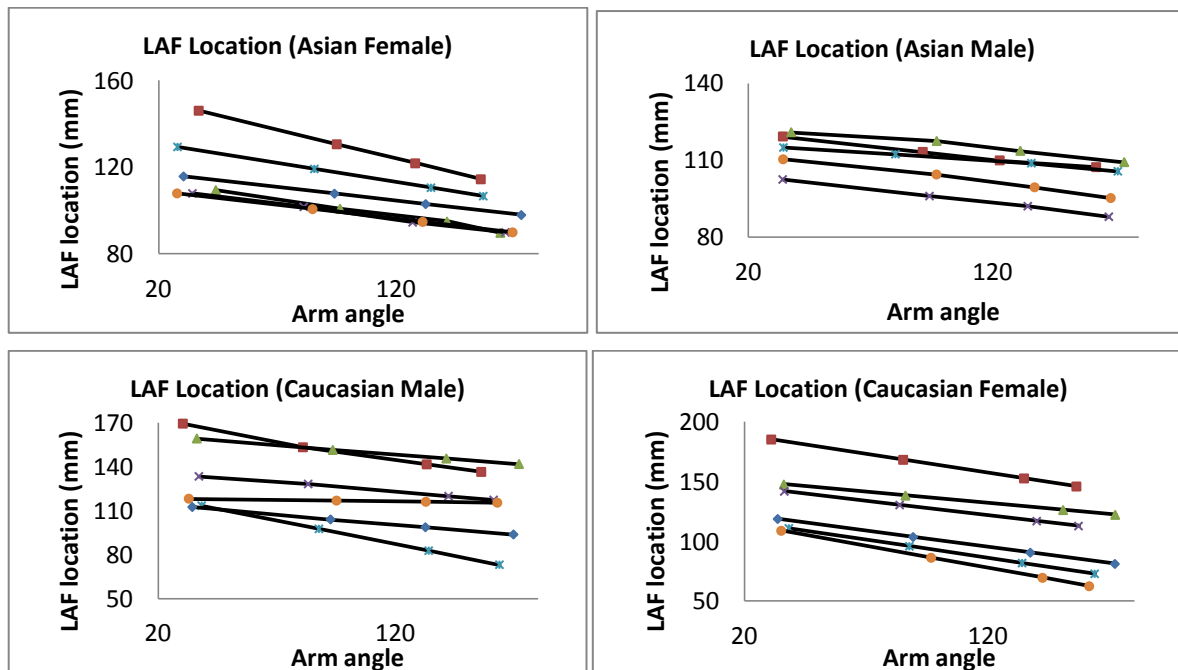


Figure 295. LAF locations are charted for each key posture and each participant in the groups

The results show that the locations of UAF and LAF generally changed linearly throughout the range of arm movement. This finding supports the outcome of the previous study in section 9.5.1. The results also show that the linear relationship for the locations of UAF and LAF was specific for

each participant. Thus, to enable a specific representation of the linear relationship for each participant, the mathematical equation below was adopted:

$$y_n = mx_n + b$$

$$m = \frac{(y_2 - y_1)}{(x_2 - x_1)}, \quad b = y_1 - m \times x_1$$

where:

- x_n = UAF or LAF location at n°
- y_n = n°
- x_1 = UAF or LAF location for fully extended arm
- y_1 = angle of fully extended arm
- x_2 = UAF or LAF location for fully flexed arm
- y_2 = angle of fully flexed arm i.e. 35°

9.10.1.4 Database item number 6: A mathematical equation that captured the relationship of UAF- UAM and LAF-LAM

To determine the mathematical equation that captured the relationship of UAF-UAM and LAF-LAM, the locations of UAF, UAM, LAM and LAF of all key postures were required from each participant. Table 37 shows an example of these locations for the Asian Female group.

Table 37. Data to establish the relationship of UAF-UAM and LAF-LAM for Asian Female group

Asian Female								
	Participant 1				Participant 2			
	Full extension	135	90	Full flexion	Full extension	135	90	Full flexion
UAF location (mm)	119.86	124.38	126.99	137.26	97.05	99.02	101.33	104.06
UAM location (mm)	54.64	63.81	84.38	101.54	41.47	49.93	62.09	72.82
UAM/UAF	0.46	0.51	0.66	0.74	0.43	0.50	0.61	0.70
LAF location (mm)	114.41	121.77	130.59	146.09	89.64	94.86	100.77	109.39
LAM location (mm)	68.63	86.64	99.05	116.91	45.86	58.48	70.03	91.59
LAM/LAF	0.60	0.71	0.76	0.80	0.51	0.62	0.69	0.84
	Participant 3				Participant 4			
	Full extension	135	90	Full flexion	Full extension	135	90	Full flexion
UAF location (mm)	90.90	93.67	97.41	102.46	110.84	113.86	117.08	125.76
UAM location (mm)	47.39	57.77	71.08	82.60	60.49	69.22	83.43	94.15
UAM/UAF	0.52	0.62	0.73	0.81	0.55	0.61	0.71	0.75
LAF location (mm)	89.88	94.50	101.67	107.88	106.63	110.51	119.18	129.34
LAM location (mm)	44.79	55.63	72.30	87.72	55.23	64.91	82.59	99.26
LAM/LAF	0.50	0.59	0.71	0.81	0.52	0.59	0.69	0.77
	Participant 5				Participant 6			
	Full extension	135	90	Full flexion	Full extension	135	90	Full flexion
UAF location (mm)	89.48	94.02	99.18	104.18	97.13	100.11	103.36	106.28
UAM location (mm)	44.84	60.17	73.97	84.37	49.10	57.36	70.67	82.30
UAM/UAF	0.50	0.64	0.75	0.81	0.51	0.57	0.68	0.77
LAF location (mm)	89.88	94.71	100.61	107.88	97.88	102.93	107.75	115.73
LAM location (mm)	46.27	60.84	79.64	88.48	50.76	67.94	77.41	90.23
LAM/LAF	0.51	0.64	0.79	0.82	0.52	0.66	0.72	0.78

To capture the relationship of UAF-UAM and LAF-LAM, the ratio of UAM to UAF and the ratio of LAM to LAF were charted for all key postures. The results are shown in Figure 296, for UAF-UAM, and in Figure 297, for LAF-LAM. The results show that, throughout the range of arm movement, the ratio of UAM to UAF and the ratio of LAM to UAF generally followed a two degree polynomial regression. Coefficients of these regressions were then stored in the database to predict the location of UAM and LAM once the locations of UAF and LAF were known.

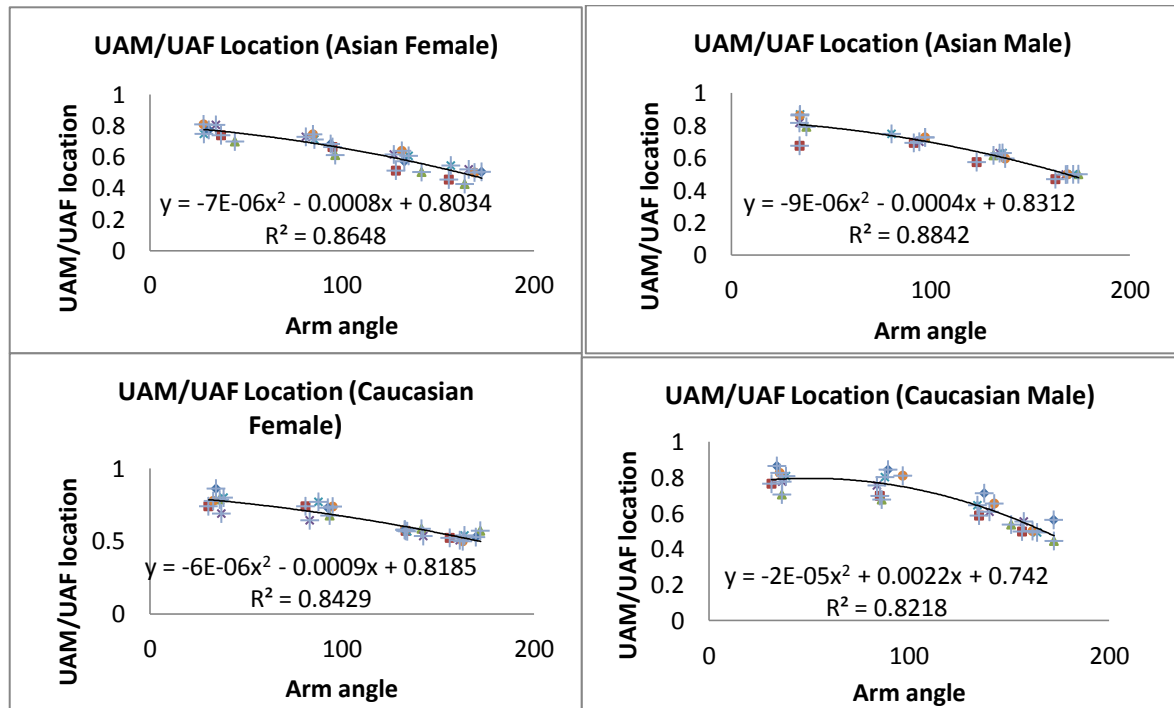


Figure 296. Relationship between UAF and UAM throughout the range of arm movement for each gender and race

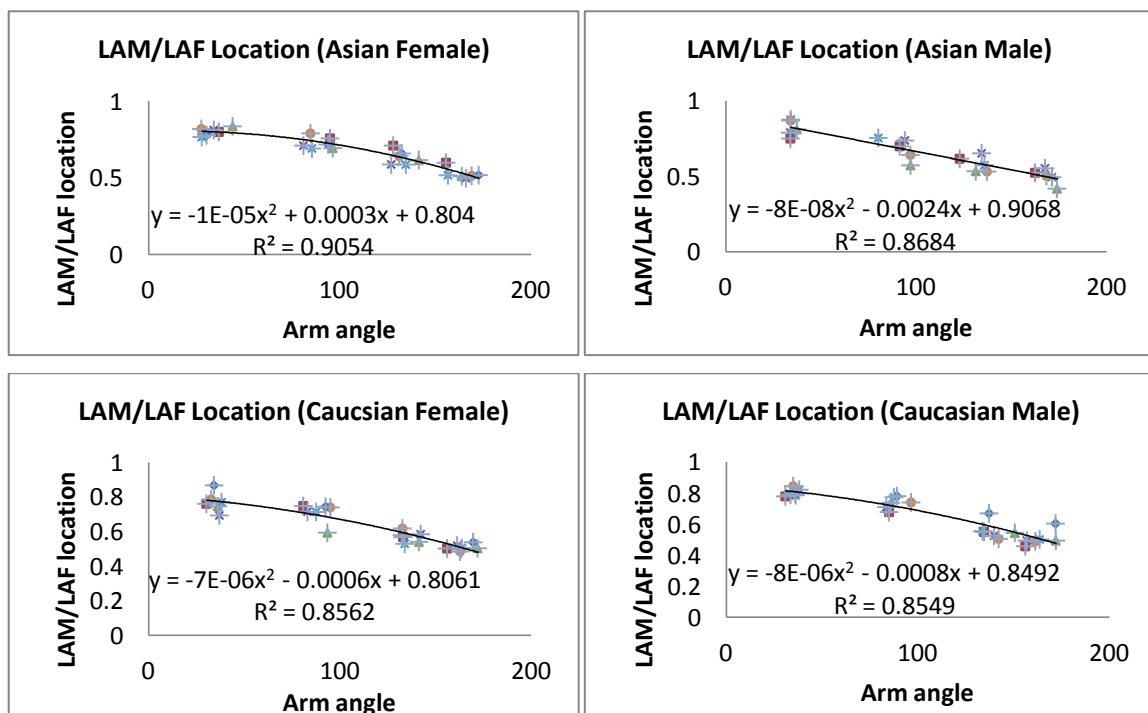


Figure 297. Relationship between LAF and LAM throughout the range of arm movement for each gender and race

9.10.1.5 Discussions

As shown in section 9.10.1.1 to 9.10.1.4, a set of mathematical equations were successfully extracted from the data collected in section 9.9. Regression analysis was used to generate the mathematical equations in section 9.10.1.1, 9.10.1.2 and 9.10.1.4. In section 9.10.1.1, with BMI and upper arm length as the input values, multiple regressions were used to predict the locations of UAF of a fully extended and flexed arm.

In section 9.10.1.2 and 9.10.1.4, linear regressions were used to predict the locations of LAF, UAF and LAM. According to Mendes and Mosley (2006), for regression analysis, an R^2 of 0.7 was required before they could be used for subsequent analysis. In this research, 21 out of 24 of the R^2 regression analysis result showed that they were able to account for at least 75% of the variation in the data. Considering that the regression analyses were created based on a limited number of data (5 or 6 data for each race and gender), the results show the potential and suitability of the regression analysis as a tool to predict the locations of UAF, UAM, LAM and LAF.

However, Mendes and Mosley (2006) also stated that the R^2 value should be obtained from a sufficient number of data. They believed that a combination of a small number of data and large number of variables might result in failure to capture the true relationship between variables. Thus, for future studies, this research suggests that additional data is collected to re-establish the mathematical equations in section 9.10.1.1, 9.10.1.2 and 9.10.1.4. The rule of thumb for regression analysis suggests that at least 10 data points should be available for each variable in order to fully capture the true relationship between variables (Davis, 2011). As the multiple regressions in section 9.10.1.1 involved three variables i.e. BMI, upper arm length and the locations of UAF; it is suggested that at least 30 participants should be allocated for each race and gender.

9.10.2 Data processing for database items that were linked to the shape of five key cross sections

Database items linked to the locations of UAF, UAM, LAM and LAF were database item numbers 7 to 10. For these database items the shapes of the five key cross sections were needed. To express the shape of the five key cross sections, an existing procedure in section 8.1.3 was partly adopted. The existing procedure, shown in Figure 298, indicated that 3D scan data with its joint information and side-front view photographs were simultaneously required to correctly locate and orientate digitised key cross sections. In the existing procedure, this step was then followed by determining sample points of a cross section and their distances towards the bone point i.e. the intersection between the cross section's plane and the bone. This meant that the sampling points' distances were dependent on the bone point location. As the aim of the database was to solely compare the cross sections' shape, a way to express its shape independently from any other factor was required.

Therefore, for the database, sample points of a cross section and their distances was obtained from the centre of the cross section' bounding box.

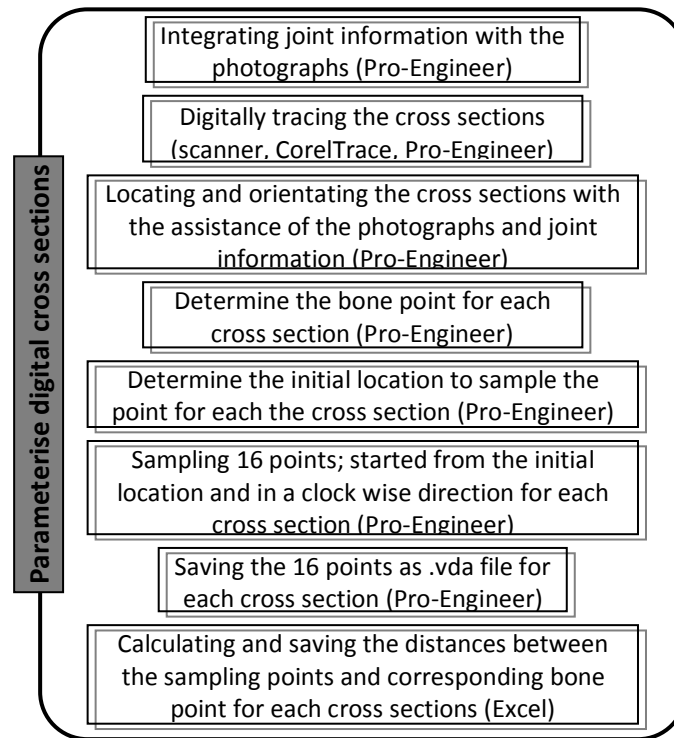


Figure 298. Existing procedure to express the shape of cross sections which was partly adopted

Figure 299 illustrates the difference in obtaining and calculating distances of sampling points using a bone point and a bounding box centre. Once the distances were acquired, they could be used to determine database item numbers 7 to 10. The complete list of the distances of sampling points for all participants are given in appendix D (supplied in the accompanying CD).

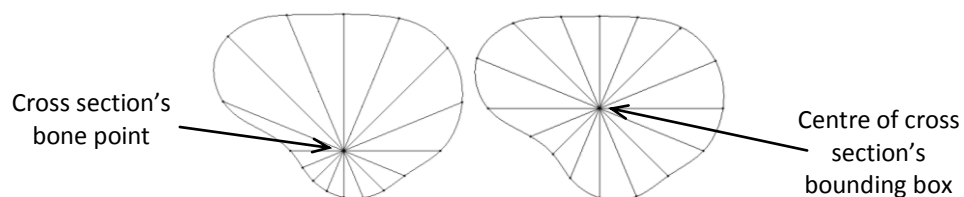


Figure 299. Left image shows obtaining sample points from the bone point, right image shows obtaining sampled point from the centre of the cross section's bounding box

9.10.2.1 Database item number 7: Ratio values of maximum vertical and horizontal dimension of UAF-UAM and LAF-LAM for fully extended arms

Figure 300 shows the steps to acquire the ratio values for the maximum vertical and horizontal dimensions of UAF-UAM and LAF-LAF for a fully extended arm. As shown in Figure 300, the coordinates of 16 sample points were recreated based on the result of the partial application of the existing procedure in section 8.1.3 i.e. key cross section's 16 sample points and their unit vectors. The coordinates were then utilised to create a Bspline curve. The creation of Bspline curves allowed

the extraction of the maximum vertical and horizontal dimensions for UAF, UAM, LAM and LAF. Once these dimensions were acquired, the ratio was then calculated.

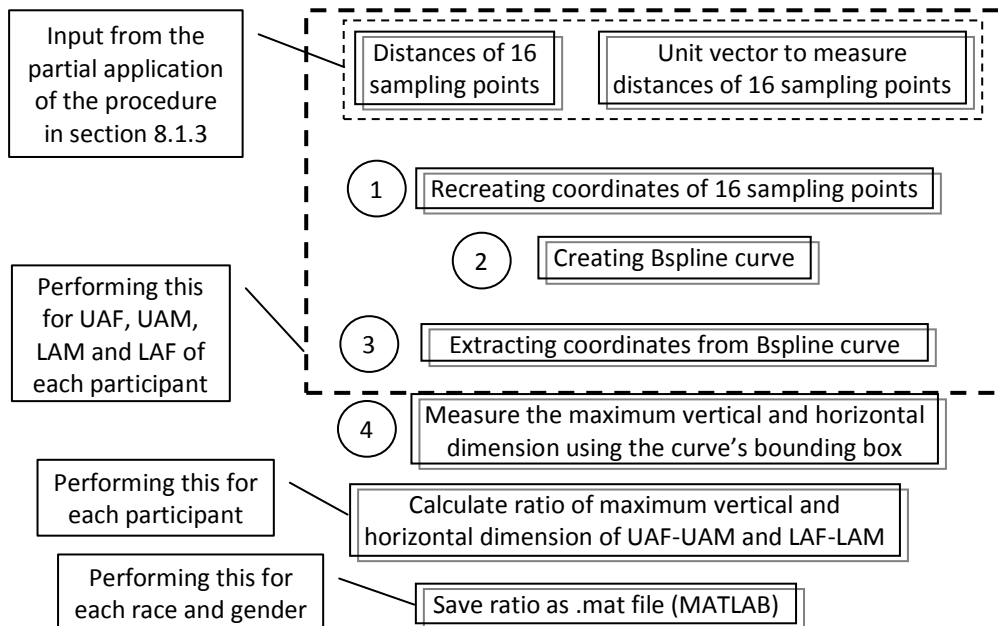


Figure 300. Steps to obtain ratio values of maximum vertical and horizontal dimension of UAF-UAM and LAM-LAF for fully extended arms

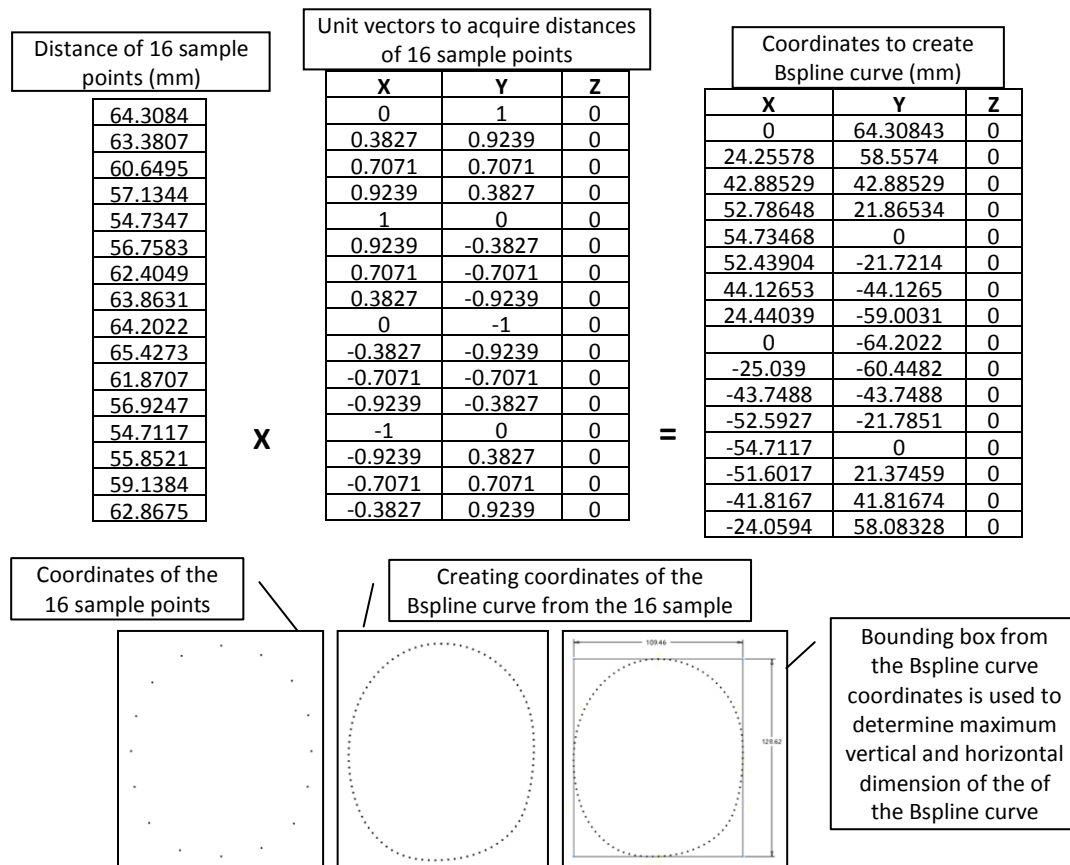


Figure 301. Example of the result from step 1 to 4 which were shown in Figure 300

All of the steps shown in Figure 300 were performed in Matlab. An example of the results from steps 1 to 4 is shown in Figure 301. The final result i.e. ratio of UAF-UAM and LAF-LAM for a fully

extended arm, is shown in Table 38 for each gender and race. These ratios were then stored in the database.

Table 38. Ratio of UAF-UAM for each gender and race

Asian Female		Participant					
		1	2	3	4	5	6
UAF-UAM	horizontal dimension (x)	1.0488	0.9905	1.0198	1.0592	0.9944	1.0756
	vertical dimension (y)	1.1821	1.1444	1.1531	1.1075	1.129	1.1577
LAF-LAM ratio	horizontal dimension (x)	0.8126	0.8458	0.8794	0.8882	0.8483	0.8788
	vertical dimension (y)	0.8902	0.898	0.9193	0.9624	0.896	0.9346
Asian Male		Participant					
		1	2	3	4	5	
UAF-UAM	horizontal dimension (x)	0.991	0.9624	0.9751	0.9402	0.939	
	vertical dimension (y)	1.1471	1.0974	1.1211	1.1312	1.1113	
LAF-LAM ratio	horizontal dimension (x)	0.9499	0.9349	0.9433	0.8707	0.9014	
	vertical dimension (y)	0.976	0.9785	0.9797	0.9924	1.0378	
Caucasian Female		Participant					
		1	2	3	4	5	6
UAF-UAM	horizontal dimension (x)	1.1347	1.0701	1.0595	0.9761	1.0228	1.0285
	vertical dimension (y)	1.1569	1.0486	1.0873	1.1366	1.1765	1.1615
LAF-LAM ratio	horizontal dimension (x)	0.7887	0.7738	0.8256	0.9785	0.9222	0.8923
	vertical dimension (y)	0.8482	0.8632	0.9187	0.9808	0.9341	0.9274
Caucasian Male		Participant					
		1	2	3	4	5	6
UAF-UAM	horizontal dimension (x)	1.05	1.0828	1.0558	0.9772	0.9071	0.9503
	vertical dimension (y)	1.1956	1.1676	1.1641	1.1535	1.1584	1.0847
LAF-LAM ratio	horizontal dimension (x)	0.8344	0.8299	0.9018	0.9875	0.9638	0.9025
	vertical dimension (y)	0.9479	0.8921	0.9319	0.9856	1.0107	0.9539

9.10.2.2 Database item number 8: The four vertical and horizontal dimensions of UAF, UAM, LAM and LAF cross sections for each key posture from all individuals in the database

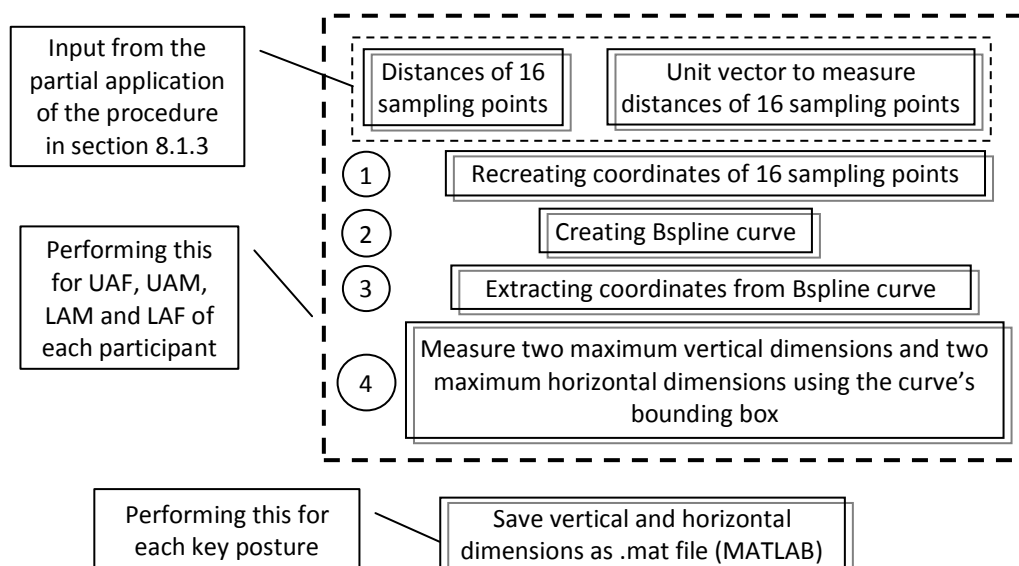


Figure 302. Steps to acquire two vertical and horizontal dimension of UAF, UAM, LAM and LAF

Figure 302 shows the steps to acquire the values for the four vertical and horizontal dimensions of UAF, UAM, LAM and LAF for all key postures. Steps 1 to 3 were exactly the same as the steps to obtain the ratio values of UAF-UAM and LAF-LAM. For step 4, a bounding box was created from the extracted coordinates of the Bspline curve. However, instead of obtaining one overall vertical and one overall horizontal dimension, two dimensions were acquired. The two dimensions were measured from the centre of the bounding box to the relevant boundary of the bounding box. Using the same Bspline coordinates from the previous example, Figure 303 shows the two horizontal and two vertical dimensions of the Bspline coordinates. Table 39 shows an example of the results for the four vertical and horizontal dimensions of UAF, UAM, LAM and LAF from fully extended arms for Asian female group. These dimensions were then stored in the database.

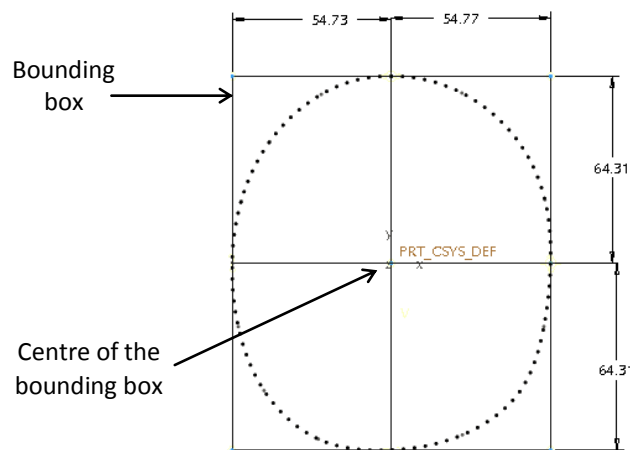


Figure 303. An example of quadrant vertical and horizontal dimensions for UAF of a fully extended arm

Table 39. Vertical and horizontal dimension for UAF, UAM, LAM and LAF for fully extended arm for Asian female group

		Participant 1	Participant 2	Participant 3	Participant 4	Participant 5	Participant 6
UAF	x ₁ (mm)	54.7728	39.2085	35.8187	39.3273	34.1084	34.5011
	x ₂ (mm)	-54.7309	-39.3036	-35.8512	-39.2482	-34.1187	-34.4154
	y ₁ (mm)	64.3084	46.751	41.5075	44.04	39.2787	40.1436
	y ₂ (mm)	-64.3066	-46.8298	-41.6145	-43.839	-39.2776	-40.117
UAM	x ₁ (mm)	52.3041	39.5812	35.1105	37.1369	34.268	31.9429
	x ₂ (mm)	-52.1058	-39.6837	-35.1684	-37.0462	-34.3406	-32.1284
	y ₁ (mm)	54.4636	40.8621	36.1107	39.8449	34.8093	34.8149
	y ₂ (mm)	-54.3426	-40.9126	-35.9733	-39.5028	-34.7727	-34.5148
LAM	x ₁ (mm)	48.799	39.6872	35.6222	39.5064	37.06	36.5162
	x ₂ (mm)	-46.318	-40.1319	-35.5811	-39.5471	-37.2874	-36.1491
	y ₁ (mm)	34.4805	32.9081	27.8396	33.056	32.6931	28.7703
	y ₂ (mm)	-44.2727	-32.8371	-27.8393	-33.0625	-32.6354	-28.6021
LAF	x ₁ (mm)	38.685	33.6845	31.3957	35.1139	31.6042	31.8544
	x ₂ (mm)	-38.6033	-33.8291	-31.2213	-35.0997	-31.4659	-32.0068
	y ₁ (mm)	35.0433	29.6041	25.5876	31.8773	29.3185	26.9065
	y ₂ (mm)	-35.0642	-29.4351	-25.5991	-31.752	-29.2183	-26.7165

9.10.2.3 Database item number 9: Transformed values of 16 sampling points' distances of E cross sections toward its centre for fully extended arms

The transformation of the 16 sampling points' distances of the E cross section toward its centre for fully extended arms used an application of PCA to reduce the number of data to be stored in the database. The PCA application was performed in MATLAB and the steps are shown in Figure 304.

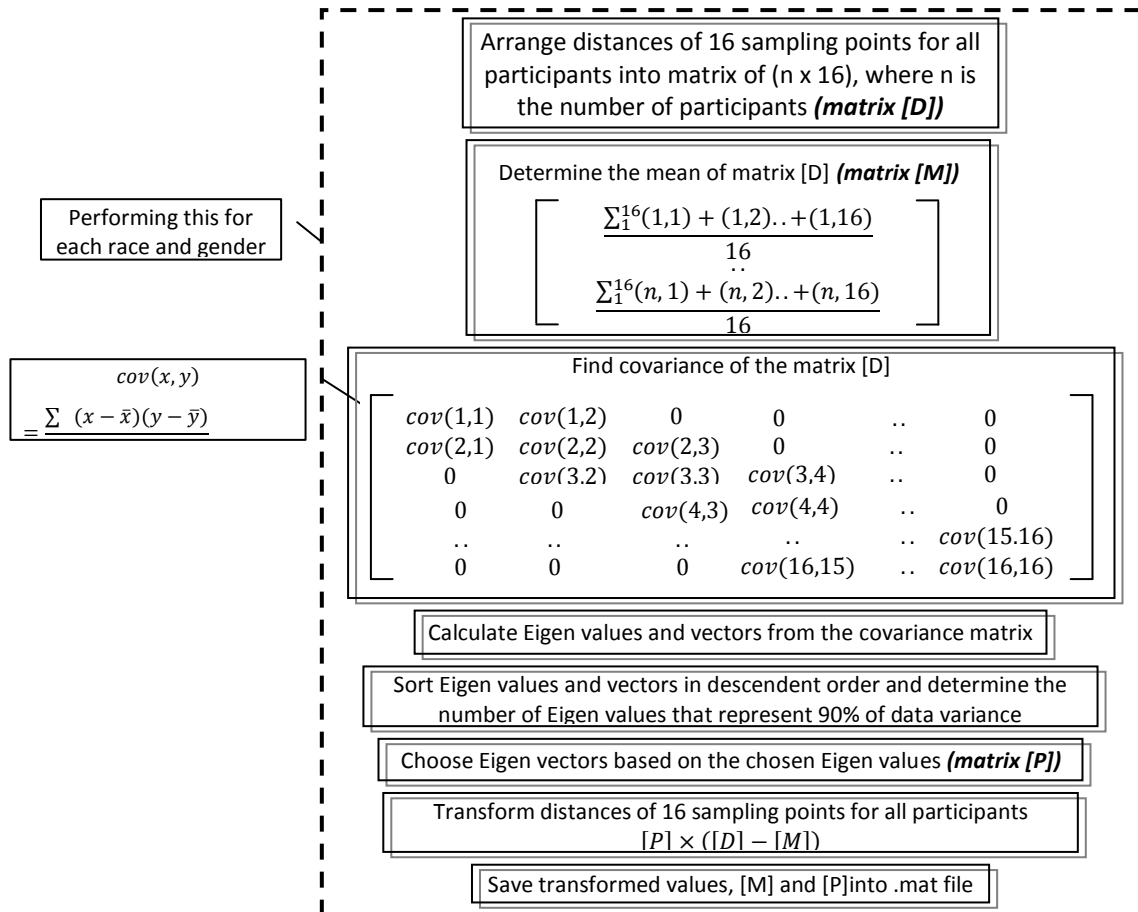


Figure 304. Steps to obtain transform values of distances from E sampling points

Firstly, 16 sampling points from all participants were arranged into $[n \text{ participants} \times 16]$ i.e. **matrix [D]** and its mean was calculated i.e. **matrix [M]**. The next step was to calculate covariance which represents data variation from the 16 sampling points. Eigen values and vectors, which identified the pattern of maximum variability within the data, were then calculated from the covariance matrix. Once the number of Eigen values and corresponding Eigen vectors i.e. **matrix [P]** to be used were determined, the distances of the 16 sampling points from the E cross section were transformed into new values.

The transformation result for each gender and race is shown in Table 40 and the graphs of the transformed values for each race and gender are shown in Figure 305. The result shows that only one principal component was required for Asian females, Asian males and Caucasian female groups. Hence, only one transformed value represented the E cross section distances for each participant in these groups. For Caucasian male groups, two transformed values were required to represent 90%

variance in the dataset. For each race and gender, the transformed values, $matrix[M]$ and corresponding Eigen vectors were then stored in the database.

Table 40. Transformed values of E cross sections' distances

Transformed Values						
	part. 1	part. 2	part. 3	part. 4	part. 5	part. 6
Asian Female	45.7069	4.4792	-3.3853	-10.8368	-17.0839	-18.8801
Asian Male	52.736	-7.1624	-12.5809	-14.7619	-18.2308	
Caucasian	35.3046	26.658	14.1646	-19.3164	-22.5371	-34.2737
Caucasian Male	20.8121	1.5426	-0.959	-1.645	-9.3026	-10.4481
	0.0241	-9.0254	6.2991	5.0549	2.7916	-5.1442

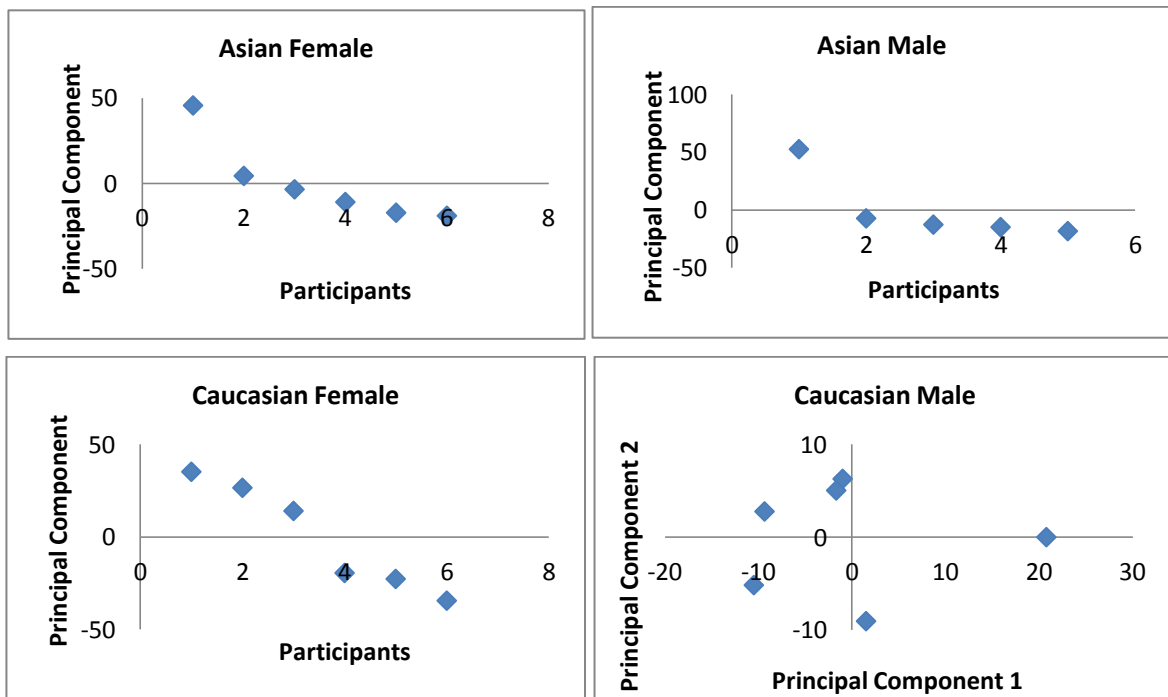


Figure 305. Transformed values of each race and gender are being charted using their principal components

9.10.2.4 Database item number 10: Transformed values of 16 sampling points' distances of E cross sections toward its centre for other key postures

The steps to transform the values of the E cross section distances for the other key postures were the same as those for fully extended arms. The only difference was the input i.e. matrix D (see Figure 303) which used the E cross section distances of other key postures instead of fully extended arms. As a result, the matrix D size was $n \times 48$, where n was the participants number and 48 was the overall number of distances from three key postures. The results of the transformation were shown in Table 41. As shown in the results, at least three principal components were required to represent the 90% data variance for each group. For each race and gender, the transformed values, the mean of 48 distances of sampling points and corresponding Eigen values were then stored in the database.

Table 41. Results of transformation of E cross sections' distances for other key postures

	Transformed Values					
	Participant 1	Participant 2	Participant 3	Participant 4	Participant 5	Participant 6
Asian Female	73.6103	-3.0187	-25.4658	3.0037	-17.2465	-30.8831
	3.8085	-10.4161	5.7343	-1.6714	-6.0238	8.5686
	-2.0402	3.9435	4.2914	6.2633	-9.6937	-2.7643
Asian Male	10.4941	21.9216	-52.8145	9.3092	11.0897	
	-10.4124	-10.2908	-1.8818	8.4195	14.1655	
	-14.1768	12.3928	2.1826	1.7976	-2.1963	
	-0.3336	2.2013	0.6479	-9.7519	7.2363	
Caucasian Female	77.2844	35.7323	11.2827	-45.6797	-27.4313	-51.1884
	-11.8042	18.7788	-3.9684	-12.1517	8.3806	0.7648
	3.3914	-6.3555	-0.502	-7.3058	7.9271	2.8448
Caucasian Male	9.7567	28.0257	10.5957	-18.3154	-5.7916	-24.2712
	17.0531	-14.4613	1.0777	-3.1098	8.4926	-9.0525
	-5.2066	-0.0689	1.4265	-11.4828	10.7914	4.5403
	0.808	-4.5059	10.5301	-4.0848	-7.2876	4.5403
	-5.7847	-1.8111	5.9541	4.1352	3.2103	-5.7039

9.10.2.5 Discussions

As shown in section 9.10.2.1 to 9.10.2.4, the required database item numbers 7 to 10 were successfully extracted from the data collected in section 9.9. In section 9.10.2.1 and 9.10.2.2, ratio values of maximum vertical and horizontal dimensions as well as the four vertical and horizontal dimensions were determined for each participant. Also, in section 9.10.2.3, sample points of the E cross sections of fully extended arms were transformed using Principal Component Analysis (PCA). The transformation allowed the 16 sample points of E cross sections to be represented with only one transformed value. This resulted in easing the process to compare the E cross section of a 3D scan with the data in the database. However, if the database is expanded as recommended in section 9.10.1.5, as the number of participants for each race and gender grow, there is a possibility that there would be more shape variations. As a result, it is possible that PCA would need more than one transformed value to represent the 16 sample points of the E cross sections. If this is the case, a more complex approach to compare the E cross section of 3D scan data and database would be needed. This research suggests the use of k-nearest neighbour as it involves a simple algorithm and hence would still be suitable for real time modelling. The k-nearest neighbour is useful in identifying how close a data point is to a group of data based on its Euclidean distance.

In section 9.10.2.4, sample points that were obtained from the E cross sections of 135°, 90° and fully flexed arms were simultaneously transformed using Principal Component Analysis (PCA). As shown in section 9.10.2.4, only 3 to 5 transformed values were required to represent the 48 sample points of the E cross sections (16 sample points for E at 135° flexion, 16 sample points for E at 90° flexion and 16 sample points for E at fully flexed). This result provided a good example of how PCA was useful in compressing the number of data. Again, any increase in the size of the database would

likely result in a corresponding increase in the shape variation of the E cross sections. This might then result in more transformed values required to represent the E cross sections of various key postures. If this was the case, this research suggests performing PCA on the E cross sections for each key posture separately. Separating the E cross sections based on key posture limits the shape variation that has to be handled by PCA and hence likely reduced the number of transformed values.

9.10.3 Data processing for database items linked to the shape of profiles

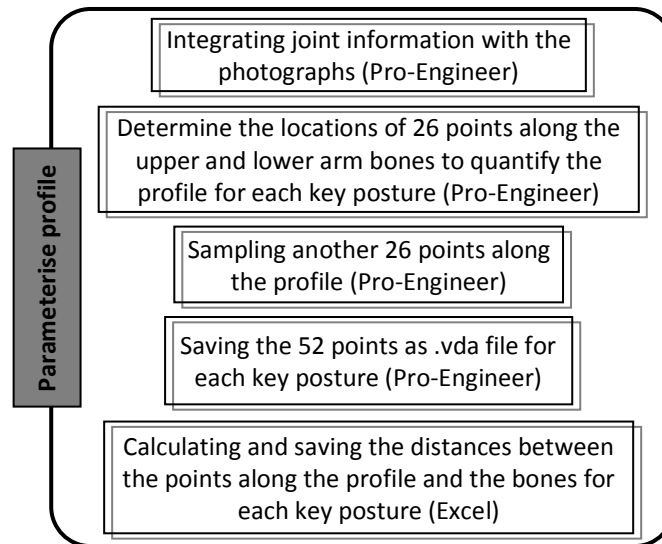


Figure 306. The existing procedure to express the shape of profiles in section 8.1.3 which was partly adopted

Database items that linked to the shape of profiles were database item numbers 11 and 12. For these database items the shapes of profiles were needed. To express the shape of profiles, an existing procedure in section 8.1.3 was partly adopted. The existing procedure, shown in Figure 306, indicated that joint information of 3D scan data and side-front view photographs were simultaneously required to create profiles. Once the profiles were created, the shapes of profiles were then expressed by calculating the distances of points on the profile towards the corresponding bone. The number and placements of these points were chosen such that they could represent different shapes of profile with the least error. Since the framework required 2/3 of the upper and lower arm profiles (see section 9.7); the number and placements of the points on the profiles should also be optimised for 2/3 of the upper and lower arm profiles. However, the number and placement of points on the profile depicted in Figure 306 was specifically aimed to express the shapes of profiles at the flesh deformation area. This meant that the number and placement of points on the profile from the existing procedure in section 8.1.3 could not be utilised. Thus, an optimum number and placement of points on the profiles had to be determined for the framework.

The number and placement of points on the profile for the framework was based on all of the database profiles i.e. 96 profiles (24 participants with 4 profiles each). The existing method to identify the optimum number and placement of points on the profile in section 7.3.2.5 was adopted.

The Matlab code of the existing method was reused with a minor change to accommodate the framework requirement i.e. using the location of 1/3 and 2/3 of upper/ lower arm length instead of the locations of UAF, UAM, LAM and LAF. The result of the Matlab code application showed that there were 33 optimum points and their locations were as the following:

- Segment 1 (2/3 – 1/3 of upper arm length): [30% 40% 60% 70% 90%]
- Segment 2 (1/3 of upper arm length - E): [20% 40% 60% 70% 80% 90%]
- Segment 3 (E-1/3 of lower arm length): [10% 20% 30% 40% 60% 70% 90%]
- Segment 4 (1/3 – 2/3 of lower arm length): [50% 70%]

Figure 307 shows the 33 optimum points on four key postures from participant 6 of the Asian female group.

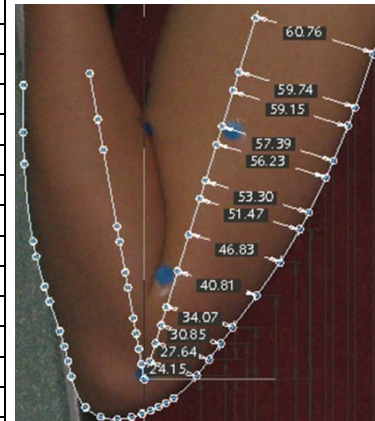


Figure 307. The 33 points on the profile for participant 6 of Asian female group

Once the optimum number and placement of points on the profile was identified, the next step was to calculate the distances between these points and the bones for each profile. The procedure shown in Figure 306 was followed. Table 42 shows an example of the profile-bone distances for the 33 points for participant 6 in the Asian female group. The complete lists of the profile-bone distances for all participants are given in appendix E (supplied in the accompanying CD). Once the profile-bone distances for the all participants were calculated, they could then be used to determine database items 11 and 12. In accordance with the requirement of the database content on number 11 and 12 in section 9.8, the application of PCA would be performed on the profile for a fully extended arm and other key postures separately. The procedure and results for each are discussed in the following.

Table 42. Example of profile distances for participant 6 from the Asian female group and an illustration of some profile distances for a fully flexed arm

Distances for profiles (mm)				
	Fully extended	135°	90°	Fully flexed
Sample point 1	59.7232	59.9058	60.6195	60.7606
Sample point 2	56.5398	55.0857	57.9964	59.7442
Sample point 3	55.1241	53.5679	56.9066	59.148
Sample point 4	51.5842	50.5404	54.2405	57.3879
Sample point 5	49.4402	48.9922	52.6211	56.2327
Sample point 6	44.507	45.7299	49.0068	53.3015
Sample point 7	41.8964	43.9814	47.1101	51.4715
Sample point 8	36.9041	40.1786	43.1255	46.8262
Sample point 9	32.9146	35.8712	38.5979	40.8086
Sample point 10	29.7153	30.9346	33.1561	34.0684
Sample point 11	27.8514	28.203	29.9941	30.8533
Sample point 12	25.2158	25.2582	26.5004	27.6381
Sample point 13	21.1303	21.9944	22.4997	24.1535
Sample point 14	15.3977	17.4419	16.8202	17.1335
Sample point 15	15.0706	16.9465	16.1336	15.7786
Sample point 16	14.781	16.57	15.8528	15.3119
Sample point 17	14.5285	16.2663	15.9653	15.6906
Sample point 18	14.3149	16.076	16.4781	17.0091
Sample point 19	14.1305	15.976	17.4757	19.6493
Sample point 20	13.9736	15.9348	19.122	23.8205
Sample point 21	13.8428	15.9973	21.1506	28.4155
Sample point 22	13.7411	16.1526	22.922	32.0445
Sample point 23	13.3082	17.6112	24.5989	35.1596
Sample point 24	13.6679	18.3429	25.3558	35.4024
Sample point 25	14.4341	18.826	25.9266	35.9269
Sample point 26	15.3757	19.2727	26.3801	36.8871
Sample point 27	17.3539	20.402	27.7677	39.2108
Sample point 28	18.3114	21.2274	28.6513	40.3148
Sample point 29	19.9614	22.9869	30.0947	41.7444
Sample point 30	20.6699	23.8017	30.4403	41.9738
Sample point 31	22.6736	25.7582	29.8784	39.5571
Sample point 32	22.0416	25.2032	28.7296	37.3442
Sample point 33	19.8686	23.03	26.1231	33.0659



9.10.3.1 Database content number 11: Transformed values of profile from fully extended arms for each race and gender

The steps to transform the values of the profile-bone distances for fully extended arms followed the description in section 9.10.2.3. The input was the profile-bone distances of the fully extended arm and the output was the transformed values of the profile-bone distances, principal components of the profile-bone distances and overall mean of the profile-bone distances. The transformed values are shown in Table 43 for each group. As shown in the results, at least three principal components were required to represent the data variance for each group. For each race and gender, the transformed values, the mean of distances of profiles and corresponding Eigen values were then stored in the database.

Table 43. Transformed values of profiles' distances for fully extended arms

Transformed profiles distances (mm)					
	Asian Female		Asian Male		
	Transformed	Transformed	Transformed	Transformed	Transformed
Participant 1	6.0038	19.1786	4.5564	-14.4227	5.1844
Participant 2	52.9272	-6.2895	-15.9861	4.0099	3.784
Participant 3	-9.6978	14.9834	-8.7352	-1.7115	-7.6362
Participant 4	-17.5594	-10.2189	11.135	2.5583	-8.4584
Participant 5	-40.1651	-6.8545	9.0299	9.566	7.1262
Participant 6	8.4914	-10.7991			
	Caucasian Female		Caucasian Male		
	Transformed	Transformed	Transformed	Transformed	Transformed
Participant 1	46.8037	20.6081	44.1513	0.6537	-8.897
Participant 2	26.7549	4.6527	9.0764	-3.0734	12.1779
Participant 3	66.9547	-19.8165	-27.4169	-5.2277	-2.2315
Participant 4	-56.1949	-2.5525	9.0188	-8.3612	0.855
Participant 5	-17.6102	-2.0076	-36.1357	2.3982	-5.7657
Participant 6	-66.7083	-0.8844	1.3061	13.6104	3.8613

9.10.3.2 Database content number 12: Transformed values of profile for the remaining key postures for each race and gender

The steps to transform the values of the profile-bone distances for the remaining key postures were the same as those used for the transformation for profile-bone distances for fully extended arms as detailed above. The input was the profile-bone distances of other key postures and the output was again: the transformed values, principal components and overall mean of profile-bone distances. The transformed values are shown in Table 44 for each group. As shown in the results, only the Caucasian female group required two principal components whereas the rest of the groups required at least three principal components. For each race and gender, the transformed values, the mean of distances of profiles and corresponding Eigen values were then stored in the database.

Table 44. Transformed values of profiles distances from other key postures

	Asian Female			Asian Male			
	Transformed values (mm)			Transformed values (mm)			
	Value 1	Value 2	Value 3	Value 1	Value 2	Value 3	Value 4
Participant 1	-12.2954	-22.6264	14.7658	-21.7469	-9.624	14.6419	-6.6066
Participant 2	101.6307	1.1966	-0.2634	-18.5604	7.7965	-16.0671	-6.5626
Participant 3	-23.6517	4.0991	16.5415	-15.8936	9.1871	2.469	13.3077
Participant 4	-28.8555	-31.9014	-17.8813	20.7939	-23.4043	-6.597	3.3576
Participant 5	-53.7192	29.1031	-4.3324	35.4069	16.0447	5.5532	-3.4961
Participant 6	16.8912	20.1291	-8.8302				
	Caucasian Female			Caucasian Male			
	Transformed values (mm)			Transformed values (mm)			
	Value 1	Value 2		Value 1	Value 2	Value 3	
Participant 1	72.1845	48.2641		59.1178	-10.8224	-10.1884	
Participant 2	54.7105	12.2431		11.0287	30.8703	-8.3406	
Participant 3	114.4781	-47.4586		-53.2621	-3.2382	10.0798	
Participant 4	-99.7086	11.249		31.7836	-32.2315	13.3395	
Participant 5	-43.7493	0.4017		-52.8161	-19.0879	-14.5263	
Participant 6	-97.9152	-24.6992		4.1481	34.5098	9.6358	

9.10.3.3 Discussions

As shown in section 9.10.3.1 and 9.10.3.2, the required database item numbers 11 to 12 were successfully extracted from the data collected in section 9.9. In section 9.10.3.1, two to three transformed values were required to represent the 33 distances between points on the profile and corresponding bones. In section 9.10.3.2, two to four transformed values were needed to represent a total of 99 distances between points on the profile and corresponding bones (33 distances for profile at 135° flexion, 33 distances for profile at 90° flexion and 33 distances for profile at a fully flexed arm). The number of transformed values for a profile was more than for the five key cross sections. This suggested that there was more shape variation in the profiles than the cross sections. Similarly to the transformed values of cross sections, as the number of participants for each race and gender grow; there is a possibility that there would be even more shape variation which would yield a larger number of transformed values. If this is the case, the transformed value could be extracted for each key posture as this would limit possible shape variations and result in a lower number of transformed values.

9.11 Software programme development

This section outlines the software programme development which allowed the application of the proposed FDM to accommodate various body sizes and types. The programming was based on the proposed framework outlined in section 9.2. The framework required four inputs: the 3D scan of a fully extended arm and the subject's race, gender and BMI; to extract information from the database. Together with the extracted data or information from the database which was created in section 9.10, these four inputs were then used to create: (1) five key cross sections for each key posture; (2) location of five key cross sections for each key posture; and (3) arm profiles for each key posture. Thus, the software programme was a means to realise the proposed prediction method in section 9.4, 9.5, 9.6 and 9.7.

The programming was created in Matlab and the full code is provided in the accompanying CD of this thesis. The programming consisted of four major parts: (1) template matching and sampling of 3D scan data; (2) predicting the five key cross sections for 135°, 90° and maximum flexion; (3) predicting profiles for 135°, 90° and maximum flexion; and (4) integration of FDM with the programming numbers 1 to 3. Each of the programming steps is discussed in the following subsections.

9.11.1 Programming for template matching and sampling of 3D scan data

The processes implemented in the programming for template matching and sampling of 3D scan data are shown in Figure 308. This programming required four inputs from the user: a 3D scan

of a fully extended arm and its joint location, gender, race and BMI. The required information from the database included: (1) the mathematical equation that captured the relationship between the location of UAF, upper arm length, and BMI for each gender and race; (2) the mathematical equation that captured the relationship between the location of UAF and LAF for a fully extended arm; (3) the mathematical equation that captured the relationship between the location of UAF and UAM; and (4) the mathematical equation that captured the relationship between LAF and LAM. The programming also used the default template information i.e. joint location and five key cross sections described in section 9.7.2.1. The output of the programme included: (1) joint coordinates of 3D scan data after template matching; (2) upper arm and lower arm bone orientation; (3) 2D coordinates of the five key cross sections of a fully extended arm from the 3D scan data; (4) the location of UAF, UAM, LAM and LAF of a fully extended arm; and (5) profile coordinates of a fully extended arm.

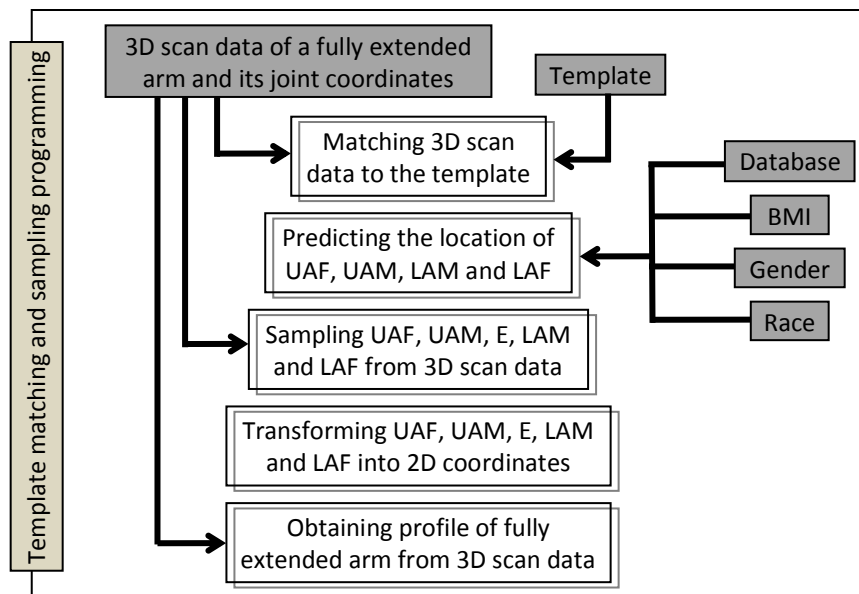


Figure 308. Processes in the programming for template matching and sampling of 3D scan data

To test whether the software programme functioned properly or not, 3D scan data from a participant in the database was used. The choice of which participant data to be used was not important as the aim was to check that the programming produced the necessary output. For the testing, the data of participant 4, from the Asian male group, was used. The data is shown in Figure 309. Joint coordinates, arm length, carrying angle and arm angle were acquired from the 3D scan data. A screenshot of the programming whilst being run is shown in Figure 310. The result after matching the 3D scan data to the template and predicting the location of UAF, UAM, LAM and LAF are shown in Figure 311. The coordinates of upper and lower arm bone orientation are also shown in Figure 311 and Figure 312. Figure 313 shows the five key cross sections which are sampled from the 3D scan data and the profile of the 3D scan data.

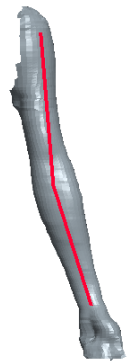

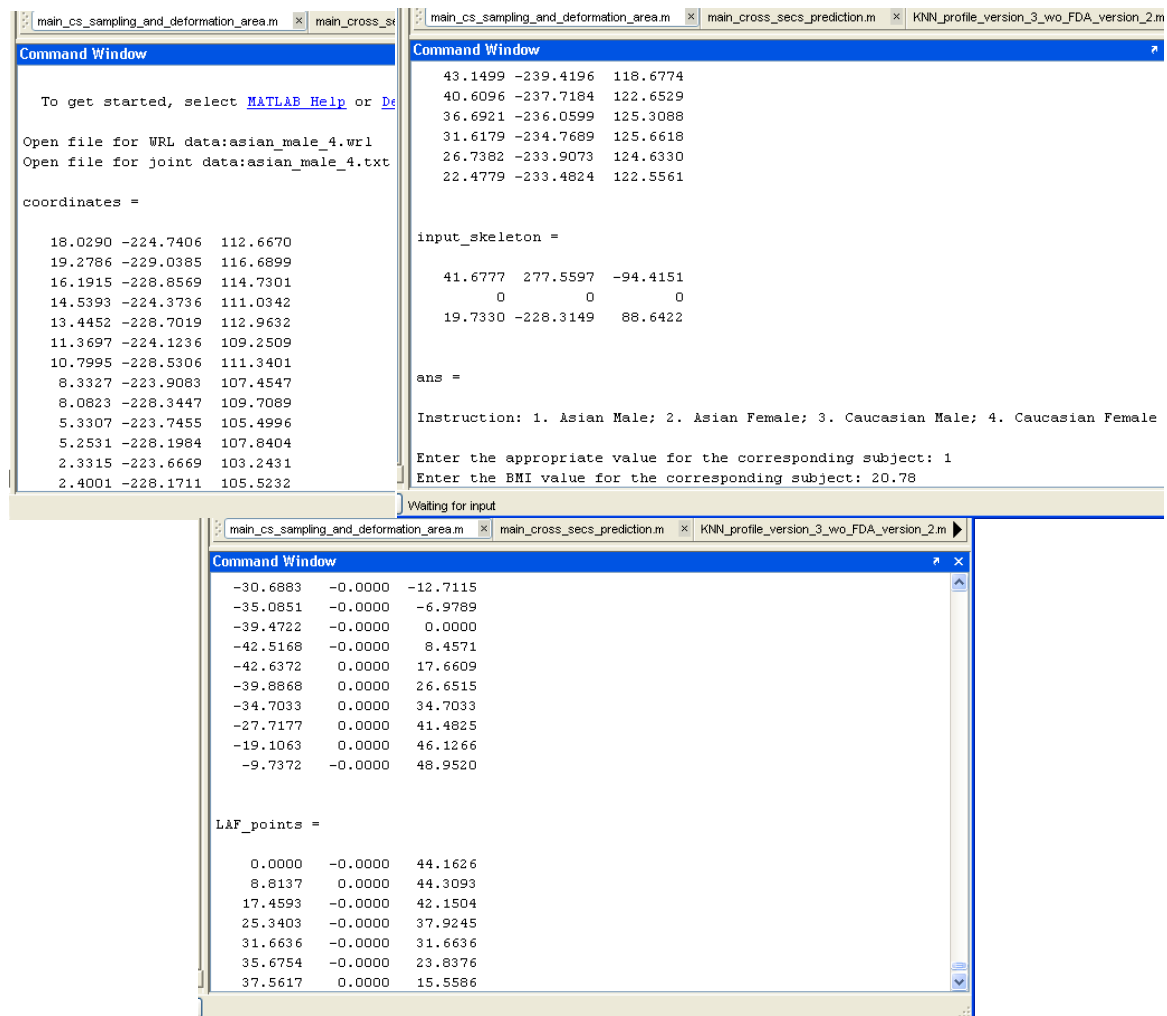
3D scan data		Joint coordinates			
			X (mm)	Y (mm)	Z (mm)
		Shoulder	195.02	1382.29	-2.94
		Elbow	219.68	1087.61	12.75
		Wrist	293.67	854.28	34.13
		BMI			
		20.77947			
		Arm Length (mm)			
		Upper arm	296.1260		
		Lower arm	245.7123		
		Carrying angle	Arm angle		
		12.5563°	167.0731°		

Figure 309. Data of participant 4 from the Asian male group



```

main_cs_sampling_and_deformation_area.m | main_cross_s... | main_cs_sampling_and_deformation_area.m | main_cross_secs_prediction.m | KNN_profile_version_3_wo_FDA_version_2.m

Command Window
To get started, select MATLAB Help or De
Open file for WRL data:asian_male_4.wrl
Open file for joint data:asian_male_4.txt

coordinates =

18.0290 -224.7406 112.6670
19.2786 -229.0385 116.6899
16.1915 -228.8569 114.7301
14.5393 -224.3736 111.0342
13.4452 -228.7019 112.9632
11.3697 -224.1236 109.2509
10.7995 -228.5306 111.3401
8.3327 -223.9083 107.4547
8.0823 -228.3447 109.7089
5.3307 -223.7455 105.4996
5.2531 -228.1984 107.8404
2.3315 -223.6669 103.2431
2.4001 -228.1711 105.5232

main_cs_sampling_and_deformation_area.m | main_cross_secs_prediction.m | KNN_profile_version_3_wo_FDA_version_2.m

Command Window
43.1499 -239.4196 118.6774
40.6096 -237.7184 122.6529
36.6921 -236.0599 125.3088
31.6179 -234.7689 125.6618
26.7382 -233.9073 124.6330
22.4779 -233.4824 122.5561

input_skeleton =

41.6777 277.5597 -94.4151
0 0 0
19.7330 -228.3149 88.6422

ans =

Instruction: 1. Asian Male; 2. Asian Female; 3. Caucasian Male; 4. Caucasian Female
Enter the appropriate value for the corresponding subject: 1
Enter the BMI value for the corresponding subject: 20.78
Waiting for input

main_cs_sampling_and_deformation_area.m | main_cross_secs_prediction.m | KNN_profile_version_3_wo_FDA_version_2.m

Command Window
-30.6883 -0.0000 -12.7115
-35.0851 -0.0000 -6.9789
-39.4722 -0.0000 0.0000
-42.5168 -0.0000 8.4571
-42.6372 0.0000 17.6609
-39.8868 0.0000 26.6515
-34.7033 0.0000 34.7033
-27.7177 0.0000 41.4825
-19.1063 0.0000 46.1266
-9.7372 -0.0000 48.9520

LAF_points =

0.0000 -0.0000 44.1626
8.8137 0.0000 44.3093
17.4593 -0.0000 42.1504
25.3403 -0.0000 37.9245
31.6636 -0.0000 31.6636
35.6754 -0.0000 23.8376
37.5617 0.0000 15.5586

```

Figure 310. Screenshot of the programming which shows the programming prompts participant's information on: (i) 3D scan and its joint data, (ii) gender and race and (iii) BMI. Screenshots also captures some of the programming's results

From observing the result of the template matching visually, it shows that the software programme was successful in manipulating the orientation of 3D scan data to conform to the template's orientation which was shown in Figure 283 in section 9.7.2.1. As shown in Figure 311, Figure 312 and Figure 313, the software programme was also successful in obtaining: 1) joint coordinates of 3D scan data after template matching; (2) upper arm and lower arm bone

orientation; (3) 2D coordinates of the five key cross sections of a fully extended arm from the 3D scan data; (4) the location of UAF, UAM, LAM and LAF of a fully extended arm; and (5) profile coordinates of a fully extended arm. Thus, based on these results, the software programme was deemed to achieve what it was aimed for.

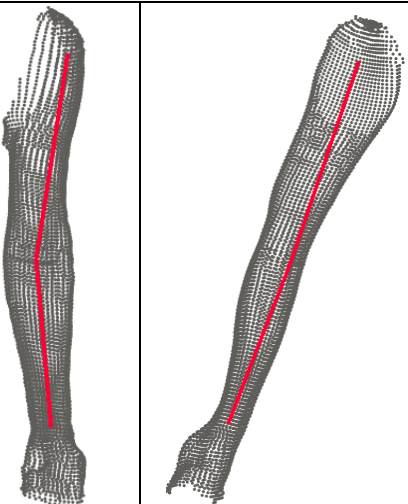

3D scan data after matching to the template		The location of UAF, UAM, LAM and LAF	Joint coordinates after matching to the template						
			X (mm)		Y (mm)		Z (mm)		
		Shoulder	41.6777		277.5597		-4.4151		
		Elbow	0		0		0		
		Wrist	9.7330		-28.3149		88.6422		
		Coordinates of the locations of UAF UAM, LAM and							
			X (mm)		Y (mm)		Z (mm)		
		UAF	15.2094		101.2900		-34.4549		
		UAM	7.7793		51.8076		-17.6229		
		LAM	3.8046		-44.0200		17.0906		
		LAF	7.9917		-92.4652		35.8992		
		Upper arm (UA) and lower arm (LA) bone orientation							
			UA (mm)			LA (mm)			
		X axis	0.99	-0.13	0.05	0.99	0.08	-0.03	
		Y axis	0.14	0.94	-0.32	0.08	-0.93	0.36	
		Z axis	0	0.32	0.95	0	0.36	0.93	

Figure 311. 3D scan data and joint coordinates of participant 4 after template matching as well as the predicted location of UAF, UAM, LAM and LAF

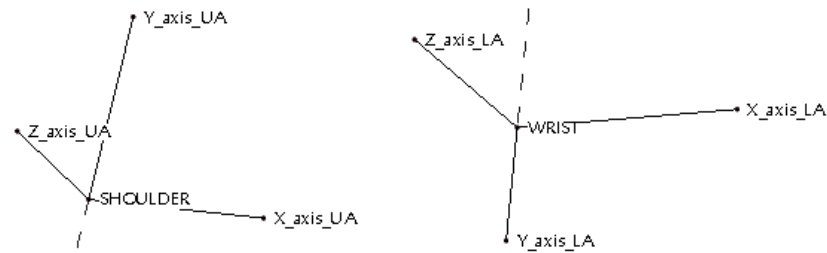


Figure 312. Orientation of upper and lower arm bones

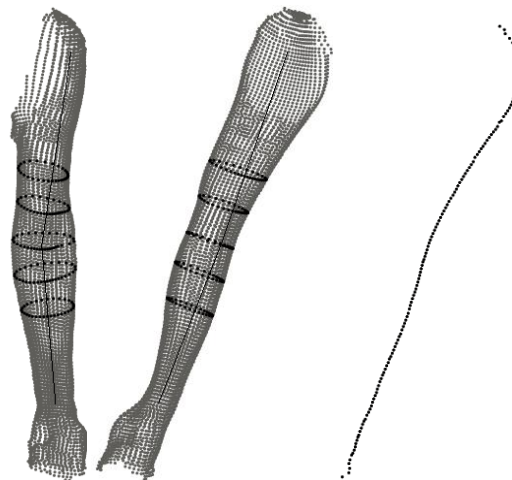


Figure 313. Examples of five key cross sections and profile which are extracted from the 3D scan data

9.11.2 Programming to predict five key cross sections for 135°, 90° and maximum flexion

The processes to be implemented in the programming to predict the five key cross sections for 135°, 90° and maximum flexion are shown in Figure 314. The figure also shows the input that was required for each process; including the output from the previous programme i.e. template matching and sampling of 3D scan data. The outputs of the programming included: (1) 3D coordinates of UAF, UAM, E, LAM and LAF for each key posture; (2) the maximum carrying angle to predict the carrying angle at any posture; (3) the cross sections of UAF, UAM, LAM, LAF and E; (4) the location of UAF, UAM, E, LAM and LAF for each key posture; and (5) the coordinates of the joint and upper/lower arm bone orientation for each key posture.

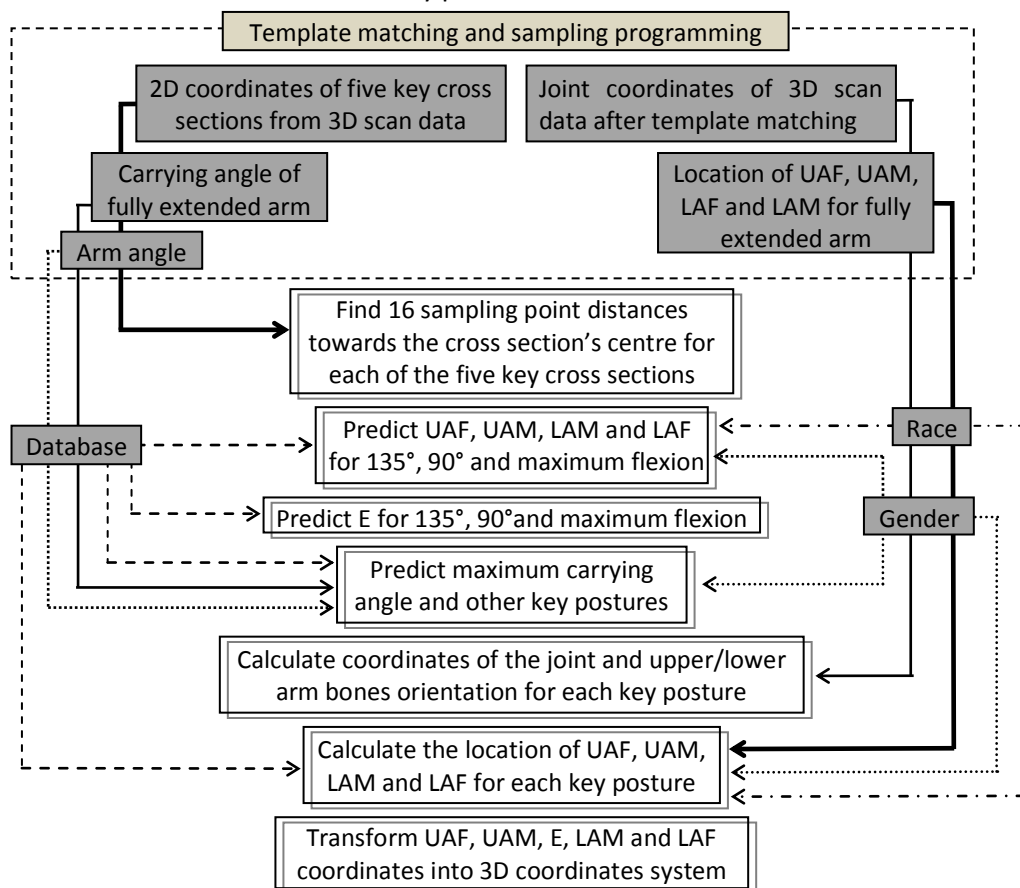


Figure 314. Processes to predict the five key cross sections for 135°, 90° and maximum flexion

To test whether the software programme functioned properly, it was tested using the data of participant 4 from the Asian male group. Figure 315 shows the result of the five key cross sections prediction. From the figure, it is apparent that the predicted cross sections generally resembled the expected shape of cross sections. For instance, UAF, LAM and LAF cross sections were of ellipsoidal shape. The figure also showed that, as the cross section prediction of UAF, UAM, LAM and LAF was mainly based on scaling the original cross sections of 3D scan data; their form was retained even for different key postures. The shape of the E cross sections for predicted key postures also resembled

the expected shape of E cross sections i.e. widening and lengthening of the sides. Based on this observation result, it was deemed that the software programme achieved what it was designed for.

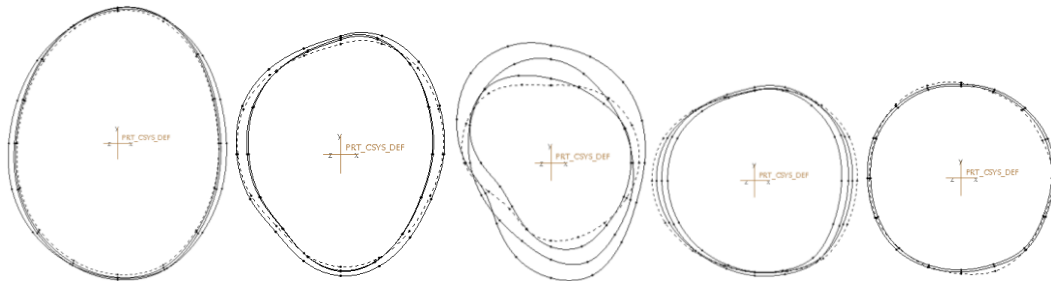


Figure 315. Predicted UAF, UAM, E, LAM and LAF for participant 4 from the Asian male group (dashed line is the original cross section from the 3D scan data, bold line is the prediction of cross sections for key posture of 135°, 90° and maximum flexion)

Table 45 shows the coordinates of the joint and upper/lower arm bone orientation as well as the coordinates of the location of UAF, UAM, LAM and LAF for each key posture. Using this information, the predicted UAF, UAM, E, LAM and LAF could be transformed into 3D coordinates. The final result of the five key cross sections' transformation was shown in Figure 316.

Table 45. Coordinates of joints and upper/lower arm bone orientation for each key posture

	Joint coordinates								
	135°			90°			Maximum flexion		
	X (mm)	Y(mm)	Z(mm)	X(mm)	Y(mm)	Z(mm)	X(mm)	Y(mm)	Z(mm)
Shoulder	41.6777	277.5597	-94.4151	41.6777	277.5597	-94.4151	41.6777	277.5597	-94.4151
Elbow	0	0	0	0	0	0	0	0	0
Wrist	27.5641	-112.858	216.5129	41.9196	72.3037	231.0616	49.125	230.5656	69.2875
	Upper arm bone orientation (the same for all key postures)								
X axis (mm)	0.9889			-0.1485			0		
Y axis (mm)	0.1407			0.9373			-0.3188		
Z axis (mm)	0.0473			0.3153			0.9478		
	Lower arm bone orientation								
	135°			90°			Maximum flexion		
X axis (mm)	0.9937	0.0519	-0.0995	0.9853	-0.0509	-0.1628	0.9798	-0.1915	-0.0575
Y axis (mm)	0.1122	-0.4593	0.8812	0.1706	0.2943	0.9404	0.1999	0.9384	0.282
Z axis (mm)	0	0.8868	0.4622	0	0.9544	-0.2986	0	0.2878	-0.9577
	The location of UAF, UAM, LAM and LAF								
	135°			90°			Maximum flexion		
	Z (mm)	X (mm)	Y (mm)	Z (mm)	X (mm)	Y (mm)	Z (mm)	X (mm)	Y (mm)
UAF	15.6239	104.0501	-35.3938	16.2054	107.9227	-36.7111	16.9161	112.6559	-38.3212
UAM	9.8382	65.5194	-22.2872	12.1995	81.2447	-27.6363	14.249	94.8935	-32.2791
LAM	6.9256	-28.3562	54.4001	13.9704	24.0964	77.005	20.241	95.0001	28.5486
LAF	11.826	-48.4201	92.892	19.3993	33.4604	106.9296	24.7596	116.2077	34.9217

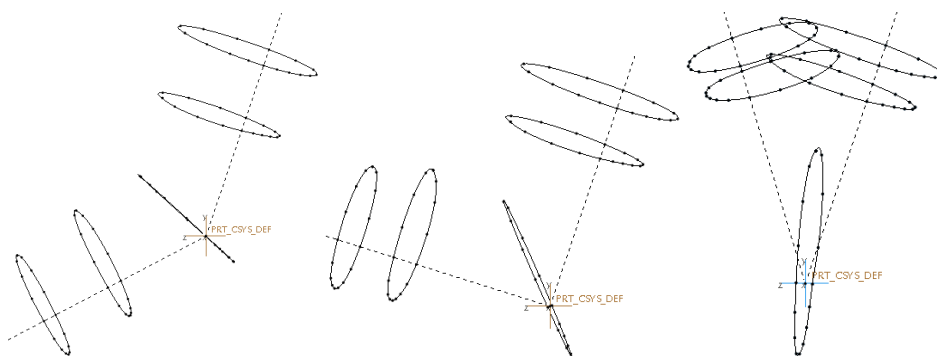


Figure 316. Transforming the predicted UAF, UAM, E, LAM and LAF into 3D coordinates

9.11.3 Programming to predict profiles at 135°, 90° and maximum flexion

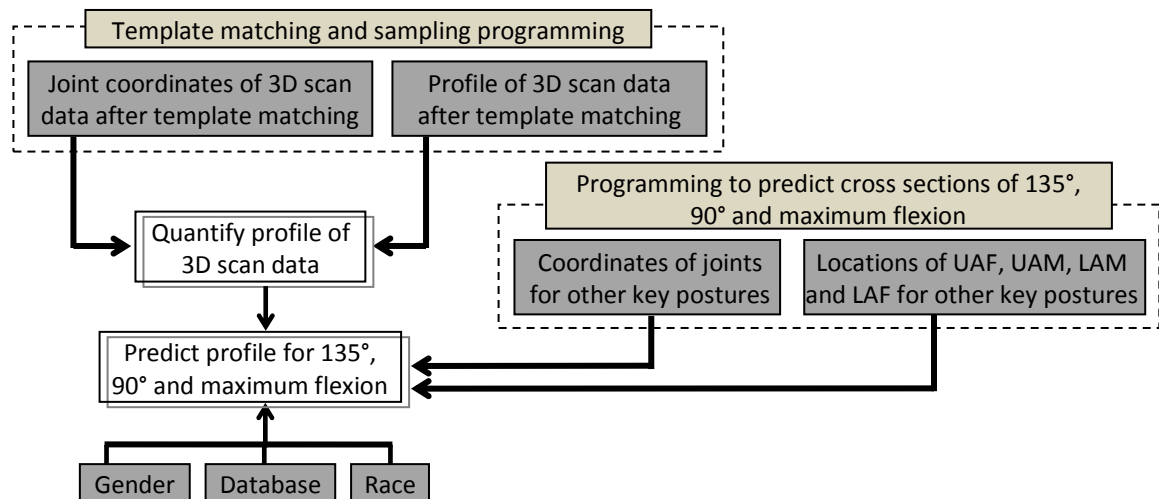


Figure 317. Processes in the programming to predict profiles of 135°, 90° and maximum flexion

The processes implemented in the programming to predict the profiles at 135°, 90° and maximum flexion are shown in Figure 317. The figure shows the input that was required for each process; including the output from the two previous programmes i.e. (1) template matching and sampling of 3D scan data; and (2) the prediction of the cross sections of 135°, 90° and maximum flexion. Using data from participant 4 of the Asian male group, the software programme was tested. The result is shown in Figure 318.

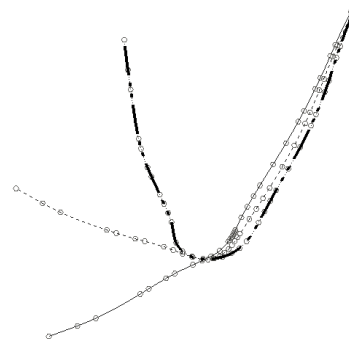


Figure 318. Results of profile prediction for 135 (thin line), 90 (dashed thin line) and maximum flexion (dashed bold line)

Figure 320 shows a side view i.e. plane Y-Z of the result of the five key cross sections and profile prediction for 135°, 90° and maximum flexion. The figure shows that the predicted five key cross sections did not coincide with the predicted profiles. In order to understand the cause of this, how the predicted five key cross sections were transformed into a 3D coordinate system needed to be investigated. In order to transform a key cross section into a 3D coordinate system, a bone point that was integrated with a cross section was required. The bone point, which was essentially the intersection between the cross section plane and the upper or lower arm bone, guided the placement of the cross section on its corresponding plane. This information was only readily available for the cross sections from 3D scan data. Since the output of the prediction for cross

sections did not provide the bone point, the current approach used the bone points from the 3D scan's cross sections to guide the placement for these predicted cross sections. Adopting this approach meant that the bone point for key cross sections for different key postures were the same. However, as illustrated in Figure 319, the bone point for a cross section was specific for each key posture. Figure 319 suggests that as the arm flexes, the bone point location for each key cross section shifts. Since the transformation of the predicted five key cross sections into a 3D coordinate system did not take into account the bone point shifting, this resulted in the incorrect placement which ultimately produces gaps between them and the corresponding profile. Figure 321 shows the result of surfaces that were created from the five key cross sections for each key posture which demonstrated that incorrect placement of five key cross sections also occurred in the front view i.e. X-Y plane.

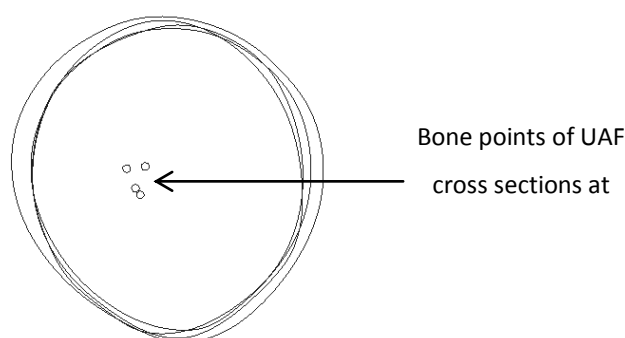


Figure 319. The bone points, which was required to guide the placement of UAF cross sections to their corresponding planes changed from one key posture to another

Observing Figure 320 and Figure 321, it was apparent that the shape of the cross sections and profiles generally resembled the expected shape for each key posture. Thus, it was clear that the problem lay on the misplacement of the cross sections and not their shape. The proposed solution was to adjust the placement of the five key cross sections for both side and front view. To adjust the placement of the five key cross sections for the side view, they would be translated so they coincided with the profile for each key posture. The translation procedure for the side view was the same as that presented in section 8.1.6. To adjust the placement of the five key cross sections for the front view, front view profiles of the 3D scan data were used to adjust the placement of UAF, UAM and E. This approach was based on the assumption that the upper arm movement was limited during the arm flexion as the arm movement was mainly concentrated on the lower arm. The adjustment was performed by 2D translation of UAF, UAM and E such that they were centred with the respect to the front view profiles.

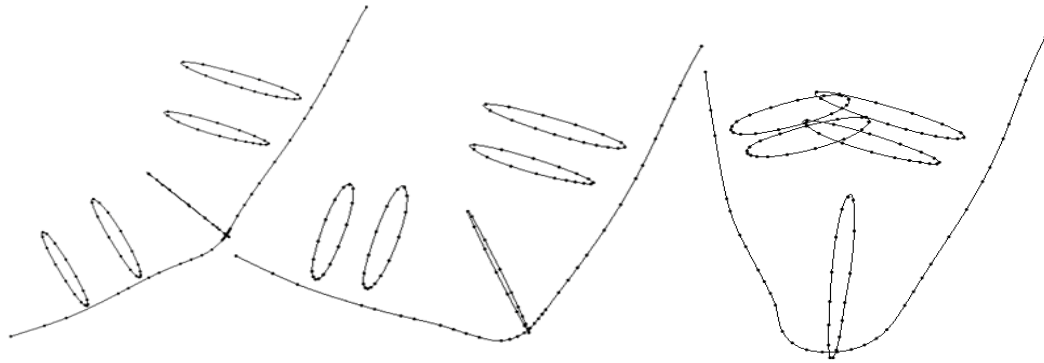


Figure 320. Cross sections do not coincide with the profiles for the predicted key postures

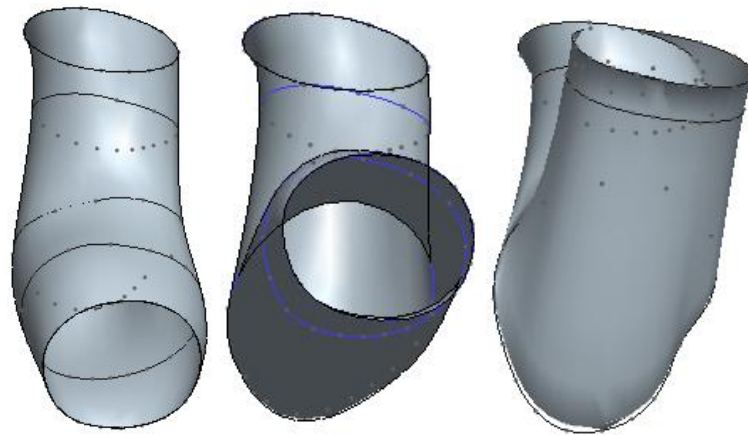


Figure 321. The effect of incorrect placement of the five key cross sections is also observable from the front view

Table 46 and Table 47 the steps to perform the translation for UAF, UAM and E. The principles of the steps were similar for UAF-UAM and E i.e. utilising the normal vector of the cross section plane to obtain $D_{cross\ section_x}$ and $D_{cross\ section_y}$ (upper arm bone for UAF-UAM and normal vector of the plane for E).

Table 46. Steps to perform translation for UAF and UAM

$\Delta = D_{UAM_y} - D_{UAM_x} \text{ where } D_{UAM_x} = D_{UAM_{x1}} + D_{UAM_{x2}}$ $UAM_{x1}^{new \text{ position}} = (0.5 \times \Delta) \times \left(\frac{\overrightarrow{UAM_{y1} UAM_{y2}}}{ UAM_{y1} UAM_{y2} } \right) + UAM_{y1}$ $\text{translation magnitude} = UAM_{x1}^{new \text{ position}} UAM_{x1} $	

Table 47. Steps to perform translation for E

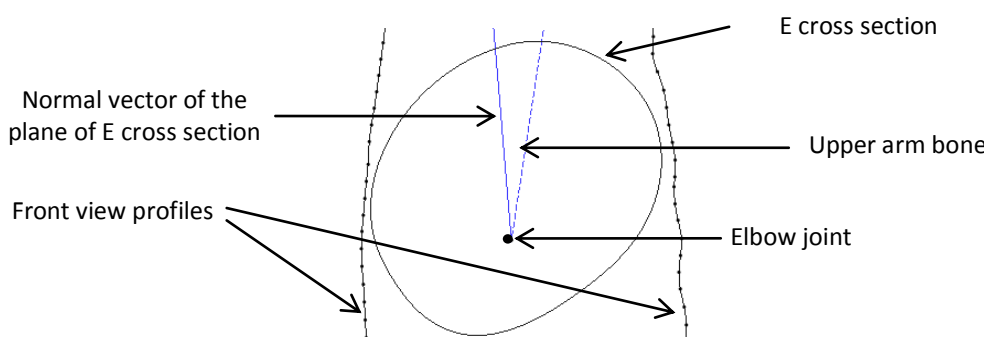
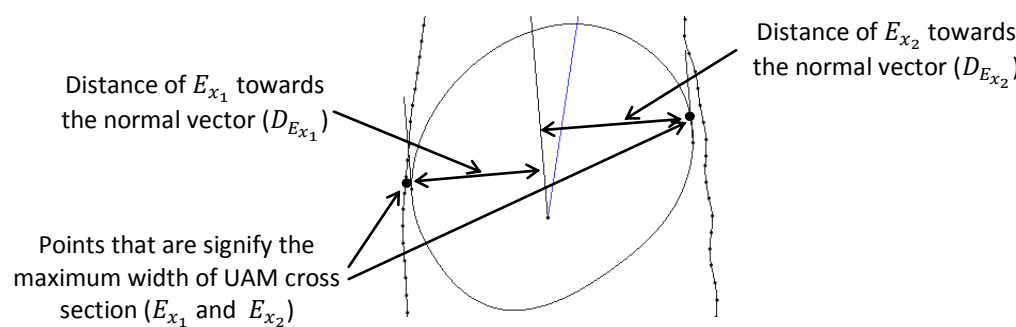
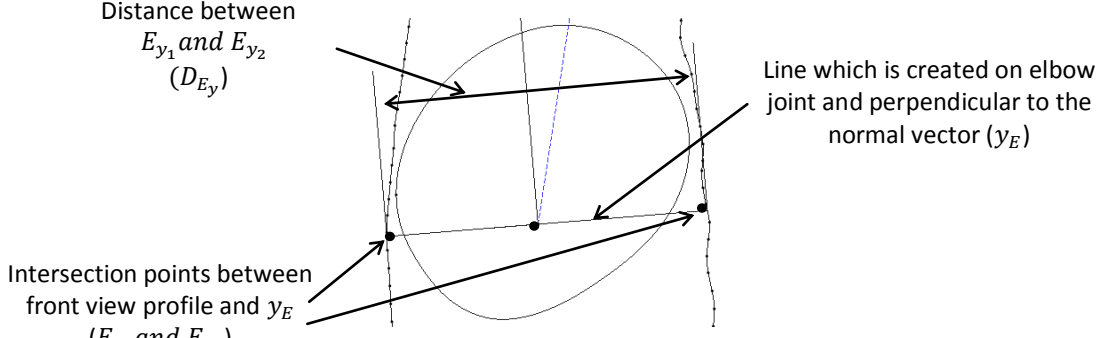
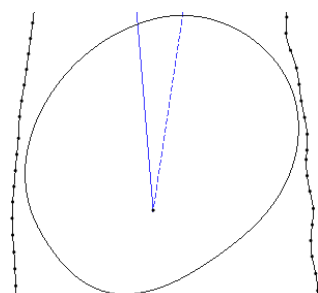
 <p>Normal vector of the plane of E cross section</p> <p>Front view profiles</p> <p>E cross section</p> <p>Upper arm bone</p> <p>Elbow joint</p>
 <p>Distance of E_{x_1} towards the normal vector ($D_{E_{x_1}}$)</p> <p>Points that signify the maximum width of UAM cross section (E_{x_1} and E_{x_2})</p> <p>Distance of E_{x_2} towards the normal vector ($D_{E_{x_2}}$)</p>
 <p>Distance between E_{y_1} and E_{y_2} (D_{E_y})</p> <p>Line which is created on elbow joint and perpendicular to the normal vector (y_E)</p> <p>Intersection points between front view profile and y_E (E_{y_1} and E_{y_2})</p>
$\Delta = D_{E_y} - D_{E_x}, \text{ where } D_{E_x} = D_{E_{x_1}} + D_{E_{x_2}}$ $E_{x_1}^{new \text{ position}} = (0.5 \times \Delta) \times \left(\frac{\overrightarrow{E_{y_1}E_{y_2}}}{ E_{y_1}E_{y_2} } \right) + E_{y_1}$ $\text{translation magnitude} = E_{x_1}^{new \text{ position}} - E_{x_1} $


Figure 322 shows the initial placement of UAF, UAM and E with respect to the front view profiles. Images at the second row were translated UAF, UAM and E, which clearly show that they were centred with respect to the front view profiles.

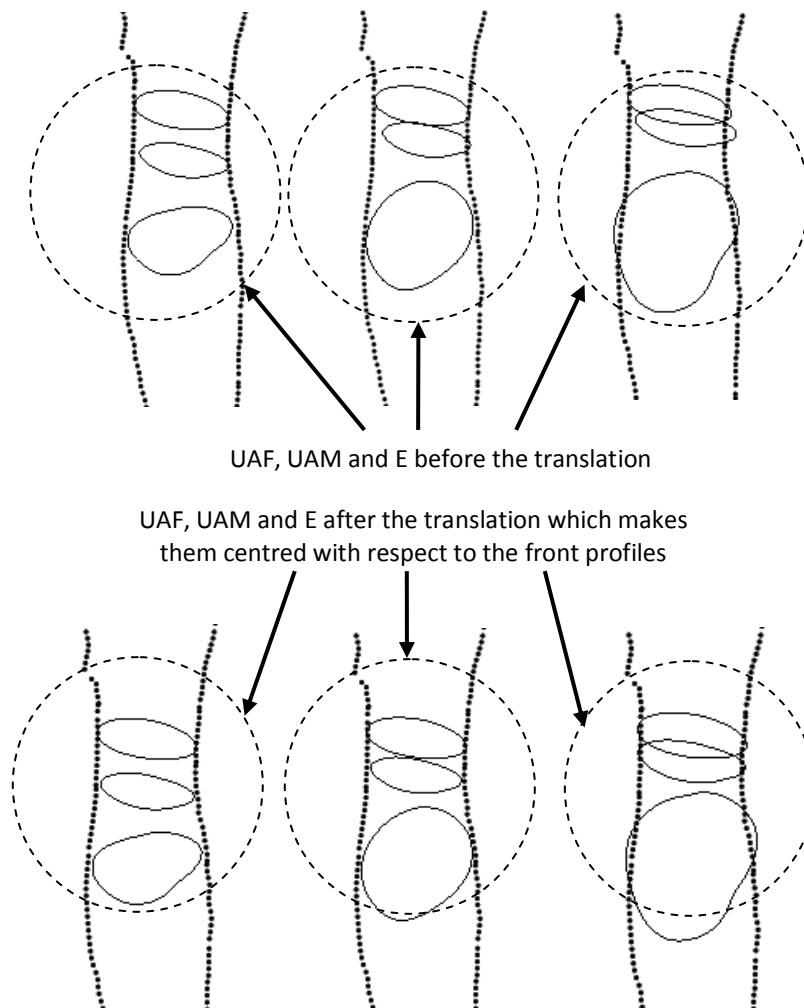


Figure 322. Using the front view profile of 3D scan data to guide translations of UAF, UAM and E to adjust their front view placement

The method of front view placement for UAF, UAM and E was not applicable to LAM and LAF due to the assumption that the upper arm movement was limited during the arm flexion as the arm movement was mainly concentrated on the lower arm. This clearly did not apply to LAM and LAF and therefore a different method of front view placement was required. To adjust the front view placement of LAM and LAF, the relative placement of LAM and LAF with respect to E for the fully extended arm was proposed to be used. This approach was based on the assumption that despite the lower arm movement, LAM and LAF placement with respect to E would remain the same. The adjustment would be performed in the 2D coordinate system by transforming E, LAM and LAF using the lower arm bone orientation. Table 48 provides an example to show the steps to translate LAM of a fully flexed arm. Based on the placement of LAM with respect to E, a ratio was calculated. This ratio i.e. $ratio_1$, was then used to determine the translation magnitude for LAM.

Table 48. Steps to translate LAM and LAF

<p>LAM cross section for fully extended arm</p> <p>LAF cross section for fully extended arm</p> <p>E cross section for fully extended arm</p> <p>Lower arm bone</p>	<p>LAM cross section of fully extended arm</p> <p>$LAM_{neu1} - E_{neu1}$</p> <p>LAM_{neu1}</p> <p>LAM_{neu2}</p> <p>E_{neu1}</p> <p>E_{neu2}</p> <p>E cross section of fully extended arm</p> $ratio_1 = \frac{LAM_{neu1} - E_{neu1}}{LAM_{neu} - E_{neu}}$ <p>where $LAM_{neu} = LAM_{neu1} + LAM_{neu2}$, $E_{neu} = E_{neu1} + E_{neu2}$</p>
<p>LAF cross section of fully flexed arm</p> <p>LAM cross section of fully extended arm</p> <p>Lower arm bone</p> <p>E cross section of fully flexed arm</p>	<p>LAF cross section of fully flexed arm</p> <p>LAM_{max1}</p> <p>LAM_{max2}</p> <p>E_{max1}</p> <p>E_{max2}</p> <p>E cross section of fully flexed arm</p>
<p>translation magnitude $= E_{max1} - (LAM_{max} - E_{max}) \times ratio_1$</p> <p>where $LAM_{max} = LAM_{max1} + LAM_{max2}$, $E_{max} = E_{max1} + E_{max2}$</p>	

The final result of front and side view adjustment for five key cross sections' placement of 135°, 90° and maximum flexion are shown in Figure 323 and Figure 324.

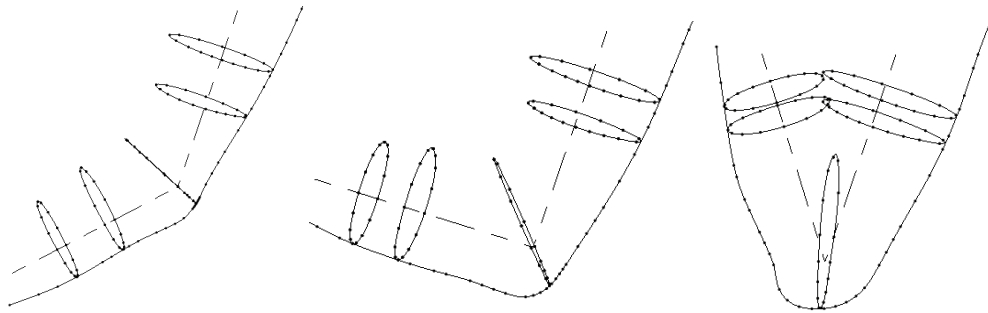


Figure 323. Final side view placement of five key cross sections for 135°, 90° and maximum flexion

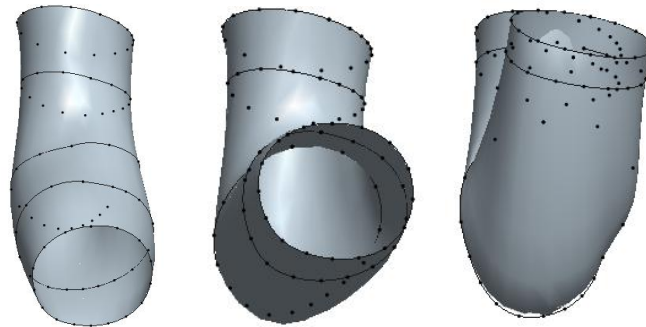


Figure 324. Final front view placement of five key cross sections for 135°, 90° and maximum flexion

9.11.4 Integration of FDM's programming with the programming from section 9.11.1, 9.11.2 and 9.11.3.

This part of the programming development was aimed to integrate programming from the new FDM and the newly developed programming in sections 9.11.1, 9.11.2 and 9.11.3. All of these software programmes were treated as subroutines. The programming in section 9.11.1 was run first and the user was prompted to key in inputs, as shown in Figure 310 (see section 9.11.1). The inputs of gender, race and BMI were used to predict the locations of UAF, UAM, LAM and LAF for all key postures. The location of UAF, UAM, LAM and LAF of a fully extended arm was then used to obtain five key cross sections from the 3D scan data. Template matching was also performed in order to obtain a profile of a fully extended arm. The inputs and outputs of programming in section 9.11.1 were subsequently passed onto the programming in section 9.11.2 and 9.11.3, which then predicted coordinates of five key cross sections and profiles for key postures other than a fully extended arm. Finally, the output of programming in sections 9.11.1, 9.11.2 and 9.11.3 were then used as the input for the FDM programming which produced elbow flesh deformation for a specified arm angle.

Figure 325 shows an example of the result from the integration of the FDM's software programme with the software programmes in section 9.11.1, 9.11.2, and 9.11.3. The result, which was based on the data of participant 4 from the Asian male group, demonstrated that the integrated

software programme was successful in generating flesh deformation for postures other than key postures.

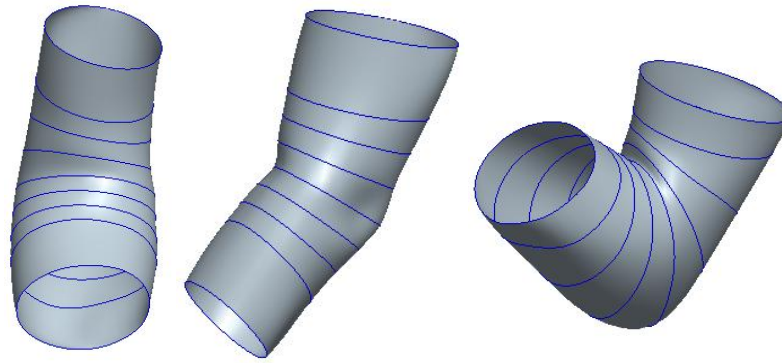


Figure 325. Examples of the result from the integration of FDM's software programme with the software programmes in section 9.11.1, 9.11.2, and 9.11.3 (arm angles, from right to left: 142°, 128° and 86°)

9.11.5 Discussions

As shown in section 9.11.1 to 9.11.4, software programmes were created to realise the proposed framework which was described in section 9.2. These programmes were tested to ensure that the software programme functioned properly. The results of the tests demonstrated that they were successful in achieving what they were aimed for and no changes were required for the proposed prediction methods in section 9.4, 9.5, 9.6 and 9.7. However, the results of the tests also showed that additional procedures were needed to correct the placement of predicted key cross sections in a 3D coordinate system. The need for these additional procedures arose because the prediction method for key cross sections in section 9.6 did not provide the bone points to guide the key cross sections' placement. The additional procedures, which used the profile and key cross sections of 3D scan data to guide the placement, involved side and front translation of the key cross sections in a 2D coordinate system. Since the additional procedures were performed in a 2D coordinate system, it did not entail complex algorithms and hence was still suitable for real time application. The result of the additional procedure's application suggested that they were successful in aiding the placement of the predicted cross sections.

9.12 Summary

A framework to accommodate the application of the new FDM was proposed and developed in this chapter. The framework was based on the usage of a database and a limited number of inputs to predict elements that are required to create the flesh deformation. The predicted elements were: (i) five key cross sections for 135°, 90° and maximum flexion; (ii) profiles for 135°, 90° and maximum flexion; and (iii) locations of the five key cross sections for all key postures and (iv) the carrying angle. The inputs for predictions were: (i) gender, race, and BMI; and (ii) 3D scan data of a fully extended arm and its joint location.

The database was designed such that it would be able to recognise the effect of different body size, type, gender and race on the new FDM's elements. To enable this, studies that investigate the effect of body sizes and types, gender and race were performed. The result was then used to refine the proposed framework and design the database content. Based on the design of the database content, data collection was performed. The database contains data from 23 individuals, which were divided into four groups i.e. Asian male, Asian female, Caucasian male and Caucasian female.

Programming which was based on the proposed framework was also developed in this chapter. The developed programming was checked for its functionality by using 3D scan data from one of the participants (participant 4) who was involved in data collection for the database. During the testing, it was found that the placement of the five key cross sections for 135°, 90° and maximum flexion were incorrect. The cause of the issue was outlined in section 9.11.3. This issue was resolved by making adjustments to the side and front view of the five key cross sections with the help of the side and front view profiles of the 3D scan data. The developed programming from this chapter would be used to validate the ability of the new FDM to accommodate flesh deformation from different body sizes and types.

10 Review of the New FDM's Ability to Accommodate Different Body Sizes and Shapes

This chapter will review the new FDM's ability to accommodate flesh deformation modelling for different body types and sizes. A report on the results of the review, which assessed the new FDM's ability to accommodate different body sizes and shapes, could also be found in Hermawati and Marshall (2009). In chapter 8, it was identified that, in order to review one of the DHM specifications i.e. ability to accommodate different body sizes and shapes, a concept which enabled application of the new FDM with minimum data acquisition from new participants was required. The concept was developed in section 9 and referred to as the framework. The framework used a database and limited numbers of inputs i.e. BMI, gender, race, and a 3D scan of a fully extended arm. The framework outputs i.e. 2D coordinates of five key cross sections, locations of five key cross sections, and profiles for each key posture as well as the range of carrying angle, were then used by the new FDM to create flesh deformation at the elbow. Thus outputs from the framework were utilised as the inputs for the new FDM. Due to this relationship a review of the new FDM's ability to accommodate different body sizes and shapes could also be viewed as a review of the framework. The methodology and the results of the review are presented in the following sections.

10.1 Methodology

In order to measure the ability of the new FDM to accommodate different body types and sizes, measurement variables were required. This research proposed accuracy and realism of flesh deformation at the elbow as the measurement variables. These variables were part of the DHM specifications and had been used to review the new FDM in chapter 8. These variables were deemed to be suitable because the utilisation of the proposed framework to provide inputs for the new FDM was expected to affect the accuracy and realism of flesh deformation. As described in the beginning of this chapter, the framework predicted 2D coordinates of five key cross sections, locations of five key cross sections, profiles for each key posture as well as the range of carrying angle based on a limited number of inputs. Any error or inaccuracies on any of these outputs would be passed on to the new FDM and hence would likely result in reduced accuracy or realism. The existing method to review flesh deformation's accuracy and realism in chapter 8 would be used. By

using the same method, it meant that the review results in this chapter were comparable to the results in chapter 8.

The accuracy review involved analysing five key cross sections and profiles for postures other than key postures. The analysis was performed through a comparison between the output of the framework and the original data. Offset measurement i.e. Euclidean distances, would be employed to measure the difference between the two. The offset measurement output was then analysed to determine the average error of the framework. In accordance with the existing method in chapter 8, the comparison was performed for each interval of the key postures i.e. full extension-135°, 135°-90° and 90°-maximum flexion. For the comparison of five key cross sections, 3D scan data was used for the first two key posture intervals whereas side view photographs were used for the last key posture interval i.e. 90°-maximum flexion. For the comparison of profiles, side view photographs were used for all key posture intervals.

The realism review involved visual observation to compare the output of the framework and the original data for postures other than key postures. Just like the accuracy review, the review for realism would also be performed for each interval of the key postures. For the first two intervals of the key postures, 3D scanned arms were used as the original data. For the last interval of the key postures i.e. 90°-maximum flexion, side view photographs were used.

Data collection from new participants was required to review the new FDM's ability to accommodate different body sizes and shapes. The new participants should be of different body types and sizes in order to show that the new FDM was able to generate flesh deformation for various body types and sizes. To comply with this need, participants of different gender and race as well as exhibiting a variety of arm length and BMI would be recruited. The types of data to be collected were determined by two factors: (i) required initial input/information for the framework and (ii) required data for the review of the framework. Taking these two factors into account, data to be collected were as the following: (1) gender; (2) race; (3) height; (4) weight; (5) 3D scan of a fully extended arm; (6) 3D scan of arm for the key interval of full extension-135°; (7) 3D scan of arm for the key interval of 135°-90°; and (8) three side view photographs for all of the key posture intervals. Data 1 to 5 were required as the inputs for the framework whereas data 6 to 8 were required for the review of the framework.

10.2 Data collection and preparation

In accordance with the methodology above, eight participants were recruited to review the framework. Two participants with different arm length and BMI represented each gender and race. It is acknowledged that data from two participants were not able to represent the full variety of arm length and BMI in each gender and race. However, in comparison to the number of participants in

the database for each gender and race, having two participants was deemed to be sufficient. Table 49 shows data from the recruited participants.

Table 49. Data from recruited participants

Asian male					
	Height (cm)	Weight (kg)	BMI	Arm Length (mm)	Arm Length Percentile
Participant	174	76.1	25.1	517	29
Participant	166	69.4	25.1	515	27
Asian female					
	Height (cm)	Weight (kg)	BMI	Arm Length (mm)	Arm Length Percentile
Participant	167	72.7	26.1	529	87
Participant	165	55.7	20.5	494	48
Caucasian Female					
	Height (cm)	Weight (kg)	BMI	Arm Length (mm)	Arm Length Percentile
Participant	158	98.1	39.3	493	6
Participant	174	60	19.8	574	89
Caucasian Male					
	Height (cm)	Weight (kg)	BMI	Arm Length (mm)	Arm Length Percentile
Participant	177.5	80.3	25.5	552	6
Participant	177	73.1	23.3	516	0.4

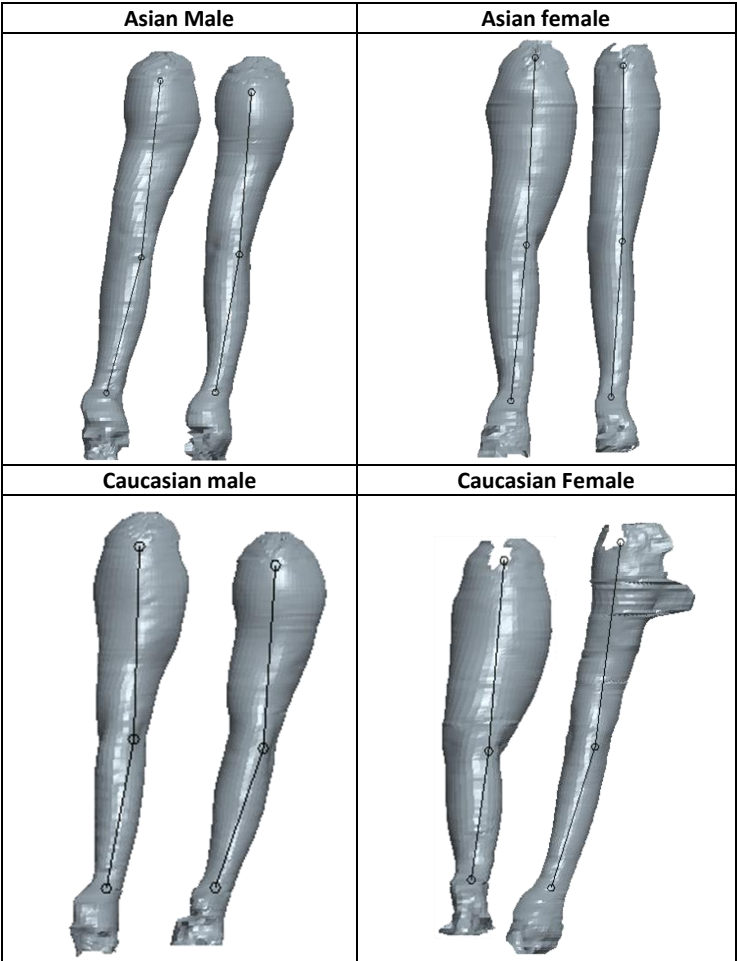


Figure 326. 3D scanned arms and their joint information of fully extended arms for all participants

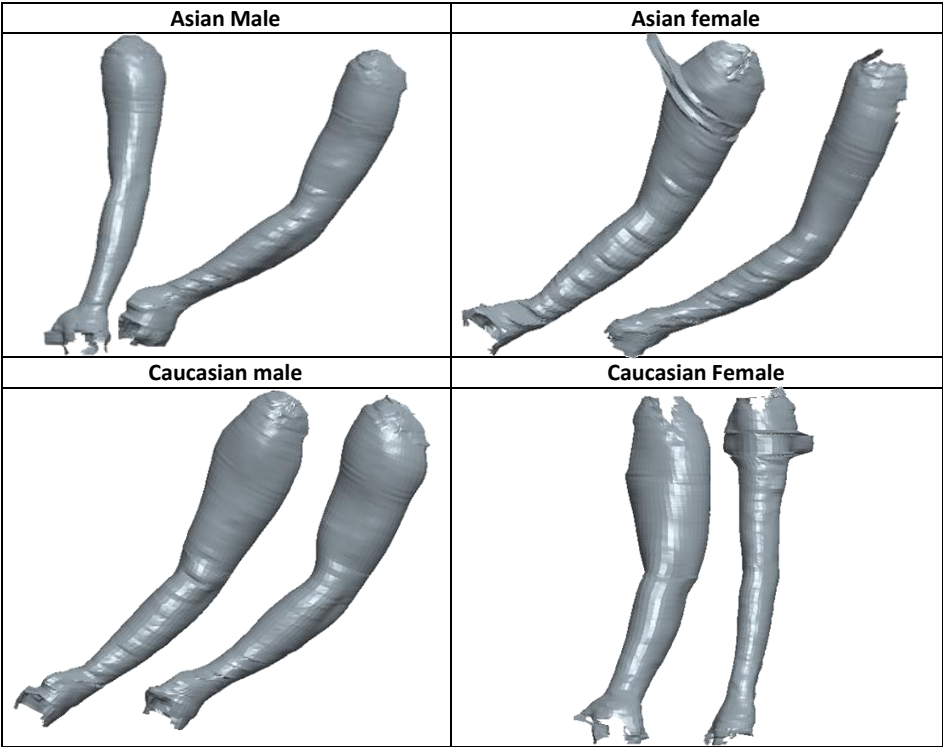


Figure 327. 3D scanned arms of all participants for arm posture in between full extension -135°

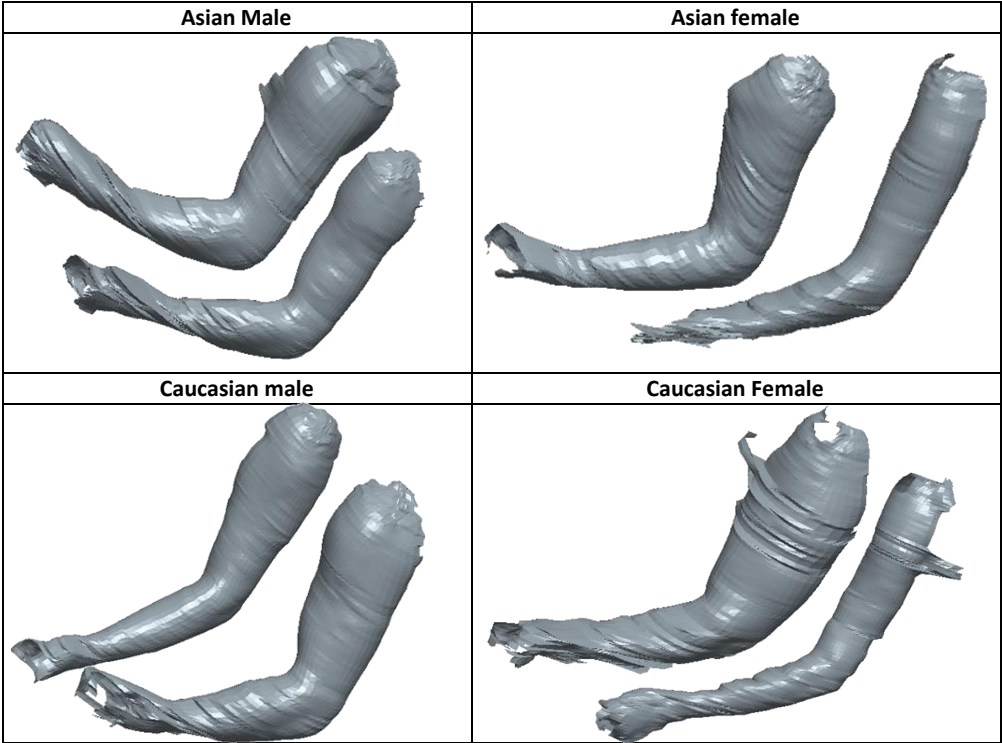


Figure 328. 3D scans of arms of all participants for arm posture in between 135°-90°

For each participant, three 3D scans were taken. The arm was scanned with a pronated wrist and only the left arm of the 3D scanned arms would be utilised for review. The 3D scan data consisted of: (i) 3D scan data while participant assumed a fully extended arm; (ii) 3D scan data while participant assumed an arm angle between a full extension-135°; and (iii) 3D scan data while participant assumed an arm angle between 135°-90°. 3D scanned arms were extracted from the 3D

scan data by following the procedure in section 5.2. For 3D scans of fully extended arms, the procedure in section 5.2 was also used to extract joint information. Figure 326 shows 3D scanned arms of all participants for fully extended arms whereas Figure 327 and Figure 328 show 3D scanned arms for postures between full extension-135° and 135°-90°, respectively. Figure 329 up to Figure 336 shows three side view photographs of all participants. A procedure in section 7.1 was followed to scale the photographs.



Figure 329. Side view photographs for participant 1 of Asian female



Figure 330. Side view photographs for participant 2 of Asian female



Figure 331. Side view photographs for participant 1 of Asian male



Figure 332. Side view photographs for participant 2 of Asian male

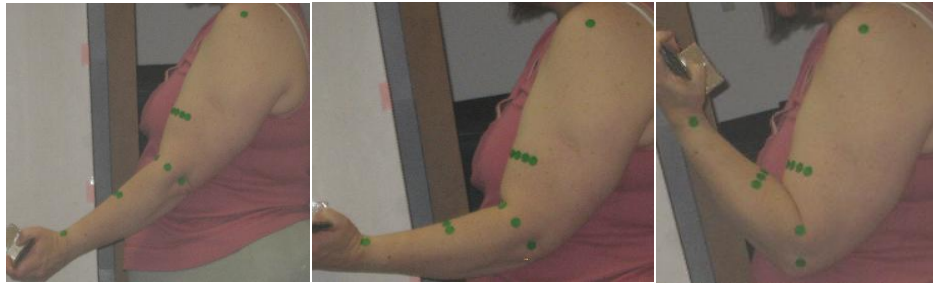


Figure 333. Side view photographs for participant 1 of Caucasian female



Figure 334. Side view photographs for participant 2 of Caucasian female



Figure 335. Side view photographs for participant 1 of Caucasian male



Figure 336. Side view photographs for participant 2 of Caucasian male

10.3 Review on the accuracy of the new FDM's ability to accommodate different body sizes and shapes

As had been suggested in section 10.1, the accuracy review of the framework to accommodate various body sizes and types could be distinguished into two parts i.e. comparison of the five key cross sections and comparison of the profiles. For both comparisons, the software programmes which were developed in chapter 9 were used to generate the required coordinates of the five key

cross sections and profiles. Both comparisons involved measuring offsets i.e. Euclidean distances between the output of the framework and the original data. The offset measurement output was then analysed to determine the average error of the proposed FDM.

10.3.1 Comparison for the five key cross sections

As described above, Matlab 7.0 was used to generate coordinates of the five key cross sections by running the software programmes which were developed in chapter 9. These coordinates, together with a 3D scanned arm (for arm angles in the range of full extension-135° and 135°-90°) or side view photographs (for arm angles in the range 90°-maximum flexion) were then visualised in Pro-Engineer Wildfire 4.0. The existing algorithm from section 8.2.1.1, which compared the five key cross sections of the proposed FDM and 3D scanned arm, was utilised to review the first two intervals of key postures i.e. full-extension-135° and 135°-90°. Following the existing approach from section 8.2.1.1, offset calculation was performed manually in Pro-Engineer Wildfire 4.0 for the last interval of key postures.

Table 50. Average error of the FDM application from the offset measurement result

	Full extension – 135°	135°-90°	90°-maximum flexion
Data to compare	FDM application and 3D scanned arm	FDM application and 3D scanned arm	FDM application and side view photograph
Average error for Asian female	2.54 mm	2.77 mm	1.77 mm
Average error for Asian male	2.87 mm	2.83 mm	3.55 mm
Average error for Caucasian female	2.82 mm	3.44 mm	3.45 mm
Average error for Caucasian male	2.47 mm	2.09 mm	1.65 mm
Average error for all groups	2.67 mm	2.78 mm	2.61 mm

Results for all intervals from each group and all groups are shown in Table 50. The average error showed a mixed result compared to the average error of the review result of the new FDM in chapter 8 i.e. 2.55 mm for full extension-135°, 2.43 for 135°-90°, and 1.29 mm for 90°-maximum flexion. This was probably caused by limited data in the database and hence limited the ability of the framework to provide closest match for the test participants. The proportion of the error level for each key posture interval was shown in Figure 337, Figure 338 and Figure 339.

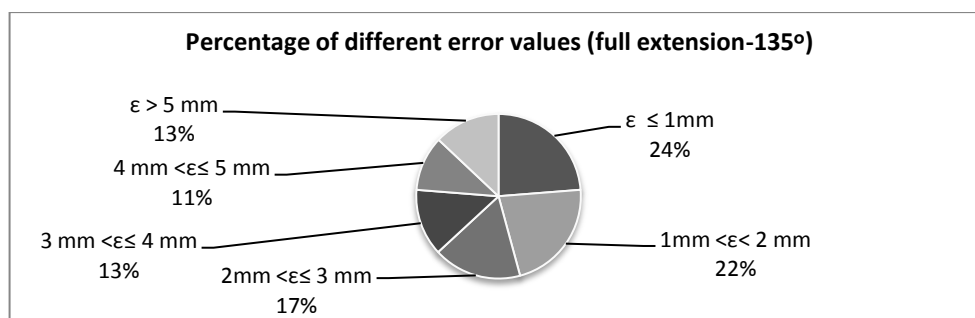


Figure 337. Proportion of different error level for the first interval of key postures i.e. maximum extension-135°

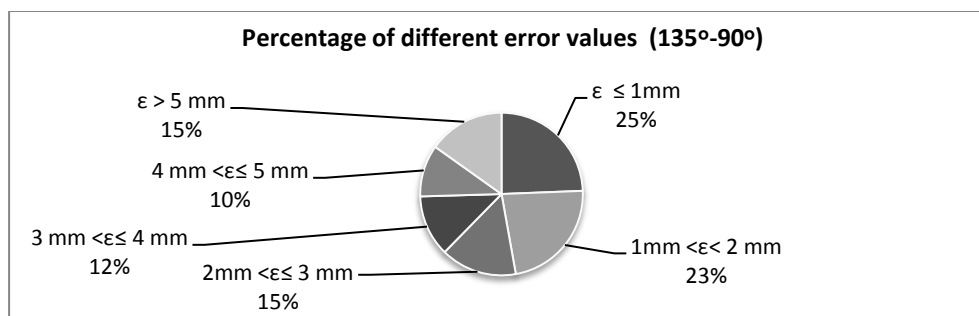


Figure 338. Proportion of different error level for the second interval of key postures i.e. 135°-90°

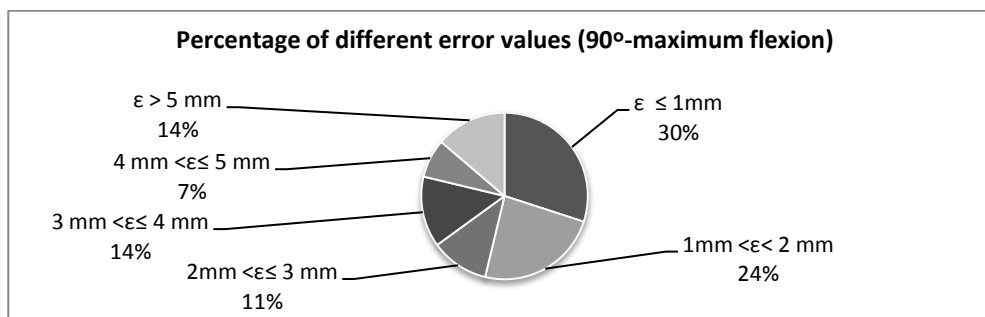


Figure 339. Proportion of different error level for the third interval of key postures i.e. 90°-maximum flexion

These figures show that an error of less than 3 mm dominated the error proportion with 63%, 63% and 65% for the first, second and third interval of the key postures. These percentages were also larger in comparison of those of the new FDM's review. This is not surprising as the average error of the framework was also larger than the new FDM's review result.

10.3.2 Comparison for the profile

Once the coordinates of the profile for each key posture's interval was generated by the software programme developed in chapter 9, the profile's offset measurements against the original data could be initiated. As discussed earlier in section 10.1, three side view photographs were used as the original data for each interval of the key postures for each participant. The existing algorithm in section 8.2.1.2 was modified to perform the offset measurement on the profile automatically. The algorithm was created in Matlab 7.0. The average of the error, which was obtained from the offset measurement, is shown in Table 51. The result showed that the average error was ≈ 2 mm for all participants with various arm angles and was larger than the new FDM's result i.e. ≈ 1 mm.

Figure 340, Figure 341, Figure 342 and Figure 343 provide some examples which show the predicted profiles and original data of each key posture's interval for four participants. Figure 340 (participant 2 of Asian female) and Figure 341 (participant 1 of Caucasian male) show predicted profiles with a smaller error i.e. between 0.52 mm – 0.82 mm and between 0.67 mm – 0.99 mm, respectively. In contrast, Figure 342 (participant 1 of Caucasian female) and Figure 343 (participant 2 of Asian male) show predicted profiles with a larger error i.e. between 1.14 mm – 2.18 mm and between 0.44 mm – 1.87 mm, respectively.

Table 51. Average error of the offset measurement for the profile interpolation

Group		Arm angle (°)	Average of the error (mm)
Asian Female	Participant 1	125; 140; 69	0.8346; 1.1299; 1.4091
	Participant 2	125; 62; 145	0.5223; 0.7832; 0.8191
Asian Male	Participant 1	107.5; 137; 56	1.0325; 0.851; 1.2892
	Participant 2	122; 152; 66	1.0152; 0.4358; 1.8684
Caucasian Female	Participant 1	99; 146; 50	1.54; 2.1796; 1.1456
	Participant 2	120; 156; 60	0.6389; 0.4801; 1.6106
Caucasian Male	Participant 1	104; 138; 53	0.7773; 0.6682; 0.9922
	Participant 2	112; 156; 60	0.6277; 0.35; 1.3249



Figure 340. The profile prediction result for participant 2 of Asian Female (bold line: prediction result, thin line: original data)

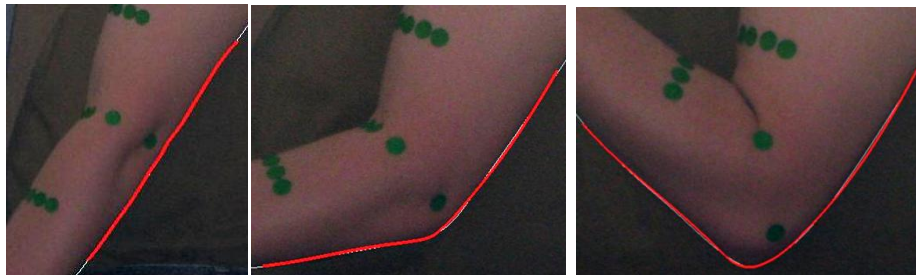


Figure 341. The profile prediction result for participant 1 of Caucasian Male (bold line: prediction result, thin line: original data)



Figure 342. The profile prediction result for participant 1 of Caucasian Female (bold line: prediction result, thin line: original data)



Figure 343. The profile prediction result for participant 2 of Asian Male (bold line: prediction result, thin line: original data)

10.3.3 Discussions on the accuracy review

The overall review on accuracy showed that flesh deformation which was created based on the framework's output generated a larger range of error than flesh deformation which was created from data that were obtained directly from participants. This was to be expected because the framework predicted the required elements to create flesh deformation from a limited number of inputs whereas the new FDM obtained these elements directly from a participant. Bearing in mind that the prediction of five key cross sections and profiles were supported by a limited number of data in the database, the review result suggested that, given a more comprehensive database, the framework had a potential to yield a higher level of accuracy.

As explained in section 8.2.1.3, due to the limited number of locations that were used to establish the flesh deformation's error, the level of error could not be used solely to describe the accuracy of the framework and it should be used in conjunction with the realism review. Furthermore, as already indicated in section 8.2.1.3, considering that the flesh deformation was a 3D object simulation, the level of error should be interpreted with care i.e. an error of x mm could mean that the surface level was elevated or reduced by up to x mm. For future study, this research suggests more locations for offset measurements and represents the offset measurements result as a 2D map. By presenting the result as a 2D map, any excessive elevation or reduction of the surface level which were unexpected could be identified and compared. However, this suggestion would only be applicable where 3D scan data were available for comparison.

10.4 Review on the realism of the new FDM's ability to accommodate different body sizes and shapes

As had been mentioned in section 10.1, a visual observation would be performed to review the realism of the new FDM's ability to accommodate different body sizes and shapes. The visual observation aimed to compare the flesh deformation of the framework with the original data. There were two types of original data which will be used i.e. 3D scanned arms for the first two intervals of key postures (arm postures between full extension-135° and between 135°-90°); and side view photographs for the last interval of key postures (90°-maximum flexion). For both comparisons, the software programmes which were developed in chapter 9 were used to create flesh deformation. The comparison result with each type of original data will be discussed in the following.

10.4.1 Comparison with the 3D scanned arm (full extension-135° and 135°-90°)

Visual observation for arm postures between full extension-135° showed that the framework captures details of the arm, particularly at the elbow area. This is shown by examples in Figure 344

from participant 1 and 2 (Asian female group) in which the indentation at the posterior of the elbow area of 3D scanned arms was replicated by the framework. Another visual observation from a different angle showed further the ability of the framework to capture details at the anterior of the elbow area. This is shown by images in Figure 345 which were taken from participant 1 of Caucasian male group and participant 1 of Caucasian female group, respectively.

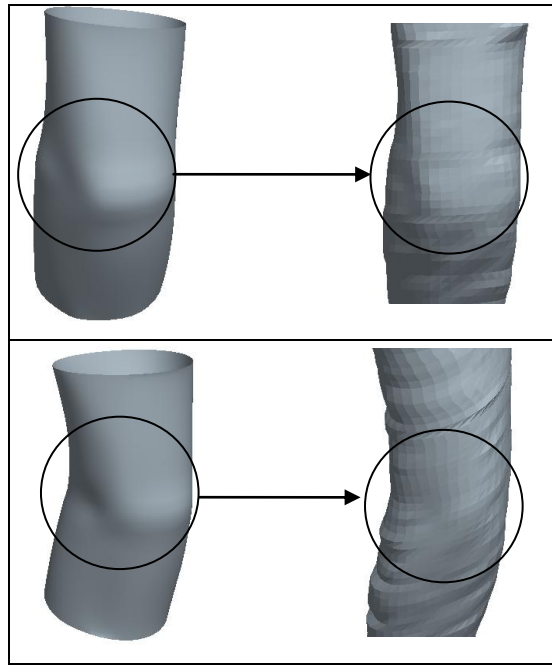


Figure 344. The framework was able to capture details at the elbow i.e. indentation at the posterior of the elbow area, which is highlighted by the solid lined circles

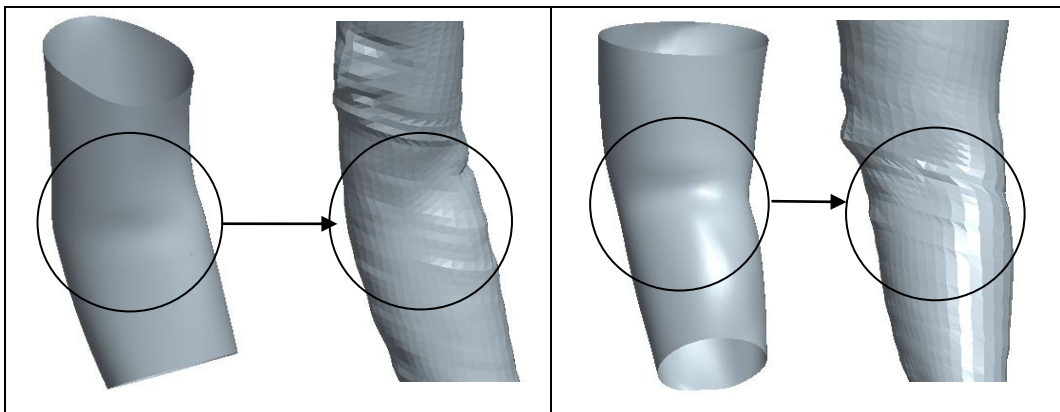


Figure 345. Visual observation shows the ability of the framework to capture details the area where the crease starts to develop as the arm flexes, which is highlighted by solid lined circles

However, it was also found that the framework produced a less realistic result for two particular participants. Figure 346, from participant 2 of Caucasian male group and participant 2 of Asian male group, shows unrealistic surface detail at the lateral area of the elbow (highlighted by solid circle lines). The surface discontinuation was likely caused by inaccurate prediction of the five key cross sections for these two participants due to their arm muscularity. Although the database strived to capture variation of body sizes and arms, current data in the database did not hold examples of five

key cross sections for overly muscular arms. An unrealistic result was also observed for participant 1 of Caucasian female group. The unrealistic result, which is highlighted by solid circle line on the leftmost image in Figure 347, was likely caused by distortion in the 3D scan of a fully extended arm and caused UAM to be larger than UAF. Because the framework was based on this particular data, any distortion would be passed on the next stages. As a result, unrealistic bulging could be observed on the upper arm of the framework result.

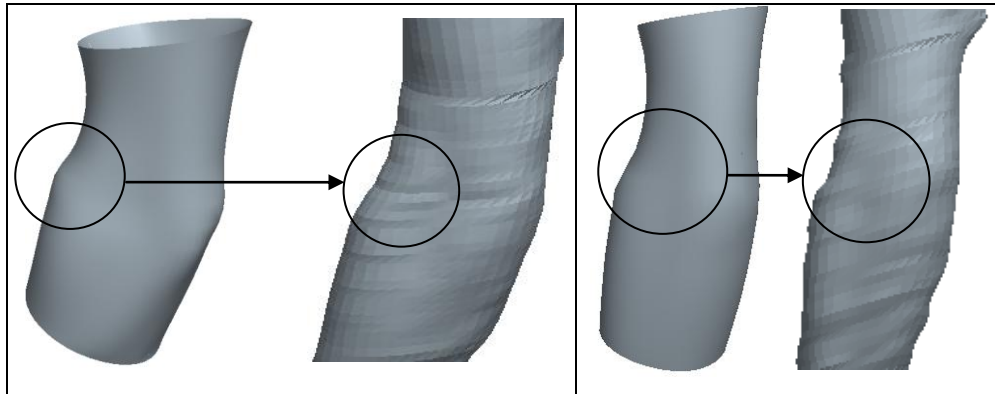


Figure 346. Sudden width changes between immediate cross sections before and after the elbow joint result in surface discontinuation (highlighted by solid lined circles)

None of the issues above were encountered in the review of the new FDM's realism (see section 8.2.2.1). This was because in the new FDM, five key cross sections of the key postures were created from manual measurements. Hence, factors that might cause unrealistic flesh deformation could be minimised. In contrast, the framework was largely dependent on the quality of the input and the ability of the database to provide a closest match.

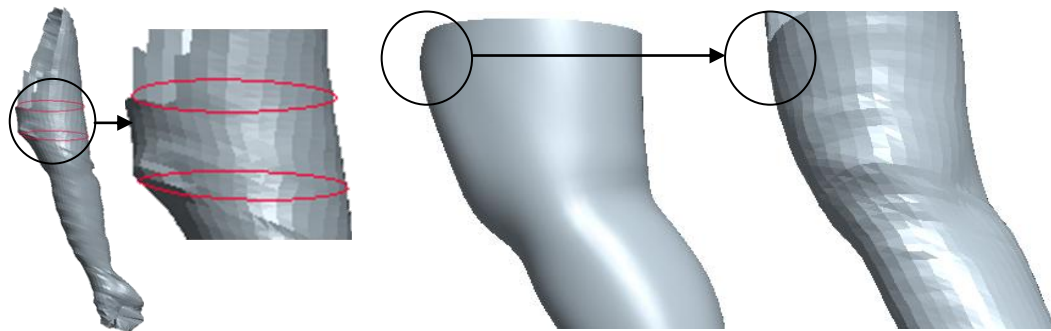


Figure 347. Distortion on the 3D scan of a fully extended arm (leftmost image) would cause unrealistic result of the framework result (middle image)

Visual observation on the second interval of the key postures i.e. between 135°-90° showed that the framework was able to capture the details at the posterior of the elbow for all participants (as highlighted by the dashed line circles in Figure 348). This result was in accordance with the result of the proposed FDM and was due to the usage of the profile. Similar to the finding of the new FDM's review, the anterior of the elbow area of the framework also showed slight discontinuities as highlighted by circle with solid lines in Figure 348.

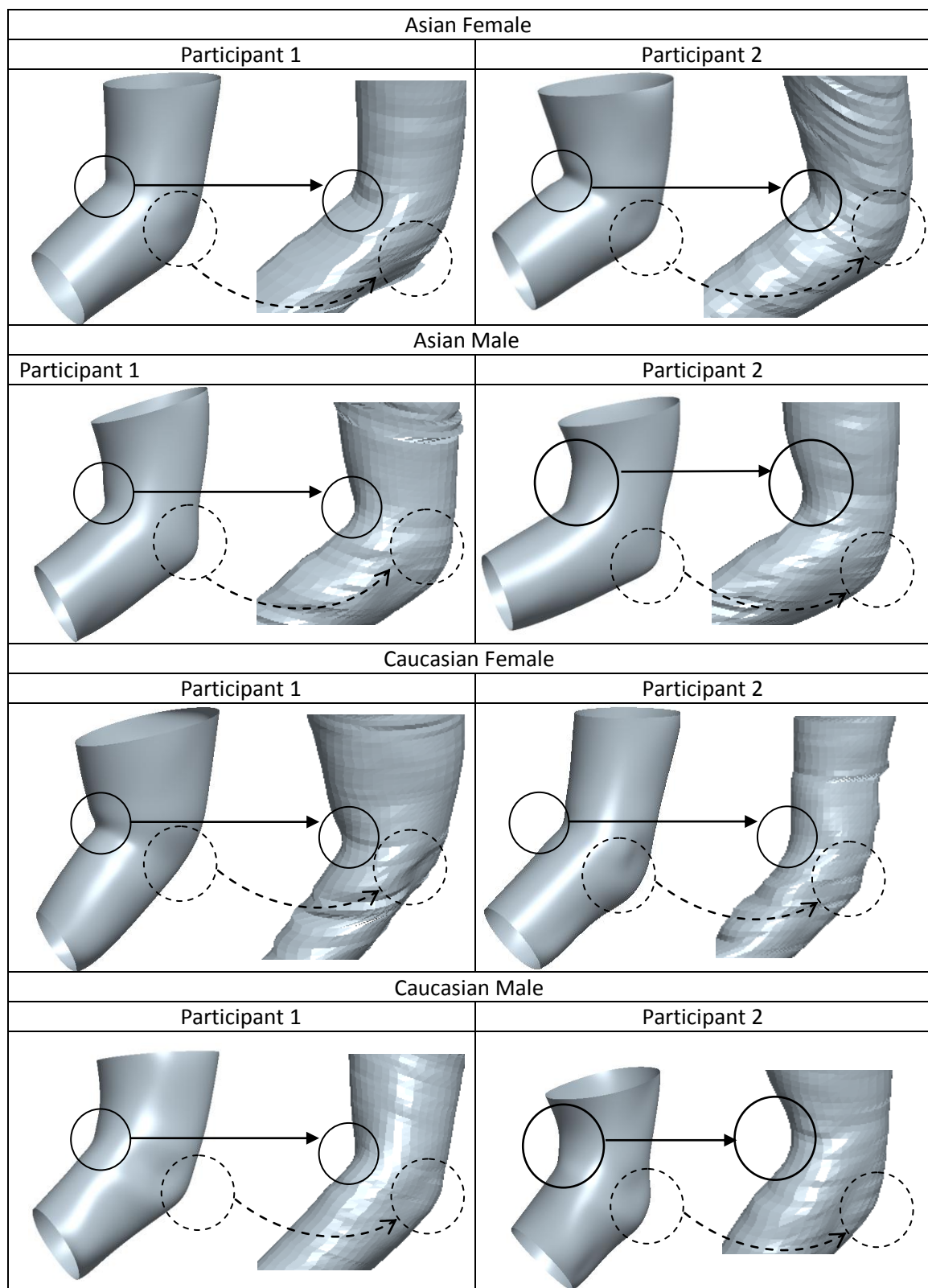


Figure 348. Visual observation on the arm postures between 135°-90° (solid lined circles highlight the anterior of the elbow area whereas the dashed lined circles highlighted the posterior of the elbow area)

From Figure 348, it was also apparent that there were surface discrepancies (highlighted by bold solid lined circles) on the anterior of the upper arm area for participant 2 of Asian male group and participant 1 of Caucasian male group. The surface discrepancies were likely a result of

inaccurate prediction of UAF, UAM and E. As had been mentioned earlier, this was likely caused by lack of examples of muscular arms in the database. As expected, unrealistic surfaces on the upper arm was also apparent for participant 1 of Caucasian female groups as shown in Figure 349. The result of the framework for this key posture interval also echoed the finding for the first key posture interval.

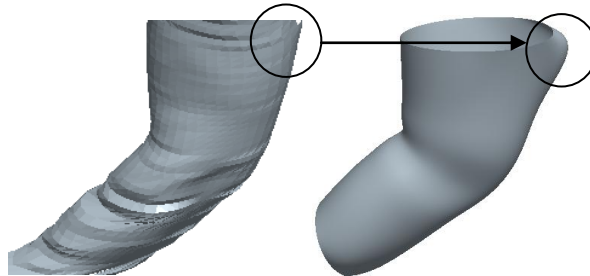


Figure 349. Further effect of distorted 3D scan of a fully extended arm on the result of the framework for arm angles between 135°-90°

10.4.2 Comparison with the side view photographs (90°-maximum flexion)

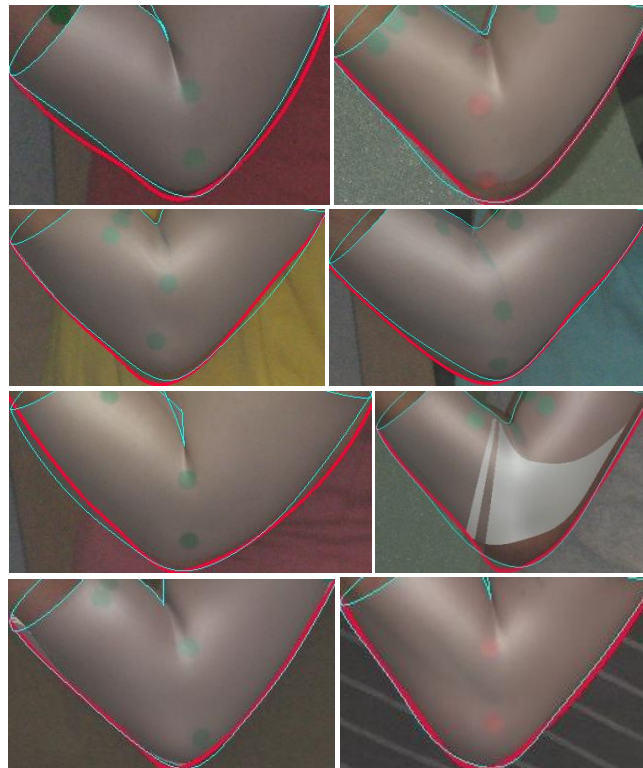


Figure 350. Shape discrepancies between predicted (thin lines) and actual (bold lines) profiles are concentrated on the elbow area for arm postures between 90°-maximum flexion

Visual observation for arm postures between 90°-maximum flexion, shown in Figure 350, demonstrated that there were shape discrepancies between the predicted profiles (thin lines) and the actual profiles (bold lines). The discrepancies, which had been identified and quantified earlier from the profile comparison result, mainly occurred at the elbow area. As shown in the figure, the discrepancies vary between participants. In comparison with the result of the new FDM's realism

review for this key posture's interval, the framework showed larger shape discrepancies. Again, this was likely caused by a limited number of available examples of profiles to be chosen from the database. The framework's ability to represent the shape at the anterior of the elbow area also showed a degree of shape discrepancies (see Figure 351). It was also identified from the review of five key cross sections' accuracy in the previous section. The largest shape discrepancies could be observed on the upper arms of participants of Asian male group. This was probably because there was no available example of UAF and UAM in the Asian male group that matched the upper arm's shapes of these two participants.

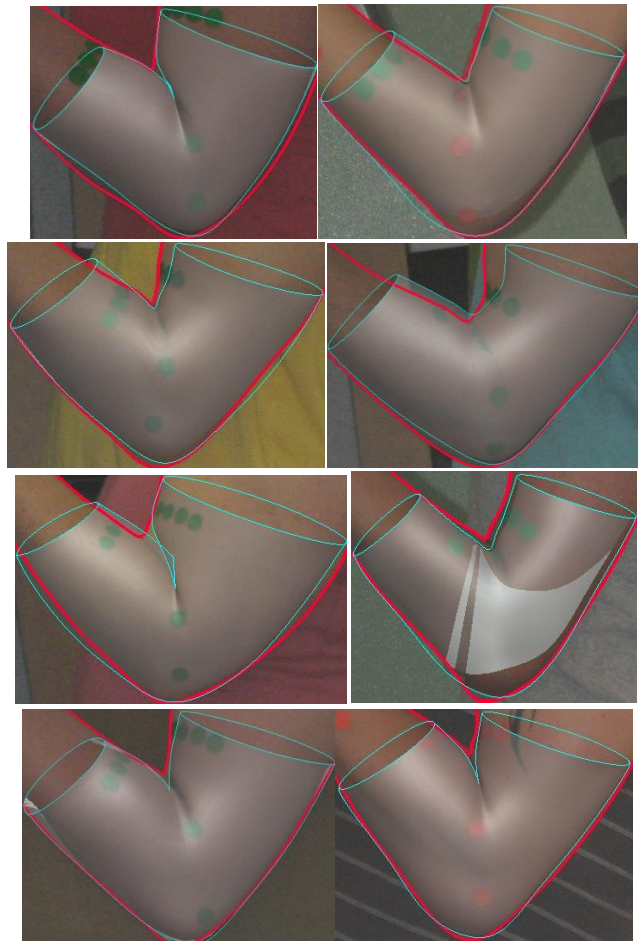


Figure 351. Shape discrepancies between predicted (thin lines) and actual (bold lines) profiles also occur on the anterior of the elbow area for arm postures between 90°-maximum flexion

Additional images, which are taken from different views and shown in Figure 352 up to Figure 371, demonstrate further the extent of realism of the framework. Figure 352 up to Figure 367, in which 3D scanned images accompanied the depiction of the result of the framework, show images for arm postures of full extension-135° and 135°-90°. Figure 368 up to Figure 371 shows the result of the framework for arm postures in the range of 90°-maximum flexion. The images from different views showed that the framework could predict the flesh deformation despite the shape discrepancies. The ability to capture details around the elbow e.g. indentation at the posterior of

the elbow, crease at the anterior of the elbow; increased the resemblance of the framework to the real arm.

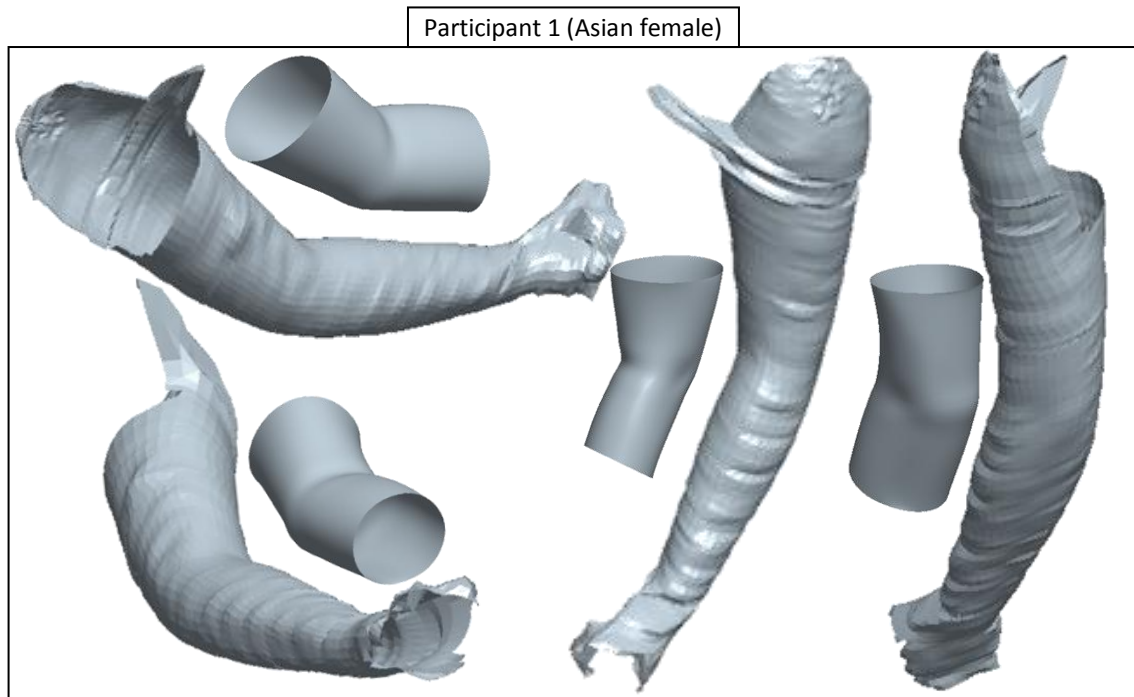


Figure 352. Images of framework's result for an arm posture between a fully extended arm-135° for participant 1 of Asian female group

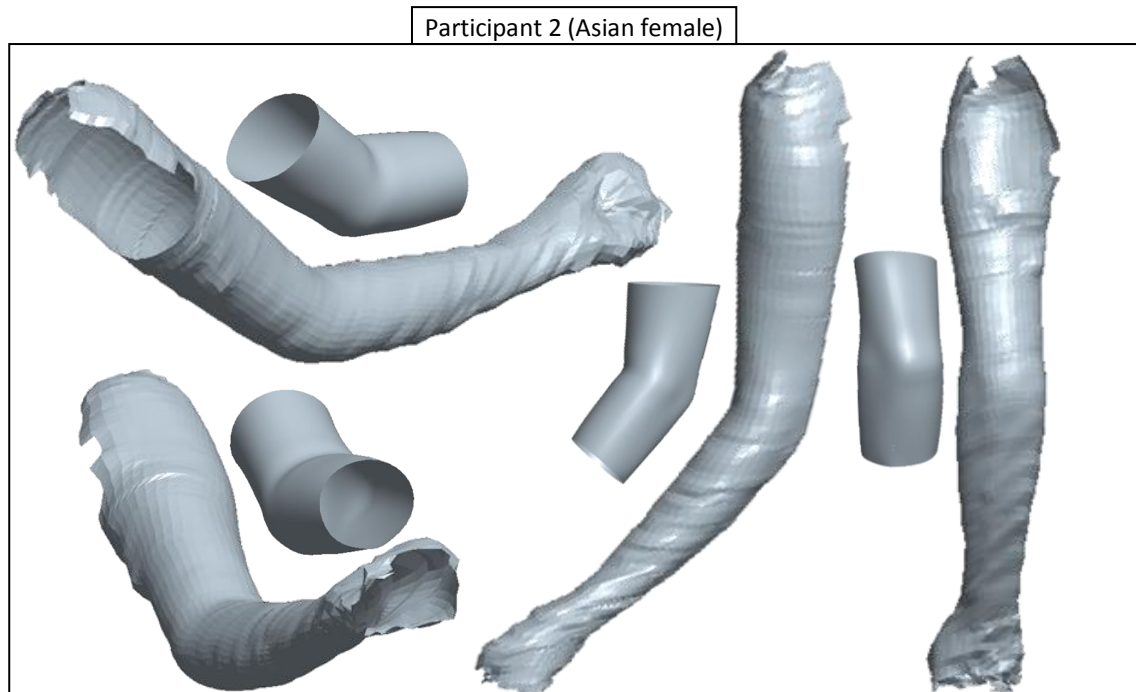


Figure 353. Images of framework's result for an arm posture between a fully extended arm-135° for participant 2 of Asian female group

Participant 1 (Asian male)

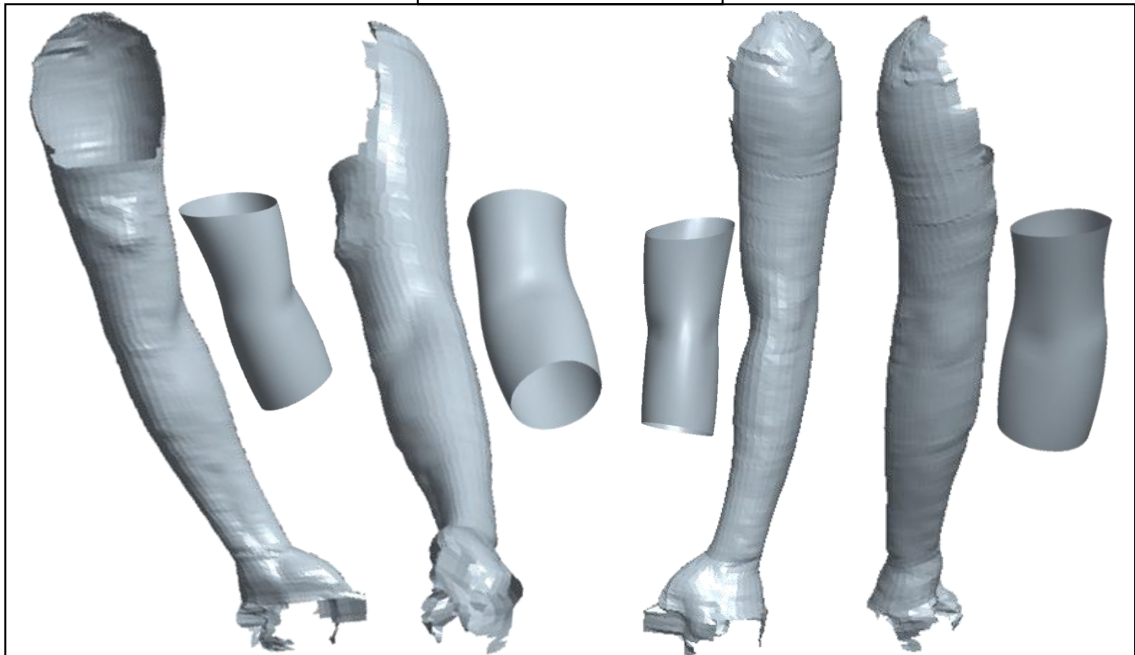


Figure 354. Images of framework's result for an arm posture between a fully extended arm-135° for participant 1 of Asian male group

Participant 2 (Asian male)

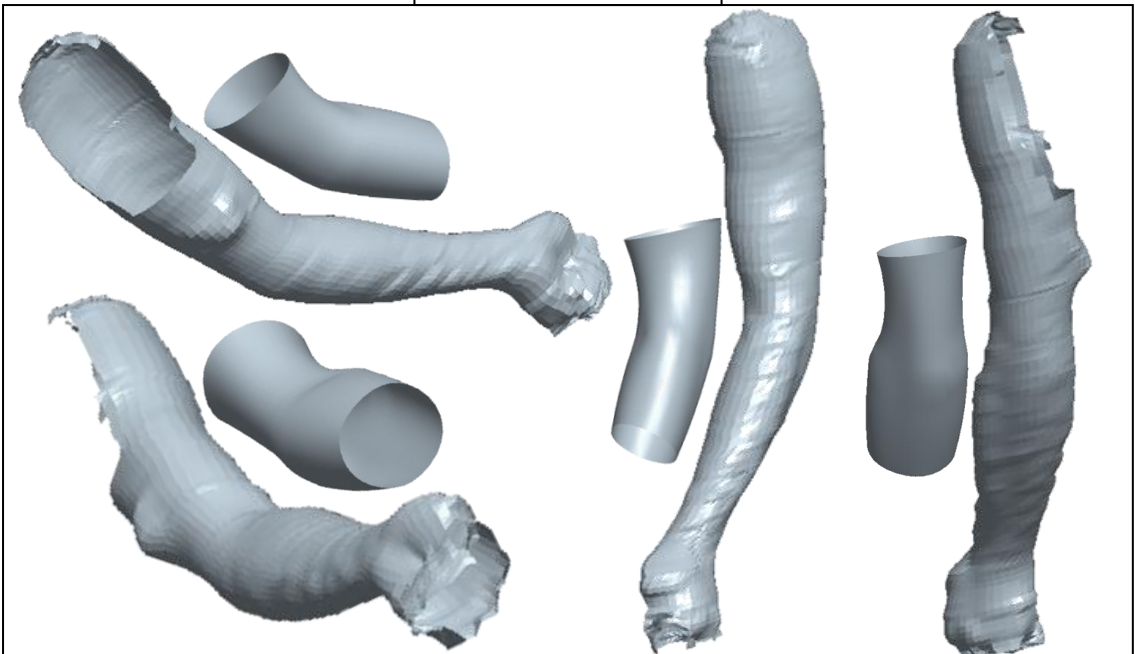


Figure 355. Images of framework's result for an arm posture between a fully extended arm-135° for participant 2 of Asian male group

Participant 1 (Caucasian female)

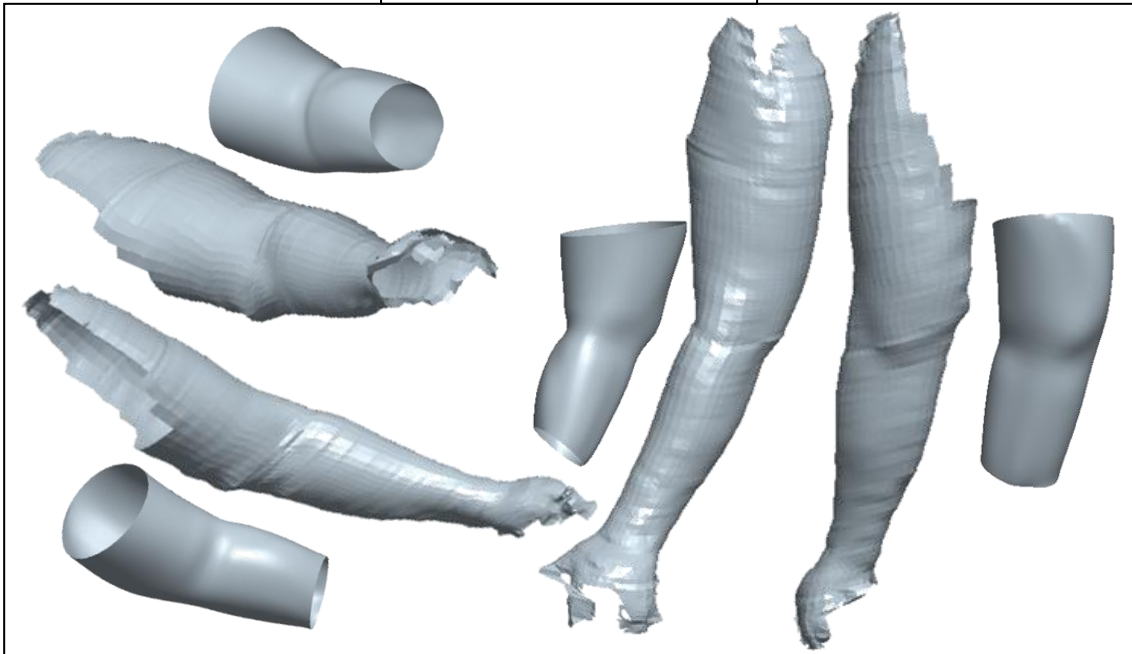


Figure 356. Images of framework's result for an arm posture between a fully extended arm-135° for participant 1 of Caucasian female group

Participant 2 (Caucasian female)

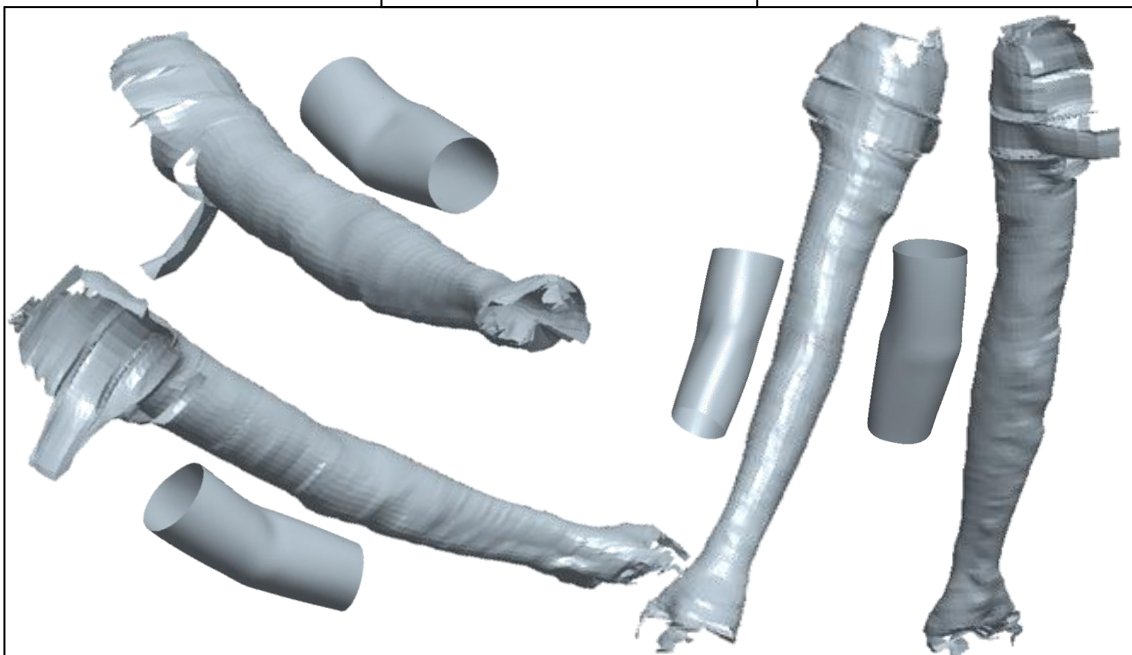


Figure 357. Images of framework's result for an arm posture between a fully extended arm-135° for participant 2 of Caucasian female group

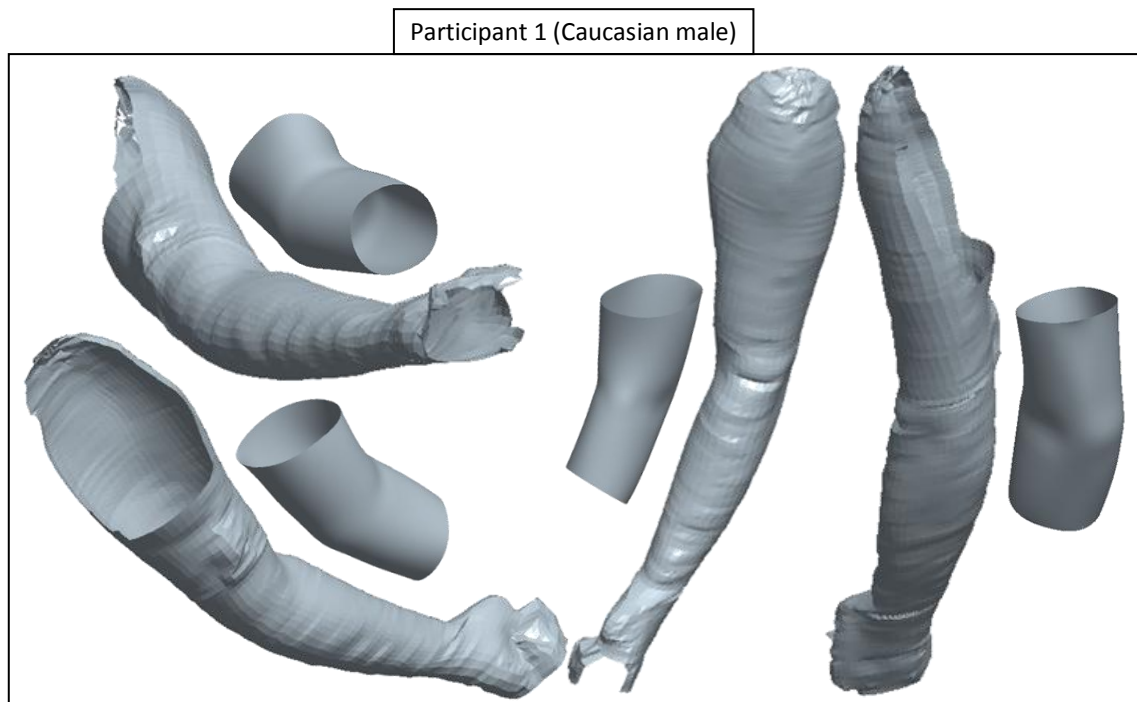


Figure 358. Images of framework's result for an arm posture between a fully extended arm-135° for participant 1 of Caucasian male group

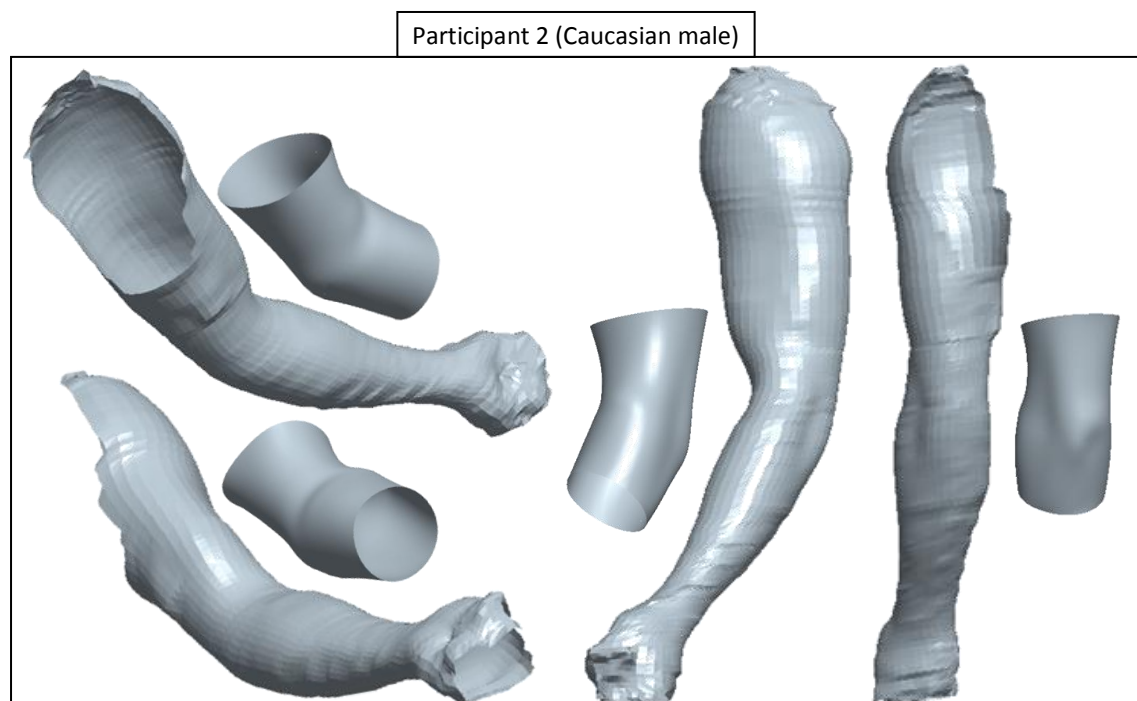


Figure 359. Images of framework's result for an arm posture between a fully extended arm-135° for participant 1 of Caucasian male group

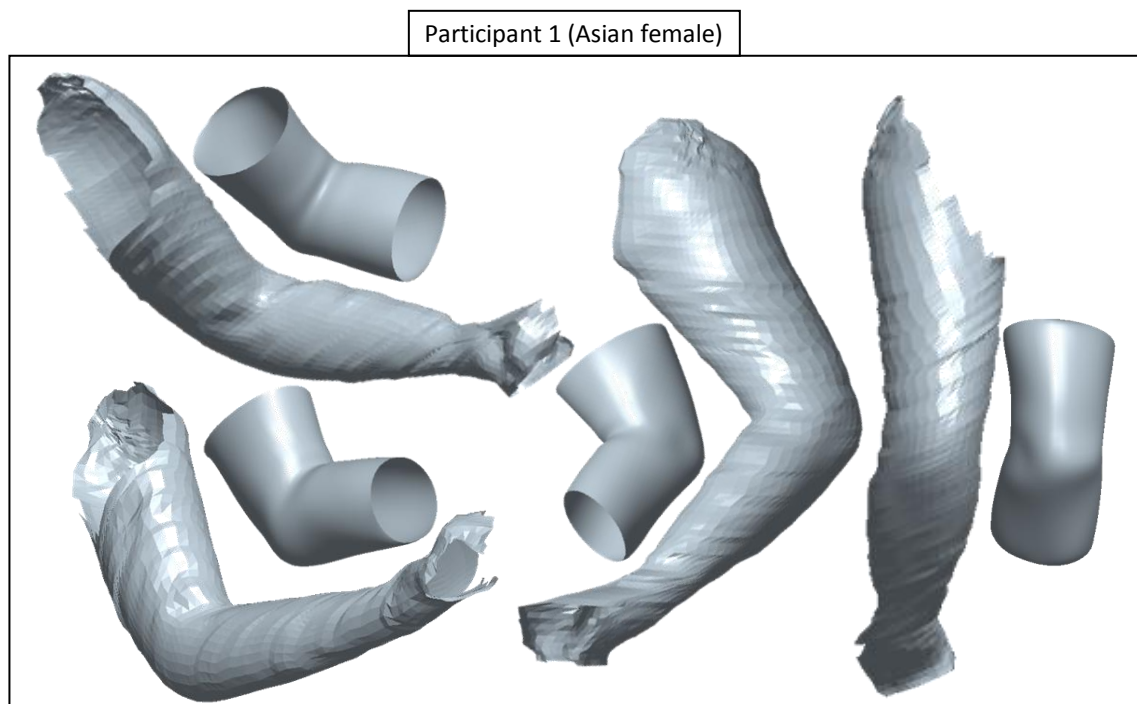


Figure 360. Images of framework's result for an arm posture between 135° - 90° for participant 1 of Asian female group

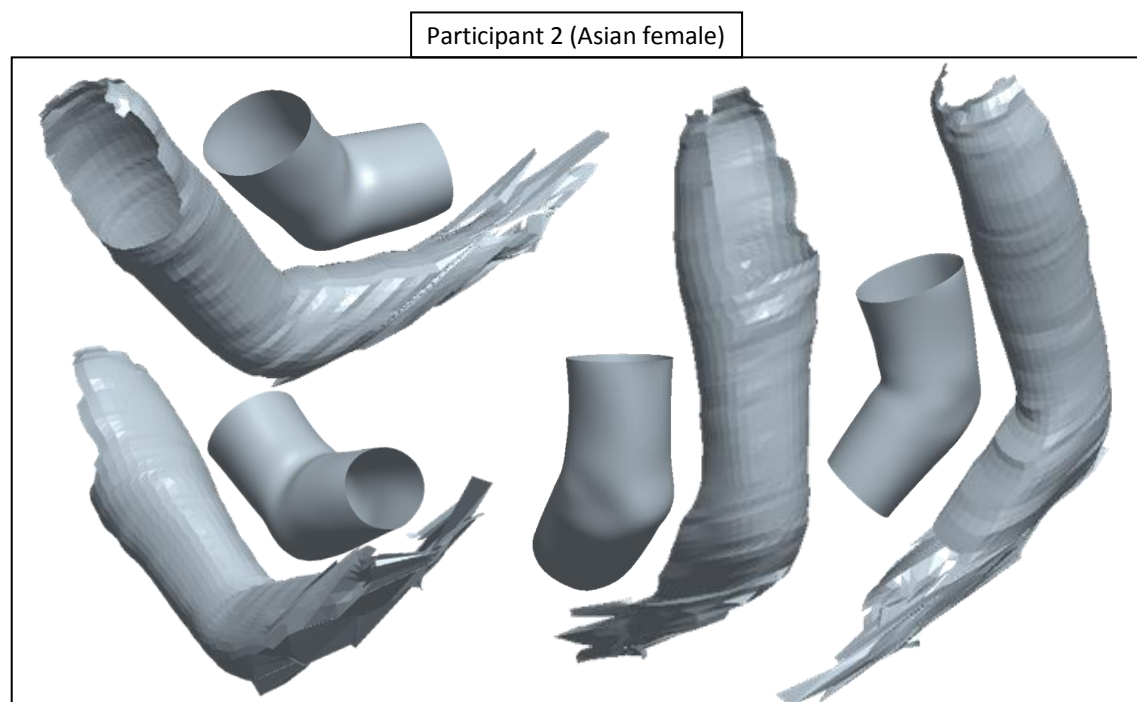


Figure 361. Images of framework's result for an arm posture between 135° - 90° for participant 2 of Asian female group

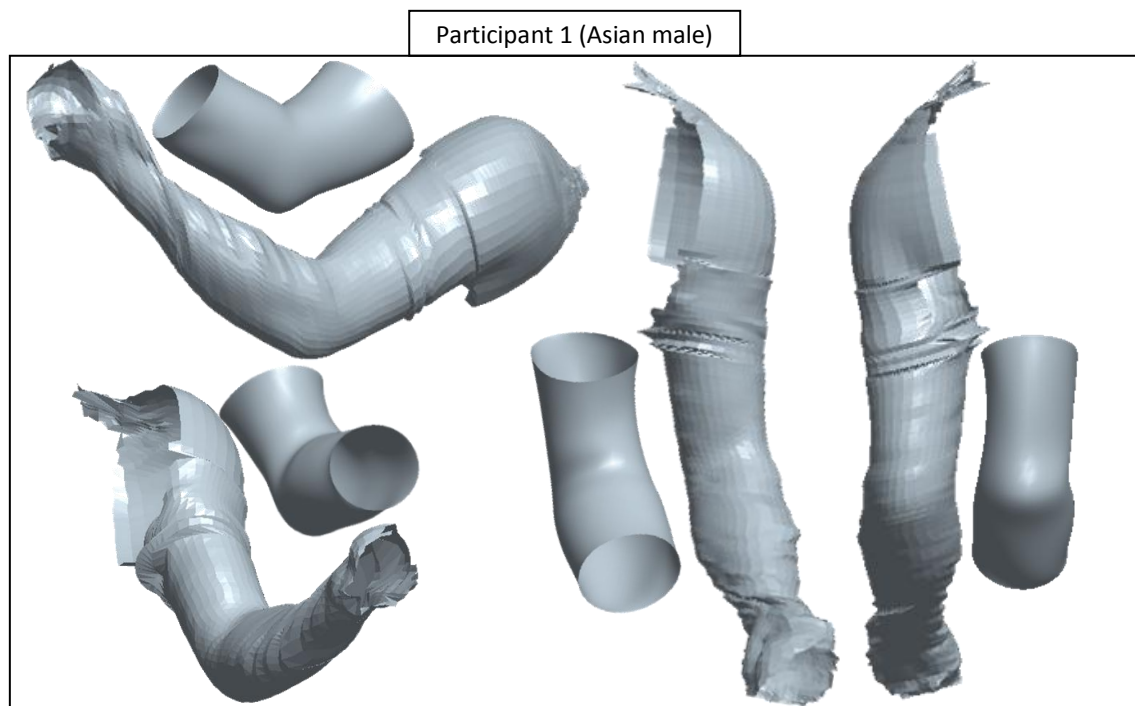


Figure 362. Images of framework's result for an arm posture between 135° - 90° for participant 1 of Asian male group

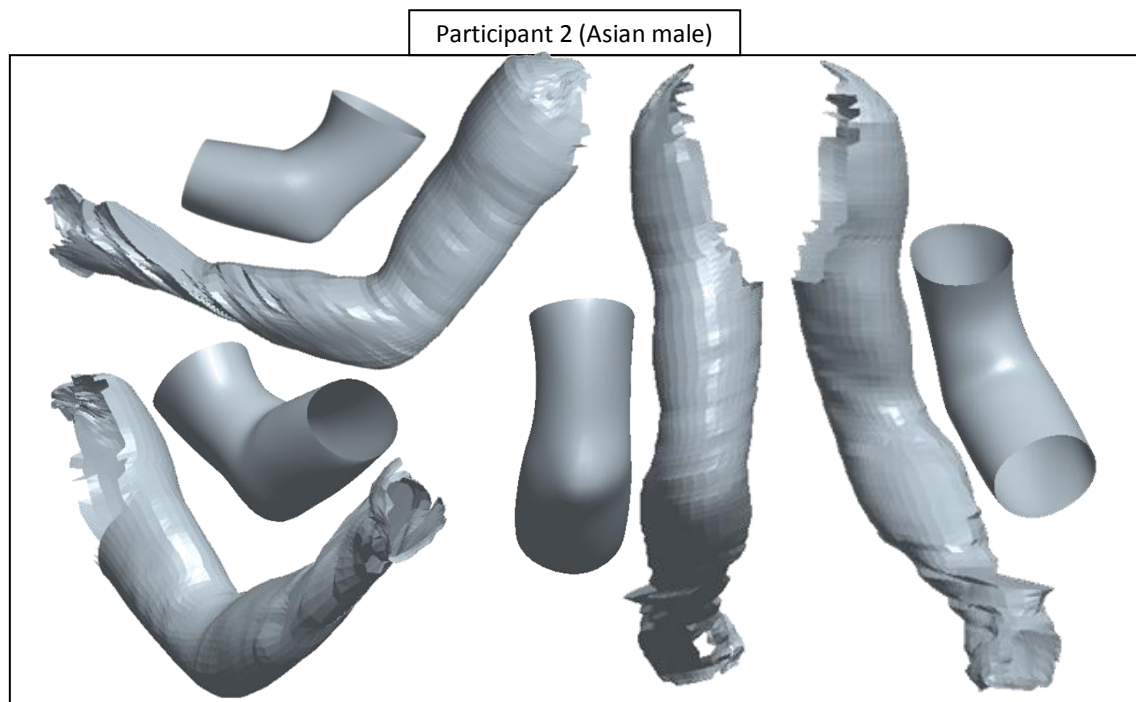


Figure 363. Images of framework's result for an arm posture between 135° - 90° for participant 2 of Asian male group

Participant 1 (Caucasian female)

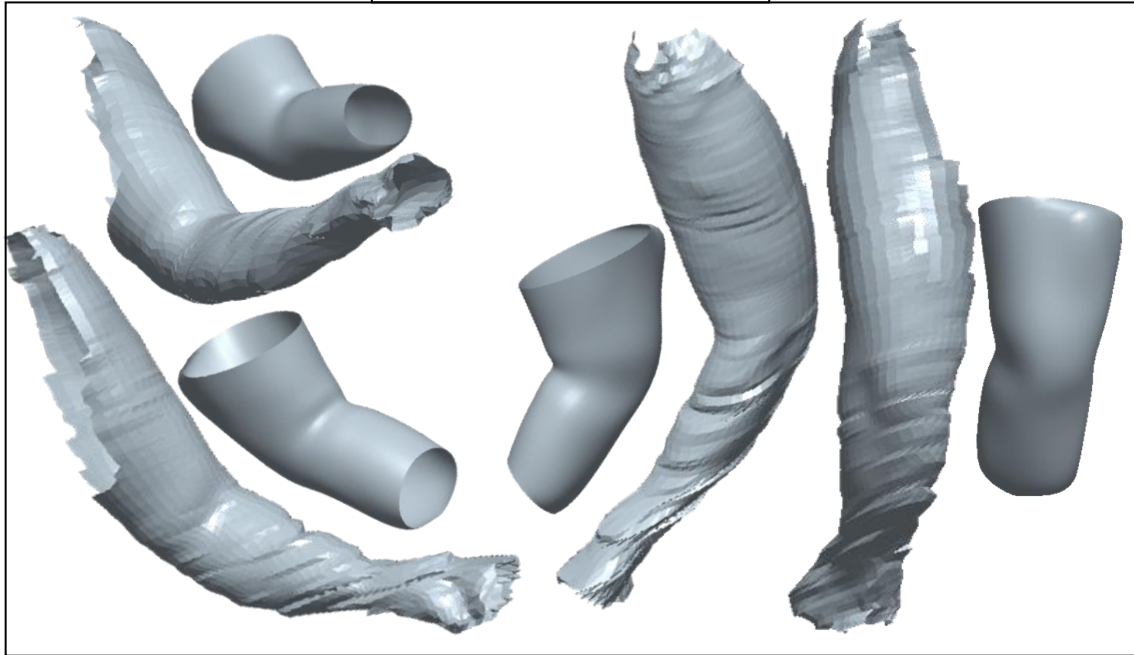


Figure 364. Images of framework's result for an arm posture between 135° - 90° for participant 1 of Caucasian female group

Participant 2 (Caucasian female)

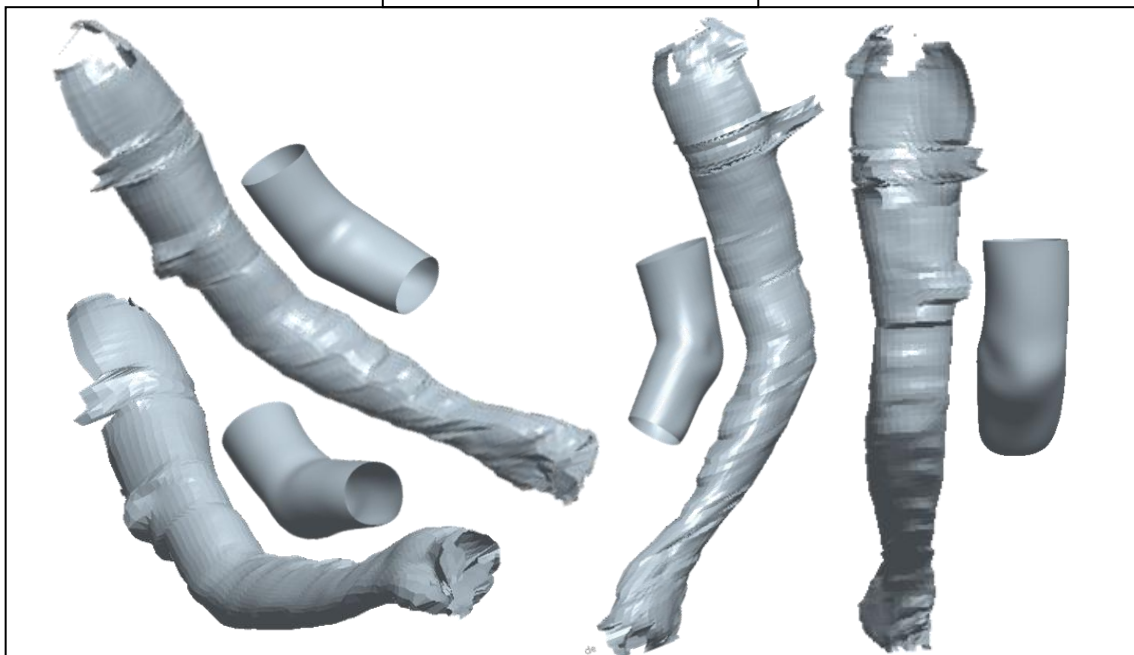


Figure 365. Images of framework's result for an arm posture between 135° - 90° for participant 2 of Caucasian female group

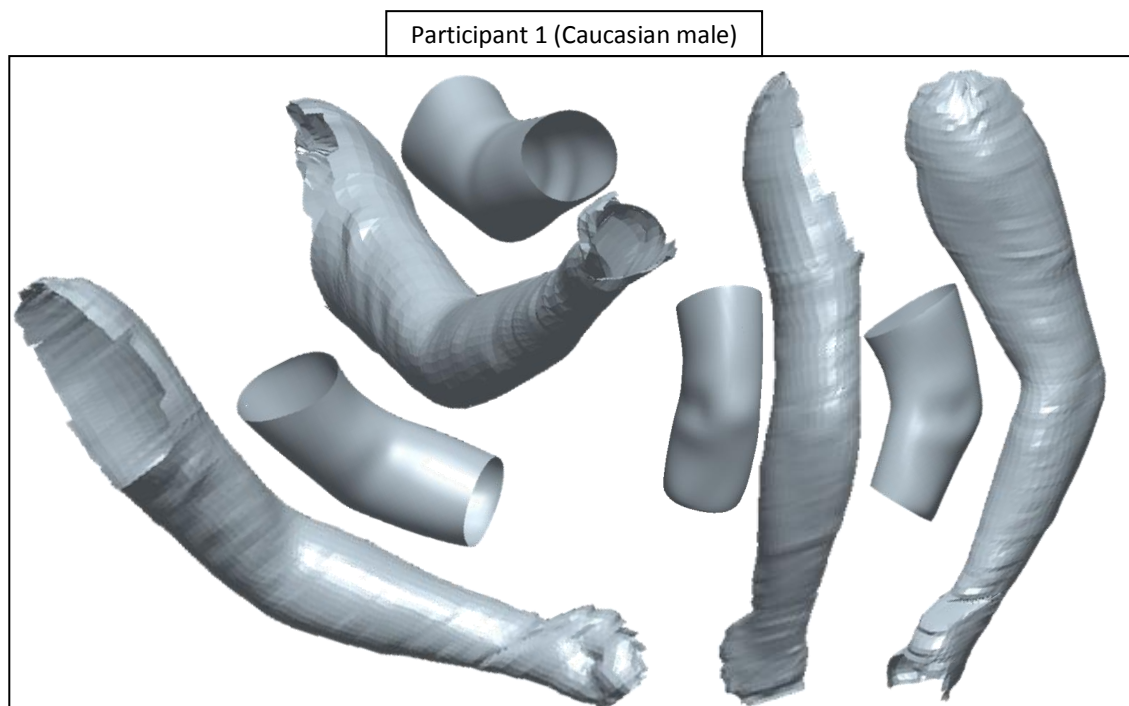


Figure 366. Images of framework's result for an arm posture between 135° - 90° for participant 1 of Caucasian male group

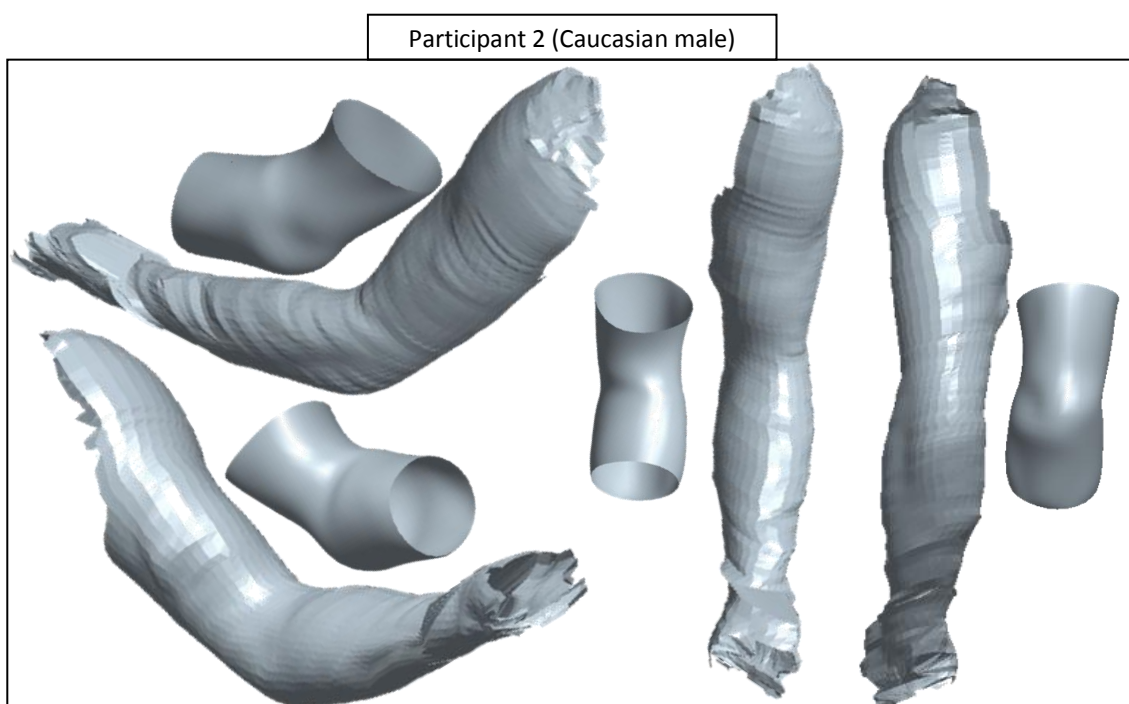


Figure 367. Images of framework's result for an arm posture between 135° - 90° for participant 2 of Caucasian male group

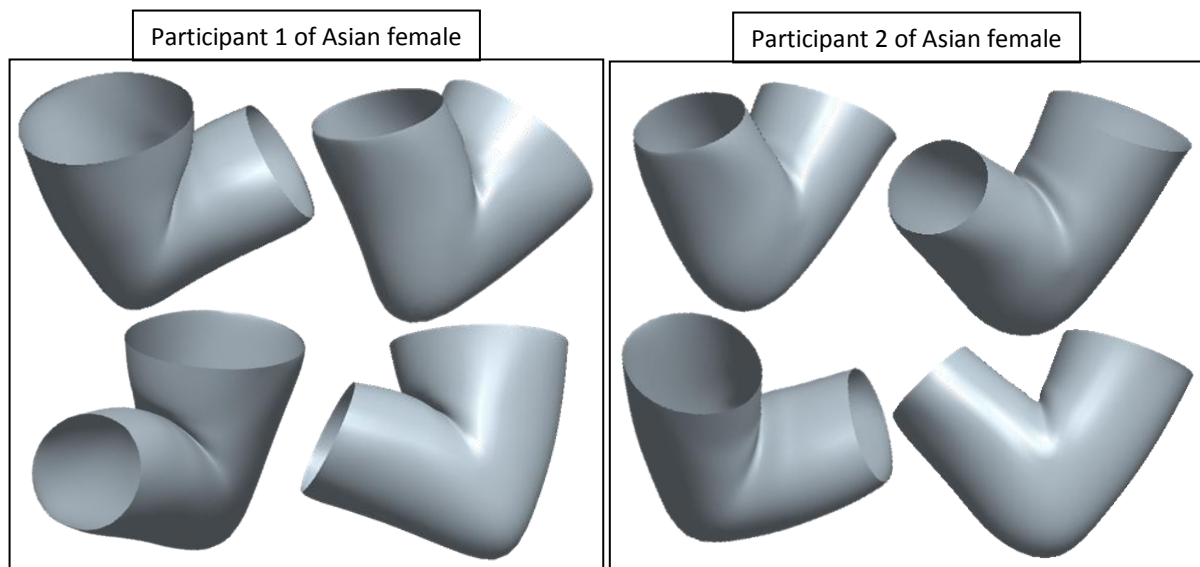


Figure 368. Images of framework's result for an arm posture between 90°-maximum flexion for Asian female group

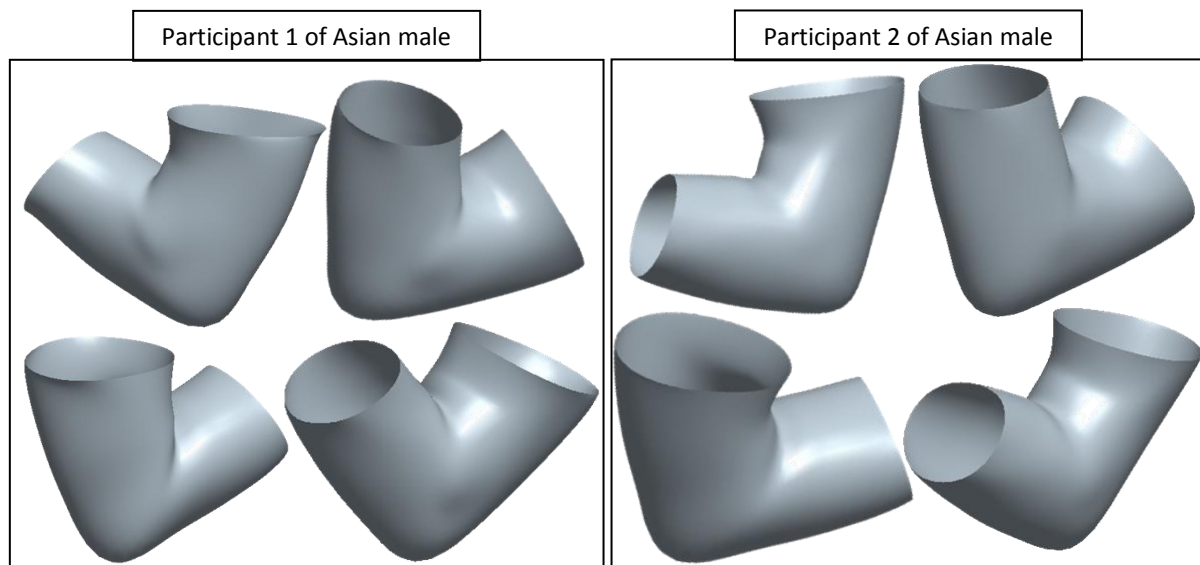


Figure 369. Images of framework's result for an arm posture between 90°-maximum flexion for Asian male group

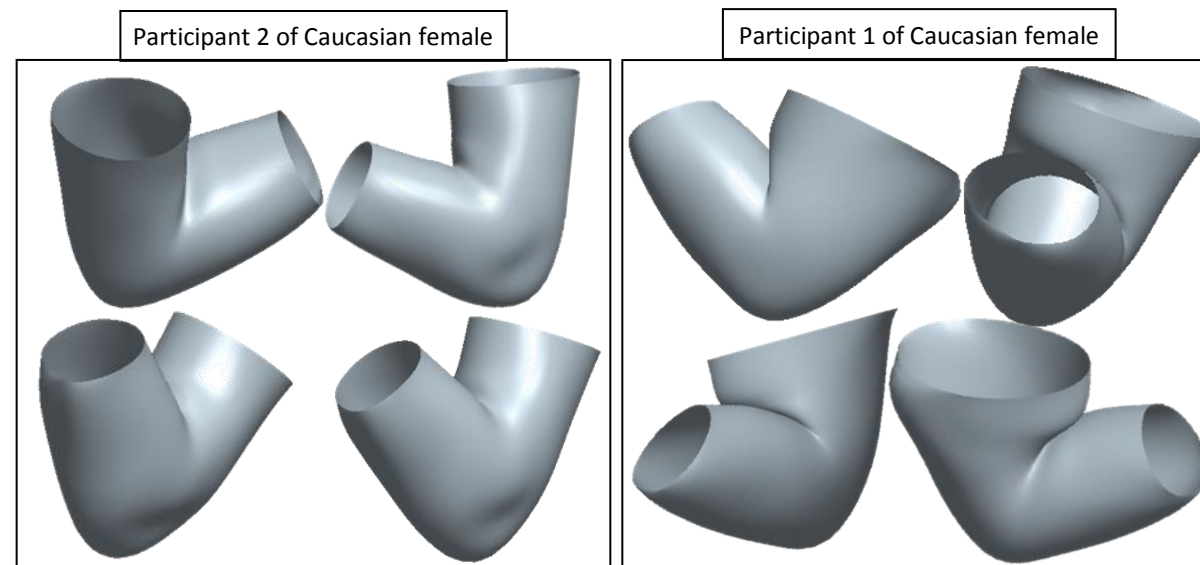


Figure 370. Images of framework's result for an arm posture between 90°-maximum flexion for Caucasian female group

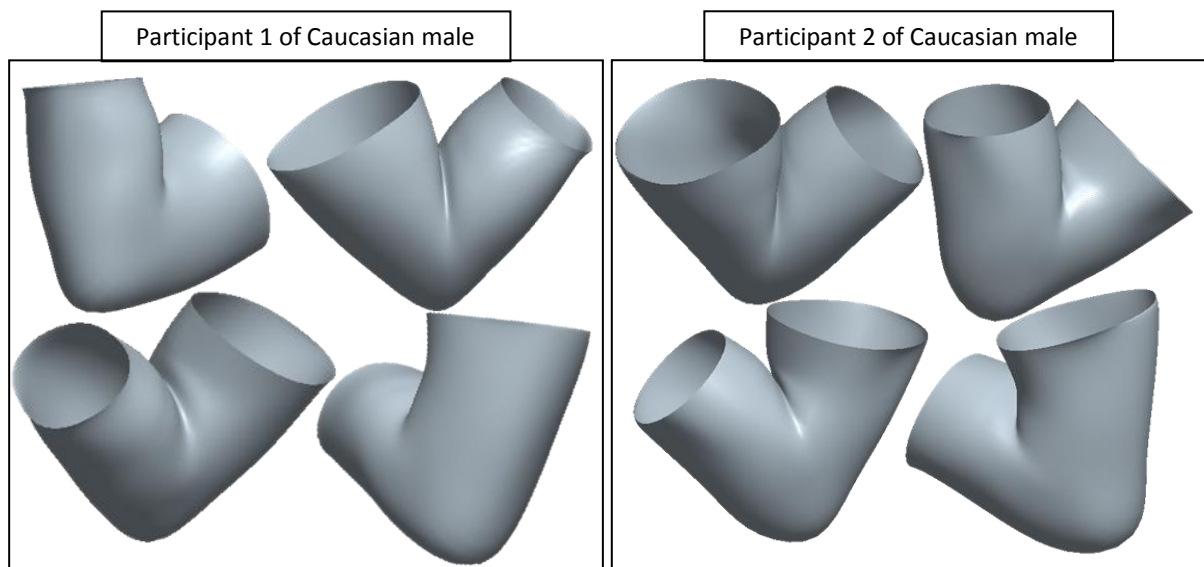


Figure 371. Images of framework's result for an arm posture between 90°-maximum flexion for Asian female group

10.4.3 Discussions on the realism review

The results of the realism review showed that the framework was able to recreate details such as the indentation at the posterior of the elbow as well as crease at the anterior of the elbow which ultimately enhanced the flesh deformation realism. However, the result of the review also showed that, in comparison to the review result in chapter 8, unrealistic flesh deformation was more likely to occur. As suggested in sections 8.2.2.1 and 10.4.2, this could either be caused by the unavailability of the closest match from the database or distortion that was possessed by the input data i.e. 3D scan data.

The overall results of the realism's review supported the findings of the accuracy's review. Both reviews suggested that flesh deformation which was created by the framework was likely to be less accurate and realistic than flesh deformation which was created from data that were obtained directly from participants. As described in the discussion of the accuracy's review in section 10.3.3, this was to be expected. The agreement between the accuracy and realism review suggested that the realism review indeed complemented the result of the accuracy review. Thus, unless a more comprehensive approach of accuracy review is performed (see section 10.3.3), this research suggests the simultaneous use of both types of review. Further discussion regarding the review of the framework is provided in chapter 11.

10.5 Summary

This chapter aimed to review the ability of the new FDM to accommodate different body sizes and types. To facilitate the review, the framework, which was developed in chapter 9, was used. The framework provided the required input for the new FDM which was then used to create flesh deformation. Two measurements variables were used to review the ability of the new FDM to

accommodate different body sizes and types. They were accuracy and realism. To assess accuracy and realism, existing methods in chapter 8 were used. These were: (1) quantifying the error level of the five key cross sections and profiles and (2) visual observation, respectively. For the purpose of review, 8 participants were recruited. The participants consisted of two Asian females, two Asian males, two Caucasian females and two Caucasian males. Three 3D scans of arms and three side view photographs were obtained for each participant. Weight and height were also obtained from each participant.

The results showed that, by utilising the framework, the new FDM was able to accommodate different body sizes and types. However, it was also shown that its accuracy and realism level were lower in comparison to the result in chapter 8. The accuracy ranged from 2.61-2.78 mm for five key cross sections of entire groups and 0.35-2.18 mm for profiles. This finding was to be expected because the input of the new FDM for this review was essentially dependent on the outputs given by the framework. Since the framework performance was in turn dependent on its ability to provide a closest match from its database, the small number of data in the database would have an effect. The review also revealed that the quality of the 3D scan of a fully extended arm also played a significant role on the performance of the framework. The review demonstrated that any distortion of the 3D scan of a fully extended arm would likely be passed on the next stage and eventually affects the creation of the flesh deformation by the new FDM.

11 Discussions

This research aimed to create flesh deformation due to joint movements in digital human models, to address the needs of ergonomics simulation. This research also limited the scope of the study into modelling the deformation at the elbow. There were four objectives of this research: (i) to review the state of the art in the use of DHM in ergonomics and body deformation; (ii) to investigate a set of specifications for DHM to guide the development of flesh deformation that suits ergonomics simulation purposes; (iii) to propose a method to create flesh deformation at the elbow joint; and (iv) to review the proposed method to deform the elbow against the set of specifications for DHM.

This research has succeeded in proposing a method for flesh deformation, the new FDM and framework, which directly addresses the needs of ergonomics simulation. The suitability for ergonomics simulation was accomplished by ensuring that the new FDM and framework comply with a set of DHM specifications which were established prior the development of the new FDM and framework. In essence, these specifications were a way to translate the needs for DHM flesh deformation for ergonomics simulation into the research. Detail discussion on the DHM specifications will be given in section 11.1.1 and 11.1.3 whereas how the new FDM and framework met the specifications has previously been addressed in section 8.2 and 10.3.

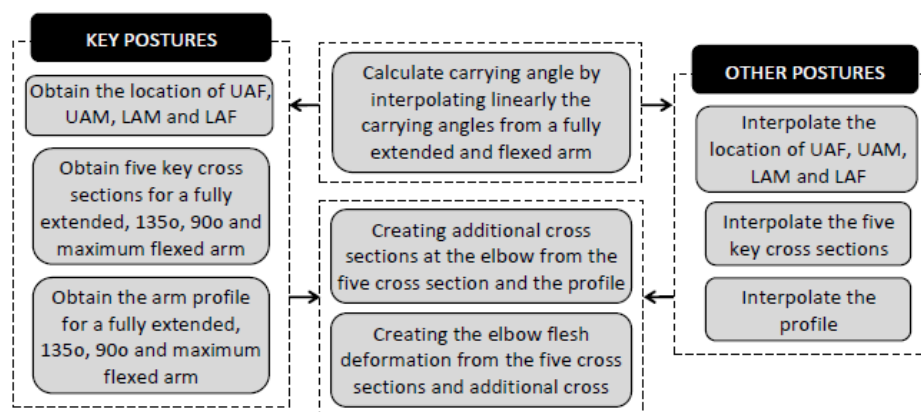


Figure 372. Mechanism of the new FDM for the elbow joint

Figure 372 shows the mechanism of the new FDM for the elbow joint. The flesh deformation possessed a number of characteristics: firstly the deformation was limited to a specific flesh deformation area; within this area the flesh form was driven by five key cross sections and a longitudinal profile. Additional cross sections were created from the five key cross sections and profile. A combination of five key cross sections and additional cross sections were then used to create the flesh deformation surface at the elbow joint. The location and shape of the five key cross

sections as well as profiles had to be provided for four key postures i.e. a fully extended arm, 135° flexion, 90° flexion and maximum flexion. From these data the location and shape of the five key cross sections as well as the profile for any other arbitrary posture e.g. 100° flexion, 60° flexion, etc. were obtained to support the flesh deformation throughout the joint range of movement.

The framework, shown in Figure 373, was developed to enable the FDM to simulate flesh deformation for a wide anthropometric range. In order to do this, the flesh deformation area, the key posture's cross sections and arm profiles had to be predicted. Five inputs were required i.e. 3D arm scan in a fully extended supine posture, height, weight, race and gender. The whole process was illustrated in chapter 9. A relationship between the flesh deformation area and body type/size was employed to predict the flesh deformation area of a 3D arm scan. A template, which was created from a predetermined 3D scan of a fully extended arm, was matched to the new 3D arm scan. Using the information from the predicted flesh deformation area, five cross sections were sampled through template matching.

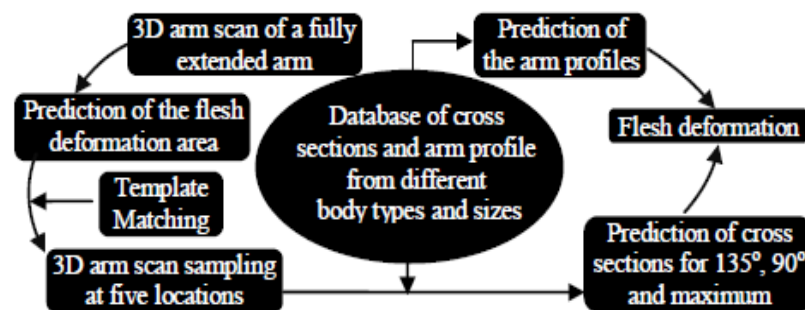


Figure 373. The mechanism for the framework

11.1 Key stages of the adopted research methodology

To achieve the aim and objectives of the research, a methodology which is shown in Figure 374 was adopted. The methodology was centred on utilising a set of specifications to develop the new FDM. This methodology was proposed to ensure that the new FDM was suitable for ergonomics modelling. The rationale behind the adopted methodology was in line with view of Badler (1997) who suggested that characteristics of DHM varied and depended on application. The figure shows how DHM specifications were generated and utilised during the development of the new FDM. The set of DHM specifications were primarily informed from the literature review (Chapter 2) and user study (Chapter 3). The approach of establishing a set of specification by means of a literature review and user study was similar to a study by Helin et al. (2007) who developed a production design simulation software platform.

As suggested in Figure 374, there were 8 key stages of the adopted research methodology. These were: (1) literature review; (2) user study; (3) establishment of DHM specifications; (4) comparison of existing FDMs and DHM specifications to determine the most suitable existing FDM;

(5) development of FDM; (6) Reviewing FDM; (7) Application of FDM (to accommodate different body sizes and types); and (8) reviewing the application of FDM (to accommodate different body sizes and types). Each of the key stages and its corresponding result are discussed in the following subsections.

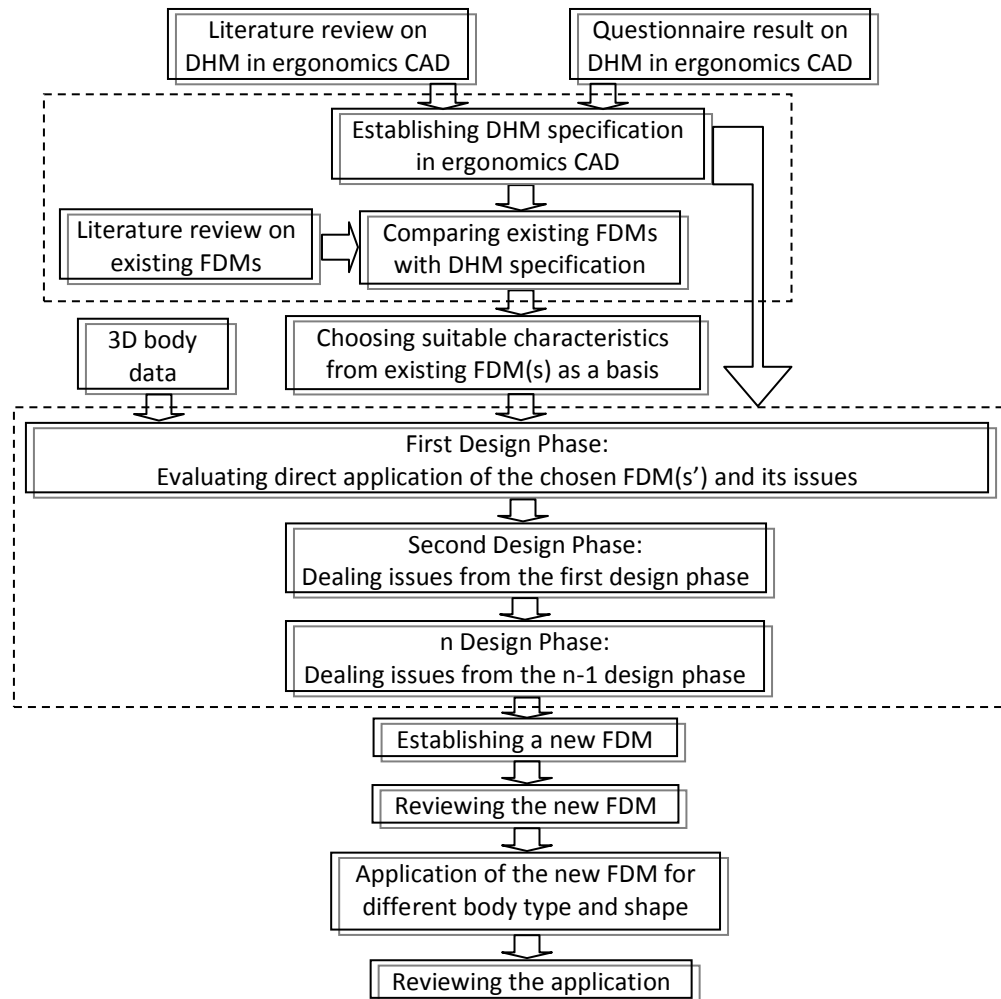


Figure 374. Adopted methodology to create a new FDM

11.1.1 The literature review

The literature review aimed to fulfil the first objective of this research i.e. to review the state of the art in the use of DHM in ergonomics and body deformation. This objective was met by performing a literature review that was focused on DHM in ergonomics application and existing approaches of flesh deformation. The literature review also covered basic theory on surface creation; DHM's joint movement and 3D body scan technology. These additional topics of literature review were added because: (1) knowledge of surface creation and DHM's joint movement were required for both understanding existing FDMs and developing a new FDM; (2) knowledge of the 3D body scan technology was required to support the intention of this research in utilising the technology.

The results of the literature review showed that:

1. *There was clearly a need of FDM that was suitable for ergonomics applications.* The literature review outlined that the ultimate aim of DHM simulation in ergonomics modelling was to limit the need to design products or workplaces with physical mock-ups or testing with real human subjects (see section 2.1.1). The literature review also showed that in order to achieve this, DHM should be able to represent a real human as closely as possible and take into account biomechanics principles, anthropometric principles, etc. (see introduction in section 2.1). As a result, DHM in ergonomics applications required fulfilment of fundamental characteristics which have been outlined in section 2.1.2. Some of the fundamental characteristics had been addressed by recent developments in existing DHM in ergonomics simulation e.g. the incorporation of motion simulation in Jack which was aimed to create a realistic and accurate motion and posture. Another example was the recent development of Vis Jack which allowed the incorporation of 3D body scan data to generate a more accurate and realistic virtual human. However, despite these latest developments, there seemed to be a lack of attention paid to the development of a realistic and yet accurate flesh deformation around the joint which would also support outer surface simulation of the human skin surface which has been identified as one of DHM fundamental characteristics by both Seidl and Bubb (2005) and Weigner et al. (2007). In addition to this, a study by Lämkuhl et al. (2007) showed that simulation of the human skin surface did affect the user's engagement with ergonomics applications. Furthermore, they also argued that the request for a more human-like virtual human was present. Further literature review also revealed that there has been substantial research to increase simulation of the human skin surface in computer graphics (see section 2.2). However, the adopted flesh deformation methods by existing DHM in ergonomics simulation were limited to only a few examples. JACK adopted free-form deformation (Azuola et al., 1994) whereas RAMSIS adopted a combination of rigid flesh deformation and torsion deformation for vertices around the joint (Bandouch et al., 2008). SANTOS (Abdel-Malek et al., 2006) adopted linear skinning which involved assigning weights to the outer skin surface based on the outer skin surface relationship with the nearby skeleton. All of the above adopted methods produce flesh deformation that was purely based on sculpting the form with less regard taken of ergonomics principles e.g. conformance to anthropometry. This was in contrast to the concept of DHM in ergonomics modelling which was largely targeted at accuracy based on certain principles such as biomechanics and anthropometry, amongst others. Badler (1997) also indicated that the characteristics of DHM vary and depend on application. This suggested that, because a method to simulate an outer skin surface for DHM in games/entertainment would not necessarily be

suitable for ergonomics applications, an alternative method to simulate the outer skin surface which was suitable for ergonomics modelling was required. With respect to methods for flesh deformation modelling at the joint for ergonomics simulation, the literature review suggested that there were limited, if any, research publications which attempted to address this issue.

2. *There were 6 potential DHM specifications that were found to be relevant for DHM in ergonomics application.* The literature review revealed that accuracy was essential in ergonomics simulation (see section 2.1). This was likely due to DHM's role as a scientific tool to evaluate the accommodation of a product or workplace. The importance of taking into account processing time had also been identified from the literature review. This was reflected from the general processes in performing analysis with existing ergonomics applications which required the posturing of DHM to be performed within a short time scale i.e. real time modelling. Another aspect, which was also found in the literature review and related to "real time" and "accuracy", was "whole body modelling". The literature review on existing DHM for ergonomics simulation suggested that whole body modelling was the commonly adopted approach (see section 2.1.3). This was probably because the existing DHM were partly designed to accommodate anthropometric assessments of products and workspaces. Another important finding from the literature review concerned with DHM was "realism" (see section 2.1.2) which concerns the outer or visual appearance e.g. cartoon-like, fantasy creature, etc. Realism was an important part with regards to the role of ergonomics simulation as a visualisation tool which was defined as a tool to support the creation and presentation of a workplace, product or solution (Sundin and Örtengren, 2006). According to Dryer (1999), realism helped user engagement as realistic DHM were perceived to be agreeable. The literature review also suggested that user intervention in ergonomics simulation was generally limited to alteration of a DHM's posture, DHM's anthropometric features, and type of ergonomics analysis. Typically, the user was not normally expected to have to correct model errors, to define acceptable postures to drive flesh deformation or address unrealistic results while altering the DHM's postures. The literature review also showed that ability to model different body sizes and shapes in ergonomics simulation was crucial. This was to ensure that a product or workplace would be suitable for a variety of target users. Thus, any flesh deformation method should be applicable to accommodate different body sizes and shapes. From the literature review and current research publications, it was not clear whether current flesh deformation methods of existing DHMs have taken this into account or not. However, it was known that for linear blend skinning, which was adopted by SANTOS, it was likely that flesh deformation that took into account body sizes and shapes would be difficult to apply. This was because the relationship

between skin surfaces and corresponding bones had to be assigned and adjusted for each possible body size and shape.

Some of the potential DHM specifications above were also likely to contradict with each other. This was clearly demonstrated by the relationship of real time modelling and three of the potential DHM specifications i.e. accuracy, realism and whole body modelling. Achieving an accurate and realistic whole body model would likely result in the lengthy processing time and thus impact on the real time modelling specification. Thus, this research had to balance the conflicting needs for accuracy, realism, whole body modelling and real time modelling. This suggested that a trade off between these specifications was required.

3. Characteristics of DHM in ergonomics modelling were driven by the DHM's function and usage in ergonomics. The literature review also found that the characteristics of DHM are driven by the function and usage of human models to resolve design problems in ergonomics. For instance, realistic and accurate motion or posture was driven by the function of ergonomics simulation to evaluate working posture and work space analysis.

The first finding confirmed that there was indeed a need for research to create a FDM that was suitable for ergonomics modelling. The first finding also corroborated a number of factors that motivated this research as described in section 1.2 and identified in the early stage of the research. The second and third findings lay the foundations for the second objective of the research i.e. to investigate a set of specifications for DHM to guide the development of flesh deformation that suits ergonomics simulation purposes.

In addition to the three findings above, the literature review also revealed that 3D body scanning technology had an ability to provide 3D anthropometry dimensions (see section 2.6). Current DHM models are based on databases of 1D anthropometric dimensions. Given several anthropometric dimensions to create a specific DHM, current ergonomics applications predict the rest of anthropometric dimensions. This approach had received critics (Marshall, et al., 2003; Sundin and Örtengren, 2006, etc) and verification results shows that errors are produced (Doi and Haslegrave, 2003; Oudenhuijzen et al., 2008, etc). 3D scanning technology has the potential to address this problem (Herron, 2006) although recent research suggests standardization concerning measurements extraction would likely be required e.g. landmark determination and dimension extraction (Lu and Wang, 2008) to make this possible.

11.1.2 The user study

By reviewing existing research and publications, the literature review provided knowledge about the state of the art on the use of DHM in ergonomics and body deformation. However, this knowledge was mainly based on the researchers' point of view. To provide a full picture concerning

DHM in ergonomics and body deformation, it was important to try to capture the users' point of view as a key stakeholder in ergonomics simulation. A user study was performed to confirm and follow up the literature review's findings from the users' point of view, especially the second and third findings (see section 11.1.1). The outcome of the user study did complement the literature review's results and contribute to the establishment of DHM specifications in ergonomics modelling.

There were four objectives for the user study: (1) Users' views on the need for a realistic outer surface simulation of the human skin surface; (2) Users' views on what constitutes DHM's realism; (3) Users' views on the possible trade off of potential DHM's specifications; and (4) User's view on the importance of flesh deformation due to contact with external objects/loads and characteristics that define the overall quality of ergonomics applications. The user study was performed by mail and personal distribution of questionnaires to ergonomists in the UK and design students of the Design and Technology Department at Loughborough University, respectively. A thorough discussion of the methodology and results of the user study are given below.

11.1.2.1 The methodology of the user study

A questionnaire was chosen due to its practicality as it allows distribution through mail to ergonomists in the UK. Limitations of questionnaires were identified (see section 3.1) and appropriate measures were taken to minimise them. The *first limitation* of a questionnaire was that it was likely to provide limited and less in-depth information in comparison to a structured interview or unstructured interview. To lessen the effect of this particular limitation; in addition to closed questions, open questions were also utilised to allow further exploration of users' points of view. Based on the results of the questionnaire, the usage of open questions in this research suggested that it assisted in probing a user's point of view or attitude towards an issue. For instance, through the comments of the respondents' from the given open questions, users' views towards the relationship between accuracy and realism were revealed i.e. that there was less added value towards the ergonomics analysis outcome from a realistic looking DHM as the increase in accuracy could only be possible if the realistic looking DHM was based on sound anthropometric and biomechanics principles. The *second limitation* of a questionnaire was that it was likely to have problems with a lower return rate, typically about 10%, when distributed by mail (Stanton et al., 2005). To anticipate a possible low return rate this research took two measures. Firstly, pre-addressed envelopes with first class stamps on them were provided. Secondly, an introduction letter was also sent to accompany the questionnaire. The letter provided information about the researcher and the reason why the questionnaire was sent to each respondent. The return rate of the mailed questionnaire (i.e. 33%) suggested that both measures helped to increase the return rate of the mailed questionnaire. The *third limitation* of questionnaire was that its questions had to be

clear enough to be understood by a respondent without any assistance. To anticipate this, prior to finalising the questionnaires, two ergonomists were involved to provide feedback which was then used to optimise the clarity of the questions. The fourth limitation was that a questionnaire was prone to social desirability bias i.e. bias which is caused by the fact that participant is simply giving what the analyst wants. To minimise the impact of this limitation, the introduction of the questionnaire and the accompanying letter provided limited information about the research (see appendix A). With hindsight, in addition to the user study, an interview could also have been performed. Although this research demonstrated that a questionnaire was able to provide sufficient detail of respondents' views, an interview could potentially provide more flexibility to probe a topic of interest. For future studies, it was suggested that the mailed questionnaire was accompanied with a request to a respondent to learn her/his willingness to be contacted further for an interview.

The user study involved a total of 27 respondents, comprising of 15 ergonomists with experience in using ergonomics applications, 5 ergonomists with no experience in using ergonomics applications and 7 design students who are taught the use of ergonomics applications as part of their undergraduate studies. The choice of respondents for this research was deemed to be appropriate as it allowed views from respondents with ergonomics knowledge and various degrees of expertise in the usage of ergonomics applications. However, for future studies, it would be useful to include a wider range of respondents e.g. a design engineer in a car manufacturing company. Inclusion of a wider range of respondents would likely enable the ability to further generalise the user study's result as a more complete view of ergonomics users needs and opinions would be captured. This follows the view of Ruiter (2000) who suggested that the users of ergonomics simulation are becoming increasingly diverse. As the number of respondents in the user study was relatively small, generalization of the user study result should be performed with care. To increase the generalization possibility of the user study result, future studies should aim to recruit more respondents. It would also be worthwhile to include respondents from different countries as varied access to the latest computing technologies might affect the views of respondents.

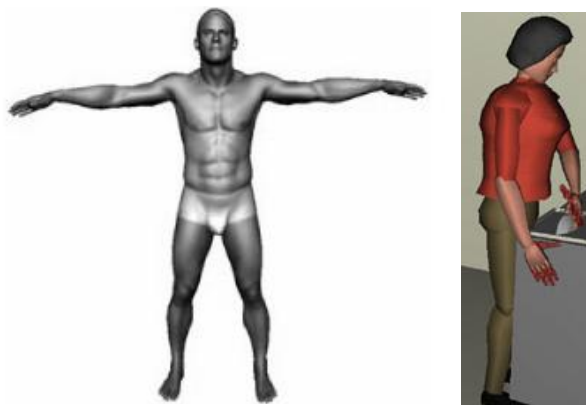


Figure 375. Two images which were used to investigate the required level of detail of a realistic DHM

Another reflection concerning this research's user study concerns the images which were used in the questionnaire regarding the level of detail of DHM and the effect of unrealistic flesh deformation at the joint. To investigate the required level of detail of DHM, two images were utilised to represent an enhancement to the detail of the whole body (i.e. accuracy must be uniform) and enhancement to the detail for certain body parts only e.g. hand, feet, head/face and torso (i.e. accuracy was not uniform). The images are shown in Figure 375. The result showed that regarding what constituted to a realistic looking DHM, respondents seemed to be less concerned about the DHM level of detail (LOD). The finding of the used study is somewhat contradictory with current research that shows level of detail affects the sense of realism (Dehn and Van Mulken, 2000). It is possible that this was because this study only used one image for each level of detail category to illustrate them. With such a limited number of images, this might result in difficulties for users to compare the realism between the two. With hindsight, several images could be used instead.



Figure 376. The image used to investigate the effect of unrealistic flesh deformation

To investigate the effect of unrealistic flesh deformation at the joint, a single image was used to demonstrate unrealistic deformation (see Figure 376). The result showed that users seemed to agree that unrealistic flesh deformation affects the sense of realism despite the usage of a single image. In this study, the given image was relatively realistic apart from the flesh deformation around the waist. Hamilton and Nowak (2009) argued that DHM users become critical of imperfections of DHM as realism increases. Thus, with hindsight, it would be interesting to investigate if users' views would remain the same if a different image is used e.g. the right image in Figure 375 where the realism contrast between the body form and flesh deformation is relatively less.

As stated at the beginning of this section, the user study was used to confirm and follow up findings from the literature review. In hindsight, the user study could also be used to find out the users' view concerning the level of importance of potential DHM specifications that were related and contradicting with each other i.e. accuracy, processing time, realism and whole body modelling. As they were later used to form DHM specifications, provision of an importance rating would likely

be useful to guide the development of flesh deformation modelling for ergonomics simulation quantitatively. An importance rating would have been useful to guide tradeoffs that were made during development, however without any weighting for specifications a balanced approach was taken.

11.1.2.2 Discussion of the user study's results

Despite the limitations of the user study's methodology, the user study achieved its four objectives. The following points discuss the user study results and demonstrate how each of the user study results contributed to achieving a particular objective:

1. Users' views on the need for a realistic outer surface simulation of the human skin surface.

This objective was met by presenting and analysing questions in the second and fourth section of the questionnaire. There are three main findings for this objective:

- *The respondents believed that flesh deformation modelling would be part of the future of DHM in ergonomics application.* This finding confirmed the need for research to improve outer surface simulation of the human skin surface from the users' point of view. The respondents' comments highlighted the contrast between the rapid advances of DHM in gaming industry/other application and DHM in ergonomics application; and suggested adoption where appropriate. Their comments supported findings from Lämkuil et al. (2007) which suggested that the need for a more human-like virtual human.
- *The respondents considered flesh deformation modelling to be less important or desirable than other characteristics.* This finding was in line with the trend found in the literature review in section 2.1.4 which suggested that current research was dedicated more to deal with other characteristics. The respondents' comments suggested that, in order to simulate flesh deformation modelling, separate applications were used. For instance, to simulate flesh deformation modelling at the joint, some of the respondents used the Poser software. The possibility of working around the problem to simulate flesh deformation explained why current researchers and respondents viewed flesh deformation modelling as less urgent than other characteristics. However, the need to utilize other applications also meant that a user was presented with demands to have skills to master other applications and time to simulate flesh deformation modelling in other applications. By integrating flesh deformation modelling with existing ergonomics applications, the need to utilize other applications could potentially be eliminated and fewer demands would be put on the user. It would also provide an opportunity to evaluate the effect of flesh deformation

modelling at the joint. Thus, this finding supported the need to create a flesh deformation modelling method that is suitable for ergonomics applications.

- *The respondents acknowledged that flesh deformation modelling supported the role of DHM in an ergonomics application as a visualisation tool.* This finding suggested that research in flesh deformation modelling is required in order to achieve the role of DHM in an ergonomics application as a visualisation tool. This result of the user study supported the earlier findings in the literature review regarding the need to produce a realistic DHM (see section 2.1.1) and realistic outer surface simulation of the human skin in ergonomics applications (see section 2.1.2).
2. *Users' views on what constitutes DHM's realism.* This objective was met by presenting and analysing questions in the third section of the questionnaire. There are two main findings for this objective:
- *The respondents seem to be indifferent with regards to the level of detail required for whole body modelling.* The user study suggested that partial (non-uniform) and whole body (uniform) detail enhancement did not affect realism. However this result might have been affected by the design of the user study (see section 11.1.2.1).
 - *The respondents suggested that unrealistic flesh deformation affected DHM realism.* This finding suggested the need of realistic flesh deformation to assist the overall realism of DHM. However, again there might have been elements of the design of the user study that influenced this finding (see section 11.1.2.1).
3. *Users' views on the possible trade off of potential DHM's specifications.* This objective was met by presenting and analysing questions in the third section of the questionnaire. There were two main findings for this objective:
- *The respondents stipulated that realistic outer surface simulation of the human skin surface should be based on ergonomics principles e.g. anthropometric, biomechanics, etc. and is not aimed solely to achieve a high quality of aesthetic appearance.* The respondents' view was in agreement with the finding of the literature review in section 2.1.1 which suggested that as part of DHM's role to evaluate the accommodation of a product or workplace, accuracy was of importance. The respondents' views identified the difference between the requirements for ergonomics modelling and entertainment, which was mostly aimed to achieve high quality of aesthetic appearance. The literature review on the existing DHMs of ergonomics application suggested that currently adopted flesh deformation modelling at the joint did not seem to show that they were based on anthropometric principles.

This demonstrated the need for flesh deformation modelling at the joint which took into account the specific requirements of ergonomics modelling.

- *The respondents acknowledge that a trade off on realistic and accurate DHM would likely be required to allow the ergonomists to explore different options for their analysis purposes in real time.* This finding suggested that respondents were aware of the need to compromise the level of realism and accuracy in order to achieve a real time interaction while working with DHM in an ergonomics application. The willingness of respondents to accept the trade off also suggested that real time was an important characteristic for DHM in ergonomics applications. This finding also demonstrated that users recognised realism, accuracy, and real time modelling as part of DHM specifications.

4. *User's view on the importance of flesh deformation due to contact with external objects/loads and characteristics that define the overall quality of ergonomics applications.*

This objective was met by presenting and analysing questions in the fifth and sixth sections of the questionnaire. There were four main findings for this objective:

- *The respondents believed that flesh deformation modelling due to contact with external objects/loads would be part of the future DHM in ergonomics application and that it would likely increase the accuracy of ergonomics applications.* This finding suggested that further work to simulate flesh deformation modelling due to contact with external objects/loads is envisioned by the respondents. Currently, flesh deformation modelling due to contact with external objects/loads was commonly performed on separate applications where a specific body part was anatomically modelled (Assassi et al., 2009; Lee et al., 2009; etc.) or an interaction between a specific body part was modelled parametrically (Tewari, 2000; Verver and Mooi, 2004; Moes, 2007; Grujicic et al., 2009; etc.). Therefore, a new approach to enable integration of flesh deformation modelling with existing ergonomics applications is suggested for future research.
- *The respondents believed that flesh deformation modelling should include object deformation and a majority of respondents suggested a whole body modelling implementation.* This finding provided further direction for future studies or research related to flesh deformation modelling due to contact with external objects/loads.
- *Respondents with experience of using more than one ergonomics application suggested that the realism of a DHM would affect their overall judgment of an ergonomics application provided that it offers functions similar to the existing ones.*

This finding suggested that DHM's realism is not "everything". However, it is still desired by users as it would be likely to assist the role of DHM in ergonomics applications as a visualisation tool.

The overall results of the user study indicated that they were in line with the findings of the literature review. The results of the user study related to the first and second objective clearly supported the first finding of the literature review i.e. *there was clearly a need for FDM that was suitable for ergonomics application*. The results of the user study related to the third objective also indirectly supported the second finding of the literature review i.e. *there were 6 potential DHM specifications that were found to be relevant for DHM in ergonomics application*. The users' awareness of a possible trade off between accuracy, realism, and real time modelling indirectly signified that these three attributes were relevant for DHM in ergonomics application.

The results of the user study are useful, not only for this research, but for other research which is related to DHM in ergonomics modelling, especially those that study flesh deformation modelling issues of DHM. As there have not been many research studies which look into this issue of DHM in ergonomics modelling, the findings of this research could be used as initial information for future studies. However, the small sample of the study also means that generalisation of the user study's results should be performed with care. Furthermore, generalisation of the user study's result should also take into account that a questionnaire is known to have low reliability and validity (Stanton et al., 2005). Future studies which involve a larger sample size are suggested to verify the user study's results.

11.1.3 The establishment of DHM specifications

The second objective of the research was to investigate a set of specifications for DHM to guide the development of flesh deformation that suited ergonomics simulation purposes. This objective was met by establishing DHM specifications from the result of literature review and user study (see chapter 4). In total, there were 6 DHM specifications identified. These were: (1) accuracy; (2) real time modelling; (3) realism; (4) accommodation of different body sizes and types; (5) whole body modelling; and (6) minimum user intervention. Details and discussion of each specification can be found in section 4.1 and section 11.1.1.

The 6 DHM specifications were identified through the literature review and some of them were investigated further in the user study. The approach taken in identifying the six DHM specifications from both the results of the literature review and user study were an attempt to ensure the specifications would be exhaustive. The agreement between the findings of the literature review and user study suggested that specifications such as accuracy, real time, realism, and

accommodation of body size and shape were likely to be correct. For other non-explicit specifications i.e. whole body modelling and minimum user intervention, they were inferred from the literature review on usage of existing DHM, which showed that these two specifications were the commonly accepted norms for DHM in ergonomics simulation. Nonetheless, as the final specifications were not re evaluated with users, there is a possibility that this research might have overlooked other possible specifications. Also, cross checking the specifications with users might potentially provide more detailed information or target values for some specifications. For instance: (i) what is the acceptable waiting time for users?; (ii) what is the acceptable level of realism for flesh deformation at the joint?; (iii) what is the acceptable/expected error level for flesh deformation at the joint?, etc. More detailed information on specifications would likely assist the development and review process of the proposed flesh deformation method. Thus, in hindsight, a second user study could be performed to cross check the 6 DHM specifications and investigate the expected level of performance of a DHM against each specification.

11.1.4 The comparison of existing DHMs against the DHM specifications

Having established the DHM specifications they were then used to evaluate existing FDMs to gauge their suitability for ergonomics applications. The most suitable FDM was then used as a basis to create an alternative more appropriate and tailored method of flesh deformation for ergonomics modelling. To gauge the suitability of existing FDMs, all of the DHM specifications were assigned the same level of importance or weight. It is acknowledged that this might not represent the true condition as it is possible that one DHM specification is more important than the others. Especially, as discussed in section 11.1, for some of DHM specifications such as real time and accuracy that appear to be contradictory. Increasing accuracy would likely cause a delay on processing time and vice versa. As the DHM specification is later used to assess existing methods of flesh deformation around the joint, the absence of weight/importance assignment to the DHM specification will affect the assessment outcome i.e. the most suitable FDM for ergonomics application. However, in order to ensure that a specification achieves what it is intended for, the weights have to be determined through objective measurements which would require the involvement of users to gauge the importance of specifications. Although it is possible to acquire this information, this research decided not to pursue it due to the time limitations and anticipation of the amount of work necessary in the later stages of FDM development. Nonetheless, it is acknowledged that assigning weights to the DHM specifications could give a better picture concerning the suitability of existing FDMs.

Instead of creating a completely new FDM, this research opts to build upon an existing FDM. Based on the comparison with the DHM specifications, the Shen et al. (1994) method seemed to be

the most appropriate basis for ergonomics modelling (see section 2.2.3.4 and chapter 4). To ensure a suitable scope for this research the principle of modifying an existing FDM was deemed to be the best approach. Opting to modify an existing FDM has its own advantages and disadvantages. The primary advantage is that the amount of work which is needed is reduced. As this research aimed to create a FDM that is suitable for ergonomics applications, to ensure the suitability of the proposed FDM, a set of DHM specifications had to be investigated first. This part of the investigation alone, as shown in Figure 374, required a comprehensive study involving a literature review and a user study, which had to be performed in addition to the FDM development. Also, the success rate of a modified existing DHM would likely be higher than a complete newly created FDM. Nonetheless, modification of an existing method also imposes some restrictions as possible modification would be limited by the existing method. For instance, the sweep based principle, which is the foundation of the proposed FDM of this research, is based on creating surfaces from a set of cross sections. Introducing another parameter to control the surface should take into account its effect on, and compatibility with, cross sections. In hindsight, despite this disadvantage, proposing a new FDM based on the modification of an existing FDM has proven to be an appropriate approach, resulting in the development of a means to deform the flesh at the joint of a DHM in ergonomics applications that conforms to DHM specifications.

11.1.5 The development of the new FDM

Together with the development of the framework, which will be discussed later in section 11.1.7, the development of the new FDM was aimed to fulfil the third objective of the research i.e. to propose a method to create flesh deformation at the elbow joint. The whole process of FDM development within this research could be modelled as a design process. According to Archer (1965), the process of designing followed a general pattern. Firstly, a need was identified by a designer and an artefact is planned to fulfil it. The artefact was constrained by boundary conditions set by external factors e.g. resource limitation, artefact requirements, etc. Solutions were then proposed. Lastly, examination of solutions' suitability with both the need and the boundary condition was then performed to reach a best solution. The need and boundary conditions were essentially requirements which have to be satisfied by the final design. Setting the need and boundary conditions prior to artefact development ensures that the final artefact achieves its function. In this research, the need of a new FDM was identified through both the literature review and the user study. The boundary conditions for a new FDM were set by the six DHM specifications, also established through both of the literature review and the user study. Archer's (1965, 1969) designing process was aimed for engineering design where possible solutions were well defined. Unfortunately, this was not the case with this research. Due to the complexity of the problem, a set

of solutions could not be provided and instead decisions had to be made through the process to reach a solution. This was in accordance with Marples's (1961) view which considered a design process as a sequence of major decisions from the initial statement of the problem to the proposed solution. Between major decisions, subsidiary decisions may be made in order to provide information as a basis for taking the next major decision.

The FDM development consisted of three key stages: (1) evaluating direct application of the chosen FDM and issues which come with it; (2) performing further research on the identified issues (stage 1 and 2); (3) feasibility testing. The first key stage (chapter 5) was a direct consequence of this research approach to modify an existing FDM as the basis for the new FDM. In the first stage, the compatibility of 3D scan data and the chosen existing FDM (Shen et al. (1994) method) were studied and any issues that arose were identified. The second key stage (chapter 6 and chapter 7) duly investigated these issues further. Completion of the second key stage allowed the outlining of the proposed FDM concept which subsequently underwent feasibility testing (section 8.1). During the feasibility testing, the concept of the proposed FDM was tested and modifications were made whenever required.

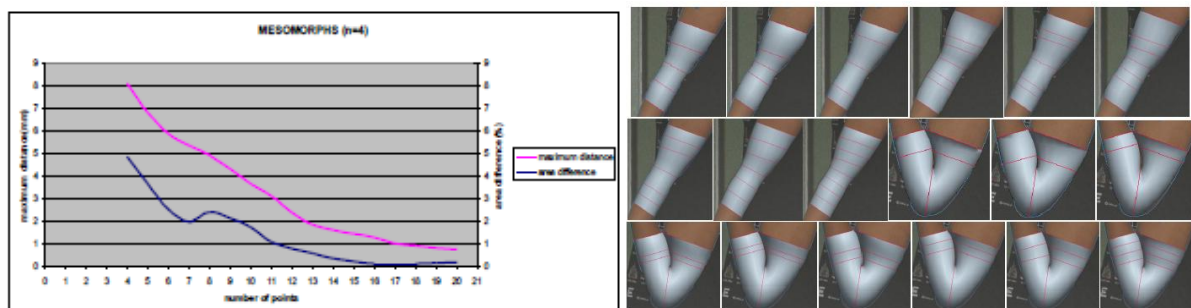


Figure 377. An example of one of the graphs for quantitative measures and example of images used for qualitative measures

As stated above, there were three key stages of the FDM development. In each key stage, major and subsidiary decisions concerning the proposed FDM were taken. Although effort was made to underpin every decision with quantitative measures, in some cases, qualitative measures, such as visual observation, were used. A clear example of quantitative measures to assist decision making is the determination of sampling points to represent five key cross sections in section 6.7. Graphs which show associated error levels for various numbers of sampling points were produced. The left image in Figure 377 shows one of the graphs. By using this graph, an optimum number of sampling points, which balances the need for accuracy and real time, was then decided. The best example of qualitative measures to assist decision making is where visual observation was used to determine the number of key cross sections (see section 6.6.2). A different number and location of cross sections were placed within the flesh deformation area and surfaces were created (see right image in Figure 377). Based on visual observation of the surface created from these cross sections,

the number of key cross sections that balanced between the need for accuracy and real time was determined. It is acknowledged that when qualitative measures such as visual observation are used, it is likely that the decision will be subjective and would indirectly affect the reliability of the design process. The key decisions in each key stage of the FDM's development and how they related to relevant DHM specifications will be discussed in detail in the following subsections.

11.1.5.1 Key decisions in the first development stage (evaluating direct application of the chosen FDM and associated issues)

In the first stage, the Shen et al. (1994) method was analysed and its compatibility with 3D scan data was investigated. There were two key decisions that were made during this stage. These were:

1. *Carrying angle.* Based on the investigation on section 5.3.1, it was found that Shen et al. (1994) did not accommodate the carrying angle even though it was shown that it was present during the arm movement. Based on the consideration that carrying angle improved accuracy and realism of DHM, this research decided to integrate carrying angle into the FDM's development. Further study in section 6.1.1, revealed that adoption of carrying angle also introduced complications as the carrying angle value was individually specific and decreased linearly as the arm flexed. This suggested that to accommodate different body types and sizes, obtaining both the carrying angle value and its decrement for every individual were required. However, as these were impractical, this research proposed a method to predict carrying angle decrement from a single carrying angle measurement of a 3D scanned arm (see section 6.1.2 - 6.1.4). To minimise the compromise on the accuracy of the prediction result, the prediction method was based on available statistically processed data of previous research by Van Roy et al. (2005) .

With hindsight, the adoption of a carrying angle could be considered as a stepping stone to improve the accuracy and realism of DHM modelling for ergonomics simulation. To the extent of the knowledge of this research there were no existing FDMs that took into account carrying angle. For a future study, the prediction method of carrying angle's linear decrement could be refined by acquiring raw data from a range of participants to provide objective values that represent the needs of ergonomics simulation.

Plane orientation of the cross section at elbow. Based on the investigation of the plane orientation of the cross section at the elbow in section 5.3.2.3, it was found that the plane orientation did not have a linear relationship with respect to the arm angle (see Figure 378). This was in contrast with Shen et al. (1994) approach that adopted a linear relationship. As this finding directly affected the elbow and thus any simplification on this area could affect both the accuracy and realism. Based on this consideration, this research

decided to adopt a non-linear relationship between the plane orientation of the elbow and the arm angle. However, this research also acknowledged that utilising this non-linear relationship itself was itself a form of a simplification. The non-linear relationship was established through analysis of participant data which, although captured the general behaviour of the data, might not be fully representative of all data.

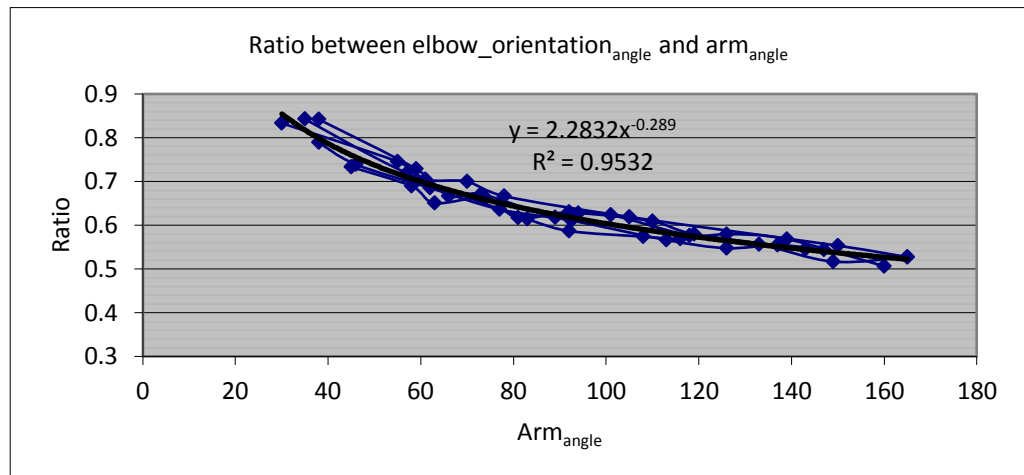


Figure 378. Non-linear relationship between arm angle and the plane orientation of the cross section at the elbow

On reflection, the use of the non-linear relationship shown in Figure 378, does to some extent, allow depiction of the natural behaviour of a cross section at the elbow. To further refine the relationship between arm angle and the plane orientation of a cross section at the elbow, either 3D scanned arms or a combination of side-view photographs should be used in any future study. Currently, the relationship between arm angle and the plane orientation of a cross section at the elbow was established from side view photographs which meant that the established relationship was limited to the 2D perspective. Also, markers that identified the plane orientation of the cross section at the elbow could be added to ease the tracking of the plane's orientation changes. In addition to this, any future study should also collect data from a larger number of participants in order to capture the true relationship between arm angle and the plane orientation of a cross section at the elbow. As a starting point this research suggests the use of data from a minimum of 20 participants, following the rule of thumb to establish regression linear relationship which required at least 10 data points for each variable in order to fully capture the true relationship between variables (Davis, 2011).

11.1.5.2 Key decisions in the second development stage (performing further research on the identified issues)

In the second stage, issues that emerged in the first stage were investigated. The second stage comprised of two chapters i.e. chapter 6 and chapter 7. The key decisions that were made during this stage were:

1. *Key postures.* The concept of key postures was introduced in section 6.3.3. This concept was put forward in response to the finding in section 5.3.2.5 which showed that procedures to drive flesh deformation in the Shen et al. (1994) method were not suitable for ergonomics modelling. The concept of key postures was inspired by the “examples based” approach (see section 2.2.4) which was an approach to deform flesh at the joint through interpolation or approximation from a set of examples that represented different stages of flesh deformation. In comparison to the Shen et al. (1994) approach, the key postures concept was more suitable in complying with two of the DHM specifications i.e. accuracy and accommodating different body types and sizes. In the Shen et al. (1994) method, the flesh deformation was driven by a swelling function that was adjusted such that it could produce muscle bulging or swelling that “looked right”. Furthermore, the swelling function would have to be specified for each body type or size in order to accommodate different body types or sizes. This was in contrast to the key postures concept where flesh deformation was based on the key postures taken from examples from real people. The key postures concept was also related to another DHM specification i.e. real time modelling. To ensure that the balance between real time modelling and accuracy was reached, the appropriate number of key postures which captured different stages of flesh deformation was established based on the study of the behaviour of flesh deformation in section 6.3. Since the key posture interpolation had to be performed in real time, linear interpolation of key postures was chosen. This decision was based on the consideration that linear interpolation put less demand on the processing time because it only involved simple computation. Details of the protocols for key posture interpolation is addressed and discussed in detail in section 7.3.

The concept of using key postures enabled this research to address several DHM specifications at once i.e. accuracy, realism, accommodating different body types or sizes and real time modelling. This was supported by the review result of the proposed FDM which was detailed and discussed in section 8.2.1.3, 8.2.2.3, 8.2.4.2 and chapter 10.

2. *Wire and side-front view photographs approach.* In section 6.3.1, it was shown that the [TC]² NX-12 body scanner could not produce 3D scanned arm for arm angles $\leq 90^\circ$ flexion. This meant that data for key postures would not be available for arm angles $\leq 90^\circ$ flexion.

As a result, an alternative approach to provide data for key postures was proposed in section 6.4. The alternative approach was achieved by exploring various solutions to acquire cross sections of an arm (see section 6.4.1). The exploration was performed to ensure that advantages and disadvantages of each solution were studied and used to choose the best solution. Five possible solutions were reviewed i.e. MRI, handheld laser scanner, 3D motion capture, arm casting and a combination of circling wire and photographs. Based on the advantages and disadvantages of each possible solution, a combination of circling wire and photographs were chosen. The chosen solution involves circling the wire around the arm at the key postures and is followed by taking photographs of the arm from the sagittal and frontal planes. This choice was deemed to be the best option as it was easily accessible and practical i.e. only requiring a semi-rigid but also flexible wire and two digital cameras. However, as shown in section 6.4.1, the chosen solution was not without its disadvantages. The first disadvantage was the risk of flesh compression by the wire itself, which was minimised by checking that each circled wire was a balance between form fitting and essentially 'loose' and thus not compressing the flesh. The second disadvantage was that a significant amount of data pre-processing would be required to capture the form. This was minimised by utilising CorelTrace which allows automatic tracing of a .jpg file and file conversion that is compatible with Pro-Engineer Wildfire 4.0. The third disadvantage concerned the need for an additional method to incorporate joint location information, which was resolved by embedding joints from the 3d scanned arm onto the side and front view photographs (see section 7.1). Integration of joint locations into the wire and side view photographs was addressed and discussed in section 7.1.

The wire and side-front view photographs proved to be an adequate choice. This was supported by the result of review on accuracy and realism which was outlined and discussed in detail in section 8.2.1.3 and 8.2.2.3. However, there is a strong possibility that the new FDM could produce a higher level of accuracy and realism if 3D scan data was available. Furthermore, the availability of 3D scan data would likely reduce the amount of data processing to obtain cross sections from each key posture because they could be obtained simply by applying the approach described in section 5.3.2.1.

3. *Cross sections.* The Shen et al. (1994) method was based on utilisation of cross sections to create the surface of a body part. There were several characteristics associated with cross sections i.e. their location, their number, their representation and their plane orientation. All of these characteristics were addressed in section 6.5, 6.6, and 6.7. Five key cross

sections (UAF, UAM, E, LAM and LAF), which were represented by 16 sample points for each, were established to balance the need for accuracy, realism and real time modelling. The method to determine this number of key cross sections and sample points was discussed in the paragraph related to Figure 377. UAF was located at the upper arm boundary of the flesh deformation area (FDA) i.e. the area where the upper and lower arm met at full flexion, whereas LAF was located at the lower arm boundary of the FDA. UAM and LAM were located at the middle UAF-E and LAF-E region where E was located at the elbow joint. UAF, UAM, LAM and LAF were located perpendicular with respect to the upper or lower arm bones. Figure 379 shows the location and plane orientation of UAF, UAM, LAM and LAF as well as the UAF-E and LAF-E region. The plane orientation of UAF, UAM, LAM and LAF prompted the need to create additional cross sections which subsequently required provision of profiles. The additional cross sections allowed provision of greater detail around the elbow area which in turn helped to improve the accuracy and realism of the proposed FDM. The detail of the additional cross sections and profiles were addressed and discussed in section 7.2.

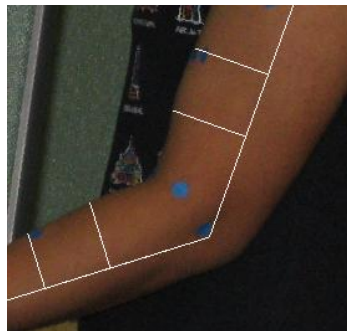


Figure 379. Location and orientation of UAF, UAM, LAM and LAF

The idea of utilising five key cross sections to create additional cross sections had its own advantages and disadvantages. Utilising five key cross sections meant that the amount of data collection was minimised while at the same time maximising the data usage of five key cross sections. Utilising five key cross sections also meant that, as additional cross sections were derived from five key cross sections, the quality of additional cross sections were dependent on the quality of the corresponding five key cross sections. This was partly minimised by the use of a profile which helped to ensure that additional cross sections followed details at the elbow.

Table 52 summarises the difference between the concept of cross sections utilised in this research and the Shen et al. (1994) method. The difference was caused by two factors that were closely related: (1) procedures to drive flesh deformation; and (2) the availability of cross sections. The adoption of key posture interpolation as a procedure to drive flesh

deformation demanded the provision of cross sections for each key posture. However, as the 3D body scanner was unable to provide this, an alternative approach of wire and side-front photographs were employed. This, in turn, limited the possible plane orientation for cross sections along the upper/lower arm bones and prompted the need for additional cross sections. This suggested that this research concept of cross sections was an indirect result of the limitation of the chosen approach to acquire cross sections. Thus, once the 3D body scanner technology could provide cross sections for key postures, it would be worthwhile to re-visit the cross sections' concept of the proposed FDM. Re-visiting the concept will likely result in the need to alter or modify some of the characteristics of the cross sections. For instance, the availability of appropriate 3D body scanner technology could provide more freedom to extract cross sections at various plane orientations and locations. This means that, with the same number of key cross sections, their orientation and location could be optimised such that the flesh deformation could be modelled more accurately and realistically. There is even a possibility that the number of additional cross sections could be reduced and hence reducing the amount of processing time for the new FDM.

Table 52. Difference of cross sections concept between the new FDM and the Shen et al. (1994) method

<i>The new FDM</i>	<i>The Shen et al. (1994) method</i>
4. <i>Five key cross sections</i>	8. <i>More than five key cross sections</i>
5. <i>Non-uniformly located along the upper/lower arm bones</i>	9. <i>Uniformly located along the upper/lower arm bones</i>
6. <i>Plane orientations of cross sections along the upper/lower arm bone were perpendicular to the upper/lower arm bones</i>	10. <i>Plane orientation of cross sections along the upper/lower arm bone were not perpendicular to the upper/lower arm bones and had to be adjusted every time arm angle changes</i>
7. <i>Creation of additional cross sections around the elbow area for every arm angle</i>	11. <i>No additional cross sections</i>

The cross section's concept that was applied in this research was able to support the key postures concept, resulting in the ability to model flesh deformation for any arm angle, as demonstrated from the review of the proposed FDM in section 8.2.1.3 and 8.2.2.3.

11.1.5.3 Key decisions in the third development stage (feasibility testing).

In the third stage, the feasibility of the whole concept of the proposed FDM was evaluated. The feasibility test, outlined in detail in section 8.1, was performed by creating a software programme that followed the concept of the proposed FDM. The key decisions that were made during this stage were: (1) adjustment of the placement of five key cross sections to match the profile; (2) utilisation of the cross sections of 90° flexion as a reference for cross sections interpolation for 90°-maximum flexion key posture interval; and (3) addition of another set of points to the points that signified the

maximum width of the arm. As detailed discussion was already provided in section 8.1, the key decisions for this stage would not be discussed further in here.

11.1.5.4 Reflection on the development process of the new FDM

On reflection, the process of FDM development was far more complex than initially anticipated. The complexity arose in the second development stage when it was found that the chosen 3D body scanner was unable to provide the required data for each key posture. In section 6.4, a set of alternative methods to capture key cross sections were reviewed. However, the review did not provide sufficient detail to anticipate the effects that each of the alternative methods would have on the elements of FDM. This resulted in the need to address the limitation that arose from the chosen method (e.g. the orientation of the cross section) which subsequently demanded more investigations (e.g. creation of additional cross sections). Thus, in hindsight, the process of FDM development would likely be more efficient if the review in section 6.4 was performed in depth and the subsequent amount of work or effort required of each method was identified beforehand.

As shown in chapters 5, 6 and 7, the process of FDM development in this research clearly demonstrated how, for each element of the DHM specifications, attempts to balance the fulfilment of relevant DHM specifications were made. This process was in agreement with the design model that was proposed by Evans (1959). Evans modelled the design process as a “design spiral” where design issues were considered in sequence and in more detail as the design progressed around the spiral, until a single design that fulfilled and balanced the constraints was reached. Wynn and Clarkson (2005) stated that Evan’s spiral design had an ability to address a fundamental problem in design i.e. making trade-offs between many interdependent factors and variables as the design progressed around the spiral. As shown later in the review of FDM, the FDM indeed showed potential to address all of the DHM specifications. However, despite this advantage, considering the scale of the investigations that were involved in this research, it was apparent that this approach was time consuming as each element of the FDM had to go through the design spiral. In hindsight, if time is a constraint, this method should be adopted with care by providing as much detail as possible in the initial stage of the design process e.g. the amount of work and the length of the time required at each stage.

As described in section 11.1.5.3, a software programme was created at the last stage of the development process to allow the feasibility testing of the new FDM. In other words, the concept of the new FDM was only tested once it was finalised. On reflection, considering the amount of effort related to the creation of the software programme, this was probably the best option. Although creation of a piece wise software programme at each stage would allow testing of the new FDM concept at different stages, there is a possibility that continual modification would be required to

synchronise them e.g. input and output parameters. In addition to this, testing the concept of the new FDM during the early stages is unlikely to identify problems that might occur due to the interaction of the elements of the new FDM, as was demonstrated in the third key stage of development process.

11.1.6 The review of FDM

The review of FDM and the review of the framework, which will be discussed later in section 11.1.8, were performed to fulfil the fourth objective of the research i.e. to review the proposed method to deform the elbow against the set of specifications for DHM. As the result of the FDM's review was already discussed in section 8.2 and 10.3, this subsection focuses only on discussion of the methodology for the review of the FDM. The aim of the FDM review was to verify whether the new FDM fulfilled the DHM specifications identified. The method of review of the new FDM was categorised into three types: (i) specifications that do not require the integration of the proposed FDM into an existing ergonomics CAD system; (ii) specifications that require further research work; and (iii) specifications that require the integration of the proposed FDM into an existing ergonomics CAD system. Each category of reviewing method is discussed below:

1. The first type of reviewing method is applicable to accuracy, realism and minimum user intervention. All of these specifications can be evaluated with the software programme that was produced during the feasibility testing in section 8.1. A mixture of quantitative and qualitative analysis was used to review the accuracy, realism and minimum user intervention. For the review of realism and accuracy, the software programme was used to create flesh deformation which was then compared to the corresponding data of either a 3D scanned arm or side view photographs. By comparing the created flesh deformation with the original corresponding data, it could be argued that the review of accuracy and realism was performed objectively i.e. based on observable phenomenon. However, as recommended in section 8.2.2.3, for the realism review, it would also be beneficial to present the created flesh deformation to users so that they could provide feedback regarding its realism.

To review the minimum user intervention, the software programme was used to demonstrate the extent of user intervention required to create flesh deformation. This was then compared to the definition of minimum user intervention, which was described in section 4.1.6. Thus, it could be argued that the review of minimum user intervention was also an objective review.

2. The second type of reviewing method is applicable to accommodation of different body types and shapes. Apart from requiring further research work, this type of reviewing

method is essentially similar to the first type of reviewing method in that the review could be performed by producing flesh deformation only for the elbow joint. The further research work is achieved by creating the proposed framework and detail discussion will be given in section 11.5.

3. The third type of review would require integration into an existing ergonomics CAD system (e.g. SAMMIE, JACK, RAMSIS, etc.) in order to establish sufficient confidence about the proposed method. Specifications that fall into this category are real time modelling and whole body modelling. There are two requirements in order to allow the integration of the new FDM into an existing ergonomics CAD system. The first requirement is full access to an ergonomics CAD system's underlying geometry and associated software code. Access to the system would allow the analysis of the existing system which then enables the new FDM to be embedded within it. The second requirement is coding language adjustment of the new FDM. This level of integration is deemed to be beyond the scope of this research as fulfilling both requirements would need substantial resources. Therefore, an alternative method of reviewing i.e. a "retrospective analysis" was employed. The alternative method is essentially a pragmatic review of the perceived effectiveness of the new FDM against the real time and whole body modelling specifications. This approach is based on the assumption that had the proposed FDM been integrated with an existing ergonomics CAD, the outcome would satisfy the corresponding specifications because the development of the proposed FDM has been constantly guided by them. It is acknowledged that this is less than ideal and its result relies heavily on the validity of the above assumption. Thus, it was suggested that in the future studies, effort should be made to integrate the new FDM with an existing DHM modelling platform.

The current approach of the review was mainly performed for each specification. For future studies, it was suggested that an integrated review should be performed. This could likely be achieved through an integration of the new FDM into an existing DHM modelling platform. In addition to providing an opportunity to review real time and whole body modelling specifications as described in (iii), the integration would also allow direct observation on how the specifications were balanced, especially for those that contradicted each other such as real time modelling against whole body modelling, accuracy and realism. Nonetheless, the adopted methodology of the review has been successful in showing either the ability or the potential of the new FDM in fulfilling five of the DHM specifications, as described further in section 8.2 and 10.3, resulting in the partial completion of the fourth research objective.

As suggested, the development of the FDM had either the ability or the potential to fulfil the DHM specifications. Meanwhile, the discussion in section 11.1.5, concerning key decisions on each key stage, demonstrated that DHM specifications assisted the decision making and subsequently determined the course of the FDM development. Thus, as DHM specifications essentially summarise the key features of ergonomics applications, it could be argued that using DHM specifications to guide the development of the FDM led to an ability to produce a FDM that suited ergonomics modelling. However, to give a definitive answer, a future study that allowed the interaction of users and the new FDM should be performed.

11.1.7 The development of the framework (the application of FDM to accommodate flesh deformation for different body types and sizes)

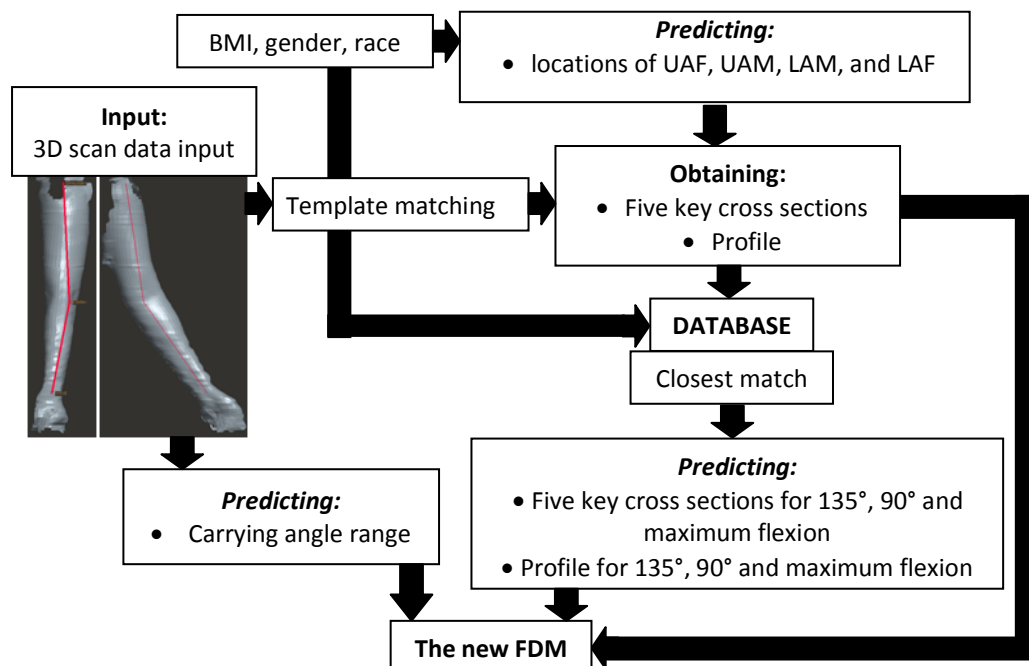


Figure 380. Depiction of processes in the framework

As described in the beginning of this chapter, a so called “framework” was developed to enable the FDM to simulate flesh deformation for a wide anthropometric range. Similarly to the new FDM development, the framework development could also be considered as a design process. Whilst the design process in the new FDM development was guided by a set of DHM specifications, the design process for the framework was driven by an aim to transform a limited number of inputs into the required outputs. The solution for this problem was inspired by the concept of database utilisation in existing ergonomics applications where a database is used to predict output from a given input. The best example of the aforementioned database concept is where, given a limited number of 2D anthropometric dimensions, an anthropometric database is used to predict anthropometric dimensions to build a three dimensional whole body model. Adopting this concept, the framework

also used a database to transform a limited number of inputs (BMI, gender, race and 3D scan of a fully extended arm) into a series of outputs (2D coordinates of five key cross sections, locations of five key cross sections, profiles and the range of carrying angle). These outputs were then used by the new FDM to generate flesh deformation. Thus, the outputs of the framework were the inputs for the new FDM. This process is shown in Figure 373.

There were three key components of the framework: 1) the input of the framework; 2) the database of the framework; and 3) the prediction methods to produce the outputs of the framework. Each of these key issues will be discussed in the following.

11.1.7.1 The inputs of the framework

The initial inputs of the framework consisted of: (i) 3D scan of a fully extended arm; (ii) race; (iii) gender; and (iv) BMI. Each of the initial inputs will be discussed in the following:

1. *3D scan of a fully extended arm.* The 3D scan of a fully extended arm was chosen for two reasons: (i) it was easier to acquire as no arm angle measurement was involved; and (ii) movement artefacts were minimised due to the provision of hand supports which are employed to capture the image of a fully extended arm within the scanner.

The framework required the 3D scan of a fully extended arm to be represented as a polygon surface and accompanied by joint locations (shoulder, elbow and wrist). Although this research directly specified the need for a 3D scan of a fully extended arm, any realistic fully extended arm that fulfilled these two requirements could be used. This is beneficial because a fully extended arm that was created in graphics simulation software such Maya, 3ds Max, etc. or created from a synthesis of features from different body types and sizes could also be utilised as the input of the framework.

2. *Race.* The choice of race was mainly based on the assumption that race affected body size and introduced differences on the arm length, arm circumference, etc. Walker (1993) suggested that a different race would exhibit different body size and proportions. In section 9.5.1, 9.6.1 and 9.7.1, it was shown that body size did affect the flesh deformation area (FDA), five key cross sections as well as profiles, respectively. Given two persons of different race with similar body size and BMI, this research also hypothesized that their flesh deformation would be dissimilar due to the differences in their muscle fat ratio. Haidet et al. (2010) reported that race also affected body composition and body fat topography (distribution). They argued that this eventually influenced the interpretation of the relationship between BMI to body fat percentage across different races. Ishida et al. (1994), who compared body composition and body fat topography between Japanese and Caucasian females, found that the distribution of subcutaneous fat might be specific to ethnic origin.

They also reported that, even when matched for stature and body mass, Japanese women had less muscle development than Caucasians. A similar result was reported by Wagner and Heyward (2001) who compared the body fat composition and distribution between Caucasian and Black race.

This research opted to use race as one of the initial inputs of the framework due to the limited resources. In hindsight, this is probably a better option than using nationality as one of the inputs of the framework. This was because there is likely a variation of races even among the same nationality. However, as mixing between races occurs, categorising people based on their race could be difficult. Thus, for future studies, this research suggests further exploration to identify the significance of the effect of race on flesh deformation at the elbow. If the effect was found to be insignificant, it will provide an opportunity to simplify data collection and categorisation of the framework's database.

3. *Gender.* Flesh deformation was likely to be affected by muscle fat ratio. As gender affected the muscle fat ratio (Malina et al., 2004), gender was also chosen as initial information. A study by Malina (1996) suggested that females have more subcutaneous fat than men and there was a significant difference in the distribution of subcutaneous adipose fat between males and females. He found that, opposite to females, males accumulated more fat on the trunk than on the extremities. Although this research's hypothesis was based on existing studies; for future study, this research suggests further investigation of gender significance on the flesh deformation at the elbow. If muscle fat ratio between genders was found to not affect the flesh deformation at a joint, gender could be omitted and data collection/categorisation for the database could be simplified.
4. *BMI.* The final initial information required was BMI which was a type of index to classify whether someone is underweight, normal, overweight or obese. BMI was used to represent body types (somatotype) and was mainly chosen due to its simplicity i.e. only weight and height are required to calculate it. The main drawback of BMI was its inability to distinguish weight associated with fat and muscle.

In contrast with BMI, Carter and Heath (1990) provided a more extensive approach to categorise body types. Body type was expressed as three numeral ratings such as 3.5 - 5 - 1. Each number described a value of a particular component of physique i.e. Endomorphy, Mesomorphy and Ectomorphy. Somatotype categorisation was based on dominant component(s) of physique. In order to acquire the numeral ratings, comprehensive measurements were required. The required measurements were weight, height, skinfolds (triceps skinfold, subscapular skinfold, supraspinale skinfold, medial calf skinfold), breadths

(biepicondylar humerus breadth, biepicondylar femur breadth) and girths (upper arm girth, flexed and tensed, standing calf girth). It is acknowledged that the Heath and Carter method would provide better definition of somatotype than BMI. However, the amount of measurements which were required would make Carter and Heath's (1990) approach inefficient for the framework. A simpler measurement that could be used in conjunction with BMI is waist circumference. A study by Gill et al. (2003) shows that a conjunction usage of BMI and waist circumference could be used to detect obesity and hence distinguish weight associated with fat and muscle. Another measurement that could also be possibly used is neck circumference. A study by Ben-Noun et al. (2001) showed that neck circumference could be used to screen overweight and obese in adults. A similar finding was also found in children (Nafiu et al., 2010).

There is a possibility that, in addition to the aforementioned initial input above, other factors which might affect variation of flesh deformation at the elbow could be used as part of the framework's initial inputs. For instance, age could be considered as one of the initial input of the framework. Ohkawa et al. (2005) suggested that age affected the muscle fat ratio. If a suitable pattern could be extracted for the influence of additional factors such as age; it is believed that the framework has the flexibility to be developed further to accommodate such additional inputs. Other factors that could affect variation of flesh deformation concern the topography of body fat. The subscapular to triceps skinfold thickness ratio could be used to indicate the level of body fat that is distributed centrally i.e. the trunk and peripherally i.e. the limbs (Sardinha and Teixeira, 2005). Another measure that could be used to indicate body fat topography is waist to hip ratio (WHR). The ratio of waist to hip ratio is a common index for upper versus lower body fat distribution and is used to determine whether an individual has upper or lower body fat tendency (Hussey, 2005).

11.1.7.2 The database of the framework

As stated above, the framework was inspired by existing ergonomics application systems which utilised a database to provide 2D anthropometry data in order to generate DHMs of different body types and sizes. The framework's database stored various information such as five key cross sections and profiles of individuals with different body types and sizes, the equation required to predict the locations of UAF, UAM, LAM and LAF and the general carrying angle range for both genders. Given the inputs from a new person (BMI, race, gender and 3D scan of a fully extended arm with its joint information), the database would provide the best match for the inputs which was then used to predict the required information to create flesh deformation (five key cross sections for all key postures, locations of five key cross sections for all key postures, profiles for all key postures and the range of carrying angle). From this description, it was clear that the database utilisation

substantially minimised the amount and complexity of data collection to model flesh deformation from a new person.

In order to provide the best match for the inputs, the database should be built on a sufficient number of data. These data should capture most of possible variations of body sizes and shapes that existed for each race and gender. To determine the necessary sample size for the database, the guideline that is given in ISO 15535:2006 (ISO, 2006) could be followed. The guideline suggests the use of the coefficient of variation of a key anthropometric dimension from existing anthropometric surveys. For the framework, the key anthropometric dimension could either be arm length or BMI. The equation below shows how the coefficient of variation and sample size could be calculated:

$$\text{Coefficient of variation (CV)} = \frac{\text{Standard deviation}}{\text{Mean}} \times 100$$

$$\text{Minimum sample size} = \left[z \text{ value of confidence level} \times \frac{CV}{\text{margin of error}} \right]^2 \times 1.534^2$$

This research suggests the utilisation of arm length as the key dimension because, based on existing data, arm length appears to produce a larger coefficient of variation than BMI. Hence, the minimum number of sample size which is calculated based on arm length will likely be more than sufficient to represent the BMI variation for each race and gender. Using anthropometric arm length data from Sri Lanka and British nationals, Table 53 shows the minimum sample size required for each race and gender with confidence level value sets to 90 % (z value of 1.645) and margin of error sets to 5% (0.05). However, as shown in Table 53, the minimum sample size is large. Thus, it is suggested that further research should be done to establish the appropriate sample size based on the performance of the framework.

Table 53. Suggested minimum number of sample size for the framework's database

	Minimum sample size
Asian female	464
Asian male	397
Caucasian female	420
Caucasian male	411

With the current limitation of 3D body scanners to produce images of arms for any posture $\geq 90^\circ$ flexion, a large data collection would likely require a lot of resources. This is because cross sections and profiles would have to be collected manually with the combination of wire-photographs, or other suitable alternative approach, and the result would have to be processed semi-automatically. With the use of different 3D scanning technology than the [TC]² NX-12 scanner employed in this research, or the improvement of this technology in the future it is hoped this difficulty could be resolved.

11.1.7.3 The prediction methods to produce outputs of the framework

The prediction method to produce outputs of the framework essentially provided answers to the question “Given the initial information of race, gender, BMI and 3D scan of a fully extended arm with its joint information, how could we produce the range of carrying angle, the coordinates and locations of five key cross sections and the coordinates of profiles for all key postures?”. The prediction methods were proposed based on a series of studies which were described in sections 9.4, 9.5.1, 9.6.1 and 9.7.1. Whenever required, data from the five participants which were involved in the development of the new FDM were used to perform the studies. The result of the studies demonstrated that BMI and arm length indeed affected the locations of UAF, UAM, LAM and LAF, the five key cross sections as well as the profiles. This finding provided further support to the initial assumption regarding the effect of BMI and arm length made during the early stage of the framework development.

The prediction methods of the framework consisted of four parts: (i) a prediction method for the range of carrying angle; (ii) a prediction method for the location of UAF, UAM, LAM and LAF for all key postures; (iii) a prediction method for five key cross sections for 135°, 90° and maximum flexion; and (iv) a prediction method for 135°, 90° and maximum flexion. Each of these methods is discussed separately in the following:

1. *A prediction method for the range of carrying angle.* The range of carrying angle was the result of subtraction between the carrying angle at full extension and the carrying angle at full flexion. Since the carrying angle at full extension could be extracted from a 3D scanned arm, only the carrying angle at full flexion needed to be estimated. The method was based on the existing data from Van Roy et al. (2005) and the carrying angle at full flexion. Table 54 shows the adopted data from Van Roy et al. (2005) whereas Figure 381 shows the method.

Table 54. Data from Van Roy et al. (2005) which was used to assist the prediction of the carrying angle for full flexion

Carrying angle	Female	Male
Full extension	Minimum = 11.9, maximum = 21	Minimum = 4.2, maximum = 15.1
Full flexion	Minimum = -0.7, maximum = 3.9	Minimum = -1.1, maximum 5.8

As shown in Figure 381, the method only required extraction of the carrying angle and gender from a 3D scan of a fully extended arm. As this information was available from the inputs of the framework, the method was appropriate for the framework’s requirement i.e. being able to synthesise required outputs from a limited number of inputs. Thus, this method was deemed to be suitable for the framework. To the extent of this research’s knowledge, this research was the first to attempt proposing a prediction method to determine the range of carrying angle based on the carrying angle of full extension and

existing data. It is acknowledged that the use of this generic existing data is not ideal. However, as previously discussed in section 6.1.2, obtaining this data requires an in-depth and complex measurement of the carrying angle which will be disproportionate to the main aims of the research, especially considering the limited resources.

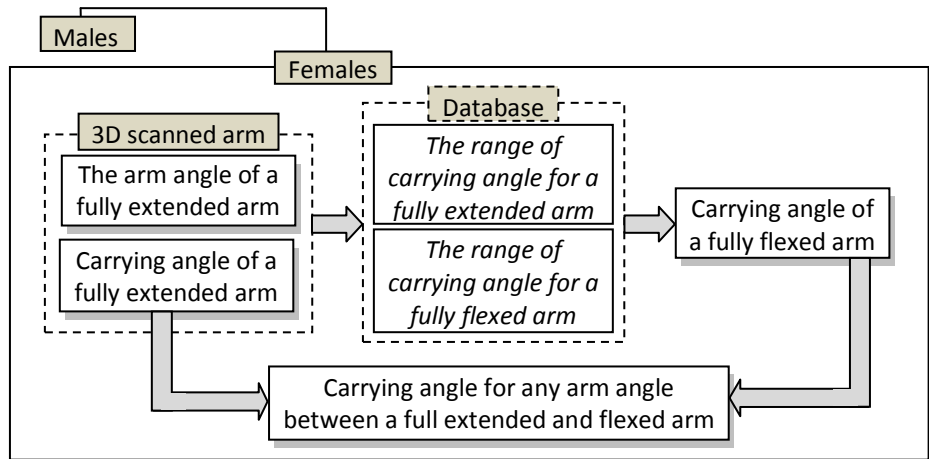


Figure 381. The prediction method to determine the carrying angle for an arm posture other than a fully extended arm

As described above, the carrying angle at full extension and data from Van Roy et al. (2005) was used to guide the estimation of the carrying angle at full flexion. Their data fixed the limit for the possible estimated values of the carrying angle at full flexion i.e. between -0.7° and 3.9° for female; and between -1.1° and 5.8° for male. Since their data was based on 10 participants for each gender, there was a strong likelihood that the values above did not fully represent the variation of the carrying angle at full flexion. A comparison with the data from Zampagni et al. (2008) suggests that greater variation does exist (see Table 55). However, data from Zampagni et al. (2008) was not used in this research because no information regarding the gender of the volunteers in their study was given. For future studies, given that a more comprehensive data is available, the current data from Van Roy et al. (2005) could be replaced.

Table 55. Data from Zampagni et al. (2008) study

Volunteer	Full extension	Full flexion
1	13.43±0.06	-6.34±0.2
2	20.36±0.1	-10.5±0.4
3	16.29±0.12	-2.5±0.2
4	17.29±0.06	-3.4±0.2
5	17.49±0.4	-0.29±0.3
6	15.24±0.5	-3.57±0.3
7	17.45±0.65	0.98±0.23

As discussed in section 7.1.5, if side-front view photographs of all key postures and 3D scans of a fully extended arm with its joint information were available, the carrying angle at all key postures could be obtained. For future study, since the required data were available from

the participants that were involved for the database, a comparison between the prediction results of the method and the range of carrying angle from these participants could be made.

2. A prediction method for the locations of UAF, UAM, LAM and LAF. Figure 382 shows the prediction method for the locations of UAF, UAM, LAM and LAF. As shown in the figure, the prediction method only required BMI and arm length. As such, this method was deemed to be suitable for the framework as the required information could be obtained from the inputs.

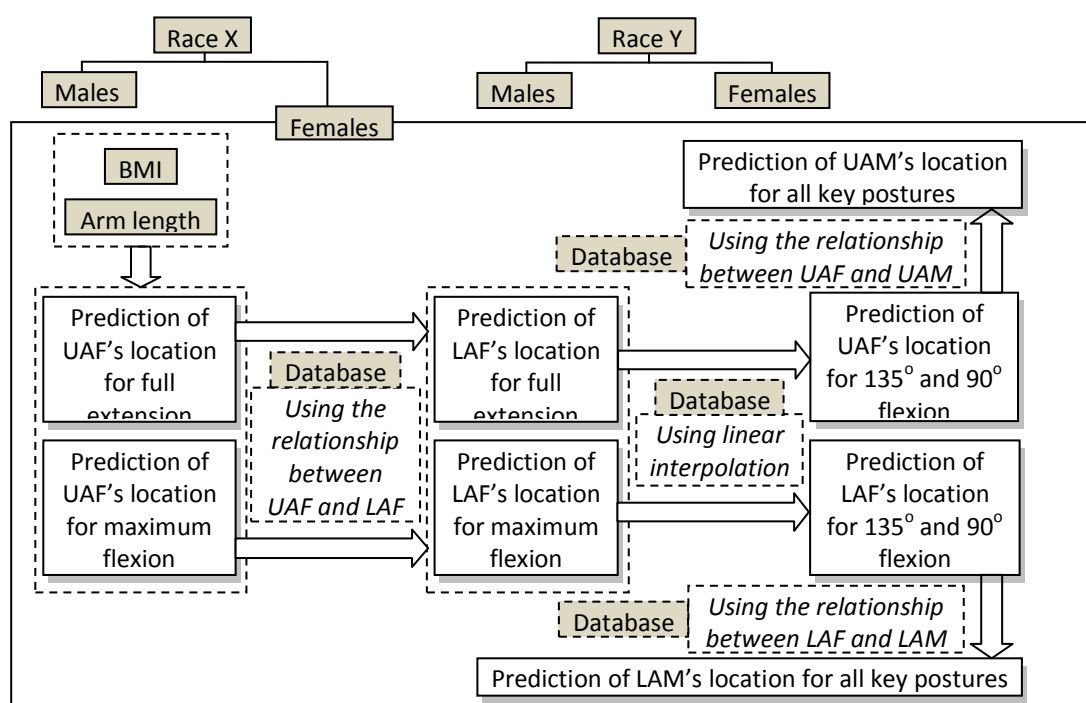


Figure 382. The prediction methods for the location of UAF, UAM, LAM and LAF

A closer observation of the figure suggests that the overall output of the prediction was determined by the ability to predict the locations of UAF at full extension and flexion. This means that any error that occurred during the prediction of the UAF's location at full extension and flexion could result in inaccuracies for subsequent prediction stages. Thus, it is of importance that the relationships which were used to predict the locations of UAF at full extension and flexion were accurate. Since this research established these relationships based on a limited number of data, further data collection is recommended. As suggested in section 9.10.1.5, a minimum of 30 data sets is needed. Once additional data collection is provided, it could be used to re-establish the relationships which were used to predict the locations of UAF at full extension and flexion. Currently, this research utilised multi regression as a means to establish the relationship between BMI, arm length and the locations of UAF at full extension. Although 5 out of 8 regressions could account for at least

75% of the variation in the data ($R^2 > 0.75$), it will be interesting to know whether other method such as k-nearest neighbour will perform better. Having additional data will provide an opportunity to investigate this issue further.

3. *A prediction method for the five key cross sections.* The prediction method for five key cross sections was divided into two parts: i) the prediction method for UAF, UAM, LAM and LAF cross sections and ii) the prediction method for E cross sections. Figure 383 shows the prediction method for UAF, UAM, LAM and LAF. The prediction method was based on finding a closest match and used the closest match to modify the UAF, UAM, LAM and LAF of a 3D scanned arm. For UAF and UAM, their closest match was found by determining the ratio of UAF's size to UAM's size (vertical and horizontal dimensions) and comparing this value with those of the participants' data in the database. A similar approach was also applicable for LAF and LAM. The ratio was used in order to accommodate the relationship that existed between these cross sections which was found during the studies in section 9.6.1. The review results on the accuracy showed that the method could predict UAF, UAM, LAM and LAF with averaged error that ranged between 1.65 mm and 3.55 mm. Bearing in mind that, the new FDM in chapter 8 had an averaged error that ranged between 0.56 mm and 3.74 mm whilst using five key cross sections of all key postures that were acquired directly from a participant, the prediction method's performance was deemed to be suitable for the framework.

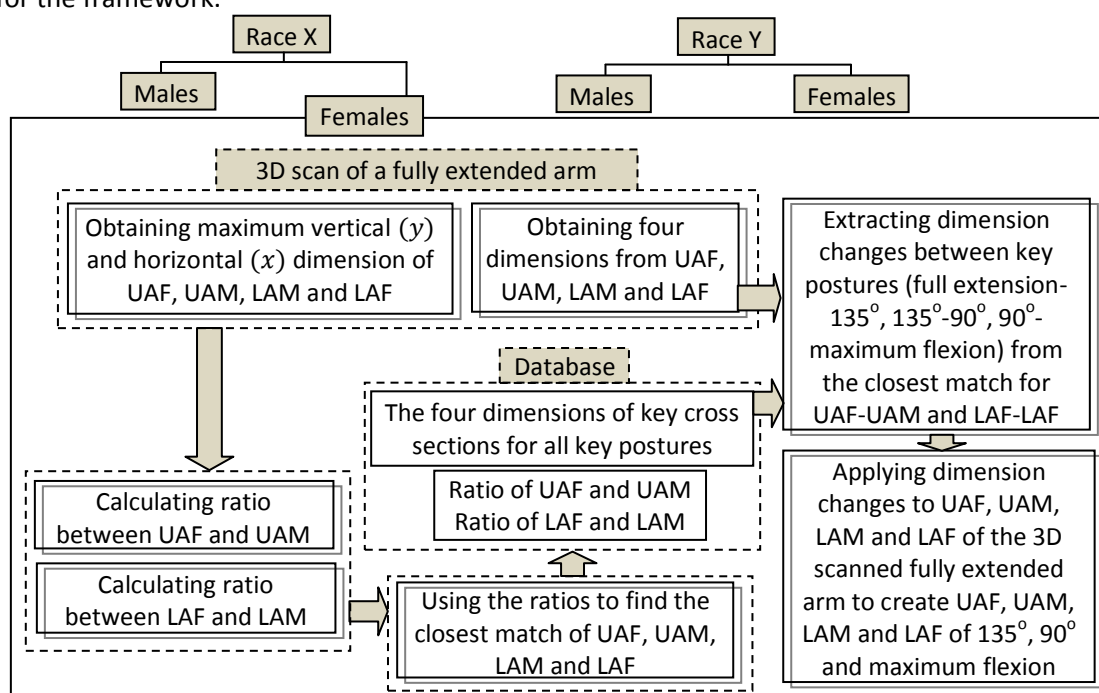


Figure 383. The prediction method for UAF, UAM, LAM and LAF

The current approach of finding a closest match was mainly driven by the relationship that existed between UAF and UAM or LAM and LAF. As shown in Figure 383, the dimension

changes of cross sections between key postures are extracted from the closest match data and are then used to adjust the cross sections of the input data. Having this current approach meant that the cross sections of the input data and the closest match could be of different sizes even though they have similar ratio values. However, because the dimension changes of the closest match were applied directly to the input data; this also meant that the input and the closest match would have exactly the same dimension changes even if their cross sections were not similar size. In other words, the dimension changes are regarded as an absolute value. For instance, given two individuals of a similar body type but of different statures; if the individual with a small stature has the dimension changes of x cm, the dimension changes for an individual with a big stature will also be x cm; even though the individual with small stature has smaller cross sections than the individual with big stature. Since there is a strong possibility that the dimension changes are dependent on or relative to the size of cross sections; in hindsight, in addition to using the ratio values, the process of finding closest match could have also used the size of cross sections. A further exploration on this issue is suggested.

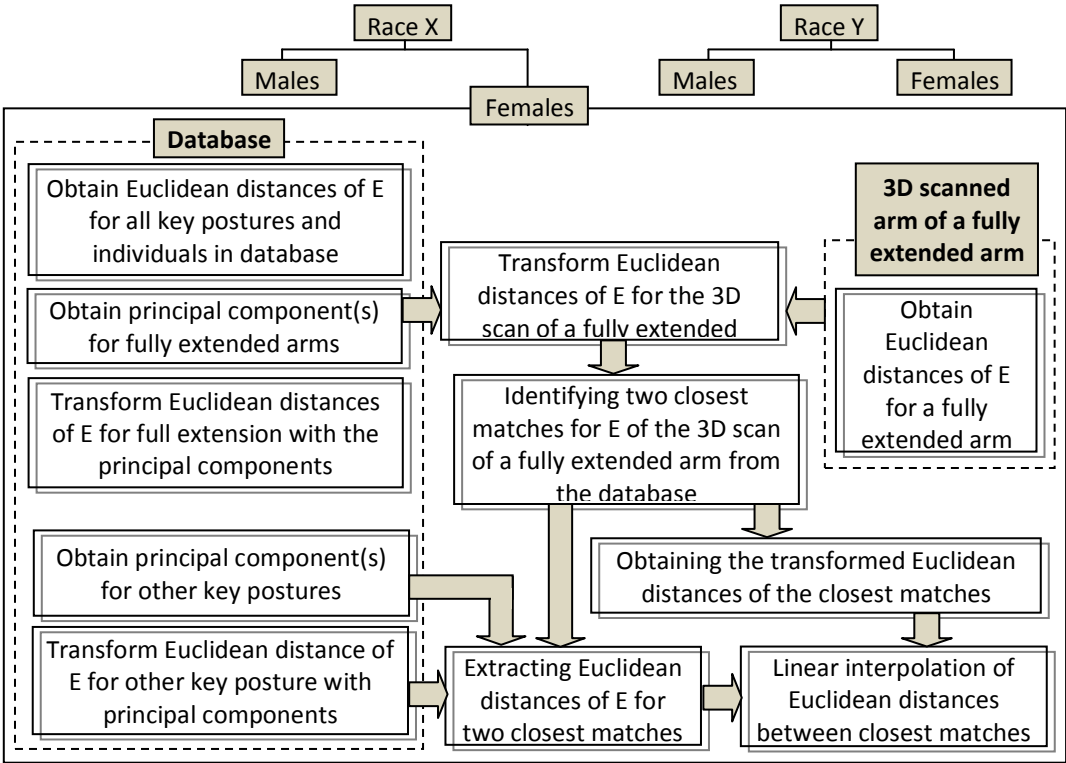


Figure 384. The prediction method for E cross sections

Figure 384 shows the prediction method for E cross sections. The prediction method was based on finding the two closest matches for the E cross section of a 3D scan of a fully extended arm and using them to create new E cross sections at 135°, 90°, and maximum flexion through interpolation. The whole method was founded by the use of PCA which

permitted value transformation of the distances of sampling points of E cross sections. The value transformation allowed the shape of E to be expressed in a mere 1 or 2 values (instead of 16 distance values) and provided a means to compare the shape of E cross section of the 3D scan data with those of participants in the database. Due to the distinct shape of E cross section, any unwanted deformities on the E cross section would likely to be directly observable. Since this was not found during the review of realism of the framework, this suggested that the prediction method was suitable for the framework. As described above, the prediction of the E cross sections used two matches instead of one. This was because the search for the closest match adopted the k-nearest neighbour approach where the use of more than one closest neighbour is suggested in order to decrease the rate of error (Matignon, 2007). The k-nearest neighbour is adopted because it is simple and yet powerful approach for scattered data (Sumathi and Sivanandam, 2006), which is likely to occur once more E cross sections data is added to the framework's database. This tendency has already been shown by the PCA components of E cross sections from the Caucasian males group (see Figure 385). The simplicity of the approach also meant that it could support the real time DHM specification.

Currently, the E cross section of the input is obtained with 3D scanner whereas the E cross sections of the database are obtained with the use of wire and side view photographs. Although the review result showed that the prediction method was satisfactory; in hindsight, the search for the closest match should have been based on data that were acquired with a similar method. Differences in data acquisition method might yield discrepancies which could eventually affect the subsequent data processing and contribute to the overall error of the prediction method. Ensuring that the input and the database are obtained with the same method would likely improve the result of the prediction method.

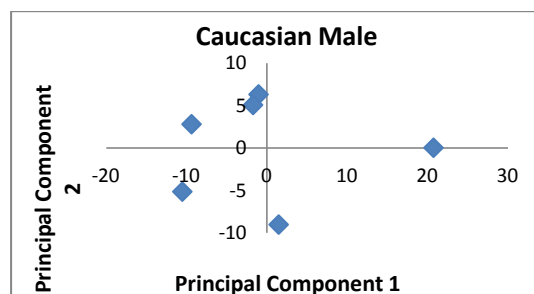


Figure 385. Principal components of E cross sections for Caucasian male group which show the tendency towards scattered data

4. *A prediction method for the profiles.* The prediction method for the profiles was shown in Figure 386. As shown in Figure 386, a template was introduced in the profiles' prediction method. The template, which was the output of the integration between joint information

and digitised cross section in section 7.1.3, was used to ensure that a profile from a 3D scan of a fully extended arm was obtained from a similar orientation view as that of a side view photograph of a fully extended arm. As described in the preliminary studies of the prediction method in section 9.7.1, it was of importance that this requirement was satisfied because the profile of the 3D scan data would be compared to the profiles in the database which were acquired from side view photographs. Similarly to the prediction method for E cross sections, PCA was also used to determine the closest match for the profile of a 3D scan of a fully extended arm. The closest match's profile at 135° was then modified to provide profiles at 135°, 90° and maximum flexion for the 3D scan data. Figure 387 shows the process that involved in the modification of the closest match's profile at 135°.

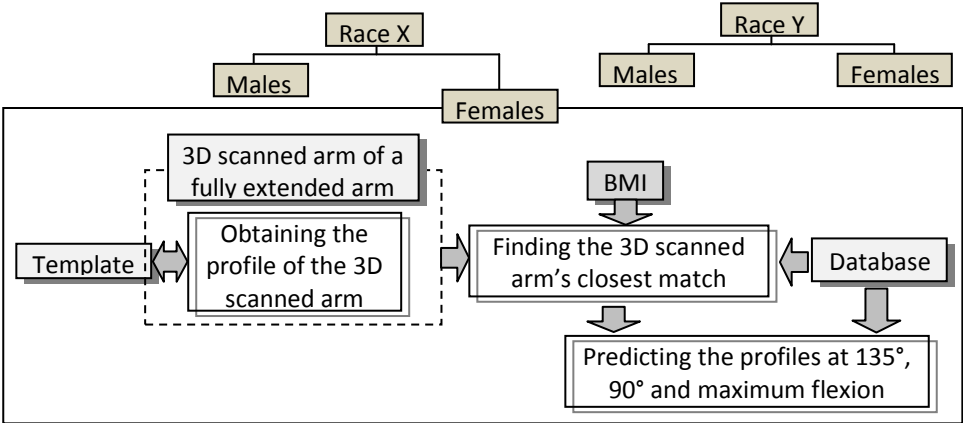


Figure 386. The proposed prediction method for profiles

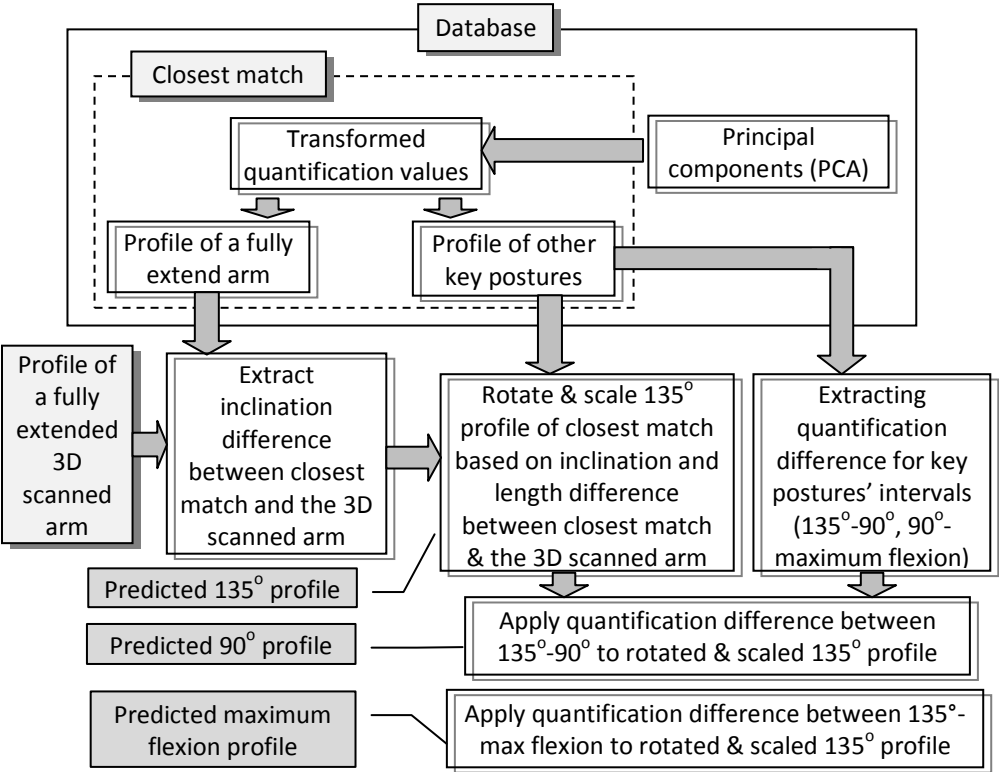


Figure 387. The process to modify closest match's profile at 135° in order to provide profiles at 135°, 90° and maximum flexion for the 3D scan data

The accuracy review of the profiles showed that the prediction method had a range of error which was between 0.35 mm and 2.1796 mm. In contrast, profiles that were predicted based on data that were acquired directly from a participant had an averaged error that ranged between 0.31 mm and 1.12 mm (see 8.2.1.2). Bearing in mind that the profile prediction method was solely based on the profile of a single set of 3D scan data, the proposed prediction method's performance was deemed to be satisfactory. Furthermore, the prediction result, shown in Figure 388, demonstrates that, given a closest match is found from the database, the prediction method had the ability to generate a profile that resembles the original data. However, the significantly larger range of error than that of the new FDM suggested that there is an opportunity for further improvement. As shown in Figure 387, the current prediction method for the profiles utilised a combination of data from the 3D body scanner and side view photographs to modify the closest match data. Although efforts were made to ensure their compatibility e.g. template utilisation, discrepancies due to the method differences in obtaining data might still exist. Thus, this research recommends the sole use of 3D scan data as this will minimise this problem and likely improve the performance of the prediction method.

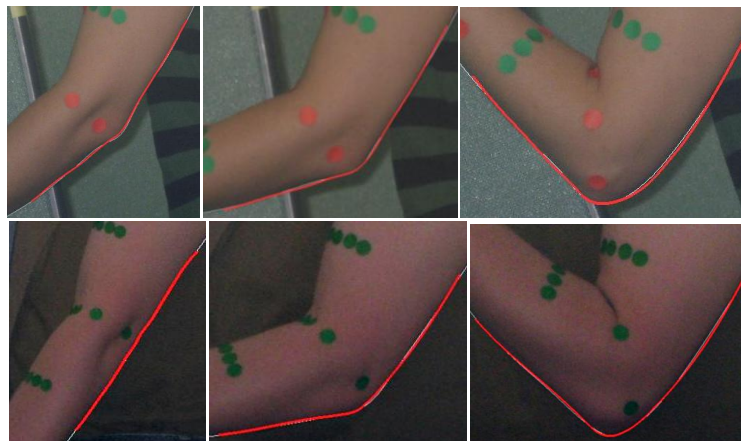


Figure 388. Top: the profile prediction result for participant 2 of Asian female and bottom: the profile prediction result for participant 1 of Caucasian Male (bold line: prediction result, thin line: original data)

11.1.8 The review of the framework

As described in section 10.1, the review of the framework was performed by measuring the accuracy and realism of the flesh deformations which were created based on the outputs of the framework. These two measurement variables were chosen because the accuracy and realism of flesh deformation were expected to be affected by the quality of the framework's outputs. The review result later confirmed this by showing a generally larger range of error for both five key cross sections and profiles, which ultimately yielded a less realistic flesh deformation. Thus, the review result suggested that the chosen measurement variables for the review were suitable for the purpose of this research.

In hindsight, in addition to reviewing the accuracy based on how well cross sections and profiles were predicted, this research should also review the prediction result for carrying angle and the locations of UAF, UAM, LAM and LAF. This was because as shown in section 11.1.1, besides predicting five key cross sections and profiles, the framework also predicted the carrying angle and the locations of UAF, UAM, LAM and LAF. The additional reviews could potentially provide an opportunity to study the framework's ability to predict them and subsequently complement the accuracy's and realism's reviews. This research suggests the use of the procedure in section 7.1.5 to obtain the carrying angle for the original data and compare it with the framework's prediction of the carrying angle. For the review of the locations of UAF, UAM, LAM and LAF; side view photographs could be utilised. This research suggests limiting the review only for the location of UAF and LAF because they are easier to identify and measure on the side view photographs than the locations of UAM and LAM.

11.2 The advantages and disadvantages of the new FDM

The new FDM offered two advantages. The first one was its ability to simulate the effect of carrying angle on the flesh deformation at the elbow. It appears that the existing methods of flesh deformation for ergonomics applications make no reference to the carrying angle for the elbow flesh deformation. The ability to simulate the effect of carrying angle was of importance as it has the potential to improve the accuracy and realism of DHM. This was supported by the study of Allen et al. (2006) which showed that without the use of the carrying angle, they were unable to fit the skeleton (the joints and bones of a digital human model) to 3D scan data.

Another advantage of the new FDM was its ability to actually take into account the effect of different body sizes and types on the flesh deformation. This ability was achieved by the utilisation of the framework which would predict the deformation of cross sections and profiles specifically for a required body size and body type. Santos (Abdel-Malek et al., 2006), which proclaimed to be the DHM frontier for ergonomics applications, uses linear blend skinning for their flesh deformation. As described in section 4.2.3., linear blend skinning would likely need adjustment of the weight for the vertices in order to create realistic and accurate flesh deformation, especially when different body types and sizes were involved. However, since no reference about this was found for Santos, it was possible that Santos did not specifically take into account the effect of different body sizes and types on flesh deformation. This was probably because it was initially developed for ergonomics simulation in the armed forces where the differences in body size and types were likely to be less varied. Thus, to the extent of this research knowledge, the existing method of flesh deformation in ergonomics applications does not appear to adopt approaches where special adjustments towards the effect of body types and sizes are made.

However, despite the advantages above, the new FDM also had a number of disadvantages. The first disadvantage was the fact that it required an extensive amount of data and effort to establish the parameter for flesh deformation as well as simulation of body size and types' effects. The extensive amount of data meant that it could limit the new FDM application for other body parts. It could also potentially make establishing FDM for the whole body more complex. Another disadvantage of the new FDM was that its usage was likely to be limited to ergonomics applications because it was aimed to satisfy the need for DHM in ergonomics applications where the level of user intervention was restricted. The last disadvantage of the new FDM was that its ability to simulate flesh deformation for a wider range of anthropometry was dependent on the framework. Thus, any inherent inaccuracies of the framework will be passed on to the new FDM and affect the overall accuracy and realism of the new FDM. However, this could be minimised by ensuring that there is sufficient data in the database, as discussed in section 11.1.7.2.

11.3 The advantages and disadvantages of the framework

The framework, which was essentially the tool for the new FDM to simulate flesh deformation of different body sizes and types, had three advantages. The first advantage of the framework was the ability to produce flesh deformation which is relatively accurate and realistic for any body size and shape based on a limited set of data inputs. This was clearly advantageous as this would enable simulating the effect of flesh deformation of various body size and shape with ease. Currently, as discussed in section 11.2, this feature does not appear to be accommodated by existing DHMs in ergonomics simulation. The second advantage was that it could be used with various 3D data as its input. As described in section 11.1.7.1, although this research specified the use of 3D scan data of an arm, the framework could actually be used with other types of data as long as the data was represented with a polygon surface and equipped with the joint locations. In addition to allowing the use of 3D data which was created on graphics simulation software such Maya, 3D data which was created from a synthesis of features from different body types and sizes could also be used. Creation of a human body or body part by synthesising features from different body types and sizes has gained popularity in the recent years. Several research studies have been successful in generating different body types and sizes by studying and then synthesising features of different body types and sizes (Seo and Thalmann, 2003; Anguelov et al., 2005). Currently, to the extent of this research's knowledge, human body synthesising has not been integrated into existing ergonomics applications. However, judging from its versatility in producing various human body type and sizes from a given parameter, it is likely that human body synthesis will be an important tool for ergonomics simulation in the future. Thus, the compatibility of the framework's with the human body synthesis would likely render its usability even in the future. The last advantage of the

framework is the ability to expand its framework to accommodate a special population if required. For instance, a special database could be created to accommodate flesh deformation at the elbow for older people.

11.4 Research contribution and limitation

This research's contributions to the field of research in DHM for ergonomics simulation are as the following:

- *Method to perform flesh deformation at the elbow joint that either meets or has the potential to meet the specifications for DHM in ergonomics simulation application.* This is the main contribution of this research. As it had been identified in the literature review, existing methods to deform the flesh around the joint are less suitable for ergonomics applications as they focused on either a visually convincing flesh deformation, which was not necessarily accurate, or anatomically correct flesh deformation, which requires a lengthy processing time and is mostly suitable for partial body modelling. However, as shown in the literature review and user study, ergonomics modelling demands a balance between accuracy, processing time, realism, whole body modelling, and the ability to accommodate different body sizes and shapes. In addition to this, as opposed to graphics simulation software such as Maya, ergonomics modelling also requires a limited user intervention i.e. the user is not expected to have to correct unrealistic flesh deformation, etc. This research fills this gap through the proposed method to perform flesh deformation that meets or has the potential to meet the requirements above.
- *DHM specifications for ergonomics modelling.* This is the second contribution of this research. Six DHM specifications were identified and established through a combination of literature review and user study. These were: (1) accuracy; (2) real time modelling; (3) realism; (4) accommodation of different body sizes and types; (5) whole body modelling; and (6) minimum user intervention. The DHM specifications were useful, not only for this research, but can also be used to support other research which is aimed to improve DHM in ergonomics modelling. This is because the DHM specifications are generic i.e. only capturing the basic requirements of any DHM feature that is aimed to be integrated in DHM in ergonomics modelling. For instance, the DHM specifications above could be applicable to guide developing methods for DHM posture simulation, movement simulation, interaction with objects, etc.
- *A database approach to create automatic elbow flesh deformation for different body types and sizes.* The third contribution of this research is a flesh deformation method that has the potential to accommodate different body types and sizes. This is achieved by utilising a

database which essentially provides examples of relevant data that are then matched to the input data. Using a database approach, flesh deformation from any body size and type/shape could be produced. The database approach provides an alternative method to the current “example based” approach which utilises a set of 3D scan data to produce whole body flesh deformation (Allen et al., 2006). The currently used “example based” approach could only be applied for that particular example set of 3D scan data. This is because flesh deformation is highly dependent on the body size and type/shape and hence limits the applicability of synthesis results.

- *Integration of carrying angle into the movement and flesh deformation modelling of an elbow.* The carrying angle permits the forearms to clear the hips in swinging movements during walking and is important when carrying objects as it would affect how an individual would hold an object (Zampagni, 2008). The new FDM fully integrates the effect of the carrying angle which to the extent of this research knowledge, is not accommodated in any existing DHM in ergonomics applications as it is not featured in 2D anthropometry databases.
- *Integration of 3D scanning technology into DHM’s flesh deformation that is suitable for ergonomics modelling.* The proposed flesh deformation method of this research is facilitated by the use of 3D body scanning technology. This research will not be the first research which integrates the use of 3D body scanning technology in ergonomics modelling. This research is also not the first research which utilises 3D body scanning to develop flesh deformation around the joint. However, it is believed that there has been no other research that integrates 3D body scanning technology to develop flesh deformation around the joint which is suitable for ergonomics modelling. Thus, this research will specifically fill this gap, and is complementary to existing research which has made use of 3D body scanning technology to create DHM for ergonomics modelling.

Despite the above contributions, this research also has some limitations. Further research could be aimed to address these limitations. The limitations are as the following:

- *Non-automatic application of the new FDM and framework for joints other than the elbow joint.* The new FDM and framework required establishment of: (i) flesh deformation area; (ii) number and locations of key cross sections; (iii) key postures; and (iv) key cross sections and profiles for key postures. In order to establish all of the above, studies would have to be carried out for other joints. More extensive studies would also be required for the application of the new FDM and framework on a shoulder joint as it is far more complex than an elbow joint.

- *More than one database would be required in order to simulate flesh deformation for whole body modelling.* The new FDM and framework requires provision of a database to predict key cross sections and profiles of the 3D scanned arm. This means that, in order to create whole body flesh deformation at joints, a database would be required for each joint. Furthermore, as the new FDM and framework are aimed to recognise the effect of body size and shapes on flesh deformation, the content of each database should endeavour to represent variety of body size and shapes. In this research; features such as gender, race and BMI were used to capture variation of body size and shapes. However, it is possible that there are other features as well e.g. age. The addition of features would likely increase the generalisation of the framework; however it will also increase the number of data to collected, analysed and stored.
- *Most decisions which led to the establishment of the new FDM and framework were based on analysis of a small number of data.* As had been explained in the earlier part of the discussion chapter, the new FDM and framework could be likened as a design process. Each stage of design required decisions on multiple issues. Resolution of these issues involves data collection and data analysis. Ideally, data analysis should be based on a sufficient number of data to allow capturing the real behaviour of the data. Provision of a sufficient number of data would likely minimise the effects of data variations that occur due to chance. During the development, it was hard to foresee whether the steps taken would be efficient i.e. whether certain data could be re-used to resolve issues on the next stage of design, etc. However, in hindsight, more data collection should be performed on studies about: (i) establishing the relationship between arm angles and orientation of elbow planes; (ii) establishing effect of race and gender on the elements of new FDM e.g. cross sections shapes and locations, profiles, etc.; (iii) establishing relationship between flesh deformation area, race, gender, etc.; and (iv) establishing relationship between locations of UAF, UAM, LAM and LAF cross sections.

11.5 Future studies

There are two studies that are relevant to the FDM methodology of this research. These were 1) application of the FDM methodology to other joints and 2) application of the FDM to support flesh deformation due to external forces. Each of the relevant study is addressed in the following.

11.5.1 Application of the FDM methodology to other joints

The new FDM and framework detailed in this thesis are focused on elbow flesh deformation. However, as whole body modelling is also one of the DHM specifications, this method is also

developed with this specification in mind. An elbow's degree of freedom is on par with the degree of freedom from a knee or finger knuckles. This means that similar steps to establish elbow flesh deformation are also applicable for the knees or finger knuckle flesh deformation. Thus to apply the method to those joints the steps would be: (i) determination of flesh deformation area; (ii) determine the number and locations of key cross sections; (iii) determine the number of key postures; and (iv) determine the profile. Although it is possible to directly adopt values and findings from the new FDM, it is strongly suggested that further studies are conducted in order to achieve as high a level of accuracy and realism as possible.

The wrist joint, ankle joint, hip joint and shoulder joint are considered to be more complex due to their increased degrees of freedom. For joints that are capable of complex movements, such as the shoulder joint, Shen et al. (1994) proposed the use of a so called "dynamic trimmed surface". The dynamic trimmed surface is essentially a shoulder patch that connects the torso and arms. In Shen et al. (1994), the dynamic trimmed surface which connects to the torso is adjusted based on a modification of the parameters affected by the movement of the shoulder joint. The use of a shoulder patch in the Shen et al. (1994) is somewhat similar to the new FDM where flesh deformation is contained within a pre-determined area i.e. flesh deformation area (FDA).

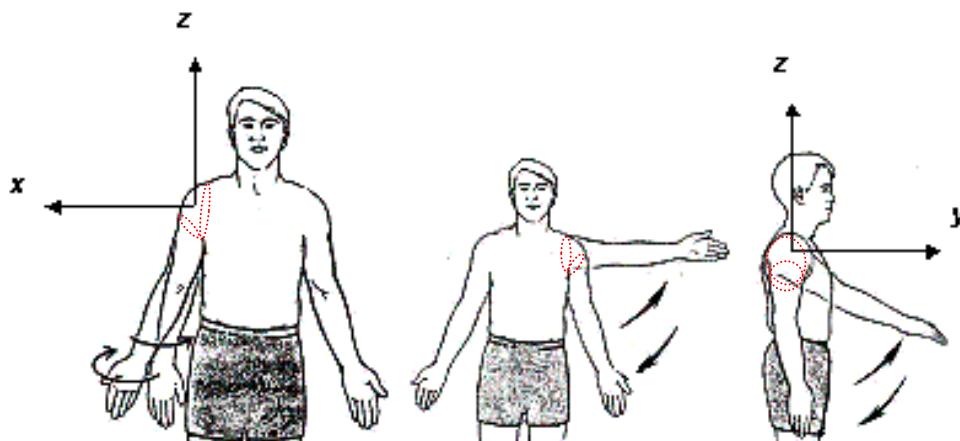


Figure 389. Creating key cross sections for each type of joint movement for the shoulder, from left to right: outward-inward medial rotation; adduction-abduction; and flexion-extension

Following the principles set by the new FDM, a set of key postures could also be used to direct the flesh deformation. As there are three types of joint movements for the shoulder i.e. flexion-extension, adduction-abduction and outward-inward medial rotation, a set of cross sections at key postures, which cover the full range of movement, could be assigned for each. Figure 389 shows the three types of joint movement for the shoulder and illustrates an example of how the shoulder flesh deformation is bounded by two key cross sections. Once the cross sections at key postures are established, they could then be used to interpolate cross sections for an arm angle other than the key postures. However, as most of a shoulder joint movement is a combination of the three types of

the movements above, simply assigning cross sections for each type of joint movement would not be sufficient. Given a certain posture of the shoulder joint angle, using the Euler angle principle, it could be expressed as a combination of three types of rotation i.e. rotation about X, rotation about Y and rotation about Z. This principle could be used to decompose a shoulder joint movement into the three types of joint movement above i.e. flexion-extension, adduction-abduction and outward-inward medial rotation. Based on the decomposed angle above, the final cross sections could be interpolated from cross sections of each type of joint movements. Hence, the final cross sections to create the flesh deformation surface for shoulder takes into account the key cross sections of different type of movements.

In the new FDM, a profile is introduced to produce a more refined detail of the flesh deformation. A profile and additional cross sections would also be likely required for a shoulder joint. However, it is difficult to suggest how many and what they should be based on until a surface is created from key cross sections interpolation. The suggested modification for the application of the new FDM on a shoulder joint is mainly based on an approximation and it is possible that more studies would be required to establish some of these issues.

As encountered in this research, the 3D body scanner is likely to encounter difficulties in providing 3D data when occlusion occurs and thus result in difficulties to obtain cross sections from shoulder joints. However, in contrast to the elbow joint, a circling wire to acquire cross sections at the shoulder joint is unlikely to be the solution because it will be quite difficult to circle the wire around the torso. To overcome this problem, the method of Allen et al. (2002) could be adopted. They utilised a template, which consisted of a polygonal surface representation of the skin and skeleton, to match the posture and size of segments (e.g. arm length, torso length, etc) of a 3D scan. The use of a template allowed automatic hole filling and approximation of the missing surface of 3D scan data. Since their method focused more on realism, whether their method is accurately approximate the missing surface of 3D scan data or not is unknown. An alternative method is to use a motion capture. A study by Hong et al. (2010) used 200 markers to capture skin deformation at the shoulder. With such a high number of markers, their method provides a realistic and presumably accurate skin deformation. However, due to the extent of the markers involved, their method could potentially be time consuming. Providing that there are enough resources, this research recommends the adoption of Hong et al. (2010) method to acquire cross sections from shoulder joint as it is potentially more accurate in capturing flesh deformation.

11.5.2 Application of the FDM methodology to support flesh deformation due to external forces

Another area of study that is closely related to this research is flesh deformation due to external forces. Although further work will likely be required, this research envisages that the new FDM has a potential to support flesh deformation due to external forces. Given that the area where the external forces are applied is known, additional cross sections could subsequently be created in this particular area. Subsequently, similar to the current concept of the new FDM, the effect of the external forces on the flesh could then be simulated by deforming the cross sections in the corresponding area. The deformation of the cross sections could likely be simulated by studying how flesh deforms under different types and amounts of external force and applying this knowledge to deform the cross sections. Shin and Badler (2002) used this relationship to simulate flesh deformation due to external forces. However, instead of using cross sections to simulate the flesh deformation, their study used a finite element model that was created from an outer surface/skin representation of an arm. The indentation skin tests, which established the relationship between the applied load (forces) and the depth of skin indentation, was used to assign material properties to the finite element model. Figure 390 shows an example of their study results. A potential challenge, for the application of the FDM methodology to support flesh deformation due to external forces, is likely to be minimising the processing time which is required to create and deform the additional cross sections at the affected area. Similar to the current approach of the new FDM, an optimum number and method to deform the cross sections will need to be investigated in order to ensure that a balance between relevant DHM specifications are achieved.



Figure 390. Simulation of flesh deformation at the lower arm due to external force application on the skin (adapted from Shin and Badler (2002))

An alternative to the approach above is to apply volume preservation on the specific area where external force is applied. Rohmer et al. (2008) utilised local volume preservation to a given 3D model which consisted of outer surface/skin representation and skeleton. The local volume preservation allowed flesh deformation to be contained in the limited area and thus created a more realistic behaviour of flesh deformation. However, since Rohmer's approach was aimed to accommodate a linear blend skinning method (see section 2.2.3.1), the adoption of local volume preservation to the FDM methodology will likely require a substantial amount of studies. Some of the anticipated studies include: 1) establishing a similar study of indentation skin test to identify and

localise the affected area, 2) establishing a method to establish volume at the specific area where external force is applied.

Due to the level of complexity involved in simulating flesh deformation due to external forces, there is a strong likelihood that the simulation has to be done for each body segment until the advancement of the technology allows otherwise.

12 Conclusions and Future Studies

This chapter concludes this PhD thesis by revisiting the research's aims and objectives and linking them with the research's key findings and/or results. This is then followed by highlighting the directions for future research.

12.1 Conclusions

The aim of this research was to develop a methodology to simulate body deformation due to joint movements which suited the needs of ergonomics simulations. To anticipate the large scope of the study, the PhD research was focused on modelling a single joint, the elbow. The aim was achieved by proposing a new FDM and a so-called 'framework' which were developed based on established specifications to ensure their suitability to the needs of ergonomics simulations. The aim of the research was supported by four objectives. Key findings and/or results for each objective of the research are described in the following.

Research objective 1: To review the state of the art on topics of the use of DHM in ergonomics and body deformation

- A thorough literature review that was focused on DHM in ergonomics application and existing method of flesh deformation was performed.
- The literature review on DHM in ergonomics application suggested that there were six important attributes of a DHM which distinguished DHM in ergonomics modelling from other types of DHM e.g. DHM for entertainment purposes. These were: (i) accuracy; (ii) realistic appearance of a DHM; (iii) real time modelling; (iv) DHM accommodation of different body types and sizes; (v) limited or minimum user intervention; and (vi) whole body modelling.
- The literature review revealed there was a research need to develop realistic flesh deformation modelling of DHM in ergonomics modelling.

Research objective 2: To develop a set of specifications for DHM to guide the development of flesh deformation modelling of the elbow that suits the needs of ergonomic simulation

- By means of a questionnaire survey, a user study was performed to elicit the views of the 27 end users of DHM for ergonomics simulation.
- The results of the user study supported the findings of the literature review and demonstrated that users considered accuracy, realism and real time modelling as important attributes for a

DHM in ergonomics applications. Since the number of respondents in the user study was relatively small, generalization of the user study result should be performed with care.

- Combining the results of the literature review and the user study, the six important attributes from the literature review were established as the specifications for DHM in ergonomics applications. These specifications were used to guide and evaluate the development of flesh deformation of the elbow to ensure its suitability with the ergonomics simulation.
- Although this research utilised the user study as a means to follow up the literature review findings, the user study could also be used to find out the users' view concerning the level of importance of potential DHM specifications that were related and contradicting with each other i.e. accuracy, processing time, realism and whole body modeling.

Research objective 3: To propose a method to create flesh deformation at the elbow joint that suits the needs of ergonomic simulation

- The development of the new FDM was based on modification of the Shen et al. (1994) method which was found to satisfy the DHM specifications to a greater degree than other existing methods of flesh deformation. The Shen et al. (1994) method deformed cross sections to simulate flesh deformation on the arm.
- The new FDM was initially aimed to fully utilise 3D scanned arm data. However, it was found that the 3D body scanner used (TC² NX-12) was unable to provide 3D scanned arm data for arm flexion $\geq \approx 90^\circ$. To overcome this issue, wires were circled around the arm to obtain cross sections and side-front view photographs were used to determine the orientation and location of these cross sections.
- The new FDM was limited to a specific flesh deformation area (FDA). The flesh deformation within this area was driven by five key cross sections and a longitudinal profile of four key postures (a fully extended arm, 135° flexion, 90° flexion and maximum flexion). The new FDM also integrated the carrying angle in order to accurately represent the joint movement of the elbow. Throughout the development of the new FDM, the DHM specifications guided the decision process.

Research objective 4: To review the proposed method to deform the elbow against the set of specifications for DHM

- The review of the new FDM against each of the DHM specifications is as the following:
 1. **Accuracy.** The review showed that the new FDM had an average error level that was less than 3 mm. The level of error suggested that for evaluation of product design or

work space where the tolerance value of error level was higher than 3 mm e.g. between 0.5-1 cm, the proposed FDM would likely be sufficiently accurate. However, for a critical safety modelling where flesh deformation was of paramount importance, a 3 mm error level might not be sufficient.

2. **Realism.** The overall result of realism seemed to show that the proposed FDM could produce a detailed flesh deformation around the elbow, capable of capturing subtle details at both the anterior and posterior of the elbow.
3. **Accommodation of different body types and sizes.** The framework was developed to allow the review of the new FDM's ability to accommodate different body types and sizes. The framework essentially predicted information (five key cross sections, profiles, locations of five key cross sections and carrying angle) that were required by the new FDM to create flesh deformation at the elbow from a limited number of inputs. The framework consisted of three important parts i.e. the inputs, the database and the prediction methods.

The overall result of the review showed that the new FDM, through the framework's utilisation, could accommodate flesh deformation modelling of different body types and sizes with a larger range of error and a lesser realism than flesh deformation which was created from data that were obtained directly from participants. Bearing in mind that the review was based on a limited number of data in the database, the result showed that the new FDM and the framework had a potential to simulate flesh deformation of a wider anthropometric range.

4. **Minimum user intervention.** The review result showed that the new FDM fulfilled the two main criteria which were related to minimum user intervention: (i) user intervention was limited to specifying or modifying the DHM feature to accommodate different postures, body size, body shapes, etc; and (ii) no direct modification of any parameter was necessary to create the flesh deformation.
5. **Real time modelling.** The retrospective analysis for real time modelling, which focused on two factors i.e. the amount of data and complexity of processing that had to be handled in real time, demonstrated that efforts were made in this research to minimise the amount of data and complexity of processing to be handled in real time. The retrospective analysis for real time modelling also showed that the new FDM had a potential to conform the real time modelling specification.
6. **Whole body modelling.** Since the proposed FDM was based on the concept that was put forward by Shen et al. (1994) method which was successfully applied for a whole

body modelling, it could be assumed that the proposed FDM could also be applied for the whole body modelling. Thus, hypothetically, had the proposed FDM been integrated with an existing ergonomics CAD, the proposed FDM could also be utilised to perform a whole body modelling. Ways to achieve this for other joints have been discussed in Chapter 11.

In this research, the inability of the scanning system i.e. [TC]² NX-12 body scanner, to capture the necessary data to support FDM was identified. The research also revealed that there was lack of standards regarding the accepted accuracy level of DHM simulation in ergonomics application. Furthermore, there were also no sufficient guidelines on how to establish the level of accuracy or other specifications that are related to DHM simulation in ergonomics such as realism and real time.

12.2 Future applications and studies

The new FDM and framework were designed such that it could simulate flesh deformation for different body types and sizes as accurately as possible. As such, the new FDM and framework have the potential to be applied commercially in high value areas of apparel and garment design in which the effects of gender, body type and size upon flesh deformation at joints needs to be considered. The need for high value apparel and garment design is commonly found in the field of health and safety (e.g. personal protective equipment), military (e.g. design of military uniform), aerospace (e.g. space suits) and leisure (e.g. diving suits).

This research has already given suggestions for future studies throughout the thesis. Thus, this section would only focus on suggestions that were deemed to be of the greatest importance. These include: i) a suggestion to integrate the new FDM and its framework with an existing platform of ergonomics application; ii) the expansion of the framework's database such that it could be more comprehensive; and iii) modelling the flesh deformation due to the movement of the elbow joint with additional load.

The first suggestion was deemed to be of priority as its execution will provide a more thorough analysis on the capability of the new FDM to simulate flesh deformation at the elbow. As described in section 11.1.6, this will require full access to the source code for an existing platform of ergonomics application. Since most of the existing platforms of ergonomics application are commercially based, this research acknowledges that gaining the access could be quite challenging.

The second suggestion for the future studies involves additional data collection for the database. This suggestion was also deemed to be important as its execution will provide a further insight into the ability of the new FDM to simulate flesh deformation for a wider range of anthropometry. However, as described in section 11.1.7.2, the collection of additional data is not trivial, requiring a considerable amount of resources and the need to address the limitations of 3D

body scanning systems. Once the above suggestion of future studies were performed, efforts could then be directed to apply the new FDM for other joints with a similar range of movement with the elbow and followed by the application of the new FDM for joints with a more complex range of movements.

The third suggestion for the future studies is direct consequence of the focus of this research i.e. modelling flesh deformation due to the movement of the elbow joint *without* additional load (see section 1.4). This suggestion was required because additional load e.g. due to lifting an object, would likely induce more muscle contractions at both upper and lower arms; and this would likely result in different flesh deformation than that of current new FDM and framework. By studying the effect of various loads on flesh deformation, a parameter to link the loads and five key cross sections could be proposed e.g. a scale factor for five key cross sections. The results could then be integrated into the new FDM and framework.

References

- Abdel-Malek, J., Yang J., Marler, T., Beck, S., Mathai, A., Zhou, X., Patrick, A. and Arora, J., 2006. Towards a new generation of virtual humans. *International Journal of Human Factors modelling and simulation*, 1(1), pp. 3-39.
- Adams., B., Wicke, M., Ovsjanikov, M., Wand, M., Seidel, H. P., Guibas, L. J., 2010. Meshless shape and motion design for multiple deformable objects. *Computer Graphics Forum*, 29(1), pp. 43-59.
- Allen, B., Curless, B. and Popovic, Z., 2002. Articulated body deformation from range scan data. *ACM Transactions on Graphics*, 21(3), pp. 612-619.
- Allen, B., Curless, B. Popovic, Z., 2003. The space of human body shapes: Reconstruction and parameterization from range scans. *ACM Transactions on Graphics*, 22(3), pp. 587-594.
- Allen, B., Curless, B., Popovic, Z., and Hertzmann, A., 2006. Learning a correlated model of identity and pose-dependent body shape variation for real-time synthesis. *Proceedings of the 2006 ACM SIGGRAPH/Eurographics symposium on Computer animation*, pp. 147-156.
- Andreoni, G., Santambrogio, G. C., Rabuffetti, M., and Pedotti, A., 2002. Method for the analysis of posture and interface pressure of car drivers. *Applied Ergonomics*, 33, pp. 511-522.
- Anguelov, D., Srinivasan, P., Koller, D., Thrun, S. and Rodgers, J., 2005. SCAPE: Shape Completion and Animation of People. *ACM Transactions on Graphics*, 24, pp. 408-416.
- Archer, B., 1965. *Systematic Methods for Designers*, London, The Design Council.
- Assassi, L., Charbonnier, C., Schmid, J., Volino, P., and Magnenat-Thalmann, N., 2009. From MRI to anatomical simulation of the hip joint. *Computer Animation and Virtual Worlds*, 20 (1), pp. 53-66.
- Autodesk, 2011. <http://usa.autodesk.com/adsk/servlet/pc/index?siteID=123112&id=13577897>
- Azuola, F., Badler, N. I., Ho, P., Kakadiaris, I., Metaxas, D., and Ting, B., 1994. Building anthropometry based virtual models, *Proceedings of the IMAGE VII Conference*, available online: <http://repository.upenn.edu/hms/54>
- WHO Expert Consultation, 2004. Appropriate body-mass index for Asian populations and its implications for policy and intervention strategies. *The LANCET*, 363, pp. 157-163.
- Badler, N., C. B. Phillips and B. L. Webber, 1993. *Simulating Humans: Computer Graphics, Animation and Control*, Oxford University Press, New York.
- Badler, N., 1997. Real time virtual humans. *Proceedings International Conference on Digital Media Futures*, Bradford, UK.
- Bandouch, J., Engstler, F., and Beetz, M., 2008. Accurate Human Motion Capture Using an Ergonomics-Based Anthropometric Human Model. *Proceedings of the 5th international conference on Articulated Motion and Deformable Objects*, ACM.

- Bapu, P., Evans, S., Kitka, P., Korna, M. and McDaniel, J., 1981. User's guide for COMBIMAN programs. Technical Report No. AFAMRL-TR-80-91, University of Dayton Research Institute, USAF Report.
- Barone, S. and Curcio, A., 2004. A computer-aided design-based system for posture analyses of motorcycles. *Journal of Engineering Design*, 15(6), pp. 581-595.
- Ben-Noun, L., Sohar, E., Laor, A., 2001. Neck circumference as a simple screening measure for identifying overweight and obese patients. *Obesity Research*, 9, pp. 470-477.
- Blakeley, F. M., 1980. CYBERMAN. Chrysler Corporation, Detroit, Michigan.
- Blanchonette, P., 2010. Jack Human Modelling Tool: A Review. A technical report DSTO-TR-2364. Available online: <http://hdl.handle.net/1947/10032>
- Boeing Company, 1970. Cockpit geometry evaluation-phase II. Final Reports, Seattle, Washington.
- Boozer, T., and Raschke, U., 1998. Using 3D human modeling tools in the design of a commercial aircraft interior: A case study. In Kumar, S. (ed.), *Advances in Occupational Ergonomics and Safety 2*, IOS Press, pp. 814-817.
- Brace, I., 2008. *Questionnaire Design: How to plan, structure and write survey material for effective market research*, Kogan Page Ltd., London UK.
- Burdea, G. C., and Coiffet, P., 2003. *Virtual Reality Technology*. John Wiley and Sons, Inc., Hoboken, New Jersey.
- Capell, S., Green, S., Curless, B., Duchamp, T. and Popović, Z., 2002. Interactive skeleton-driven dynamic deformations. *ACM Transactions on Graphics*, 21(3), pp. 586-593.
- Carey, E.J. and Gallwey, T.J., 2002. Evaluation of human postures with computer aids and virtual workplace designs. *International Journal of Production Research*, 40(4), pp. 825-843.
- Catmull, E. and Clark, J., 1978. Recursively generated b-spline surfaces on arbitrary topological meshes. *Computer Aided Design*, 10(6), pp. 350-355.
- Carter, J.E.L. and Heath, B.H., 1990. *Somatotyping - Development and Applications*. Cambridge University Press.
- CDC, 2011. Applications Manual for the Revised NIOSH Lifting Equation. Available online: <http://www.cdc.gov/niosh/docs/94-110/> [accessed 30 October 2011]
- CEN, 2003. Ergonomics: Computer Manikins and Body Templates, Part 1: General Requirements, CEN/TC 122, ISO/FDIS 15536-1:2003. Manuscript of the final draft, European Standard prEN ISO 15536-1, European Committee for Standardization, Brussels, Belgium.
- CEN, 2007. Ergonomics: Computer Manikins and Body Templates, Part 2: Verification of functions and validation of dimensions for computer manikin systems, CEN/TC 122, ISO/FDIS 15536-2:2007. Manuscript of the final draft, European Standard prEN ISO 15536-2, European Committee for Standardization, Brussels, Belgium.

- Chadwick, J.E., Haumann, D.R. and Parent, R.E., 1989. Layered construction for deformable animated characters. *Proceedings of the 16th annual conference on Computer Graphics and Interactive Techniques*, New York, USA, pp. 243-252.
- Chaffin, D.B., 2001. *Digital Human Modeling for Vehicle and Workplace Design*. Society of Automotive Engineers, Inc., Warrendale, PA.
- Chaffin, D. B., 2002. On simulating human reach motions for ergonomics analyses. *Human Factors and Ergonomics in Manufacturing*, 12(3), pp. 235-247.
- Chaffin, D.B., 2005. Improving digital human modelling for proactive ergonomics in design. *Ergonomics*, 48(5), pp. 478-491.
- Chaffin, D. B., 2007. Human motion simulation for vehicle and workplace design. *Human Factors and Ergonomics in Manufacturing*, 17(5), pp. 475-484.
- Committee of Human Factors, 1998. Anthropometric models. In Kroemer, K. H. E., Snook, S. H., Meadows, S. K., and Deutsch, S. (ed.), *Ergonomics Models of Anthropometry, Human Biomechanics and Operator-Equipment Interfaces: Proceedings of a workshop*, National Academy Press, Washington DC, pp. 4-19.
- Davis, J. H., 2011. *Statistics for Compensation: A Practical Guide to Compensation Analysis*. John y, Wiley and Sons, Inc., New Jersey, pp. 285.
- D'appuzo, N., 2006. Overview of 3D surface digitization technologies in Europe. *Proceedings of SPIE-IS&T Electronic Imaging*, San Jose, USA.
- Debril, J., Pudlo, P., Menceur, M. O. A. E, Gorce, P., and Lepoutre, F. X., 2007. Human articulation efforts estimation in the automobile vehicle accessibility movement: a pilot study. *Proceedings of the 1st international conference on Digital human modelling*, pp. 23-32.
- Dehn, D. M., and Van Mulken, S., 2000. The impact of animated interface agents: a review of empirical research. *International Journal of Human-Computer Studies*, 52(1), pp. 1-22.
- Doi, M. A. C., and Haslegrave, C. M., 2003. Evaluation of JACK for investigating postural behaviour at sewing machine workstations. *Proceedings of the Digital Human Modeling Conference*, Society of Automotive Engineers, Montreal, Canada.
- Dong, D, Wang. L., and Yuan, X., 2007. Experimental research on human body motion simulation based on the motion capture technology. *Proceedings of the 1st international conference on Digital human modeling*, pp. 42-47.
- Dong, F., Clapworthy, G.J., Krokos, M.A. and Yao, J., 2002. An anatomy-based approach to human muscle modeling and deformation. *IEEE Transaction on Visualization and Computer Graphics*, 8(2), pp. 154-170.

- Doo, D., and Sabin, M., 1978. Behaviour of recursive division surfaces near extraordinary points, *Computer-Aided Design*, 10, pp. 356-360.
- Dooley, M., 1982. Anthropometric modelling programs: A survey. *IEEE Computer Graphics and Applications*. IEEE Computer Society, 2(9), pp. 7-25
- Dryer, D. C., 1999. Getting personal with computers: How to design personalities for agents. *Applied Artificial Intelligence*, 12(3), pp. 273-295.
- Dyn, N., Levin, D. and Gregory, J., 1990. A butterfly subdivision scheme for surface interpolation with tension control. *ACM Transactions on Graphics*, 9(2), pp. 160-169.
- Eldrege, S. A., 1996. *Mask Improvisation for Actor Training and Performance: The Compelling Image*. Northwestern University, Chicago.
- Ergonomics Society , 2007. <http://www.ergonomics.org.uk/rc-directory> [accessed 30 October 2011]
- Evans, J. H., 1959. Basic Design Concepts. *Naval Engineers Journal*, 21.
- Fetter, W., 1982. A progression of human figures simulated by computer graphics. *IEEE Computer Graphics and Applications*, 2 (9), pp. 9-13.
- Feyen, R., Yili, L., Chaffin, D., Jimmerson, G. and Brad, J., 2000. Computer-aided ergonomics: A case study of incorporating ergonomics analyses into workplace design. *Applied Ergonomics*, 31(3), pp. 227-334.
- Fritzsche, F., and Bubb, H., 2007. Prediction of discomfort during arm movements. *Proceedings of Human Computer Interactions*, pp. 66-73.
- Fulder, T., Pizmoht, P., Polajnar, A. and Leber, M., 2005. Ergonomically designer workstation based on simulation of worker's movements. *International Journal of Simulation Modeling*, 4(1), pp. 27-34.
- Gibson, I., Rosen, D. W., Stucker, B., 2010. *Additive Manufacturing Technologies: Rapid Prototyping to Direct Digital*. Springer, New York, USA, pp. 341-343.
- Gill, T., Chittleborough, C., Taylor, A., Ruffin, R., Wilson, D., Phillips, P., 2003. Body mass index, waist hip ratio, and waist circumference: Which measure to classify obesity?. *Sozial- und Praventivmedizin*, 48, 3, pp. 191-198.
- Golden, D., Wojcicki, J., Jhee, J. T., Gilpin, S. L. , Sawyer, J. R., and Heyman, M. B., 2008. Body mass index and elbow range of motion in a healthy pediatric population. *Journal of Pediatric Gastroenterology and Nutrition*, 46, pp. 196-201.
- Gordon, C. and Bradtmiller, B., 1996. Interobserver error in a large scale anthropometrics survey. *American Journal of Human Biology*, 4, pp. 253-263.
- Goto, A., Moritomo, H., and Murase, T., 2004. In vivo elbow biomechanical analysis during flexion: Three dimensional motion analysis using magnetic resonance imaging. *Journal of Shoulder and Elbow Surgery*, 13, pp. 441-447.

- Green, R. (2000). A Generic Process for Human Model Analysis. Proceedings of the Digital Human Modeling Conference, Munich, Germany. SAE 2000-01-2167.
- Grujicic, M., Pandurangan, B., Arakere, G., He, T., and Xie, X., 2009. Seat-cushion and soft-tissue material modeling and a finite element investigation of the seating comfort for passenger-vehicle occupants. *Materials and Design*, 30(10), pp. 4273-4285.
- Guo, Q. and Liu, Y., 2007. Hand grasping motion simulation for astronauts training. *Lecture Notes in Computer Science*, 4561, pp. 101-109.
- Guo, X. and Qin, H., 2005. Real time meshless deformation. *Computer Animation and Virtual Worlds*, 16, pp. 189-200.
- Guo, Z. and Wong, K. C., 2005. Skinning with deformable chunks. *Computer Graphics Forum*, 24(3), pp. 373-381.
- Hamilton, M. A., and Nowak, K. L., 2009. The role of realism and anthropomorphism in the selection of avatars. *Proceedings of the 12th Annual International Workshop on Presence, The International Society for Presence Research*.
- Haidet, J., Demirci, C., and Arslanian, S. A., 2010. Racial differences in childhood obesity: pathogenesis and complications. In Freemark, M. (ed.), *Pediatric Obesity: Etiology, Pathogenesis and Treatment*, Springer Science+Business Media.
- Hearn, D. and Baker, M.P., 1994. *Computer Graphics*, Prentice Hall Inc., New Jersey.
- Helin, K., Viitaniemi, J., Montonen, J., Aromaa, S., and Määttä, 2007. Digital human model based participatory design method to improve work tasks and workplaces. *Lecture Notes in Computer Science*, 4561, pp. 847-855.
- Hermawati, S., and Marshall, R., 2007. Virtual human models for ergonomic product design and development. *Proceedings of International Conference on Product Design and Development*, Yogyakarta, Indonesia.
- Hermawati, S., and Marshall, R., 2008. Realistic flesh deformation for digital humans. *Proceedings of SAE Digital Human Modeling for Design and Engineering Conference*, Pittsburgh, USA.
- Hermawati, S., and Marshall, R., 2009. Realistic elbow flesh deformation based on anthropometrical data for ergonomics modeling. *Lecture Notes in Computer Science*, 5620, pp. 632-641.
- Herron, R. E., 2006. Anthropometric database. In Karwowski, W., *International Encyclopedia of Ergonomics and Human Factors*, CRC Press, pp.
- Hong, Q. Y., Park, S. I., and Hodgins, J. K., 2010. A data-driven segmentation for the shoulder complex. *Computer Graphics Forum*, 29(2), pp. 537-544.
- Human Solutions GmbH., 2011. http://www.human-solutions.com/automotive/index_en.php. [accessed 30 October 2011]

- Hussey, J., 2005. Measurement of physical fitness and habitual physical activity. In Gormley, J., and Hussey, J. (eds.), *Exercise therapy in prevention and treatment of disease*, Blackwell Publishing Ltd, Oxford, pp. 79-101.
- Hyun, D.E., Yoon, S.H., Kim, M.S. and Jüttler, B., 2003. Modeling and deformation of arms and legs based on ellipsoidal sweeping. *Proceedings of the 11th Pacific Conference on Computer Graphics and Applications*, Canada, pp. 204-212.
- Hyun, D.E., Yoon, S.H., Chang, J.W., Seong, J.K., Kim, M.S. and Jüttler, B., 2005. 3D modeling of the human upper limb including the biomechanics of joints, muscles and soft tissues. *The Visual Computer*, 21, pp. 542-550.
- Ishida, Y., Kanehisa, H., Kondo, M., Fukunaga, T., Carroll, J. F., Pollock, M. L., Graves, J. E., and Legget, S. H., 1994. Body fat and muscle thickness in Japanese and Caucasian females. *American Journal of Human Biology*, 6 (6), pp. 711-718.
- International Standards Organization, ISO 15535:2006 – General Requirements for Establishing Anthropometric Databases, 2006, Geneva: International Organization for Standardization.
- Istook, C. L. and Hwang, S.J., 2001. 3D body scanning systems with application to the apparel industry. *Journal of Fashion Marketing and Management*, 5(2), pp. 120-132.
- James, T., 1989. *The Prop Builder's Molding and Casting Handbook*. F+W Publications Inc., Cincinnati, Ohio.
- Johansson, A. and Åström, L., 2004. How to use computer manikins and motion capture. Master Thesis, Lulea University of Technology, Department of Human Work and Sciences, Division of Industrial Design. Available online <http://epubl.luth.se/1402-1617/2004/278/LTU-EX-04278-SE.pdf>
- Jolliffe, I.T., 2002. *Principal Component Analysis*, Springer-Verlag, New York.
- Ju, T., Zhou, Q., Panne M., Cohen-Or, D. and Neumann, U., 2008. Reusable skinning templates using cage based deformations. *ACM Transactions on Graphics*, 27(5), article 122.
- Kasap, M., Chaudhuri, P. and Magnenat-Thalmann, N., 2009. Fast EMG-data driven skin deformation. *Computer Animation and Virtual Worlds*, 20, pp. 153-161.
- Karhu, O., Kansi, P. and Kuorinka, I., 1977. Correcting working postures in industry: A practical method for analysis. *Applied Ergonomics*, 8, pp. 199-201.
- Kavan, L., Collins, S., Žára, J. and O'Sullivan, C., 2008. Geometric skinning with approximate dual quaternion blending. *ACM Transactions on Graphics*, 27(4), article 105.
- Khare, G.N., Goel, S.C., Saraf, S.K., Singh, G. and Mohanty, C., 1999. New observations on carrying angle. *Indian Journal of Medical Sciences*, 53, pp. 61-67.
- Kingsley, E., Schofield, N. and Case, K., 1981. SAMMIE – A computer aid for man-machine modeling. *Computer Graphics*, 15, pp. 163-169.

- Kurihara, T. and Miyata, N., 2004. Modeling deformable human hands from medical images. Proceedings of the 2004 Eurographics/ACM SIGGRAPH Symposium on Computer Animation, pp. 355-363.
- Laitila, L. (2005). Datormannequinprogram som verktyg vid arbetsplatsutformning – en kritisk studie av programanvändning. Licentiate thesis (in Swedish – abstract in English), Lulea University of Technology, Department of Human Work and Sciences, Division of Industrial Design.
- Lämkkull, D., Hanson, L., and Örtengren, R., 2007. The influence of virtual human model appearance on visual ergonomics posture evaluation. *Applied Ergonomics*, 38, pp. 713-722.
- Landreneau, E. and Schaefer, S., 2010. Poisson-based weight reduction of animated meshes. *Computer Graphics Forum*, 29 (6), pp. 1945-1954.
- Lee, S., Sifakis, E. and Terzopoulos, D., 2009. Comprehensive biomechanical modelling and simulation of the upper body. *ACM Transactions in Graphics*, 28(4), pp. 1–17.
- Lee, J. and Kim, M., 2007. Human hand adaptation using sweeps: Generating animatable hand models. *Computer Animation and Virtual Worlds*, 18, pp. 505-516.
- Lee, J., Kim, M. and Yoon, S., 2009. Patches: character skinning with local deformation layer. *Computer Animation and Virtual worlds*, 20, pp. 321-331.
- Lerch, T., MacGillivray, M. and Domina, T., 2007. 3D laser scanning: A model of multidisciplinary research. *Journal of Textile and Apparel, Technology and Management*, 5(4).
- Lewis, J.P., Cordner, M. And Fong, N., 2000. Pose space deformation: A unified approach to shape interpolation and skeleton-driven deformation. Proceedings of the 27th annual conference on Computer Graphics and Interactive Techniques, ACM Press/Addison-Wesley Publishing Co., pp. 165-172.
- Li, K. and Zhang, X., 2007. The strength factor in digital human modelling and simulation: a case for a new framework. Proceeding of the 1st international conference on Digital human modelling, pp. 144-146.
- Lieu, D. K. and Sorby, S., 2009. Visualization, Modeling and Graphics for Engineering Design. Delmar, Cengage Learning.
- Lo, B., 2010. Ethical Issue in Clinical Research: A Practical Guide. Lippincott Williams and Wilkins, Philadelphia, USA.
- Locket, J. F., Assmann, E., Green, R., Reed, M. P., Rascke, R., and Verriest, J. P., 2005. Digital human modeling research and development user needs panel. Proceedings of SAE Digital Human Modelling for Design and Engineering Symposium, SAE, Iowa City.
- Loop, C., July 1994. Smooth spline surfaces over irregular meshes. Proceedings of SIGGRAPH 1994 Conference, ACM SIGGRAPH, pp. 303-310.

- Lu, J., and Wang, M., 2008. Digital human modeling and scanner based anthropometry. In Duffy, V. G. (ed.), *Handbook of Digital Human Modeling Research for Applied Ergonomics and Human Factors Engineering*, CRC Press.
- Luttgens, K. and Hamilton, N., 1997. *Kinesiology: Scientific Basis of Human Motion*, Brown and Benchmark, Madison NY.
- Makehuman.org, 2011. <http://www.makehuman.org/> [accessed 30 October 2011]
- Malina, R. M., 1996. Regional body composition: Age, sex and ethnic variation. In: Roche, A. F., Heymsfield, S. B., Lohman, T.G. (eds.), *Human Body Composition*, Champaign, pp. 217-55.
- Malina, R. M, Bourchard, C., and Bar-Or, O., 2004. Growth, maturation and physical activity, *Human Kinetics*, USA, pp. 150-154.
- Maurel, W. and Thalmann, D., 1998. 3D Modeling of the Human Upper Limb including the Biomechanics of Joints, Muscles and Soft Tissues. PhD thesis, Ecoles Polytechniques fédérale de Lausanne.
- Marple, D., 1961. The decisions of engineering design. *IEEE Transactions of Engineering Management*, 2, pp. 55-71.
- Marshall, R., Case, K., Porter, J.M., Gyi, D.E. and Sims, R.E., 2003. Virtual Task Analysis in 'Design for All'. In Campbell, R.I. and Balci, N.O. (ed.), *Virtual Engineering Applications for Design and Product Development*, Media Services, Loughborough University, European Virtual Engineering Network (EVEN) , Trinity College Dublin, Ireland, pp. 235-242.
- Marshall, R., Porter, J. M., Case, K., Sims, R., Gyi, D. E., 2004. Using HADRIAN for eliciting virtual user feedback in 'design for all'. *Proceedings of the Institution of Mechanical Engineers, Part B: Journal of Engineering Manufacture*, 218 (9), Sage Publications, pp. 1203-1210.
- Matignon, R., 2007. *Data Mining Using SAS Enterprise Miner™*, John Wiley and Sons, New Jersey, pp. 460.
- McAtamney, L. and Corlett, E.N., 1993. RULA: A survey method for the investigation of work-related upper limb disorders. *Applied Ergonomics*, 24(2), pp. 91-99.
- McKinnon, L. and Istook, C., 2002. Body scanning: The effects of subject respiration and foot positioning on the data integrity of scanned measurements. *Journal of Fashion Marketing and Management*, 6 (2), pp. 103-121.
- Mehta, C. R., and Tewari, V. K., Seating discomfort for tractor operators-a critical review. *International Journal of Industrial Ergonomics*, 25(6), pp. 661-674.
- Menache, A., 2010. *Understanding Motion Capture for Computer Animation*. Elsevier Inc., Burlington, USA.
- Mendes, E., and Mosley, N., 1998. *Web Engineering*. Springer-Verlag Berlin, pp. 94-95.

- Merry, B., Marais, P. and Gain, J., 2006. Animation space: A truly linear framework for character animation. *ACM Transactions on Graphics*, 25(4), pp. 1400-1423.
- Mohr, A., and Gleicher, M., 2003. Building efficient, accurate character skins from examples. *Proceedings of International Conference on Computer Graphics and Interactive Techniques*, ACM, New York , pp. 562-568.
- Mohr, A., Tokheim, L. and Gleicher, M., 2003. Direct manipulation of interactive character skins, *Proceedings of the 2003 symposium on Interactive 3D graphics*, ACM Press New York, NY, USA, pp. 27-30.
- Moes, C. C. M., 2007. Variation in sitting pressure distribution and location of the points of maximum pressure with rotation of the pelvis, gender and body characteristics. *Ergonomics*, 50(4), pp. 536-561.
- Morrissey, M., 1998. Human-centric design. *Mechanical Engineering*, 120(7), pp. 60-62.
- Nafiu, O. O., burke, C. B., Lee, J., Voepel-Lewis, T., malviya, S., Tremper, K. K., 2010. Neck circumference as a screening measure for identifying children with high body mass index. *Pediatrics*, 126 (2), pp. 306-310.
- Narayan, K. L, Rao, K. M., Sarcar, M. M. M., 2008. *Computer Aided Design and Manufacturing*, Prentice hall of India Private Limited, New Delhi.
- Naumann, A. and Roetting, M., 2007. Digital human modeling for design and evaluation of human-machine systems. *MMI-Interaktiv*, 12, pp. 27-35.
- Nedel, L.P. and Thalmann, D., 2000. Anatomic modelling of deformable human bodies. *The Visual Computer*, 16, pp. 306-321.
- NexGen Ergonomics Inc., 2011. <http://www.nexgenergo.com/ergonomics/mqpro.html>. [accessed 30 October 2011]
- Ohkawa, S., Odamaki, M., Ikegaya, N., Hibi, I., Miyaji, K., and Kumagai H., 2005. Association of age with muscle mass, fat mass and fat distribution in non-diabetic haemodialysis patients. *Nephrol Dial Transplant*, 20(5), pp. 945-951.
- Oudenhuijzen, A., Zehner, G. F., and Hudson, J. A., 2008. Verification and validation of human modelling system. In Duffy, V. G. (ed.), *Handbook of Digital Human Modeling Research for Applied Ergonomics and Human Factors Engineering*, CRC Press.
- Paraskevas, G., Papadopoulos, A., Papaziogas, B., Spanidou, S., Argiriadou, H., and Gigis, J., 2004. Study of the carrying angle of the human elbow joint in full extension: a morphometric analysis. *Surgical and Radiologic Anatomy*, 26(1), pp. 19-23.
- Peebles, L., and Norris, B. J., 1998. *ADULTDATA: The Handbook of Adult Anthropometric and Strength Measurements*. Department of Trade and Industry, London.

- Phillips, C. and Badler, N. I., 1988. Jack: A Toolkit for manipulating articulated figures. ACM/SIGGRAPH Symposium on User Interface Software, Banff, Canada, pp. 221-229.
- Porter, J.M., Freer, M., Case, K. and Bonney, M.C., 1995. Computer aided ergonomics and workplace design. In: J.R. Wilson and E.N. Corlett (ed.), *Evaluation of Human Work: A Practical Ergonomics Methodology*, 2nd edn., London: Taylor and Francis, pp. 574-620.
- Porter, J.M., Marshall, R., Freer, M., and Case, K., 2004. SAMMIE: A computer aided ergonomics design tool. In Delleman, N. J., Haslegrave, C. M., and Chaffin, D. B. (ed.), *Working postures and movements: Tools for evaluation and engineering*, CRC Press, Florida, pp. 454-462.
- PTC, 2011. <http://www.ptc.com/appserver/mkt/products/home.jsp?k=403> [accessed 30 October 2011]
- Pushkar, J., Meyer, M., DeRose, T., Green, B. and Sanocki, T., 2007. Harmonic coordinates for character articulation. *ACM Transactions on Graphics*, 26(3), article 71.
- Ranjan, P., 2006. *Principles of Multimedia*. Tata McGraw-Hill, New Delhi, India, pp. 691.
- Raschke, U., 2004. The Jack simulation tool, In: N.J. Delleman, C.M. Haslegrave, and D.B. Chaffin (ed.), *Working Postures and Movements: Tools for Evaluation and Engineering*, CRC Press, Florida, pp. 431-437.
- Reed, M. P. And Parkinson, M.B., 2008. Modeling variability in torso shape for chair and seat design. *Proceedings of ASME 2008 International Design Engineering Technical Conferences and Computers and Information in Engineering Conference*, New York, USA, pp. 561-569.
- Rhee, T., Lewis, J.P. and Neumann, U., 2006. Real time weighted pose-space deformation on the GPU. *Computer Graphics Forum*, 25(3), pp. 439-448.
- Robinette, K., Daanen, H.A.M. and Zehner, G., 2004. Three-dimensional anthropometry. In: Delleman, N., Chaffin, D. and Haslegrave, C. (ed.), *Working Postures and Movements: Tools for Evaluation and Engineering*, CRC Press, pp. 30-49.
- Rohmer, D., Hahmann, S. and Cani, M., 2008. Local volume preservation for skinned characters. *Computer Graphics Forums*, 27 (7), pp. 1919-1927.
- Ruiter I.A., 2000. Anthropometric man-models, handle with care. In: K. Landau (ed.), *Ergonomic Software Tools in Product and Workplace Design*, Stuttgart, Verlag ERGON GmbH, pp. 94-99.
- SAE International, 2011. CAESAR- The most comprehensive source for body measurement data. Available online: <http://store.sae.org/caesar/>
- Safework Inc., 2011. <http://www.3ds.com/products/delmi/solutions/human-modeling/> [accessed 30 October 2011]
- SAMMIE-CAD Limited, 2011. <http://www.lboro.ac.uk/departments/cd/research/groups/erg/sammie/home.htm> [accessed 30 October 2011]

- SantosHuman™ Inc., 2010. <http://www.santoshumaninc.com/software-suite/engine/> [accessed 30 October 2011]
- Sardinha, L. B., and Teixeira, P. J., 2005. Measuring adiposity and fat distribution in relation to health. In: Heymsfield, S.B., Lohman, T. G., Wang, Z. M., and Going, S. B. (eds), *Human Body Composition*, Champaign, IL, pp. 177–201.
- Scheepers, F., Parent, R.E , Carlson, W. E., and May, S. F., 1997. Anatomy-based modeling of the human musculature. *Proceedings of 24th Conference on Computer Graphics and Interactive Techniques*, pp. 163-172.
- Schneider, P. J. and Eberly, D. H., 2003. *Geometric Tools for Computer Graphics*, Elsevier Science, San Francisco, USA.
- Sederberg, T.W. and Parry, S.R., 1986. Free-form deformation of solid geometric models. *Proceedings of the 13th annual conference on Computer Graphics and Interactive Techniques*, ACM Press New York, NY, pp. 151-160.
- Seager, S. L., and Slabaugh, M. R., 2011. *Chemistry for Today: General, Organic and Biochemistry*. Brooks/Cole Cengage Learning, Belmont, USA, pp. 317.
- Seidl, A., 1997. RAMSIS: A New CAD-tool for Ergonomic Analysis of Vehicles Developed for the German Automotive Industry. *Automotive Concurrent/Simultaneous Engineering SAE Special Publications*.
- Seidl, A., 2004. The RAMSIS and ANTHROPOS human simulation tools. In Delleman, N. J., Haslegrave, C. M., and Chaffin, D. B. (ed.), *Working postures and movements: Tools for evaluation and engineering*, CRC Press, Florida, pp. 446.
- Seidl, A. and Bubb, H., 2005. Standards in Anthropometry. In: Karwowski, W. (ed.), *Handbook of Standards and Guidelines in Ergonomics and Human Factors*, CRC Press, pp. 169-196.
- Seo, H. and Thalmann, N., 2003. An automatic modelling of human bodies from sizing parameters. *Proceedings of the 2003 symposium on Interactive 3D Graphics*, ACM Press New York, NY, pp. 19-26.
- Sharp, B., 2000. Implementing Subdivision Surface Theory. *Game Developer Magazine*, February Issue, UBM TechWeb, San Francisco.
- Shen, J., Magnenat-Thalmann, N., Thalmann, D., 1994. Human skin deformation from cross sections. *Proceedings of Computer Graphics International 1994*, pp. 612–619.
- Shi, X., Zhou, K., Tong, Y., Desbrun, M., Bao, H. and Guo, B., 2008. Example based dynamic skinning in real time. *ACM Transactions on Graphics*, 27(3), article 29.
- Shin, H., and Badler, N. I., 2002. Modelling deformable human arm for constrained research analysis. In *Proceedings of the Digital Human Modelling Conference*, Munich, pp. 217-228.

- Siemens PLM software, 2011.
http://www.plm.automation.siemens.com/en_us/products/tecnomatix/assembly_planning/jack/index.shtml [accessed 30 October 2011]
- Sloan P-P. J., Rose, C. F., and Cohen, M. F., 2001. Shape by example. Proceedings of the symposium on Interactive 3D graphics, pp. 135-143.
- Stanton, N. A., Salmon, . M., Walker, G. H., Baber, C., Jenkins, D. P., 2005. Human factors methods: A practical guide for engineering and designs, Ashgate Publishing Limited, England.
- Sueda, S., Kaufman, A., and Pai, D. K., 2008. Musculotendon simulation for hand animation. ACM Transaction in Graphics, 27(3), article 83.
- Summer, R. W., Schmid, J. and Pauly, M., 2007. Embedded deformation for shape manipulation. ACM Transaction in Graphics, 26(3), article 80.
- Sundin, A., Christmansson, M., and Larsson, M., 2004. A different perspective in participatory ergonomics in product development improves assembly work in the automotive industry. International Journal of Industrial Ergonomics, 33, pp. 1- 14.
- Sumathi, S., and Sivanandam, S. N., 2006. Introduction to Data Mining and its Applications, Springer-Verlag, Berlin, pp. 14.
- Sundin, A. and Sjöberg, H., 2002. How are computer manikins used in Sweden?. Proceedings of 34th Annual Congress of the Nordic Ergonomics Society, Kolmården, pp. 745-750.
- Sundin, A. and Örtengren, R., 2006. Digital Human modelling for CAE applications. In: Salvendy, G. (ed.), Handbook of Human Factors and Ergonomics, John Wiley & Sons, 3rd Edition, pp. 1053-1078.
- Tan, H., 2007. Costume of Craftwork on a Budget. Elsevier, Inc., Oxford, UK.
- Tang, Y. M., 2010. Modeling skin deformation using boundary element method. Computer Aided Design and Applications, 7(1), pp. 101-108.
- [TC]², 2011. <http://www.tc2.com/index.html> [accessed 30 October 2011]
- Tewari, V. K., and Prasad N., 2000. Optimum seat pan and back-rest parameters for a comfortable tractor seat. Ergonomics, 43(2), pp. 167-186.
- The Mathworks, 2009. <http://www.mathworks.com/products/matlab/description1.html>
- Tost, D. and Pueyo, X., 1988. Human body animation: A survey. The Visual Computer, 3, pp. 254-264.
- Van Roy P, Baeyens JP, Fauvart D, Lanssiers R, and Clarijs, J. P., 2005. Arthro-kinematics of the elbow: study of the carrying angle. Ergonomics, 48(11), pp. 1645-1656.
- Vassilev, T. and Spanlang, B., Sep. 2002. A mass-spring model for real time deformable solids. Proceedings of East-West Vision 2002, Graz, Austria, pp. 149-154.

- Verver, M. M., and Mooi, H. G., 2004. Seating comfort simulation and H-point prediction. Proceedings of the 10th International MADYMO Users Meeting, Amsterdam.
- Vugt, H. C., Konijn, E. A., Hoorn, J. F., Keur, I., Eliens, A., 2007. Realism is not all! User engagement with task-related interface characters. *Interacting with Computers*, 19, pp. 267-280.
- Walker, R. A., 1993. The impact of racial variation on human engineering design criteria, *NAPA Bulletin*, 13(1), pp. 7-21.
- Wagner, D. R., and Heyward, V. H., 2000. Measures of body composition in blacks and whites: a comparative review, 71 (6), pp. 1392-1402.
- Wang, X., Chateauroux, E., Nicolas, C., 2007. A data-based modeling approach of reach capacity and discomfort for digital human models. *Proceedings of Human Computer Interactions*, pp. 215-223.
- Wang, X.C., and Phillips, C., 2002. Multiweight enveloping: Least square approximation techniques for skin animation. *Proceedings of ACM SIGGRAPH/Eurographics Symposium on Computer Animation*, ACM, New York, pp. 129-138.
- Watkins, J., 2010. Structure and functions of the musculoskeletal system. *Human Kinetics*, Champaign, ILL, pp. 40.
- Wegner, D., Chiang, J., Kemmer, B., Lämkuhl, D. and Roll, R., 2007. Digital human modeling requirements and standardization. *Proceedings of Digital Human Modeling for Design and Engineering Conference and Exhibition*, SAE, Seattle.
- WHO, 1995. Physical status: the use and interpretation of anthropometry. Report of a WHO Expert Committee, WHO Technical Report Series 854, Geneva.
- WHO, 2000. Obesity: preventing and managing the global epidemic. Report of a WHO Consultation, WHO Technical Report Series 894, Geneva.
- Wichert, A., Marcos-Suarez, P., Vereczkei, A., Seitz, T., Bubb, H., and Feussner, H., 2004. Improvement of the ergonomic situation in the integrated operating room for laparoscopic operations. *International Congress Series* 1268, pp. 842-846.
- Wilhelms, J. and Gelder, A. V., 1997. Anatomically based modeling. *Proceedings of 24th annual conference on Computer Graphics and Interactive Techniques*, pp. 173-180.
- Winkelbach, S., Molkenstruck, S., and Wahl, F. M., 2006. Low-cost laser range scanner and fast surface registration approach. In Franke, K., Müller, K. R., Nickolar, B. and Schafer, R. (eds.), *DAGM 2006*, LNCS, 4174, pp. 718-728.
- Wynn, D.C. and Clarkson, P.J., 2005. Models of Designing. In Clarkson, P. J. and Eckert, C. M. (eds.), *Design Process Improvement - A Review of Current Practice*, Springer.
- Yang, J., 2008. Research for applied ergonomics and human factors engineering. In Duffy, V. G (ed.), *Handbook of Digital Human Modelling*, pp. 29-1 – 29-23.

- Yang, X., Somasekharan, A. and Zhang, J. J., 2006. Curve Skeleton skinning for human and creature characters. *Computer Animation and virtual worlds*, 17, pp. 281-292.
- You, L. H., Yang, X. and Zhang, J. J., 2008. Dynamic skin deformation with characteristic curves. *Computer Animation and Virtual Worlds*, 19, pp. 433-444.
- Zampagni, M. L., Casino, D., Zaffagnini, S., Visani, A. A., and Marcacci, M., 2008. Trend Of The Carrying Angle During Flexion-Extension Of The Elbow Joint: A Pilot Study. *Orthopedics*, 31(1): 76.
- Zampagni, M. L., Dona, G., Motta, M., Martelli, S., Benelli, P., and Marcacci, M., 2006. A new method for anthropometric acquisition of the upper extremity parameters in elite master swimmers. *Journal of Mechanics in Medicine and Biology*, 6(1), pp. 1-11.
- Zhang, X. and Chaffin, D. B., 2000. A three dimensional dynamic posture prediction model for simulating in-vehicle seated reaching movements: development and validation. *Ergonomics*, 43, pp. 1314-1330.
- Zheng, G., Li, W., Ogunbona, P., Dong, L., and Kharitonenko, I., 2007. Human motion simulation and action corpus. *Proceedings of the 1st international conference on Digital human modelling*, pp. 314-322.

APPENDIX A: Questionnaire for user study

Questionnaire on digital human usage for ergonomics CAD modelling

The use of digital human is a key component of ergonomics modelling. Several case studies reported the successful use of various digital human models to improve the physical ergonomics of different designs. Currently, the existing digital humans in various ergonomics applications are varied in terms of their realism, accuracy etc.

This questionnaire is part of a PhD study which aims to investigate the usage of digital human models in ergonomics CAD software. Any information that will be given will be treated as strictly confidential and will only be used for the purpose of this research.

Age _____ :

Occupation _____ :

Sex _____ : Female [☐] Male [☐]

PART I : EXPERIENCE RELATED TO ERGONOMICS CAD SOFTWARE USAGE

1. What types of CAD ergonomics software e.g. SammieCAD, Jack, Ramsis, Anthropos, MannequinPro etc, have you ever used?

Software name	Version (if applicable)	Duration of usage

2. What types of analysis/activity (e.g. postural analysis, fit and reach assessment) have you used the CAD ergonomics software for within the last 3-5 years?

Software name	Type of analysis

PART II : PERCEPTION OF THE IMPORTANCE OF DIFFERENT CRITERIA RELATED TO DIGITAL HUMAN MODEL

Please rate the importance of the following criteria for digital human model (DHM) in ergonomics modelling by *placing a cross [X] in the appropriate box*. The description for each criteria is also given for further clarification. You are also allowed to add your own criteria at the end.

DHM's appearance				
No	Criteria	Description		Relevancy to previous experiences
1.	Natural and realistic looking postures/motion	How important is the visual accuracy of the postures and motions that the DHM adopts (e.g. reach).	<input type="checkbox"/> Essential <input type="checkbox"/> Important <input type="checkbox"/> Desirable <input type="checkbox"/> Unimportant	Have you used or would like to have used this function in any of your ergonomics analysis? <input type="checkbox"/> Used <input type="checkbox"/> Like to have used <input type="checkbox"/> Neither
2.	Realistic appearance	How important is a visually realistic flesh form for the DHM.	<input type="checkbox"/> Essential <input type="checkbox"/> Important <input type="checkbox"/> Desirable <input type="checkbox"/> Unimportant	Have you used or would like to have used this function in any of your ergonomics analysis? <input type="checkbox"/> Used <input type="checkbox"/> Like to have used <input type="checkbox"/> Neither
3	Level of details of realistic appearance	How important are realistic body details for the DHM (e.g. head, hands, feet, legs/arm, torso).	<input type="checkbox"/> Essential <input type="checkbox"/> Important <input type="checkbox"/> Desirable <input type="checkbox"/> Unimportant	Have you used or would like to have used this function in any of your ergonomics analysis? <input type="checkbox"/> Used <input type="checkbox"/> Like to have used <input type="checkbox"/> Neither
4.	Realistic and accurate joint flesh deformation	How important is visually realistic flesh deformation at the joint when the DHM	<input type="checkbox"/> Essential <input type="checkbox"/> Important	Have you used or would like to have used this function in any of your

		posture changes.	<input type="checkbox"/> Desirable <input type="checkbox"/> Unimportant	ergonomics analysis? <input type="checkbox"/> Used <input type="checkbox"/> Like to have used <input type="checkbox"/> Neither
5.	DHM's flesh interaction with external forces	How important is the ability of the DHM's flesh to react to external loads e.g. flesh deformation of the buttocks/thigh in a sitting posture.	<input type="checkbox"/> Essential <input type="checkbox"/> Important <input type="checkbox"/> Desirable <input type="checkbox"/> Unimportant	Have you used or would like to have used this function in any of your ergonomics analysis? <input type="checkbox"/> Used <input type="checkbox"/> Like to have used <input type="checkbox"/> Neither
DHM's size and shape				
No	Criteria	Description		
6.	Shape flexibility	How important is the provision of data to be able to transform the DHM to represent any possible human body shape.	<input type="checkbox"/> Essential <input type="checkbox"/> Important <input type="checkbox"/> Desirable <input type="checkbox"/> Unimportant	Have you used or would like to have used this function in any of your ergonomics analysis? <input type="checkbox"/> Used <input type="checkbox"/> Like to have used <input type="checkbox"/> Neither
7.	Size flexibility	How important is the provision of data to be able to transform the DHM to represent any possible human size.	<input type="checkbox"/> Essential <input type="checkbox"/> Important <input type="checkbox"/> Desirable <input type="checkbox"/> Unimportant	Have you used or would like to have used this function in any of your ergonomics analysis? <input type="checkbox"/> Used <input type="checkbox"/> Like to have used <input type="checkbox"/> Neither
DHM's function				
No	Criteria	Description		

8.	Postural/biomechanical analysis	How important is postural/biomechanical analysis to assess whether a particular design may result in injury related to musculoskeletal disorders.	<input type="checkbox"/> Essential <input type="checkbox"/> Important <input type="checkbox"/> Desirable <input type="checkbox"/> Unimportant	Have you used or would like to have used this function in any of your ergonomics analysis? <input type="checkbox"/> Used <input type="checkbox"/> Like to have used <input type="checkbox"/> Neither
7.	Reach and fit analysis	How important is the ability to simulate whether a DHM fits i.e. adequate clearance, in a virtual environment set and is able to reach any specified object.	<input type="checkbox"/> Essential <input type="checkbox"/> Important <input type="checkbox"/> Desirable <input type="checkbox"/> Unimportant	Have you used or would like to have used this function in any of your ergonomics analysis? <input type="checkbox"/> Used <input type="checkbox"/> Like to have used <input type="checkbox"/> Neither
10.	Hand grip and strength	How important is the analysis on the fitness of hand tools in terms of comfort, efficiency and required strength of use.	<input type="checkbox"/> Essential <input type="checkbox"/> Important <input type="checkbox"/> Desirable <input type="checkbox"/> Unimportant	Have you used or would like to have used this function in any of your ergonomics analysis? <input type="checkbox"/> Used <input type="checkbox"/> Like to have used <input type="checkbox"/> Neither
11.	Visual sight line	How important is the ability to show the DHM's field of vision.	<input type="checkbox"/> Essential <input type="checkbox"/> Important <input type="checkbox"/> Desirable <input type="checkbox"/> Unimportant	Have you used or would like to have used this function in any of your ergonomics analysis? <input type="checkbox"/> Used <input type="checkbox"/> Like to have used <input type="checkbox"/> Neither
12	Field of view on a mirror	How important is the ability to show the DHM's field of vision on a mirror.	<input type="checkbox"/> Essential	Have you used or would like to have used this function in any of your

			<input type="checkbox"/> Important <input type="checkbox"/> Desirable <input type="checkbox"/> Unimportant	ergonomics analysis? <input type="checkbox"/> Used <input type="checkbox"/> Like to have used <input type="checkbox"/> Neither
Miscellaneous				
No	Criteria	Description		
13.	Adding variety of clothing, helmets, etc.	How important is the ability to add clothing and accessories to assess their fitness and effects on motion restriction.	<input type="checkbox"/> Essential <input type="checkbox"/> Important <input type="checkbox"/> Desirable <input type="checkbox"/> Unimportant	Have you used or would like to have used this function in any of your ergonomics analysis? <input type="checkbox"/> Used <input type="checkbox"/> Like to have used <input type="checkbox"/> Neither
14.	Other criteria:		<input type="checkbox"/> Essential <input type="checkbox"/> Important <input type="checkbox"/> Desirable <input type="checkbox"/> Unimportant	Have you used or would like to have used this function in any of your ergonomics analysis? <input type="checkbox"/> Used <input type="checkbox"/> Like to have used <input type="checkbox"/> Neither
15.	Other criteria:		<input type="checkbox"/> Essential <input type="checkbox"/> Important <input type="checkbox"/> Desirable <input type="checkbox"/> Unimportant	Have you used or would like to have used this function in any of your ergonomics analysis? <input type="checkbox"/> Used <input type="checkbox"/> Like to have used <input type="checkbox"/> Neither

PART III : PERCEPTION OF THE REQUIRED LEVEL OF DETAIL FOR A REALISTIC LOOKING DIGITAL HUMAN MODEL

For part III and IV, the term “realistic looking” does not include flesh deformation due to physical contact with objects e.g. buttock deformation while sitting.

1. For each statement, please placing a cross [X] in one of the boxes.

<div data-bbox="635 481 997 817" data-label="Image"> </div> <p>a) A realistic looking DHM should be represented by enhancing the details of the whole body (i.e. accuracy must be uniform).</p> <p>[] Strongly agree [] Agree [] Neutral [] Disagree [] Strongly Disagree</p>	
<div data-bbox="766 969 884 1301" data-label="Image"> </div> <p>b) A realistic looking DHM should be represented by enhancing the details for <u>certain body parts</u> only e.g. hand, feet, head/face and torso (i.e. accuracy is not uniform)</p> <p>[] Strongly agree [] Agree [] Neutral [] Disagree [] Strongly Disagree</p>	
<div data-bbox="694 1487 1031 1845" data-label="Image"> </div> <p>c) Unrealistic joint flesh deformation affects the overall level of DHM's realism.</p> <p>[] Strongly agree [] Agree [] Neutral [] Disagree [] Strongly Disagree</p>	

2. Bearing in mind the “realistic looking” definition above, what other aspects should be considered to create a realistic looking DHM?

3. The more accurate and realistic a digital human model (whole body), the more likely it will take time to render/manipulate it. For ergonomics modelling applications, do you think that a waiting time would be inconvenient for you in the situation in which a real time interaction is required (e.g. manipulating the posture) ?
- ☐ YES ☐ NO ☐ POSSIBLY

Please explain.

4. If your answer is YES to question 3, i.e. waiting time is inconvenient for you, would you be willing to compromise by having a less accurate but still a realistic looking digital human model?
- ☐ YES ☐ NO ☐ POSSIBLY

Please explain.

5. If your answer is NO or POSSIBLY to question 3 i.e. a waiting time is convenient for you, is waiting time dependent on the type of activity?
- ☐ YES ☐ NO ☐ POSSIBLY

Please explain.

PART IV : PERCEPTION OF THE IMPACT OF A REALISTIC LOOKING DIGITAL HUMAN MODEL

1. Do you think that more realistic looking DHMs will be part of the future trends of DHM's characteristics in ergonomics CAD software?
- ☐ YES ☐ NO ☐ POSSIBLY

Please explain.

2. Do you think that a realistic looking DHM would improve the accuracy of ergonomics analyses, e.g. reach and fit analysis?

☐ YES ☐ NO ☐ POSSIBLY

Please explain.

3. Do you think that a realistic looking DHM would be useful for aesthetic purposes e.g. presentations and visualisations to clients?

☐ YES ☐ NO ☐ POSSIBLY

Please explain.

4. Disregarding all other issues such as pricing, ease of use, etc., would a realistic looking DHM affect your choice of ergonomics CAD software?

☐ YES ☐ NO ☐ POSSIBLY

Please explain.

PART V : PERCEPTION OF THE IMPORTANCE OF FLESH DEFORMATION DUE TO CONTACT WITH EXTERNAL OBJECTS/LOADS

1. Do you think that flesh deformation due to contact with external objects e.g. flesh deformation on the buttocks in a sitting posture, will be part of the future trends of DHM's characteristics in ergonomics CAD software?

☐ YES ☐ NO ☐ POSSIBLY

Please explain.

2. Do you think that flesh deformation due to external forces or contact with other objects will improve the accuracy for ergonomics analysis, e.g. reach and fit analysis?

☐ YES ☐ NO

Please explain.

3. If your answer is YES to question 2, do you think that the flesh deformation should be accompanied by object deformation as well?

[] YES [] NO

Please explain.

4. Is it important that the flesh deformation, due to contact with external objects, should be implemented for the whole body?

[] YES [] NO

If your answer is YES, please explain.

If your answer is NO, which parts of the body are most important?

PART VI : PERCEPTION OF THE CHARACTERISTICS THAT DEFINE THE OVERALL QUALITY OF ERGONOMICS CAD SOFTWARE

If you have used more than one CAD ergonomics software package, what characteristics affect your judgement about the overall quality of ergonomics CAD software?

Thank you for your time!!

Your responses are very important to this research.

Contact:

Setia Hermawati

Design and Technology

Loughborough University, UK

Tel : +44 (0)1509228315

Email : s.hermawati@lboro.ac.uk

*APPENDIX B: Result of digital cross sections
parameterisation for participants for the review of the new
FDM*

UAF											
A full extension	39.5797	49.50011	55.63955	55.7712	52.9025	135 flexion	39.8847	48.35183	56.4402	58.0455	51.6633
	44.6262	50.22956	55.2385	60.5575	55.4484		44.3919	51.80329	58.4907	61.7575	54.1502
	46.6677	46.89639	50.25542	60.1201	52.1914		45.9091	50.53342	53.2543	59.5702	51.5833
	46.5392	44.51125	44.20867	55.9715	45.3997		45.6727	46.26564	46.2648	56.0891	46.8110
	46.3397	43.13367	40.67106	52.9074	41.1117		45.9204	44.12934	42.1713	52.0117	42.8745
	47.2889	40.85708	38.66513	52.3780	39.7785		48.6021	42.13665	40.8810	48.3463	40.4765
	45.7826	38.30655	38.96874	50.0756	37.5636		49.4395	40.14512	41.5333	44.8701	38.0349
	44.2649	34.29286	41.07453	43.0896	35.0374		45.3967	38.05554	40.7023	42.1463	36.2945
	38.5698	29.62025	40.75947	35.8670	33.5366		39.9482	32.62017	37.8333	39.8958	34.6439
	32.0981	26.92066	36.92553	31.2383	32.1052		34.4483	27.14536	34.9434	34.9006	32.0152
	27.1242	25.96687	33.46113	28.9974	31.3013		29.8826	24.37304	34.3135	31.4251	29.5765
	25.0526	25.19397	32.9178	28.6601	31.5249		26.9659	22.83309	33.7943	30.1349	29.1587
	25.1929	25.49316	34.35537	30.0741	32.8509		25.9471	23.39224	33.3965	30.9835	30.8639
	26.541	27.80626	38.45255	33.4207	36.0984		26.7711	26.10309	35.9974	34.1586	34.3727
	29.2484	34.39055	45.08487	39.0618	41.8829		29.5967	32.62267	41.5906	40.0902	38.5709
	33.7486	44.15087	51.29435	47.3858	48.0815		34.4454	41.70865	49.6705	48.7376	45.7788
90 flexion	40.3234	44.54719	57.09024	58.81077	53.0975	A full flexion	38.6662	32.2798	47.17094	55.41804	49.5087
	43.1643	48.08719	57.01914	63.33062	55.3986		42.0331	37.29796	48.44335	56.65598	49.3911
	44.1408	48.40798	51.37689	62.74062	52.9104		45.9294	40.21561	49.03443	58.45573	49.3327
	45.3079	47.02629	45.10781	56.61641	47.5605		48.5247	43.26008	48.81065	59.0384	47.6303
	47.8791	45.25003	40.64052	51.89744	42.3184		50.0971	47.14877	48.85565	58.03302	45.525
	51.0597	44.61685	37.69253	50.23911	39.4312		51.4433	52.05694	49.86686	57.53512	44.5936
	52.9219	45.00805	36.19334	49.77332	37.9641		54.0783	55.15368	51.51265	55.04054	44.3761
	49.5242	43.91766	36.04787	45.84011	36.3826		52.8063	53.69099	51.92189	51.4038	44.9387
	42.8243	40.23202	36.78353	38.77866	35.1936		46.6779	49.1296	49.94534	45.73246	45.3757
	37.2003	33.303	36.55158	32.84993	32.941		40.2503	41.65164	47.59975	38.92782	44.3109
	32.4837	26.77789	35.62189	28.45182	30.2713		35.3684	32.83626	45.11135	35.54139	43.3987
	29.7381	23.36616	34.91949	26.49121	29.4556		32.4651	27.11911	43.98028	34.69707	43.3527
	28.9119	22.41243	36.07012	26.98758	30.7999		31.5188	24.34787	42.99985	36.29214	44.3967
	29.697	23.66625	40.28752	30.09841	34.5486		32.2217	23.70138	42.69365	40.49474	46.3462
	31.9835	27.71388	47.27213	36.54387	40.8006		33.8148	24.83397	43.54636	46.80782	48.5269
	35.7864	35.93973	53.73463	47.07533	47.5325		35.9746	27.69724	45.45724	53.37694	49.8613

UAM											
A full extension	42.8169	50.3282	55.42372	57.7972	49.8905	135 flexion	41.2165	41.20849	53.2882	48.6550	51.3131
	44.968	53.72784	52.81383	60.3678	48.0077		43.2641	42.8872	53.6267	52.3692	49.0286
	45.453	51.36893	48.25585	59.3532	45.5551		43.1695	44.7128	49.8342	54.7607	45.4517
	44.5849	44.45781	42.80729	53.3295	40.3223		42.1371	44.66669	42.6040	52.5926	41.9733
	41.4857	36.01601	36.6032	45.5023	34.1862		42.3967	42.12227	37.4407	45.9600	40.1218
	37.571	29.79409	32.19381	38.6260	29.9085		42.2563	42.3021	35.4217	39.2863	38.6449
	33.6769	26.00494	29.97234	32.7984	28.0255		40.4366	41.09956	34.5947	32.6905	36.4581
	30.5187	23.15314	29.08795	28.7735	27.6397		37.9142	35.24147	34.3519	25.9083	34.2273
	27.9355	21.65307	28.93611	26.7790	27.1631		33.497	30.64858	33.9076	23.5701	33.3998
	25.7957	22.31978	29.03543	25.8889	27.1435		29.8802	27.19515	32.3673	23.9892	34.3606
	24.5428	24.63192	30.34323	26.5810	28.6759		27.683	25.22473	31.9607	26.4566	35.0802
	24.714	28.38691	32.9454	28.8813	31.8556		26.6372	24.77034	31.7455	30.5884	35.2718
	26.6147	31.57041	37.38759	32.2568	36.1685		26.7405	25.57289	32.8855	36.0533	36.0541
	30.0872	34.83667	44.13772	37.8429	41.0021		28.3698	28.18612	35.7377	40.9519	39.5168
	34.2477	40.92786	49.53604	45.7638	46.2167		31.7279	32.3105	41.1192	44.8174	45.1298
	38.4174	46.86116	53.61041	53.0884	49.3197		36.7244	37.09735	49.7223	46.8922	50.1943
90 flexion	36.3557	40.57915	50.53942	56.1682	52.711	A full flexion	20.9456	20.98079	37.35518	33.67977	49.5087
	40.2897	43.78543	50.54217	60.56608	52.199		23.6636	23.27297	37.90139	38.16875	49.3911
	42.565	44.2395	46.53439	59.06781	48.5559		31.8823	29.12179	39.56828	46.64934	49.3327
	43.7447	43.76241	41.66615	54.26493	43.4416		44.6221	37.20376	42.66584	54.34785	47.6303
	44.6162	43.41861	38.96045	50.24637	39.2521		48.9853	44.55459	46.42508	57.79632	45.525
	45.8595	43.40786	37.90805	45.7104	35.4641		50.8187	49.19	49.79649	57.7725	44.5936
	47.4814	43.32973	37.49033	42.05339	33.0136		51.0061	53.58661	50.89794	54.40653	44.3761
	46.1616	41.3324	37.07189	37.60156	33.2423		49.6788	52.55627	49.29626	47.38868	44.9387
	40.8739	37.91087	36.57915	31.93007	33.4824		44.8083	46.55015	49.16541	42.89037	45.3757
	34.838	30.80345	35.56984	27.25276	33.3598		38.8781	38.21427	51.41606	40.60881	44.3109
	29.7986	26.58325	35.00777	24.91191	33.5973		34.9253	31.88124	50.59073	39.70996	43.3987
	26.4329	24.57319	35.55926	24.82987	33.6105		32.9817	28.0124	49.28494	39.38698	43.3527
	24.8709	24.28733	37.55692	27.10147	34.7125		31.1153	25.97805	45.80261	39.10954	44.3967
	25.046	25.65296	41.14846	31.64531	38.1218		28.389	24.19064	42.20334	38.44241	46.3462
	26.991	29.12212	45.77232	38.29476	43.8929		24.3026	22.56962	39.41467	36.71698	48.5269
	30.9899	34.85184	49.35749	48.37729	49.9098		21.2748	21.09798	37.78098	33.78202	49.8613

E											
A full extension	28.30287	33.26593	34.57603	35.0820	33.16234	135 flexion	31.38215	35.57871	37.9257	39.8465	35.4252
	30.25548	35.79496	36.3549	36.4554	34.33664		32.85049	34.93032	39.2430	40.3044	35.4725
	34.71619	40.33049	40.71183	40.0437	37.57507		35.63748	35.93622	42.7293	41.0012	35.8986
	38.14259	43.64458	44.60605	43.6989	40.54987		37.08604	38.51247	44.0239	40.7578	37.0514
	37.50193	43.3176	44.66952	46.2854	41.75948		37.97895	39.74001	42.6452	41.0246	38.1405
	34.18297	40.30057	41.32464	46.9156	40.92705		37.22117	38.8368	40.6092	41.7039	38.2570
	29.45078	36.962	37.56999	42.0832	36.78893		35.4629	40.27708	39.3520	42.8618	37.6350
	29.32758	35.40209	36.57085	37.3859	33.72789		33.76265	38.5624	40.0320	43.1309	37.3271
	27.47342	31.29842	33.13645	33.2548	33.40779		28.68805	29.82908	37.9202	35.7400	33.5847
	23.18327	26.67513	26.1183	28.0796	33.73637		23.38591	27.21051	33.3152	33.3068	27.5062
	19.92921	24.71358	22.93907	26.9401	32.17028		22.74046	28.67399	30.6663	35.6538	25.0014
	22.6214	30.38309	29.62193	32.5355	32.7603		29.38427	33.26397	32.4366	38.8994	29.6711
	33.83145	42.21428	44.30104	46.5077	40.79611		37.59852	38.70316	39.3514	40.7492	37.6029
	40.23437	43.54708	43.83024	47.1361	44.0978		38.86933	41.01576	46.4801	42.8759	40.8426
	37.03879	38.48096	39.76903	42.3284	41.24642		36.50622	40.95581	48.4802	43.2739	39.3343
	30.44848	33.61837	35.82657	37.0866	35.89015		32.67742	37.75886	41.9464	41.2793	36.1707
90 flexion	38.24129	43.27918	46.94079	47.05771	46.63623	A full flexion	44.21448	52.54985	56.9689	49.0584	47.39202
	36.82584	38.14609	44.81418	44.02187	42.68492		41.38571	48.417	57.06679	48.9468	46.45007
	35.96863	35.55725	42.83968	41.52629	38.93375		39.52088	45.63997	54.05186	49.4957	45.53891
	35.55748	35.8368	40.80592	39.95341	37.26419		38.93205	44.57091	49.1168	50.0762	43.47263
	35.65484	38.80323	39.20769	40.76225	37.67457		37.51494	44.34585	44.31605	49.9552	39.76275
	35.93935	42.21454	39.10788	41.63639	39.84032		36.03489	47.21946	41.83279	49.5121	39.44397
	35.48453	44.84634	41.34345	42.21324	42.53285		39.4841	53.60559	44.46276	51.0116	43.21564
	37.90569	46.15706	45.37939	45.63115	45.61381		45.74994	56.46702	52.93973	52.6536	48.79686
	38.21719	42.31307	45.972	47.39716	46.21797		43.24876	51.38319	56.03005	46.8692	45.77362
	33.04465	35.10925	36.92627	41.39142	39.7261		37.82973	46.29518	53.06744	42.1055	41.63269
	30.69971	32.85078	33.42628	36.43003	36.31792		31.81004	37.77112	43.64956	36.0339	36.72385
	32.12521	34.4904	33.64948	35.89567	35.8071		30.14578	36.45185	39.75875	37.5426	33.82656
	34.89862	38.81669	37.10503	39.14787	37.54396		34.226	40.51993	43.9097	49.6449	38.57794
	37.73433	42.95999	43.04888	45.14057	40.88482		41.09882	48.16106	48.34276	52.5725	44.42135
	39.75017	46.68167	47.82549	49.55563	44.43531		45.65268	54.85514	52.06762	51.7652	47.674
	39.71261	47.03045	48.6805	49.64009	46.6765		46.55299	55.56077	54.82895	50.1556	47.73884

LAM											
A full extension	41.0946	41.57594	49.94349	54.5174	40.7759	135 flexion	37.0547	39.92015	49.0003	48.7319	40.6490
	41.3809	44.03856	49.84536	53.2305	39.141		37.3318	42.68317	49.0760	52.4757	38.0564
	41.2556	47.2462	48.30856	52.9111	38.0467		37.3448	47.11895	46.7979	54.7638	35.6940
	38.5028	46.11102	41.85145	49.9510	35.2037		35.659	49.85619	41.3420	52.4641	33.8128
	32.1732	41.04333	32.03689	44.4534	31.0455		32.8076	45.21056	35.6187	45.7522	31.1681
	23.1101	33.95005	24.09362	37.8752	26.7227		28.722	39.61741	31.5723	39.1486	28.0303
	17.7236	28.72481	19.10901	31.4843	23.6068		24.2847	34.99776	28.5989	32.4615	25.2634
	15.1595	23.08488	17.28066	25.4220	22.0213		21.567	29.85448	25.7119	25.7971	23.3306
	14.5617	19.03436	17.22004	22.4879	22.0477		20.7539	25.85015	23.3392	23.5502	22.5803
	15.5938	18.20282	17.98338	22.3610	24.4218		22.022	24.94911	23.1394	24.0306	23.7052
	18.5098	20.93245	20.44729	24.7307	29.1047		26.0671	26.60887	25.7666	26.5455	27.0873
	24.117	29.43894	28.1037	29.6286	36.5006		32.4965	32.40764	31.5961	30.7211	33.3217
	32.2739	40.92829	39.93293	36.8234	44.9046		37.0871	36.89347	39.7900	36.2023	41.8182
	38.2644	46.37572	51.42253	44.8443	49.3755		38.7708	39.20189	47.3398	41.0654	46.2312
	41.0792	44.50255	56.29419	51.6283	47.4771		38.2808	39.56045	51.3247	44.9044	46.5073
	41.3207	41.82602	52.73411	55.7042	43.7549		37.3011	38.76333	50.0589	46.9249	43.3564
90 flexion	35.5669	41.57743	51.37178	45.73355	41.9943	A full flexion	29.7472	35.75743	35.80422	36.02981	36.4303
	35.4121	43.93573	50.48232	47.26528	40.2636		33.5462	36.45837	36.30794	38.18965	36.5435
	36.8934	45.88974	47.60997	50.10014	37.1679		36.7002	40.49292	39.26254	41.82857	36.7906
	37.7186	47.25419	43.80692	53.88623	33.4022		38.9285	46.25967	43.35889	46.15115	37.9479
	36.2301	46.08561	40.48709	55.63068	29.5875		39.4747	49.23031	45.76266	49.93883	39.1427
	32.1688	41.29426	37.00918	53.91597	26.3672		35.7669	50.13936	45.65588	49.60321	35.8773
	26.6727	36.49208	32.24669	42.2222	24.4161		28.2453	41.03854	40.92308	43.46919	31.6629
	23.4295	32.02424	27.58819	32.3901	24.34		22.4842	33.13673	35.61347	38.31001	27.7474
	22.4541	27.268	25.13398	27.4362	25.4815		20.6355	30.13512	34.40166	37.76835	26.3945
	23.4085	24.72953	25.38289	25.7971	27.7684		21.6609	31.96032	36.65703	40.03768	28.5218
	26.0414	25.92848	27.85719	26.55114	31.2966		24.9727	34.23761	40.28178	44.53257	35.8779
	29.7183	30.12418	32.90771	29.5268	36.1276		29.5216	35.54779	44.75117	47.55305	42.2508
	33.3667	33.88051	40.04813	34.47071	41.0576		32.5582	37.77879	48.3515	47.97651	42.2227
	36.0663	36.91468	45.60669	38.98893	43.2447		32.0536	39.17301	48.808	42.1674	40.2974
	37.0887	39.44943	48.42936	42.29089	43.7648		29.8148	37.36748	42.32964	36.585	37.9499
	36.572	40.63765	50.65621	44.69844	43.0683		28.6169	36.22987	37.16915	35.26908	36.6871

LAF											
A full extension	33.5462	40.1356	43.74902	48.3488	29.8855	135 flexion	30.7445	35.28694	40.1518	40.9004	32.6331
	34.9228	41.4351	42.71927	49.2332	27.0465		31.8346	36.4613	41.4718	44.6762	33.2334
	36.6706	42.66523	42.63137	48.6665	24.7798		33.3446	39.39208	41.9606	48.9175	34.4651
	36.9026	42.78304	40.86658	46.6997	23.8541		34.4518	42.65265	40.5136	50.8386	35.5551
	33.4843	39.0465	36.25442	43.4316	25.2071		32.6959	44.04419	37.7616	49.7336	34.9534
	28.319	33.35962	29.8548	40.3160	27.543		29.2844	41.71914	34.6930	45.6869	30.8835
	22.9382	29.55489	25.2448	36.0704	28.9071		25.8083	35.84897	32.0778	37.8972	26.6624
	18.3686	26.5655	22.35902	30.1949	28.5904		21.434	31.70101	28.0859	31.7543	23.6216
	17.2519	25.37128	21.83567	27.5901	28.4469		20.1032	29.91596	26.1625	28.8990	22.3284
	18.2532	24.48958	23.82546	27.9202	31.1664		21.5551	29.7375	27.0454	28.2223	23.3432
	20.8299	25.99882	28.13758	30.3977	35.3084		24.891	31.4082	29.5133	29.0545	26.0008
	24.5508	30.84476	33.0141	33.8940	38.1538		27.8968	33.27836	32.4017	31.1965	28.8520
	27.9398	36.55178	39.79595	38.7030	39.3116		30.1329	34.19706	34.8832	33.5751	30.5223
	30.6751	40.08408	45.42902	41.6004	39.2304		30.9849	34.92975	37.8327	35.1203	31.2337
	32.2117	40.08595	45.77182	45.6695	36.7255		30.2791	35.86801	38.4576	36.7297	31.8960
	32.8527	39.4891	44.56388	47.3072	33.2691		30.145	35.84172	38.9945	38.4690	32.2211
90 flexion	27.9794	35.74052	38.59318	37.43596	32.8125	A full flexion	26.6149	33.20618	31.42683	33.38957	35.6966
	28.5211	37.23758	38.93456	41.62376	32.9001		30.1781	34.71812	31.74573	33.67085	35.9443
	30.2973	39.94966	39.14143	46.43186	32.9446		33.3977	37.62337	33.78208	35.60556	35.6862
	31.3817	42.8967	39.74571	51.6523	32.2291		35.2123	40.94111	36.81762	39.4487	34.8994
	31.1861	44.53086	40.09657	54.72146	30.2537		35.2356	44.94662	40.035	42.63699	34.3295
	29.5641	43.05326	38.32195	51.87007	27.2732		33.3155	45.74173	42.87158	42.97034	33.624
	26.2366	38.42249	33.62922	43.95153	24.5193		26.8681	40.81568	39.93903	40.2472	31.2451
	23.0884	33.25664	29.52951	34.90963	23.0866		21.8622	33.07867	34.93804	36.30102	28.3536
	21.6921	29.15326	28.62556	31.05982	23.0941		19.8715	30.74269	33.61614	35.45952	26.831
	22.7079	25.42337	30.02135	28.66141	24.6489		20.2698	31.78924	36.17427	37.87349	29.0053
	25.1811	24.1994	32.89385	27.37057	27.8242		23.1924	32.0718	39.49376	40.62832	33.2025
	27.7831	24.67726	35.51099	27.53232	32.2619		26.2697	33.46222	42.2696	41.9213	36.9208
	29.7831	26.1641	36.35402	28.55655	33.7556		27.6215	33.19866	43.23632	41.85896	38.6482
	30.4679	29.09911	35.92523	30.13075	33.4116		27.073	33.56655	40.06256	40.63227	37.918
	29.8129	32.99582	35.95269	31.68581	32.827		25.5983	33.43827	35.9836	37.16247	35.8947
	28.6492	34.82504	37.25042	33.95098	32.6425		25.2168	33.10299	32.85089	34.42105	35.1727

APPENDIX C: Distances between points along profiles and bones for the participants for the review of the new FDM

	(mm)			
	Full extension	135°	90°	Maximum flexion
Participant 1	41.3508	42.7562	45.6706	48.3861
	36.3665	39.8202	44.0215	47.6969
	34.0656	38.4611	43.2618	47.3259
	30.3415	36.181	42.0219	46.6715
	23.3626	28.8322	34.8878	38.975
	21.9174	27.2649	33.1402	36.794
	20.2941	25.7042	31.1591	34.3621
	15.8753	22.4369	26.1574	28.4375
	12.6816	19.4375	21.3125	20.4025
	12.5028	18.7901	20.2956	17.7345
	12.3365	18.2698	19.7462	16.1019
	12.1817	17.8391	19.5204	15.4062
	12.0475	17.5024	19.3828	15.4682
	11.9279	17.2818	19.1056	16.1816
	11.8178	17.138	18.753	17.4136
	11.7168	17.0985	18.5139	18.8579
	11.634	17.1694	18.5795	20.2558
	10.8753	17.8593	19.9339	21.779
	10.7782	18.0419	20.4601	21.5041
	11.0159	18.098	20.7708	21.9637
	11.9958	18.3348	21.2173	23.8414
	12.5151	18.5512	21.4437	24.4663
	14.0124	19.5805	22.4911	24.7461
	15.2742	20.2477	22.4698	24.5451
	16.2466	20.4727	22.2663	24.4271
	17.3844	20.4126	21.6077	24.1718
Participant 2	29.5789	39.2628	46.0484	51.7267
	24.2744	34.9937	44.2118	50.9076
	22.2917	33.0784	43.3228	50.5217
	19.745	30.0365	41.8577	49.9175
	17.1798	22.7709	33.2607	40.8437
	16.8098	21.449	31.2586	38.896
	16.3972	20.2147	29.1826	37.0486
	15.4116	18.0734	24.8267	33.4436
	15.2023	17.1188	21.7864	29.5583
	15.2176	17.0805	21.5704	28.7513
	15.2392	17.1087	21.9104	28.3375
	15.2671	17.2147	22.7903	28.3862
	15.3015	17.4088	24.1353	28.9766
	15.3497	17.6768	25.759	30.2873
	15.4067	18.0186	27.3351	32.2919
	15.4704	18.4362	28.769	33.6238
	15.5411	18.9489	30.0841	33.339
	16.9337	21.8075	32.3497	32.3449
	18.1859	23.0067	32.5374	33.415
	19.0855	23.471	32.3737	34.9011
	19.9577	23.3326	32.135	37.9175
	20.0962	23.1382	32.4792	39.2743
	20.6259	22.969	33.9803	39.3054

	(mm)			
	Full extension	135°	90°	Maximum flexion
	21.6897	23.9711	34.0736	38.6417
	22.3854	24.6584	34.0727	38.2904
	23.908	25.9629	33.9538	37.5625
Participant 3	41.3373	44.1249	45.9579	50.3159
	35.0512	41.1019	44.631	49.5843
	32.4779	39.7303	43.8893	49.1491
	28.3347	37.282	42.5944	48.35
	22.7195	27.5345	36.2336	40.081
	22.2029	25.5634	34.6958	38.0167
	21.0875	23.8867	32.7656	35.9148
	14.9598	21.8997	27.6601	30.5517
	13.9773	21.6721	23.6213	22.2591
	13.9902	21.7831	23.1539	20.1561
	14.0046	21.9429	23.0165	19.0858
	14.0203	22.1304	23.139	18.8187
	14.0376	22.3199	23.4455	19.2625
	14.0563	22.4819	23.821	20.4432
	14.0764	22.5564	24.0834	22.3396
	14.0981	22.5961	24.0346	24.6942
	14.1254	22.643	23.8128	26.1891
	15.2909	22.5794	23.33	26.5326
	15.683	21.8667	22.8667	26.2923
	14.9762	21.1781	22.6354	26.7393
	13.8357	21.0424	23.2199	30.0629
	14.1683	21.4314	23.9569	31.7215
	16.1791	23.3949	26.7789	33.7838
	18.5085	24.4462	27.5432	33.5494
	19.6286	24.8911	27.8401	33.3644
	21.5056	25.7115	28.2541	32.8946
Participant 4	41.0328	44.3335	45.1887	48.3813
	34.5872	41.0651	43.046	46.3441
	32.2756	39.5916	42.1348	45.3781
	29.497	37.248	40.6902	43.789
	25.1253	28.4956	31.4894	33.9401
	24.022	26.3168	28.9825	31.5857
	22.7178	24.1148	26.22	29.115
	18.1292	19.9674	19.8114	23.3983
	14.7893	16.894	15.162	16.7837
	14.5972	16.4379	14.5699	15.5157
	14.4284	16.0723	14.245	14.9988
	14.2732	15.7999	14.1862	15.1024
	14.1309	15.6145	14.3355	15.8572
	14.0111	15.5145	14.6876	17.3082
	13.9117	15.5006	15.2578	19.6129
	13.8232	15.5741	16.035	22.9768
	13.7452	15.7385	17.0291	27.2154
	13.342	16.8902	20.3746	32.0674
	13.8934	17.2877	20.9459	31.7012
	15.3891	17.6745	21.5453	31.5998
	18.8532	19.1694	23.6139	34.5083
	19.8711	20.2914	24.9645	36.2488
	22.5102	23.8957	30.0336	37.831

	(mm)			
	Full extension	135°	90°	Maximum flexion
	25.6806	25.5785	31.2255	37.1712
	27.1624	26.3856	31.5904	36.6933
	28.9528	27.7768	31.7764	35.456
Participant 5	39.3813	42.5854	45.5618	46.81
	34.6141	40.1714	44.5785	46.4383
	32.7791	39.1111	44.1081	46.2265
	30.4379	37.4562	43.3121	45.8077
	28.2235	31.5079	36.5907	39.6533
	27.7933	30.0453	34.5794	37.5623
	27.1796	28.5808	32.3195	35.0949
	24.8252	25.4329	27.1173	28.5677
	21.9588	22.8955	22.9769	21.9626
	21.5356	22.4296	22.2585	20.8377
	21.1446	22.0811	22.0153	20.5695
	20.7836	21.8415	22.1635	20.9483
	20.4547	21.6562	22.621	21.8986
	20.1574	21.5701	23.2125	23.3493
	19.8908	21.5457	23.7318	24.9203
	19.6646	21.6046	24.187	25.9597
	19.4587	21.731	24.6776	26.5853
	18.8455	22.4773	26.2033	27.3393
	19.5997	22.322	26.255	27.2062
	20.2229	21.9234	26.1239	27.5119
	20.2485	21.753	26.0859	29.0503
	20.3709	22.0237	26.2174	29.9465
	21.5448	23.9174	26.5866	31.9001
	23.4278	25.0209	25.8342	31.6455
	24.1241	25.205	25.2393	31.3742
	24.1775	24.7967	23.6352	30.5489

*APPENDIX D: Result of digital cross sections
parameterisation for participants for the review of the
framework*

UAF Asian Female													
A full extension	63.3552	52.9025	39.5797	40.3081	43.4182	44.8026	135 flexion	63.3866	51.6633	39.8847	43.5997	44.6406	45.2257
	58.7947	55.4484	44.6262	45.1886	42.4509	47.5678		60.1241	54.1502	44.3919	44.9607	43.6427	46.738
	54.2829	52.1914	46.6677	46.7294	39.6929	46.7221		55.0972	51.5833	45.9091	45.5599	40.4502	45.1965
	51.5648	45.3997	46.5392	46.9369	36.8504	44.0885		51.6292	46.8110	45.6727	46.5845	37.9066	43.2028
	51.3225	41.1117	46.3397	47.1937	36.3229	41.9886		51.1209	42.8745	45.9204	48.1182	37.2233	42.2228
	54.9464	39.7785	47.2889	49.3644	36.4212	39.8132		54.4292	40.4765	48.6021	48.382	38.3552	40.7499
	60.8689	37.5636	45.7826	50.7171	36.1349	38.3418		58.7668	38.0349	49.4395	48.3891	39.8336	39.8726
	59.0546	35.0374	44.2649	47.0454	36.5907	37.3203		61.6148	36.2945	45.3967	46.6175	39.1847	37.0509
	58.1587	33.5366	38.5698	42.7999	34.8169	32.5657		59.1829	34.6439	39.9482	40.2506	37.3787	33.056
	58.4123	32.1052	32.0981	37.2581	31.2799	28.2308		56.7038	32.0152	34.4483	33.0463	34.588	28.1555
	54.1963	31.3013	27.1242	30.791	29.8496	25.6004		56.0824	29.5765	29.8826	28.159	30.7105	26.1067
	49.1023	31.5249	25.0526	26.6735	29.9179	24.937		52.7816	29.1587	26.9659	25.5626	28.4975	25.1806
	48.3450	32.8509	25.1929	25.2927	31.1691	26.0156		51.1388	30.8639	25.9471	25.1952	28.7947	25.6321
	51.2219	36.0984	26.541	26.0991	33.622	28.5888		53.2597	34.3727	26.7711	27.0901	31.5572	28.2441
	56.0982	41.8829	29.2484	28.983	37.4062	32.9032		57.6279	38.5709	29.5967	31.5549	36.6008	33.6221
	61.3851	48.0815	33.7486	33.9207	41.2022	39.2996		62.1897	45.7788	34.4454	38.7348	42.1254	40.0055
90 flexion	58.5352	53.0975	40.3234	40.7224	42.1786	44.2594	A full flexion	59.6195	49.5087	38.6662	38.813	33.6774	43.0775
	58.2486	55.3986	43.1643	45.4513	42.0741	45.5246		57.7213	49.3911	42.0331	39.5784	34.2043	43.1446
	55.308	52.9104	44.1408	48.2694	39.7052	44.6783		56.0187	49.3327	45.9294	41.2684	35.9209	42.6125
	52.6423	47.5605	45.3079	49.2697	37.5132	43.1943		55.5842	47.6303	48.5247	43.755	38.2919	42.194
	52.719	42.3184	47.8791	50.4328	37.0592	43.2011		57.05	45.525	50.0971	45.4211	40.6495	43.6605
	57.8135	39.4312	51.0597	52.5279	37.9978	44.0237		60.7906	44.5936	51.4433	47.3569	42.905	43.7569
	64.7063	37.9641	52.9219	53.9059	40.2189	43.4556		66.1682	44.3761	54.0783	50.6578	46.5126	43.9974
	67.812	36.3826	49.5242	50.5666	41.238	42.6895		71.0447	44.9387	52.8063	53.779	47.7349	45.0129
	65.6673	35.1936	42.8243	44.6505	39.2932	37.8822		72.9457	45.3757	46.6779	51.1397	45.955	41.9252
	60.4358	32.941	37.2003	34.4651	36.2827	31.5269		71.482	44.3109	40.2503	45.8943	43.8551	37.1816
	54.3284	30.2713	32.4837	27.0252	33.6272	27.1643		67.5994	43.3987	35.3684	43.7909	41.964	33.7489
	49.6838	29.4556	29.7381	23.2795	31.6809	24.9003		63.4919	43.3527	32.4651	41.5802	38.3134	32.2852
	47.1224	30.7999	28.9119	22.3947	31.4795	24.834		62.4555	44.3967	31.5188	38.3326	35.699	32.8147
	47.1087	34.5486	29.697	23.9382	33.3768	27.1062		62.8852	46.3462	32.2217	36.2202	34.5904	34.9811
	49.8128	40.8006	31.9835	27.8148	37.086	31.9734		62.4377	48.5269	33.8148	35.9234	34.4532	38.2142
	54.9148	47.5325	35.7864	33.7762	40.3509	38.7193		61.1791	49.8613	35.9746	37.4383	34.1127	41.6062

UAM Asian Female													
A full extension	62.9549	49.8905	42.8169	41.8255	44.5255	47.7512	135 flexion	59.1911	51.3131	41.2165	41.5702	44.3512	46.4
	62.3797	48.0077	44.968	48.7638	43.7987	47.1886		58.3134	49.0286	43.2641	48.0151	43.0886	45.5308
	59.9503	45.5551	45.453	53.046	40.6887	43.311		56.0554	45.4517	43.1695	51.8325	39.3472	42.9604
	56.2481	40.3223	44.5849	53.182	34.4682	38.2263		53.6077	41.9733	42.1371	52.6172	35.4034	39.6842
	52.3276	34.1862	41.4857	52.3274	28.7887	32.3951		52.3411	40.1218	42.3967	50.9603	33.3332	37.0818
	48.0008	29.9085	37.571	49.2472	24.8275	27.7968		52.4462	38.6449	42.2563	50.1753	33.2763	34.8425
	43.6951	28.0255	33.6769	43.1383	22.8795	24.6565		52.2453	36.4581	40.4366	46.1855	33.843	32.4281
	41.6854	27.6397	30.5187	36.7986	22.7973	22.4927		50.6134	34.2273	37.9142	38.9459	32.9785	29.5613
	41.5281	27.1631	27.9355	31.3577	24.2856	20.9271		48.6563	33.3998	33.497	31.7404	32.2224	26.7177
	42.7751	27.1435	25.7957	25.6164	26.2369	19.6467		46.8908	34.3606	29.8802	25.7526	32.0608	23.915
	43.5872	28.6759	24.5428	21.8394	27.4762	19.4503		45.9657	35.0802	27.683	21.6156	31.4231	22.222
	43.8772	31.8556	24.714	20.0845	28.676	21.0618		46.1129	35.2718	26.6372	19.6	30.4766	22.2634
	45.5566	36.1685	26.6147	20.1075	31.7076	24.937		47.5904	36.0541	26.7405	19.4109	30.7766	24.1638
	50.2624	41.0021	30.0872	21.9982	37.072	30.9094		50.2219	39.5168	28.3698	21.1043	32.891	28.2238
	57.4367	46.2167	34.2477	26.2466	41.5777	37.5881		53.7177	45.1298	31.7279	25.2733	36.908	34.7867
	61.2514	49.3197	38.4174	33.4502	44.5842	43.0949		57.2551	50.1943	36.7244	32.6941	42.011	43.0742
90 flexion	56.3767	52.711	36.3557	38.2616	41.9353	42.1559	A full flexion	38.9188	49.5087	20.9456	20.1389	24.0649	26.9483
	56.5646	52.199	40.2897	43.8901	41.9058	42.6891		40.3746	49.3911	23.6636	22.8446	25.3276	28.2444
	55.1651	48.5559	42.565	47.5612	39.4116	40.8927		43.5993	49.3327	31.8823	28.3586	27.7603	32.2086
	54.0401	43.4416	43.7447	47.7049	36.6919	38.8378		49.9013	47.6303	44.6221	37.0708	31.7476	37.7736
	54.412	39.2521	44.6162	48.3255	35.4086	38.5841		57.641	45.525	48.9853	46.3239	38.0004	42.2312
	56.6966	35.4641	45.8595	51.9816	35.5848	37.9913		64.2263	44.5936	50.8187	51.4982	42.98	42.7506
	58.2642	33.0136	47.4814	53.0017	36.8384	35.6472		68.2111	44.3761	51.0061	55.2532	42.8911	42.5325
	57.8078	33.2423	46.1616	47.3659	37.4962	33.9212		67.8419	44.9387	49.6788	53.0515	43.0564	40.8138
	55.7616	33.4824	40.8739	39.8114	36.3769	33.6706		65.9364	45.3757	44.8083	49.0205	43.2303	39.6276
	52.2741	33.3598	34.838	30.9157	34.1808	30.9509		65.1357	44.3109	38.8781	47.8252	43.7185	39.0807
	47.9987	33.5973	29.7986	24.8627	32.1993	27.2701		63.7556	43.3987	34.9253	44.2479	43.0149	37.3803
	44.9035	33.6105	26.4329	21.202	30.7024	25.4835		59.6149	43.3527	32.9817	36.7425	40.0761	35.942
	43.7484	34.7125	24.8709	19.8939	30.542	25.4104		53.1015	44.3967	31.1153	29.5125	36.0768	34.1915
	45.0635	38.1218	25.046	20.8677	32.1686	27.1673		46.4244	46.3462	28.389	23.9891	32.3899	32.04
	48.6879	43.8929	26.991	24.6286	35.4772	31.4617		41.5341	48.5269	24.3026	20.7442	28.1604	29.6867
	53.2314	49.9098	30.9899	31.2839	39.1987	37.5664		39.0776	49.8613	21.2748	19.5221	24.9635	27.7413

E Asian Female													
A full extension	43.6265	33.16234	28.30287	31.58018	32.53596	28.55176	135 flexion	44.8596	35.4252	31.38215	33.90832	35.19522	33.177
	44.7190	34.33664	30.25548	32.87977	32.90452	29.69989		46.0287	35.4725	32.85049	34.87242	34.39937	32.29817
	48.8698	37.57507	34.71619	37.35965	34.83669	34.28896		49.1769	35.8986	35.63748	37.18884	33.83732	32.7121
	52.7575	40.54987	38.14259	41.34999	37.23017	37.7719		52.5202	37.0514	37.08604	39.97287	33.91562	34.211
	53.9672	41.75948	37.50193	41.05459	37.54473	37.55699		53.0299	38.1405	37.97895	41.93074	35.06303	34.4895
	54.1787	40.92705	34.18297	36.52562	34.2486	34.01847		49.7784	38.2570	37.22117	41.22499	35.9081	33.63067
	49.2430	36.78893	29.45078	34.08384	32.18582	30.19754		46.7219	37.6350	35.4629	37.87171	36.50904	33.31056
	46.5220	33.72789	29.32758	32.99569	32.88503	29.23569		45.7483	37.3271	33.76265	36.87963	37.15498	35.52579
	42.3558	33.40779	27.47342	31.36547	32.10851	27.68533		43.4670	33.5847	28.68805	29.33638	33.03614	29.8898
	37.3803	33.73637	23.18327	28.63254	27.47619	23.7945		35.9880	27.5062	23.38591	25.23031	26.44505	26.51089
	34.0699	32.17028	19.92921	26.03424	23.95546	23.2865		38.8620	25.0014	22.74046	26.61757	24.48078	27.2396
	38.5091	32.7603	22.6214	31.33039	27.13306	28.29595		47.8163	29.6711	29.38427	32.92485	27.60611	30.83428
	50.6977	40.79611	33.83145	40.41127	36.44491	37.34492		53.1881	37.6029	37.59852	40.73866	33.19098	34.24456
	56.8380	44.0978	40.23437	43.01034	39.23269	38.4179		53.1924	40.8426	38.86933	42.11563	37.95497	35.689
90 flexion	53.3913	41.24642	37.03879	38.71563	36.8455	35.01974	A full flexion	49.5872	39.3343	36.50622	39.41041	38.33032	34.986
	46.8628	35.89015	30.44848	33.84754	33.99873	30.79111		46.0001	36.1707	32.67742	35.30771	36.51296	34.16034
	48.35246	46.63623	38.24129	43.84171	43.16001	37.21261		55.66811	47.39202	44.21448	48.08351	43.99584	41.78844
	46.58469	42.68492	36.82584	40.27815	41.44677	35.43293		54.65936	46.45007	41.38571	45.86415	43.65448	38.9516
	46.10054	38.93375	35.96863	37.30145	37.86459	34.43198		54.80461	45.53891	39.52088	44.32913	43.04257	37.35139
	47.33097	37.26419	35.55748	36.07794	34.94305	35.15904		56.31731	43.47263	38.93205	44.07169	42.18568	36.89171
	48.76173	37.67457	35.65484	36.67773	33.93119	35.4801		59.30865	39.76275	37.51494	45.1544	41.26766	37.0868
	48.96775	39.84032	35.93935	38.84454	34.02396	35.05022		60.3676	39.44397	36.03489	45.68153	41.53512	37.50553
	47.2215	42.53285	35.48453	40.91891	35.17707	34.3449		58.12566	43.21564	39.4841	46.90906	45.73826	40.42493
	48.78487	45.61381	37.90569	44.11146	39.13237	36.19915		57.07221	48.79686	45.74994	49.09596	47.44812	44.36954
	48.29794	46.21797	38.21719	43.54543	42.47106	36.6673		53.75631	45.77362	43.24876	47.56616	42.0141	41.23042
	44.46392	39.7261	33.04465	38.91059	36.25509	32.49429		46.12735	41.63269	37.82973	41.37672	37.6792	38.18209
	43.13123	36.31792	30.69971	36.54857	33.36318	30.89002		43.21532	36.72385	31.81004	34.42409	31.34231	32.58028
	45.01982	35.8071	32.12521	35.80602	32.401	31.77412		49.61174	33.82656	30.14578	33.25551	33.65513	29.37672
	48.61159	37.54396	34.89862	36.74062	33.40466	34.36546		57.79067	38.57794	34.226	41.42076	40.63332	32.91307
	50.61351	40.88482	37.73433	39.80154	36.32086	37.43939		63.03936	44.42135	41.09882	49.39635	43.3286	40.24001
	51.19499	44.43531	39.75017	44.40313	40.16045	38.99672		61.32583	47.674	45.65268	52.58949	43.24535	45.14865
	50.49339	46.6765	39.71261	45.62524	43.08531	38.54362		57.81856	47.73884	46.55299	50.53784	43.67616	44.71589

LAM Asian Female													
A full extension	55.9348	40.7759	41.0946	42.8108	46.1044	43.4992	135 flexion	47.3554	40.6490	37.0547	40.767	37.2959	36.8249
	56.6106	39.141	41.3809	46.5638	42.1946	42.1935		50.1783	38.0564	37.3318	41.7314	35.9489	36.2597
	54.6966	38.0467	41.2556	50.0748	37.8828	39.4192		52.3234	35.6940	37.3448	43.7046	35.0334	37.0646
	49.1452	35.2037	38.5028	49.4995	33.5332	33.5113		53.3578	33.8128	35.659	45.2096	34.0824	36.8693
	42.7794	31.0455	32.1732	44.1669	28.0508	25.7939		50.2287	31.1681	32.8076	45.8934	32.4085	33.3565
	36.2259	26.7227	23.1101	36.2997	22.6563	20.0867		44.3671	28.0303	28.722	42.1231	29.8442	29.3426
	29.5321	23.6068	17.7236	29.8601	19.5305	16.1821		38.3535	25.2634	24.2847	34.0382	26.6647	25.9455
	24.6371	22.0213	15.1595	24.9611	18.3356	14.1601		33.6462	23.3306	21.567	28.7234	25.3812	23.7803
	22.6872	22.0477	14.5617	20.1147	18.4683	13.6609		31.1183	22.5803	20.7539	27.1634	24.8558	22.9322
	23.6796	24.4218	15.5938	16.786	19.8295	14.6151		30.8088	23.7052	22.022	27.9299	25.1608	23.6585
	28.1503	29.1047	18.5098	16.4463	23.0932	17.5123		32.6986	27.0873	26.0671	29.4422	27.6464	26.2305
	35.9565	36.5006	24.117	18.8965	29.4892	23.7287		35.9429	33.3217	32.4965	31.4165	32.458	30.0989
	45.7019	44.9046	32.2739	24.4882	38.3241	34.0696		39.3952	41.8182	37.0871	33.603	37.2739	34.2596
	53.3601	49.3755	38.2644	32.4421	46.7052	44.9829		41.7621	46.2312	38.7708	36.3164	40.665	37.1012
	56.8414	47.4771	41.0792	38.917	50.0877	47.0817		43.2790	46.5073	38.2808	38.9393	40.8768	38.2243
90 flexion	56.8565	43.7549	41.3207	41.6219	49.2417	45.4389	A full flexion	44.8204	43.3564	37.3011	40.3813	39.2588	37.7141
	47.117	41.9943	35.5669	39.4167	31.1082	31.4019		39.807	36.4303	29.7472	31.1773	18.5336	19.5858
	46.1366	40.2636	35.4121	42.0389	30.5489	30.9876		43.5212	36.5435	33.5462	36.7373	19.0302	22.4772
	46.7831	37.1679	36.8934	46.7922	30.575	31.4514		47.5919	36.7906	36.7002	42.1931	21.0405	28.06
	47.4547	33.4022	37.7186	50.1949	31.4266	32.3428		52.0222	37.9479	38.9285	44.5859	24.6948	34.4212
	44.2534	29.5875	36.2301	50.0144	33.3112	33.1923		54.6312	39.1427	39.4747	45.9725	30.275	39.2087
	40.045	26.3672	32.1688	46.6893	33.7183	32.0678		53.7913	35.8773	35.7669	44.9393	35.253	41.3332
	36.1207	24.4161	26.6727	39.3162	31.9931	30.0231		48.1431	31.6629	28.2453	39.4189	35.9307	39.7006
	31.8971	24.34	23.4295	32.7888	30.0482	28.0746		43.4802	27.7474	22.4842	32.5805	36.0406	37.4408
	30.029	25.4815	22.4541	29.5514	30.0666	27.5338		42.2874	26.3945	20.6355	30.4269	35.5173	36.7062
	31.3056	27.7684	23.4085	28.9113	31.1474	28.8604		44.9145	28.5218	21.6609	31.0093	38.492	37.676
	34.5149	31.2966	26.0414	29.0688	32.5282	31.8345		51.143	35.8779	24.9727	32.6781	44.1443	39.134
	38.6864	36.1276	29.7183	29.7454	34.0072	35.5067		51.7762	42.2508	29.5216	33.7807	49.1377	38.4383
	43.041	41.0576	33.3667	30.9603	35.2026	39.016		44.9283	42.2227	32.5582	32.8614	47.6769	32.5905
	46.574	43.2447	36.0663	32.6836	35.4862	39.864		38.0137	40.2974	32.0536	30.6901	37.199	25.5274
	48.5109	43.7648	37.0887	34.8615	34.4895	36.8092		35.6582	37.9499	29.8148	28.8542	26.0801	20.759
	48.7943	43.0683	36.572	37.1391	32.6163	33.5229		36.5041	36.6871	28.6169	28.6049	20.2236	19.0051

LAF Asian Female													
A full extension	41.0889	29.8855	33.5462	34.0957	37.0077	35.2344	135 flexion	34.6881	32.6331	30.7445	32.5445	28.873	31.6243
	41.3938	27.0465	34.9228	37.0921	35.5221	33.7357		37.6072	33.2334	31.8346	34.892	29.4833	31.3056
	42.1596	24.7798	36.6706	40.5676	33.7829	32.5728		42.6448	34.4651	33.3446	38.3631	31.052	30.9027
	42.1188	23.8541	36.9026	43.0702	31.3235	31.3769		47.3437	35.5551	34.4518	41.0466	31.419	30.6023
	40.1440	25.2071	33.4843	45.0836	27.8103	28.7424		47.2360	34.9534	32.6959	41.928	30.761	30.1138
	36.8775	27.543	28.319	40.0198	24.2712	24.6794		42.3434	30.8835	29.2844	41.3938	30.1266	28.8033
	33.2772	28.9071	22.9382	33.3109	22.1165	20.9646		36.1362	26.6624	25.8083	35.9788	29.0642	25.8598
	30.4106	28.5904	18.3686	29.5077	21.2193	18.6334		32.2564	23.6216	21.434	30.7558	27.2677	23.3586
	28.8438	28.4469	17.2519	27.664	21.3146	18.039		30.8119	22.3284	20.1032	28.9464	25.6768	23.2637
	28.7326	31.1664	18.2532	25.8463	22.6009	19.6314		31.1003	23.3432	21.5551	28.7368	25.8187	24.8111
	30.1659	35.3084	20.8299	24.8894	25.1936	24.201		32.6135	26.0008	24.891	29.2232	27.7853	27.4028
	33.0429	38.1538	24.5508	25.3646	28.9352	30.5802		34.4042	28.8520	27.8968	30.0021	30.1416	30.1296
	36.0321	39.3116	27.9398	26.509	32.9425	33.6745		35.4207	30.5223	30.1329	30.895	31.035	32.2315
	38.8412	39.2304	30.6751	28.0058	35.8102	35.4975		35.8293	31.2337	30.9849	31.7337	30.8758	32.457
	41.8739	36.7255	32.2117	29.7588	36.9388	36.4485		35.0962	31.8960	30.2791	31.5207	30.0564	32.1333
	42.2641	33.2691	32.8527	31.7533	37.4428	36.3733		34.2424	32.2211	30.145	31.4177	29.2143	31.931
90 flexion	37.9754	32.8125	27.9794	29.9345	24.0649	26.4108	A full flexion	32.0354	35.6966	26.6149	28.3889	17.9978	18.4084
	39.4145	32.9001	28.5211	34.7359	24.465	27.2734		34.5287	35.9443	30.1781	34.8687	17.6761	20.8267
	41.5247	32.9446	30.2973	41.4364	26.1523	28.6843		38.4436	35.6862	33.3977	41.2393	19.034	25.1026
	41.5025	32.2291	31.3817	47.3402	28.7851	30.0353		42.9621	34.8994	35.2123	43.699	21.8577	30.0084
	39.0424	30.2537	31.1861	50.3717	31.4254	29.9184		46.5892	34.3295	35.2356	43.7073	26.0211	34.2138
	35.2779	27.2732	29.5641	47.2264	32.9179	29.0896		47.1916	33.624	33.3155	42.1566	30.5102	36.9057
	31.9539	24.5193	26.2366	39.7626	30.8634	28.2669		44.1311	31.2451	26.8681	35.311	34.0601	36.615
	29.8603	23.0866	23.0884	31.8271	29.4537	27.6759		38.6811	28.3536	21.8622	29.0716	35.5632	34.7757
	29.4526	23.0941	21.6921	28.7182	29.9583	27.7959		36.8353	26.831	19.8715	26.2926	34.96	33.5829
	31.0011	24.6489	22.7079	28.2462	31.8671	29.1181		39.2084	29.0053	20.2698	25.5428	37.8736	33.4058
	33.928	27.8242	25.1811	28.0037	33.6756	31.9539		42.1672	33.2025	23.1924	25.4546	42.3984	32.6739
	36.7595	32.2619	27.7831	27.231	33.7117	33.8805		42.6415	36.9208	26.2697	26.1093	43.3061	30.7248
	39.1227	33.7556	29.7831	26.4621	32.1994	33.0091		41.9268	38.6482	27.6215	27.1083	39.2691	27.3902
	40.805	33.4116	30.4679	26.787	29.994	30.4527		37.6283	37.918	27.073	26.2225	32.8026	22.3473
	39.6362	32.827	29.8129	27.5669	27.511	27.9536		33.1323	35.8947	25.5983	24.7068	25.8638	19.0162
	38.1938	32.6425	28.6492	28.0828	25.1768	26.5651		31.4095	35.1727	25.2168	25.1676	20.5091	17.8445

UAF Asian Male											
A full extension	55.7712	55.63955	43.26953	53.65218	49.50011	135 flexion	58.0455	56.4402	42.26707	52.16558	48.35183
	60.5575	55.2385	48.68945	55.71532	50.22956		61.7575	58.4907	47.3568	54.2835	51.80329
	60.1201	50.25542	51.00618	52.82641	46.89639		59.5702	53.2543	47.59948	50.1845	50.53342
	55.9715	44.20867	49.29173	45.63886	44.51125		56.0891	46.2648	45.9615	44.44744	46.26564
	52.9074	40.67106	45.16949	40.12073	43.13367		52.0117	42.1713	44.59751	41.19514	44.12934
	52.3780	38.66513	40.64458	37.13202	40.85708		48.3463	40.8810	44.6314	40.58	42.13665
	50.0756	38.96874	36.15535	35.65734	38.30655		44.8701	41.5333	43.49351	40.05252	40.14512
	43.0896	41.07453	31.44485	31.32171	34.29286		42.1463	40.7023	40.56425	38.65168	38.05554
	35.8670	40.75947	27.59313	27.91006	29.62025		39.8958	37.8333	36.03707	36.26139	32.62017
	31.2383	36.92553	24.08563	26.39379	26.92066		34.9006	34.9434	30.61298	33.06215	27.14536
	28.9974	33.46113	21.53334	25.56247	25.96687		31.4251	34.3135	26.85263	30.18093	24.37304
	28.6601	32.9178	20.41046	26.40756	25.19397		30.1349	33.7943	24.88562	29.03837	22.83309
	30.0741	34.35537	20.77895	29.08357	25.49316		30.9835	33.3965	24.41638	31.0822	23.39224
	33.4207	38.45255	22.85201	33.07057	27.80626		34.1586	35.9974	25.32364	34.85772	26.10309
	39.0618	45.08487	27.11746	38.52927	34.39055		40.0902	41.5906	28.27976	40.01025	32.62267
	47.3858	51.29435	34.27102	46.38782	44.15087		48.7376	49.6705	34.08196	47.33287	41.70865
90 flexion	58.81077	57.09024	38.09956	52.75838	44.54719	A full flexion	55.41804	47.17094	37.51497	42.72645	32.2798
	63.33062	57.01914	46.8498	51.4309	48.08719		56.65598	48.44335	40.05237	42.09533	37.29796
	62.74062	51.37689	50.45707	47.1686	48.40798		58.45573	49.03443	42.2141	41.17449	40.21561
	56.61641	45.10781	50.58004	44.0154	47.02629		59.0384	48.81065	44.11621	40.84678	43.26008
	51.89744	40.64052	48.98882	41.19385	45.25003		58.03302	48.85565	47.74778	42.07449	47.14877
	50.23911	37.69253	46.43534	39.64154	44.61685		57.53512	49.86686	52.14814	45.2688	52.05694
	49.77332	36.19334	46.36992	39.40119	45.00805		55.04054	51.51265	54.92067	48.38641	55.15368
	45.84011	36.04787	44.95238	39.01117	43.91766		51.4038	51.92189	53.606	48.33247	53.69099
	38.77866	36.78353	38.43217	37.88799	40.23202		45.73246	49.94534	48.85524	46.69633	49.1296
	32.84993	36.55158	32.27875	35.69109	33.303		38.92782	47.59975	40.11986	43.7173	41.65164
	28.45182	35.62189	27.84662	31.30346	26.77789		35.54139	45.11135	33.12446	39.94859	32.83626
	26.49121	34.91949	24.86621	28.6615	23.36616		34.69707	43.98028	29.10554	37.19379	27.11911
	26.98758	36.07012	23.29749	28.9009	22.41243		36.29214	42.99985	27.48512	36.60885	24.34787
	30.09841	40.28752	23.66009	31.70287	23.66625		40.49474	42.69365	28.1994	37.69873	23.70138
	36.54387	47.27213	26.56624	38.74296	27.71388		46.80782	43.54636	30.84048	38.96463	24.83397
	47.07533	53.73463	31.10263	47.66105	35.93973		53.37694	45.45724	34.15772	40.80417	27.69724

UAM Asian Male											
A full extension	57.7972	55.42372	46.33686	52.65467	50.3282	135 flexion	48.6550	53.2882	44.03234	49.57948	41.20849
	60.3678	52.81383	49.63541	51.43255	53.72784		52.3692	53.6267	47.41186	49.80788	42.8872
	59.3532	48.25585	49.45608	48.56641	51.36893		54.7607	49.8342	47.38151	46.12072	44.7128
	53.3295	42.80729	46.978	42.80685	44.45781		52.5926	42.6040	44.00822	42.83909	44.66669
	45.5023	36.6032	41.84219	34.33888	36.01601		45.9600	37.4407	40.61028	37.70301	42.12227
	38.6260	32.19381	35.12766	27.21931	29.79409		39.2863	35.4217	37.58955	34.61973	42.3021
	32.7984	29.97234	28.38951	25.40258	26.00494		32.6905	34.5947	34.30391	32.4159	41.09956
	28.7735	29.08795	23.43979	25.57514	23.15314		25.9083	34.3519	30.85758	31.09679	35.24147
	26.7790	28.93611	20.2862	25.14907	21.65307		23.5701	33.9076	26.17825	30.78695	30.64858
	25.8889	29.03543	17.99212	25.01919	22.31978		23.9892	32.3673	23.17427	28.61913	27.19515
	26.5810	30.34323	17.46582	26.07913	24.63192		26.4566	31.9607	21.56775	26.58135	25.22473
	28.8813	32.9454	18.96419	29.12719	28.38691		30.5884	31.7455	22.09678	27.16863	24.77034
	32.2568	37.38759	22.67003	34.6078	31.57041		36.0533	32.8855	24.00614	29.58636	25.57289
	37.8429	44.13772	28.51684	41.67959	34.83667		40.9519	35.7377	27.20807	33.75418	28.18612
90 flexion	45.7638	49.53604	34.53271	46.04377	40.92786	A full flexion	44.8174	41.1192	32.22837	40.6379	32.3105
	53.0884	53.61041	40.42553	49.32203	46.86116		46.8922	49.7223	38.27336	46.63952	37.09735
	56.1682	50.53942	37.52055	45.74145	40.57915		33.67977	37.35518	29.05032	36.92862	20.98079
	60.56608	50.54217	44.85803	45.61101	43.78543		38.16875	37.90139	31.76153	37.05986	23.27297
	59.06781	46.53439	47.71608	41.26502	44.2395		46.64934	39.56828	35.24284	38.41568	29.12179
	54.26493	41.66615	48.40625	38.28774	43.76241		54.34785	42.66584	39.48932	40.74567	37.20376
	50.24637	38.96045	46.17439	38.37293	43.41861		57.79632	46.42508	46.36443	43.19297	44.55459
	45.7104	37.90805	44.25132	38.36083	43.40786		57.7725	49.79649	51.33905	45.33179	49.19
	42.05339	37.49033	42.78112	37.1197	43.32973		54.40653	50.89794	52.21932	46.32413	53.58661
	37.60156	37.07189	38.77191	35.5885	41.3324		47.38868	49.29626	50.74815	47.00738	52.55627
	31.93007	36.57915	33.57686	35.04315	37.91087		42.89037	49.16541	46.72541	46.00327	46.55015
	27.25276	35.56984	28.5277	33.62462	30.80345		40.60881	51.41606	39.98185	41.63651	38.21427
	24.91191	35.00777	25.09394	31.53115	26.58325		39.70996	50.59073	33.35035	38.02143	31.88124
	24.82987	35.55926	22.95108	28.97329	24.57319		39.38698	49.28494	28.33302	35.98228	28.0124
	27.10147	37.55692	22.10935	28.05558	24.28733		39.10954	45.80261	25.81104	35.24589	25.97805
	31.64531	41.14846	22.53161	29.30005	25.65296		38.44241	42.20334	25.25539	35.68213	24.19064
	38.29476	45.77232	24.63295	33.17245	29.12212		36.71698	39.41467	25.68958	36.7591	22.56962
	48.37729	49.35749	29.74654	39.88915	34.85184		33.78202	37.78098	27.05477	37.06462	21.09798

E Asian Male											
A full extension	35.0820	34.57603	49.257	34.84122	33.26593	135 flexion	39.8465	37.9257	35.55234	36.86808	35.57871
	36.4554	36.3549	51.4847	37.75841	35.79496		40.3044	39.2430	35.26848	35.24007	34.93032
	40.0437	40.71183	57.1048	42.76079	40.33049		41.0012	42.7293	36.01641	35.81138	35.93622
	43.6989	44.60605	62.4443	45.98015	43.64458		40.7578	44.0239	37.25725	38.91446	38.51247
	46.2854	44.66952	64.325	43.92413	43.3176		41.0246	42.6452	37.9833	38.89226	39.74001
	46.9156	41.32464	62.5204	38.16756	40.30057		41.7039	40.6092	37.99438	38.48633	38.8368
	42.0832	37.56999	56.4136	34.72651	36.962		42.8618	39.3520	38.49859	38.57931	40.27708
	37.3859	36.57085	52.2985	34.95066	35.40209		43.1309	40.0320	38.05792	39.60874	38.5624
	33.2548	33.13645	46.9458	34.98668	31.29842		35.7400	37.9202	33.08607	36.59561	29.82908
	28.0796	26.1183	38.3488	31.26481	26.67513		33.3068	33.3152	28.01578	30.93348	27.21051
	26.9401	22.93907	35.3832	29.45007	24.71358		35.6538	30.6663	24.83715	26.47196	28.67399
	32.5355	29.62193	44.0002	36.42816	30.38309		38.8994	32.4366	28.02789	26.2184	33.26397
	46.5077	44.30104	64.2304	44.38032	42.21428		40.7492	39.3514	36.43682	33.61784	38.70316
	47.1361	43.83024	64.3654	44.17678	43.54708		42.8759	46.4801	40.06046	42.74447	41.01576
	42.3284	39.76903	58.0799	39.6645	38.48096		43.2739	48.4802	39.62049	45.33251	40.95581
	37.0866	35.82657	51.5651	35.53106	33.61837		41.2793	41.9464	37.45961	41.41768	37.75886
90 flexion	47.05771	46.94079	44.2104	45.30642	43.27918	A full flexion	49.0584	56.9689	30.62143	50.70168	52.54985
	44.02187	44.81418	40.69867	41.92187	38.14609		48.9468	57.06679	33.1465	49.44192	48.417
	41.52629	42.83968	37.37945	38.88447	35.55725		49.4957	54.05186	38.03431	49.56457	45.63997
	39.95341	40.80592	34.87428	38.90013	35.8368		50.0762	49.1168	41.23051	48.37098	44.57091
	40.76225	39.20769	33.92379	40.48055	38.80323		49.9552	44.31605	39.92154	46.35058	44.34585
	41.63639	39.10788	36.11903	42.82855	42.21454		49.5121	41.83279	36.83784	46.03511	47.21946
	42.21324	41.34345	37.87696	45.02365	44.84634		51.0116	44.46276	33.7474	49.91768	53.60559
	45.63115	45.37939	39.64255	47.3133	46.15706		52.6536	52.93973	31.68969	53.39751	56.46702
	47.39716	45.972	43.74595	41.89162	42.31307		46.8692	56.03005	30.40737	49.64008	51.38319
	41.39142	36.92627	41.74198	37.10794	35.10925		42.1055	53.06744	26.22479	43.35482	46.29518
	36.43003	33.42628	38.22983	35.98348	32.85078		36.0339	43.64956	23.47173	36.70461	37.77112
	35.89567	33.64948	34.98553	37.51705	34.4904		37.5426	39.75875	24.48068	34.05132	36.45185
	39.14787	37.10503	34.00817	40.16633	38.81669		49.6449	43.9097	35.8325	41.47633	40.51993
	45.14057	43.04888	36.04598	43.13484	42.95999		52.5725	48.34276	42.2932	50.33227	48.16106
	49.55563	47.82549	40.47271	45.78215	46.68167		51.7652	52.06762	38.0144	56.32806	54.85514
	49.64009	48.6805	44.32293	46.67709	47.03045		50.1556	54.82895	32.56698	55.4788	55.56077

LAM Asian Male											
A full extension	54.5174	49.94349	45.54114	48.40932	41.57594	135 flexion	48.7319	49.0003	41.25422	45.5217	39.92015
	53.2305	49.84536	47.28719	49.39635	44.03856		52.4757	49.0760	42.48608	44.47413	42.68317
	52.9111	48.30856	50.0769	51.41693	47.2462		54.7638	46.7979	47.32391	45.3651	47.11895
	49.9510	41.85145	47.29397	49.29976	46.11102		52.4641	41.3420	49.34782	46.88866	49.85619
	44.4534	32.03689	39.73662	42.52274	41.04333		45.7522	35.6187	43.70827	45.25673	45.21056
	37.8752	24.09362	31.40351	34.10345	33.95005		39.1486	31.5723	36.54809	40.35252	39.61741
	31.4843	19.10901	24.59686	27.1177	28.72481		32.4615	28.5989	29.89149	33.05109	34.99776
	25.4220	17.28066	20.6157	23.77507	23.08488		25.7971	25.7119	25.0251	27.57294	29.85448
	22.4879	17.22004	18.05662	22.95212	19.03436		23.5502	23.3392	22.24384	24.48857	25.85015
	22.3610	17.98338	16.75309	24.56062	18.20282		24.0306	23.1394	21.18935	23.91105	24.94911
	24.7307	20.44729	17.03605	29.31075	20.93245		26.5455	25.7666	22.96302	25.97038	26.60887
	29.6286	28.1037	19.41021	38.49437	29.43894		30.7211	31.5961	28.17581	31.17791	32.40764
	36.8234	39.93293	25.72594	48.472	40.92829		36.2023	39.7900	35.13958	40.26869	36.89347
	44.8443	51.42253	36.99893	52.27367	46.37572		41.0654	47.3398	39.3131	50.77548	39.20189
	51.6283	56.29419	45.11614	50.91704	44.50255		44.9044	51.3247	41.08626	52.52202	39.56045
	55.7042	52.73411	46.25248	49.06554	41.82602		46.9249	50.0589	40.86089	48.74126	38.76333
90 flexion	45.73355	51.37178	37.56992	42.4864	41.57743	A full flexion	36.02981	35.80422	24.90453	32.15349	35.75743
	47.26528	50.48232	38.9683	43.1653	43.93573		38.18965	36.30794	28.27953	34.72122	36.45837
	50.10014	47.60997	41.04597	45.89548	45.88974		41.82857	39.26254	37.53459	38.8911	40.49292
	53.88623	43.80692	43.80082	47.28645	47.25419		46.15115	43.35889	46.30041	42.20614	46.25967
	55.63068	40.48709	46.11693	44.95016	46.08561		49.93883	45.76266	48.47526	44.17099	49.23031
	53.91597	37.00918	43.83166	40.66031	41.29426		49.60321	45.65588	46.78579	45.62712	50.13936
	42.2222	32.24669	37.67357	35.64091	36.49208		43.46919	40.92308	41.6102	46.51125	41.03854
	32.3901	27.58819	31.54264	32.04244	32.02424		38.31001	35.61347	37.38005	43.36559	33.13673
	27.4362	25.13398	27.06591	31.3742	27.268		37.76835	34.40166	35.2505	39.73902	30.13512
	25.7971	25.38289	25.57421	32.52132	24.72953		40.03768	36.65703	37.90811	39.40898	31.96032
	26.55114	27.85719	26.08378	34.48111	25.92848		44.53257	40.28178	41.98562	41.26042	34.23761
	29.5268	32.90771	28.3303	38.40104	30.12418		47.55305	44.75117	41.02019	43.87832	35.54779
	34.47071	40.04813	32.2873	43.49768	33.88051		47.97651	48.3515	36.53448	45.93084	37.77879
	38.98893	45.60669	37.07795	45.80232	36.91468		42.1674	48.808	31.21685	45.41086	39.17301
	42.29089	48.42936	38.27749	46.48258	39.44943		36.585	42.32964	27.4797	38.42508	37.36748
	44.69844	50.65621	37.76421	43.96178	40.63765		35.26908	37.16915	24.91262	33.26562	36.22987

LAF Asian Male											
A full extension	48.3488	43.74902	41.92091	43.90369	40.1356	135 flexion	40.9004	40.1518	35.0793	39.27027	35.28694
	49.2332	42.71927	44.27433	44.7199	41.4351		44.6762	41.4718	37.99032	38.7412	36.4613
	48.6665	42.63137	45.4958	44.77164	42.66523		48.9175	41.9606	41.46823	40.51499	39.39208
	46.6997	40.86658	44.5144	42.74487	42.78304		50.8386	40.5136	43.58622	42.98132	42.65265
	43.4316	36.25442	40.14105	39.16218	39.0465		49.7336	37.7616	42.55983	42.09325	44.04419
	40.3160	29.8548	33.37897	34.58747	33.35962		45.6869	34.6930	37.53146	38.72092	41.71914
	36.0704	25.2448	26.04336	30.86176	29.55489		37.8972	32.0778	30.77344	35.15	35.84897
	30.1949	22.35902	20.2551	28.17346	26.5655		31.7543	28.0859	25.6387	31.95176	31.70101
	27.5901	21.83567	18.57065	26.83018	25.37128		28.8990	26.1625	23.88302	28.89374	29.91596
	27.9202	23.82546	18.80675	27.65991	24.48958		28.2223	27.0454	23.75957	28.29669	29.7375
	30.3977	28.13758	20.08355	30.69302	25.99882		29.0545	29.5133	25.92652	30.48619	31.4082
	33.8940	33.0141	23.15025	35.72612	30.84476		31.1965	32.4017	29.52661	34.50035	33.27836
	38.7030	39.79595	28.85827	41.78106	36.55178		33.5751	34.8832	32.4169	39.10932	34.19706
	41.6004	45.42902	34.38819	45.15854	40.08408		35.1203	37.8327	34.42109	42.35993	34.92975
	45.6695	45.77182	37.91378	44.76194	40.08595		36.7297	38.4576	34.25182	42.82811	35.86801
	47.3072	44.56388	39.65544	43.65878	39.4891		38.4690	38.9945	33.95366	41.20755	35.84172
90 flexion	37.43596	38.59318	33.32003	36.19286	35.74052	A full flexion	33.38957	31.42683	24.44422	31.56118	33.20618
	41.62376	38.93456	35.17318	37.18627	37.23758		33.67085	31.74573	25.98048	33.31074	34.71812
	46.43186	39.14143	39.09037	40.35789	39.94966		35.60556	33.78208	30.8286	37.08061	37.62337
	51.6523	39.74571	42.36077	44.54114	42.8967		39.4487	36.81762	38.579	39.81959	40.94111
	54.72146	40.09657	44.83872	47.1353	44.53086		42.63699	40.035	45.36384	42.54745	44.94662
	51.87007	38.32195	44.83508	46.3036	43.05326		42.97034	42.87158	44.20475	42.46665	45.74173
	43.95153	33.62922	38.20077	41.11431	38.42249		40.2472	39.93903	39.17961	41.01403	40.81568
	34.90963	29.52951	31.37449	36.50101	33.25664		36.30102	34.93804	35.42738	39.98135	33.07867
	31.05982	28.62556	27.44929	34.48577	29.15326		35.45952	33.61614	34.05382	39.489	30.74269
	28.66141	30.02135	27.38142	35.17559	25.42337		37.87349	36.17427	34.36573	40.00751	31.78924
	27.37057	32.89385	29.7955	36.34918	24.1994		40.62832	39.49376	36.10291	40.88135	32.0718
	27.53232	35.51099	32.45219	37.58033	24.67726		41.9213	42.2696	37.81913	41.98551	33.46222
	28.55655	36.35402	32.21693	37.98939	26.1641		41.85896	43.23632	36.53236	42.48796	33.19866
	30.13075	35.92523	31.43453	38.05781	29.09911		40.63227	40.06256	32.32376	40.66069	33.56655
	31.68581	35.95269	32.4405	38.18599	32.99582		37.16247	35.9836	28.26818	36.94688	33.43827
	33.95098	37.25042	33.04505	36.90459	34.82504		34.42105	32.85089	25.56441	32.86118	33.10299

UAF Caucasian Female													
A full extension	69.3094	57.88313	53.09827	38.16811	45.20852	39.6094	135 flexion	70.1311	58.8725	52.36982	41.18644	46.28101	41.83007
	69.8159	57.9154	52.62958	37.86523	44.54191	37.78342		70.1018	59.1215	51.79468	40.57762	44.18341	39.05235
	68.5017	55.35213	50.80717	37.10297	42.06285	35.74319		68.7022	55.9118	50.30973	38.24771	41.52772	35.65956
	64.9590	52.80759	48.43229	35.59849	39.32622	33.97488		65.3502	52.2804	48.20967	35.79336	39.30301	33.33839
	63.0748	52.19726	47.07207	34.65218	37.54707	33.86538		63.3405	51.8953	46.99538	35.40781	38.50682	32.61807
	63.6977	54.00167	47.14831	34.69259	38.13073	36.02602		63.5727	54.1156	47.16725	36.77686	39.52859	34.25484
	66.3425	57.534	50.45729	35.73092	41.56542	38.00873		66.0291	57.7828	48.61585	39.58735	42.33609	38.15316
	68.1632	58.77713	53.6379	37.37227	45.59753	39.01077		68.5011	58.2046	50.91022	42.09401	45.7539	41.90246
	69.4489	57.93401	52.82126	38.20073	44.82796	39.6883		70.1237	58.9242	52.3507	40.88446	46.12764	41.70211
	68.1836	57.67675	50.95476	36.97616	43.1842	38.75858		68.6244	56.2025	51.75425	38.87101	43.3892	38.7899
	66.9014	54.49302	48.22445	35.21868	41.04776	36.44726		66.4916	54.0691	49.23162	36.78171	40.65604	36.22678
	64.5684	52.91047	46.25539	34.37602	38.73739	34.53245		63.8364	52.6142	47.73471	34.75851	38.62739	33.34836
	63.1410	52.23561	46.96888	34.60602	37.61569	34.08694		63.2811	51.9957	47.00439	34.96623	38.39268	32.57576
	63.6486	52.95947	48.78144	35.97911	37.96152	35.30528		65.6800	52.8781	48.72955	37.42803	40.45037	34.23153
	65.9486	54.38028	50.25335	38.30127	39.84245	37.8002		68.3273	54.7953	51.60977	39.45171	44.02753	37.16031
	68.5301	56.2443	51.40375	39.11432	43.07421	39.63305		70.0392	56.9668	52.44079	40.83016	46.54147	40.28776
90 flexion	70.05517	62.20964	53.77081	42.30538	46.47509	42.39487	A full flexion	71.87376	62.98006	52.71383	43.23786	45.516	42.90884
	67.46454	59.98337	52.7457	42.03751	43.86002	40.00273		71.62928	62.92489	52.72057	42.84801	43.93802	40.58265
	65.30411	56.48674	50.68367	39.98305	40.28108	37.20035		69.8093	59.5322	52.31642	41.92065	42.17988	38.51764
	64.02652	53.84745	48.91892	37.75751	37.39206	35.25651		68.06508	55.03484	51.46911	40.38817	40.63447	37.46824
	62.01101	53.07774	48.36309	36.60677	36.8511	35.23416		67.52298	54.20834	51.14129	39.95752	40.18903	37.2264
	62.17561	54.85474	49.36288	37.66248	38.71768	36.48166		68.27504	56.93011	53.04302	40.96371	41.20168	37.8162
	65.53475	58.91982	51.43201	40.29605	42.43684	38.73319		70.0732	60.75787	55.82419	42.97751	43.44544	39.13861
	67.71796	60.08657	53.15992	41.85475	46.17412	41.42171		71.8944	63.80505	54.80179	44.15496	45.54277	41.34349
	70.15091	62.27529	53.77237	42.26062	46.44297	42.56581		71.65934	62.73398	52.67357	43.00108	45.59338	43.00968
	68.46794	59.67051	52.17281	40.42504	43.13292	40.57975		69.82469	61.42156	53.34709	40.57418	44.21788	41.16913
	64.45016	56.51562	49.64867	38.0486	39.54776	37.86819		69.86294	58.91825	53.25936	38.82333	41.47914	38.97039
	62.14573	54.05377	48.57102	36.38564	37.24802	35.62278		68.69147	56.01441	51.95537	38.42371	40.01049	37.83443
	62.16346	53.08344	48.35631	36.4726	36.82328	35.20544		67.46967	54.24787	51.15644	39.59507	40.10461	37.22849
	63.90179	54.4424	49.48455	38.20118	38.86054	37.00484		66.98686	54.37751	51.73882	41.99283	41.82634	38.04233
	67.34321	58.16242	51.83707	39.9384	42.85763	39.98049		68.77762	57.01885	52.56234	44.04807	44.67732	40.34404
	69.87195	62.37353	53.43254	41.29835	46.64404	42.64443		71.28093	60.91315	52.80663	44.3477	46.14385	42.52406

UAM Caucasian Female													
A full extension	59.7184	55.267	48.59355	33.67552	38.35995	34.19447	135 flexion	62.4139	55.2152	48.91775	36.96416	40.50269	36.77361
	56.8651	53.23003	47.45813	34.23552	38.14427	34.29591		60.8272	53.6507	47.12897	36.64952	38.14184	35.66171
	57.4109	50.97242	46.66993	34.8092	37.93828	34.04985		58.6237	51.7536	46.07941	36.5512	36.44025	34.34468
	56.6841	49.66597	45.14177	35.30387	37.38726	33.62761		56.6513	49.7957	45.58125	36.135	35.86581	32.64383
	55.7055	48.79759	44.44987	35.53054	36.80056	33.16958		55.4306	48.2185	44.49301	35.66809	36.14529	32.03414
	55.8275	49.13416	46.28424	35.42485	37.29982	32.99807		56.1074	48.2894	44.73551	35.45837	36.65679	33.69584
	56.4355	50.97105	48.88899	34.83458	38.32718	32.90486		58.5516	50.0976	46.63022	35.42602	37.7596	36.14994
	59.8112	53.3476	49.97675	33.69079	38.23771	33.30775		60.3304	51.9645	48.30909	36.2275	39.72915	37.21852
	60.0939	55.30878	48.69049	33.64705	38.35242	34.16559		62.4741	54.8101	48.94526	36.9884	40.77918	36.77887
	58.8617	53.78131	47.92347	34.28433	37.6233	34.0516		61.3106	54.6329	48.87285	36.29663	39.808	36.25773
	57.0149	51.88359	45.30465	34.03577	37.39742	33.05707		59.0986	51.5939	47.61523	34.78378	38.21614	34.37708
	56.2676	50.18226	43.92636	34.18038	36.94844	32.7749		56.3642	48.8791	46.14029	34.15525	36.59522	32.61832
	55.5817	48.81305	44.3271	35.45237	36.76233	33.14264		55.4017	48.1944	44.37568	35.39661	36.12725	32.11163
	55.8464	50.26183	46.28983	35.58123	37.83227	33.78143		57.7066	50.4426	44.559	36.93888	37.56843	32.79517
	58.1183	52.986	48.5934	34.89431	38.49267	34.21772		61.0884	53.4118	46.6024	37.81689	39.88107	34.28722
	60.0409	55.09996	49.45354	34.00542	38.60442	34.17254		62.6716	55.0774	48.38753	37.63471	41.51308	36.05446
90 flexion	66.29488	59.38603	48.56757	38.72978	44.07691	38.11048	A full flexion	60.25523	54.5581	46.24726	34.13064	36.49023	38.06006
	63.43506	58.29966	48.33373	38.69803	40.69945	36.42702		60.75485	55.33452	47.11607	35.2729	37.32182	37.75721
	61.18417	54.36027	47.63625	37.6983	36.33986	34.32087		62.74835	56.17516	48.83884	36.39568	37.9436	36.61657
	59.64369	50.49889	46.63104	35.86102	34.16654	32.39546		63.68261	55.52337	50.01028	36.74488	38.26632	36.49166
	59.8182	48.06956	46.04745	34.97546	34.30404	32.28193		63.8632	54.32324	50.26648	36.09893	38.68104	37.21557
	61.70649	48.97952	46.1133	35.50352	36.93665	33.8576		63.17122	53.2723	50.35013	35.41725	39.11302	37.75651
	63.73775	53.47517	47.12847	37.33142	41.29421	35.58843		61.97787	52.96222	49.80173	35.69195	38.76568	38.29239
	66.01168	57.20651	48.47622	38.64718	44.53037	37.99007		60.65214	54.42915	47.76545	34.76313	37.40881	38.61519
	66.6642	59.38655	48.64164	38.57562	43.86701	38.06498		60.22704	54.58911	46.21038	34.17385	36.50531	37.91457
	66.00373	55.78982	48.52138	36.88324	41.24576	35.785		61.40971	55.36417	46.75089	34.69195	37.04931	36.75747
	64.67658	51.78662	48.03899	34.90093	38.13263	33.05164		63.18551	55.19399	48.9452	35.41769	38.84205	36.56152
	61.54183	48.9311	46.38955	33.77413	35.09005	32.32914		64.32385	54.56625	50.48447	36.06114	39.45089	36.91044
	59.91734	48.18247	46.01412	34.69575	34.51473	32.40574		63.83707	54.41453	50.22495	36.181	38.68712	37.24522
	61.71728	49.69875	47.49188	36.42404	36.75652	33.42215		62.67511	55.09952	49.41253	35.92153	39.01062	38.01414
	65.44916	52.61794	49.97315	37.74098	41.38472	35.70082		61.14387	56.52764	48.48359	35.19357	38.53328	39.34883
	68.10951	56.07713	50.15553	38.46852	44.0467	37.73846		60.84574	56.20036	47.14679	34.3068	36.86559	39.11179

E Caucasian Male													
A full extension	39.5344	38.51597	39.63667	36.94223	40.10488	35.99091	135 flexion	41.7672	45.2195	41.48009	40.25611	44.71258	41.28424
	42.0357	42.31074	41.69442	39.08518	41.82686	38.84531		41.9423	44.7630	40.83196	39.33188	43.68574	39.82689
	44.8745	50.76113	44.83821	42.70616	45.38401	44.06344		44.0943	46.4421	42.27802	39.94994	43.72083	40.10458
	47.6152	56.72402	46.88902	44.03996	48.42455	46.79485		46.2686	50.4199	45.08308	41.27156	44.62379	41.58244
	47.9564	55.85816	47.56637	43.01049	48.41386	45.80989		46.2853	54.2066	47.70298	42.52852	46.25174	43.72448
	44.5153	50.94401	46.96325	40.66919	44.70258	41.62099		44.2990	52.7653	46.86978	42.59347	48.78007	45.60104
	40.1695	47.45579	44.50328	38.37362	41.86313	38.32463		43.1794	48.8314	43.15786	42.35096	50.25171	46.88724
	39.1072	42.25331	42.54187	37.30577	41.88768	37.66655		43.5082	46.4508	42.18578	43.03121	48.39612	45.6986
	39.7612	36.52357	34.71437	36.84742	37.2055	34.55409		38.1132	44.4598	40.681	38.28198	41.66503	34.6384
	35.5504	33.35183	29.10453	33.98474	30.72617	28.87665		28.7114	36.5418	33.73764	31.99849	31.64296	28.84878
	36.5870	37.76305	28.51875	33.60547	28.16816	27.48594		27.7933	35.5290	31.68911	29.49681	27.37864	28.46059
	44.1512	46.90337	37.27696	36.92881	35.75124	34.63895		31.4310	42.7473	34.76318	35.12691	30.80818	32.12459
	48.0511	55.40252	46.42461	42.01157	46.90896	45.00675		39.9503	52.6480	43.89837	41.2953	42.89906	39.45315
	45.8797	55.11399	49.03477	45.46193	49.59738	47.20212		50.2350	54.6292	50.90082	44.86318	49.59391	47.5977
90 flexion	41.6808	47.31138	46.32815	44.87801	45.63272	43.18126	A full flexion	49.8495	51.0546	49.11483	45.74171	49.13138	49.27909
	39.2149	40.35225	41.45759	39.41217	41.47598	37.49935		44.9798	47.5986	44.38614	43.38149	46.71964	45.35858
	49.20649	53.87124	53.39456	49.62808	51.42327	49.34068		59.83099	55.76831	62.32987	49.93396	59.36215	52.03317
	46.2515	52.04194	51.64041	45.63345	47.0368	46.71829		57.05368	56.05615	59.19729	47.05004	56.57703	54.06757
	44.59705	49.94679	49.36677	42.17619	42.78467	42.21593		54.48353	57.53144	55.32523	46.2765	53.68752	54.04615
	44.79341	47.92618	46.54386	39.7655	39.8852	39.7457		53.94217	57.88809	52.59223	47.72857	51.31247	50.19135
	46.17044	46.78026	44.61423	39.75053	39.08263	38.33088		54.98401	54.40637	50.43254	49.05273	49.89987	44.69424
	47.72587	47.81094	44.53978	41.7131	40.58913	38.45394		56.79265	50.8178	48.64965	49.31727	49.79626	42.27685
	49.58271	50.36903	47.01931	44.05096	44.03031	41.33139		59.11646	49.75547	50.18325	50.64171	55.1686	44.06401
	50.99387	54.13756	51.75414	46.91355	50.43996	47.26881		63.59399	53.67978	57.94856	50.90049	61.34478	49.78349
	48.97347	53.26411	53.20081	50.24798	51.14158	48.58751		58.98093	55.92649	61.03531	50.6428	56.41265	51.9004
	43.1899	52.26088	46.61598	43.12961	42.89808	38.64626		52.28504	57.05395	53.2665	47.51471	49.36282	49.05186
	40.0741	45.53528	42.52389	37.38458	36.72704	33.73598		42.2986	53.76403	44.52221	42.97631	38.91832	44.55571
	41.73499	42.49888	41.57915	35.62901	35.26787	33.16103		44.01531	48.75117	44.09621	39.65856	38.32091	39.39194
	45.50119	45.06135	43.36043	37.61217	37.3499	35.91703		52.67383	53.79838	50.09922	44.11865	45.95722	44.58875
	48.77995	49.83274	48.30611	43.20572	42.25678	41.57562		58.68199	58.65338	53.14238	53.10966	53.97744	49.2505
	51.15774	52.32238	54.83781	49.57589	48.19003	47.24327		61.40422	61.01239	57.03701	57.53385	59.66239	50.35308
	51.78624	54.08561	55.72969	51.76078	52.43578	49.65449		61.56411	59.11377	60.82787	54.32263	60.86115	50.70091

LAM Caucasian Female													
A full extension	42.4222	40.66661	38.09012	28.94929	31.30895	29.16473	135 flexion	42.9180	38.9228	38.26586	31.68031	31.47669	29.49753
	44.1230	41.00189	37.83725	30.7861	32.15783	29.48221		43.8787	39.7209	37.88468	32.425	31.99449	29.71182
	44.6845	42.04932	39.34688	34.68576	34.35657	31.03098		45.8275	41.8898	39.51581	34.76408	33.9594	30.89384
	46.1457	43.71669	42.37567	37.55346	37.03662	33.47826		47.3754	44.9407	41.75234	37.11803	36.7826	32.8387
	49.2020	46.71218	45.26189	36.22673	37.41955	34.81932		48.8667	45.3313	43.97717	37.48409	37.61844	34.55278
	49.9443	49.48646	46.53833	34.22278	36.17596	33.78106		50.3321	43.1971	44.7446	36.21019	36.33629	35.19217
	47.9284	47.0076	44.74627	32.17888	34.32268	30.95256		47.7250	40.2347	43.44026	34.73125	33.75324	34.3671
	44.5060	42.82908	40.09296	29.94687	32.62936	29.5755		43.9915	38.4575	40.5975	33.38584	32.17375	30.9307
	42.5925	40.64323	38.18058	28.96951	31.21653	29.17791		42.9183	38.7973	38.56184	31.12262	31.42418	29.49773
	44.5932	42.21136	39.94994	30.40702	31.22429	29.45815		44.6157	40.6610	40.29976	29.81243	31.12307	30.94006
	48.1309	45.13157	43.92787	32.98332	32.91127	31.06944		49.1577	44.0671	43.11768	31.18214	32.59402	34.09407
	49.3558	46.19217	46.74398	36.58478	36.00142	33.49329		50.7433	46.1420	44.30233	34.76408	35.66934	35.93448
	49.5380	47.55195	45.23284	36.47158	37.44581	34.8177		48.8109	45.2958	44.18494	37.427	37.59282	34.45198
	47.6981	45.86251	43.71414	34.66523	36.19439	34.1565		46.8451	43.0582	44.39899	37.40724	36.76006	33.66625
90 flexion	44.5300	42.83392	42.02409	31.9634	33.78753	32.10221	A full flexion	44.7095	40.5580	43.01354	35.52917	33.95718	31.91938
	42.2401	40.9522	39.6067	29.46631	31.90592	30.14608		43.3357	39.1594	40.49488	32.93941	32.1183	30.20838
	42.26604	39.49742	38.36134	32.98635	31.07199	28.9542		38.29255	41.35342	35.99474	30.76776	28.13433	26.82751
	43.33929	40.80762	37.96793	32.34401	31.41035	29.78967		39.92855	41.59297	37.89126	32.48112	28.85762	28.59102
	45.26446	42.98958	39.14161	32.84309	32.91468	31.9651		43.9691	43.07841	41.6253	36.41543	32.56716	32.44786
	47.61703	44.5795	42.64138	34.42498	34.43501	33.91579		48.49822	45.39993	45.05163	39.19608	37.23499	35.72731
	50.21691	45.86273	44.8063	36.55229	36.20925	35.36439		50.34374	48.50875	47.44159	40.22432	39.99205	37.11118
	51.67011	46.21101	44.19292	37.84156	38.46067	35.96357		48.75974	50.58272	47.72088	39.05211	39.80049	35.94702
	49.08759	44.48102	41.74083	37.36124	37.62761	35.30155		44.73354	47.60007	44.49199	36.29822	35.24682	32.72465
	44.20843	41.62118	38.91861	34.83989	33.06161	30.92419		40.52315	42.65042	38.13719	32.80266	30.14306	28.14136
	42.28612	39.03853	38.36219	33.0402	31.12274	28.87369		38.14936	41.37066	36.06477	30.73634	28.30212	26.70186
	44.04121	37.49157	40.43601	33.40384	32.37243	29.85818		39.11262	42.97958	37.60903	32.37702	29.25957	28.60762
	48.06983	38.19466	42.55145	34.97786	34.95029	33.02418		42.45308	45.79463	41.46886	35.28247	32.21377	32.39037
	51.85137	41.88452	43.63078	36.64247	36.0899	36.1144		47.34832	47.94233	45.83992	38.17234	36.58087	35.75182
	49.93934	45.80468	44.77935	36.80227	36.69517	35.17695		50.3481	49.07185	47.57126	40.19799	39.8902	37.06089
	46.37844	45.44026	45.11514	36.23143	37.03236	33.54016		48.0705	47.31138	45.83832	39.01176	39.74075	34.50399
	43.96043	43.40429	43.48075	35.63119	35.95216	31.58602		43.33184	45.10122	41.9807	35.30268	34.98135	30.6107
	42.42128	40.70808	40.2799	34.35815	32.87619	29.78354		39.42699	42.76142	37.19947	32.05482	30.32357	27.57158

LAF Caucasian Female													
A full extension	36.2485	34.83747	35.01402	28.42681	29.10156	27.02737	135 flexion	35.1782	32.2839	33.42811	30.28106	29.0769	26.10673
	36.2163	32.84286	35.03636	29.17271	29.41521	27.35731		35.6189	32.7861	33.58994	30.7043	29.48206	26.26462
	37.0642	32.08573	35.87391	31.34297	31.57459	28.63382		36.6971	34.7285	34.47967	32.62448	31.06413	27.68923
	38.3744	33.33337	36.85777	34.06139	33.66415	30.18325		38.4153	37.0267	35.98608	35.40652	33.40967	29.84176
	39.0270	36.18249	37.47469	35.75496	34.53301	31.05875		40.0911	38.2705	37.36056	36.20329	34.64423	31.65388
	39.2735	38.32629	39.04476	35.49095	33.6997	31.19086		41.2696	37.4209	38.32305	34.4616	34.0028	30.49115
	38.4936	38.62222	39.24256	32.28364	32.19493	30.91869		40.6529	35.8887	37.60617	32.02943	31.27112	28.31367
	37.2065	36.41791	36.14442	29.55163	30.19483	28.66331		37.4286	33.7903	34.80762	30.52633	29.56888	26.7366
	36.2447	35.09458	34.99807	28.40202	29.21098	27.01228		35.1235	32.2580	33.31035	30.29036	29.0708	26.13666
	36.8247	35.91084	36.62086	28.79607	30.41986	27.79144		37.3009	32.8394	35.1311	31.0432	29.16667	27.62745
	38.5842	37.14475	38.81388	31.1742	33.02573	29.95245		42.1148	34.9450	37.1695	32.60957	30.53501	29.85712
	39.6584	36.88895	39.19262	34.28305	34.63222	31.40819		41.5463	37.1685	37.989	34.54971	32.83457	30.7363
	38.9770	36.82867	37.21498	35.77101	34.51573	31.03599		40.0828	38.2697	37.37084	36.17183	34.58754	31.66563
	38.0167	36.97699	36.10354	35.60819	33.73631	30.2471		38.7642	37.7058	35.85431	35.85441	33.86169	31.21798
90 flexion	37.0397	36.78949	35.7074	33.33319	32.34224	28.74398	A full flexion	37.0557	35.7597	34.30935	33.8816	31.23416	29.45423
	36.4918	36.16668	35.54257	29.69529	30.5845	27.5115		35.5042	33.5706	33.51417	31.42938	29.61448	27.28752
	35.39635	33.89883	33.99202	30.42118	27.99244	26.01315		35.02722	35.21434	35.78303	30.7445	27.56544	24.13273
	35.94823	34.41184	35.13812	31.17412	28.14505	25.80801		34.85941	35.63621	36.5361	30.91559	27.91332	25.23637
	37.53507	35.68854	37.50867	32.90908	29.42812	27.11423		36.83489	37.23755	38.18881	32.00128	29.36978	27.90499
	39.91708	37.82214	40.32506	34.77578	31.49906	29.04365		40.03445	39.47588	39.95952	33.40652	31.75041	30.63423
	42.24965	40.16767	41.93374	36.01811	33.63378	30.92296		42.98515	40.31745	41.39894	34.67901	34.77077	32.10483
	41.84756	40.55223	41.42542	34.93241	34.3652	31.8702		44.1976	39.87121	41.5274	34.85225	36.05142	32.39238
	39.57904	38.29069	38.38123	32.85103	32.53812	31.20371		40.74407	38.27134	40.18472	34.11433	33.82455	29.69164
	36.49773	35.20437	34.95715	31.2754	29.3207	27.58422		36.76885	36.18103	37.42656	32.39221	29.34747	25.93288
	35.39585	33.76686	33.98332	30.42121	28.01547	25.88525		35.19968	35.21503	35.70375	30.68932	27.56453	24.01006
	36.51202	34.21641	35.30077	31.7143	29.23704	27.30167		36.64121	36.22678	36.37624	32.32761	28.28007	25.19158
	40.0993	37.56186	38.28406	34.91492	31.96625	30.36454		39.91966	38.70387	38.56232	34.45863	30.93842	28.41784
	42.63484	39.59378	40.87866	36.40097	33.72514	31.61533		42.62795	40.62695	40.67768	34.92805	34.5818	31.34936
	42.16848	40.27784	41.93924	35.88322	33.83781	31.32037		43.39759	40.25223	41.40259	34.71817	35.21883	32.20245
	39.99309	39.35329	41.06533	34.16761	32.75892	30.30168		41.89413	38.99782	39.58861	34.05588	33.88796	30.92385
	37.82712	37.69479	38.45082	32.69128	30.90219	28.62781		39.29521	37.20516	37.64193	33.02446	31.42008	27.95312
	36.11474	35.28381	35.18383	31.17746	28.94979	27.15806		36.87045	35.75569	36.23664	31.60659	28.88906	25.18699

UAF Caucasian Male													
A full extension	59.9570	59.90526	55.70867	43.27856	46.2051	43.45469	135 flexion	59.3997	62.0216	58.24413	44.28459	48.0226	45.87149
	55.9134	58.81144	53.47238	42.7693	44.8671	43.0508		57.3054	60.7492	54.86365	41.54555	45.58551	44.11346
	51.2905	56.36934	49.83328	40.38451	42.80557	41.10635		53.9474	56.9957	50.67444	38.94135	42.00692	41.43423
	47.9619	53.03548	46.90436	38.10784	40.45498	39.30207		51.1583	52.9443	47.20008	37.33459	39.36201	39.34177
	47.1993	50.75196	45.93532	37.61165	39.83022	38.38605		50.4477	51.3341	46.07107	37.24306	39.18539	38.77116
	49.7840	51.73397	48.19922	38.63353	41.9031	38.97543		51.6504	53.0555	48.26232	38.71229	42.22542	40.07301
	54.1215	54.05052	52.36348	40.40739	45.37102	41.55072		53.8937	56.7335	53.14308	40.96622	46.51029	42.93165
	57.5900	58.96906	55.22661	42.52114	45.50252	42.94649		57.9075	60.3679	57.57154	42.97553	49.11563	45.02206
	60.1598	59.8006	55.60586	43.16706	46.14268	43.45707		59.4870	61.9930	58.42565	44.65881	47.87525	45.78752
	57.6634	58.36912	52.42814	41.02377	45.73106	43.25669		57.1081	59.9386	55.94763	42.49004	45.07531	42.7628
	51.5290	56.64176	48.89537	39.13093	42.42757	41.34877		54.3483	55.4561	51.05011	40.05199	41.77279	40.72662
	47.9927	53.34752	46.2013	37.56767	40.50869	38.93004		50.8714	52.6798	47.11486	38.40583	39.58286	39.03311
	47.2445	50.74159	45.84307	37.58806	39.84113	38.37195		50.3429	51.2869	46.04197	37.29771	39.38654	38.73145
	49.4698	51.33157	48.27983	38.51742	41.80701	39.5825		52.7274	51.5505	48.31065	38.54561	41.73433	40.2913
	54.6709	54.93734	52.40852	40.17433	44.8337	41.27436		56.6568	54.4101	53.30258	42.09632	45.51739	43.01624
	59.5120	58.35786	55.10092	42.09108	46.52189	42.70711		59.5785	59.1504	57.888	44.83557	48.25588	45.53976
90 flexion	62.0202	61.68343	59.38182	48.03114	48.6245	44.31345	A full flexion	66.91576	60.66159	60.54829	46.77598	51.20041	44.55993
	59.9445	58.56142	57.1822	44.92757	44.95026	42.85046		64.4801	60.68528	57.52258	45.88866	50.25945	43.28803
	55.78784	54.18645	52.34553	40.96908	41.10305	40.8141		59.95143	58.86815	53.28327	43.83188	48.75301	42.17794
	51.48711	51.20471	47.7952	38.33012	39.1704	39.26094		56.29431	55.33547	50.54567	41.9808	47.05232	41.14779
	49.25821	51.26333	46.52973	38.5357	39.24004	38.86728		55.58931	52.5607	50.01646	41.8626	46.94336	40.83067
	50.93734	52.07261	49.12164	40.84316	40.84971	39.72892		57.88604	54.18639	52.05537	42.97785	48.45475	42.16151
	56.43983	55.0714	53.20946	44.29426	44.64536	41.54281		62.74738	57.73458	56.24275	44.70984	50.45342	43.95931
	61.93083	60.10525	57.04134	48.01091	48.95024	43.32324		67.75968	60.25777	60.73704	46.02926	51.73154	44.73159
	61.47922	61.63194	59.39695	47.94319	48.85034	44.32407		66.74868	60.60193	60.2427	46.69751	51.22747	44.58164
	56.37216	59.17069	57.16981	44.84679	48.07645	43.28327		64.92335	59.59799	57.47395	44.27475	50.62996	43.87653
	52.92617	56.48394	52.4607	41.50804	43.13494	40.44495		61.09558	58.00362	54.44366	42.67938	49.35771	42.20135
	50.44008	53.11305	47.51216	39.27475	39.5215	38.74922		57.3265	54.56254	51.63472	41.92686	47.85232	41.48739
	49.28349	51.271	46.49476	38.78659	39.1831	38.80363		55.64153	52.56014	50.05153	41.88251	46.99539	40.84281
	50.90984	52.67413	49.09805	40.38643	41.18561	40.20901		56.96638	53.49406	51.3514	42.78253	47.85782	41.15017
	55.28693	56.6974	54.84497	44.22381	45.09739	42.40491		61.19286	56.79324	56.00705	44.38391	50.64378	43.10304
	59.91353	60.5165	59.27713	47.8016	48.90098	44.00934		65.19288	59.41505	59.61747	46.01659	51.75505	44.56944

UAM Caucasian Male													
A full extension	50.0796	51.24838	47.84666	37.43715	39.86985	40.04266	135 flexion	51.3884	55.5406	52.98574	40.18546	43.84703	41.32483
	47.5209	51.2507	47.38359	38.02595	40.69493	40.15709		49.8385	53.6560	49.75251	39.81526	43.17384	40.50875
	45.3649	50.17031	45.34873	39.03494	42.27719	40.64816		48.2216	50.6250	45.71417	38.94292	42.23555	39.54243
	44.6242	48.63327	43.51622	39.31283	43.67619	40.34561		46.6215	48.0312	43.01089	37.42126	41.51621	38.40803
	44.9753	47.00272	43.50244	38.4095	43.97544	40.38704		45.6057	47.0936	42.9683	36.66685	41.33471	37.58125
	46.6944	47.46471	44.78449	38.03669	43.11919	40.86204		45.8484	48.1144	45.242	37.31079	43.1027	37.77014
	49.4957	48.38686	46.45449	38.6096	42.25258	40.68142		48.0391	50.3752	48.45561	39.11552	44.89705	39.14302
	50.5516	51.10998	47.95764	38.5696	41.01085	40.88404		51.2072	52.9174	51.6116	40.89904	45.48344	40.78996
	50.2732	51.16775	47.77899	37.34548	39.80744	40.01673		51.4657	55.5583	53.03345	40.16217	43.3693	41.36226
	50.3926	49.04332	46.29743	37.20343	39.49555	40.04799		49.6244	53.7028	50.85853	39.55679	41.24675	39.88203
	48.1915	48.599	44.60853	37.59095	40.3688	40.27747		46.4439	51.1030	47.32545	38.01255	40.0943	37.62745
	45.9713	48.6995	43.37431	38.00068	42.81518	40.314		45.8927	48.2657	44.55103	36.74964	40.59293	36.73243
	45.0535	46.63894	43.49925	38.48935	43.99369	40.39751		45.6143	47.0941	43.15003	36.62771	41.35281	37.37388
	45.9851	46.36751	44.56027	38.92654	43.42146	40.77136		47.0734	48.3204	44.68895	37.83555	42.30038	39.41395
90 flexion	48.7805	47.80071	45.3663	39.38941	42.84515	41.06614	A full flexion	49.9136	51.6670	48.58856	39.46231	42.88673	41.46498
	50.9032	49.49591	46.78919	38.67421	41.27264	40.75671		51.8476	54.9431	51.80391	40.07085	43.46248	42.00939
	57.17716	57.36782	55.19043	45.34646	47.48816	41.58326		51.81754	52.09658	49.75516	40.62121	44.56701	38.42292
	54.73188	56.71928	51.00328	43.27986	44.86301	40.64114		52.54643	52.00242	49.52158	40.61427	45.09343	39.25767
	50.74563	54.02265	46.73048	40.09398	41.94699	40.09127		52.95522	53.23942	49.69724	41.71431	46.05029	39.98203
	47.53799	50.04239	44.15869	37.82044	39.67399	39.10177		53.25534	53.13364	49.45923	42.44375	46.72244	40.91174
	46.39559	48.76413	43.82359	37.56932	39.09196	38.78462		53.32158	52.68466	49.34315	41.98798	46.9396	39.57378
	48.22491	49.63453	46.36679	39.63803	40.64371	39.61276		52.75429	52.7075	49.71774	41.14344	46.95443	38.66577
	52.41224	52.04473	49.86035	43.15615	44.06648	40.26771		53.10313	52.72096	51.30758	42.02926	47.41218	38.3893
	55.79477	55.55344	52.54756	44.77965	46.98387	40.76194		53.93799	52.65092	51.84954	41.74231	46.59722	38.89637
	57.21645	57.15111	55.29141	45.34909	47.63243	41.72854		51.45136	52.01921	49.21797	40.51432	44.50649	38.39326
	54.90346	58.18596	51.38712	44.78626	46.49021	41.31951		52.08136	50.88436	48.21841	39.46127	45.22024	38.03962
	51.43102	53.6871	46.95272	40.68123	43.57586	39.76278		53.25857	51.04195	49.12746	40.02203	46.1674	38.43351
	48.19216	50.11947	44.42295	38.01178	39.96918	38.56833		53.51297	51.98065	49.74541	40.90984	46.42989	39.51887
	46.37913	48.78767	43.91873	37.63414	39.0236	38.72627		53.30066	52.6119	49.34362	41.9824	46.91811	39.82704
	47.83008	49.65223	45.52125	39.24832	40.92915	40.07175		52.01222	54.56998	50.44907	42.90317	47.38722	40.20735
	52.23254	53.276	48.64824	42.20814	43.97718	42.00132		51.1219	56.12247	51.31293	43.1736	47.1682	40.52621
	56.47289	56.37042	53.07568	44.65567	47.07692	42.84876		51.25108	53.95256	50.51118	42.08515	45.82116	39.10721

E Caucasian Male													
A full extension	39.5344	38.51597	39.63667	36.94223	40.10488	35.99091	135 flexion	41.7672	45.2195	41.48009	40.25611	44.71258	41.28424
	42.0357	42.31074	41.69442	39.08518	41.82686	38.84531		41.9423	44.7630	40.83196	39.33188	43.68574	39.82689
	44.8745	50.76113	44.83821	42.70616	45.38401	44.06344		44.0943	46.4421	42.27802	39.94994	43.72083	40.10458
	47.6152	56.72402	46.88902	44.03996	48.42455	46.79485		46.2686	50.4199	45.08308	41.27156	44.62379	41.58244
	47.9564	55.85816	47.56637	43.01049	48.41386	45.80989		46.2853	54.2066	47.70298	42.52852	46.25174	43.72448
	44.5153	50.94401	46.96325	40.66919	44.70258	41.62099		44.2990	52.7653	46.86978	42.59347	48.78007	45.60104
	40.1695	47.45579	44.50328	38.37362	41.86313	38.32463		43.1794	48.8314	43.15786	42.35096	50.25171	46.88724
	39.1072	42.25331	42.54187	37.30577	41.88768	37.66655		43.5082	46.4508	42.18578	43.03121	48.39612	45.6986
	39.7612	36.52357	34.71437	36.84742	37.2055	34.55409		38.1132	44.4598	40.681	38.28198	41.66503	34.6384
	35.5504	33.35183	29.10453	33.98474	30.72617	28.87665		28.7114	36.5418	33.73764	31.99849	31.64296	28.84878
	36.5870	37.76305	28.51875	33.60547	28.16816	27.48594		27.7933	35.5290	31.68911	29.49681	27.37864	28.46059
	44.1512	46.90337	37.27696	36.92881	35.75124	34.63895		31.4310	42.7473	34.76318	35.12691	30.80818	32.12459
	48.0511	55.40252	46.42461	42.01157	46.90896	45.00675		39.9503	52.6480	43.89837	41.2953	42.89906	39.45315
	45.8797	55.11399	49.03477	45.46193	49.59738	47.20212		50.2350	54.6292	50.90082	44.86318	49.59391	47.5977
90 flexion	41.6808	47.31138	46.32815	44.87801	45.63272	43.18126	A full flexion	49.8495	51.0546	49.11483	45.74171	49.13138	49.27909
	39.2149	40.35225	41.45759	39.41217	41.47598	37.49935		44.9798	47.5986	44.38614	43.38149	46.71964	45.35858
	49.20649	53.87124	53.39456	49.62808	51.42327	49.34068		59.83099	55.76831	62.32987	49.93396	59.36215	52.03317
	46.2515	52.04194	51.64041	45.63345	47.0368	46.71829		57.05368	56.05615	59.19729	47.05004	56.57703	54.06757
	44.59705	49.94679	49.36677	42.17619	42.78467	42.21593		54.48353	57.53144	55.32523	46.2765	53.68752	54.04615
	44.79341	47.92618	46.54386	39.7655	39.8852	39.7457		53.94217	57.88809	52.59223	47.72857	51.31247	50.19135
	46.17044	46.78026	44.61423	39.75053	39.08263	38.33088		54.98401	54.40637	50.43254	49.05273	49.89987	44.69424
	47.72587	47.81094	44.53978	41.7131	40.58913	38.45394		56.79265	50.8178	48.64965	49.31727	49.79626	42.27685
	49.58271	50.36903	47.01931	44.05096	44.03031	41.33139		59.11646	49.75547	50.18325	50.64171	55.1686	44.06401
	50.99387	54.13756	51.75414	46.91355	50.43996	47.26881		63.59399	53.67978	57.94856	50.90049	61.34478	49.78349
	48.97347	53.26411	53.20081	50.24798	51.14158	48.58751		58.98093	55.92649	61.03531	50.6428	56.41265	51.9004
	43.1899	52.26088	46.61598	43.12961	42.89808	38.64626		52.28504	57.05395	53.2665	47.51471	49.36282	49.05186
	40.0741	45.53528	42.52389	37.38458	36.72704	33.73598		42.2986	53.76403	44.52221	42.97631	38.91832	44.55571
	41.73499	42.49888	41.57915	35.62901	35.26787	33.16103		44.01531	48.75117	44.09621	39.65856	38.32091	39.39194
	45.50119	45.06135	43.36043	37.61217	37.3499	35.91703		52.67383	53.79838	50.09922	44.11865	45.95722	44.58875
	48.77995	49.83274	48.30611	43.20572	42.25678	41.57562		58.68199	58.65338	53.14238	53.10966	53.97744	49.2505
	51.15774	52.32238	54.83781	49.57589	48.19003	47.24327		61.40422	61.01239	57.03701	57.53385	59.66239	50.35308
	51.78624	54.08561	55.72969	51.76078	52.43578	49.65449		61.56411	59.11377	60.82787	54.32263	60.86115	50.70091

LAM Caucasian Male													
A full extension	37.8781	40.72224	42.83606	35.22039	38.9198	33.74513	135 flexion	38.9129	41.4836	42.13198	36.31391	41.82	35.83179
	37.7071	42.75449	41.95675	37.24237	40.38585	34.67853		39.3896	42.7491	42.09171	37.53739	42.44736	36.83768
	40.0046	46.75544	42.29086	41.49753	44.29368	38.62419		41.5521	45.7414	43.26756	40.32537	43.89083	38.67551
	44.6009	50.66429	43.69954	44.67068	49.48196	43.76737		44.1886	48.9556	45.08173	43.5293	46.21895	41.06372
	45.7795	52.59487	45.38515	44.20109	50.60663	45.8833		45.4484	51.6554	46.0617	45.37319	48.59405	42.82076
	43.3018	52.23966	47.86684	42.71413	47.79195	44.12836		45.4918	50.4492	45.38842	46.31682	48.21984	43.53494
	40.3474	49.39514	46.69745	38.24462	42.31005	39.31948		44.5447	47.5241	44.89984	44.11569	45.47087	43.02661
	38.1833	43.4153	44.33034	35.96566	40.21935	35.52704		41.2471	44.3245	43.5825	38.80268	43.64022	38.04944
	37.9353	40.53539	42.94883	35.09337	38.23218	33.70985		38.9092	41.4639	42.03487	36.23627	41.28067	35.83189
	39.1336	40.64178	43.7863	34.20928	33.6761	34.14606		39.5558	42.5572	41.46441	36.57517	38.61436	37.38914
	40.9238	44.01793	45.44096	35.69907	33.04187	37.52225		41.8264	45.9784	42.66702	38.56058	38.402	40.63572
	43.2873	50.13363	46.50228	40.95761	39.08605	42.59194		44.9134	49.8726	44.43143	42.36767	42.23497	43.33184
	45.8369	52.73435	45.93098	44.24002	48.98221	45.76899		45.4370	51.7054	45.9754	45.41008	47.38365	42.74068
	44.6514	50.14037	46.16906	43.4273	51.59856	45.11492		44.6352	49.9031	46.31858	44.88848	50.78095	40.92531
	41.3096	45.22539	46.16022	39.98358	47.0572	40.67913		42.7827	46.0742	45.33396	41.37987	47.77568	38.35773
	39.1263	41.55918	44.37598	36.22982	41.33462	35.84749		40.3198	42.8193	43.55146	37.48682	43.49145	36.29447
90 flexion	40.13201	41.77282	41.47203	35.65565	42.97591	37.25221	A full flexion	40.43116	40.88061	40.5157	36.04359	37.50465	36.16532
	39.87626	41.90774	42.12534	35.28228	42.48184	37.08672		40.23421	42.65053	40.22894	36.76382	40.20643	36.4179
	40.65103	44.50366	44.67474	36.89804	42.52719	38.09269		41.21478	45.31212	42.06247	41.21807	45.52674	39.30763
	42.4198	47.91064	46.64827	40.49111	43.82722	40.65384		43.43072	48.53974	45.57562	46.22593	49.6783	42.85917
	44.53874	50.23227	47.53774	45.04829	46.18167	43.52233		45.17278	51.22256	48.78636	47.10803	50.03268	45.88922
	46.73219	50.77041	47.49011	46.04272	47.74716	44.47642		47.66681	51.84905	50.20005	44.30068	48.23379	47.421
	47.18477	47.95191	44.97017	43.03087	47.48456	44.1804		47.48173	49.47722	48.17894	40.50049	44.02066	44.33677
	42.33718	43.68689	42.62736	37.98914	45.53003	40.4466		42.68329	43.25853	42.92225	37.36094	39.46597	38.87645
	40.09389	42.01681	41.40955	35.84053	41.91311	34.27483		40.44831	40.76443	40.86466	36.22423	37.35685	36.13019
	40.50203	43.44096	40.96438	37.39621	37.15886	31.97052		42.34665	43.45143	42.98645	37.62149	40.58417	36.80616
	42.53773	46.5612	42.63253	41.46163	35.09188	33.44936		46.0131	47.83827	46.07094	41.18542	46.71425	40.15226
	44.25342	49.54214	45.33572	44.86132	37.55363	37.97692		45.62565	50.64327	47.73035	45.28939	50.08392	44.20945
	44.8676	50.34265	47.47406	45.65173	43.99315	43.48083		45.50486	51.27199	48.86301	47.16885	49.91432	46.22933
	44.23892	48.82843	47.47203	43.78482	49.55497	44.13638		44.70307	47.70871	50.69589	46.76411	46.46557	43.91713
	42.70522	46.24227	45.51022	40.49557	49.15087	42.8656		42.9217	42.89369	49.84538	43.4927	41.81512	41.03741
	41.16551	44.0966	43.00975	37.56403	44.94446	39.44478		41.38993	40.73138	43.94679	38.54527	38.36695	38.20207

LAF Caucasian Male													
A full extension	35.9976	36.34907	39.89802	34.69664	39.30853	32.22676	135 flexion	35.3759	34.6456	40.35026	36.11123	40.87161	32.30363
	36.2016	37.13039	38.88656	36.47627	40.52247	33.53557		35.8305	35.5121	39.81263	37.57449	41.31163	32.88838
	36.7793	38.74829	38.72606	41.11804	43.32801	37.0273		36.9071	38.6862	40.14194	39.84399	42.51951	34.54186
	37.3882	40.86219	39.58898	43.96599	46.4466	40.53798		37.7988	41.7582	40.49335	42.13744	44.07354	36.99233
	38.1278	43.29315	41.203	43.57855	48.64081	41.35358		38.4291	42.4963	40.7068	43.95662	44.9277	39.24201
	39.2956	45.07682	42.91023	41.66944	47.70422	39.18456		39.1875	41.8414	41.74828	43.66913	45.34896	39.98243
	38.5415	43.22403	44.38198	39.14772	43.81961	35.92178		39.4509	39.5691	42.37	41.10217	44.75147	37.828
	36.5441	38.74375	42.16638	36.11814	40.35601	33.32917		37.3697	36.2426	41.63294	37.85026	42.2785	33.6882
	35.9798	36.33636	39.97674	34.67695	39.30855	32.18369		35.2137	34.5600	40.33558	36.16117	40.86803	32.24496
	37.0663	37.35154	41.23433	35.35641	40.33198	32.19064		36.3227	37.0503	39.73815	37.14504	42.39727	33.95445
	38.5018	39.40038	41.91681	38.81872	43.09853	34.51462		38.5024	40.6957	40.09299	39.70737	44.85354	36.88087
	38.6326	42.69762	41.4298	42.64279	46.67411	38.93745		39.2359	42.6615	40.43822	42.85901	45.72625	39.30915
	38.2255	43.70692	41.42382	43.75658	48.69392	41.33443		38.3408	42.4661	40.6944	43.98282	44.85834	39.42521
	38.3986	42.39092	41.77863	42.36329	46.71944	41.29094		37.5444	41.3881	41.97618	42.17534	43.71819	38.81789
90 flexion	37.6829	39.34145	41.67696	38.99533	43.47796	38.4134	A full flexion	36.9124	38.7726	42.61624	39.26272	42.49927	36.20114
	36.5585	37.05865	40.92397	35.83623	40.53677	33.87279		35.9125	36.0599	41.60537	36.58476	41.40685	33.33631
	33.70992	35.84533	37.40458	33.98394	41.14494	32.19333		35.11908	36.39768	37.65637	35.54953	36.37706	33.22246
	34.16854	37.11808	39.1251	34.59688	40.03941	33.23559		35.45618	36.552	37.91624	36.86513	36.55252	35.06271
	36.15822	39.20618	41.26007	36.26765	41.05612	36.23258		36.75914	38.97889	39.46556	40.45051	38.70475	37.65661
	38.60205	41.48836	42.62344	39.03265	43.46221	38.77228		37.84539	41.96031	41.58173	43.45701	41.62905	40.31897
	39.81011	42.99591	43.18862	42.45265	45.76218	40.57175		39.32066	43.62178	43.0008	43.69146	44.0647	40.55936
	39.83815	43.24109	42.24131	42.39222	47.54624	40.64236		40.62736	43.28262	42.88387	42.6934	45.33228	40.59198
	38.34259	41.09098	40.47245	38.28673	47.35467	38.16404		40.21475	40.81623	40.91046	40.36769	43.58623	38.02022
	35.62442	37.63106	38.17737	34.52801	44.49355	34.70096		36.21165	38.10614	38.58784	36.256	39.09428	34.62637
	33.50465	35.85349	37.3456	33.85621	38.94579	31.56288		34.99091	36.63302	37.68284	35.54984	36.24699	33.42923
	33.57341	37.24788	39.27756	35.88941	35.01158	31.80464		36.75595	38.52821	38.58005	36.48457	39.26474	34.69707
	35.79033	41.28664	41.38386	39.35643	35.89042	34.39844		38.88227	42.80644	40.4544	39.36289	44.12047	37.8054
	38.60541	43.37035	42.73309	42.12682	41.29152	37.56804		40.31447	43.9308	42.23537	42.14094	44.91364	40.36028
	39.8238	42.96028	43.19139	42.74543	45.91695	40.51401		39.23731	43.63095	43.0097	43.74046	44.30464	40.42607
	39.38573	41.32707	43.00606	41.68421	46.19352	40.68494		38.47024	42.48665	41.65024	42.7665	43.58271	38.09248
	37.42759	38.57251	41.31663	38.06293	44.77707	37.26779		38.09923	40.40113	40.01427	39.85878	40.81942	35.07178
	35.02816	36.38745	38.52525	35.03432	43.06086	33.5466		36.07785	38.47358	38.66328	36.84322	37.95824	33.02422

APPENDIX E: Distances between points along profiles and bones for the participants for the review of the new FDM

	mm								
	full flexion	135	90	full flexion		full flexion	135	90	full flexion
Participant 1	52.482	52.5422	50.0099	50.8046	Participant 2	73.407	78.6166	74.7655	77.4274
	47.5544	49.197	47.8268	49.3244		67.6127	70.8345	70.9489	73.8037
	46.4136	48.0144	47.2021	48.9445		65.3752	68.535	69.6074	73.0561
	44.4102	45.5834	46.0698	48.2531		60.9083	64.3754	66.7373	71.6945
	43.274	44.3775	45.5349	47.8635		58.7593	62.4189	65.2039	70.7324
	40.2343	42.0059	44.3528	46.7764		54.4682	58.5235	61.9555	67.8149
	38.3533	40.8304	43.6276	46.0102		52.314	56.5198	60.2135	65.8428
	34.2668	38.3153	41.7459	44.043		47.9439	52.2511	56.3179	60.9339
	30.4955	35.4063	39.0884	41.4371		43.2696	47.4065	51.438	54.7621
	27.7633	31.734	35.4781	37.9127		38.517	41.5708	45.0946	47.3596
	26.8616	29.7152	33.2356	35.512		36.1457	38.1778	41.2122	43.133
	26.0424	27.7383	30.706	32.589		33.3395	34.3632	36.8321	38.4591
	24.8498	25.8326	27.8754	28.9825		29.5753	30.2169	32.0392	33.2043
	21.8235	23.0731	23.3493	21.9429		23.3825	24.5432	24.8065	22.8668
	21.5047	22.6495	22.5611	20.5101		22.6563	23.5979	23.3089	20.5881
	21.2135	22.3363	22.2566	20.0121		22.0124	22.797	22.2487	19.5567
	20.9436	22.1312	22.3485	20.2382		21.4101	22.1	21.5769	19.4942
	20.697	21.9798	22.7386	21.1045		20.863	21.4796	21.1896	20.3205
	20.4733	21.913	23.2681	22.5501		20.3815	20.9268	21.072	22.1656
	20.269	21.9085	23.7927	24.2239		19.9475	20.4563	21.2528	25.1146
	20.0948	21.9839	24.2745	25.5451		19.5682	20.1394	21.663	28.8741
	19.9377	22.1331	24.6728	26.0869		19.2412	19.9575	22.1642	32.129
	19.3755	22.8192	25.6667	26.9122		17.6448	20.6751	23.5559	35.2851
	19.8642	22.5836	25.7417	27.1156		17.8965	21.9011	24.3235	36.3152
	20.1797	22.6035	25.8259	27.4642		18.7361	23.1501	24.959	37.4769
	20.7093	22.8884	25.9483	27.9381		19.6468	24.2409	25.5697	38.6948
	21.8744	23.4814	25.9652	29.0704		21.4165	26.0527	27.39	41.5977
	22.3712	23.7793	26.0067	29.6078		22.4455	27.0161	28.5126	43.2369
	23.3468	24.5974	26.4502	30.4559		24.7758	28.9618	30.5168	45.9832
	23.702	25.0382	26.6998	30.7521		25.9456	29.8012	31.1879	46.8895
	23.7416	24.5701	25.2605	30.0296		29.0308	31.2648	30.3599	46.2563
	23.2469	23.5074	23.9477	28.5724		28.8561	30.5463	29.562	43.8517
	22.0782	21.537	21.4849	26.0084		27.6664	28.6318	27.713	39.6076
Participant 3	48.2401	50.572	49.13	50.4686	Participant 4	51.1301	48.7047	48.9334	48.6951
	44.1825	46.9843	46.4728	48.8337		48.5615	46.7754	48.2884	48.4796
	43.2118	45.7368	45.6735	48.2566		47.3186	46.0142	47.873	48.3971
	41.3349	43.0327	44.0838	46.9858		44.2373	44.3526	46.6939	48.0201
	40.1981	41.6393	43.2491	46.269		42.4836	43.4063	45.9201	47.6511
	37.1361	38.8753	41.3959	44.516		38.6091	41.1853	44.0039	46.404
	35.2301	37.5246	40.3417	43.4087		36.4789	39.8868	42.8683	45.4829
	31.0511	34.7626	37.8966	40.6661		31.9133	36.8639	40.253	43.0381
	27.2511	31.7545	34.9315	37.1732		27.4978	33.3349	37.1668	39.7539
	24.5064	28.1963	31.2516	33.0824		23.4961	29.4308	33.5654	35.6976
	23.5683	26.2892	29.0596	30.7158		21.5807	27.3897	31.4558	33.3923
	22.778	24.419	26.6432	27.9825		19.6493	25.3217	29.0178	30.8515
	21.596	22.6248	23.9538	24.6438		16.9285	23.12	26.1167	27.9009
	18.7913	20.4451	19.9562	18.7303		12.7126	19.35	21.1263	20.4118
	18.591	20.2453	19.4493	17.9796		12.5392	18.6869	20.1418	17.8672
	18.4051	20.1388	19.357	18.01		12.3827	18.1537	19.6232	16.3275
	18.2345	20.1337	19.6469	18.6638		12.2405	17.7099	19.4286	15.6967

	mm								
	full flexion	135	90	full flexion		full flexion	135	90	full flexion
	18.0799	20.1791	20.3211	20.0137		12.1165	17.3613	19.3302	15.7993
	17.9379	20.302	21.3473	22.2067		12.007	17.1344	19.0954	16.5283
	17.8076	20.4738	22.633	25.1561		11.9087	16.9841	18.7666	17.7357
	17.6971	20.7066	24.0205	28.2645		11.821	16.9393	18.5437	19.0607
	17.5968	20.9931	25.2227	30.3305		11.7492	17.0024	18.6577	20.4621
	17.1213	22.2301	27.332	32.1219		10.8458	17.7704	20.1113	22.0603
	17.4614	22.2599	27.6372	32.5517		10.6975	17.8976	20.6416	21.6036
	17.7239	22.4963	27.7666	33.0054		11.1558	17.7705	20.889	21.4443
	18.2879	22.8972	27.8574	33.5181		12.0309	17.7756	21.0404	21.8074
	19.5444	23.5636	27.8654	34.5806		13.8669	18.318	21.4567	23.2984
	20.0398	23.8789	27.966	35.0897		14.6824	18.7207	21.7311	24.0018
	20.9188	24.7582	28.6349	35.8643		16.161	19.4823	22.2572	24.8924
	21.2414	25.2619	29.018	36.0325		16.9035	19.8027	22.4183	25.1154
	21.4865	25.1909	28.1967	33.9646		19.4759	20.3623	21.4792	24.7425
	21.0757	24.2432	26.9502	32.0464		19.4542	19.7909	20.6328	24.1559
	20.1154	22.2295	24.2157	28.6663		18.9638	18.7482	19.561	23.1193
Participant 5	42.982	44.4233	46.3561	47.5419		59.8045	60.0595	59.9924	61.8292
	41.237	41.7287	44.2933	46.7125		56.1364	55.0816	57.2665	59.8441
	40.3846	40.7482	43.459	46.1234		54.4944	53.5202	56.1806	59.1894
	38.0015	38.3317	41.3425	44.3982		50.7895	50.3335	53.5632	57.5632
	36.498	36.9252	40.0065	43.3184		48.8354	48.6615	52.0014	56.4623
	32.9176	33.8484	36.8813	40.7058		44.7365	45.1103	48.4864	53.4937
	30.8374	32.226	35.167	39.1155		42.5788	43.2276	46.5864	51.5935
	26.2772	28.8609	31.5794	35.1916		38.0555	39.2426	42.545	46.8803
	22.0651	25.3559	28.0121	30.2592		33.4915	34.9153	38.1563	40.9611
	18.5545	21.8499	24.3555	25.2377		29.1022	30.2335	33.151	34.4998
	16.9773	20.1141	22.3824	23.0497		26.9339	27.6995	30.2721	31.3297
	15.5578	18.3767	20.2393	20.8894		24.5776	24.9396	27.0681	28.0529
	13.4807	16.5881	17.7442	18.4129		21.3352	21.947	23.4543	24.4069
	10.2036	14.4938	14.1564	13.6706		16.2548	18.0101	18.0949	17.0819
	10.214	14.4132	13.8773	12.9797		15.8742	17.5068	17.2416	15.5408
	10.2185	14.4179	13.917	12.9216		15.5356	17.1178	16.7443	14.913
	10.228	14.5026	14.2697	13.4883		15.2214	16.8151	16.5784	15.0941
	10.2428	14.6627	14.9664	14.8776		14.9397	16.5963	16.7059	16.165
	10.2544	14.9196	16.0702	17.4492		14.692	16.4661	17.168	18.4148
	10.2647	15.2184	17.6799	21.5696		14.4692	16.3973	18.0817	22.1814
	10.2724	15.5707	19.6653	26.7698		14.2729	16.4323	19.3674	27.1258
	10.2824	15.9749	21.6387	31.2152		14.1068	16.5626	20.7559	31.5549
	9.6956	17.9418	25.4258	34.6566		12.9058	18.0686	23.7387	35.2673
	9.502	18.5033	26.3153	34.8547		12.8689	19.1052	24.724	35.7952
	9.7934	18.8517	26.5973	35.039		13.4877	19.9243	25.2279	36.3828
	10.5982	19.1616	26.6522	35.4915		14.4018	20.5915	25.5565	37.2012
	12.3487	19.8355	26.871	36.6619		16.2603	21.8379	26.6527	39.2897
	13.0314	20.2231	27.1718	37.2156		17.1829	22.538	27.426	40.41
	14.1073	21.0942	28.1168	37.8605		19.0333	23.9457	28.9717	42.0875
	14.6254	21.5727	28.5834	37.7969		19.9721	24.5936	29.5551	42.4566
	16.588	22.657	28.8544	34.3374		22.9297	26.1873	29.5462	40.1288
	16.5459	22.1919	28.0068	32.5215		22.882	25.7309	28.8398	38.0887
16.2066	20.7938	25.9236	29.3128		22.1653	24.2636	27.1002	34.4834	

	mm								
	full flexion	135	90	full flexion		full flexion	135	90	full flexion
Participant 1	52.8392	52.6433	54.7094	55.3305	Participant 2	59.1448	59.622	60.3997	61.9913
	47.6657	48.7101	50.9986	53.384		55.4119	56.9893	58.2849	60.8431
	45.4286	47.6968	50.2315	53.2899		53.9764	55.5717	57.0758	59.9266
	40.307	45.4157	48.8993	53.2209		50.0436	52.0467	54.1233	57.6721
	37.6874	44.0663	48.2102	52.9707		47.1212	50.0174	52.4067	56.3384
	32.7421	40.939	46.4847	51.5767		39.5492	45.5383	48.5449	53.1689
	30.4022	39.1325	45.3235	50.4568		35.7014	43.1329	46.4341	51.3099
	25.8981	34.9764	42.2239	47.3967		30.0453	38.1476	41.9542	47.063
	21.7611	30.17	38.2133	43.4122		26.7643	33.1123	37.2401	42.6304
	18.686	25.1978	33.5165	39.2227		24.0075	28.2447	32.4477	38.6224
	17.6862	22.8304	30.9467	37.2799		22.3304	25.9463	30.0721	36.5268
	16.9	20.6614	28.2625	35.4295		20.9134	23.7459	27.6739	34.0862
	15.9581	18.7284	25.4545	33.5329		20.4098	21.7835	25.0645	30.9991
	15.1828	17.1188	21.7864	29.5583		19.364	20.1309	21.2348	24.5677
	15.194	17.0805	21.5704	28.7513		19.309	20.0013	20.8283	23.2474
	15.212	17.1087	21.9104	28.3375		19.2646	19.9492	20.823	22.7537
	15.2369	17.2147	22.7903	28.3862		19.2332	19.967	21.1635	22.8676
	15.2688	17.4088	24.1353	28.9766		19.2134	20.0543	21.7901	23.583
	15.3149	17.6768	25.759	30.2873		19.204	20.2129	22.618	24.9389
	15.3702	18.0186	27.3351	32.2919		19.2048	20.4453	23.5104	27.0811
	15.4325	18.4362	28.769	33.6238		19.214	20.7547	24.3683	29.929
	15.5019	18.9489	30.0841	33.339		19.2284	21.1449	25.2609	31.8267
	17.8979	22.5999	32.3977	32.2697		19.5919	23.4926	28.1488	32.8896
	19.483	23.499	32.5027	33.0991		20.0337	24.369	28.9593	33.5711
	20.0978	23.3884	32.2864	34.3378		20.4021	24.8542	29.4453	34.5027
	20.3028	23.0829	32.1053	35.6739		20.9716	25.0308	29.7019	35.2765
	20.8305	22.8743	32.8685	38.2896		23.1575	25.4028	29.9857	36.6495
	21.2754	23.2292	33.4042	39.4441		24.267	25.9124	30.2527	37.3189
	22.4573	24.4968	33.9946	40.5336		26.0925	27.8704	31.0854	38.5614
	23.1485	25.2083	34.0724	40.2693		26.8247	28.9669	31.617	39.0271
	25.21	26.7457	32.5789	35.7506		28.3854	29.7729	33.5637	37.6021
	24.746	25.6215	30.1842	33.6051		27.4581	28.0186	32.2452	34.5286
	23.0603	22.8936	25.6716	29.8517		24.4734	24.9554	28.1037	29.2426
Participant 3	57.8514	58.9411	57.7132	58.7436	Participant 4	48.5355	45.235	45.6991	47.2142
	54.5917	54.3117	54.2474	55.5488		48.4602	46.4113	46.7633	49.8824
	53.1293	52.8777	53.4228	54.7727		47.7671	46.4144	46.7952	50.3456
	48.9467	49.671	51.5275	53.6794		45.1428	45.5989	46.4626	50.5202
	46.0978	47.666	50.2327	53.0275		43.4171	44.728	46.0325	50.234
	39.285	42.8062	46.8552	50.6801		39.4947	42.3594	44.5368	48.8809
	35.771	40.0799	44.8244	48.8529		37.303	41.0389	43.4357	47.8239
	29.8487	34.4336	40.1435	43.9255		32.6332	37.9243	40.768	45.0107
	25.5074	29.3069	34.8311	38.0287		28.0961	33.5904	38.0803	41.5376
	22.2358	25.4776	29.6982	33.5235		24.1973	27.9977	35.1582	37.6424
	21.1825	23.616	27.6527	31.4946		23.2554	25.4143	33.2311	35.6202
	20.1143	21.5099	26.0978	29.0869		21.92	23.3101	30.7768	33.36
	18.2408	19.5039	24.7796	26.1508		17.5941	22.0203	27.8734	30.3852
	17.3969	18.454	21.9239	22.0543		13.7516	21.6721	23.6213	22.2591
	17.4228	18.5265	21.3879	22.1285		13.7171	21.7831	23.1539	20.1561
	17.4507	18.6885	21.2254	22.9653		13.6892	21.9429	23.0165	19.0859
	17.491	18.9469	21.464	24.3146		13.67	22.1304	23.139	18.8187

	17.5415	19.2933	22.1008	25.9909	13.6584	22.3199	23.4455	19.2625
	17.5943	19.7063	23.091	28.1918	13.653	22.4819	23.821	20.4432
	17.6499	20.1907	24.3391	31.1753	13.6535	22.5564	24.0834	22.3396
	17.7105	20.7412	25.7573	34.5317	13.6583	22.5961	24.0346	24.6942
	17.7766	21.3405	27.1889	36.783	13.6713	22.643	23.8128	26.1891
	19.4387	23.3989	29.1894	38.0369	15.1266	22.429	23.2942	26.6735
	18.9864	23.3619	29.4352	38.1003	14.8498	21.5086	22.814	26.3141
	17.9751	23.3384	29.6314	38.0719	14.8003	20.9102	22.6282	26.3625
	17.9111	23.3407	29.6785	38.0603	15.5218	21.0372	22.8523	26.8187
	18.9701	23.5207	29.5313	38.1485	16.6028	22.1805	24.3949	29.347
	19.738	23.8741	29.4093	38.1784	17.3444	22.8062	25.2755	30.7706
	21.0957	25.1344	29.1986	38.0405	19.1076	23.8996	26.6592	32.7928
	21.6411	25.834	29.103	37.8178	19.9836	24.3662	27.1808	33.3621
	22.8904	26.1658	28.1317	34.6905	22.5462	26.2814	28.3863	33.3203
	22.4233	24.8774	26.8638	32.6058	22.9163	26.6954	28.0826	32.4565
	21.1278	22.2539	23.8741	29.0985	23.3087	26.046	26.8823	30.3458
Participant 5	47.0014	48.4732	48.114	49.841				
	47.0108	48.6462	49.1553	50.7471				
	46.4818	48.1538	48.7355	50.4602				
	44.5058	46.4766	46.9289	49.1394				
	43.0275	45.3152	45.7349	48.159				
	39.1643	42.4423	43.1402	45.6323				
	37.0519	40.7779	41.7399	44.0938				
	33.2254	37.103	38.5687	40.5422				
	29.993	33.1165	34.6785	36.4199				
	26.5891	28.3982	29.7688	31.7694				
	24.8978	25.6819	26.8678	29.26				
	23.0789	22.9927	23.6342	26.6089				
	19.8957	20.466	20.0814	23.4688				
	14.9656	16.894	15.162	16.7837				
	14.8105	16.4379	14.5699	15.5157				
	14.6747	16.0723	14.245	14.9988				
	14.5468	15.7999	14.1862	15.1024				
	14.4271	15.6145	14.3355	15.8572				
	14.3261	15.5145	14.6876	17.3082				
	14.242	15.5006	15.2578	19.6129				
	14.1666	15.5741	16.035	22.9768				
	14.0999	15.7385	17.0291	27.2154				
	13.9408	17.0171	20.3301	32.0056				
	15.0655	17.4665	20.893	31.8878				
	17.2048	18.0832	21.4402	31.5835				
	18.9749	19.2191	22.2208	31.6949				
	21.4244	21.9821	24.529	34.0953				
	22.5537	23.0662	25.867	35.6191				
	25.0011	24.7303	28.4225	37.5206				
	26.2213	25.4535	29.5133	37.9096				
	29.6346	28.3261	31.7084	36.5804				
	29.6593	28.37	30.9374	34.8838				
	28.3519	26.9027	29.2632	31.5532				

	mm								
	full flexion	135	90	full flexion		full flexion	135	90	full flexion
Participant 1	81.3459	84.0558	86.5737	88.7123	Participant 2	73.2788	77.3717	78.9283	79.8842
	80.5806	82.329	84.8348	86.7868		71.6488	75.7882	77.505	78.7117
	79.6504	80.9705	83.5205	85.3095		70.5801	74.6379	76.4514	77.7519
	76.1813	76.7089	79.6438	81.7657		67.4147	71.1918	73.3966	75.1873
	73.7782	74.0134	77.2265	79.8031		65.3991	69.0092	71.4832	73.6548
	68.0931	68.1805	71.8924	75.5841		60.7369	64.1	67.1635	70.1409
	65.0265	65.2932	69.1288	73.2355		58.1893	61.5365	64.8571	68.1317
	59.0445	59.4995	63.4951	67.8606		52.9123	56.2312	59.9762	63.5323
	53.0243	53.3428	57.5931	61.2261		47.3477	50.5909	54.5877	57.948
	45.9799	46.1057	50.7347	52.895		41.2667	44.2116	48.2993	51.0509
	42.027	42.0968	46.5668	47.878		38.1432	40.7417	44.6431	46.9338
	38.0065	37.9235	41.7413	42.1459		35.0997	37.1749	40.5577	42.2506
	33.3995	33.5043	36.2302	35.3838		31.7654	33.559	35.9752	36.7786
	25.5239	25.5144	26.5615	21.8908		26.4788	27.8737	28.0465	25.4218
	24.8141	24.0546	24.1909	18.8789		25.9363	26.8557	26.1511	22.7252
	24.1392	22.7451	22.4686	17.3327		25.4324	25.9441	24.8648	21.4238
	23.5038	21.6305	21.1884	16.8046		24.9699	25.1598	24.0525	21.1612
	22.9411	20.6554	20.2881	17.104		24.5607	24.4762	23.6604	21.7867
	22.4134	19.8749	19.7065	18.1765		24.1821	23.9189	23.6188	23.3815
	21.9473	19.2771	19.4716	20.0682		23.8542	23.4817	23.8928	26.0907
	21.5245	18.8818	19.5935	22.978		23.5686	23.1749	24.4526	29.4279
	21.1574	18.6558	20.1447	26.7661		23.3284	22.9774	25.3161	31.967
	18.7365	19.2295	23.762	33.7271		21.6753	22.8177	28.6194	36.8512
	19.0816	20.3132	25.9173	34.9725		20.541	22.9894	30.1159	37.9883
	20.1236	21.0323	27.6259	35.9171		20.63	23.2867	31.2624	38.9609
	21.3558	21.9346	29.0278	37.1548		21.7543	24.0189	32.2466	40.0803
	24.5534	24.9638	31.6215	40.7232		24.5579	26.469	34.159	42.8368
	26.3604	26.7633	32.871	42.5139		25.8846	27.8217	35.0976	44.1056
	29.6847	30.3372	35.267	45.3441		28.3645	30.3511	36.7764	45.8215
	31.085	31.8786	36.3676	46.3599		29.4287	31.3777	37.4426	46.2145
	34.2413	34.3159	39.2849	47.3844		31.382	32.5806	37.9188	44.1992
	33.6136	33.4292	38.4248	46.0751		30.6931	31.6141	36.5038	42.0517
	31.3866	32.0882	35.6939	42.775		28.8642	29.9278	33.3328	37.841
Participant 3	76.9548	79.6512	79.9251	78.2322	Participant 4	52.9211	54.0126	55.0037	57.122
	76.1459	79.5539	79.5711	78.6467		48.6642	50.2668	52.642	55.3822
	75.4382	78.8677	78.9923	78.5337		46.9356	48.9157	51.5211	54.4552
	73.5452	76.5985	77.3013	77.3988		43.0671	45.7956	48.4863	52.2535
	72.3356	75.0213	76.1637	76.4393		41.0058	44.0513	46.69	50.9752
	69.165	70.9684	73.147	73.7595		36.886	40.3382	43.0543	48.0611
	67.1462	68.5595	71.2393	72.1204		34.8509	38.4464	41.3839	46.3951
	62.085	63.2247	66.631	68.346		30.7936	34.6102	38.2151	42.6154
	55.9981	57.4844	61.0324	63.8398		26.7065	30.6426	34.6818	38.21
	49.8676	51.3569	54.7384	58.2917		22.651	26.3168	30.058	33.1354
	47.0328	48.0722	51.4308	54.9569		20.9263	24.0899	27.2825	30.2737
	44.2963	44.6999	48.0032	51.178		19.5647	21.9466	24.2048	27.0668
	41.5509	41.4459	44.2613	46.8689		18.2251	20.0348	20.8596	23.3222
	37.6578	37.8703	37.2559	36.4413		16.7916	17.3802	16.3799	16.5545
	37.0271	37.1961	35.2751	33.4039		16.6838	17.0478	16.0127	15.3645
	36.4679	36.573	33.9339	32.0334		16.5876	16.7907	16.087	14.8936
	35.9803	35.9909	33.1391	31.9858		16.5055	16.6144	16.6029	15.0291

	35.5444	35.4596	32.8488	33.0878		16.4389	16.5128	17.5091	15.7746
	35.1489	34.9546	33.019	35.7261		16.3834	16.5131	18.668	17.0753
	34.8208	34.4891	33.617	40.3727		16.3386	16.5912	19.8572	18.7962
	34.5602	34.0489	34.6552	45.1257		16.3082	16.7723	20.8584	20.9179
	34.3548	33.6239	36.129	45.601		16.2916	17.0525	21.5698	23.4117
	32.4218	31.0723	40.5163	49.0032		16.5034	18.9134	22.0805	24.8382
	26.806	29.5516	42.011	50.7678		17.0056	19.3735	21.668	24.5724
	24.5681	29.2194	42.9389	52.3604		17.5657	19.5385	21.5619	24.5503
	26.0925	29.92	43.5965	53.7663		18.0523	19.8321	21.9001	24.8293
	30.0565	32.2928	44.8238	55.9909		18.8397	20.7349	23.0233	26.1518
	31.3118	33.4149	45.4615	56.6476		19.2568	21.1905	23.5811	26.967
	33.4297	35.2609	46.4414	56.6281		20.3836	21.8735	24.3908	28.4587
	34.2869	35.9173	46.6519	55.8822		20.9748	22.0481	24.5864	29.02
	35.1078	36.0837	43.563	47.588		21.6427	21.4652	24.161	29.0731
	34.0308	34.8056	40.84	43.579		21.2329	20.8076	23.4043	27.7217
	32.1147	32.2888	36.0439	36.7823		20.3104	19.5601	21.7749	25.3543
Participant 5	61.7693	61.2164	62.1324	63.4193	Participant 6	50.9123	50.2373	50.3364	51.1251
	58.6889	58.3753	60.2424	62.1401		46.3642	46.9052	48.4081	50.2103
	57.2715	57.169	59.2296	61.3616		44.5481	45.7877	47.5565	49.7974
	53.8235	54.1738	56.4434	59.3212		40.5045	43.4435	45.3423	48.531
	51.8622	52.4153	54.7578	58.076		38.3651	42.158	44.036	47.6516
	47.6662	48.5148	51.1667	55.1434		34.1521	39.2206	41.3307	45.3686
	45.4707	46.4569	49.3861	53.4469		32.1102	37.5691	40.0388	43.9997
	40.927	42.1889	45.7712	49.5832		28.133	34.0385	37.4098	40.8941
	36.1721	37.7173	41.6604	45.0368		24.2152	30.3791	34.159	37.3933
	31.268	32.8425	36.5525	39.6849		20.3304	26.6557	29.898	33.527
	28.9896	30.2894	33.5865	36.6049		18.6938	24.8132	27.525	31.4097
	26.9583	27.7693	30.339	33.1382		17.4417	23.0995	25.0626	29.0687
	24.847	25.4305	26.7916	29.1093		16.2114	21.7793	22.4927	26.4003
	21.9486	22.2899	21.4833	21.1831		14.9652	21.054	19.3246	21.1984
	21.6509	21.8227	20.6566	19.4923		14.9012	21.0782	19.2424	20.1359
	21.3792	21.4295	20.3258	18.7675		14.8435	21.1379	19.5832	19.8063
	21.1362	21.1145	20.4596	18.8277		14.7949	21.2163	20.4018	20.1581
	20.9243	20.8723	21.008	19.6272		14.7589	21.3339	21.6547	21.2151
	20.7324	20.7206	21.8581	21.2078		14.7314	21.4881	23.2044	23.0755
	20.5697	20.6439	22.8421	23.5769		14.7099	21.6627	24.7889	25.7385
	20.4356	20.6586	23.8045	26.3155		14.6981	21.8714	26.1736	28.4402
	20.3293	20.7577	24.6738	28.4374		14.6967	22.1205	27.2167	29.6889
	19.7362	21.5861	26.1971	30.5909		15.0871	22.9945	27.7617	29.4676
	19.107	21.6468	26.3382	30.8493		16.1373	22.5053	26.9281	29.2687
	19.2373	21.7328	26.5548	31.2315		16.9509	22.2644	26.4155	29.3989
	20.0297	22.1477	27.0196	31.8078		17.3482	22.4424	26.4162	29.6644
	21.7733	23.4852	28.244	33.4472		17.8631	22.9586	26.9557	30.3531
	22.5621	24.1581	28.8562	34.2798		18.2123	23.0788	27.2496	30.7021
	24.2162	25.2494	29.7877	35.513		19.2615	22.9466	27.4498	31.106
	24.9836	25.6022	30.0349	35.813		19.833	22.7121	27.2691	31.0226
	26.0732	25.3442	29.2062	34.0946		20.5	21.1161	24.5118	27.7731
	25.5083	24.5389	28.0145	32.165		20.149	20.34	23.1172	25.4829
	24.1994	23.0091	25.6346	28.7804		19.3089	18.6919	20.8545	21.9734

	mm								
	full flexion	135	90	full flexion		full flexion	135	90	full flexion
Participant 1	71.6115	71.4019	72.2804	73.6692	Participant 2	63.639	58.7184	60.9513	62.5855
	69.6056	70.5202	71.7737	74.04		61.4818	59.3486	62.0125	63.7427
	68.3791	69.6217	71.133	73.5923		59.8767	59.0179	61.7412	63.6912
	65.0606	67.1005	69.0799	71.9673		56.0293	57.5803	60.2155	62.8595
	63.0069	65.511	67.6624	70.8202		53.8183	56.4512	59.132	62.0925
	58.1948	61.6776	64.0812	67.8343		48.8374	53.3614	56.3172	59.7917
	55.3976	59.3803	61.9002	66.0175		46.1204	51.4124	54.5066	58.2307
	48.8629	53.8469	56.8028	61.648		40.4935	46.6946	50.032	54.1391
	41.3415	46.6788	50.9296	56.2547		34.8883	40.9016	44.4875	48.679
	34.5017	39.2415	44.442	49.6406		29.2882	34.8688	38.0332	41.7954
	32.5044	36.4432	40.7423	45.7253		26.0743	32.3048	34.4339	37.8091
	31.3745	34.5593	36.6873	41.2674		22.4486	30.2485	30.5349	33.396
	29.2433	32.9454	32.3637	36.0719		19.2248	28.1841	26.3169	28.2918
	25.016	29.7434	26.4727	25.5554		17.5182	24.9287	20.2832	18.4445
	24.6853	29.1957	25.8113	23.157		17.4956	24.4396	19.4821	16.4967
	24.4002	28.7564	25.8306	21.8766		17.4849	24.0452	19.1813	15.58
	24.1574	28.3751	26.4136	21.5271		17.4806	23.7064	19.2849	15.5025
	23.9511	28.0646	27.5642	22.1695		17.4784	23.4305	19.7029	16.2758
	23.7821	27.8234	29.0363	23.9693		17.4827	23.2257	20.272	17.9534
	23.6594	27.6184	30.1018	26.6484		17.4964	23.0548	20.721	20.8453
	23.5937	27.5091	29.8028	28.4771		17.5113	22.955	21.1155	25.4839
	23.5664	27.4662	28.9117	29.5829		17.5357	22.8949	21.8869	30.7036
	23.9363	27.5312	28.5101	32.1314		18.081	22.6608	25.4452	36.0223
	24.5785	27.3396	28.8223	32.7912		18.5354	22.4885	26.448	36.3923
	25.812	27.6474	29.5311	33.6777		19.542	22.9487	26.8842	36.9434
	27.196	28.4236	30.5108	34.9317		20.6087	23.7658	27.2337	38.0126
	29.69	30.6042	32.6077	37.8046		22.4569	26.0939	28.9846	40.806
	30.7129	31.6949	33.4312	39.0591		23.3239	27.4757	30.0905	42.1709
	32.2161	33.3474	34.4731	40.6636		24.8526	30.1648	32.0702	44.2679
	32.6971	33.8097	34.7254	40.9627		25.5542	31.2662	32.8393	44.8676
	32.4205	32.735	33.3241	38.9396		28.0828	32.5541	33.737	43.9018
	31.3967	31.1091	31.335	36.8853		28.4855	31.4713	32.5296	41.9803
	29.3101	27.848	27.2779	32.7673		28.7048	29.2267	29.7158	37.5868
Participant 3	52.527	49.9261	50.5814	53.3766	Participant 4	64.624	68.9726	68.4179	71.1942
	48.5493	47.4465	49.1261	53.403		61.4854	65.8986	66.1712	70.9751
	47.015	46.4272	48.51	53.3048		59.7504	64.5018	65.296	70.5469
	43.3915	44.0096	47.1554	52.6898		55.5582	61.1678	63.3124	69.1068
	41.2938	42.5971	46.4865	52.1456		53.1479	59.2612	62.1635	68.0776
	36.6718	39.4111	44.9934	50.5172		47.8166	55.0195	59.3866	65.353
	34.2495	37.6818	44.0678	49.3871		44.9334	52.6978	57.691	63.6565
	29.5289	34.0815	41.5855	46.4536		38.9051	47.6658	53.5728	59.584
	25.0868	30.6581	37.7823	42.5856		32.745	41.9335	48.2964	54.6145
	20.9035	27.21	32.589	38.0188		27.0355	35.8626	41.8527	48.8073
	19.2974	25.213	30.0885	35.6119		24.6803	33.0326	38.4542	45.566
	18.2204	23.0427	27.8629	33.1652		22.6165	30.4902	35.0804	42.0597
	18.1719	21.3442	25.8426	30.6322		20.8785	28.5339	31.7839	38.2843
	18.6741	21.1373	23.0165	26.3607		19.5209	26.6275	27.5361	31.2602
	18.7429	21.383	22.8208	25.9586		19.4803	26.4621	27.1774	29.8578
	18.8224	21.7208	23.019	26.1311		19.4566	26.3974	27.4119	29.3622
	18.9084	22.1552	23.6013	26.8834		19.4503	26.4225	28.1962	29.6638

	18.9978	22.6471	24.4938	28.3499		19.4524	26.5298	29.6251	30.8319
	19.1021	23.147	25.783	30.7755		19.4757	26.6874	31.7432	33.2747
	19.22	23.6568	27.6752	34.1036		19.5194	26.9033	34.2112	36.6071
	19.3481	24.1359	30.0806	37.099		19.5893	27.1717	35.7358	37.6191
	19.4768	24.6065	32.3382	38.5396		19.6694	27.4935	36.1605	36.4135
	20.4498	25.9172	35.3957	38.1055		21.1827	28.475	36.1883	35.607
	20.5101	25.7356	35.0181	38.2199		22.5246	28.2693	35.9857	36.1951
	20.5269	25.9038	34.4371	38.9189		23.4702	28.8453	36.1582	37.1935
	20.7106	26.3476	34.2405	39.7829		24.1993	29.8313	36.8141	38.3166
	21.8767	27.2162	34.7123	41.3041		25.5539	31.3291	38.0176	40.1778
	22.6545	27.5325	35.0872	41.7476		26.1606	31.6273	38.3466	40.7058
	23.9522	27.9683	35.6842	41.8667		27.0809	31.5907	38.4928	40.872
	24.3363	28.0706	35.8674	41.6056		27.3678	31.3488	38.3563	40.607
	24.3372	27.7867	34.8844	38.0379		27.2514	29.4027	35.5069	37.1015
	23.3502	27.0903	33.2523	36.0544		26.4439	28.1526	33.32	35.0267
	21.279	24.9576	30.161	32.8995		24.9621	25.0721	29.1101	31.839
Participant 5	47.2388	50.1621	51.1699	52.5386	Participant 6	55.4132	57.9294	59.6682	62.3511
	43.467	47.684	49.5021	52.0713		53.9674	58.0743	60.4573	63.6346
	42.3345	46.5882	48.7825	51.7124		53.2413	57.6748	60.1891	63.7248
	39.5855	44.1383	47.2597	50.6469		51.254	56.0789	58.7702	63.1732
	37.9148	42.8077	46.4034	49.9647		49.936	54.84	57.8468	62.5072
	34.1029	39.9628	44.5393	48.2992		46.6099	51.4893	55.412	60.2911
	32.0764	38.3745	43.5281	47.3137		44.6607	49.4657	53.7589	58.6856
	28.1188	34.7256	41.1582	44.9963		40.3559	44.8943	49.4551	54.3483
	24.3698	30.6489	38.0362	42.1405		35.7448	39.775	43.7001	48.4651
	20.7364	26.907	34.1584	38.7624		30.9033	34.2163	36.5817	41.1531
	19.5741	25.5038	32.2765	36.8827		28.5555	31.3428	32.7347	37.0492
	19.1781	24.524	30.5717	34.8224		26.3385	28.525	28.725	32.6546
	19.7037	24.0778	29.0277	32.448		24.0078	25.7368	24.4973	27.7927
	20.0697	24.8624	26.7536	27.5367		21.3354	22.2671	18.5528	19.0732
	20.0854	25.1838	26.7249	26.7898		21.1447	21.8267	17.7336	17.5327
	20.1195	25.6152	27.2145	26.5423		20.9872	21.4698	17.3294	17.0129
	20.161	26.1297	28.1606	26.8768		20.8429	21.1827	17.288	17.3001
	20.2137	26.6773	29.3767	28.0702		20.7218	20.9736	17.5966	18.334
	20.2805	27.198	30.6438	30.1721		20.6086	20.849	18.3156	20.3226
	20.365	27.6604	31.771	32.6627		20.5184	20.7985	19.4699	23.7942
	20.4564	28.0706	32.684	34.1417		20.4289	20.8199	21.05	29.05
	20.5544	28.4545	33.401	33.9306		20.3673	20.8869	22.9254	34.6287
	20.3847	29.8944	33.3694	32.1876		18.4529	20.7922	28.2008	39.8811
	19.0225	29.7205	32.1183	32.2764		16.0376	20.613	29.5407	40.2453
	18.5563	28.989	31.5288	33.0752		16.2166	21.5966	29.8568	40.7676
	18.7572	28.6005	31.6049	34.0368		17.4922	22.8884	29.9872	41.7553
	20.4443	29.0597	32.4812	36.078		20.6139	25.2725	31.3246	44.0515
	21.5965	29.553	32.8487	36.8138		22.2937	26.3861	32.3244	45.1025
	23.5762	30.2052	33.1819	37.2201		25.268	28.5898	34.2444	46.73
	24.2245	30.2414	33.2193	36.9297		26.5318	29.5709	35.0046	47.2192
	24.9319	28.8179	31.8678	32.7885		30.4849	31.2665	35.7831	46.2201
	24.0448	27.6094	29.7945	30.7168		31.0886	30.5365	34.764	44.3403
	21.7488	24.8202	26.1419	27.3117		30.8367	28.6789	32.2146	40.284